World Journal of
Clinical Cases

World Journal of *Clinical Cases*

Contents

Contents

Contents

Contents

ABOUT COVER

Editorial Board Member of *World Journal of Clinical Cases*, Shu-Pin Huang, MD, Associate Professor, Attending Doctor, Director, Department of Urology, Kaohsiung Medical University, Kaohsiung 807, Taiwan

AIMS AND SCOPE

World Journal of Clinical Cases (*World J Clin Cases*, *WJCC*, online ISSN 2307-8960, DOI: 10.12998) is a peer-reviewed open access academic journal that aims to guide clinical practice and improve diagnostic and therapeutic skills of clinicians.

   The primary task of *WJCC* is to rapidly publish high-quality Case Report, Clinical Management, Editorial, Field of Vision, Frontier, Medical Ethics, Original Articles, Meta-Analysis, Minireviews, and Review, in the fields of allergy, anesthesiology, cardiac medicine, clinical genetics, clinical neurology, critical care, dentistry, dermatology, emergency medicine, endocrinology, family medicine, gastroenterology and hepatology, *etc*.

INDEXING/ABSTRACTING

The *WJCC* is now indexed in PubMed, PubMed Central, Science Citation Index Expanded (also known as SciSearch®), and Journal Citation Reports/Science Edition. The 2019 Edition of Journal Citation Reports cites the 2018 impact factor for *WJCC* as 1.153 (5-year impact factor: N/A), ranking *WJCC* as 99 among 160 journals in Medicine, General and Internal (quartile in category Q3).

RESPONSIBLE EDITORS FOR THIS ISSUE

Bone alterations in inflammatory bowel diseases

Dolores Sgambato, Francesca Gimigliano, Cristiana De Musis, Antimo Moretti, Giuseppe Toro, Emanuele Ferrante, Agnese Miranda, Domenico De Mauro, Lorenzo Romano, Giovanni Iolascon, Marco Romano

ORCID number: Dolores Sgambato (0000-0002-7501-3792); Francesca Gimigliano (0000-0002-1905-6405); Cristiana De Musis (0000-0001-7011-5047); Antimo Moretti (0000-0002-4598-2891); Giuseppe Toro (0000-0002-8560-721X); Emanuele Ferrante (0000-0001-5612-0560); Agnese Miranda (0000-0003-4682-9087); Domenico De Mauro (0000-0002-4484-0963); Lorenzo Romano (0000-0002-6581-7930); Giovanni Iolascon (0000-0002-0976-925X); Marco Romano (0000-0002-3271-349X).

Dolores Sgambato, Cristiana De Musis, Emanuele Ferrante, Agnese Miranda, Domenico De Mauro, Marco Romano, Departments of Precision Medicine and Polyspecialistic Internal Medicine, University of Campania ''Luigi Vanvitelli'' and University Hospital, Naples 80131, Italy

Francesca Gimigliano, Department of Physical and Mental Health, University of Campania "Luigi Vanvitelli", Naples 80131, Italy

Antimo Moretti, Giuseppe Toro, Giovanni Iolascon, Department of Medical and Surgical Specialties and Dentistry, University of Campania "Luigi Vanvitelli", Naples 80131, Italy

Lorenzo Romano, Surgical Digestive Endoscopy, Department of Clinical Medicine and Surgery, Federico II University, Naples 80131, Italy

Corresponding author: Marco Romano, MD, Professor, Departments of Precision Medicine and Polyspecialistic Internal Medicine, University of Campania ''Luigi Vanvitelli'' and University Hospital. University of Campania "Luigi Vanvitelli", Via Pansini 5, Naples 80131, Italy. marco.romano@unicampania.it
Telephone: +39-081-5665718
Fax: +39-081-5665714

Abstract

Inflammatory bowel diseases (IBDs) are characterized by a multifactorial partially unknown etiology that involves genetic, immunological and environmental factors. Up to 50% of IBD patients experience at least one extraintestinal manifestation; among them is the involvement of bone density which is referred to as metabolic bone disease (MBD), including osteopenia and osteoporosis. Bone alterations in IBDs population appear to have a multifactorial etiology: Decreased physical activity, inflammation-related bone resorption, multiple intestinal resections, dietary malabsorption of minerals and vitamin D deficiency, genetic factors, gut-bone immune signaling interaction, steroid treatment, microbiota and pathogenic micro-organisms interaction, and dietary malabsorption of minerals, that, all together or individually, may contribute to the alteration of bone mineral density. This review aims to summarize the prevalence and pathophysiology of metabolic bone alterations in IBD subjects outlining the main risk factors of bone fragility. We also want to underline the role of the screening and prophylaxis of bone alterations in Crohn's disease and ulcerative colitis patients and the importance of treating appropriately MBD.

Key words: Inflammatory bowel diseases; Bone alterations; Bone mineral density;

Osteoporosis; Osteopenia; Ulcerative colitis; Crohn's disease

Core tip: Up to 50% of inflammatory bowel disease (IBD) patients experience at least one extraintestinal manifestation; among them is the involvement of bone density which is referred to as metabolic bone disease (MBD), including osteopenia and osteoporosis. Bone alterations in IBD population appear to have a multifactorial etiology. This review summarizes the prevalence and pathophysiology of metabolic bone alterations in IBD subjects outlining the main risk factors of bone fragility. We also want to underline the role of the screening and prophylaxis of bone alterations in Crohn's disease and ulcerative colitis patients and the importance of treating appropriately MBD.

INTRODUCTION

Inflammatory bowel diseases (IBDs) are mainly represented by Crohn's disease (CD) and ulcerative colitis (UC), both characterized by a multifactorial, partially unknown etiology that involves genetic, immunological and environmental factors including intestinal microbiota[1]. A dysregulated immune response to an unknown trigger leading to a sustained pro-inflammatory response within the gastrointestinal (GI) tract seems to play a major pathogenic role. Also, 10%-40% of IBD patients may suffer from at least one extraintestinal manifestation (EIM)[2], even before the occurrence of the intestinal disease[3].

Among the most frequent EIMs, there are those affecting the musculoskeletal system and in particular the bone tissue, such as osteoporosis (OP)[4].

OP is a systemic disease characterized by an increased risk of fractures even after a low energy trauma (fragility fracture). The reduction of bone strength is a consequence of a decrease in bone mineral density (BMD) and a deterioration in bone quality[5]. According to the World Health Organization the operational diagnosis of OP is based on BMD values equal or lower than 2.5 standard deviations (SD) from the average values for young healthy women (T-score < -2.5 SD) in post-menopausal women and men aged ≥ 50 years, while, osteopenia is defined by BMD values between -1 to -2.5 SD (T-score -1< and > -2.5).

BMD is measured trough dual-energy X-ray absorptiometry (DXA)[6,7]; T-score is a parameter comparing the BMD of a given patient with the average bone density of young healthy adults of the same sex, while, Z-score compares each BMD with the average BMD of a person with the same age and sex[8].

OP is classified into two main groups: Primary (or idiopathic) and secondary. The first one is the most common and includes juvenile, postmenopausal and senile OP. Secondary OP might be caused by several conditions (*i.e.*, endocrine, hematological, GI, rheumatic or renal diseases) that negatively affect bone metabolism leading to poor bone strength. Other causes might be the chronic use of some medications, particularly glucocorticoids (GCs), anticoagulants, and anticonvulsants[9,10]. Therefore, the term "secondary OP" refers to all those clinical conditions in which the bone involvement is a consequence of the primary disease or results from the related treatments (*i.e.*, GCs). Secondary OP affects about 60% of males and more than 50% of premenopausal women[11,12].

In IBD population, there are several pathological mechanisms that might result in low BMD and poor bone strength, thus leading to OP.

This review aims to summarize the prevalence and pathophysiology of metabolic bone alterations in IBD subjects outlining their main risk factors. We also underline the role of the screening and prophylaxis of BMD in CD and UC patients and the importance of early treatment.

EPIDEMIOLOGY

OP is one of the most common noncommunicable diseases[13] and its incidence is increasing worldwide[14]. According to Svedbom *et al*[15], 22 million women and 5.5 million men were estimated to have OP in Europe, with a reported incidence of 3.5 million new osteoporotic fractures in 2010, (620000 hip fractures, 520000 vertebral fractures, 560000 forearm fractures and 1800000 fractures in other skeletal sites). OP and its consequences (*i.e.*, fractures) carry a considerable economic burden on the health care systems[15] and, in particular, the socioeconomic costs of an osteoporotic hip fracture are equivalent to those of myocardial infarction and stroke[16].

In IBD subjects, the prevalence of low BMD ranges from 22% to 77% and that of fragility fractures from 17% to 41%[17]. These wide ranges across different studies might be explained by the small number of samples and by the heterogeneity of the studies and of the populations.

Several studies have been performed to describe the relationship between IBD and bone alterations. Sheth *et al*[2] showed that both osteopenia and OP are frequently associated with IBD, ranging from 32% to 36% for osteopenia and from 7% to 15% for OP. The same study reported an increased relative risk of fragility fractures in CD patients and a prevalence of < 0.5% for osteonecrosis, a clinical condition characterized by the death of the bone tissue, commonly described as a complication of steroid therapy in IBD patients. A study of Boubaker *et al*[18] reported that in a Tunisian group of 67 patients, OP represented the most frequent EIM in CD patients with a prevalence of low BMD at hip and spine in 31.8% and 40.9% of cases, respectively. OP is strongly associated with CD in females, thus suggesting that female gender might be one of the risk factors for bone loss in IBD. A prospective study in Romania found osteopenia in 48.07% of UC patients and in 56.41% of CD patients, while OP was shown in 18.26% of UC patients and in 15.38% of CD patients[19]. A Swiss IBD cohort study performed on 877 patients showed a prevalence of bone density alteration in 20% of IBD patients and identified, by multivariate logistic regression analysis, corticosteroid usage, long disease duration and perianal disease as independent risk factors[4]. A Japanese study reported that two-thirds of IBD patients showed a loss of BMD, with a prevalence of OP of about 13% in their cohort of patients with mean age of 43 years. The prevalence of OP is more frequent in Western IBD population than in the Asiatic one[20] and, therefore, the prevalence of bone metabolism alterations generally varies depending on study population, location and design of the study performed.

Notably, the risk of fragility fractures seems to be increased in IBD population[21] although the literature shows controversial results. Recently, Komaki *et al*[22] showed that there was no increase in the risk of overall fractures in IBD patients, but they reported more fractures at the spine, associated with steroids therapy.

Pediatric IBDs seem to show a similar association with osteopenia and OP as in adults. In fact, it is known that children with IBD have a higher risk of low BMD[23]. The overall prevalence of osteopenia and OP in pediatric and young IBDs patients seems to vary from 20% to 50%[24]. A recent study suggested a positive association between BMD and physical activity and between low BMD and fractures in the childhood[25]. Incidence of fragility fractures is higher in the young IBD population and is likely to be associated to the use of GC[26,27]. Pediatric CD patients appear to be more severely compromised than those with UC, probably because CD inhibits linear growth more frequently than UC[28].

CD and UC, while being both classified as IBDs, show considerable differences in the anatomic location and distribution of the intestinal lesions as well as in the underlying pathogenic mechanisms. This might have an influence on the incidence of bone alterations in each condition. Bjarnason *et al*[29] described no significant differences in T scores for spine or hip between patients with CD and those with UC. On the other side, in a study by Jahnsen *et al*[30], BMD resulted significantly reduced in CD subjects at all measured sites compared with UC patients, and healthy subjects. Interestingly, the authors did not describe significant differences in BMD between UC and healthy subjects. Ardizzone *et al*[46], in Italy, evaluated differences between CD and UC with respect to the pathogenic mechanisms underlying bone loss. Crohn's Disease Activity Index (CDAI)[31] and Truelove and Witts' Score[32] were used to grade disease activity of CD and UC, respectively. The distribution of normal, osteopenic and osteoporotic BMD values among CD and UC showed no significant differences also between patients with different disease activity. Also, in a study conducted in Sri-Lanka, there were no significant statistical differences in the frequency of OP between CD and UC, whereas the occurrence of OP among IBDs patients (13.5%) was higher than in healthy controls[33]. Recently, Vázquez *et al*[34] did not find any difference between patients with CD and those with UC regarding the prevalence of alterations of bone density.

The discrepancy between different studies may be due to variability in patient selection, differences in the methods used to evaluate bone density, and the body sites studied at DEXA (*i.e.*, radius *vs* lumbar spine or hip).

PATHOPHYSIOLOGY

Both bone quality and quantity (BMD) depend on physiological mechanisms, such as bone modeling and remodeling that in turn are regulated by biochemical and mechanical factors, including osteoprotegerin (OPG), receptor activator of nuclear factor kappa-B ligand (RANKL), receptor activator of nuclear factor kappa-B (RANK), and weight bearing activities. In particular, the RANKL secreted by osteoblasts binds to the RANK receptor, located on pre-osteoclasts and mature osteoclasts, inducing osteoclast proliferation, activity and survival. OPG, a molecule secreted by oste-oblasts, modulates bone turnover by inhibiting the binding of RANKL to RANK. The balance between OPG and RANKL release regulates osteoclast activity that in turn can be influenced by several hormones and cytokines, including vitamin D, estrogens, testosterone, GCs, parathormone (PTH), as well as pro-inflammatory mediators, such as interleukin-1 (IL-1) and tumor necrosis factor-alfa (TNFα). In OP, an imbalance between the serum levels of OPG and RANKL occurs, with excessive bone resorption and impaired bone formation, with consequent overall reduction of bone mass[35].

Other key modulators of bone turnover are the Wnt/β-catenin signaling and sclerostin, which acts mainly on osteoblasts and osteocytes. Sclerostin is a glycopro-tein produced almost exclusively by osteocytes and its expression is influenced by many factors, including serum PTH and mechanical loading[36]. Animal studies have shown that the mechanical load reduces serum sclerostin, whereas unloading increases the transcription of *SOST*, the gene encoding for sclerostin. Once secreted, sclerostin through osteocyte canalicular system reaches the bone lining cells (capable of activation into mature osteoblasts), where it binds to specific co-receptors (LRP-5 and -6) to inhibit the Wnt pathway, with consequent reduction of osteoblastogenesis and bone formation. On the contrary, a reduction in sclerostin levels is associated with an activation of the Wnt/β-catenin pathway with subsequent enhancement of osteoblast activity and survival[37]. Moreover, there is a correlation between hyperscle-rostinemia and bone loss in subjects forced to prolonged immobilization, thus supporting the key role of sclerostin in the development of OP following reduced mechanical load[38].

Among the most frequent secondary forms of OP, GCs use has been shown to decrease the number of osteoblast precursors and to increase the apoptosis of mature osteoblasts. The reduction in osteoblast differentiation is in partly mediated by the inhibition of the Wnt/β-catenin pathway along with increased expression of sclerostin, that antagonizes the Wnt signaling[39]. On the other hand, GCs decrease also osteoclast proliferation, although their activity tends to increase, through both the increase in RANKL and the reduction of OPG levels[40]. During GCs therapy, bone loss occurs rapidly with BMD reduction of 6%-12% within the first year, followed by a constant and gradual loss throughout the treatment period[41]. These two pathways are the basis of the most modern pharmacological approaches to OP: A human mono-clonal antibody against the RANKL (denosumab) and a humanized monoclonal antibody that targets sclerostin (romosozumab).

Among the most frequent causes of secondary OP there are GI disorders, including IBDs. Chronic gut inflammation in IBD may contribute to OP through the activation of T lymphocytes resulting in enhanced release of inflammatory cytokines, such as TNFα, that modulates the OPG/RANKL/RANK pathway thus inducing bone loss[42] (Figure 1). Moreover, TNFα enhances sclerostin production that results in decreased bone formation. Interestingly, in patients affected by CD, bone loss occurs before GCs administration, supporting the detrimental role of systemic inflammation on bone health[43].

There is a close relationship between bone and GI system that allows calcium absorption and bone mineralization; the GI tract may communicate with bone tissue through different mechanisms such as blood, nerves and immune cells, defining a characteristic gut-to-bone signaling axis that involves also incretins, serotonin and GI microbiota[44] (Figure 2).

Although in the general population female sex, early menopause, hormonal imbalance, smoke and old age are the main risk factors correlated with the onset of metabolic bone disease (MBD), in IBD patients the main risk factor seems to be the prolonged use of GCs[45,46]. Activity and severity of gut inflammation, intestinal malabsorption and calcium and vitamin D deficiency are also directly involved in the loss of BMD[47,48]. In particular, in CD the involvement of the terminal ileum may affect
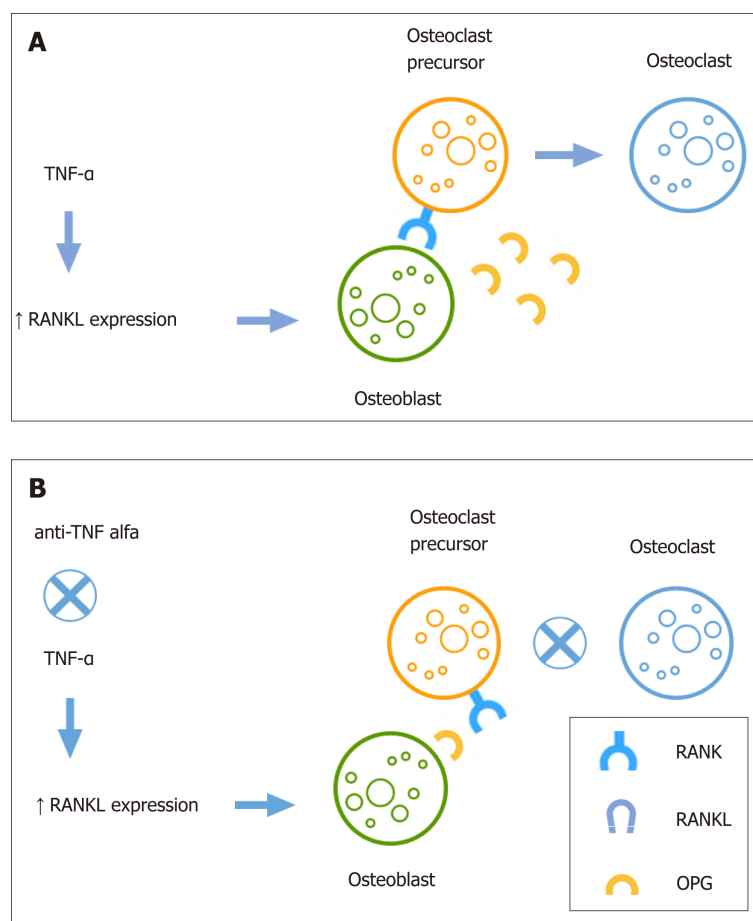
Figure 1 Modulation of osteoclast differentiation by serum TNF-α and anti-TNF-α treatment. A: TNF-α influences osteoclast precursor differentiation and bone resorption activity inducing RANKL expression on osteoblast cells and preventing the binding of OPG; B: Anti-TNF-α treatment reduces RANKL expression resulting in decrease of osteoclast differentiation and bone resorption.

the bile salt enterohepatic circulation thus leading to a reduced absorption of vitamin D. Chronic inflammation seems to have a key role in the reduction of BMD as suggested in some studies that show that rat models with colitis have a drastic loss of trabecular bone and a suppression of bone formation. At resolution of colitis with mucosal healing, the bone formation regresses to normal levels. During gut inflammation some mediators that alter the deposition of new bone matrix mediated by osteoblasts are produced, such as IL-6 and RANKL[49].

Untreated inflammation may be the main determinant for the loss of BMD in IBDs. In fact, a study by Ghosh *et al*[43] showed that CD patients have very low T-scores at the diagnosis before any drug therapy. Several studies in last years have also demonstrated that the usage of anti-TNF agents seems to have a positive effect on BMD[50] (see below). Recent studies suggest a role for the inflammatory process in the alteration of bone metabolism through the involvement of immune system cells, however it is not clear whether the inflammation is directly involved in the loss of BMD or if other factors contribute to the decline of BMD in IBD patients.

Bone alterations in IBD population appear to have a multifactorial etiology: Genetic factors, gut-bone immune signaling interaction, inflammation-related bone resorption, multiple intestinal resections, microbiota and pathogenic micro-organisms interaction, and dietary malabsorption of minerals[51,52] (Figure 2).

However, the main factor that seems to directly affect bone metabolism, with consequent reduction in BMD values, is corticosteroid treatment. In the following paragraphs we will summarize the evidence linking these factors to BMD deterioration in IBD patients.

Main risk factors

Genetic factors: The literature concerning the genetic predisposition to OP in IBD patients appears rather contradictory. A number of polymorphic sites apparently associated with the increased risk of bone loss in IBD patients such as *IL-6* and *IL-1ra* have already been described[53]. Todhunter *et al*[54] showed that the polymorphisms
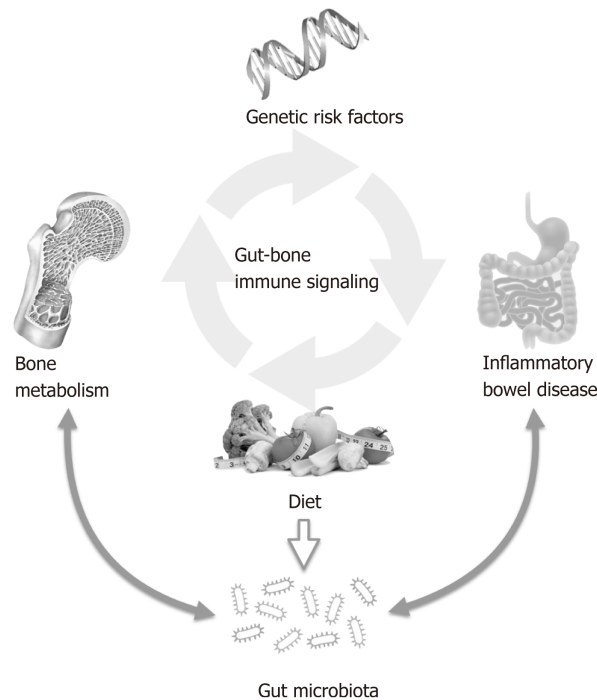
Figure 2 Gut-bone immune signaling: interplay between different factors which may affect bone metabolism in patients with inflammatory bowel diseases.

identified in some genes such as *COL1A1* and *IL-6* seems to influence BMD in IBD patients, particularly those with CD. Nemetz *et al*[55] showed also an increased risk of bone loss in patients with *IL1B* polymorphism (*IL1B-511*2*) associated with hypersecretion of *IL1B*.

One of the latest genetic factors associated with OP development is OPG encoded by the gene *TNFRS11B*, where the polymorphism c.-223C>T in 5' UTR region was identified as strongly related to OP in postmenopausal women. However, the genotyping analysis did not show unequivocal association between c.-223C>T of *TNFRS11B* and a predisposition to OP in IBD patients, although this polymorphism is more frequent in IBD patients than in healthy controls[56]. Krela-Kaźmierczak *et al*[56] studied the relationship between different polymorphic variants of *TGFB*1 and bone loss in IBD, finding no significant differences in BMD values or in the risk of fragility fractures between UC and CD patients and healthy controls with different polymorphic variants of the *TGFB1* gene. Moreover, no association between the 29T>C polymorphic variant of *TGFB1* and BMD of spongy bone and cortical bones was found[57].

The gene encoding for bone morphogenetic protein 2 (BMP2) was analyzed using restriction fragments length polymorphisms (RFLPs) to determine the association among the incidence of 570 A>T polymorphism, BMD alterations, and the incidence of fractures in IBD patients. The analysis revealed no significant association between this polymorphism and changes in bone metabolism in both UC and CD patients[58].

An interesting and recent theory correlates the presence of genetic alterations that might affect the ability to respond to endoplasmic reticulum (ER) stress and normal bone tissue physiology in IBD patients. A recent meta-analysis focused on the association between the genes involved in the response to unfolded proteins (UPR) and ER stress, which could directly correlate with the pathogenesis of IBDs[59]. It was suggested that the same defects in the Paneth cells inherent in UPR may also be present in bone cells, both osteoblasts and osteoclasts (although this has not yet been confirmed in IBD)[60]. Although its polymorphic variant seems to have no direct association with BMD, BMP2 activates the UPR during osteogenesis[61] allowing the production of RANKL[62]. In conclusion, during osteoblast differentiation ER stress is induced and activates also the PERK-eIF2α-ATF4 pathway that appears as a potential target against bone diseases[61]. To date, the association between genetic factors and bone alterations in IBD patients is not clear and other risk factors must be taken into account, such as those related to nutrition and lifestyle, as well as the ethno-demographic characteristics.

Gut-bone immune signaling: Bone structure depends on the balance between osteoblasts activity, specialized in the deposition of new bone matrix and osteoclasts, responsible for the resorption of bone tissue. Mounting evidence suggests an immunological involvement in the alteration of bone metabolism[63]. Activated CD4+ cells appear to be important actors in the bone loss related to IBD. In fact, in mice models, bone marrow CD4+ cells producing IL-17 and TNF-α migrate into the bone marrow during the inflammation, promoting the recruitment of monocytes as osteoclast progenitors, thus contributing to the bone loss[64]. Ashcroft *et al*[65] reported that activated T cells, producing RANKL, are accumulated in the bone marrow during intestinal inflammation.

As already discussed, osteoclastogenesis is guided by the RANK-RANKL pathway and by the RANKL/OPG ratio. OPG produced by osteoblasts works as a decoy receptor for RANKL, thus interfering with osteoclast activation. Li *et al*[66] suggested that lymphocytes might work as key regulators of bone metabolism by interfering with this pathway. In particular, they found that over 60% of OPG is produced by B lymphocytes and that T lymphocytes stimulate OPG production by osteoblasts via CD40L/CD40 co-stimulation. Finally, they showed that B-cells as well as CD40 or CD40L knockout mice developed OP and OPG deficiency[66].

Current knowledge strongly suggests a dynamic interplay between skeletal and immune system which is referred to as osteoimmunology. IL-17-producing helper T cells [T(H)17] induce RANKL, stimulating osteoclastogenesis through nuclear factor of activated T cells cytoplasmic 1 (NFATc1)[67]. There is evidence of activation of NFAT2 in lamina propria mononuclear cells of subjects with UC[68].

All these studies seem to show, in IBD, a direct involvement of immune system in the bone loss, mainly due to CD4+ cells that appear osteoclastogenic during inflammation.

Microbiota and pathogenic micro-organisms: The human microbiota consists of a set of about 100 trillion of commensal micro-organisms belonging to different species, which express a genome of about a hundred times greater than that expressed by the host's cells. There is evidence that alterations of the microbiota composition influence the healthy state of the host[69].

In particular, an immune response to an altered intestinal microbiota or an alteration of the immune response leading to its activation in the face of a normal intestinal microbiota both leading to a sustained inflammatory process, have been suggested as the main pathogenic mechanisms for the development of IBD[70].

Several studies suggest a key role for microbiota in the alteration of BMD. Irwin *et al*[71] reported a close correlation between *H. hepaticus* infection and bone loss. McCabe *et al*[72] showed that treating healthy male mice with *Lactobacillus reuteri* enhanced bone density and suppressed basal TNFα mRNA levels in male mice, but not in females. They also showed that probiotics increased male trabecular bone parameters, as mineral density in the distal femur metaphyseal region as well as in the lumbar vertebrae and increased osteoblast serum markers in male mice, although no effect on bone parameters in females was found[72]. Furthermore, Schepper *et al*[73] investigated the effect of antibiotic treatment on gut and bone health in mice models. They found an increase in the Firmicutes/Bacteroidetes ratio, in the intestinal permeability, and a reduction of femoral trabecular bone volume. Treating the mice with *L. reuteri* reduced the post-antibiotic elevation of the Firmicutes/Bacteroidetes ratio and prevented bone loss. Antibiotic-induced dysbiosis was associated with decreased osteoblast and increased osteoclast activities[73].

Recently, Naser *et al*[74] showed that the inflammation associated to *Mycobacterium avium subspecies paratuberculosis* (MAP) infection results in elevation of under-carboxylated osteocalcin (ucOC) and downregulation of active osteocalcin (OC) in CD patients. This suggest that MAP infection may serve as a trigger factor in the development of OP in CD patients.

Nutrition and vitamin deficiency: Nutritional alterations and vitamins or minerals deficiency due to inadequate diet intake and/or malabsorption correlate with a low BMD and may contribute to the development of osteopenia and OP both in UC and CD patients. Lim *et al*[75] assessed the nutritional status of 41 IBD patients with or without malnutrition and showed significantly higher serum C-reactive protein (CRP) and lower serum calcium in the malnourished group. No significant differences between malnourished and normal group were found as to BMD although lower bone density was more frequent in malnourished group. Also, Azzopardi *et al*[47] found a significant correlation between body mass index (BMI) and BMD of IBD patients[76].

Many studies measured calcium daily intake in IBD patients. Silvennoinen *et al*[77] assessed calcium intake and measured BMD in IBD patients and controls. They found

that, although the daily intake of calcium was lower in IBD subjects than in controls, especially in male patients, there was no significant correlations between calcium deficiency and BMD[77]. Vernia *et al*[78] analyzed by means of a questionnaire the dietary calcium intake in 187 IBD patients. They confirmed that calcium intake is frequently lower in IBD patients; moreover, most of the patients adopted some arbitrary dietary restrictions (*i.e.*, avoidance of milk or dairy products) which increased the risk of OP[78]. Calcium supplements as well as vitamin D administration showed an improvement of BMD at lumbar spine in osteoporotic patients with IBD. On the contrary, fluoride supplementation does not seem to provide any benefit to IBD patients[79].

Vitamin D has systemic functions; it acts on regulation of the innate and adaptive immune responses and modulates calcium homeostasis involved in bone metabolism. In IBD patients a vitamin D deficiency negatively affects the immune system inducing dysregulation and inflammation-associated loss of BMD[80]. Vitamin D deficiency is more frequent in IBD patients than in the general population[81]. Del Pinto *et al*[82], in a meta-analysis involving 14 studies, with 938 IBD patients and 953 controls, showed that 64% of IBD patients had lower vitamin D serum levels than controls. Interestingly, UC appeared to be associated with more than double the odds of vitamin D deficiency compared to healthy controls. A recent study, aimed at evaluating the absorption of orally administered vitamin D in CD patients compared with healthy controls, showed a great variability in the bioavailability of vitamin D(2) in CD patients although no significant differences between patients with different location of disease or among those with or without previous surgery were found. Moreover, 24 h after an oral load of vitamin D(2), the authors reported that the ability of absorption in CD patients was on average 30% lower than in normal subjects ($P < 0.001$)[83]. Based on most of the studies, it seems reasonable that measurement of serum vitamin D levels should be included in the follow up of IBD patients both adults and children. In fact, in pediatric IBD patients a vitamin D deficiency may enhance the odds of developing osteopenia or OP[84].

IBD patients might also have a reduced absorption of vitamin K, especially CD patients with an involvement of distal ileum. Besides playing a major role in coagulation processes vitamin K prevents bone resorption, inhibiting the production of prostaglandin E2 by osteoclasts, so its deficiency may affect BMD, as reported in both adults and pediatric patients[80]. However, the role of vitamin K in bone metabolism is controversial and the routine supplementation is not widely accepted yet[85].

Glucocorticoid therapy: A major risk factor associated to bone metabolism alterations in IBD patients is GC therapy, which in several occasions is administered without additional vitamin D or calcium supplementation[4]. GCs are still largely used in IBD patients with moderate or severe disease[86]. GC therapy causes a biphasic bone loss, firstly with a rapid decrease of BMD of about 6% to 12% in the first year, and after, with an annual loss of about 3% for as long as the therapy is administered[87] associated with an increase of the fracture risk in the first 3 mo, which can reach a percentage as high as 75%. The fracture risk then decreases in the first 3 mo after GC withdrawal, before any significant improvement in BMD values[88]. GCs cause a reduction in the cortical thickness and an increased cortical porosity in mice models, associated with increased osteoclast number at the endocortical surface. Osteoclast formation in trabecular bone depends on the production of RANKL by osteocytes as well as by the increase in cortical bone resorption induced by mechanical unloading or by dietary calcium deficiency. *In vitro* models showed that GC therapy directly increases the production of RANKL and reduces OPG expression levels in stromal cells and osteoblasts[89]. Also, Hofbauer *et al*[90] reported that RANKL inhibition prevented GC-induced bone loss.

Piemontese *et al*[91] examined the effects of prednisolone on cortical bone in mice lacking RANKL production in osteocytes. Prednisolone increased osteoclast number at the endocortical surface, increased cortical porosity, and reduced cortical thickness in control mice, but none of these effects were found in mice lacking RANKL in osteocytes. Moreover, in cortical bone organ cultures and primary osteoblasts, dexamethasone suppressed OPG without any variation of RANKL levels. Therefore, based on these observations, OPG, rather than RANKL, seems to play a major role in the endocortical resorption.

OPG-mediated bone loss prevention acts through the inhibition of RANK-RANKL pathway and reduction of osteocytes apoptosis, induced by GCs. Weinstein *et al*[41], both *in vivo* and *in vitro*, studied the effect of OPG administration, with or without the fragment crystallizable region of Ig heavy chains (OPG-Fc), on the bone loss and on the apoptosis of osteocytes, with or without GCs administration. They showed that in mice treated with prednisolone combined with OPG-Fc or only with OPG-Fc there

was a decreased expression of both receptors of cathepsin K and OC, which are markers of osteoclast number. Moreover, OPG-Fc administration preserved the BMD at spine compared with animals who received only prednisolone. The authors also reported an increase of vertebral strength of about 29% in mice receiving OPG-Fc compared to those receiving OPG-Fc combined with prednisone. Finally, OPG-Fc administration, alone or combined with prednisolone, decreased the number of osteoclasts of about 7% and 5% respectively, compared with placebo group. Prednisolone also induced an increase of the osteocytes apoptosis of about 335%, which was prevented by OPG-Fc administration. This supports the concept that OPG administration may prevent the reduction of BMD, of vertebral cortical thickness, and of osteocytes viability induced by GCs[41].

In conclusion, GC therapy is a major determinant of bone mass alteration in IBD patients. New generation GCs, such as budesonide or beclometasone, which show a very efficient hepatic first pass metabolism may represent a valid alternative to conventional GCs in order to try to minimize GC detrimental effect in general and on bone structure in particular[92,93].

DISEASE SEVERITY/ACTIVITY AND BONE MINERAL DENSITY

Calcium is an essential ion for bone formation and its only source is diet. The absorption of dietary calcium is a vitamin D-dependent process[94]. In the distal part of the intestine, 70%-80% of the ingested calcium is absorbed (mostly in the ileum)[95] through the action of Vitamin D receptor which is expressed in all segments of the small and large intestine with the highest levels reported in the cecum and colon. In patients with extensive intestinal resection, calcium absorption has been reported to be significantly higher when the colon is preserved[96]. In IBD, different segments of the intestine may be involved by the inflammatory process and the subsequent alterations of the absorptive processes have been suggested to be an important determinant of bone loss[97,98]. Several studies evaluated the correlation between disease extension or activity according to the Montreal classification for IBD[99] and BMD. In 1997, Bjarnason *et al*[29] reported that there were no significant differences in T scores for spine or hip within the patient subgroups according to disease location. Also, Jahnsen *et al*[30] assessed BMD in 60 patients with CD in 60 patients with UC and in 60 healthy subjects. Patients with CD had similar BMD, independently on whether the colon or the small intestine was involved. Furthermore, no differences were described between patients with CD with or without small bowel resection. In addition, no correlations between the length of small bowel resected and BMD were found. Finally, in the UC patients there was no influence of disease location and extension on MBD. More recently, the same results have been described by Vázquez *et al*[34] on 107 patients with IBDs (53 with CD and 54 with UC) with different location of the disease. The extension and the location of the disease did not seem to influence BMD loss or vertebral fractures prevalence. In a study conducted in 99 consecutive CD outpatients, Cravo *et al*[100] assessed disease activity by Harvey–Bradshaw Index (HBI). With a multivariate analysis, they described a direct and significant association between age (above 40 years), chronic active disease (HBI 4), previous colonic surgeries and the presence of OP. Both small bowel and colonic resection were similarly associated to OP. This might be explained by the major impact of inflammation due to disease severity in respect to the reduction of mineral absorption induced by short bowel syndrome, as initially hypothesized. Moreover, to support the role of chronic inflammation in the pathogenesis of bone loss, patients with active disease (HBI > 4) and those with a penetrating or structuring disease, which are usually more aggressive phenotypes, were also those with the highest rate of OP.

More recently, Lima *et al*[101] evaluated the correlation between disease severity and BMD in 68 patients with UC and 60 with CD of 17-40 years of age. About half CD patients had an ileocolonic disease (53.3%) while 29 subjects (48.3%) had non-stricturing non-penetrating disease and 33.3% had perianal disease, according to Montreal classification. In the UC group, 29 patients (44.6%) had extensive UC according to the Montreal classification[99]. The authors described a higher incidence of osteopenia in UC and CD patients than controls (OR = 14.93/OR = 24.38, respectively). At multivariate analysis in CD group, low BMD was associated with sex (M > F), perianal disease, penetrating behavior and age at diagnosis > 40 years, while, no association was described between BMD and disease activity. In the UC group, low BMD was significantly associated to sex (M > F) and left colitis. Therefore, disease activity does not seem to be a major determinant of bone density alteration in CD and UC patients, while disease severity seems to be associated with osteopenia in IBD

patients. It must be emphasized that only 0.02% of UC patients and 0.26% of CD patients had active disease at the time DEXA was performed, and, therefore, the remission of the disease might have been be associated with an increase in BMD.

TNF-/ANTI-TNF- THERAPY AND BONE DENSITY ALTERATIONS

IBD is an immune-mediated inflammatory condition characterized by activation of different inflammatory pathways and abnormal secretion of different cytokines such as TNF-α[102].

Anti-TNF-α is the first available biologic therapy for IBD and, currently, its effects on BMD are not known. Moreover, it is not clear whether the effects of anti-TNFα agents on bone health are the consequence of a direct interference with the process of bone modeling or if these effects are simply due to a decreased disease activity and subsequent improvement of mineral absorption.

As previously mentioned, two members of TNF superfamily, RANKL OPG, are the key regulators of bone remodeling. RANKL, derived by osteoblasts, stimulates formation of mature osteoclasts while OPG, produced by osteoblasts, is a competitor that inhibits the interaction between RANKL and its receptor[103]. TNF-α is a main actor of osteoclastogenesis by inducing activation of NF-κ B transcription and, also, reducing bone formation through the inhibition of osteoblast differentiation[104]. Moreover, it increases the survival of osteoclasts by protecting them against apoptosis[105] while it induces apoptosis of osteoblasts to reduce bone formation[106]. Therefore, TNF-α not only plays a central role in the pathogenesis of IBD but is also involved in bone metabolism, promoting bone resorption through regulation of osteoclast activity (Figure 1). As described by Azuma *et al*[107], TNF-α directly induces the differentiation of osteoclast progenitors into mature osteoclast playing an important role in local osteolysis in chronic inflammatory diseases. Based on this, many studies have evaluated the effect of infliximab, a chimeric (*i.e.*, half human and half murine) anti-TNF agent, on bone metabolism investigating serum bone marker, BMD or incidence of bone fractures. Only one study assessed the impact of adalimumab, another all human anti-TNF agent, on bone metabolism. In a Belgian study[108], authors evaluated markers of bone formation and resorption at eight weeks from the beginning of infliximab therapy in comparison with healthy controls. In their cohort, regardless of patients' clinical response, anti-TNF-α increased bone formation and, in the majority of patients, strongly decreased bone resorption. In a one year follow up study[109], after starting therapy, the mean BMD resulted to be increased significantly in CD patients without any correlation with concurrent corticosteroid therapy. So, the authors suggested that amongst the factors inducing bone loss in CD, the inflammatory disease process might be predominant over the effects of treatment with prednisone. This might be especially relevant in CD patients who need to continue steroid therapy despite concurrent immunomodulatory therapy.

In 24 patients with active CD treated with infliximab, Ryan *et al*[110] described a significant increase of bone alkaline phosphatase, a marker of bone formation, and OC, a bone specific calcium-binding protein produced by osteoblasts, which persisted up to 4 wk after the end of treatment. As underlined by other authors, the benefits occurred independently of the clinical response of CD to biological treatment. On the other side, Miheller *et al*[111] dosed serum OC and CrossLaps (bCL), a degradation product of collagen, in 27 patients with fistulizing CD treated with anti-TNF-α. In the group of patients who responded to therapy, but not in those who did not, serum bCL concentrations were significantly decreased from week 0 to week 6, while a statistically significant increase was described for OC, thus suggesting that the beneficial effect of anti-TNF therapy was related to the amelioration of the underlying inflammatory process.

More recently, a 7-year follow-up longitudinal prospective cohort study by Maldonado-Pérez *et al*[112] evaluated the role of anti-TNF-α in decreasing fracture risk or modifying BMD in IBD patients. The authors described no difference in the incidence of vertebral fracture and value of bone mass between the group of patients treated with anti-TNF-α and the control group which did not receive biological treatment. Despite the biological-treated patients had received GC therapy for a longer period of time compared to the control group, new fractures were more common and more severe in the control, nonbiological-treated group. After 7 years of follow-up, bone mass increased significantly in the spine and in the femoral neck in patients treated with anti-TNF-α, compared to subjects who did not receive biological therapy.

Only one study[113] evaluated the impact of adalimumab therapy on bone

metabolism. Parathyroid hormone, vitamin D, bone formation and resorption marker, pro- and anti-inflammatory OPG, and sRANKL were measured in healthy controls and in CD patients pre- and post-treatment with adalimumab. Moreover, viability and differentiation of human osteoblasts (hFOB 1.19) cells after exposure to sera from CD patients pre- and post-adalimumab treatment was also analyzed. Following adalimumab therapy, a rapid increase in bone formation markers (OC and procollagen type 1 N-terminal pro-peptide) and a not significant decrease of a bone resorption marker (C-telopeptide of type-1 collagen) were observed. In the *in vitro* study, osteoblasts exposed to sera of CD patients before adalimumab therapy showed consistently higher levels of viability and lower levels of ALP compared to control group suggesting a greater viability of osteoblasts associated to a lower osteoblast function likely due to an inflammatory-driven response. After treatment, serum of CD patients induced higher levels of ALP in hFOB cells probably due to an improvement of their functionality.

In conclusion, anti-TNF seems to improve BMD in IBD patients both through a direct beneficial effect on bone metabolism and through the improvement in the underlying intestinal inflammatory process. Whether other biologic agents now available for the treatment of IBD, such as vedolizumab or ustekinumab, have any effect on bone metabolism needs to be determined.

DIAGNOSIS OF OSTEOPOROSIS

Diagnosis of OP should be based on patient clinical history, physical examination, BMD measurements, and laboratory investigations[17]. In particular, because changes in bone metabolism are frequently associated with the evolution of IBD and may have a negative impact on the patient's quality of life, assessment of BMD in all IBD patients is essential to prevent and treat appropriately MBDs. The gold standard for its assessment is DXA. Changes in BMD values are key determinants to evaluate treatment efficacy at follow-up. Moreover, FRAX algorithm by combining all the fracture risks with the hip BMD value can quantify the 10-year risk of experiencing a fragility fracture[114]. Laboratory tests are necessary not only to exclude secondary forms of OP but also for the bone metabolism assessment. They should include biochemical markers of bone turnover and vitamin D status that might provide additional information regarding the patient fracture risk.

Moreover, increase in the incidence of BMD loss supports the recommendation to screen patients with IBD at an early stage of the disease. Screening recommendation of European Crohn and Colitis Organization (ECCO)[115] does not differ from those for the general population. It considers risk factors such as postmenopausal state, ongoing corticosteroid treatment, cumulative corticosteroid use > 3 mo, history of low-trauma fracture and age. Moreover, annual DXA scans is recommended in patients receiving long-term steroid therapy (in particular when there are others risk factors) if the T-score approaches the threshold for treatment with bisphosphonates (BPs) (T-score < −1.5 SD)[116].

THE PHARMACOLOGICAL MANAGEMENT OF OP

The aim of the management of OP is to reduce the risk of fragility fractures in individuals at high-risk. Therefore, pharmacological intervention thresholds should be based on the assessment of this risk deriving from the integration of densitometric data with other important clinical factors as determined by the FRAX[116]. Approved pharmacological treatments for the management of OP can be classified into two categories: anti-resorption (or anti-catabolic) and anabolic drugs. Among anti-catabolic drugs, biphosphonates (BPs) blocking the osteoclastic activity, manage to reduce the bone remodeling process with a consequent increase in bone density. Alendronate and risedronate are the most commonly used for the prevention of vertebral and non-vertebral fractures (including hip) based on strong scientific evidence of efficacy[117]. However, they have reduced compliance and persistence to prolonged therapy, due to daily or weekly administration regimens and possible gastro-intestinal adverse events. Zoledronic acid is a BP intravenously administered with documented efficacy in reducing the risk of vertebral, non-vertebral and hip fractures[117]. A meta-analysis of studies on BPs use in IBD patients showed that these drugs are effective in case of low BMD reducing the risk of vertebral but not of non-vertebral fracture[118]; so, the use of BPs should be recommended for fracture prevention in IBD patients taking always into account the possible adverse effects of treatment.

A powerful inhibitor of bone resorption is denosumab, a human monoclonal antibody capable of neutralizing RANKL, a cytokine that interacts with the RANK receptor on the membrane of preosteoclasts and mature osteoclasts, affecting their recruitment, maturation and survival. A dose of 60 mg subcutaneously every 6 months is sufficient to strongly inhibit osteoclastic activity and to reduce the risk of vertebral and non-vertebral fractures (including hip). Unlike BPs, discontinuation of denosumab is followed by a sharp increase in bone turnover and a rapid loss of BMD. Therefore, discontinuation of denosumab generally requires the patient to initiate BPs treatment at an appropriate dosage as soon as possible[119].

Among anabolic drugs, teriparatide, the active fragment of PTH (1-34 PTH) is the most widely used. It can stimulate both bone formation and resorption, with a predominant effect on the neoformation (anabolic window) which is evident above all during the first 12 mo of treatment. It is generally used as a second line anti-osteoporotic drug in case of intolerance or resistance to other anti-resorption agents and as first choice in case of severe OP in patients with multiple fragility fractures[17].

All clinical guidelines agree that the pharmacological therapy of OP, independently of the prescribed treatment, should always be supplemented by the administration of vitamin D and, in case of nutritional deficient intake, of calcium[120].

ECCO guidelines[115] suggest, some recommendations concerning the management of bone alterations in IBD population (Table 1).

CONCLUSION

The prevalence of OP and/or fragility fractures in IBD patients is controversial because of different factors, such as different study population and study design, and location of the disease. Moreover, some aspects still need to be clarified, particularly the correlation between the increased risk of fragility fractures in subjects affected by IBD.

Changes in bone metabolism are frequently associated with the evolution of IBD and may have a negative impact on the patient's quality of life.

In this context, even understanding the pathophysiological milieu seems to be quite challenging. For example, the genetic background predisposing to the development of osteopenia and OP, specific for IBD patients, since the strongly multifactorial nature of these diseases, does not allow to evaluate its pathogenic role without considering other factors, such as nutrition, lifestyle, or more simply, pharmacological therapy for IBD. On the other side, increasing evidence suggests a gut-bone signaling pathway, which is responsible for a close cross-talk between the musculoskeletal and the GI system, and whose alteration may potentially correlate with the evolution of this type of EIMs. Furthermore, because of the emerging role of intestinal microbiota in the pathogenesis of IBDs, a direct impact of dysbiotic commensal microflora on bone metabolism, as shown in the healthy population, seems to be possible. A schematic diagram summarizing the pathophysiologic mechanism, including molecular mechanisms, underlying BMD alteration in IBD patients is shown in Figure 3.

The nutritional aspects, always considered among the main factors capable of triggering bone alterations, appear once again crucial, especially regarding the intake of calcium and vitamin D, the lack of which, both in adults and children, shows a direct correlation with the increased probability of developing bone fragility, specifically linked to osteoporomalacic findings. For this reason, it is important to include the evaluation of serum vitamin D levels and of nutritional status in IBD patients, both in active phase and remission of disease, in order to avoid the establishment of malnutrition that may increase the onset of comorbidity.

Pharmacotherapy of IBD might play a major role in bone metabolism. GCs are the main determinants of bone alterations and their prolonged use is associated with OP, osteopenia and increased risk of fractures. Therefore, their use should be limited and, whenever possible, new generation corticosteroids with a safer profile should be used. Finally, anti-TNF agents seem to improve bone health in IBD patients both by directly interfering with the metabolic pathways involved in bone modeling and by decreasing the disease activity and severity. Whether new biologic agents exert any beneficial effect on bone tissue in IBD patients remains to be determined.

Finally, and more important, a thorough evaluation of bone metabolism including serological markers should be part of the follow-up of IBD patients in order to prevent and/or promptly treat any bone alteration which may alter their quality of life and increase the risk of fractures.

Table 1 European Crohn and Colitis Organization guidelines for the management of bone alterations in inflammatory bowel diseases population

ECCO guidelines for the management of bone alterations in IBD population	
Life style recommendations	Physical exercise; Stopping smoking; and adequate dietary calcium (1 g/daily)
Vitamin and mineral supplements	Calcium (500-1000 mg/daily); Vitamin D (dose of ~1000 IU daily, or higher dose if known vitamin D deficiency) supplement for prophylaxis in patients receiving systemic steroid therapy; Calcium and vitamin D supplement if the T score is lower than -1.5
Treatment recommendations	More intensive treatment in patients with a history of pre-existing fracture; Regular use of BPs and other therapies in subjects with underlying disease activity particularly in young and postmenopausal women or those with previous spontaneous fractures

ECCO: European Crohn and Colitis Organization; IBD: Inflammatory bowel diseases.
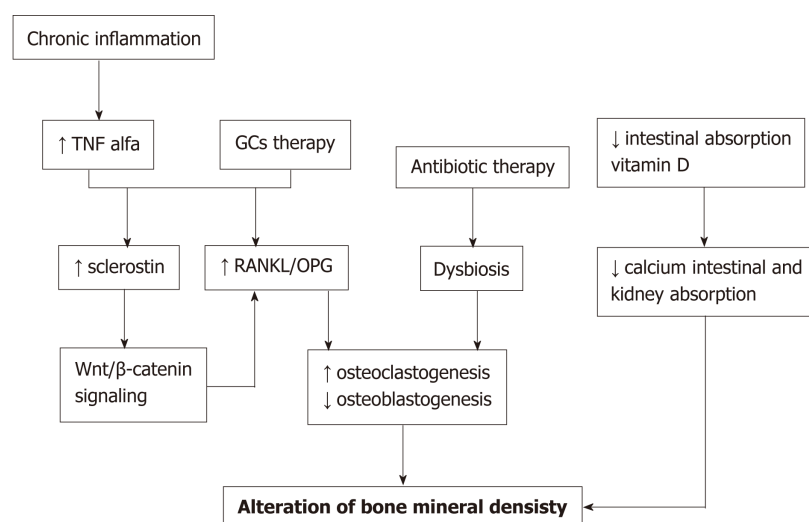
Figure 3 Diagramatic representation of the pathogenic mechanisms involved in alteration of bone mineral density in inflammatory bowel diseases.

REFERENCES

1   **Ferreira PVALS**, Cavalcanti AS, Silva GAPD. Linear growth and bone metabolism in pediatric patients with inflammatory bowel disease. *J Pediatr (Rio J)* 2019; **95** Suppl 1: 59-65 [PMID: 30562479 DOI: 10.1016/j.jped.2018.11.002]

2   **Sheth T**, Pitchumoni CS, Das KM. Musculoskeletal manifestations in inflammatory bowel disease: a revisit in search of immunopathophysiological mechanisms. *J Clin Gastroenterol* 2014; **48**: 308-317 [PMID: 24492406 DOI: 10.1097/MCG.0000000000000067]

3   **Vavricka SR**, Rogler G, Gantenbein C, Spoerri M, Prinz Vavricka M, Navarini AA, French LE, Safroneeva E, Fournier N, Straumann A, Froehlich F, Fried M, Michetti P, Seibold F, Lakatos PL, Peyrin-Biroulet L, Schoepfer AM. Chronological Order of Appearance of Extraintestinal Manifestations Relative to the Time of IBD Diagnosis in the Swiss Inflammatory Bowel Disease Cohort. *Inflamm Bowel Dis* 2015; **21**: 1794-1800 [PMID: 26020601 DOI: 10.1097/MIB.0000000000000429]

4   **Schüle S**, Rossel JB, Frey D, Biedermann L, Scharl M, Zeitz J, Freitas-Queiroz N, Kuntzen T, Greuter T, Vavricka SR, Rogler G, Misselwitz B; Swiss IBD cohort study. Widely differing screening and treatment practice for osteoporosis in patients with inflammatory bowel diseases in the Swiss IBD cohort study. *Medicine (Baltimore)* 2017; **96**: e6788 [PMID: 28562531 DOI: 10.1097/MD.0000000000006788]

5   Consensus development conference: diagnosis, prophylaxis, and treatment of osteoporosis. *Am J Med* 1993; **94**: 646-650 [PMID: 8506892 DOI: 10.1016/0002-9343(93)90218-E]

6   **Kanis JA**, McCloskey EV, Johansson H, Oden A, Melton LJ, Khaltaev N. A reference standard for the description of osteoporosis. *Bone* 2008; **42**: 467-475 [PMID: 18180210 DOI: 10.1016/j.bone.2007.11.001]

7   World Health Organization – WHO Criteria for Diagnosis of Osteoporosis [Internet]. 4BoneHealth 2018. Available from: http://www.4bonehealth.org/education/world-health-organization-criteria-diagnosis-osteoporosis/

8   **Baim S**, Binkley N, Bilezikian JP, Kendler DL, Hans DB, Lewiecki EM, Silverman S. Official Positions of the International Society for Clinical Densitometry and executive summary of the 2007 ISCD Position Development Conference. *J Clin Densitom* 2008; **11**: 75-91 [PMID: 18442754 DOI: 10.1016/j.jocd.2007.12.007]

9   **Maggi S**, Noale M, Giannini S, Adami S, Defeo D, Isaia G, Sinigaglia L, Filipponi P, Crepaldi G; ESOPO Study Group. Quantitative heel ultrasound in a population-based study in Italy and its relationship with

fracture history: the ESOPO study. *Osteoporos Int* 2006; **17**: 237-244 [PMID: 16142503 DOI: 10.1007/s00198-005-1985-2]

10   **World Health Organization (WHO)**. Guidelines for preclinical evaluation and clin-ical trials in osteoporosis [Internet]. 1998; Available from: http://www.who.int/iris/handle/10665/42088

11   **Tarantino U**, Iolascon G, Cianferotti L, Masi L, Marcucci G, Giusti F, Marini F, Parri S, Feola M, Rao C, Piccirilli E, Zanetti EB, Cittadini N, Alvaro R, Moretti A, Calafiore D, Toro G, Gimigliano F, Resmini G, Brandi ML. Clinical guidelines for the prevention and treatment of osteoporosis: summary statements and recommendations from the Italian Society for Orthopaedics and Traumatology. *J Orthop Traumatol* 2017; **18**: 3-36 [PMID: 29058226 DOI: 10.1007/s10195-017-0474-7]

12   **Khosla S**. Update in male osteoporosis. *J Clin Endocrinol Metab* 2010; **95**: 3-10 [PMID: 20056806 DOI: 10.1210/jc.2009-1740]

13   **Johnell O**, Kanis JA. An estimate of the worldwide prevalence and disability associated with osteoporotic fractures. *Osteoporos Int* 2006; **17**: 1726-1733 [PMID: 16983459 DOI: 10.1007/s00198-006-0172-4]

14   **Cooper C**, Cole ZA, Holroyd CR, Earl SC, Harvey NC, Dennison EM, Melton LJ, Cummings SR, Kanis JA; IOF CSA Working Group on Fracture Epidemiology. Secular trends in the incidence of hip and other osteoporotic fractures. *Osteoporos Int* 2011; **22**: 1277-1288 [PMID: 21461721 DOI: 10.1007/s00198-011-1601-6]

15   **Svedbom A**, Hernlund E, Ivergård M, Compston J, Cooper C, Stenmark J, McCloskey EV, Jönsson B, Kanis JA, EU Review Panel of IOF. Osteoporosis in the European Union: a compendium of country-specific reports. *Arch Osteoporos* 2013; **8**: 137 [PMID: 24113838 DOI: 10.1007/s11657-013-0137-0]

16   **Piscitelli P**, Iolascon G, Argentiero A, Chitano G, Neglia C, Marcucci G, Pulimeno M, Benvenuto M, Mundi S, Marzo V, Donati D, Baggiani A, Migliore A, Granata M, Gimigliano F, Di Blasio R, Gimigliano A, Renzulli L, Brandi ML, Distante A, Gimigliano R. Incidence and costs of hip fractures vs strokes and acute myocardial infarction in Italy: comparative analysis based on national hospitalization records. *Clin Interv Aging* 2012; **7**: 575-583 [PMID: 23269863 DOI: 10.2147/CIA.S36828]

17   **Ali T**, Lam D, Bronze MS, Humphrey MB. Osteoporosis in inflammatory bowel disease. *Am J Med* 2009; **122**: 599-604 [PMID: 19559158 DOI: 10.1016/j.amjmed.2009.01.022]

18   **Boubaker J**, Feki M, Hsairi M, Fekih M, Kaabachi N, Filali A, Mebazaa A. [Osteoporosis and inflammatory bowel disease: prevalence and risk factors in Tunisian patients]. *Gastroenterol Clin Biol* 2003; **27**: 901-907 [PMID: 14631305]

19   **Dumitrescu G**, Mihai C, Dranga M, Prelipcean CC. Bone mineral density in patients with inflammatory bowel disease from north-eastern Romania. *Rev Med Chir Soc Med Nat Iasi* 2013; **117**: 23-28 [PMID: 24505888]

20   **Naito T**, Yokoyama N, Kakuta Y, Ueno K, Kawai Y, Onodera M, Moroi R, Kuroha M, Kanazawa Y, Kimura T, Shiga H, Endo K, Nagasaki M, Masamune A, Kinouchi Y, Shimosegawa T. Clinical and genetic risk factors for decreased bone mineral density in Japanese patients with inflammatory bowel disease. *J Gastroenterol Hepatol* 2018; **33**: 1873-1881 [PMID: 29603369 DOI: 10.1111/jgh.14149]

21   **Targownik LE**, Bernstein CN, Leslie WD. Inflammatory bowel disease and the risk of osteoporosis and fracture. *Maturitas* 2013; **76**: 315-319 [PMID: 24139749 DOI: 10.1016/j.maturitas.2013.09.009]

22   **Komaki Y**, Komaki F, Micic D, Ido A, Sakuraba A. Risk of Fractures in Inflammatory Bowel Diseases: A Systematic Review and Meta-Analysis. *J Clin Gastroenterol* 2019; **53**: 441-448 [PMID: 29672437 DOI: 10.1097/MCG.0000000000001031]

23   **Lopes LH**, Sdepanian VL, Szejnfeld VL, de Morais MB, Fagundes-Neto U. Risk factors for low bone mineral density in children and adolescents with inflammatory bowel disease. *Dig Dis Sci* 2008; **53**: 2746-2753 [PMID: 18351466 DOI: 10.1007/s10620-008-0223-0]

24   **Bryant RV**, Schultz CG, Ooi S, Goess C, Costello SP, Vincent AD, Schoeman SN, Lim A, Bartholomeusz FD, Travis SPL, Andrews JM. Obesity in Inflammatory Bowel Disease: Gains in Adiposity despite High Prevalence of Myopenia and Osteopenia. *Nutrients* 2018; 10 [PMID: 30200405 DOI: 10.3390/nu10091192]

25   **Nobile S**, Grand RJ, Pappa HM. Risk factors for low bone mineral density in pediatric inflammatory bowel disease: the positive role of physical activity. *Eur J Gastroenterol Hepatol* 2018; **30**: 471-476 [PMID: 29438136 DOI: 10.1097/MEG.0000000000001076]

26   **Ward LM**, Ma J, Rauch F, Benchimol EI, Hay J, Leonard MB, Matzinger MA, Shenouda N, Lentle B, Cosgrove H, Scharke M, Konji VN, Mack DR. Musculoskeletal health in newly diagnosed children with Crohn's disease. *Osteoporos Int* 2017; **28**: 3169-3177 [PMID: 28791436 DOI: 10.1007/s00198-017-4159-0]

27   **Huber AM**, Gaboury I, Cabral DA, Lang B, Ni A, Stephure D, Taback S, Dent P, Ellsworth J, LeBlanc C, Saint-Cyr C, Scuccimarri R, Hay J, Lentle B, Matzinger M, Shenouda N, Moher D, Rauch F, Siminoski K, Ward LM; Canadian Steroid-Associated Osteoporosis in the Pediatric Population (STOPP) Consortium. Prevalent vertebral fractures among children initiating glucocorticoid therapy for the treatment of rheumatic disorders. *Arthritis Care Res (Hoboken)* 2010; **62**: 516-526 [PMID: 20391507 DOI: 10.1002/acr.20171]

28   **Sylvester FA**, Gordon CM, Thayu M, Burnham JM, Denson LA, Essers J, Ferrari S, Gupta N, Hewison M, Koletzko S, McCabe L, Pappa H, Sanderson I, Ward L, Zanotti S. Report of the CCFA pediatric bone, growth and muscle health workshop, New York City, November 11-12, 2011, with updates. *Inflamm Bowel Dis* 2013; **19**: 2919-2926 [PMID: 23974992 DOI: 10.1097/MIB.0b013e3182a5a004]

29   **Bjarnason I**, Macpherson A, Mackintosh C, Buxton-Thomas M, Forgacs I, Moniz C. Reduced bone density in patients with inflammatory bowel disease. *Gut* 1997; **40**: 228-233 [PMID: 9071937 DOI: 10.1136/gut.40.2.228]

30   **Jahnsen J**, Falch JA, Aadland E, Mowinckel P. Bone mineral density is reduced in patients with Crohn's disease but not in patients with ulcerative colitis: a population based study. *Gut* 1997; **40**: 313-319 [PMID: 9135518 DOI: 10.1136/gut.40.3.313]

31   **Best WR**, Becktel JM, Singleton JW, Kern F. Development of a Crohn's disease activity index. National Cooperative Crohn's Disease Study. *Gastroenterology* 1976; **70**: 439-444 [PMID: 1248701 DOI: 10.1016/S0016-5085(76)80163-1]

32   **TRUELOVE SC**, WITTS LJ. Cortisone in ulcerative colitis; final report on a therapeutic trial. *Br Med J* 1955; **2**: 1041-1048 [PMID: 13260656 DOI: 10.1136/bmj.2.4947.1041]

33   **de Silva AP**, Karunanayake AL, Dissanayaka TG, Dassanayake AS, Duminda HK, Pathmeswaran A, Wickramasinghe AR, de Silva HJ. Osteoporosis in adult Sri Lankan inflammatory bowel disease patients. *World J Gastroenterol* 2009; **15**: 3528-3531 [PMID: 19630109 DOI: 10.3748/wjg.15.3528]

34   **Vázquez MA**, Lopez E, Montoya MJ, Giner M, Pérez-Temprano R, Pérez-Cano R. Vertebral fractures in

patients with inflammatory bowel disease compared with a healthy population: a prospective case-control study. *BMC Gastroenterol* 2012; **12**: 47 [PMID: 22584049 DOI: 10.1186/1471-230X-12-47]

35   **Lacey DL**, Boyle WJ, Simonet WS, Kostenuik PJ, Dougall WC, Sullivan JK, San Martin J, Dansey R. Bench to bedside: elucidation of the OPG-RANK-RANKL pathway and the development of denosumab. *Nat Rev Drug Discov* 2012; **11**: 401-419 [PMID: 22543469 DOI: 10.1038/nrd3705]

36   **Moester MJ**, Papapoulos SE, Löwik CW, van Bezooijen RL. Sclerostin: current knowledge and future perspectives. *Calcif Tissue Int* 2010; **87**: 99-107 [PMID: 20473488 DOI: 10.1007/s00223-010-9372-1]

37   **Robling AG**, Niziolek PJ, Baldridge LA, Condon KW, Allen MR, Alam I, Mantila SM, Gluhak-Heinrich J, Bellido TM, Harris SE, Turner CH. Mechanical stimulation of bone in vivo reduces osteocyte expression of Sost/sclerostin. *J Biol Chem* 2008; **283**: 5866-5875 [PMID: 18089564 DOI: 10.1074/jbc.M705092200]

38   **Gaudio A**, Pennisi P, Bratengeier C, Torrisi V, Lindner B, Mangiafico RA, Pulvirenti I, Hawa G, Tringali G, Fiore CE. Increased sclerostin serum levels associated with bone formation and resorption markers in patients with immobilization-induced bone loss. *J Clin Endocrinol Metab* 2010; **95**: 2248-2253 [PMID: 20305005 DOI: 10.1210/jc.2010-0067]

39   **Gifre L**, Ruiz-Gaspà S, Monegal A, Nomdedeu B, Filella X, Guañabens N, Peris P. Effect of glucocorticoid treatment on Wnt signalling antagonists (sclerostin and Dkk-1) and their relationship with bone turnover. *Bone* 2013; **57**: 272-276 [PMID: 23981659 DOI: 10.1016/j.bone.2013.08.016]

40   **Humphrey EL**, Williams JH, Davie MW, Marshall MJ. Effects of dissociated glucocorticoids on OPG and RANKL in osteoblastic cells. *Bone* 2006; **38**: 652-661 [PMID: 16298558 DOI: 10.1016/j.bone.2005.10.004]

41   **Weinstein RS**. Clinical practice. Glucocorticoid-induced bone disease. *N Engl J Med* 2011; **365**: 62-70 [PMID: 21732837 DOI: 10.1056/NEJMcp1012926]

42   **Briot K**, Geusens P, Em Bultink I, Lems WF, Roux C. Inflammatory diseases and bone fragility. *Osteoporos Int* 2017; **28**: 3301-3314 [PMID: 28916915 DOI: 10.1007/s00198-017-4189-7]

43   **Ghosh S**, Cowen S, Hannan WJ, Ferguson A. Low bone mineral density in Crohn's disease, but not in ulcerative colitis, at diagnosis. *Gastroenterology* 1994; **107**: 1031-1039 [PMID: 7926456 DOI: 10.1016/0016-5085(94)90227-5]

44   **McCabe LR**, Parameswaran N. Understanding the gut-bone Signaling Axis: Mechanism and therapeutics implications.. 2017 [DOI: 10.1007/978-3-319-66653-2]

45   **Rossini M**, Adami S, Bertoldo F, Diacinti D, Gatti D, Giannini S, Giusti A, Malavolta N, Minisola S, Osella G, Pedrazzoni M, Sinigaglia L, Viapiana O, Isaia GC. Guidelines for the diagnosis, prevention and management of osteoporosis. *Reumatismo* 2016; **68**: 1-39 [PMID: 27339372 DOI: 10.4081/reumatismo.2016.870]

46   **Van Assche G**, Dignass A, Reinisch W, van der Woude CJ, Sturm A, De Vos M, Guslandi M, Oldenburg B, Dotan I, Marteau P, Ardizzone A, Baumgart DC, D'Haens G, Gionchetti P, Portela F, Vucelic B, Söderholm J, Escher J, Koletzko S, Kolho KL, Lukas M, Mottet C, Tilg H, Vermeire S, Carbonnel F, Cole A, Novacek G, Reinshagen M, Tsianos E, Herrlinger K, Oldenburg B, Bouhnik Y, Kiesslich R, Stange E, Travis S, Lindsay J; European Crohn's and Colitis Organisation (ECCO). The second European evidence-based Consensus on the diagnosis and management of Crohn's disease: Special situations. *J Crohns Colitis* 2010; **4**: 63-101 [PMID: 21122490 DOI: 10.1016/j.crohns.2009.09.009]

47   **Azzopardi N**, Ellul P. Risk factors for osteoporosis in Crohn's disease: infliximab, corticosteroids, body mass index, and age of onset. *Inflamm Bowel Dis* 2013; **19**: 1173-1178 [PMID: 23511037 DOI: 10.1097/MIB.0b013e31828075a7]

48   **Jahnsen J**, Falch JA, Mowinckel P, Aadland E. Bone mineral density in patients with inflammatory bowel disease: a population-based prospective two-year follow-up study. *Scand J Gastroenterol* 2004; **39**: 145-153 [PMID: 15000276 DOI: 10.1080/00365520310007873]

49   **Bernstein CN**, Leslie WD, Leboff MS. AGA technical review on osteoporosis in gastrointestinal diseases. *Gastroenterology* 2003; **124**: 795-841 [PMID: 12612917 DOI: 10.1053/gast.2003.50106]

50   **Veerappan SG**, O'Morain CA, Daly JS, Ryan BM. Review article: the effects of antitumour necrosis factor-α on bone metabolism in inflammatory bowel disease. *Aliment Pharmacol Ther* 2011; **33**: 1261-1272 [PMID: 21521250 DOI: 10.1111/j.1365-2036.2011.04667.x]

51   **Yang BR**, Choi NK, Kim MS, Chun J, Joo SH, Kim H, Lee J. Prevalence of extraintestinal manifestations in Korean inflammatory bowel disease patients. *PLoS One* 2018; **13**: e0200363 [PMID: 29990326 DOI: 10.1371/journal.pone.0200363]

52   **Von Tirpitz C**, Pischulti G, Klaus J, Rieber A, Brückel J, Böhm BO, Adler G, Reinshagen M. [Pathological bone density in chronic inflammatory bowel diseases--prevalence and risk factors]. *Z Gastroenterol* 1999; **37**: 5-12 [PMID: 10091278]

53   **Schulte CM**, Dignass AU, Goebell H, Röher HD, Schulte KM. Genetic factors determine extent of bone loss in inflammatory bowel disease. *Gastroenterology* 2000; **119**: 909-920 [PMID: 11040178 DOI: 10.1053/gast.2000.18158]

54   **Todhunter CE**, Sutherland-Craggs A, Bartram SA, Donaldson PT, Daly AK, Francis RM, Mansfield JC, Thompson NP. Influence of IL-6, COL1A1, and VDR gene polymorphisms on bone mineral density in Crohn's disease. *Gut* 2005; **54**: 1579-1584 [PMID: 16009674 DOI: 10.1136/gut.2005.064212]

55   **Nemetz A**, Tóth M, García-González MA, Zágoni T, Fehér J, Peña AS, Tulassay Z. Allelic variation at the interleukin 1beta gene is associated with decreased bone mass in patients with inflammatory bowel diseases. *Gut* 2001; **49**: 644-649 [PMID: 11600466 DOI: 10.1136/gut.49.5.644]

56   **Krela-Kaźmierczak I**, Kaczmarek-Ryś M, Szymczak A, Michalak M, Skrzypczak-Zielińska M, Drwęska-Matelska N, Marcinkowska M, Eder P, Łykowska-Szuber L, Wysocka E, Linke K, Słomski R. Bone Metabolism and the c.-223C > T Polymorphism in the 5'UTR Region of the Osteoprotegerin Gene in Patients with Inflammatory Bowel Disease. *Calcif Tissue Int* 2016; **99**: 616-624 [PMID: 27639566 DOI: 10.1007/s00223-016-0192-9]

57   **Krela-Kaźmierczak I**, Michalak M, Wawrzyniak A, Szymczak A, Eder P, Łykowska-Szuber L, Kaczmarek-Ryś M, Drwęska-Matelska N, Skrzypczak-Zielińska M, Linke K, Słomski R. The c.29T>C polymorphism of the transforming growth factor beta-1 (TGFB1) gene, bone mineral density and the occurrence of low-energy fractures in patients with inflammatory bowel disease. *Mol Biol Rep* 2017; **44**: 455-461 [PMID: 28993955 DOI: 10.1007/s11033-017-4131-2]

58   **Krela-Kazmierczak I**, Wawrzyniak A, Szymczak A, Eder P, Lykowska-Szuber L, Michalak M, Drweska-Matelska N, Kaczmarek-Rys M, Skrzypczak-Zielinska M, Szalata M, Slomski R. Bone mineral density and the 570A>T polymorphism of the bone morphogenetic protein 2 (BMP2) gene in patients with inflammatory bowel disease: a cross-sectional study. *J Physiol Pharmacol* 2017; **68**: 757-764 [PMID: 29375051]

59   **Cleynen I**, Boucher G, Jostins L, Schumm LP, Zeissig S, Ahmad T, Andersen V, Andrews JM, Annese V, Brand S, Brant SR, Cho JH, Daly MJ, Dubinsky M, Duerr RH, Ferguson LR, Franke A, Gearry RB, Goyette P, Hakonarson H, Halfvarson J, Hov JR, Huang H, Kennedy NA, Kupcinskas L, Lawrance IC, Lee JC, Satsangi J, Schreiber S, Théâtre E, van der Meulen-de Jong AE, Weersma RK, Wilson DC; International Inflammatory Bowel Disease Genetics Consortium, Parkes M, Vermeire S, Rioux JD, Mansfield J, Silverberg MS, Radford-Smith G, McGovern DP, Barrett JC, Lees CW. Inherited determinants of Crohn's disease and ulcerative colitis phenotypes: a genetic association study. *Lancet* 2016; **387**: 156-167 [PMID: 26490195 DOI: 10.1016/S0140-6736(15)00465-1]

60   **Wu Y**, Yang M, Fan J, Peng Y, Deng L, Ding Y, Yang R, Zhou J, Miao D, Fu Q. Deficiency of osteoblastic Arl6ip5 impaired osteoblast differentiation and enhanced osteoclastogenesis via disturbance of ER calcium homeostasis and induction of ER stress-mediated apoptosis. *Cell Death Dis* 2014; **5**: e1464 [PMID: 25321471 DOI: 10.1038/cddis.2014.427]

61   **Saito A**, Ochiai K, Kondo S, Tsumagari K, Murakami T, Cavener DR, Imaizumi K. Endoplasmic reticulum stress response mediated by the PERK-eIF2(alpha)-ATF4 pathway is involved in osteoblast differentiation induced by BMP2. *J Biol Chem* 2011; **286**: 4809-4818 [PMID: 21135100 DOI: 10.1074/jbc.M110.152900]

62   **Tohmonda T**, Yoda M, Mizuochi H, Morioka H, Matsumoto M, Urano F, Toyama Y, Horiuchi K. The IRE1α-XBP1 pathway positively regulates parathyroid hormone (PTH)/PTH-related peptide receptor expression and is involved in pth-induced osteoclastogenesis. *J Biol Chem* 2013; **288**: 1691-1695 [PMID: 23235147 DOI: 10.1074/jbc.C112.424606]

63   **Arron JR**, Choi Y. Bone versus immune system. *Nature* 2000; **408**: 535-536 [PMID: 11117729 DOI: 10.1038/35046196]

64   **Ciucci T**, Ibáñez L, Boucoiran A, Birgy-Barelli E, Pène J, Abou-Ezzi G, Arab N, Rouleau M, Hébuterne X, Yssel H, Blin-Wakkach C, Wakkach A. Bone marrow Th17 TNFα cells induce osteoclast differentiation, and link bone destruction to IBD. *Gut* 2015; **64**: 1072-1081 [PMID: 25298539 DOI: 10.1136/gutjnl-2014-306947]

65   **Ashcroft AJ**, Cruickshank SM, Croucher PI, Perry MJ, Rollinson S, Lippitt JM, Child JA, Dunstan C, Felsburg PJ, Morgan GJ, Carding SR. Colonic dendritic cells, intestinal inflammation, and T cell-mediated bone destruction are modulated by recombinant osteoprotegerin. *Immunity* 2003; **19**: 849-861 [PMID: 14670302 DOI: 10.1016/S1074-7613(03)00326-1]

66   **Li Y**, Toraldo G, Li A, Yang X, Zhang H, Qian WP, Weitzmann MN. B cells and T cells are critical for the preservation of bone homeostasis and attainment of peak bone mass in vivo. *Blood* 2007; **109**: 3839-3848 [PMID: 17202317 DOI: 10.1182/blood-2006-07-037994]

67   **Nakashima T**, Takayanagi H. Osteoimmunology: crosstalk between the immune and bone systems. *J Clin Immunol* 2009; **29**: 555-567 [PMID: 19585227 DOI: 10.1007/s10875-009-9316-6]

68   **Shih TC**, Hsieh SY, Hsieh YY, Chen TC, Yeh CY, Lin CJ, Lin DY, Chiu CT. Aberrant activation of nuclear factor of activated T cell 2 in lamina propria mononuclear cells in ulcerative colitis. *World J Gastroenterol* 2008; **14**: 1759-1767 [PMID: 18350607 DOI: 10.3748/wjg.14.1759]

69   **Fukuda S**, Ohno H. Gut microbiome and metabolic diseases. *Semin Immunopathol* 2014; **36**: 103-114 [PMID: 24196453 DOI: 10.1007/s00281-013-0399-z]

70   **Tomasello G**, Tralongo P, Damiani P, Sinagra E, Di Trapani B, Zeenny MN, Hussein IH, Jurjus A, Leone A. Dismicrobism in inflammatory bowel disease and colorectal cancer: changes in response of colocytes. *World J Gastroenterol* 2014; **20**: 18121-18130 [PMID: 25561781 DOI: 10.3748/wjg.v20.i48.18121]

71   **Irwin R**, Lee T, Young VB, Parameswaran N, McCabe LR. Colitis-induced bone loss is gender dependent and associated with increased inflammation. *Inflamm Bowel Dis* 2013; **19**: 1586-1597 [PMID: 23702805 DOI: 10.1097/MIB.0b013e318289e17b]

72   **McCabe LR**, Irwin R, Schaefer L, Britton RA. Probiotic use decreases intestinal inflammation and increases bone density in healthy male but not female mice. *J Cell Physiol* 2013; **228**: 1793-1798 [PMID: 23389860 DOI: 10.1002/jcp.24340]

73   **Schepper JD**, Collins FL, Rios-Arce ND, Raehtz S, Schaefer L, Gardinier JD, Britton RA, Parameswaran N, McCabe LR. Probiotic Lactobacillus reuteri Prevents Postantibiotic Bone Loss by Reducing Intestinal Dysbiosis and Preventing Barrier Disruption. *J Bone Miner Res* 2019; **34**: 681-698 [PMID: 30690795 DOI: 10.1002/jbmr.3635]

74   **Naser A**, Qasem A, Naser SA. Mycobacterial infection influences bone biomarker levels in patients with Crohn's disease. *Can J Physiol Pharmacol* 2018; **96**: 662-667 [PMID: 29638140 DOI: 10.1139/cjpp-2017-0700]

75   **Lim H**, Kim HJ, Hong SJ, Kim S. Nutrient intake and bone mineral density by nutritional status in patients with inflammatory bowel disease. *J Bone Metab* 2014; **21**: 195-203 [PMID: 25247157 DOI: 10.11005/jbm.2014.21.3.195]

76   **Leslie WD**, Miller N, Rogala L, Bernstein CN. Body mass and composition affect bone density in recently diagnosed inflammatory bowel disease: the Manitoba IBD Cohort Study. *Inflamm Bowel Dis* 2009; **15**: 39-46 [PMID: 18623166 DOI: 10.1002/ibd.20541]

77   **Silvennoinen J**, Lamberg-Allardt C, Kärkkäinen M, Niemelä S, Lehtola J. Dietary calcium intake and its relation to bone mineral density in patients with inflammatory bowel disease. *J Intern Med* 1996; **240**: 285-292 [PMID: 8946811 DOI: 10.1046/j.1365-2796.1996.25862000.x]

78   **Vernia P**, Loizos P, Di Giuseppantonio I, Amore B, Chiappini A, Cannizzaro S. Dietary calcium intake in patients with inflammatory bowel disease. *J Crohns Colitis* 2014; **8**: 312-317 [PMID: 24090907 DOI: 10.1016/j.crohns.2013.09.008]

79   **Abitbol V**, Mary JY, Roux C, Soulé JC, Belaiche J, Dupas JL, Gendre JP, Lerebours E, Chaussade S; Groupe D'etudes Thérapeutiques des Affections Inflammatoires Digestives (GETAID). Osteoporosis in inflammatory bowel disease: effect of calcium and vitamin D with or without fluoride. *Aliment Pharmacol Ther* 2002; **16**: 919-927 [PMID: 11966500 DOI: 10.1046/j.1365-2036.2002.01247.x]

80   **Ghishan FK**, Kiela PR. Vitamins and Minerals in Inflammatory Bowel Disease. *Gastroenterol Clin North Am* 2017; **46**: 797-808 [PMID: 29173522 DOI: 10.1016/j.gtc.2017.08.011]

81   **Zhang YZ**, Li YY. Inflammatory bowel disease: pathogenesis. *World J Gastroenterol* 2014; **20**: 91-99 [PMID: 24415861 DOI: 10.3748/wjg.v20.i1.91]

82   **Del Pinto R**, Pietropaoli D, Chandar AK, Ferri C, Cominelli F. Association Between Inflammatory Bowel Disease and Vitamin D Deficiency: A Systematic Review and Meta-analysis. *Inflamm Bowel Dis* 2015; **21**: 2708-2717 [PMID: 26348447 DOI: 10.1097/MIB.0000000000000546]

83   **Farraye FA**, Nimitphong H, Stucchi A, Dendrinos K, Boulanger AB, Vijjeswarapu A, Tanennbaum A, Biancuzzo R, Chen TC, Holick MF. Use of a novel vitamin D bioavailability test demonstrates that

vitamin D absorption is decreased in patients with quiescent Crohn's disease. *Inflamm Bowel Dis* 2011; **17**: 2116-2121 [PMID: 21910173 DOI: 10.1002/ibd.21595]

84 **Levin AD**, Wadhera V, Leach ST, Woodhead HJ, Lemberg DA, Mendoza-Cruz AC, Day AS. Vitamin D deficiency in children with inflammatory bowel disease. *Dig Dis Sci* 2011; **56**: 830-836 [PMID: 21222159 DOI: 10.1007/s10620-010-1544-3]

85 **Palermo A**, Tuccinardi D, D'Onofrio L, Watanabe M, Maggi D, Maurizi AR, Greto V, Buzzetti R, Napoli N, Pozzilli P, Manfrini S. Vitamin K and osteoporosis: Myth or reality? *Metabolism* 2017; **70**: 57-71 [PMID: 28403946 DOI: 10.1016/j.metabol.2017.01.032]

86 **Dubois-Camacho K**, Ottum PA, Franco-Muñoz D, De la Fuente M, Torres-Riquelme A, Díaz-Jiménez D, Olivares-Morales M, Astudillo G, Quera R, Hermoso MA. Glucocorticosteroid therapy in inflammatory bowel diseases: From clinical practice to molecular biology. *World J Gastroenterol* 2017; **23**: 6628-6638 [PMID: 29085208 DOI: 10.3748/wjg.v23.i36.6628]

87 **LoCascio V**, Bonucci E, Imbimbo B, Ballanti P, Adami S, Milani S, Tartarotti D, DellaRocca C. Bone loss in response to long-term glucocorticoid therapy. *Bone Miner* 1990; **8**: 39-51 [PMID: 2306553 DOI: 10.1016/0169-6009(91)90139-Q]

88 **Van Staa TP**, Laan RF, Barton IP, Cohen S, Reid DM, Cooper C. Bone density threshold and other predictors of vertebral fracture in patients receiving oral glucocorticoid therapy. *Arthritis Rheum* 2003; **48**: 3224-3229 [PMID: 14613287 DOI: 10.1002/art.11283]

89 **Hofbauer LC**, Gori F, Riggs BL, Lacey DL, Dunstan CR, Spelsberg TC, Khosla S. Stimulation of osteoprotegerin ligand and inhibition of osteoprotegerin production by glucocorticoids in human osteoblastic lineage cells: potential paracrine mechanisms of glucocorticoid-induced osteoporosis. *Endocrinology* 1999; **140**: 4382-4389 [PMID: 10499489 DOI: 10.1210/endo.140.10.7034]

90 **Hofbauer LC**, Zeitz U, Schoppet M, Skalicky M, Schüler C, Stolina M, Kostenuik PJ, Erben RG. Prevention of glucocorticoid-induced bone loss in mice by inhibition of RANKL. *Arthritis Rheum* 2009; **60**: 1427-1437 [PMID: 19404943 DOI: 10.1002/art.24445]

91 **Piemontese M**, Xiong J, Fujiwara Y, Thostenson JD, O'Brien CA. Cortical bone loss caused by glucocorticoid excess requires RANKL production by osteocytes and is associated with reduced OPG expression in mice. *Am J Physiol Endocrinol Metab* 2016; **311**: E587-E593 [PMID: 27460899 DOI: 10.1152/ajpendo.00219.2016]

92 **Rutgeerts P**, Löfberg R, Malchow H, Lamers C, Olaison G, Jewell D, Danielsson A, Goebell H, Thomsen OO, Lorenz-Meyer H. A comparison of budesonide with prednisolone for active Crohn's disease. *N Engl J Med* 1994; **331**: 842-845 [PMID: 8078530 DOI: 10.1056/NEJM199409293311304]

93 **D'Haens G**, Verstraete A, Cheyns K, Aerden I, Bouillon R, Rutgeerts P. Bone turnover during short-term therapy with methylprednisolone or budesonide in Crohn's disease. *Aliment Pharmacol Ther* 1998; **12**: 419-424 [PMID: 9663720 DOI: 10.1046/j.1365-2036.1998.00321.x]

94 **Christakos S**, Dhawan P, Porta A, Mady LJ, Seth T. Vitamin D and intestinal calcium absorption. *Mol Cell Endocrinol* 2011; **347**: 25-29 [PMID: 21664413 DOI: 10.1016/j.mce.2011.05.038]

95 **Wasserman RH**. *Vitamin D and intestinal absorption of calcium: a view and over-view*. In: P JW, Feldman D, Glorieux F, editors. Vitamin D. San Diego 2005; 411–428 [DOI: 10.1016/B978-012252687-9/50027-9]

96 **Xue Y**, Fleet JC. Intestinal vitamin D receptor is required for normal calcium and bone metabolism in mice. *Gastroenterology* 2009; **136**: 1317-1327, e1-e2 [PMID: 19254681 DOI: 10.1053/j.gastro.2008.12.051]

97 **Vogelsang H**, Ferenci P, Woloszczuk W, Resch H, Herold C, Frotz S, Gangl A. Bone disease in vitamin D-deficient patients with Crohn's disease. *Dig Dis Sci* 1989; **34**: 1094-1099 [PMID: 2743850 DOI: 10.1007/BF01536381]

98 **Tromm A**, Rickels K, Hüppe D, Wiebe V, May B. [Osteopenia in chronic inflammatory bowel diseases. Results of a cross-sectional study using quantitative computerized tomography]. *Leber Magen Darm* 1994; **24**: 23-26, 29-30 [PMID: 8145623]

99 **Satsangi J**, Silverberg MS, Vermeire S, Colombel JF. The Montreal classification of inflammatory bowel disease: controversies, consensus, and implications. *Gut* 2006; **55**: 749-753 [PMID: 16698746 DOI: 10.1136/gut.2005.082909]

100 **Cravo M**, Guerreiro CS, dos Santos PM, Brito M, Ferreira P, Fidalgo C, Tavares L, Pereira AD. Risk factors for metabolic bone disease in Crohn's disease patients. *Inflamm Bowel Dis* 2010; **16**: 2117-2124 [PMID: 20848459 DOI: 10.1002/ibd.21297]

101 **Lima CA**, Lyra AC, Mendes CMC, Lopes MB, Coqueiro FG, Rocha R, Santana GO. Bone mineral density and inflammatory bowel disease severity. *Braz J Med Biol Res* 2017; **50**: e6374 [PMID: 29069227 DOI: 10.1590/1414-431X20176374]

102 **Holleran G**, Lopetuso L, Petito V, Graziani C, Ianiro G, McNamara D, Gasbarrini A, Scaldaferri F. The Innate and Adaptive Immune System as Targets for Biologic Therapies in Inflammatory Bowel Disease. *Int J Mol Sci* 2017; 18 [PMID: 28934123 DOI: 10.3390/ijms18102020]

103 **Takahashi N**, Udagawa N, Suda T. A new member of tumor necrosis factor ligand family, ODF/OPGL/TRANCE/RANKL, regulates osteoclast differentiation and function. *Biochem Biophys Res Commun* 1999; **256**: 449-455 [PMID: 10080918 DOI: 10.1006/bbrc.1999.0252]

104 **Theill LE**, Boyle WJ, Penninger JM. RANK-L and RANK: T cells, bone loss, and mammalian evolution. *Annu Rev Immunol* 2002; **20**: 795-823 [PMID: 11861618 DOI: 10.1146/annurev.immunol.20.100301.064753]

105 **Kaji K**, Katogi R, Azuma Y, Naito A, Inoue JI, Kudo A. Tumor necrosis factor alpha-induced osteoclastogenesis requires tumor necrosis factor receptor-associated factor 6. *J Bone Miner Res* 2001; **16**: 1593-1599 [PMID: 11547829 DOI: 10.1359/jbmr.2001.16.9.1593]

106 **Tsuboi M**, Kawakami A, Nakashima T, Matsuoka N, Urayama S, Kawabe Y, Fujiyama K, Kiriyama T, Aoyagi T, Maeda K, Eguchi K. Tumor necrosis factor-alpha and interleukin-1beta increase the Fas-mediated apoptosis of human osteoblasts. *J Lab Clin Med* 1999; **134**: 222-231 [PMID: 10482306 DOI: 10.1016/S0022-2143(99)90201-9]

107 **Azuma Y**, Kaji K, Katogi R, Takeshita S, Kudo A. Tumor necrosis factor-alpha induces differentiation of and bone resorption by osteoclasts. *J Biol Chem* 2000; **275**: 4858-4864 [PMID: 10671521 DOI: 10.1074/jbc.275.7.4858]

108 **Franchimont N**, Putzeys V, Collette J, Vermeire S, Rutgeerts P, De Vos M, Van Gossum A, Franchimont D, Fiasse R, Pelckmans P, Malaise M, Belaiche J, Louis E. Rapid improvement of bone metabolism after infliximab treatment in Crohn's disease. *Aliment Pharmacol Ther* 2004; **20**: 607-614 [PMID: 15352908 DOI: 10.1111/j.1365-2036.2004.02152.x]

109   **Bernstein M**, Irwin S, Greenberg GR. Maintenance infliximab treatment is associated with improved bone mineral density in Crohn's disease. *Am J Gastroenterol* 2005; **100**: 2031-2035 [PMID: 16128948 DOI: 10.1111/j.1572-0241.2005.50219.x]

110   **Ryan BM**, Russel MG, Schurgers L, Wichers M, Sijbrandij J, Stockbrugger RW, Schoon E. Effect of antitumour necrosis factor-alpha therapy on bone turnover in patients with active Crohn's disease: a prospective study. *Aliment Pharmacol Ther* 2004; **20**: 851-857 [PMID: 15479356 DOI: 10.1111/j.1365-2036.2004.02097.x]

111   **Miheller P**, Muzes G, Zagoni T, Toth M, Racz K, Tulassay Z. Infliximab therapy improves the bone metabolism in fistulizing Crohn's disease. *Dig Dis* 2006; **24**: 201-206 [PMID: 16699279 DOI: 10.1159/000091299]

112   **Maldonado-Pérez MB**, Castro-Laria L, Caunedo-Álvarez A, Montoya-García MJ, Giner-García M, Argüelles-Arias F, Romero-Gómez M, Vázquez-Gámez MÁ. Does the Antitumor Necrosis Factor-α Therapy Decrease the Vertebral Fractures Occurrence in Inflammatory Bowel Disease? *J Clin Densitom* 2019; **22**: 195-202 [PMID: 30205986 DOI: 10.1016/j.jocd.2018.07.010]

113   **Veerappan SG**, Healy M, Walsh BJ, O'Morain CA, Daly JS, Ryan BM. Adalimumab Therapy Has a Beneficial Effect on Bone Metabolism in Patients with Crohn's Disease. *Dig Dis Sci* 2015; **60**: 2119-2129 [PMID: 25732718 DOI: 10.1007/s10620-015-3606-z]

114   **Kanis JA**, Johnell O, Oden A, Johansson H, McCloskey E. FRAX and the assessment of fracture probability in men and women from the UK. *Osteoporos Int* 2008; **19**: 385-397 [PMID: 18292978 DOI: 10.1007/s00198-007-0543-5]

115   **Harbord M**, Annese V, Vavricka SR, Allez M, Barreiro-de Acosta M, Boberg KM, Burisch J, De Vos M, De Vries AM, Dick AD, Juillerat P, Karlsen TH, Koutroubakis I, Lakatos PL, Orchard T, Papay P, Raine T, Reinshagen M, Thaci D, Tilg H, Carbonnel F; European Crohn's and Colitis Organisation. The First European Evidence-based Consensus on Extra-intestinal Manifestations in Inflammatory Bowel Disease. *J Crohns Colitis* 2016; **10**: 239-254 [PMID: 26614685 DOI: 10.1093/ecco-jcc/jjv213]

116   **Scott EM**, Gaywood I, Scott BB. Guidelines for osteoporosis in coeliac disease and inflammatory bowel disease. British Society of Gastroenterology. *Gut* 2000; **46** Suppl 1: i1-i8 [PMID: 10647595 DOI: 10.1136/gut.46.suppl_1.I1]

117   **Black DM**, Rosen CJ. Postmenopausal Osteoporosis. *N Engl J Med* 2016; **374**: 2096-2097 [PMID: 27223157 DOI: 10.1056/NEJMc1602599]

118   **Melek J**, Sakuraba A. Efficacy and safety of medical therapy for low bone mineral density in patients with inflammatory bowel disease: a meta-analysis and systematic review. *Clin Gastroenterol Hepatol* 2014; **12**: 32-44.e5 [PMID: 23981521 DOI: 10.1016/j.cgh.2013.08.024]

119   **Papapoulos S**, Chapurlat R, Libanati C, Brandi ML, Brown JP, Czerwiński E, Krieg MA, Man Z, Mellström D, Radominski SC, Reginster JY, Resch H, Román Ivorra JA, Roux C, Vittinghoff E, Austin M, Daizadeh N, Bradley MN, Grauer A, Cummings SR, Bone HG. Five years of denosumab exposure in women with postmenopausal osteoporosis: results from the first two years of the FREEDOM extension. *J Bone Miner Res* 2012; **27**: 694-701 [PMID: 22113951 DOI: 10.1002/jbmr.1479]

120   **Nuti R**, Brandi ML, Checchia G, Di Munno O, Dominguez L, Falaschi P, Fiore CE, Iolascon G, Maggi S, Michieli R, Migliaccio S, Minisola S, Rossini M, Sessa G, Tarantino U, Toselli A, Isaia GC. Guidelines for the management of osteoporosis and fragility fractures. *Intern Emerg Med* 2019; **14**: 85-102 [PMID: 29948835 DOI: 10.1007/s11739-018-1874-2]

Extrahepatic hepcidin production: The intriguing outcomes of recent years

Raêd Daher, Thibaud Lefebvre, Hervé Puy, Zoubida Karim

Raêd Daher, Thibaud Lefebvre, Hervé Puy, Zoubida Karim, Université Paris Diderot, Bichat site, Paris 75018, France

Raêd Daher, Thibaud Lefebvre, Hervé Puy, Zoubida Karim, Inflammation Research Center (CRI), INSERM U1149/ERL CNRS 8252, Paris 75018, France

Raêd Daher, Thibaud Lefebvre, Hervé Puy, Zoubida Karim, Laboratory of Excellence, GR-Ex, Paris 75018, France

Corresponding author: Zoubida Karim, PhD, Professor, Université Paris Diderot, Faculté de Médecine Site Bichat, 16 rue Henri-Huchard, Paris 75018, France. zoubida.karim@inserm.fr
Telephone: +33-1-57277559

Abstract

Hepcidin is the hyposideremic hormone regulating iron metabolism. It is a defensin-like disulfide-bonded peptide with antimicrobial activity. The main site of hepcidin production is the liver where its synthesis is modulated by iron, inflammation and erythropoietic signaling. However, hepcidin locally produced in several peripheral organs seems to be an important actor for the maintenance of iron homeostasis in these organs. This review highlights the presence of peripheral hepcidin and its potential functions. Understanding the role of extrahepatic hepcidin could be of great physiological and therapeutic importance for several specific pathologies.

Key words: Hepcidin; Extrahepatic hepcidin; Iron metabolism; Bacterial infection; Inflammation

Core tip: Hepcidin is the key regulator of iron homeostasis and is involved in iron-related disorders, namely anemia of inflammation and primary and secondary hemochromatosis. Since the discovery of its hyposideremic role, considerable efforts were made to explore iron handling by hepcidin. Almost all these studies focused on the liver because this organ was shown to be the major source of systemic hepcidin. However, interesting pending data showed an extrahepatic production of hepcidin in several organs, but the involvement of this peripheral hepcidin in local and overall iron homeostasis remains unknown. Thus, we think that those in the field should: (1) Consider the presence of endogenous hepcidin in the peripheral organs; and (2) Be interested in the involvement of hepcidin in other physiological and pathological mechanisms, in particular antimicrobial activity, acid secretion regulation, immune inflammatory response, *etc*.

INTRODUCTION

Iron is one of the most abundant metals in the planet with the potential of high toxicity to living cells. Highly active cells need iron for their metabolic activity because iron exhibits an optimal chemical property for electron transfer, facilitating biochemical reactions between different atoms and molecules. The toxicity of iron is due to induction of reactive oxygen species, which at high levels leads to cellular damage[1].

In the body, 60% of iron is incorporated into hemoglobin, while 10% to 15% are found in muscle myoglobin and cytochromes. Circulating iron, related to transferrin, represents only 1%. Under physiological conditions, the liver and macrophages of the reticuloendothelial system are the main iron storage and recycling sites. One to two milligrams of iron are lost daily by sweating and desquamation of skin and intestinal cells, and in women by menstrual bleeding. This small amount is totally recovered by intestinal absorption of heme and non-heme iron, which takes place in the duodenal enterocytes[2].

There is no effective mechanism for iron excretion. As a result, the exogenous iron supplied to the body is not eliminated and may accumulate in a toxic way in the tissues.

BODY IRON METABOLISM

Dietary iron (Fe) III is reduced to FeII by duodenal cytochrome B reductase located in the brush borders of the enterocytes[3]. FeII is then transported through divalent metal transporter 1 (named DMT1 or SLC11A2)[4] and is exported to blood *via* ferroportin (FPN or SLC40A1), which shares no homology with DMT1 and is localized at the basolateral pole of the enterocytes[5]. The export of iron by FPN requires a ferroxidase activity provided by the enzymes hephastin and/or ceruloplasmin allowing transferrin (Tf) to bind the circulating iron in the form of FeIII. Most cells in the body can assimilate Tf-bound iron through the ubiquitous transferrin receptor 1 (TfR1) that has a high affinity for the Tf-FeIII complex. After TfR1-mediated endocytosis, iron is released from Tf in the intracellular endosomes at acidic pH. The released FeIII is then reduced to FeII by a reductase, for example the six epithelial transmembrane antigen of the prostate 3 in erythroid cells. FeII is then transported to the cytosol through DMT1 localized in these endosomes. Erythroid cells of the bone marrow are the largest consumers of iron. About one billion iron atoms (20 to 30 mg) are used daily to form hemoglobin in newly produced erythrocytes. Macrophages of the spleen and liver recover heme iron from senescent erythrocytes after phagocytosis and catabolism of heme by the enzyme heme oxygenase[6]. The mobilizable iron is thus recycled to the plasma for redistribution to tissues. FPN is essential for the export of iron by macrophages[7].

In all cells, unused iron is stored in a non-reactive form due to ferritin (Ft). FeII could be delivered to Ft by cytoplasmic chaperones, such as poly (rC)-binding protein 1[8]. Ft is a protein complex consisting of 24 subunits of two types called heavy and light ferritins. Each complex is capable of storing up to 4500 iron atoms, which are easily mobilized when needed. A secreted form of Ft, low in iron, is found in the plasma. This serum Ft, used clinically to evaluate iron stores, is composed mainly of light subunits, some of which are glycosylated. In the majority of cases, serum Ft concentrations correlate with tissue stores of iron except under certain conditions where the synthesis of Ft is mainly due to inflammation. Indeed, Ft stimulated by inflammatory cytokines[9] is widely recognized as a marker of acute and chronic inflammation.

REGULATION OF IRON METABOLISM

Intracellular regulation

Intracellular iron homeostasis is ensured by the iron response element (IRE)-iron regulatory protein (IRP) system that controls the post-transcriptional expression of several iron proteins (TfR1, DMT1, FPN, Ft, and ALAS2; the first enzyme involved in heme biosynthesis in erythroid cells)[10-13]. IREs are hairpin-like RNA motifs that serve as specific binding sites for IRPs. IRPs are soluble cytosolic proteins whose activity varies according to the intracellular iron concentration. There are two IRPs: IRP1 and IRP2 with a sequence identity of 56%[14]. The IRE-IRP interaction stabilizes the mRNA when the IRE motifs are located in the 3'-UTR region, such as for TfR1, and imposes a steric constraint on the translation of the protein when IRE motifs are located in the 5'-UTR region. This results in an increase in transferrin-related iron acquisition when intracellular iron levels are low. A decrease in FPN and ferritin expression also occurs because iron export and intracellular iron storage are not appropriate in this condition.

Systemic regulation

Hepcidin was initially identified as an antimicrobial peptide[15] (see section below). Yet since 2001, it is considered to be the master regulator of iron balance in humans by decreasing iron absorption and increasing iron retention in macrophages and Kupffer cells[16,17]. The mechanism by which hepcidin inhibits these iron effluxes has been well studied in macrophages, where hepcidin binds to FPN and leads to its internalization and degradation in lysosomes[18,19]. In duodenal cells, studies have reported a different mechanism. Indeed, hepcidin was shown to decrease duodenal transepithelial iron transport without internalization of FPN from the plasma membrane[20-22]. In these cells, hepcidin leads to a decrease in the protein expression of DMT1 rather than that of FPN[21]. Recently, the non-internalization of FPN following hepcidin treatment was also shown in other cellular contexts[23,24]. Zhang *et al*[23] first observed that FPN was highly expressed in mature red blood cells lacking the proteasomal degradation pathway. In these mature red blood cells, hepcidin was shown to inhibit iron export but did not change FPN abundance similarly to what we have previously observed in duodenal enterocytes[21]. Studies on hepcidin-FPN interactions in the transfected HEK293T cell line and *Xenopus* oocytes also confirmed that hepcidin binding is able to block iron export without causing FPN internalization[24]. Thus, it seems that depending on the cellular and membrane environment hepcidin binding may block iron efflux acting either on FPN activity and/or on its abundance at the cell membrane. Moreover, in the duodenum, a permanent increase in hepcidin, as in a transgenic mouse model for example, has been shown to ultimately reduce FPN abundance by mechanisms that remain to be explored[25].

HEPCIDIN PRODUCTION

Hepcidin is synthesized in the liver as a pre-propeptide of 84 amino acids (aa); it then undergoes successive proteolytic cleavage to produce the 25-aa bioactive form, which is secreted in plasma. Being a low-molecular-weight peptide, hepcidin is assumed to be rapidly excreted by the kidney[26,27], where it is supposed to be taken up and degraded by the renal proximal tubule. Indeed, hepcidin was first isolated from human urine and named according to its synthetic site (hep-) and its antibacterial properties shown *in vitro* (-cidin). The mass spectroscopy studies have shown the presence of urinary 25-aa hepcidin as well as shorter forms (22 aa and 20 aa) that are supposed to be degradation products with still unknown functions[28]. Hepcidin exhibits a cysteine-rich structure reminiscent of four disulfide bridges defensins with *in vitro* antimicrobial activity[15,26,29], suggesting ancestral innate defense properties against invasive bacteria. Hepcidin structure is characteristic of peptides able to disrupt bacterial membranes and is similar to other antimicrobial peptides such as defensins. Hepcidin may also limit bacterial proliferation by decreasing iron in plasma and extracellular fluids. With regards to this immune activity, hepcidin synthesis was shown to be highly induced by inflammatory signals such as IL-6, allowing it to play a major role in the anemia associated with chronic diseases and inflammation[30-33]. Hepcidin is also induced in the liver in response to lipo-polysaccharide (LPS) through activin B and SMAD-signaling, but this pathway is still debatable[34-37].

Hepcidin is mainly, but not exclusively, produced and secreted by the liver. Indeed, several studies have shown that hepcidin is locally synthesized by multiple other tissues including kidney[38], macrophages[39,40], stomach[41], adipose tissue[42], brain[43], heart[44] and pancreas[45]. Iron is essential for the normal function of these organs. In addition, hepcidin was found in atypical biological fluids as bile, ascitic and pleural, and cerebrospinal liquid[46,47]. The functions carried out by this extrahepatic hepcidin

are not completely known but this concern has gained increased attention in recent years. Some related findings will be discussed below.

Hepatic hepcidin

Serum levels of hepcidin are mostly correlated with the levels of liver hepcidin expression[48] demonstrating that hepatic hepcidin is the key regulator of systemic iron balance. This was obviously demonstrated in mouse models with either total or liver-specific ablation of the hepcidin gene[49,50]. Liver-specific knockout (KO) mice were shown to fully recapitulate the severe iron overload phenotype observed in the total KO mice with increased plasma iron and massive parenchymal iron accumulation.

The regulation of hepatic synthesis of hepcidin is extremely complex and responds to multiple signals, some of which are still unclear. Indeed, the synthesis of hepcidin is stimulated by the high intake of iron and by inflammation, while it is repressed by iron deficiency and by all the pathological situations that stimulate the erythropoietic activity (anemia, bleeding, hemolysis, dyserythropoiesis and erythropoietin injections).

Hepatic hepcidin is regulated by iron-mediated pathways through a complex of integral hemochromatosis proteins. Hemojuvelin (HJV) was first identified as the mutated protein in the majority of juvenile hemochromatosis[51]. The absence of HJV leads to a severe deficit in hepcidin production. HJV acts as a co-receptor with bone morphogenetic proteins (BMPs), enhancing activation of the SMAD pathway in response to binding of BMPs to their receptor (BMPR). BMP6 plays a major role in this pathway and in the stimulation of hepatic hepcidin by iron. In mice, the ablation of the *Bmp6* gene causes severe iron overload[52]. In humans, we and others[53-57] recently identified heterozygous mutations localized in the propeptide of the BMP6 protein leading to mild to moderate hemochromatosis. The BMP6 pathway is negatively controlled by matriptase 2 that interrupts the binding of BMP6 on its BMPR in hepatocytes[58-61]. The BMP6 pathway also seems to be a target of erythroferrone, the erythroid factor that represses hepcidin when erythropoiesis is pathologically stimulated[62].

The study of the different forms of genetic hemochromatosis has demonstrated the role of the human hemochromatosis protein (HFE) and transferrin receptor 2 (TfR2) in the regulation of hepcidin by iron. The forms of adult hemochromatosis are due to mutations of the *HFE* gene for the most common forms, or TfR2 for rarer forms and are characterized by a lack of activation of hepcidin in response to iron overload[63]. Mice deficient in *Hfe* or patients with *HFE* mutations have a low hepcidin mRNA level in the liver despite their iron overload. A model has been proposed in which HFE, TfR2 and HJV interact with each other at the hepatocyte membrane to form an "iron-sensing complex"[64]. When transferrin saturation in serum increases, holo-transferrin shifts HFE from its binding to TfR1, which allows its interaction with TfR2 and activates transcription of hepcidin-encoding gene. Thus, TfR2 acts as a sensor of the transferrin saturation (serum iron) and BMP6 as a tissue iron sensor activating hepcidin synthesis by interaction with HJV during excessive accumulation of iron in hepatocytes[65,66].

Extrahepatic hepcidin

Hepcidin expression in the kidney: In 2005, using immunocytochemistry assays, Kulaksiz *et al*[38] observed for the first time that hepcidin was expressed in the kidney, namely in the cortical thick ascending limb (cTAL) and connecting tubules and to a lesser extent in the collecting ducts. Hepcidin was absent in the proximal tubule and descending and ascending thin limbs[38]. It was localized at the apical surface of the renal epithelial cells, which suggests that renal hepcidin is eliminated in the urine after an autocrine/paracrine action on renal tubules. Using microdissected and isolated renal tubules, we also confirmed that hepcidin is preferentially expressed throughout the distal nephron, particularly in the TAL[67]. Interestingly, the distal nephron expresses DMT1 and FPN transporters at the apical and the basolateral membrane, respectively and was described to be the site of the reabsorption of non-heme iron in kidney[68-71]. Using mouse models with defects in hepcidin production (hepcidin KO and HJV KO mice), our group had clearly shown that non-heme iron accumulated in this distal nephron particularly the TAL[71]. In the TAL cell line, we found that vectorial transport of iron was decreased following exogenous hepcidin treatment[21]. In addition, similarly to what we observed in intestine[21], hepcidin was able to decrease DMT1 both *in vivo* using kidney sections from hepc-/- mice and *in vitro* using TAL cells. All together, these reports highlight a new role of hepcidin in the control of renal iron transport and accumulation and suggest that local synthesis of hepcidin within renal tubules may play a crucial role in this effect. Hepcidin seems to specifically target the distal nephron rather than the proximal tubule. We investigated the importance of hepcidin in the protection of kidneys against urinary tract

infection[67]. We developed an experimental urinary tract infection model and showed that hepcidin KO mice inoculated with the gram-negative CFT073 strain exhibited higher renal bacterial load than infected wildtype mice as well as a significant attenuation of renal inflammatory profile. Hepcidin KO mice showed a marked alkalization of urine associated with repression of both Atp4a and Atp12a proton pumps. Pre-treatment of wildtype mice with hepcidin considerably reduced renal colonization by the CFT073 strain and restored the acidic pH of urine. *In vitro* experiments proved the bacteriostatic activity of hepcidin against UroPathogenic *Escherichia coli* because the bacterial growth was inhibited in the presence of this peptide. Interestingly, we found that CFT073 repressed renal hepcidin expression in infected mice through reduction of SMAD signaling. These results indicate that hepcidin plays a role in the fight against UroPathogenic *Escherichia coli* infection and that UroPathogenic *Escherichia coli* might target renal hepcidin to attenuate its global antibacterial activity in the early phase of a UTI[67].

Hepcidin expression in macrophages: Macrophages play a central role in iron recycling and consequently in establishing iron balance. Initial studies from Liu *et al*[39] demonstrated that the reticuloendothelial system (RES, namely liver Kupffer and spleen macrophages) was able to produce hepcidin following LPS-induced inflammation in mice and upon treatment of mouse splenic adherent cells by LPS. This RES-produced hepcidin was independent of the iron pool of the cells because *in vivo* iron loading has been shown to induce hepcidin production in liver without increase in hepcidin mRNA in the spleen. In addition, when splenic cells were treated *in vitro* with ferric ammonium citrate, there was again no increase in splenic hepcidin mRNA expression. Peyssonnaux *et al*[40] also investigated the ability of macrophages to endogenously synthesize hepcidin *in vitro* and *in vivo* following bacterial infections. They found that intraperitoneal bacterial challenge was able to increase hepcidin expression in splenic macrophages *via* the LPS-mediated Toll-like receptor 4 pathway. In addition to RES, hepcidin was shown to be produced by alveolar macrophages at a low level when not stimulated but at a high level when exposed to LPS *in vitro* and *in vivo*[72,73]. In agreement with these previous data, Sow *et al*[74] also showed a strong induction of hepcidin mRNA expression in several macrophage cell lines infected with mycobacteria and/or treated with the inflammatory cytokine IFN-γ.

The physiological significance of local hepcidin expression in macrophages is not yet fully determined but the hypothesis is that RES-produced hepcidin may contribute by greatly increasing the regulatory pool of hepcidin around liver Kupffer cells and spleen macrophages as well as other macrophages residing in tissues frequently confronted by infection. Increased local hepcidin might potentiate the retention of iron during conditions of inflammation and infection particularly since FPN is strongly expressed at the cell surface of these cells. These findings strongly suggested that macrophage hepcidin could play a role in host defense by acting on FPN expression and consequently limiting the availability of iron to invading bacteria.

Recently, we described the involvement of RES-produced hepcidin in iron metabolism dysregulation in Gaucher disease (GD), an inherited deficiency of the lysosomal enzyme glucocerebrosidase leading to accumulation of glucosylceramide in tissues including the spleen and the liver[75]. In order to understand the unexplained hyperferritinemia frequently reported in Gaucher disease patients, Perl's staining of spleen and bone marrow smears was performed. Analysis revealed iron accumulation in the lipid-laden macrophages also called Gaucher cells. Using an *in vitro* model of Gaucher cells, we have shown that hepcidin production was induced in these macrophages, and FPN protein was consequently internalized from the plasma membrane. Thus, hyperferritinemia in Gaucher disease could be related to the sequestration of iron in Gaucher cells due to local production and an autocrine action of hepcidin in these cells.

Hepcidin expression in the stomach: The gut is an additional organ that produces hepcidin[41]. In the stomach, hepcidin was found in the gastric fundus and corpus, more precisely, in parietal cells. *In vitro*, gastric hepcidin was upregulated upon treatment with IL6 and in response to bacterial infection. In humans, gastric hepcidin level was elevated during bacterial infection and then normalized after successful eradication. In addition, acid secretion in hepcidin KO mice was markedly reduced due to repression of Atp4a proton pump, and this was associated with gastric bacterial overgrowth. Thus, this original study was the first to show that hepcidin is a gastric factor essential for acid secretion and fight against *Helicobacter* bacterial invasion.

Hepcidin expression in adipose tissue: Hepcidin synthesis in adipose tissue was reported by Bekri *et al*[42] in severely obese patients with low-grade systemic

inflammatory disorder[42]. mRNA level of adipose tissue hepcidin was correlated with multiple indexes of inflammation (IL6, C-reactive protein). This observation was also confirmed by *in vitro* studies using cultured adipose tissue explants, where IL6 was shown to promote hepcidin expression. Thus, adipose tissue hepcidin is suggested to exacerbate the iron deficiency and iron deficiency anemia observed in the majority of obese patients. In this context, it is not clear whether adipose tissue hepcidin contributes to increased pool of systemic hepcidin, but one can suppose that adipose tissue may provide a high concentration of local hepcidin around intestinal cells and inhibit iron absorption *via* an autocrine/paracrine mechanism. Yet, numerous studies have been conducted to explore the role of hepcidin secreted by adipose tissue in obesity hypoferremia. Several high-fat diet mouse models were developed for that purpose, but the results remained highly controversial[76-80].

Hepcidin expression in the brain: Iron has a role in oxidative metabolism and is a cofactor in the synthesis of myelin and neurotransmitters. It is thus essential for normal neurological function. The presence of hepcidin in the brain was shown by Zechel *et al*[43]. Using different RNA and protein detection techniques, the cellular distribution of hepcidin in murine brain was investigated. Results showed a widespread distribution of this peptide in different brain areas. Many other reports described the presence of brain hepcidin production although to a lesser extent with protein levels higher than mRNA levels, suggesting that the liver is partially responsible in addition to locally produced hepcidin[81,82].

Hepcidin expression in the brain is induced by inflammation. LPS and IL6 are known as major actors in inflammation-induced mechanisms. LPS was described as an indirect inductor of hepcidin expression in astrocytes *via* upregulated IL6 expression in microglia[83,84]. However, other experiments showed a direct upregulation of hepcidin by LPS in glial cells[85].

Recently, we investigated iron metabolism in the brain of a mouse model of Sanfilippo syndrome (mucopolysaccharidosis type III) where the progressive accumulation of heparan sulfate oligosaccharides induced microglia and astrocytes to produce pro-inflammatory cytokines leading to severe neuroinflammation[86]. We found that iron accumulation in mucopolysaccharidosis type III mice mainly affected the cerebral cortex where hepcidin expression was higher than in wildtype mice. This increase was correlated with low expression of FPN and consequently brain iron retention. We showed *in vitro* that heparan sulfate oligosaccharides are directly responsible for the induction of hepcidin and a decrease in FPN level when added to microglia and to a lesser extent to astrocytes. Our results showed that microglia play a key role in brain hepcidin overexpression, and the regulation of brain hepcidin may be dependent on or independent of inflammation.

Because hepcidin may act as an antimicrobial peptide in the brain, we investigated hepcidin production in cerebrospinal fluid during infectious meningitis. Using a liquid chromatography tandem mass spectrometry method[48], we compared hepcidin signal in cerebrospinal fluid of 5 patients diagnosed for viral meningitis *versus* 5 patients with bacterial meningitis. In viral infection, hepcidin signal was very low nearing the background level in the same range as healthy patients (Figure 1). By contrast, cerebrospinal fluid hepcidin was significantly increased in bacterial meningitis. These observations were different from what was observed in the liver where hepcidin was induced by both bacterial and viral infections, suggesting again that hepcidin plays tissue-specific roles[87]. The most frequent pathogens in community-acquired bacterial meningitis are pneumococcus and meningococcus, which are gram-negative germs and LPS producers[88]. Thus, like what was described in the kidney[67] and elsewhere[89], brain hepcidin must be more sensitive to gram-negative bacteria and induced through the LPS/Toll-like receptor signal transduction pathway.

Hepcidin expression in the heart: Iron is essential for normal heart function; however, the dysregulation of cardiac iron homeostasis may be deleterious. Merle *et al*[44] performed the first analysis of hepcidin expression and its regulation in rat heart. They reported that hepcidin is expressed in cardiomyocytes, and it is regulated in response to hypoxia and inflammation, which strongly suggests that this peptide may play an important role in cardiac diseases. Quantification of hepcidin postulated the heart as the organ with the highest hepcidin level next to the liver[15,90]. Ge *et al*[91] studied the effect of hepcidin on FPN expression in cardiomyocytes. Using a cardiomyocyte cell line, they demonstrated that local hepcidin was able to reduce FPN level and iron export from these cells. Studies conducted by Lakhal-Littleton *et al*[92] strongly supported these data. Indeed, they first confirmed that FPN is expressed in cardiomyocytes and demonstrated that its cardiac-specific deletion leads to fatal cardiac iron overload. To go further, they generated mice with cardiomyocyte-specific
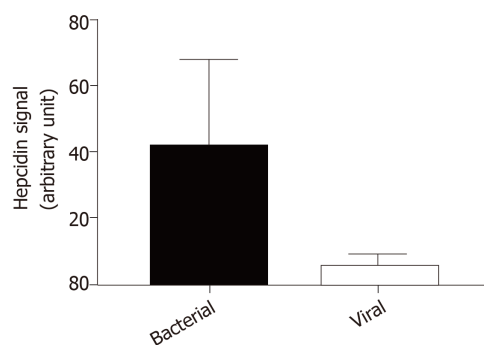
Figure 1 Hepcidin signals measured by liquid chromatography tandem mass spectrometry in cerebrospinal fluid of patients with bacterial meningitis and viral meningitis (*n* = 5 per group). Hepcidin signal is expressed in arbitrary unit, corresponding to the ratio of the area under the curve of hepcidin signal on the area under the curve of internal standard (heavy hepcidin). According to the Mann-Whitney test the difference was significant (*P* = 0.0076).

hepcidin deletion or knock-in of hepcidin-resistant FPN. They found that both models maintained normal systemic iron homeostasis but developed fatal cardiac dysfunction as a consequence of cardiomyocyte iron deficiency[93]. Thus, they provided evidence for a cell-autonomous role of hepcidin in cardiac iron homeostasis.

Hepcidin expression in the pancreas: Data published by Kulaksiz *et al*[45] demonstrated that hepcidin is expressed in the pancreas of rat and human. Further analysis showed that it was localized in β-cells of the islets of Langerhans. In addition, the *in vitro* experiments performed in this study demonstrated that the expression of hepcidin in β-cells is directly regulated by iron.

Iron is important for normal insulin secretion. However, excess of iron have been shown to affect β-cell function in hemochromatosis models[94-96], causing iron accumulation in the islets, decreased insulin secretion and increased apoptosis. In contrast, iron pool decrease was shown to protect from diabetes and loss of β-cell function in the obese (ob/ob) mouse model[97]. Both DMT1 and FPN are expressed in β-cells. In β-cell-specific DMT1 KO islets, glucose-stimulated insulin secretion was reduced[98]. These observations suggested that hepcidin produced by β-cells may be involved in an intrinsic regulation of pancreas iron and in their function in glucose homeostasis.

CONCLUSION

Although only some organs have been addressed in this review, there is a number of studies describing the production of hepcidin in many others such as lungs[99,100], prostate[101], placenta[102,103] and retina[104]. Our hypothesis is that peripheral hepcidin is intended for an innate immune response including a defense against bacterial invasion. However, under local or systemic inflammatory conditions, the induction of this peripheral hepcidin may contribute to target tissue damage due to local accumulation of toxic iron and apoptosis. Nevertheless, despite considerable advances recently, further explorations deserve to be rapidly achieved to deeply investigate the cellular mechanisms and functions of peripheral hepcidin as well as its regulation in the different organs.

REFERENCES

1   **Valko M**, Jomova K, Rhodes CJ, Kuča K, Musílek K. Redox- and non-redox-metal-induced formation of free radicals and their role in human disease. *Arch Toxicol* 2016; **90**: 1-37 [PMID: 26343967 DOI: 10.1007/s00204-015-1579-5]

2   **Chung J**, Wessling-Resnick M. Molecular mechanisms and regulation of iron transport. *Crit Rev Clin Lab Sci* 2003; **40**: 151-182 [PMID: 12755454 DOI: 10.1080/713609332]

3   **McKie AT**, Barrow D, Latunde-Dada GO, Rolfs A, Sager G, Mudaly E, Mudaly M, Richardson C, Barlow D, Bomford A, Peters TJ, Raja KB, Shirali S, Hediger MA, Farzaneh F, Simpson RJ. An iron-regulated ferric reductase associated with the absorption of dietary iron. *Science* 2001; **291**: 1755-1759 [PMID: 11230685 DOI: 10.1126/science.1057206]

4   **Gunshin H**, Mackenzie B, Berger UV, Gunshin Y, Romero MF, Boron WF, Nussberger S, Gollan JL, Hediger MA. Cloning and characterization of a mammalian proton-coupled metal-ion transporter. *Nature* 1997; **388**: 482-488 [PMID: 9242408 DOI: 10.1038/41343]

5   **Abboud S**, Haile DJ. A novel mammalian iron-regulated protein involved in intracellular iron metabolism. *J Biol Chem* 2000; **275**: 19906-19912 [PMID: 10747949 DOI: 10.1074/jbc.M000713200]

6   **Delaby C**, Pilard N, Hetet G, Driss F, Grandchamp B, Beaumont C, Canonne-Hergaux F. A physiological model to study iron recycling in macrophages. *Exp Cell Res* 2005; **310**: 43-53 [PMID: 16095591 DOI: 10.1016/j.yexcr.2005.07.002]

7   **Donovan A**, Lima CA, Pinkus JL, Pinkus GS, Zon LI, Robine S, Andrews NC. The iron exporter ferroportin/Slc40a1 is essential for iron homeostasis. *Cell Metab* 2005; **1**: 191-200 [PMID: 16054062 DOI: 10.1016/j.cmet.2005.01.003]

8   **Shi H**, Bencze KZ, Stemmler TL, Philpott CC. A cytosolic iron chaperone that delivers iron to ferritin. *Science* 2008; **320**: 1207-1210 [PMID: 18511687 DOI: 10.1126/science.1157643]

9   **Wei Y**, Miller SC, Tsuji Y, Torti SV, Torti FM. Interleukin 1 induces ferritin heavy chain in human muscle cells. *Biochem Biophys Res Commun* 1990; **169**: 289-296 [PMID: 2350350 DOI: 10.1016/0006-291x(90)91466-6]

10   **Wilkinson N**, Pantopoulos K. The IRP/IRE system in vivo: insights from mouse models. *Front Pharmacol* 2014; **5**: 176 [PMID: 25120486 DOI: 10.3389/fphar.2014.00176]

11   **Hentze MW**, Caughman SW, Rouault TA, Barriocanal JG, Dancis A, Harford JB, Klausner RD. Identification of the iron-responsive element for the translational regulation of human ferritin mRNA. *Science* 1987; **238**: 1570-1573 [PMID: 3685996]

12   **Casey JL**, Hentze MW, Koeller DM, Caughman SW, Rouault TA, Klausner RD, Harford JB. Iron-responsive elements: regulatory RNA sequences that control mRNA levels and translation. *Science* 1988; **240**: 924-928 [PMID: 2452485]

13   **Müllner EW**, Kühn LC. A stem-loop in the 3' untranslated region mediates iron-dependent regulation of transferrin receptor mRNA stability in the cytoplasm. *Cell* 1988; **53**: 815-825 [PMID: 3370673]

14   **Rouault TA**. The role of iron regulatory proteins in mammalian iron homeostasis and disease. *Nat Chem Biol* 2006; **2**: 406-414 [PMID: 16850017 DOI: 10.1038/nchembio807]

15   **Krause A**, Neitz S, Mägert HJ, Schulz A, Forssmann WG, Schulz-Knappe P, Adermann K. LEAP-1, a novel highly disulfide-bonded human peptide, exhibits antimicrobial activity. *FEBS Lett* 2000; **480**: 147-150 [PMID: 11034317]

16   **Pigeon C**, Ilyin G, Courselaud B, Leroyer P, Turlin B, Brissot P, Loréal O. A new mouse liver-specific gene, encoding a protein homologous to human antimicrobial peptide hepcidin, is overexpressed during iron overload. *J Biol Chem* 2001; **276**: 7811-7819 [PMID: 11113132 DOI: 10.1074/jbc.M008923200]

17   **Nicolas G**, Bennoun M, Devaux I, Beaumont C, Grandchamp B, Kahn A, Vaulont S. Lack of hepcidin gene expression and severe tissue iron overload in upstream stimulatory factor 2 (USF2) knockout mice. *Proc Natl Acad Sci U S A* 2001; **98**: 8780-8785 [PMID: 11447267 DOI: 10.1073/pnas.151179498]

18   **Nemeth E**, Tuttle MS, Powelson J, Vaughn MB, Donovan A, Ward DM, Ganz T, Kaplan J. Hepcidin regulates cellular iron efflux by binding to ferroportin and inducing its internalization. *Science* 2004; **306**: 2090-2093 [PMID: 15514116 DOI: 10.1126/science.1104742]

19   **Delaby C**, Pilard N, Gonçalves AS, Beaumont C, Canonne-Hergaux F. Presence of the iron exporter ferroportin at the plasma membrane of macrophages is enhanced by iron loading and down-regulated by hepcidin. *Blood* 2005; **106**: 3979-3984 [PMID: 16081696 DOI: 10.1182/blood-2005-06-2398]

20   **Chaston T**, Chung B, Mascarenhas M, Marks J, Patel B, Srai SK, Sharp P. Evidence for differential effects of hepcidin in macrophages and intestinal epithelial cells. *Gut* 2008; **57**: 374-382 [PMID: 17965061 DOI: 10.1136/gut.2007.131722]

21   **Brasse-Lagnel C**, Karim Z, Letteron P, Bekri S, Bado A, Beaumont C. Intestinal DMT1 cotransporter is down-regulated by hepcidin via proteasome internalization and degradation. *Gastroenterology* 2011; **140**: 1261-1271.e1 [PMID: 21199652 DOI: 10.1053/j.gastro.2010.12.037]

22   **Chung B**, Chaston T, Marks J, Srai SK, Sharp PA. Hepcidin decreases iron transporter expression in vivo in mouse duodenum and spleen and in vitro in THP-1 macrophages and intestinal Caco-2 cells. *J Nutr* 2009; **139**: 1457-1462 [PMID: 19549758 DOI: 10.3945/jn.108.102905]

23   **Zhang DL**, Wu J, Shah BN, Greutélaers KC, Ghosh MC, Ollivierre H, Su XZ, Thuma PE, Bedu-Addo G, Mockenhaupt FP, Gordeuk VR, Rouault TA. Erythrocytic ferroportin reduces intracellular iron accumulation, hemolysis, and malaria risk. *Science* 2018; **359**: 1520-1523 [PMID: 29599243 DOI: 10.1126/science.aal2022]

24   **Aschemeyer S**, Qiao B, Stefanova D, Valore EV, Sek AC, Ruwe TA, Vieth KR, Jung G, Casu C, Rivella S, Jormakka M, Mackenzie B, Ganz T, Nemeth E. Structure-function analysis of ferroportin defines the binding site and an alternative mechanism of action of hepcidin. *Blood* 2018; **131**: 899-910 [PMID: 29237594 DOI: 10.1182/blood-2017-05-786590]

25   **Viatte L**, Nicolas G, Lou DQ, Bennoun M, Lesbordes-Brion JC, Canonne-Hergaux F, Schönig K, Bujard H, Kahn A, Andrews NC, Vaulont S. Chronic hepcidin induction causes hyposideremia and alters the pattern of cellular iron accumulation in hemochromatotic mice. *Blood* 2006; **107**: 2952-2958 [PMID: 16339398 DOI: 10.1182/blood-2005-10-4071]

26   **Park CH**, Valore EV, Waring AJ, Ganz T. Hepcidin, a urinary antimicrobial peptide synthesized in the liver. *J Biol Chem* 2001; **276**: 7806-7810 [PMID: 11113131 DOI: 10.1074/jbc.M008922200]

27   **Ganz T**, Olbina G, Girelli D, Nemeth E, Westerman M. Immunoassay for human serum hepcidin. *Blood* 2008; **112**: 4292-4297 [PMID: 18689548 DOI: 10.1182/blood-2008-02-139915]

28   **Kemna EH**, Tjalsma H, Podust VN, Swinkels DW. Mass spectrometry-based hepcidin measurements in serum and urine: analytical aspects and clinical implications. *Clin Chem* 2007; **53**: 620-628 [PMID: 17272487 DOI: 10.1373/clinchem.2006.079186]

29   **Hunter HN**, Fulton DB, Ganz T, Vogel HJ. The solution structure of human hepcidin, a peptide hormone with antimicrobial activity that is involved in iron uptake and hereditary hemochromatosis. *J Biol Chem* 2002; **277**: 37597-37603 [PMID: 12138110 DOI: 10.1074/jbc.M205305200]

30   **Nemeth E**, Rivera S, Gabayan V, Keller C, Taudorf S, Pedersen BK, Ganz T. IL-6 mediates hypoferremia of inflammation by inducing the synthesis of the iron regulatory hormone hepcidin. *J Clin Invest* 2004; **113**: 1271-1276 [PMID: 15124018 DOI: 10.1172/JCI20945]

31   **Wrighting DM**, Andrews NC. Interleukin-6 induces hepcidin expression through STAT3. *Blood* 2006; **108**: 3204-3209 [PMID: 16835372 DOI: 10.1182/blood-2006-06-027631]

32   **Nicolas G**, Chauvet C, Viatte L, Danan JL, Bigard X, Devaux I, Beaumont C, Kahn A, Vaulont S. The gene encoding the iron regulatory peptide hepcidin is regulated by anemia, hypoxia, and inflammation. *J Clin Invest* 2002; **110**: 1037-1044 [PMID: 12370282 DOI: 10.1172/JCI15686]

33   **Ganz T**, Nemeth E. Iron sequestration and anemia of inflammation. *Semin Hematol* 2009; **46**: 387-393 [PMID: 19786207 DOI: 10.1053/j.seminhematol.2009.06.001]

34   **Canali S**, Core AB, Zumbrennen-Bullough KB, Merkulova M, Wang CY, Schneyer AL, Pietrangelo A, Babitt JL. Activin B Induces Noncanonical SMAD1/5/8 Signaling via BMP Type I Receptors in Hepatocytes: Evidence for a Role in Hepcidin Induction by Inflammation in Male Mice. *Endocrinology* 2016; **157**: 1146-1162 [PMID: 26735394 DOI: 10.1210/en.2015-1747]

35   **Besson-Fournier C**, Latour C, Kautz L, Bertrand J, Ganz T, Roth MP, Coppin H. Induction of activin B by inflammatory stimuli up-regulates expression of the iron-regulatory peptide hepcidin through Smad1/5/8 signaling. *Blood* 2012; **120**: 431-439 [PMID: 22611157 DOI: 10.1182/blood-2012-02-411470]

36   **Besson-Fournier C**, Gineste A, Latour C, Gourbeyre O, Meynard D, Martin P, Oswald E, Coppin H, Roth MP. Hepcidin upregulation by inflammation is independent of Smad1/5/8 signaling by activin B. *Blood* 2017; **129**: 533-536 [PMID: 27903526 DOI: 10.1182/blood-2016-10-748541]

37   **Wang RH**, Li C, Xu X, Zheng Y, Xiao C, Zerfas P, Cooperman S, Eckhaus M, Rouault T, Mishra L, Deng CX. A role of SMAD4 in iron metabolism through the positive regulation of hepcidin expression. *Cell Metab* 2005; **2**: 399-409 [PMID: 16330325 DOI: 10.1016/j.cmet.2005.10.010]

38   **Kulaksiz H**, Theilig F, Bachmann S, Gehrke SG, Rost D, Janetzko A, Cetin Y, Stremmel W. The iron-regulatory peptide hormone hepcidin: expression and cellular localization in the mammalian kidney. *J Endocrinol* 2005; **184**: 361-370 [PMID: 15684344 DOI: 10.1677/joe.1.05729]

39   **Liu XB**, Nguyen NB, Marquess KD, Yang F, Haile DJ. Regulation of hepcidin and ferroportin expression by lipopolysaccharide in splenic macrophages. *Blood Cells Mol Dis* 2005; **35**: 47-56 [PMID: 15932798 DOI: 10.1016/j.bcmd.2005.04.006]

40   **Peyssonnaux C**, Zinkernagel AS, Datta V, Lauth X, Johnson RS, Nizet V. TLR4-dependent hepcidin expression by myeloid cells in response to bacterial pathogens. *Blood* 2006; **107**: 3727-3732 [PMID: 16391018 DOI: 10.1182/blood-2005-06-2259]

41   **Schwarz P**, Kübler JA, Strnad P, Müller K, Barth TF, Gerloff A, Feick P, Peyssonnaux C, Vaulont S, Adler G, Kulaksiz H. Hepcidin is localised in gastric parietal cells, regulates acid secretion and is induced by Helicobacter pylori infection. *Gut* 2012; **61**: 193-201 [PMID: 21757452 DOI: 10.1136/gut.2011.241208]

42   **Bekri S**, Gual P, Anty R, Luciani N, Dahman M, Ramesh B, Iannelli A, Staccini-Myx A, Casanova D, Ben Amor I, Saint-Paul MC, Huet PM, Sadoul JL, Gugenheim J, Srai SK, Tran A, Le Marchand-Brustel Y. Increased adipose tissue expression of hepcidin in severe obesity is independent from diabetes and NASH. *Gastroenterology* 2006; **131**: 788-796 [PMID: 16952548 DOI: 10.1053/j.gastro.2006.07.007]

43   **Zechel S**, Huber-Wittmer K, von Bohlen und Halbach O. Distribution of the iron-regulating protein hepcidin in the murine central nervous system. *J Neurosci Res* 2006; **84**: 790-800 [PMID: 16933319 DOI: 10.1002/jnr.20991]

44   **Merle U**, Fein E, Gehrke SG, Stremmel W, Kulaksiz H. The iron regulatory peptide hepcidin is expressed in the heart and regulated by hypoxia and inflammation. *Endocrinology* 2007; **148**: 2663-2668 [PMID: 17363462 DOI: 10.1210/en.2006-1331]

45   **Kulaksiz H**, Fein E, Redecker P, Stremmel W, Adler G, Cetin Y. Pancreatic beta-cells express hepcidin, an iron-uptake regulatory peptide. *J Endocrinol* 2008; **197**: 241-249 [PMID: 18434354 DOI: 10.1677/JOE-07-0528]

46   **Arnold J**, Sangwaiya A, Manglam V, Geoghegan F, Thursz M, Busbridge M. Presence of hepcidin-25 in biological fluids: bile, ascitic and pleural fluids. *World J Gastroenterol* 2010; **16**: 2129-2133 [PMID: 20440853]

47   **Delaby C**, Bros P, Vialaret J, Moulinier A, Delatour V, Gabelle A, Lehmann S, Hirtz C. Quantification of hepcidin-25 in human cerebrospinal fluid using LC-MS/MS. *Bioanalysis* 2017; **9**: 337-347 [PMID: 28106476 DOI: 10.4155/bio-2016-0240]

48   **Lefebvre T**, Dessendier N, Houamel D, Ialy-Radio N, Kannengiesser C, Manceau H, Beaumont C, Nicolas G, Gouya L, Puy H, Karim Z. LC-MS/MS method for hepcidin-25 measurement in human and mouse serum: clinical and research implications in iron disorders. *Clin Chem Lab Med* 2015; **53**: 1557-1567 [PMID: 25781546 DOI: 10.1515/cclm-2014-1093]

49   **Lesbordes-Brion JC**, Viatte L, Bennoun M, Lou DQ, Ramey G, Houbron C, Hamard G, Kahn A, Vaulont S. Targeted disruption of the hepcidin 1 gene results in severe hemochromatosis. *Blood* 2006; **108**: 1402-1405 [PMID: 16574947 DOI: 10.1182/blood-2006-02-003376]

50   **Zumerle S**, Mathieu JR, Delga S, Heinis M, Viatte L, Vaulont S, Peyssonnaux C. Targeted disruption of hepcidin in the liver recapitulates the hemochromatotic phenotype. *Blood* 2014; **123**: 3646-3650 [PMID: 24646470 DOI: 10.1182/blood-2014-01-550467]

51   **Papanikolaou G**, Samuels ME, Ludwig EH, MacDonald ML, Franchini PL, Dubé MP, Andres L, MacFarlane J, Sakellaropoulos N, Politou M, Nemeth E, Thompson J, Risler JK, Zaborowska C, Babakaiff R, Radomski CC, Pape TD, Davidas O, Christakis J, Brissot P, Lockitch G, Ganz T, Hayden MR, Goldberg YP. Mutations in HFE2 cause iron overload in chromosome 1q-linked juvenile hemochromatosis. *Nat Genet* 2004; **36**: 77-82 [PMID: 14647275 DOI: 10.1038/ng1274]

52   **Meynard D**, Kautz L, Darnaud V, Canonne-Hergaux F, Coppin H, Roth MP. Lack of the bone morphogenetic protein BMP6 induces massive iron overload. *Nat Genet* 2009; **41**: 478-481 [PMID: 19252488 DOI: 10.1038/ng.320]

53   **Daher R**, Kannengiesser C, Houamel D, Lefebvre T, Bardou-Jacquet E, Ducrot N, de Kerguenec C, Jouanolle AM, Robreau AM, Oudin C, Le Gac G, Moulouel B, Loustaud-Ratti V, Bedossa P, Valla D, Gouya L, Beaumont C, Brissot P, Puy H, Karim Z, Tchernitchko D. Heterozygous Mutations in BMP6 Pro-peptide Lead to Inappropriate Hepcidin Synthesis and Moderate Iron Overload in Humans. *Gastroenterology* 2016; **150**: 672-683.e4 [PMID: 26582087 DOI: 10.1053/j.gastro.2015.10.049]

54   **Le Gac G**, Gourlaouen I, Ka C, Férec C. The p.Leu96Pro Missense Mutation in the BMP6 Gene Is Repeatedly Associated With Hyperferritinemia in Patients of French Origin. *Gastroenterology* 2016; **151**: 769-770 [PMID: 27590690 DOI: 10.1053/j.gastro.2016.03.054]

55   **Bignell P**, Atoyebi W, Robson K. Heterozygous BMP6 Variants Coupled With HFE Variants. *Gastroenterology* 2016; **151**: 769 [PMID: 27591421 DOI: 10.1053/j.gastro.2016.02.088]

56   **Piubelli C**, Castagna A, Marchi G, Rizzi M, Busti F, Badar S, Marchetti M, De Gobbi M, Roetto A, Xumerle L, Suku E, Giorgetti A, Delledonne M, Olivieri O, Girelli D. Identification of new BMP6 pro-peptide mutations in patients with iron overload. *Am J Hematol* 2017; **92**: 562-568 [PMID: 28335084 DOI: 10.1002/ajh.24730]

57   **Kleven MD**, Enns CA, Zhang AS. Bone Morphogenetic Protein-6 Mutations Take Their Place in Iron Overload Diseases. *Gastroenterology* 2016; **150**: 556-559 [PMID: 26820052 DOI: 10.1053/j.gastro.2016.01.016]

58   **Du X**, She E, Gelbart T, Truksa J, Lee P, Xia Y, Khovananth K, Mudd S, Mann N, Moresco EM, Beutler

E, Beutler B. The serine protease TMPRSS6 is required to sense iron deficiency. *Science* 2008; **320**: 1088-1092 [PMID: 18451267 DOI: 10.1126/science.1157121]

59   **Guillem F**, Kannengiesser C, Oudin C, Lenoir A, Matak P, Donadieu J, Isidor B, Méchinaud F, Aguilar-Martinez P, Beaumont C, Vaulont S, Grandchamp B, Nicolas G. Inactive matriptase-2 mutants found in IRIDA patients still repress hepcidin in a transfection assay despite having lost their serine protease activity. *Hum Mutat* 2012; **33**: 1388-1396 [PMID: 22581667 DOI: 10.1002/humu.22116]

60   **De Falco L**, Sanchez M, Silvestri L, Kannengiesser C, Muckenthaler MU, Iolascon A, Gouya L, Camaschella C, Beaumont C. Iron refractory iron deficiency anemia. *Haematologica* 2013; **98**: 845-853 [PMID: 23729726 DOI: 10.3324/haematol.2012.075515]

61   **Silvestri L**, Guillem F, Pagani A, Nai A, Oudin C, Silva M, Toutain F, Kannengiesser C, Beaumont C, Camaschella C, Grandchamp B. Molecular mechanisms of the defective hepcidin inhibition in TMPRSS6 mutations associated with iron-refractory iron deficiency anemia. *Blood* 2009; **113**: 5605-5608 [PMID: 19357398 DOI: 10.1182/blood-2008-12-195594]

62   **Nai A**, Rubio A, Campanella A, Gourbeyre O, Artuso I, Bordini J, Gineste A, Latour C, Besson-Fournier C, Lin HY, Coppin H, Roth MP, Camaschella C, Silvestri L, Meynard D. Limiting hepatic Bmp-Smad signaling by matriptase-2 is required for erythropoietin-mediated hepcidin suppression in mice. *Blood* 2016; **127**: 2327-2336 [PMID: 26755707 DOI: 10.1182/blood-2015-11-681494]

63   **Pietrangelo A**. Hereditary hemochromatosis--a new look at an old disease. *N Engl J Med* 2004; **350**: 2383-2397 [PMID: 15175440 DOI: 10.1056/NEJMra031573]

64   **D'Alessio F**, Hentze MW, Muckenthaler MU. The hemochromatosis proteins HFE, TfR2, and HJV form a membrane-associated protein complex for hepcidin regulation. *J Hepatol* 2012; **57**: 1052-1060 [PMID: 22728873 DOI: 10.1016/j.jhep.2012.06.015]

65   **Babitt JL**, Huang FW, Wrighting DM, Xia Y, Sidis Y, Samad TA, Campagna JA, Chung RT, Schneyer AL, Woolf CJ, Andrews NC, Lin HY. Bone morphogenetic protein signaling by hemojuvelin regulates hepcidin expression. *Nat Genet* 2006; **38**: 531-539 [PMID: 16604073 DOI: 10.1038/ng1777]

66   **Parrow NL**, Fleming RE. Bone morphogenetic proteins as regulators of iron metabolism. *Annu Rev Nutr* 2014; **34**: 77-94 [PMID: 24995692 DOI: 10.1146/annurev-nutr-071813-105646]

67   **Houamel D**, Ducrot N, Lefebvre T, Daher R, Moulouel B, Sari MA, Letteron P, Lyoumi S, Millot S, Tourret J, Bouvet O, Vaulont S, Vandewalle A, Denamur E, Puy H, Beaumont C, Gouya L, Karim Z. Hepcidin as a Major Component of Renal Antibacterial Defenses against Uropathogenic Escherichia coli. *J Am Soc Nephrol* 2016; **27**: 835-846 [PMID: 26293821 DOI: 10.1681/ASN.2014101035]

68   **Wareing M**, Ferguson CJ, Green R, Riccardi D, Smith CP. In vivo characterization of renal iron transport in the anaesthetized rat. *J Physiol* 2000; **524** Pt 2: 581-586 [PMID: 10766935]

69   **Wolff NA**, Liu W, Fenton RA, Lee WK, Thévenod F, Smith CP. Ferroportin 1 is expressed basolaterally in rat kidney proximal tubule cells and iron excess increases its membrane trafficking. *J Cell Mol Med* 2011; **15**: 209-219 [PMID: 20015204 DOI: 10.1111/j.1582-4934.2009.00985.x]

70   **Ferguson CJ**, Wareing M, Ward DT, Green R, Smith CP, Riccardi D. Cellular localization of divalent metal transporter DMT-1 in rat kidney. *Am J Physiol Renal Physiol* 2001; **280**: F803-F814 [PMID: 11292622 DOI: 10.1152/ajprenal.2001.280.5.F803]

71   **Moulouel B**, Houamel D, Delaby C, Tchernitchko D, Vaulont S, Letteron P, Thibaudeau O, Puy H, Gouya L, Beaumont C, Karim Z. Hepcidin regulates intrarenal iron handling at the distal nephron. *Kidney Int* 2013; **84**: 756-766 [PMID: 23615502 DOI: 10.1038/ki.2013.142]

72   **Nguyen NB**, Callaghan KD, Ghio AJ, Haile DJ, Yang F. Hepcidin expression and iron transport in alveolar macrophages. *Am J Physiol Lung Cell Mol Physiol* 2006; **291**: L417-L425 [PMID: 16648237 DOI: 10.1152/ajplung.00484.2005]

73   **Deschemin JC**, Mathieu JRR, Zumerle S, Peyssonnaux C, Vaulont S. Pulmonary Iron Homeostasis in Hepcidin Knockout Mice. *Front Physiol* 2017; **8**: 804 [PMID: 29089902 DOI: 10.3389/fphys.2017.00804]

74   **Sow FB**, Florence WC, Satoskar AR, Schlesinger LS, Zwilling BS, Lafuse WP. Expression and localization of hepcidin in macrophages: a role in host defense against tuberculosis. *J Leukoc Biol* 2007; **82**: 934-945 [PMID: 17609338 DOI: 10.1189/jlb.0407216]

75   **Lefebvre T**, Reihani N, Daher R, de Villemeur TB, Belmatoug N, Rose C, Colin-Aronovicz Y, Puy H, Le Van Kim C, Franco M, Karim Z. Involvement of hepcidin in iron metabolism dysregulation in Gaucher disease. *Haematologica* 2018; **103**: 587-596 [PMID: 29305416 DOI: 10.3324/haematol.2017.177816]

76   **Gotardo ÃM**, dos Santos AN, Miyashiro RA, Gambero S, Rocha T, Ribeiro ML, Gambero A. Mice that are fed a high-fat diet display increased hepcidin expression in adipose tissue. *J Nutr Sci Vitaminol (Tokyo)* 2013; **59**: 454-461 [PMID: 24418880]

77   **Citelli M**, Fonte-Faria T, Nascimento-Silva V, Renovato-Martins M, Silva R, Luna AS, Silva SV, Barja-Fidalgo C. Obesity promotes alterations in iron recycling. *Nutrients* 2015; **7**: 335-348 [PMID: 25569627 DOI: 10.3390/nu7010335]

78   **Sonnweber T**, Ress C, Nairz M, Theurl I, Schroll A, Murphy AT, Wroblewski V, Witcher DR, Moser P, Ebenbichler CF, Kaser S, Weiss G. High-fat diet causes iron deficiency via hepcidin-independent reduction of duodenal iron absorption. *J Nutr Biochem* 2012; **23**: 1600-1608 [PMID: 22444869 DOI: 10.1016/j.jnutbio.2011.10.013]

79   **Dongiovanni P**, Lanti C, Gatti S, Rametta R, Recalcati S, Maggioni M, Fracanzani AL, Riso P, Cairo G, Fargion S, Valenti L. High fat diet subverts hepatocellular iron uptake determining dysmetabolic iron overload. *PLoS One* 2015; **10**: e0116855 [PMID: 25647178 DOI: 10.1371/journal.pone.0116855]

80   **Pini M**, Rhodes DH, Fantuzzi G. Hematological and acute-phase responses to diet-induced obesity in IL-6 KO mice. *Cytokine* 2011; **56**: 708-716 [PMID: 21996012 DOI: 10.1016/j.cyto.2011.09.015]

81   **Raha-Chowdhury R**, Raha AA, Forostyak S, Zhao JW, Stott SR, Bomford A. Expression and cellular localization of hepcidin mRNA and protein in normal rat brain. *BMC Neurosci* 2015; **16**: 24 [PMID: 25896789 DOI: 10.1186/s12868-015-0161-7]

82   **Vela D**. Hepcidin, an emerging and important player in brain iron homeostasis. *J Transl Med* 2018; **16**: 25 [PMID: 29415739 DOI: 10.1186/s12967-018-1399-5]

83   **You LH**, Yan CZ, Zheng BJ, Ci YZ, Chang SY, Yu P, Gao GF, Li HY, Dong TY, Chang YZ. Astrocyte hepcidin is a key factor in LPS-induced neuronal apoptosis. *Cell Death Dis* 2017; **8**: e2676 [PMID: 28300826 DOI: 10.1038/cddis.2017.93]

84   **Qian ZM**, He X, Liang T, Wu KC, Yan YC, Lu LN, Yang G, Luo QQ, Yung WH, Ke Y. Lipopolysaccharides upregulate hepcidin in neuron via microglia and the IL-6/STAT3 signaling pathway. *Mol Neurobiol* 2014; **50**: 811-820 [PMID: 24659348 DOI: 10.1007/s12035-014-8671-3]

85   **Urrutia P**, Aguirre P, Esparza A, Tapia V, Mena NP, Arredondo M, González-Billault C, Núñez MT. Inflammation alters the expression of DMT1, FPN1 and hepcidin, and it causes iron accumulation in

central nervous system cells. *J Neurochem* 2013; **126**: 541-549 [PMID: 23506423 DOI: 10.1111/jnc.12244]

86   **Puy V**, Darwiche W, Trudel S, Gomila C, Lony C, Puy L, Lefebvre T, Vitry S, Boullier A, Karim Z, Ausseil J. Predominant role of microglia in brain iron retention in Sanfilippo syndrome, a pediatric neurodegenerative disease. *Glia* 2018; **66**: 1709-1723 [PMID: 29624734 DOI: 10.1002/glia.23335]

87   **Rodriguez R**, Jung CL, Gabayan V, Deng JC, Ganz T, Nemeth E, Bulut Y. Hepcidin induction by pathogens and pathogen-derived molecules is strongly dependent on interleukin-6. *Infect Immun* 2014; **82**: 745-752 [PMID: 24478088 DOI: 10.1128/IAI.00983-13]

88   **Fitch MT**, Abrahamian FM, Moran GJ, Talan DA. Emergency department management of meningitis and encephalitis. *Infect Dis Clin North Am* 2008; **22**: 33-52, v-vi [PMID: 18295682 DOI: 10.1016/j.idc.2007.10.001]

89   **Michels KR**, Zhang Z, Bettina AM, Cagnina RE, Stefanova D, Burdick MD, Vaulont S, Nemeth E, Ganz T, Mehrad B. Hepcidin-mediated iron sequestration protects against bacterial dissemination during pneumonia. *JCI Insight* 2017; **2**: e92002 [PMID: 28352667 DOI: 10.1172/jci.insight.92002]

90   **Vela D**. Balance of cardiac and systemic hepcidin and its role in heart physiology and pathology. *Lab Invest* 2018; **98**: 315-326 [PMID: 29058707 DOI: 10.1038/labinvest.2017.111]

91   **Ge XH**, Wang Q, Qian ZM, Zhu L, Du F, Yung WH, Yang L, Ke Y. The iron regulatory hormone hepcidin reduces ferroportin 1 content and iron release in H9C2 cardiomyocytes. *J Nutr Biochem* 2009; **20**: 860-865 [PMID: 19027283 DOI: 10.1016/j.jnutbio.2008.07.014]

92   **Lakhal-Littleton S**, Wolna M, Carr CA, Miller JJ, Christian HC, Ball V, Santos A, Diaz R, Biggs D, Stillion R, Holdship P, Larner F, Tyler DJ, Clarke K, Davies B, Robbins PA. Cardiac ferroportin regulates cellular iron homeostasis and is important for cardiac function. *Proc Natl Acad Sci U S A* 2015; **112**: 3164-3169 [PMID: 25713362 DOI: 10.1073/pnas.1422373112]

93   **Lakhal-Littleton S**, Wolna M, Chung YJ, Christian HC, Heather LC, Brescia M, Ball V, Diaz R, Santos A, Biggs D, Clarke K, Davies B, Robbins PA. An essential cell-autonomous role for hepcidin in cardiac iron homeostasis. *Elife* 2016; **5** [PMID: 27897970 DOI: 10.7554/eLife.19804]

94   **Cooksey RC**, Jouihan HA, Ajioka RS, Hazel MW, Jones DL, Kushner JP, McClain DA. Oxidative stress, beta-cell apoptosis, and decreased insulin secretory capacity in mouse models of hemochromatosis. *Endocrinology* 2004; **145**: 5305-5312 [PMID: 15308612 DOI: 10.1210/en.2004-0392]

95   **Lunova M**, Schwarz P, Nuraldeen R, Levada K, Kuscuoglu D, Stützle M, Vujić Spasić M, Haybaeck J, Ruchala P, Jirsa M, Deschemin JC, Vaulont S, Trautwein C, Strnad P. Hepcidin knockout mice spontaneously develop chronic pancreatitis owing to cytoplasmic iron overload in acinar cells. *J Pathol* 2017; **241**: 104-114 [PMID: 27741349 DOI: 10.1002/path.4822]

96   **Altamura S**, Kessler R, Gröne HJ, Gretz N, Hentze MW, Galy B, Muckenthaler MU. Resistance of ferroportin to hepcidin binding causes exocrine pancreatic failure and fatal iron overload. *Cell Metab* 2014; **20**: 359-367 [PMID: 25100063 DOI: 10.1016/j.cmet.2014.07.007]

97   **Cooksey RC**, Jones D, Gabrielsen S, Huang J, Simcox JA, Luo B, Soesanto Y, Rienhoff H, Abel ED, McClain DA. Dietary iron restriction or iron chelation protects from diabetes and loss of beta-cell function in the obese (ob/ob lep-/-) mouse. *Am J Physiol Endocrinol Metab* 2010; **298**: E1236-E1243 [PMID: 20354157 DOI: 10.1152/ajpendo.00022.2010]

98   **Hansen JB**, Tonnesen MF, Madsen AN, Hagedorn PH, Friberg J, Grunnet LG, Heller RS, Nielsen AØ, Størling J, Baeyens L, Anker-Kitai L, Qvortrup k, Bouwens L, Efrat S, Aalund M, Andrews NC, Billestrup N, Karlsen AE, Holst B, Pociot F, Mandrup-Poulsen T. Divalent metal transporter 1 regulates iron-mediated ROS and pancreatic β cell fate in response to cytokines. *Cell Metab* 2012; **16**: 449-461 [PMID: 23000401 DOI: 10.1016/j.cmet.2012.09.001]

99   **Frazier MD**, Mamo LB, Ghio AJ, Turi JL. Hepcidin expression in human airway epithelial cells is regulated by interferon-γ. *Respir Res* 2011; **12**: 100 [PMID: 21810240 DOI: 10.1186/1465-9921-12-100]

100   **Chen QX**, Song SW, Chen QH, Zeng CL, Zheng X, Wang JL, Fang XM. Silencing airway epithelial cell-derived hepcidin exacerbates sepsis induced acute lung injury. *Crit Care* 2014; **18**: 470 [PMID: 25096529 DOI: 10.1186/s13054-014-0470-8]

101   **Tesfay L**, Clausen KA, Kim JW, Hegde P, Wang X, Miller LD, Deng Z, Blanchette N, Arvedson T, Miranti CK, Babitt JL, Lin HY, Peehl DM, Torti FM, Torti SV. Hepcidin regulation in prostate and its disruption in prostate cancer. *Cancer Res* 2015; **75**: 2254-2263 [PMID: 25858146 DOI: 10.1158/0008-5472.CAN-14-2465]

102   **Evans P**, Cindrova-Davies T, Muttukrishna S, Burton GJ, Porter J, Jauniaux E. Hepcidin and iron species distribution inside the first-trimester human gestational sac. *Mol Hum Reprod* 2011; **17**: 227-232 [PMID: 21177636 DOI: 10.1093/molehr/gaq101]

103   **Roperto S**, Russo V, Urraro C, Cutarelli A, Perillo A, De Falco F, Roperto F. Expression of hepcidin and ferroportin in full term placenta of pregnant cows. *Theriogenology* 2017; **103**: 90-97 [PMID: 28780484 DOI: 10.1016/j.theriogenology.2017.07.031]

104   **Gnana-Prakasam JP**, Martin PM, Mysona BA, Roon P, Smith SB, Ganapathy V. Hepcidin expression in mouse retina and its regulation via lipopolysaccharide/Toll-like receptor-4 pathway independent of Hfe. *Biochem J* 2008; **411**: 79-88 [PMID: 18042040 DOI: 10.1042/BJ20071377]

Neoadjuvant endocrine therapy: A potential strategy for ER-positive breast cancer

Li-Tong Yao, Mo-Zhi Wang, Meng-Shen Wang, Xue-Ting Yu, Jing-Yi Guo, Tie Sun, Xin-Yan Li, Ying-Ying Xu

ORCID number: Li-Tong Yao (0000-0001-9233-5331); Mo-Zhi Wang (0000-0002-0297-2052); Meng-Shen Wang (0000-0002-3190-6062); Xue-Ting Yu (0000-0002-1463-7630); Jing-Yi Guo (0000-0001-8857-2254); Tie Sun (0000-0002-7234-9100); Xin-Yan Li (0000-0003-0710-0293); Ying-Ying Xu (0000-0003-4924-9379).

Conflict-of-interest statement: The authors have no conflict of interest.

Li-Tong Yao, Mo-Zhi Wang, Meng-Shen Wang, Xue-Ting Yu, Jing-Yi Guo, Tie Sun, Xin-Yan Li, Ying-Ying Xu, Department of Breast Surgery, the First Affiliated Hospital of China Medical University, Shenyang 110001, Liaoning Province, China

Corresponding author: Ying-Ying Xu, PhD, Professor, Department of Breast Surgery, the First Affiliated Hospital of China Medical University, No. 155, North Nanjing Street, Shenyang 110001, Liaoning Province, China. xuyingying@cmu.edu.cn

Telephone: +86-24-83282741
Fax: +86-24-22703578

Abstract

A potential strategy for patients with estrogen receptor (ER)-positive breast cancer is necessary to replace neoadjuvant chemotherapy which has limited benefit. Neoadjuvant endocrine therapy (NAE) has been indicated to be a favorable alternate approach to downstage large or locally advanced breast cancer in ER-positive, human epidermal growth factor receptor 2 (HER2)-negative (ER+/HER2-) patients, especially postmenopausal women. Previous studies have demonstrated the efficacy of various endocrine agents in NAE. Aromatase inhibitors (AIs) have proven superiority over tamoxifen as a suitable choice to optimize treatment efficacy. Fulvestrant was recently reported as an effective agent, similar to AIs. Furthermore, the addition of targeted agents exerts synergistic antiproliferative effects with endocrine agents and rapidly improves response rates in both endocrine sensitive and resistant tumors. The neoadjuvant platform provides a unique opportunity to define the appropriate strategy and address the mechanisms of endocrine resistance. In addition, the predictive value of biomarkers and genomic assays in NAE is under investigation to evaluate individual effects and validate biomarker-based strategies. In this review, we discuss the most relevant evidence on the potential of NAE for ER+ breast cancer. The current understanding also offers new insights into the identification of the optimal settings and valuable predictive tools of NAE to guide clinical treatment decisions and achieve beneficial therapeutic effects.

Key words: Breast cancer; Neoadjuvant endocrine therapy; Neoadjuvant chemotherapy; Aromatase inhibitor; Palbociclib; Ki67; Genomic assay

Core tips: Neoadjuvant endocrine therapy (NAE), either alone or combined with other therapies, is a valuable alternate approach to ER-positive breast cancer. Our objective is

to define the optimal settings for suitable individuals, including optimal treatment duration, endocrine agents, and targeted agents in NAE. The identification of correct patients for NAE remains unknown and requires further validation corresponding to biomarker-based strategies. This review consolidates the current relevant evidence to verify the potential value and discuss the development prospects of NAE.

INTRODUCTION

Neoadjuvant chemotherapy (NAC) has been defined as a standard treatment option for localized or locally advanced breast cancer. NAC is used to downgrade and downsize the tumor, which can decrease the extent of surgery and increase the likelihood of breast-conserving surgery (BCS). Moreover, it can improve the long-term prognosis for patients whose operative specimen showed a pathological complete response (pCR)[1,2]. Clinical evidence has demonstrated that the status of hormone receptor (HR) and human epidermal growth factor receptor 2 (HER2) leads to a corresponding response and efficacy of NAC[3]. However, patients with estrogen receptor (ER)-positive, HER2-negative (ER+/HER2-) breast cancer show limited results from NAC, with a lower pCR and poor objective response rate (ORR)[4]. Thus, an alternate neoadjuvant approach is required for breast cancer of this subtype. There is now increasing data that neoadjuvant endocrine therapy (NAE) may be a more appropriate treatment strategy than NAC[5].

Traditionally, NAE has been reserved for locally advanced breast cancer in chemotherapy intolerant or feeble senior patients due to its indolent clinical response and difficulties in efficacy evaluation[6]. However, since the development of third-generation aromatase inhibitors (AIs), several studies were conducted to evaluate the effects of NAE on ER+ breast cancer[7,8]. Neoadjuvant AI has comparable efficacy to NAC in terms of pCR, ORR, and BCS, suggesting the feasibility of this well-tolerated strategy, mainly for postmenopausal patients[9]. The choice of chemotherapy or endocrine therapy (ET) as neoadjuvant treatment depends on disease characteristics and patient subtypes. We will discuss the most relevant clinical trials to illustrate whether NAE, either monotherapy or combination therapy, can serve as a potential option in patients with ER+/HER2- breast cancer.

Furthermore, optimal NAE settings can optimize treatment response and achieve the maximum therapeutic effect for ER+ breast cancer[10]. Emerging evidence has revealed the efficacy of different endocrine agents in presurgical application, including AIs, tamoxifen, and fulvestrant. The identification of optimal agents can result in tailored treatment for both postmenopausal and premenopausal patients. Combining targeted agents with AI or fulvestrant yields promising effects for postmenopausal patients with advanced or metastatic breast cancer[11,12]. The results are being translated to neoadjuvant settings and provide possibilities to fulfill the requirements of drug resistance mechanism exploration and new drug development[13]. Available neoadjuvant endocrine settings are generally favorable for ER+ breast cancer patients, but not all patients benefit equally. The neoadjuvant period can provide a usable platform for tumors to receive biopsy on treatment, leading to the exploration of predictive tools that can screen suitable individuals and select treatment options in breast cancer[14,15]. Current evidence suggested that compared with traditional tumor staging, biomarkers, especially Ki67, and genomic assays offered more accurate prediction information. This evidence provides novel insight into the development of biomarker-based strategies in NAE.

In this review, we will detail the most relevant evidence to verify the potential role of NAE. We identify optimal settings, including optimal duration, optimal endocrine agents, and optimal targeted agents, and then evaluate the prognostic role of biomarkers and genomic assays in NAE. NAE can act as a prospective strategy and scientific platform for optimizing treatment efficacy, screening suitable individuals, and investigating mechanisms of drug resistance in ER+/HER2- breast cancer.

NAE AS A POTENTIAL APPROACH IN THE NEOADJUVANT SETTING

NAE monotherapy

Several studies have already proved that NAE had a similar beneficial therapeutic effect to NAC for ER+ breast cancer (Table 1). A phase II clinical trial published by Semiglazov *et al*[16] suggested that there was no significant difference between the NAC arm (doxorubicin plus paclitaxel) and NAE arm (anastrozole or exemestane) in terms of clinical response (63.6% *vs* 64.5%), ultrasound response (46% *vs* 40%), or mammographic response (63% *vs* 60%). In comparison with the NAC arm, the NAE arm showed an improved BCS rate (24% *vs* 33%, P = 0.058). Similar results were provided in the GEICAM/2006-03 trial between the NAC arm (epirubicin, cyclophosphamide, and docetaxel) and NAE arm (exemestane) in both clinical response rate (CRR 66% *vs* 48%, P = 0.075) and BCS rate (47% *vs* 56%, P = 0.2369)[5]. Meanwhile, a subgroup analysis suggested that NAC had a clear advantage over NAE in premenopausal women (CRR, 75% and 44%, P = 0.027), whereas in postmenopausal women, this advantage disappeared.

Regarding the safety of neoadjuvant settings, grade 3/4 toxicity was more common in NAC therapy than in NAE therapy (47% *vs* 9%, P < 0.001)[5]. The recent, multicenter NEOCENT trial also proposed that the NAC group had more serious adverse effects (AEs), such as alopecia, vomiting, stomatitis, and anemia, than the NAE group, affirming the safety and tolerability of NAE[17]. Furthermore, a meta-analysis including five randomized controlled trials with 538 patients, of whom 267 (49.6%) received NAE and 271 (50.4%) underwent NAC, can be considered the best evidence. This meta-analysis indicated that NAE was as efficacious as NAC in clinical response and increased the rates of BCS and wide local excision, with better tolerability[9]. Given the efficacy and low toxicity correlated with NAE, this treatment option as a potential alternative treatment strategy to NAC, especially in postmenopausal patients, was encouraged.

NAE combination therapy

Based on this promising knowledge of NAE, neoadjuvant chemo-endocrine therapy (NCET), which combined NAE and NAC, was a potential treatment option for hormone-sensitive patients (Table 1). NCET has been explored in comparison with either NAE or NAC therapy. Nakayama *et al*[18] compared the efficacy between the single-agent anastrozole group and the anastrozole plus UFT (tegafur/uracil) group in the Neo-ACET BC trial. There was a greater tendency of tumor degeneration in the NCET group than in the NAE group, although the study was halted due to altered liver function. A recent trial enrolled 63 primary invasive breast cancer patients with initial exemestane treatment followed by response-dependent addition of cyclophosphamide. The results suggested that the clinical response of nonresponders was improved to be comparable to that of responders by the addition of cytotoxic agents to the endocrine agents (CRR for nonresponders and responders at weeks 24 and 36; 54% *vs* 85% and 71% *vs* 71%)[19]. NECT has a broad-range antitumor activity and favorable efficacy over NAE monotherapy.

In comparison with NAC and NECT, Mohammadianpanah *et al*[20] indicated that the addition of letrozole simultaneously with neoadjuvant FAC (5-fluorouracil, doxorubicin, and cyclophosphamide) therapy significantly increased clinical and pathologic response rates compared with chemotherapy alone. The CSCSG-036 trial confirmed that concurrent NAC and estrogen deprivation provided higher effectiveness in ER+ breast cancer (CRR, 84.8% *vs* 72.6%, P = 0.02), especially for those with high Ki67 expression (91.2% *vs* 68.7%, P = 0.001)[21]. Similar toxicities were observed in the NCET and NAC arms, further supporting the role of NCET as a potential neoadjuvant treatment option. Owing to its promising clinical response and acceptable toxicity, NCET has shown great development prospects for ER+/HER2- breast cancer patients.

OPTIMAL SETTING OF NAE

To understand the optimal settings for NAE, we will discuss clinical trials to identify the optimal duration, endocrine agents, and targeted agents (Tables 2 and 3).

Optimal duration of NAE

The duration of NAE treatment in most clinical trials was approximately 4-6 mo, based on experience; however, some investigators noted that this common duration might not be sufficient to achieve the best results in tumor shrinkage[22-24]. Several

Table 1 Neoadjuvant endocrine therapy and neoadjuvant chemo-endocrine therapy as potential approaches in the neoadjuvant settings

Clinical trial	Treatment arms (*n*)	Duration	Primary endpoint	ORR	BCS rate
Semiglazov *et al*[16], 2007	(A) NAE: EXE 25 mg/d or ANA 1 mg/d (121); (B) NAC: doxorubicin 60 mg/m² pluspaclitaxel 200 mg/m² (118)	3 mo	OR by clinical palpation	64% *vs* 64% (*P* > 0.5)	33% *vs* 24 (*P* = 0.58)
Alba *et al*[5], 2012	(A) NAE: EXE 25 mg/d (41-47); (B) NAC: Epirubicin 90 mg/m² plus cyclophosphamide 600 mg/m² then docetaxel 100 mg/ m² (EC-T) (41-48)	24 wk	OR by MRI	48% *vs* 66% (*P* = 0.075)	56% *vs* 47 (*P* = 0.2369)
Palmieri *et al*[17],2014 (NEOCENT)	(A) NAE: LET 2.5 mg/d (22); (B) NAC: 5-fluorouracil 500 mg/m², epirubicin 100 mg/m² plus cyclophosphamide 500 mg/m² (FE100C) (22)	18-23 wk	OR by ultrasound and mammography	59.1% *vs* 54.5% (*P* = 0.32)	
Nakayama *et al*[18], 2018 (Neo-ACET BC)	(A) NAE: ANA 1mg/d (29); (B) NCET: ANA 1mg/d plus tegafur/uracil (UFT) 270 mg/m² (28)	24 wk	OR by MRI and CT	39.3% *vs* 14.3% (*P* = 0.0683)	
Sato *et al*[19], 2018	(A) NAE: EXE 25mg/d (14); (B) NCET: EXE 25 mg/d plus cyclophosphamide 50 mg/d (42)	24 wk	OR by clinical palpation	85% *vs* 54% (at weeks 24); 71% *vs* 71% (at weeks 36)	No increased rate shown
Mohammadianpanah *et al*[20], 2012	(A) NCT: 5-fluorouracil 600 mg/m², doxorubicin 60 mg/m², and cyclophosphamide 600 mg/m² (FAC) (51); (B) NCET: letrozole 2.5 mg/d plus FAC (50)	9–13 wk	OR by clinical palpation	10.2% *vs* 25.5% (*P* = 0.049)	
Yu *et al*[21], 2019 (CSCSG-036)	(A) NCT: EC-T or FEC-T (124); (B) NCET: letrozole 2.5 mg/d plus EC-T or FEC-T (Tleuprorelin) (125)	8-9 wk	OR by MRI	72.6% *vs* 84.8% (*P* = 0.02)	

NAE: Neoadjuvant endocrine therapy; NAC: Neoadjuvant chemotherapy; NCET: Neoadjuvant chemo-endocrine therapy; EXE: Exemestane; ANA: Anastrozole; LET: Letrozole; OR: Objective response; BCS: Breast-conserving surgery.

clinical trials were established to assess the optimal duration of neoadjuvant AIs that would permit tumor regression and BCS eligibility for initially unsuitable patients[23]. A study comparing the tumor size of patients receiving exemestane treatment at 3 and 6 months revealed that extended exemestane therapy had a potential to significantly reduce tumor volume[25]. A phase IV clinical trial verified this conclusion with a slightly larger number of participants and suggested that 7.5-mo neoadjuvant letrozole therapy was optimal to achieve beneficial shrinkage in tumor volume and facilitate BCS, in comparison with 4-month conventional treatment[22]. Overall, long-term neoadjuvant treatment achieves further tumor reduction and increases the feasibility of the BCS rate, but the optimal treatment duration for NAE is still unknown and needs to be further investigated.

Optimal endocrine agents for NAE

In the following paragraph, we will review clinical trials that were conducted to evaluate the efficacy of different endocrine agents and identify the optimal choice in both premenopausal and postmenopausal patients.

Neoadjuvant AIs *vs* tamoxifen: Clinical evidence favoring the three third-generation AIs, letrozole, anastrozole, and exemestane, rather than tamoxifen, in neoadjuvant treatment was established in several randomized clinical trials for ER+ breast cancer. For both the CRR and BCS, letrozole was superior to tamoxifen and had less toxicity, as shown in the P024 trial[7]. There was no statistically significant difference between

Table 2 The optimal duration and optimal endocrine agents of neoadjuvant endocrine therapy

Clinical trial	Patient characteristics	Treatment arms (*n*)	Duration	Primary endpoint	ORR	BCS rate
Krainick-Strobel *et al*[23], 2008	ER+ and/or PR+; Postmenopausal	LET 2.5 mg/d (33)	4-8 mo	OR by clinical palpation, mammography, ultrasound, and BCS	55% *vs* 24% at 4 and > 4 mo	71% *vs* 80% at 4 and > 4 mo
Fontein *et al*[25], 2014	ER+; Postmenopausal	EXE (102)	3 mo *vs* 6 mo	OR by clinical palpation at 3 and 6 months	58.7% *vs* 68.3%	61.8% *vs* 70.6% (*P* = 0.012)
Carpenter *et al*[22], 2014	ER+ and/or PR+; Postmenopausal	LET 2.5 mg/d (146)	3–12 mo	Optimal duration to permit BCS	-	7.5 mo
Eiermann *et al*[7], 2001 (PO24)	ER+ and/or PR+; Postmenopausal	(A) LET 2.5 mg/d (162); (B) TAM 20 mg/d (223)	4 mo	OR by clinical palpation	55% *vs* 36% (*P* < 0.001)	45% *vs* 35% (*P* = 0.022)
Smith *et al*[26], 2005 (IMPACT)	ER+; Postmenopausal	(A) ANA 1 mg/d (113); (B) TAM 20 mg/d (108)	12 wk	OR by ultrasound	37% *vs* 36% (*P* < 0.087)	41% *vs* 31% (*P* = 0.23)
Catalioth *et al*[27], 2006 (PROACT)	ER+ and/or PR+; Postmenopausal	(A) ANA 1 mg/d (228); (B) TAM 20 mg/d (223)	3 mo	OR by ultrasound	50.0% *vs* 46.2% (*P* = 0.037)	38.1% *vs* 29.9% (*P* = 0.11)
Semiglazov *et al*[16], 2015	ER+ and/or PR+; Postmenopausal	(A) EXE (76); (B) TAM (75)	3 mo	OR by clinical palpation	76.3% *vs* 40% (*P* = 0.05)	36.8% *vs* 20% (*P* = 0.05)
Kuter *et al*[29], 2012 (NEWEST)	ER+; Postmenopausal	(A) FUL 500 mg/mo (109); (B) FUL 250 mg/mo (102)	16 wk	Expression of Ki67	17.4 *vs* 11.8% at week 4; 22.9 *vs* 20.6% at week 16	-
Quenel-Tueux *et al*[30], 2015	ER+; Postmenopausal	(A) ANA 1 mg/d (61); (B) FUL 500 mg/mo (59)	6 mo	OR by clinical palpation	58.9% *vs* 53.8%	58.9% *vs* 50%
Guarneri *et al*[31], 2014 (CARMINA 02)	ER+ and/or PR+ Her2-; Postmenopausal	(A) ANA 1 mg/d (59); (B) FUL 500 mg/mo (57)	6 mo	OR by clinical palpation	52.6% *vs* 36.8%	57.6% *vs* 50% (*P* = 0.5 not significant)
Ellis *et al*[32], 2011 (ACOSOG Z1031)	ER+ (Allred score 6-8) postmenopausal T2-T4cN0-3M0	(A) EXE 25 mg/d(124); (B) LET 2.5 mg/d (128); (C) ANA 1 mg/d(125);	16-18 wk	OR by clinical palpation	69.1% *vs* 62.9% *vs* 74.8%	45.2% *vs* 40% *vs* 48.7%
Torrisi *et al*[33], 2007	ER+ T2-T4N0N2; premenopausal	LET 2.5 mg/d plus GnRHa 11.25 mg/3 mo (32)	4 mo	OR by clinical palpation	50%	47%
Masuda *et al*[34], 2012 (STAGE)	ER+ and/or PR+ Her2-; Premenopausal	(A) ANA 1 mg/d (goseretin 3.6 mg/mo) (98); (B) TAM 20 mg/d (goseretin 3.6 mg/mo) (99)	24 wk	OR by ultrasound	70.4% *vs* 50.5% (*P* = 0.004)	85.7% *vs* 67.6%
Dellapasqua *et al*[35], 2019 (TREND)	ER+ and/or PR+ Her2-; Premenopausal	(A) Triptorelin + letrozole (26); (B) degarelix + letrozole (25)	6 mo	Time to optimal OFS	46.2% *vs* 44.0%	52.2% *vs* 42.3%

ER: Estrogen receptor; PR: Progesterone receptor; EXE: Exemestane; ANA: Anastrozole; LET: Letrozole; FUL: Fulvestrant; TAM: Tamoxifen; OR: Objective response; OFS: Ovarian function suppression; BCS: Breast-conserving surgery.

anastrozole and tamoxifen in ORR; however, anastrozole was more effective than tamoxifen in certain clinical subgroups of patients in the IMPACT and PROACT trials[26,27]. Semiglazov *et al*[16] proved that the exemestane group exhibited higher CRR and BCS rates than the tamoxifen group, but there was no difference in the effectiveness, as shown by ultrasound and mammography. A meta-analysis of seven randomized trials further demonstrated the efficacy of neoadjuvant AIs. There was significantly higher clinical and radiological response rates (OR = 1.69 and 1.49, respectively, *P* < 0.001) and BCS rate (OR = 1.62, *P* < 0.001) in the AI arm than in the tamoxifen arm[10]. As illustrated, neoadjuvant AIs treatment possessed better efficacy than tamoxifen.

Neoadjuvant AIs *vs* fulvestrant: Fulvestrant is a selective ER degrader that is recommended by NCCN guidelines as first-line ET for HR+ metastatic breast cancer after progression on TAM or AI[28]. Limited reports have appraised the appropriate

Table 3 The optimal targeted agents

Clinical trial	Treatment arms (*n*)	Duration	Primary endpoint	Response (Primary endpoint)
Johnston *et al*[37], 2019 (PALLET)	(A) LET 14 w (103); (B) LET 2 w followed by LET + PAL 12 w (68); (C) PAL 2 w followed by LET + PAL (69); (D) LET + PAL 14 w (67); LET:2.5 mg/d PAL: 125 mg/d	14 wk	Clinical response by ultrasound and median log-fold change in Ki-67 expression	A *vs* B + C + D: 54.3% *vs* 49.5% (*P* = 0.2), -2.2 *vs* -4.1(*P* < 0.001)
Ma *et al*[38], 2017 (NeoPalAna)	ANA 1 mg/d (plus goserelin if premenopausal) followed by PAL 125 mg/d on C1D1 (50)	5 mo	CCCA (Ki67 < 2.7%) on palbociclib plus anastrozole	C1D1 *vs* C1D15: 26% *vs* 87% (*P* < 0.001)
Arnedos *et al*[40], 2018 (POP)	(A) PAL 125 mg/d (74); (B) placebo (26)	14 d	Antiproliferative response, defined as lnKi67 < 1 at day five	58% *vs* 12% (*P* < 0.001)
Curigliano *et al*[42], 2016 (MONALEESA-1)	(A) LET 2.5 mg/d (2); (B) LET 2.5 mg/d + RIB 400 mg/d (6); (C) LET 2.5 mg/d + RIB 600 mg/d (3)	14 d	mean decreases in the Ki67-positive cell fraction from baseline	(A) 69% (range 38%-100%); (B) 96% (range 78%-100%); (C) 92% (range 75%-100%)
Neo-MONARCH	(A) ANA 2 w; (B) abemaciclib 2 w; (C) ANA + abemaciclib 2 w followed by ANA+ abemaciclib 12 w	14 wk	Changes in Ki67 expression	Reduced Ki67 in patients 15% *vs* 59% *vs* 66%
Ma *et al*[46], 2017	ANA 1 mg/d (plus goserelin if premenopausal) followed by MK-2206 125 mg/w (16)	4 mo	pCR rate	0%
Baselga *et al*[48], 2009	(A) LET 2.5 mg/d+ placebo; (B) LET 2.5 mg/d+ everolimus 10 mg/d	4 mo	OR by clinical palpation	68.1% *vs* 59.1% (*P* = 0.062)

ER: Estrogen receptor; PR: Progesterone receptor; LET: Letrozole; ANA: Anastrozole; PAL: Palbociclib; RIB: Ribociclib; OR: Objective response; CCCA: Complete cell-cycle arrest; pCR: Pathological complete response; BCS: Breast-conserving surgery.

treatment dosing and clinical value of fulvestrant in NAE. The phase II NEWEST trial reported that 500 mg fulvestrant was significantly related to greater early reduction in the levels of ER (-25.0% *vs* -13.5%, *P* = 0.0002) and Ki67 (-78.8% *vs* -47.4%, *P* < 0.0001) than 250 mg. Meanwhile, individuals also had better responses at the recommended 500 mg dose (CRR at week 16, 22.9% *vs* 20.6%)[29]. A high-dose regimen of fulvestrant would improve clinical response and biological activity for ER+ breast cancer in NAE. Together with the same dose-dependent advantages in adjuvant settings, we support the application of 500 mg fulvestrant in future clinical practice.

To determine the efficacy of fulvestrant, a short-term neoadjuvant study first compared the biological activity of fulvestrant plus anastrozole treatment *vs* either agent alone. Quenel-Tueux *et al*[30] evaluated the utility of these two agents in 120 postmenopausal breast cancer patients who were not eligible for primary BCS, with different results. They demonstrated that the fulvestrant arm yielded equal effectiveness as the anastrozole arm in both objective response rate (53.8% *vs* 58.9%) and BCS rate (50.0% *vs* 58.9%)[30]. The CARMINA 02 trial also showed that the efficacy and tolerability of fulvestrant were similar to those of anastrozole[31]. These outcomes suggested the excellent therapeutic effects of fulvestrant and encouraged further exploration to verify whether it can serve as an ideal agent to replace well-recognized and valuable AIs in neoadjuvant therapy.

Choice of different aromatase inhibitors: To explore the choice of the beneficial AIs, the ACOSOG Z1031A trial involved 377 postmenopausal women with stage II/III ER+ (Allred score, 6 to 8) breast cancer. These patients were randomized to treatment with presurgical exemestane, letrozole, or anastrozole for 16 wk. The three AIs had clinically and biologically equivalent effects, as the CRR was 60%, 72%, and 68% and the geometric mean percentage change in Ki67 was 87.2%, 82.1%, and 78%, respectively[32]. Thus, the clinical and biological efficacy did not significantly differ among the three AIs in neoadjuvant settings.

Optimal endocrine agents for premenopausal patients: Current limited data encouraged the efficacy of AI plus ovarian function suppression (OFS) in neoadjuvant endocrine settings for premenopausal patients. Torrisi *et al*[33] confirmed the efficacy of NAE with letrozole plus gonadotropin-releasing hormone (GnRH) analogue in

premenopausal breast cancer patients. Over half of the patients achieved clinical response, and none of patients progressed during treatment[33]. The STAGE trial randomized 204 premenopausal patients into either the neoadjuvant anastrozole arm or tamoxifen arm, accompanied by goserelin, for 24 wk. They indicated the superiority of anastrozole over tamoxifen by assessing CRR (70.4 *vs* 50.5%, *P* = 0.004) and BCS (86% *vs* 68%)[34]. Furthermore, the suitable selection of OFS has been discussed in premenopausal individuals. The TREND trial was conducted to evaluate the efficacy of degarelix (a GnRH antagonist) *vs* triptorelin (a GnRH agonist) in patients receiving neoadjuvant letrozole. Individuals treated with degarelix responded more quickly in inducing optimal OFS than those receiving triptorelin[35]. This finding supported the use of additional studies to assess whether degarelix optimizes treatment efficacy in neoadjuvant treatment and to screen for the optimal agents for OFS. In conclusion, AI plus OFS is a suitable selection in NAE for premenopausal patients, and it demands prospective validation in more clinical trials.

Optimal targeted agents of NAE

The application of targeted agents was supported to promote endocrine response and reveal drug resistance mechanisms. We will review the promising antiproliferative effects of targeted agents, including cyclin-dependent kinase (CDK) 4/6 inhibitors and phosphatidylinositol 3-kinase (PI3K)/AKT/mammalian target of rapamycin (mTOR) pathway inhibitors.

CDK 4/6 inhibitors: CDK 4/6 inhibitors are suppressors of the cell cycle from G1 to S phase. By inducing retinoblastoma protein (Rb) hypophosphorylation, they effectively inhibit mitosis and thus subsequently prevent cell proliferation and tumor progression (Figure 1)[36]. CDK4/6 inhibitors in combination with endocrine therapies have yielded a good prognosis and clinical benefits for ER+ patients, and provoked thoughts about applying CDK4/6 inhibitors in NAE. The following several paragraphs will review clinical trials discussing the efficacy of CDK4/6 inhibitors, especially palbociclib, and addressing the mechanisms of drug resistance.

Newly published in 2018, PALLET, the largest phase II clinical study, has obtained worldwide focus for its concern with efficacy evaluation of a CDK4/6 inhibitor in NAE. In this trial, patients were randomized to letrozole monotherapy or letrozole plus palbociclib therapy for 14 weeks. The combination group showed remarkable superiority over letrozole monotherapy, with larger change in Ki67 (-4.1 *vs* -2.2), higher rate of complete cell-cycle arrest (CCCA, 90% *vs* 59%), and greater cleaved poly(ADP-ribose) polymerase (c-PARP, -0.80 *vs* -0.42), indicating that the combination of palbociclib and letrozole could induce the suppression of cell proliferation[37]. In NeoPalAna single arm trial, patients received neoadjuvant anastrozole, adding palbociclib on cycle 1 day 1 (C1D1) and leaving study if Ki67 was > 10% on C1D15. CCCA rate, as the primary endpoint, was significantly higher in C1D15 than C1D1 (87% *vs* 26%), and rebound of Ki67 expression occurred following withdrawal of palbociclib[38]. The significant improvement of CCCA rate and Ki67 suppression was observed in either luminal A or B subtype and with both PIK3CA mutant or wild type (WT) status, which is parallel to data from the PALOMA-3 trial[39]. Considering molecular remission, researchers pointed out that the antiproliferation effect corresponding to biomarkers was important to identify patients who might benefit and provide an effective endpoint for clinical research.

The POP trial investigated the antiproliferative action of palbociclib in the Rb phosphorylation process. Antiproliferative response, defined as lnKi67 < 1 at day 5, was the primary endpoint, and it was improved in the palbociclib arm *vs* the placebo arm (58% *vs* 12%). Greater Ki67 and phospho-Rb decrease were observed in the palbociclib group[40,41]. Phospho-Rb was related to palbociclib activity, and changes in Rb phosphorylation might be an indicator for CDK4/6 inhibitors. In the MONALEESA-1 trial, patients randomly received either letrozole alone (A) or in combination with ribociclib at different dosages (B: 400 mg/d, C: 600 mg/d). The mean decreases in the Ki67-positive cell fraction from baseline were A, 69%; B, 96%; and C, 92%; this finding indicated the possible antiproliferative effect of combined letrozole and ribociclib[42]. Regarding abemaciclib, 224 postmenopausal patients were randomly assigned to undergo neoadjuvant abemaciclib monotherapy, anastrozole monotherapy, or combination therapy for 2 weeks in the neoMONARCH trial. Abemaciclib, alone or in combination with anastrozole, reduced Ki67 in more patients than anastrozole alone (59%, 66%, and 15%, respectively)[43]. Investigators concluded that CDK 4/6 inhibitors might serve as antiproliferative agents with manageable toxicities and may be predictive of improved disease-free survival. However, this conclusion is still uncertain due to small sample sizes and limited data, and continuous application should be guaranteed to maintain this effect.
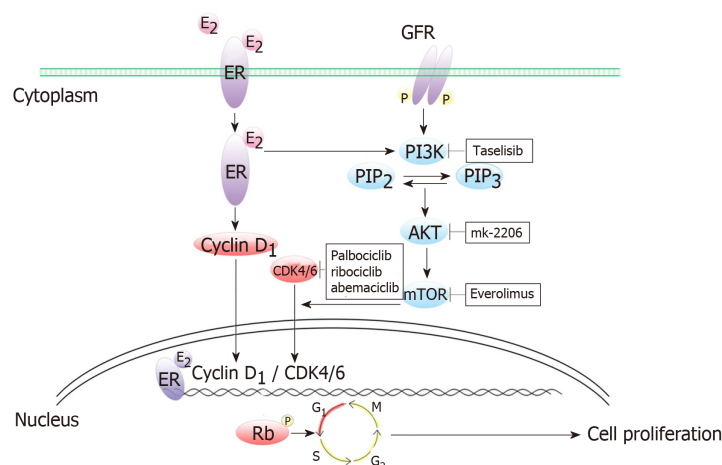
Figure 1 The crosstalk between estrogen receptor and growth factor receptor intracellular signaling pathways. Growth factor receptors (GFRs) activate the downstream PI3K/AKT/mTOR signaling pathway and the Cyclin D1/CDK4/6 complex, while the ER-E2 complex has the same effect[79]. The Cyclin D1/CDK4/6 complex drives cell proliferation by inducing Rb phosphorylation and promotes cell cycle from G1 phase to S phase in the nucleus[80]. Targeted agents against the CDK4/6 pathway and the PI3K/AKT/mTOR pathway can trigger cell cycle arrest and control tumor progression. ER: Estrogen receptor; GFR: Growth factor receptor; CDK4/6: Cyclin-dependent kinase; PI3K: Phosphatidylinositol 3-kinase; PIP2: Phosphatidylinositol 4,5-biphosphate; PIP3: Phosphatidylinositol triphosphate; mTOR: Mammalian target of rapamycin; Rb: Retinoblastoma protein.

PI3K/AKT/mTOR pathway inhibitors: The PI3K/AKT/mTOR pathway was found to be a key survival mechanism responsible for endocrine resistance (Figure 1). Regarding PIK3CA inhibitors, the LORELEI trial randomized postmenopausal patients with ER+ HER2- operable breast cancer into two arms to investigate the effect of letrozole plus taselisib *vs* letrozole plus placebo for 16 wk[44]. The primary results showed that the improvement of ORR was significantly related to the addition of taselisib in the general patient population as well as PIK3CA mutant participants compared with letrozole monotherapy. The results encouraged the antitumor value of taselisib to be investigated in further research.

In preclinical studies, MK-2206 has been proved to be an allosteric pan-AKT inhibitor[45]. A clinical trial explored whether the addition of MK-2206 to anastrozole can lead to the pCR improvement of PIK3CA mutant ER+ breast cancer. This trial selected 22 PIK3CA mutant patients, of whom 16 received the experimental drug. The combination of anastrozole and MK-2206 had no further inhibitory effect on cell proliferation and did not promote apoptosis on C1D17 compared to anastrozole monotherapy[46]. The possibility of improving the efficacy of anastrozole by adding MK-2206 is low, and we disagree with the necessity to continue studying MK-2206 in the target population.

Everolimus, an analog of rapamycin, might competitively bind to the target protein of rapamycin and block downstream signal transduction to suppress tumor cell proliferation[47]. Everolimus utility in NAE was first discussed in a 2009 phase II randomized study carried out by Baselga *et al*[48]. Postmenopausal patients with ER+ breast cancer were treated with neoadjuvant letrozole plus everolimus or letrozole monotherapy. Investigators assessed CRR (68.1% *vs* 59.1%) and calculated the percentage of patients with Ki67 < 1% (57% *vs* 30%)[48]. The everolimus group was superior to the placebo group in both endpoints, indicating the better efficacy of everolimus in NAE. Clinical trials in this area were not adequate until Wu *et al*[49] compared neoadjuvant letrozole plus everolimus with neoadjuvant chemotherapy in ER+/HER2- nonmetastatic breast cancer, and a network meta-analysis by Wang *et al*[50] in 2016 concluded that letrozole in combination with everolimus was the most effective treatment in the neoadjuvant setting. Furthermore, we can expect outcomes in several ongoing neoadjuvant studies combining AI with everolimus, in an attempt to enhance the clinical response of NAE.

BIOMARKERS AND GENOMIC ASSAYS FOR PREDICTION OF NAE BENEFIT

The molecular and genetic expression profiles measured in tumor specimens upon neoadjuvant treatment can provide a remarkable opportunity to explore predictive

tools. In the following paragraph, we will discuss the relevant research that elaborates the value of biomarkers and genomic assays and establish a potential biomarker-based strategy in neoadjuvant settings.

Ki67 and PEPI biomarkers

Ki67, as a biomarker, can be commonly expressed in all stages of the cell cycle, except for G0, and it is of great significance in measuring tumor proliferation in breast specimens[51]. Current evidence showed that the decrease of Ki67 during NAE with endocrine or targeted agents can reveal anti-proliferation effects, and Ki67 level was inversely correlated with prognosis[52,53]. We encourage a broad development prospect for biomarker-based estimates of prognosis in the neoadjuvant therapy field.

Several clinical trials discussed the relationship between prognosis and Ki67 expression at baseline or after short-term treatment. DeCensi *et al*[54] assessed the levels of Ki67 at baseline and after 4 wk of presurgical tamoxifen treatment, and the multivariable hazard ratio for baseline and posttreatment Ki67 labeling index was 1.007 (95%CI: 0.975–1.041) *vs* 1.034 (95%CI: 1.001–1.068)[54]. A PerELISA study first indicated that patients with postmenopausal ER+ breast cancer who gained a reduction in Ki67 after 2-wk neoadjuvant letrozole treatment achieved a meaningful pCR rate without chemotherapy[55]. However, a recent study showed different results at baseline. The POETIC trial compared peri-surgical AI treatment (pre- and postsurgery) with no treatment in 4000 ER+ breast cancers[56]. The results announced at the SABCS 2017 conference suggested that Ki67 levels both at baseline and after short-term therapy were both predictive of efficacy. In conclusion, sufficient evidence has demonstrated that Ki67 levels measured after short-term neoadjuvant therapy were meaningfully related to survival. Whether Ki67 level at baseline can act as a predictive tool is controversial and needs further confirmation.

The preoperative endocrine prognostic index (PEPI) combines Ki67 level with ER status, pathological tumor size, and node status in the surgical specimen following NAE[57]. The predictive role of PEPI for relapse-free survival (RFS) was discovered by Ellis *et al*[32] in the P024 trial and validated in the independent IMPACT trial. Patients with a PEPI score equal to 0 (pT1 or pT2, pN0, Ki67 ≤ 2.7%, Allred score < 2) had an extremely low risk of relapse and can be exempt from adjuvant chemotherapy, while PEPI > 0 recognizes a higher relapse risk. Recently, the predictive value of PEPI was verified in the ACOSOG Z1031B trial[32]. After a median follow-up period of 5.5 years, the incidence of recurrence in patients who completed the neoadjuvant AI period was significantly different. Kaplan-Meier analysis identified the relationship between RFS and PEPI, and the recurrence HR in patients with a PEPI score equal to 0 *vs* PEPI > 0 patients was 0.27 (*P* = 0.014). Moreover, the relapse risk was only 3.6% without chemotherapy in patients with a PEPI score equal to 0[58]. These results supported the use of the PEPI score to identify drug-sensitive or drug-resistant patients and guide tailored treatment decisions on avoiding chemotherapy.

Genomic assays

Recent evidence indicated the predictive role of genomic assays including Oncotype DX, EndoPredict, MammaPrint, BluePrint assays, and a four-gene predictive tool (Table 4).

Oncotype DX Recurrence Score assay: The Oncotype DX® Breast Recurrence Score (RS) assay is a 21-gene validated genomic tool developed by Genomic Health to assess recurrence risk for patients who received adjuvant ET with ER+/HER2- early stage breast cancer, regardless of lymph node status[59,60]. The RS assay can predict the likelihood of benefit from adding chemotherapy to ET in the adjuvant settings. A low-risk RS tended to have a greater clinical response to ET[61]. Additionally, several studies have already incorporated the RS assay in the neoadjuvant setting and illustrated that the approach can be used to guide the decision of neoadjuvant systemic therapy.

We discuss the relevant trials considering the predictive role of RS assay in NAE. Ueno *et al*[62] indicated that the low-risk group (RS < 18) was more likely to benefit from presurgical exemestane treatment than the high-risk group (RS ≥ 31) in CRR (54% *vs* 22%, *P* < 0.001) and BCS (91% *vs* 47%, *P* = 0.003). A 2017 multicenter study reported that the successful BCS rates of the low-intermediate risk group (RS 11-25) after NAE were 75% and 72%, respectively, which were higher than that of high-risk NAC[63]. NAE was found to be a scientific strategy for low-risk patients. Moreover, NAE was not inferior to NAE in midrange RS score, and this finding mirrored the results in similar adjuvant settings in the TAILORx trial[64]. Most recently, the larger, multicenter TransNEOS trial validated the feasibility of RS assay in predicting clinical response and successful BCS with neoadjuvant letrozole in 295 ER+/HER2-postmenopausal patients. The low RS-score group was considered to have an

Table 4 Genomic assays to predict outcome in neoadjuvant endocrine therapy

Genomic assay	Gene number	Genomic information	Method	Current results in NAE	Ref.
Oncotype DX®	21 (16+5)	Proliferative-related genes: *Ki67 AURKA, BIRC5, CCNB1, MYBL2*	QRT-PCR	Recurrence score; low RS results imply a greater likelihood of response to NAE	[62-63]
		Invasive-related genes: *MMP11, CTSL2*			
		Estrogen-related genes: *ESR1, PGR, BCL2, SCUBE2*			
		HER2-related genes: *ERBB2, GRB7*			
		Other genes: *GSTM1, CD68, BAG1*			
		Reference genes: *ACTB, GAPDH, RPLPO, GUS, TFRC*			
EndoPredict (EP)	12 (8+4)	Proliferative-related genes: *BIRC5, UBE2C,* DHCR7	QRT-PCR	Lower genomic risk related to favorable response.	[69]
		Estrogen-related genes: *RBBP8, IL6ST, AZGP1, MGP, STC2*			
		Reference genes: *CALM1, OAZ1, RPL37A, HBB*			
MammaPrint (and BluePrint)	70	*AA555029_RC, ALDH4A1, AP2B1, AYTL2, BBC3, C16orf61, C20orf46, C9orf30, CCNE2, CDC42BPA, CDCA7, CENPA, COL4A2, DCK, DIAPH3, DTL, EBF4, ECT2, EGLN1, ESM1, EXT1, etc.*	Microarray analysis	Distinguish breast cancer subtypes; luminal-subtype patients have a promising prognosis	[73]
Four-gene predictive model	4	Proliferative-related genes: *ASPM* and *MCM4*	QRT-PCR or IHC	Associated to RFS and BCS	[75]
		Immune-related gene: *IL6ST*			
		Apoptosis induction-related gene: *NGFRAP1*			

NAE: Neoadjuvant endocrine therapy; QRT-PCR: Quantitative real time polymerase chain reaction; IHC: Immunohistochemistry.

improved BCS rate, implying a greater likelihood of response to NAE rather than NAC (CRR: 54% *vs* 22%, $P < 0.001$)[65]. In conclusion, the Oncotype DX assay would be a significant predictive tool for providing useful information to screen patients who would benefit from neoadjuvant systematic therapy, with NAE used for low-risk group and NAC for high-risk group.

EndoPredict assay: The EndoPredict® (EP) assay is a 12-gene signature test based on eight proliferation-related and differentiation-related cancer genes and four reference genes. EP score low-risk and high-risk categories were specified in previous studies, providing a score between 0 and 15 to assess recurrence risk[66]. EPclin is a diagnostic arithmetic genomic assay derived from the EP score by integrating clinical factors including nodal status and residual tumor size, which are also involved in PEPI[67]. EP and EPclin assays were shown to be prognostic for early and late distant recurrence[68]. Chow *et al*[69] enrolled 20 eligible patients with neoadjuvant letrozole plus palbociclib treatment in four repeated cycles. The EP score was significantly reduced after NAE, and patients in the high PEPI category had high EPclin scores, indicating that EPclin might be a better predictive marker than PEPI[69]. A retrospective analysis of ABCSG 34 reported at SABCS 2017 also examined the predictive role of EP score. The results after 6 months of neoadjuvant letrozole treatment showed that 27.3% of low-risk and

7.7% of high-risk patients achieved residual cancer burden[70]. The EP assay may help guide neoadjuvant therapy. Lower genomic risk is related to a favorable response to NAE and worse response to NAC. Further studies should be conducted to verify whether EP and EPclin scores can act as alternative parameters for prognosis in NAE settings in a wide range of population.

MammaPrint and BluePrint assays: The MammaPrint® assay, a 70-gene genomic assay, was of great significance in the accurate guidance of treatment decisions for breast cancer patients in adjuvant settings[71]. BluePrint®, a molecular profile that integrates the expression levels of 80 genes, can act as a complement with MammaPrint[72]. According to MammaPrint and BluePrint assays, patients were classified into four molecular subgroups: Luminal A, Luminal B, HER2, and Basal type. The identification of chemosensitivities or endocrine sensitivities in patients with different subtypes can provide insight into the response and prognosis of neoadjuvant therapy. The NBRST trial was designed to include patients with histologically proven breast cancer for selecting optimal therapy[73]. Approximately 68% of patients with BluePrint Luminal breast cancer who received AI therapy and 29% who received tamoxifen had a clinical response in NAE. Patients with MammaPrint Luminal A-subtype tumors had similar clinical efficacy to relatively high-risk Luminal B-subtype patients (CRR: 68.6% *vs* 66.7%)[74]. We discovered that luminal-subtype patients determined by these genomic assays could be valuable candidates for NAE and had a promising prognosis. Limited research focused on MammaPrint and BluePrint prognostic assays for the effective stratification of breast cancer patients in neoadjuvant therapy; therefore, further prospective development is needed to guide clinicians' decisions.

Four-gene predictive model: A clinical trial reported by Turnbull *et al*[75] provided a four-gene predictive model combining two pretreatment genes (immune-related *IL6ST* and apoptosis-related *NGFRAP1*) and two on-treatment genes (proliferation-related *ASPM* and *MCM4*) after 2 weeks of letrozole therapy to forecast clinical response with an accuracy of 96%[75]. Another blinded independent setting of patients receiving anastrozole yielded similar results, with an accuracy of 91%. The gene signature can be significantly associated with RFS and BCS, and accurately measured and performed by PCR and immunohistochemistry, which can give confidence to guide treatment decisions and facilitate further applications[76]. Although it is a viable result as a predictive biomarker based on one small, retrospective analysis, it needs to be confirmed in large, prospective clinical trials.

DISCUSSION AND FUTURE OUTLOOK

NAE is a favorable alternate approach treatment to NAC for patients with ER+ breast cancer. Given efficacy and good tolerance associated with NAE, especially as NECT, consideration and identification of the optimal settings are of great significance for precision treatment. We consider that extended NAE therapy has a greater potential to result in tumor regression and BCS eligibility, but the optimal treatment duration remains to be further validated. The optimal endocrine agents have been widely discussed in neoadjuvant settings. For postmenopausal patients, AIs demonstrated superiority over TAM, and clinical efficacy is biologically and clinically equivalent among letrozole, anastrozole, and exemestane. For premenopausal patients, AI plus OFS is a beneficial strategy in both adjuvant and neoadjuvant settings despite limited data, as mentioned. The effective role of fulvestrant in NAE has also been indicated above. Additional relevant studies are demanded for the helpful knowledge of endocrine agents to define the most appropriate medication and investigate combination approaches in both postmenopausal and premenopausal patients in NAE.

Multiple trials have demonstrated that combination approaches with targeted agents are effective in inducing cell cycle arrest and preventing tumor progression. The potential antiproliferative effect of CDK4/6 inhibitors, especially palbociclib, has been confirmed to be broadly applicable to ER+ breast cancer patients in NAE. However, insufficient data have been published for PI3K/AKT/mTOR pathway inhibitors. Attempts to promote endocrine response and address mechanisms of both "*de novo*" and acquired endocrine resistance by application of targeted agents through specific intracellular signaling pathways are encouraged.

Apart from that, NAE will also provide a well-recognized scenario for biomarker research related to cell proliferation. The establishment of the Ki67 biomarker, which can replace the conventional clinical endpoint of tumor shrinkage, offered a feasible approach to reveal the antiproliferative effect of different drugs[77]. Moreover, Ki67

levels in postsurgical biopsies have been validated as an effective predictive tool for prognosis and facilitated the development of biomarker-based prognosis estimation. PEPI integrating four risk parameters associated with survival was further confirmed to predict RFS. The ongoing and highly anticipated ALTERNATE trial aimed to assess the validity of Ki67 level measurement following 4 wk treatment and a modification of the PEPI score prospectively responding to anastrozole, fulvestrant, or combination therapy[78]. If a biomarker-based strategy is ultimately determined, it will help guide the choice of treatment options and achieve the goal of individualized and precise treatment.

Compared with the molecular profiles, gene analysis provided more accurate information in predicting response, as the results remained the same during the treatment or washout period. The predictive role of genomic assays in NAE is in its infancy. The risk stratification through genetic analysis provided a unique opportunity to guide neoadjuvant systemic therapies. Different genomic assays could evaluate recurrence risks of individuals based on specific related genes and statistical algorithms and provided various risk stratification. Oncotype Dx has been widely recognized as the most useful potential assay in NAE to screen endocrine or chemo-sensitive individuals and divide individuals according to RS scores into low-risk, moderate-risk, and high-risk groups. Inconsistent with Oncotype Dx, Endopredict and MammaPrint assays have utility to classify candidates into high-risk and low-risk groups. Similarly, the low-risk group has a potential to benefit from NAE and exempt from adjuvant chemotherapy. Thus for, there are still insufficient retrospective and prospective studies to confirm the predictive role of genomic assays. We believe that with the publication of more clinical research results, genomic assays will become a useful predictive tool for clinicians to judge prognosis and guide clinical treatment.

CONCLUSION

In conclusion, NAE can serve as a potential strategy for ER+ breast cancer. It allows the identification of suitable individuals with a good response and guides the decisions for clinical systemic treatment. We can meet our requirements of precise treatment through this platform. Although potential strategies have been proposed, the clinical practicability is lacking validity. Further explorations with large-range populations and long-term follow-up periods are demanded to verify the value of NAE.

REFERENCES

1   **Fisher B**, Brown A, Mamounas E, Wieand S, Robidoux A, Margolese RG, Cruz AB, Fisher ER, Wickerham DL, Wolmark N, DeCillis A, Hoehn JL, Lees AW, Dimitrov NV. Effect of preoperative chemotherapy on local-regional disease in women with operable breast cancer: findings from National Surgical Adjuvant Breast and Bowel Project B-18. *J Clin Oncol* 1997; **15**: 2483-2493 [PMID: 9215816 DOI: 10.1200/JCO.1997.15.7.2483]

2   **Rastogi P**, Anderson SJ, Bear HD, Geyer CE, Kahlenberg MS, Robidoux A, Margolese RG, Hoehn JL, Vogel VG, Dakhil SR, Tamkus D, King KM, Pajon ER, Wright MJ, Robert J, Paik S, Mamounas EP, Wolmark N. Preoperative chemotherapy: updates of National Surgical Adjuvant Breast and Bowel Project Protocols B-18 and B-27. *J Clin Oncol* 2008; **26**: 778-785 [PMID: 18258986 DOI: 10.1200/JCO.2007.15.0235]

3   **Guarneri V**, Broglio K, Kau SW, Cristofanilli M, Buzdar AU, Valero V, Buchholz T, Meric F, Middleton L, Hortobagyi GN, Gonzalez-Angulo AM. Prognostic value of pathologic complete response after primary chemotherapy in relation to hormone receptor status and other factors. *J Clin Oncol* 2006; **24**: 1037-1044 [PMID: 16505422 DOI: 10.1200/JCO.2005.02.6914]

4   **Cortazar P**, Zhang L, Untch M, Mehta K, Costantino JP, Wolmark N, Bonnefoi H, Cameron D, Gianni L, Valagussa P, Swain SM, Prowell T, Loibl S, Wickerham DL, Bogaerts J, Baselga J, Perou C, Blumenthal G, Blohmer J, Mamounas EP, Bergh J, Semiglazov V, Justice R, Eidtmann H, Paik S, Piccart M, Sridhara R, Fasching PA, Slaets L, Tang S, Gerber B, Geyer CE, Pazdur R, Ditsch N, Rastogi P, Eiermann W, von Minckwitz G. Pathological complete response and long-term clinical benefit in breast cancer: the CTNeoBC pooled analysis. *Lancet* 2014; **384**: 164-172 [PMID: 24529560 DOI: 10.1016/S0140-6736(13)62422-8]

5   **Alba E**, Calvo L, Albanell J, De la Haba JR, Arcusa Lanza A, Chacon JI, Sanchez-Rovira P, Plazaola A, Lopez Garcia-Asenjo JA, Bermejo B, Carrasco E, Lluch A, GEICAM. Chemotherapy (CT) and hormonotherapy (HT) as neoadjuvant treatment in luminal breast cancer patients: results from the GEICAM/2006-03, a multicenter, randomized, phase-II study. *Ann Oncol* 2012; **23**: 3069-3074 [PMID: 22674146 DOI: 10.1093/annonc/mds132]

6   **Chiba A**, Hoskin TL, Heins CN, Hunt KK, Habermann EB, Boughey JC. Trends in Neoadjuvant Endocrine Therapy Use and Impact on Rates of Breast Conservation in Hormone Receptor-Positive Breast Cancer: A National Cancer Data Base Study. *Ann Surg Oncol* 2017; **24**: 418-424 [PMID: 27663568 DOI: 10.1245/s10434-016-5585-5]

7   **Eiermann W**, Paepke S, Appfelstaedt J, Llombart-Cussac A, Eremin J, Vinholes J, Mauriac L, Ellis M, Lassus M, Chaudri-Ross HA, Dugan M, Borgs M; Letrozole Neo-Adjuvant Breast Cancer Study Group.

Preoperative treatment of postmenopausal breast cancer patients with letrozole: A randomized double-blind multicenter study. *Ann Oncol* 2001; **12**: 1527-1532 [PMID: 11822750 DOI: 10.1023/a:1013128213451]

8   **Takei H**, Suemasu K, Inoue K, Saito T, Okubo K, Koh J, Sato K, Tsuda H, Kurosumi M, Tabei T; Saitama Breast Cancer Clinical Study Group. Multicenter phase II trial of neoadjuvant exemestane for postmenopausal patients with hormone receptor-positive, operable breast cancer: Saitama Breast Cancer Clinical Study Group (SBCCSG-03). *Breast Cancer Res Treat* 2008; **107**: 87-94 [PMID: 18043897 DOI: 10.1007/s10549-007-9529-4]

9   **Huang L**, Xu AM. Short-term outcomes of neoadjuvant hormonal therapy versus neoadjuvant chemotherapy in breast cancer: systematic review and meta-analysis of randomized controlled trials. *Expert Rev Anticancer Ther* 2017; **17**: 327-334 [PMID: 28271747 DOI: 10.1080/14737140.2017.1301208]

10   **Spring LM**, Gupta A, Reynolds KL, Gadd MA, Ellisen LW, Isakoff SJ, Moy B, Bardia A. Neoadjuvant Endocrine Therapy for Estrogen Receptor-Positive Breast Cancer: A Systematic Review and Meta-analysis. *JAMA Oncol* 2016; **2**: 1477-1486 [PMID: 27367583 DOI: 10.1001/jamaoncol.2016.1897]

11   **Walker AJ**, Wedam S, Amiri-Kordestani L, Bloomquist E, Tang S, Sridhara R, Chen W, Palmby TR, Fourie Zirkelbach J, Fu W, Liu Q, Tilley A, Kim G, Kluetz PG, McKee AE, Pazdur R. FDA Approval of Palbociclib in Combination with Fulvestrant for the Treatment of Hormone Receptor-Positive, HER2-Negative Metastatic Breast Cancer. *Clin Cancer Res* 2016; **22**: 4968-4972 [PMID: 27407089 DOI: 10.1158/1078-0432.ccr-16-0493]

12   **Shah A**, Bloomquist E, Tang S, Fu W, Bi Y, Liu Q, Yu J, Zhao P, Palmby TR, Goldberg KB, Chang CJG, Patel P, Alebachew E, Tilley A, Pierce WF, Ibrahim A, Blumenthal GM, Sridhara R, Beaver JA, Pazdur R. FDA Approval: Ribociclib for the Treatment of Postmenopausal Women with Hormone Receptor-Positive, HER2-Negative Advanced or Metastatic Breast Cancer. *Clin Cancer Res* 2018; **24**: 2999-3004 [PMID: 29437768 DOI: 10.1158/1078-0432.CCR-17-2369]

13   **Petrelli F**, Ghidini A, Pedersini R, Cabiddu M, Borgonovo K, Parati MC, Ghilardi M, Amoroso V, Berruti A, Barni S. Comparative efficacy of palbociclib, ribociclib and abemaciclib for ER+ metastatic breast cancer: an adjusted indirect analysis of randomized controlled trials. *Breast Cancer Res Treat* 2019; **174**: 597-604 [PMID: 30659432 DOI: 10.1007/s10549-019-05133-y]

14   **Ying M**, He Y, Qi M, Dong B, Lu A, Li J, Xie Y, Wang T, Lin B, Ouyang T. Value of pre-treatment biomarkers in prediction of response to neoadjuvant endocrine therapy for hormone receptor-positive postmenopausal breast cancer. *Chin J Cancer Res* 2013; **25**: 397-404 [PMID: 23997526 DOI: 10.3978/j.issn.1000-9604.2013.08.01]

15   **Goto-Yamaguchi L**, Yamamoto-Ibusuki M, Yamamoto Y, Fujiki Y, Tomiguchi M, Sueta A, Takeshita T, Iwase H. Therapeutic predictors of neoadjuvant endocrine therapy response in estrogen receptor-positive breast cancer with reference to optimal gene expression profiling. *Breast Cancer Res Treat* 2018; **172**: 353-362 [PMID: 30151737 DOI: 10.1007/s10549-018-4933-5]

16   **Semiglazov VF**, Semiglazov VV, Dashyan GA, Ziltsova EK, Ivanov VG, Bozhok AA, Melnikova OA, Paltuev RM, Kletzel A, Berstein LM. Phase 2 randomized trial of primary endocrine therapy versus chemotherapy in postmenopausal patients with estrogen receptor-positive breast cancer. *Cancer* 2007; **110**: 244-254 [PMID: 17538978 DOI: 10.1002/cncr.22789]

17   **Palmieri C**, Cleator S, Kilburn LS, Kim SB, Ahn SH, Beresford M, Gong G, Mansi J, Mallon E, Reed S, Mousa K, Fallowfield L, Cheang M, Morden J, Page K, Guttery DS, Rghebi B, Primrose L, Shaw JA, Thompson AM, Bliss JM, Coombes RC. NEOCENT: a randomised feasibility and translational study comparing neoadjuvant endocrine therapy with chemotherapy in ER-rich postmenopausal primary breast cancer. *Breast Cancer Res Treat* 2014; **148**: 581-590 [PMID: 25395314 DOI: 10.1007/s10549-014-3183-4]

18   **Nakayama T**, Sagara Y, Takashima T, Matsunami N, Masuda N, Miyoshi Y, Taguchi T, Aono T, Ito T, Kagimura T, Noguchi S. Randomized phase II study of anastrozole plus tegafur-uracil as neoadjuvant therapy for ER-positive breast cancer in postmenopausal Japanese women (Neo-ACET BC). *Cancer Chemother Pharmacol* 2018; **81**: 755-762 [PMID: 29468454 DOI: 10.1007/s00280-018-3544-5]

19   **Sato N**, Masuda N, Morimoto T, Ueno T, Kanbayashi C, Kaneko K, Yasojima H, Saji S, Sasano H, Morita S, Ohno S, Toi M. Neoadjuvant endocrine therapy with exemestane followed by response-guided combination therapy with low-dose cyclophosphamide in postmenopausal patients with estrogen receptor-positive breast cancer: A multicenter, open-label, phase II study. *Cancer Med* 2018 [PMID: 29905023 DOI: 10.1002/cam4.1600]

20   **Mohammadianpanah M**, Ashouri Y, Hoseini S, Amadloo N, Talei A, Tahmasebi S, Nasrolahi H, Mosalaei A, Omidvari S, Ansari M, Mosleh-Shirazi MA. The efficacy and safety of neoadjuvant chemotherapy +/- letrozole in postmenopausal women with locally advanced breast cancer: a randomized phase III clinical trial. *Breast Cancer Res Treat* 2012; **132**: 853-861 [PMID: 22002564 DOI: 10.1007/s10549-011-1814-6]

21   **Yu KD**, Wu SY, Liu GY, Wu J, Di GH, Hu Z, Hou YF, Chen CM, Fan L, Tang LC, Shen ZZ, Wu KJ, Zhuang ZG, Zhang HW, Shao ZM. Concurrent neoadjuvant chemotherapy and estrogen deprivation in patients with estrogen receptor-positive, human epidermal growth factor receptor 2-negative breast cancer (CBCSG-036): A randomized, controlled, multicenter trial. *Cancer* 2019 [PMID: 30892700 DOI: 10.1002/cncr.32057]

22   **Carpenter R**, Doughty JC, Cordiner C, Moss N, Gandhi A, Wilson C, Andrews C, Ellis G, Gui G, Skene AI. Optimum duration of neoadjuvant letrozole to permit breast conserving surgery. *Breast Cancer Res Treat* 2014; **144**: 569-576 [PMID: 24562823 DOI: 10.1007/s10549-014-2835-8]

23   **Krainick-Strobel UE**, Lichtenegger W, Wallwiener D, Tulusan AH, Jänicke F, Bastert G, Kiesel L, Wackwitz B, Paepke S. Neoadjuvant letrozole in postmenopausal estrogen and/or progesterone receptor positive breast cancer: a phase IIb/III trial to investigate optimal duration of preoperative endocrine therapy. *BMC Cancer* 2008; **8**: 62 [PMID: 18302747 DOI: 10.1186/1471-2407-8-62]

24   **Hojo T**, Kinoshita T, Imoto S, Shimizu C, Isaka H, Ito H, Imi K, Wada N, Ando M, Fujiwara Y. Use of the neo-adjuvant exemestane in post-menopausal estrogen receptor-positive breast cancer: a randomized phase II trial (PTEX46) to investigate the optimal duration of preoperative endocrine therapy. *Breast* 2013; **22**: 263-267 [PMID: 23587451 DOI: 10.1016/j.breast.2013.03.002]

25   **Fontein DB**, Charehbili A, Nortier JW, Meershoek-Klein Kranenbarg E, Kroep JR, Putter H, van Riet Y, Nieuwenhuijzen GA, de Valk B, Terwogt JM, Algie GD, Liefers GJ, Linn S, van de Velde CJ. Efficacy of six month neoadjuvant endocrine therapy in postmenopausal, hormone receptor-positive breast cancer patients--a phase II trial. *Eur J Cancer* 2014; **50**: 2190-2200 [PMID: 24970786 DOI: 10.1016/j.ejca.2014.05.010]

26   **Smith IE**, Dowsett M, Ebbs SR, Dixon JM, Skene A, Blohmer JU, Ashley SE, Francis S, Boeddinghaus I, Walsh G; IMPACT Trialists Group. Neoadjuvant treatment of postmenopausal breast cancer with anastrozole, tamoxifen, or both in combination: the Immediate Preoperative Anastrozole, Tamoxifen, or Combined with Tamoxifen (IMPACT) multicenter double-blind randomized trial. *J Clin Oncol* 2005; **23**: 5108-5116 [PMID: 15998903 DOI: 10.1200/jco.2005.04.005]

27   **Cataliotti L**, Buzdar AU, Noguchi S, Bines J, Takatsuka Y, Petrakova K, Dube P, de Oliveira CT. Comparison of anastrozole versus tamoxifen as preoperative therapy in postmenopausal women with hormone receptor-positive breast cancer: the Pre-Operative "Arimidex" Compared to Tamoxifen (PROACT) trial. *Cancer* 2006; **106**: 2095-2103 [PMID: 16598749 DOI: 10.1002/cncr.21872]

28   **Di Leo A**, Jerusalem G, Petruzelka L, Torres R, Bondarenko IN, Khasanov R, Verhoeven D, Pedrini JL, Smirnova I, Lichinitser MR, Pendergrass K, Garnett S, Lindemann JP, Sapunar F, Martin M. Results of the CONFIRM phase III trial comparing fulvestrant 250 mg with fulvestrant 500 mg in postmenopausal women with estrogen receptor-positive advanced breast cancer. *J Clin Oncol* 2010; **28**: 4594-4600 [PMID: 20855825 DOI: 10.1200/JCO.2010.28.8415]

29   **Kuter I**, Gee JM, Hegg R, Singer CF, Badwe RA, Lowe ES, Emeribe UA, Anderson E, Sapunar F, Finlay P, Nicholson RI, Bines J, Harbeck N. Dose-dependent change in biomarkers during neoadjuvant endocrine therapy with fulvestrant: results from NEWEST, a randomized Phase II study. *Breast Cancer Res Treat* 2012; **133**: 237-246 [PMID: 22286314 DOI: 10.1007/s10549-011-1947-7]

30   **Quenel-Tueux N**, Debled M, Rudewicz J, MacGrogan G, Pulido M, Mauriac L, Dalenc F, Bachelot T, Lortal B, Breton-Callu C, Madranges N, de Lara CT, Fournier M, Bonnefoi H, Soueidan H, Nikolski M, Gros A, Daly C, Wood H, Rabbitts P, Iggo R. Clinical and genomic analysis of a randomised phase II study evaluating anastrozole and fulvestrant in postmenopausal patients treated for large operable or locally advanced hormone-receptor-positive breast cancer. *Br J Cancer* 2015; **113**: 585-594 [PMID: 26171933 DOI: 10.1038/bjc.2015.247]

31   **Lerebours F**, Rivera S, Mouret-Reynier MA, Alran S, Venat-Bouvet L, Kerbrat P, Salmon R, Becette V, Bourgier C, Cherel P, Boussion V, Balleyguier C, Thibault F, Lavau-Denes S, Nabholz JM, Sigal B, Trassard M, Mathieu MC, Martin AL, Lemonnier J, Mouret-Fourme E. Randomized phase 2 neoadjuvant trial evaluating anastrozole and fulvestrant efficacy for postmenopausal, estrogen receptor-positive, human epidermal growth factor receptor 2-negative breast cancer patients: Results of the UNICANCER CARMINA 02 French trial (UCBG 0609). *Cancer* 2016; **122**: 3032-3040 [PMID: 27315583 DOI: 10.1002/cncr.30143]

32   **Ellis MJ**, Suman VJ, Hoog J, Lin L, Snider J, Prat A, Parker JS, Luo J, DeSchryver K, Allred DC, Esserman LJ, Unzeitig GW, Margenthaler J, Babiera GV, Marcom PK, Guenther JM, Watson MA, Leitch M, Hunt K, Olson JA. Randomized phase II neoadjuvant comparison between letrozole, anastrozole, and exemestane for postmenopausal women with estrogen receptor-rich stage 2 to 3 breast cancer: clinical and biomarker outcomes and predictive value of the baseline PAM50-based intrinsic subtype--ACOSOG Z1031. *J Clin Oncol* 2011; **29**: 2342-2349 [PMID: 21555689 DOI: 10.1200/JCO.2010.31.6950]

33   **Torrisi R**, Bagnardi V, Pruneri G, Ghisini R, Bottiglieri L, Magni E, Veronesi P, D'Alessandro C, Luini A, Dellapasqua S, Viale G, Goldhirsch A, Colleoni M. Antitumour and biological effects of letrozole and GnRH analogue as primary therapy in premenopausal women with ER and PgR positive locally advanced operable breast cancer. *Br J Cancer* 2007; **97**: 802-808 [PMID: 17712311 DOI: 10.1038/sj.bjc.6603947]

34   **Masuda N**, Sagara Y, Kinoshita T, Iwata H, Nakamura S, Yanagita Y, Nishimura R, Iwase H, Kamigaki S, Takei H, Noguchi S. Neoadjuvant anastrozole versus tamoxifen in patients receiving goserelin for premenopausal breast cancer (STAGE): a double-blind, randomised phase 3 trial. *Lancet Oncol* 2012; **13**: 345-352 [PMID: 22265697 DOI: 10.1016/S1470-2045(11)70373-4]

35   **Dellapasqua S**, Gray KP, Munzone E, Rubino D, Gianni L, Johansson H, Viale G, Ribi K, Bernhard J, Kammler R, Maibach R, Rabaglio-Poretti M, Ruepp B, Di Leo A, Coates AS, Gelber RD, Regan MM, Goldhirsch A, Colleoni M; International Breast Cancer Study Group. Neoadjuvant Degarelix Versus Triptorelin in Premenopausal Patients Who Receive Letrozole for Locally Advanced Endocrine-Responsive Breast Cancer: A Randomized Phase II Trial. *J Clin Oncol* 2019; **37**: 386-395 [PMID: 30589600 DOI: 10.1200/JCO.18.00296]

36   **Lange CA**, Yee D. Killing the second messenger: targeting loss of cell cycle control in endocrine-resistant breast cancer. *Endocr Relat Cancer* 2011; **18**: C19-C24 [PMID: 21613412 DOI: 10.1530/ERC-11-0112]

37   **Johnston S**, Puhalla S, Wheatley D, Ring A, Barry P, Holcombe C, Boileau JF, Provencher L, Robidoux A, Rimawi M, McIntosh SA, Shalaby I, Stein RC, Thirlwell M, Dolling D, Morden J, Snowdon C, Perry S, Cornman C, Batten LM, Jeffs LK, Dodson A, Martins V, Modi A, Osborne CK, Pogue-Geile KL, Cheang MCU, Wolmark N, Julian TB, Fisher K, MacKenzie M, Wilcox M, Huang Bartlett C, Koehler M, Dowsett M, Bliss JM, Jacobs SA. Randomized Phase II Study Evaluating Palbociclib in Addition to Letrozole as Neoadjuvant Therapy in Estrogen Receptor-Positive Early Breast Cancer: PALLET Trial. *J Clin Oncol* 2019; **37**: 178-189 [PMID: 30523750 DOI: 10.1200/JCO.18.01624]

38   **Ma CX**, Gao F, Luo J, Northfelt DW, Goetz M, Forero A, Hoog J, Naughton M, Ademuyiwa F, Suresh R, Anderson KS, Margenthaler J, Aft R, Hobday T, Moynihan T, Gillanders W, Cyr A, Eberlein TJ, Hieken T, Krontiras H, Guo Z, Lee MV, Spies NC, Skidmore ZL, Griffith OL, Griffith M, Thomas S, Bumb C, Vij K, Bartlett CH, Koehler M, Al-Kateb H, Sanati S, Ellis MJ. NeoPalAna: Neoadjuvant Palbociclib, a Cyclin-Dependent Kinase 4/6 Inhibitor, and Anastrozole for Clinical Stage 2 or 3 Estrogen Receptor-Positive Breast Cancer. *Clin Cancer Res* 2017; **23**: 4055-4065 [PMID: 28270497 DOI: 10.1158/1078-0432.CCR-16-3206]

39   **Cristofanilli M**, Turner NC, Bondarenko I, Ro J, Im SA, Masuda N, Colleoni M, DeMichele A, Loi S, Verma S, Iwata H, Harbeck N, Zhang K, Theall KP, Jiang Y, Bartlett CH, Koehler M, Slamon D. Fulvestrant plus palbociclib versus fulvestrant plus placebo for treatment of hormone-receptor-positive, HER2-negative metastatic breast cancer that progressed on previous endocrine therapy (PALOMA-3): final analysis of the multicentre, double-blind, phase 3 randomised controlled trial. *Lancet Oncol* 2016; **17**: 425-439 [PMID: 26947331 DOI: 10.1016/S1470-2045(15)00613-0]

40   **Arnedos M**, Bayar MA, Cheaib B, Scott V, Bouakka I, Valent A, Adam J, Leroux-Kozal V, Marty V, Rapinat A, Mazouni C, Sarfati B, Bieche I, Balleyguier C, Gentien D, Delaloge S, Lacroix-Triki M, Michiels S, Andre F. Modulation of Rb phosphorylation and antiproliferative response to palbociclib: the preoperative-palbociclib (POP) randomized clinical trial. *Ann Oncol* 2018; **29**: 1755-1762 [PMID: 29893769 DOI: 10.1093/annonc/mdy202]

41   **Finn RS**, Dering J, Conklin D, Kalous O, Cohen DJ, Desai AJ, Ginther C, Atefi M, Chen I, Fowst C, Los G, Slamon DJ. PD 0332991, a selective cyclin D kinase 4/6 inhibitor, preferentially inhibits proliferation of luminal estrogen receptor-positive human breast cancer cell lines in vitro. *Breast Cancer Res* 2009; **11**:

R77 [PMID: 19874578 DOI: 10.1186/bcr2419]

42   **Curigliano G**, Gómez Pardo P, Meric-Bernstam F, Conte P, Lolkema MP, Beck JT, Bardia A, Martínez García M, Penault-Llorca F, Dhuria S, Tang Z, Solovieff N, Miller M, Di Tomaso E, Hurvitz SA. Ribociclib plus letrozole in early breast cancer: A presurgical, window-of-opportunity study. *Breast* 2016; **28**: 191-198 [PMID: 27336726 DOI: 10.1016/j.breast.2016.06.008]

43   Abemaciclib Shows Promise for Early Breast Cancer. *Cancer Discov* 2017; **7**: 119-120 [PMID: 27986713 DOI: 10.1158/2159-8290.CD-NB2016-160]

44   **Zhang T**, Feng F, Yao Y, Qi L, Tian J, Zhou C, Dong S, Wang X, Sun C. Efficacy and acceptability of neoadjuvant endocrine therapy in patients with hormone receptor-positive breast cancer: A network meta-analysis. *J Cell Physiol* 2019; **234**: 12393-12403 [PMID: 30652307 DOI: 10.1002/jcp.28068]

45   **Ma CX**, Sanchez C, Gao F, Crowder R, Naughton M, Pluard T, Creekmore A, Guo Z, Hoog J, Lockhart AC, Doyle A, Erlichman C, Ellis MJ. A Phase I Study of the AKT Inhibitor MK-2206 in Combination with Hormonal Therapy in Postmenopausal Women with Estrogen Receptor-Positive Metastatic Breast Cancer. *Clin Cancer Res* 2016; **22**: 2650-2658 [PMID: 26783290 DOI: 10.1158/1078-0432.CCR-15-2160]

46   **Ma CX**, Suman V, Goetz MP, Northfelt D, Burkard ME, Ademuyiwa F, Naughton M, Margenthaler J, Aft R, Gray R, Tevaarwerk A, Wilke L, Haddad T, Moynihan T, Loprinzi C, Hieken T, Barnell EK, Skidmore ZL, Feng YY, Krysiak K, Hoog J, Guo Z, Nehring L, Wisinski KB, Mardis E, Hagemann IS, Vij K, Sanati S, Al-Kateb H, Griffith OL, Griffith M, Doyle L, Erlichman C, Ellis MJ. A Phase II Trial of Neoadjuvant MK-2206, an AKT Inhibitor, with Anastrozole in Clinical Stage II or III PIK3 CA-Mutant ER-Positive and HER2-Negative Breast Cancer. *Clin Cancer Res* 2017; **23**: 6823-6832 [PMID: 28874413 DOI: 10.1158/1078-0432.CCR-17-1260]

47   **Hare SH**, Harvey AJ. mTOR function and therapeutic targeting in breast cancer. *Am J Cancer Res* 2017; **7**: 383-404 [PMID: 28400999]

48   **Baselga J**, Semiglazov V, van Dam P, Manikhas A, Bellet M, Mayordomo J, Campone M, Kubista E, Greil R, Bianchi G, Steinseifer J, Molloy B, Tokaji E, Gardner H, Phillips P, Stumm M, Lane HA, Dixon JM, Jonat W, Rugo HS. Phase II randomized study of neoadjuvant everolimus plus letrozole compared with placebo plus letrozole in patients with estrogen receptor-positive breast cancer. *J Clin Oncol* 2009; **27**: 2630-2637 [PMID: 19380449 DOI: 10.1200/JCO.2008.18.8391]

49   **Wu W**, Deng H, Rao N, You N, Yang Y, Cao M, Liu J. Neoadjuvant everolimus plus letrozole versus fluorouracil, epirubicin and cyclophosphamide for ER-positive, HER2-negative breast cancer: study protocol for a randomized pilot trial. *Trials* 2017; **18**: 497 [PMID: 29070044 DOI: 10.1186/s13063-017-2228-5]

50   **Wang W**, Liu C, Zhou W, Xia T, Xie H, Wang S. Network Meta-Analysis of the Effectiveness of Neoadjuvant Endocrine Therapy for Postmenopausal, HR-Positive Breast Cancer. *Sci Rep* 2016; **6**: 25615 [PMID: 27174543 DOI: 10.1038/srep25615]

51   **Dowsett M**, Nielsen TO, A'Hern R, Bartlett J, Coombes RC, Cuzick J, Ellis M, Henry NL, Hugh JC, Lively T, McShane L, Paik S, Penault-Llorca F, Prudkin L, Regan M, Salter J, Sotiriou C, Smith IE, Viale G, Zujewski JA, Hayes DF; International Ki-67 in Breast Cancer Working Group. Assessment of Ki67 in breast cancer: recommendations from the International Ki67 in Breast Cancer working group. *J Natl Cancer Inst* 2011; **103**: 1656-1664 [PMID: 21960707 DOI: 10.1093/jnci/djr393]

52   **Gallardo A**, Garcia-Valdecasas B, Murata R, Teran R, Lopez L, Barnadas A, Lerma E. Inverse relationship between Ki67 and survival in early luminal breast cancer: confirmation in a multivariate analysis. *Breast Cancer Res Treat* 2018; **167**: 31-37 [PMID: 28865009 DOI: 10.1007/s10549-017-4486-z]

53   **Penault-Llorca F**, Radosevic-Robin N. Ki67 assessment in breast cancer: an update. *Pathology* 2017; **49**: 166-171 [PMID: 28065411 DOI: 10.1016/j.pathol.2016.11.006]

54   **DeCensi A**, Guerrieri-Gonzaga A, Gandini S, Serrano D, Cazzaniga M, Mora S, Johansson H, Lien EA, Pruneri G, Viale G, Bonanni B. Prognostic significance of Ki-67 labeling index after short-term presurgical tamoxifen in women with ER-positive breast cancer. *Ann Oncol* 2011; **22**: 582-587 [PMID: 20716629 DOI: 10.1093/annonc/mdq427]

55   **Guarneri V**, Dieci MV, Bisagni G, Frassoldati A, Bianchi GV, De Salvo GL, Orvieto E, Urso L, Pascual T, Paré L, Galván P, Ambroggi M, Giorgi CA, Moretti G, Griguolo G, Vicini R, Prat A, Conte PF. De-escalated therapy for HR+/HER2+ breast cancer patients with Ki67 response after 2 weeks letrozole: results of the PerELISA neoadjuvant study. *Ann Oncol* 2019 [PMID: 30778520 DOI: 10.1093/annonc/mdz055]

56   **Dowsett M**, Smith I, Robertson J, Robison L, Pinhel I, Johnson L, Salter J, Dunbier A, Anderson H, Ghazoui Z, Skene T, Evans A, A'Hern R, Iskender A, Wilcox M, Bliss J. Endocrine therapy, new biologicals, and new study designs for presurgical studies in breast cancer. *J Natl Cancer Inst Monogr* 2011; **2011**: 120-123 [PMID: 22043057 DOI: 10.1093/jncimonographs/lgr034]

57   **Ellis MJ**, Tao Y, Luo J, A'Hern R, Evans DB, Bhatnagar AS, Chaudri Ross HA, von Kameke A, Miller WR, Smith I, Eiermann W, Dowsett M. Outcome prediction for estrogen receptor-positive breast cancer based on postneoadjuvant endocrine therapy tumor characteristics. *J Natl Cancer Inst* 2008; **100**: 1380-1388 [PMID: 18812550 DOI: 10.1093/jnci/djn309]

58   **Ellis MJ**, Suman VJ, Hoog J, Goncalves R, Sanati S, Creighton CJ, DeSchryver K, Crouch E, Brink A, Watson M, Luo J, Tao Y, Barnes M, Dowsett M, Budd GT, Winer E, Silverman P, Esserman L, Carey L, Ma CX, Unzeitig G, Pluard T, Whitworth P, Babiera G, Guenther JM, Dayao Z, Ota D, Leitch M, Olson JA, Allred DC, Hunt K. Ki67 Proliferation Index as a Tool for Chemotherapy Decisions During and After Neoadjuvant Aromatase Inhibitor Treatment of Breast Cancer: Results From the American College of Surgeons Oncology Group Z1031 Trial (Alliance). *J Clin Oncol* 2017; **35**: 1061-1069 [PMID: 28045625 DOI: 10.1200/JCO.2016.69.4406]

59   **Dzimitrowicz H**, Mougalian S, Storms S, Hurd S, Chagpar AB, Killelea BK, Horowitz NR, Lannin DR, Harigopal M, Hofstatter E, DiGiovanna MP, Adelson KB, Silber A, Abu-Khalaf M, Chung G, Zaheer W, Abdelghany O, Hatzis C, Pusztai L, Sanft TB. Impacts of Early Guideline-Directed 21-Gene Recurrence Score Testing on Adjuvant Therapy Decision Making. *J Oncol Pract* 2017; **13**: e1012-e1020 [PMID: 29048991 DOI: 10.1200/JOP.2017.022731]

60   **Albain KS**, Barlow WE, Shak S, Hortobagyi GN, Livingston RB, Yeh IT, Ravdin P, Bugarini R, Baehner FL, Davidson NE, Sledge GW, Winer EP, Hudis C, Ingle JN, Perez EA, Pritchard KI, Shepherd L, Gralow JR, Yoshizawa C, Allred DC, Osborne CK, Hayes DF; Breast Cancer Intergroup of North America. Prognostic and predictive value of the 21-gene recurrence score assay in postmenopausal women with node-positive, oestrogen-receptor-positive breast cancer on chemotherapy: a retrospective analysis of a randomised trial. *Lancet Oncol* 2010; **11**: 55-65 [PMID: 20005174 DOI: 10.1016/S1470-2045(09)70314-6]

61 **Gluz O**, Nitz UA, Christgen M, Kates RE, Shak S, Clemens M, Kraemer S, Aktas B, Kuemmel S, Reimer T, Kusche M, Heyl V, Lorenz-Salehi F, Just M, Hofmann D, Degenhardt T, Liedtke C, Svedman C, Wuerstlein R, Kreipe HH, Harbeck N. West German Study Group Phase III PlanB Trial: First Prospective Outcome Data for the 21-Gene Recurrence Score Assay and Concordance of Prognostic Markers by Central and Local Pathology Assessment. *J Clin Oncol* 2016; **34**: 2341-2349 [PMID: 26926676 DOI: 10.1200/JCO.2015.63.5383]

62 **Ueno T**, Masuda N, Yamanaka T, Saji S, Kuroi K, Sato N, Takei H, Yamamoto Y, Ohno S, Yamashita H, Hisamatsu K, Aogi K, Iwata H, Sasano H, Toi M. Evaluating the 21-gene assay Recurrence Score® as a predictor of clinical response to 24 weeks of neoadjuvant exemestane in estrogen receptor-positive breast cancer. *Int J Clin Oncol* 2014; **19**: 607-613 [PMID: 24101215 DOI: 10.1007/s10147-013-0614-x]

63 **Bear HD**, Wan W, Robidoux A, Rubin P, Limentani S, White RL, Granfortuna J, Hopkins JO, Oldham D, Rodriguez A, Sing AP. Using the 21-gene assay from core needle biopsies to choose neoadjuvant therapy for breast cancer: A multicenter trial. *J Surg Oncol* 2017; **115**: 917-923 [PMID: 28407247 DOI: 10.1002/jso.24610]

64 **Succop P**, Bornschein R, Brown K, Tseng CY. An empirical comparison of lead exposure pathway models. *Environ Health Perspect* 1998; **106** Suppl 6: 1577-1583 [PMID: 9860917 DOI: 10.1056/NEJMoa1804710]

65 **Iwata H**, Masuda N, Yamamoto Y, Fujisawa T, Toyama T, Kashiwaba M, Ohtani S, Taira N, Sakai T, Hasegawa Y, Nakamura R, Akabane H, Shibahara Y, Sasano H, Yamaguchi T, Sakamaki K, Bailey H, Cherbavaz DB, Jakubowski DM, Sugiyama N, Chao C, Ohashi Y. Validation of the 21-gene test as a predictor of clinical response to neoadjuvant hormonal therapy for ER+, HER2-negative breast cancer: the TransNEOS study. *Breast Cancer Res Treat* 2019; **173**: 123-133 [PMID: 30242578 DOI: 10.1007/s10549-018-4964-y]

66 **Filipits M**, Rudas M, Jakesz R, Dubsky P, Fitzal F, Singer CF, Dietze O, Greil R, Jelen A, Sevelda P, Freibauer C, Müller V, Jänicke F, Schmidt M, Kölbl H, Rody A, Kaufmann M, Schroth W, Brauch H, Schwab M, Fritz P, Weber KE, Feder IS, Hennig G, Kronenwett R, Gehrmann M, Gnant M; EP Investigators. A new molecular predictor of distant recurrence in ER-positive, HER2-negative breast cancer adds independent information to conventional clinical risk factors. *Clin Cancer Res* 2011; **17**: 6012-6020 [PMID: 21807638 DOI: 10.1158/1078-0432.CCR-11-0926]

67 **Fitzal F**, Filipits M, Rudas M, Greil R, Dietze O, Samonigg H, Lax S, Herz W, Dubsky P, Bartsch R, Kronenwett R, Gnant M. The genomic expression test EndoPredict is a prognostic tool for identifying risk of local recurrence in postmenopausal endocrine receptor-positive, her2neu-negative breast cancer patients randomised within the prospective ABCSG 8 trial. *Br J Cancer* 2015; **112**: 1405-1410 [PMID: 25867274 DOI: 10.1038/bjc.2015.98]

68 **Dubsky P**, Brase JC, Jakesz R, Rudas M, Singer CF, Greil R, Dietze O, Luisser I, Klug E, Sedivy R, Bachner M, Mayr D, Schmidt M, Gehrmann MC, Petry C, Weber KE, Fisch K, Kronenwett R, Gnant M, Filipits M; Austrian Breast and Colorectal Cancer Study Group (ABCSG). The EndoPredict score provides prognostic information on late distant metastases in ER+/HER2- breast cancer patients. *Br J Cancer* 2013; **109**: 2959-2964 [PMID: 24157828 DOI: 10.1038/bjc.2013.671]

69 **Chow LWC**, Morita S, Chow CYC, Ng WK, Toi M. Neoadjuvant palbociclib on ER+ breast cancer (N007): clinical response and EndoPredict's value. *Endocr Relat Cancer* 2018; **25**: 123-130 [PMID: 29158285 DOI: 10.1530/ERC-17-0396]

70 **Rinnerthaler G**, Gampenrieder SP, Greil R. SABCS 2017: lifestyle factors, hormone receptor-positive advanced disease, liquid biopsies, and prognosis. *Memo* 2018; **11**: 208-212 [PMID: 30220928 DOI: 10.1007/s12254-018-0433-x]

71 **Beumer I**, Witteveen A, Delahaye L, Wehkamp D, Snel M, Dreezen C, Zheng J, Floore A, Brink G, Chan B, Linn S, Bernards R, van 't Veer L, Glas A. Equivalence of MammaPrint array types in clinical trials and diagnostics. *Breast Cancer Res Treat* 2016; **156**: 279-287 [PMID: 27002507 DOI: 10.1007/s10549-016-3764-5]

72 **Krijgsman O**, Roepman P, Zwart W, Carroll JS, Tian S, de Snoo FA, Bender RA, Bernards R, Glas AM. A diagnostic gene profile for molecular subtyping of breast cancer associated with treatment response. *Breast Cancer Res Treat* 2012; **133**: 37-47 [PMID: 21814749 DOI: 10.1007/s10549-011-1683-z]

73 **Whitworth P**, Stork-Sloots L, de Snoo FA, Richards P, Rotkis M, Beatty J, Mislowsky A, Pellicane JV, Nguyen B, Lee L, Nash C, Gittleman M, Akbari S, Beitsch PD. Chemosensitivity predicted by BluePrint 80-gene functional subtype and MammaPrint in the Prospective Neoadjuvant Breast Registry Symphony Trial (NBRST). *Ann Surg Oncol* 2014; **21**: 3261-3267 [PMID: 25099655 DOI: 10.1245/s10434-014-3908-y]

74 **Whitworth P**, Beitsch P, Mislowsky A, Pellicane JV, Nash C, Murray M, Lee LA, Dul CL, Rotkis M, Baron P, Stork-Sloots L, de Snoo FA, Beatty J. Chemosensitivity and Endocrine Sensitivity in Clinical Luminal Breast Cancer Patients in the Prospective Neoadjuvant Breast Registry Symphony Trial (NBRST) Predicted by Molecular Subtyping. *Ann Surg Oncol* 2017; **24**: 669-675 [PMID: 27770345 DOI: 10.1245/s10434-016-5600-x]

75 **Turnbull AK**, Arthur LM, Renshaw L, Larionov AA, Kay C, Dunbier AK, Thomas JS, Dowsett M, Sims AH, Dixon JM. Accurate Prediction and Validation of Response to Endocrine Therapy in Breast Cancer. *J Clin Oncol* 2015; **33**: 2270-2278 [PMID: 26033813 DOI: 10.1200/JCO.2014.57.8963]

76 **Sestak I**, Buus R, Cuzick J, Dubsky P, Kronenwett R, Denkert C, Ferree S, Sgroi D, Schnabel C, Baehner FL, Mallon E, Dowsett M. Comparison of the Performance of 6 Prognostic Signatures for Estrogen Receptor-Positive Breast Cancer: A Secondary Analysis of a Randomized Clinical Trial. *JAMA Oncol* 2018; **4**: 545-553 [PMID: 29450494 DOI: 10.1001/jamaoncol.2017.5524]

77 **Gellert P**, Segal CV, Gao Q, López-Knowles E, Martin LA, Dodson A, Li T, Miller CA, Lu C, Mardis ER, Gillman A, Morden J, Graf M, Sidhu K, Evans A, Shere M, Holcombe C, McIntosh SA, Bundred N, Skene A, Maxwell W, Robertson J, Bliss JM, Smith I, Dowsett M; POETIC Trial Management Group and Trialists. Impact of mutational profiles on response of primary oestrogen receptor-positive breast cancers to oestrogen deprivation. *Nat Commun* 2016; **7**: 13294 [PMID: 27827358 DOI: 10.1038/ncomms13294]

78 **Suman VJ**, Ellis MJ, Ma CX. The ALTERNATE trial: assessing a biomarker driven strategy for the treatment of post-menopausal women with ER+/Her2- invasive breast cancer. *Chin Clin Oncol* 2015; **4**: 34 [PMID: 26408301 DOI: 10.3978/j.issn.2304-3865.2015.09.01]

79 **Nwabo Kamdje AH**, Seke Etet PF, Vecchio L, Muller JM, Krampera M, Lukong KE. Signaling pathways in breast cancer: therapeutic targeting of the microenvironment. *Cell Signal* 2014; **26**: 2843-2856 [PMID: 25093804 DOI: 10.1016/j.cellsig.2014.07.034]

80 **Herrera-Abreu MT**, Palafox M, Asghar U, Rivas MA, Cutts RJ, Garcia-Murillas I, Pearson A, Guzman

M, Rodriguez O, Grueso J, Bellet M, Cortés J, Elliott R, Pancholi S, Baselga J, Dowsett M, Martin LA, Turner NC, Serra V. Early Adaptation and Acquired Resistance to CDK4/6 Inhibition in Estrogen Receptor-Positive Breast Cancer. *Cancer Res* 2016; **76**: 2301-2313 [PMID: 27020857 DOI: 10.1158/0008-5472.CAN-15-0728]

ORIGINAL ARTICLE

Basic Study

Vestigial like family member 3 is a novel prognostic biomarker for gastric cancer

Li-Hua Zhang, Zhuo Wang, Long-Hai Li, Yan-Kui Liu, Lin-Fang Jin, Xiao-Wei Qi, Chun Zhang, Teng Wang, Dong Hua

ORCID number: Li-Hua Zhang (0000-0002-0931-5039); Zhuo Wang (0000-0001-8206-6035); Long-Hai Li (0000-0003-4387-8932); Yan-Kui Liu (0000-0003-4387-8942); Lin-Fang Jin (0000-0002-2487-5886); Xiao-Wei Qi (0000-0001-7761-5095); Chun Zhang (0000-0001-6422-3367); Teng Wang (0000-0001-6092-9522); Dong Hua (0000-0001-5569-1708).

Institutional review board statement: This study was reviewed and approved by Affiliated Hospital of Jiangnan University Institutional Review Board.

Informed consent statement: Any personal item or information will not be published without explicit consent from the involved persons.

Li-Hua Zhang, Dong Hua, School of Pharmaceutical Sciences, Jiangnan University, Wuxi 214122, Jiangsu Province, China

Li-Hua Zhang, Teng Wang, Dong Hua, Department of Oncology, Affiliated Hospital of Jiangnan University, Wuxi 214062, Jiangsu Province, China

Zhuo Wang, Department of Geriatrics, Affiliated Wuxi First People's Hospital of Nanjing Medical University, Wuxi 214122, Jiangsu Province, China

Long-Hai Li, Chun Zhang, Wuxi Medical College, Jiangnan University, Wuxi 214122, Jiangsu Province, China

Yan-Kui Liu, Lin-Fang Jin, Xiao-Wei Qi, Department of Pathology, Affiliated Hospital of Jiangnan University, Wuxi 214062, Jiangsu Province, China

Corresponding author: Dong Hua, MD, PhD, Chief Doctor, Professor, Department of Oncology, Affiliated Hospital of Jiangnan University, No. 200, Huihe Road, Wuxi 214062, Jiangsu Province, China. wx89211@163.com
Telephone: +86-510-88682109
Fax: +86-510-85808820

Abstract

BACKGROUND
Vestigial like family member 3 (VGLL3) is associated with the prognosis of epithelial ovarian cancer and soft tissue sarcoma, but its role in gastric cancer (GC) is unclear.

AIM
To explore the expression pattern and clinical significance of VGLL3 in GC.

METHODS
Integrative analysis was performed on the GC transcriptome profiles and survival information deposited in the ONCOMINE, GEPIA, and ONCOLNC databases. The expression levels of VGLL3 mRNA and protein were analyzed in the freshly resected tumor and normal gastric tissues from GC patients by quantitative RT-PCR and Western blot, respectively. In addition, the *in situ* expression of VGLL3 in the GC tissues was determined by immunohistochemistry (IHC), and the patients were accordingly classified into the high and low expression groups. The correlation of VGLL3 expression status with patient prognosis was then determined by univariate and multivariate Cox

regression analyses.

RESULTS
Analysis of the ONCOMINE and GEPIA databases showed that VGLL3 was significantly up-regulated in GC tissues (P = 0.003), and associated with the tumor TNM stage (P = 0.0163). The high VGLL3 expression group had a significantly worse prognosis compared to the low expression group, as per both GEPIA (P = 0.0057) and ONCOLNC (P = 0.01). The bioinformatics results were validated by the significantly higher VGLL3 mRNA and protein levels in the GC tissues compared to the adjacent normal tissues (P < 0.001) in a cohort of 30 GC patients. Furthermore, high *in situ* expression of VGLL3 protein was associated with more advanced N and TNM stages and HER2 mutation (P < 0.05) in a cohort of 172 patients. Kaplan-Meier analysis showed that the high VGLL3 expression group had a worse prognosis compared to the low expression group (P = 0.019). Multivariate analysis showed that VGLL3 expression status was an independent risk factor for prognosis. In addition, the prognostic risk model nomogram showed that VGLL3 was the most important indicator, with an area under the receiver operating characteristic (ROC) curve (AUC) of 0.613 for 3-year survival and 0.706 for 5-year survival. Finally, the protein interaction network analysis revealed that VGLL3 is likely involved in the Hippo signaling pathway.

CONCLUSION
VGLL3 is overexpressed in GC tissues and associated with a poor prognosis, indicating its potential as a novel prognosis biomarker and therapeutic target for GC.

Key words: Vestigial like family member 3; Stomach adenocarcinoma; HER2 mutation; Gastric cancer; Bioinformatics analysis

Core tip: The present study for the first time revealed the expression of vestigial like family member 3 (VGLL3) in gastric cancer (GC) and its correlation with HER2 mutation. Overall, the findings of the present study suggest that VGLL3 is a novel prognostic biomarker for GC and highlight the significance of VGLL3 as a promising therapeutic target for GC.

INTRODUCTION

Gastric cancer (GC) is a frequently occurring malignancy of the digestive tract[1], and it was the fifth most commonly diagnosed and the third most common cause of cancer-related mortality worldwide in 2018[2]. Lack of early diagnosis and ineffective treatment options for the advanced stages are the primary reasons for the dismal 5-year survival rate of GC[3]. Therefore, it is imperative to identify novel biomarkers for early diagnosis and accurate prediction of prognosis. Vestigial like family member 3 (VGLL3) is a member of the vestigial like family of proteins[4], and is associated with epithelial ovarian cancer[5] and soft tissue sarcoma[6]. The aim of this study was to determine the expression status and prognostic utility of VGL33 in GC. To this end, we mined the transcriptomic data of GC from the ONCOMINE and GEPIA databases, and determined its correlation with the survival data from GEPIA and ONCOLINC. VGLL3 levels were upregulated in GC samples and associated with a poor prognosis. The bioinformatics data were successfully validated on the tumor and normal gastric tissues resected from GC patients. Based on the VGLL3 levels, the patients were stratified into the high and low expression groups, and a prognosis prediction model was established on the basis of VGLL3 status and clinical data. Our findings show a

strong prognostic role of VGLL3 in GC, which can potentially translate to clinical applications.

MATERIALS AND METHODS

Patients and tissue samples

A total of 172 tissue samples were obtained from gastric adenocarcinoma patients who underwent major surgery at the Affiliated Hospital of Jiangnan University between 2009 and 2012. The tissues were immediately fixed in formalin and embedded in paraffin for further analysis. In addition, fresh samples were dissected from 30 patients at the Affiliated Hospital of Jiangnan University in November 2018, and immediately stored in liquid nitrogen for molecular analysis. The mean follow-up duration was 43.1 mo and ranged from 0.2 to 86 mo. None of the patients received chemotherapy or radiotherapy before surgery[7]. The tumor stage classification was determined by three pathologists who were blinded to the patient data according to the guidelines of the American Joint Committee on Cancer (AJCC). Freshly resected tissues were obtained from 202 patients, and were fixed in formalin and embedded in paraffin. In addition, tissue specimens from 30 patients were flash frozen in liquid nitrogen. All participating clinicians and patients provided written informed consent.

Bioinformatics analysis

The VGLL3 mRNA levels in the GC and normal gastric tissues were determined by integrated analysis of the Oncomine database (www.oncomine.org)[8] using Coexpedia (www.coexpedia.org)[9]. ONCOLINC (http://www.oncolnc.org/cancer/) and Coexpedia were used to analyze the prognostic value of WISP1 in STAD. The STRING database (http://www.string-db.org) was utilized to construct the protein-protein interaction (PPI) network[10].

RNA isolation and RT-qPCR

Total RNA was extracted from frozen tissue samples using Trizol reagent (Invitrogen, Carlsbad, CA) according to the manufacturer's instructions, and reverse transcribed using the PrimeScript RT-PCR kit (Takara, Japan)[11]. RT-qPCR was performed on the ABI 7500 RealTime PCR System (Applied Biosystems, Inc. USA) using SYBR Green Master Mix (Takara, Japan), and the VGLL3 levels were normalized to β-actin. The following primers were used: Forward primer, 5'-CCAACTACAGTCACC-TCTGCTAC-3' and reverse primer, 5'-ACCACGGTGATTCCTTACTCTTG-3' for VGLL3; forward primer, 5'-CCTGTGGCATCCACGAAACT-3' and reverse primer, 5'-GAAGCATTTGCG GTGGACGAT-3' for β-actin. All reactions were performed in triplicates, and the $2^{-\Delta\Delta Ct}$ method[12] was used to quantify the relative expression levels of VGLL3.

Western blot analysis

Total protein was extracted from GC and para-cancerous tissues using the RIPA lysis buffer (Pierce, Thermo Scientifc, Cramlington, United Kingdom)[13], and quantified with the enhanced BCA protein assay kit (KeyGEN BioTECH, Jiangsu, China). Equal amount (40 mg) of proteins per sample were separated by sodium dodecyl sulfate-polyacrylamide gel electrophoresis (SD-PAGE), and then transferred to polyvinylidene difluoride membranes (Bio-Rad, Hercules, CA, United States). After blocking with 5% non-fat milk for 1 h at room temperature (RT), the membranes were incubated overnight with anti-VGLL3 (ab83555, Abcam) and β-actin (ab8226, Abcam) primary antibodies at 4 °C. After washing thrice with TBST, the membranes were incubated with HRP-conjugated secondary antibody (1:1000) for 1 h at RT. The protein bands were visualized with an ECL chemiluminescence system after short exposure to X-ray films (Kodak, Japan). Densitometric analysis was performed with Image Pro-Plus software, and the relative expression levels of VGLL3 were normalized to tubulin.

Immunohistochemistry (IHC)

The formalin-fixed tissues were dehydrated, embedded in paraffin, and cut into 5 μm thick sections. IHC was performed according to the manufacturer's protocol[14]. Briefly, the sections were heated in citrate buffer in a microwave, cooled, and incubated overnight with anti-VGLL3 antibody (1:50, clone PA5-68441, Invitrogen) at 4 °C. After labeling with the secondary antibody for 1 hour at RT, color was developed using liquid DAB substrate. Three pathologists blinded to the patient identity observed and graded VGLL3 positivity as 0, 1 (1%–29% positively-stained cells), 2 (30%–69%), or 3 (70%-100%), and the staining intensity as 0 (negative), 1 (weak staining), 2 (moderate staining), or 3 (strong staining). The immunoreactive

score (IRS) was then calculated for each sample by multiplying the staining intensity and positivity scores, and graded as: 0-1, "-"; 2-3, "+"; 4-6, "++"; and 6-9, "+++"[15]. Based on the IRS, the samples were stratified into the high (4-9) and low (0-3) VGLL3 expression groups.

Fluorescence in situ hybridization (FISH)
The tissue sections were treated with denaturing solution to denature the DNA into single strands, and hybridized with the PathVysion probes (No.36-161060, PathVysion HER-2DNA Probe Kit). After washing the unbound probe with DNA, the sections were counterstained with the nuclear dye DAPI (4′, 6 diamidino-2-phenylindole). Positive LSI HER-2/neu and CEP 17 signals were counted under a fluorescence microscope, and the ratio of the copy number of HER-2/neu gene to that of chromosome 17 was calculated.

Statistical analysis
Statistical analyses were performed with R*64 version 3.5.2 software and Graphpad 6.01. HER2 status (positive or negative) was designated on the basis of the combined FISH and IHC results as per the American Society of Clinical Oncology/College of American Pathologists Clinical Practice Guidelines. VGLL3 expression levels in the tumor and normal samples were compared by the Student's *t*-test, and the association between VGLL3 and clinico-pathological features was assessed by the chi-square test. The overall survival (OS) curve was plotted by the Kaplan-Meier method and analyzed by the log-rank test. Univariate and multivariate analyses of the prognostic factors were performed using the Cox proportional hazard regression model. A nomogram was formulated based on the results of the multivariate analysis with the package of rms in R version 3.5.2 (http://www.r-project.org/)[16]. The receiver operating characteristic (ROC) curve was plotted to determine the sensitivity and specificity of the VGLL3-based prognostic score[17], and the area under the curve (AUC) was calculated. All *P*-values were two-tailed and considered statistically significant when less than 0.05.

RESULTS

VGLL3 mRNA and protein levels are upregulated in GC samples
GEPIA database profiling showed that although VGLL3 was significantly overexpressed in GC samples of advanced TNM stages relative to those at the lower stages (*P* = 0.0163), there was no significant difference between the GC and normal tissues (*P* > 0.05). Integrated analysis of multiple VGLL3 transcriptome datasets from the ONCOMINE database, however, showed that VGLL3 was significantly overexpressed in GC (*P* = 0.003), and notably associated with a poor prognosis according to the ONCOLINC database analysis (*P* = 0.01, *n* = 378) (Figure 1). In addition, GEPIA online survival analysis further confirmed that VGLL3 was a marker of poor prognosis in GC (*P* = 0.0062, *n* = 384). To validate the *in silico* data, we analyzed the expression levels of VGLL3 in the tumor and normal gastric tissues resected from 30 GC patients, and observed significantly higher levels of VGLL3 mRNA (*P* < 0.001) and protein (*P* < 0.001) in the GC tissues compared to normal tissues (Figure 2). Taken together, VGLL3 is upregulated in GC and possibly associated with a worse prognosis.

VGLL3 is a potential prognostic factor for GC
The relationships between VGLL3 levels and the clinico-pathological characteristics of the patients are summarized in Table 1. High levels of VGLL3 were positively correlated with tumor lymph node metastasis (*P* = 0.028) and TNM stage (*P* = 0.041). In addition, the median survival time of the GC patients was significantly lower in the high VGLL3 expression group than in the low expression group (35 mo *vs* 49 mo, *P* = 0.019; Figure 3C). Univariate analysis showed that the VGLL3 expression level (*P* = 0.019) was the only significant prognostic factor of GC, whereas age, gender, differentiation, T stage, lymph node status, TNM stage, and HER2 status did not show any significant results (*P* > 0.05). After including the significant factors in the Cox proportional hazards regression model for multivariate prognostic analysis, we found that VGLL3 expression (*P* = 0.019) was an independent risk factor for GC. ROC curves were plotted to determine the power of the VGLL3 prognostic score in predicting the 3- and 5-year survival, and the AUCs were 0.613 and 0.706, respectively (Figure 3I). We constructed a PPI network of VGLL3 using the STRING database, and identified YAP1, TEAD1, WWTR1, and VGLL4 as upstream of VGLL3, and POU1F1, TEAD3, AKAP11, SYT17, CHMP28, TEAD4, and ERBBE2 (HER2) as downstream proteins (Table 2).
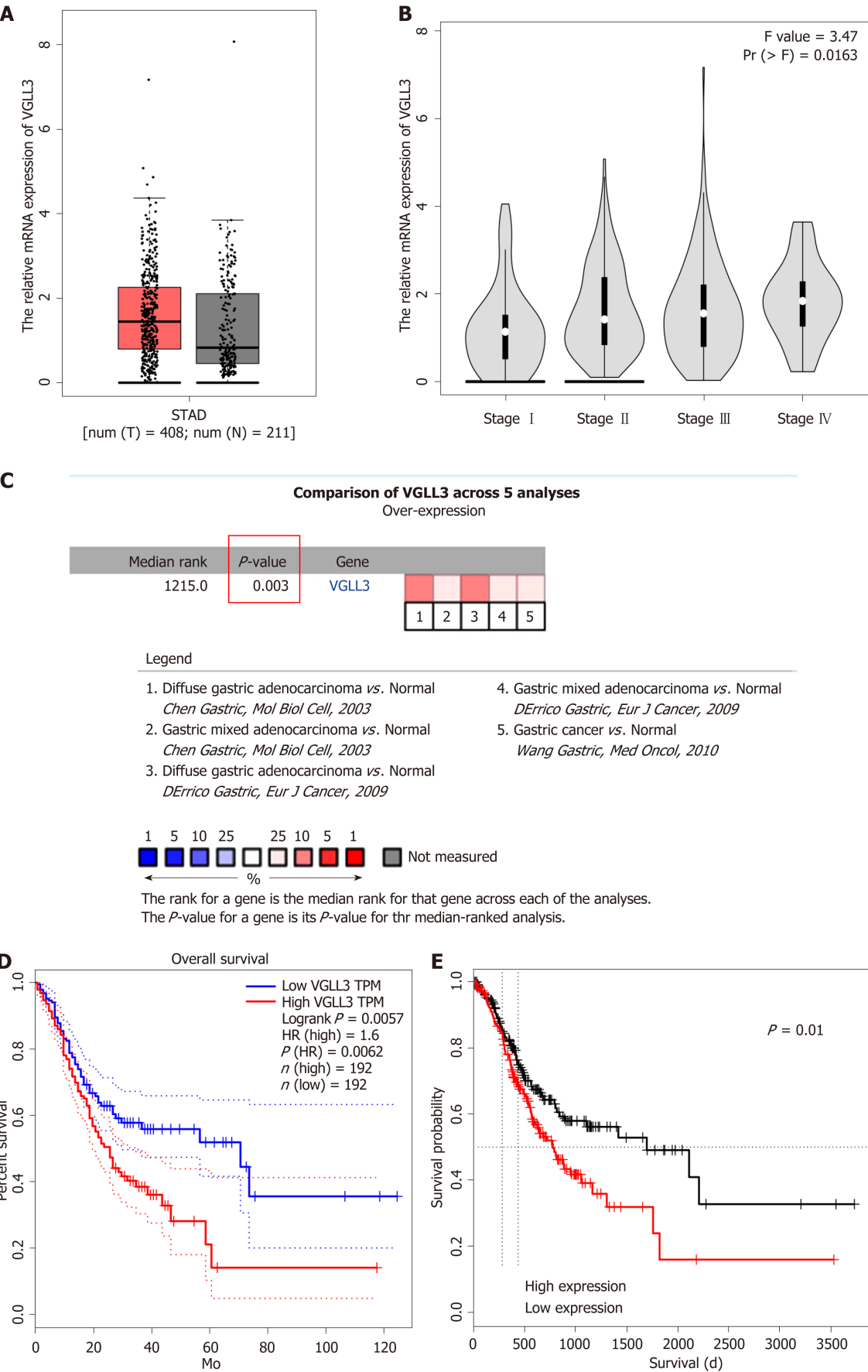
Figure 1 Vestigial like family member 3 mRNA expression levels in gastric cancer tissues determined by integrated analysis of different databases. A and B: Vestigial like family member 3 (VGLL3) expression in gastric cancer and normal gastric tissues (A) and in different TNM stages (B) in the GEPIA database; C: VGLL3 expression reported in the five published studies in the ONCOMINE database; D and E: Kaplan-Meier survival analysis of patients in the GEPIA (D) and ONCOLNC (E) databases stratified by VGLL3 expression status.
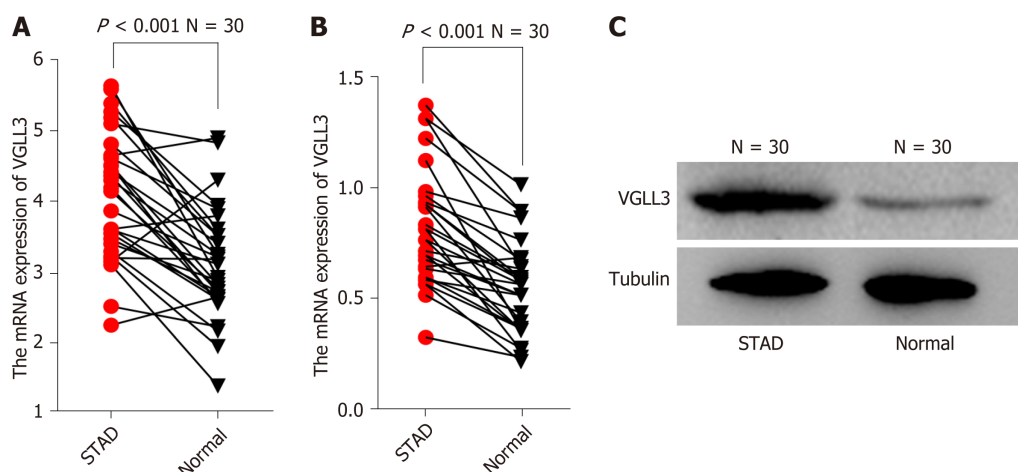
Figure 2 Vestigial like family member 3 mRNA and protein expression levels in gastric cancer. The expression of vestigial like family member 3 mRNA (A) and protein (B and C) in 30 pairs of gastric cancer and normal gastric tissues is shown.

DISCUSSION

GC is the third most common cause of cancer-related deaths worldwide, mainly due to ineffective diagnostic and therapeutic options. It is often detected at the advanced stage, and is highly heterogeneous. Therefore, novel molecular biomarkers for the early diagnosis and treatment of GC are urgently needed. VGLL3 is a member of the vestigial-like family proteins that are related to sex and maturation[18-20], and is reportedly associated with epithelial ovarian cancer and soft tissue sarcoma. Through bioinformatics data mining and integrated analysis, we found that VGLL3 mRNA was not only upregulated in the GC tissues relative to normal gastric tissues, but also significantly associated with advanced TNM stage GC and poor survival outcomes. To validate the *in silico* data, we analyzed the gastric tissues of GC patients, and found abnormally high levels of VGLL3 in the tumor relative to normal tissues. In addition, high *in situ* expression of VGLL3 was correlated with tumor lymph node metastasis, TNM stage, and HER2 mutation, but not with age, gender, differentiation, T stage, or M stage. The patients were stratified into the high and low VGLL3 expression groups, and the former showed a significantly poor survival. Univariate and multivariate analyses further indicated that VGLL3 expression and TNM stage were independent risk factors for the prognosis of GC. Finally, the respective AUCs of the 3- and 5-year survival of the VGLL3-based prognostic model were 0.613 and 0.706, indicating a somewhat imperfect predictive ability. This could be due to the insufficient number of samples and other confounding factors such as the patient's state of mind, economic status, and family environment. Taken together, we identified VGLL3 as a novel prognostic biomarker for GC.

To further elucidate the underlying molecular mechanisms, we analyzed the PPI network of VGLL3 through the STRING database, and found that the Hippo pathway was significantly enriched. In addition, the identified upstream molecules of VGLL3 are YAP1[6], TEAD1, WWTR1, VGLL4, and the downstream molecules are POU1F1, TEAD3, AKAP11, SYT17, CHMP28, and TEAD4. Interestingly, the expression level of VGLL3 was related to ERBBE2 (HER2) mutation, although the relevant mechanistic connection is unclear.

To conclude, VGLL3 is highly expressed in GC and an independent risk factor, and further studies are needed to determine its underlying mechanism. Nevertheless, VGLL3 is a novel biomarker for GC prognosis and a potential therapeutic target for this malignancy.

Table 1 Characteristics of gastric cancer patients according to vestigial like family member 3 expression status

Characteristic	Cases	High expression	Low expression	*P*-value
Age (yr)				
≤60	97	47	50	0.548
>60	75	32	43	
Gender				
Female	101	43	58	0.369
Male	71	36	35	
Differentiation				
Well	84	40	44	0.779
Poor and moderate	88	39	49	
T stage				
T1/2	91	36	55	0.105
T3/4	81	43	38	
N stage				
N0/1	95	36	59	0.028
N2/3	77	43	34	
TNM stage				
I-II	119	48	71	0.041
III-IV	53	31	22	
HER2				
Negative	89	32	57	0.010
Positive	83	47	36	

Table 2 Univariate and multivariate analyses of factors associated with overall survival

Characteristic	Univariate analysis			Multivariate analysis		
	Hazard ratio	95%CI	*P*-value	Hazard ratio	95%CI	*P*-value
Age (yr)	0.83	0.55-1.26	0.389			
Gender (Male *vs* Female)	1.31	0.87-1.96	0.194			
Differentiation (Well *vs* Poor and moderate)	0.81	0.54-1.22	0.304			
T stage (T3/4 *vs* T1/2)	1.16	0.77-1.73	0.484			
N stage (N2/3 *vs* N0/1)	0.94	0.63-1.42	0.778			
TNM stage (III/IV *vs* I/II)	1.27	0.82-1.97	0.283			
HER2 (Positive *vs* Negative)	1.19	0.79-1.8	0.392			
VGLL3 (High *vs* Low)	1.66	1.09-2.55	0.019	1.66	1.09-2.55	0.019

VGLL3: Vestigial like family member 3.
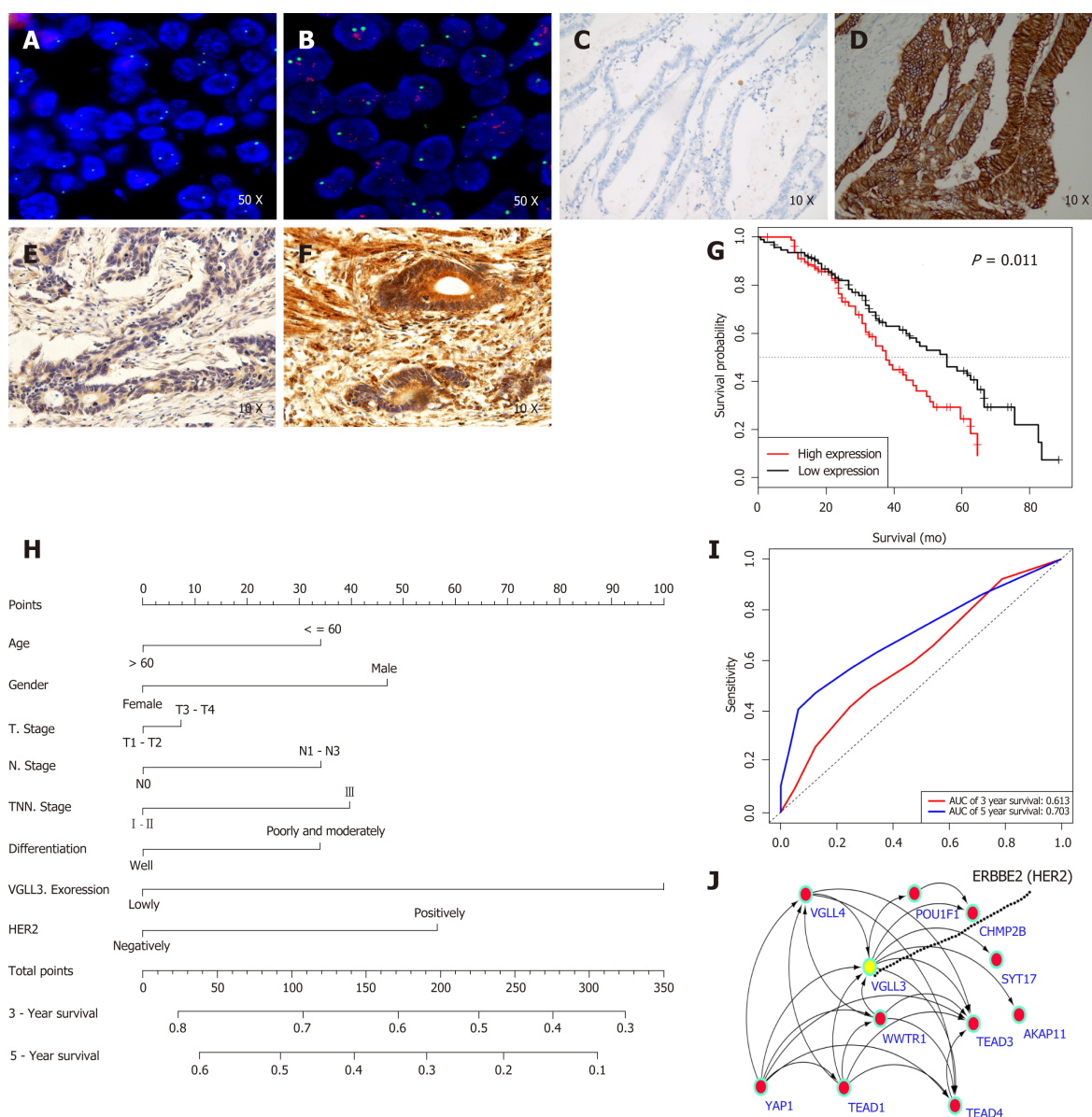
Figure 3 Prognostic value and putative molecular mechanism of vestigial like family member 3 in gastric cancer. A-D: HER2 mutation status detected by FISH (A and C) and IHC (B and D) in gastric cancer (GC) tissues; E and F: *In situ* vestigial like family member 3 (VGLL3) status in GC tissues; G: Kaplan-Meier survival analysis on patients stratified by VGLL3 expression status; H: Prognostic nomogram for gastric cancer based on VGLL3 expression status and clinical features; I: Time-dependent receiver operating characteristic curves for the combination of VGLL3-based prognostic score and clinico-pathological variables; J: Protein-protein interaction network of VGLL3 based on STRING database.

ARTICLE HIGHLIGHTS

Research background

Gastric cancer (GC) is the most prevalent gastrointestinal tract malignancy. The prognosis of GC patients remains relatively poor. It is urgent to explore prognostic markers for GC.

Research motivation

There are insufficient reports about the correlation between VGLL3 and GC.

Research objectives

The aim of the present study was to explore the expression pattern and clinical significance of VGLL3 in GC.

Research methods

It was found that VGLL3 would be a potential prognostic marker by bioinformatics analysis. To validate the *in silico* data, the authors identified the expression of VGLL3 in GC patient samples by immunohistochemistry and evaluated clinical outcomes.

Research results

Analysis of the ONCOMINE and GEPIA databases showed that VGLL3 was significantly up-regulated in GC tissues, and associated with the tumor TNM stage. In addition, the high VGLL3 expression group had a significantly worse prognosis compared to the low expression group, as per both GEPIA and ONCOLNC. The bioinformatics results were validated by the significantly higher VGLL3 mRNA and protein levels in the GC tissues compared to the adjacent normal tissues in a cohort of 30 GC patients. Furthermore, high *in situ* expression of VGLL3 protein was associated with more advanced N and TNM stages and HER2 mutation in a cohort of 172 patients. Kaplan-Meier analysis showed that the high VGLL3 expression group had a worse prognosis compared to the low VGLL3 expression group. Multivariate analysis showed that VGLL3 expression status was an independent risk factor for prognosis. In addition, the prognostic risk model nomogram showed that VGLL3 was the most important indicator, with an AUC of 0.613 for 3-year survival and 0.706 for 5-year survival. Finally, the protein interaction network analysis revealed that VGLL3 is likely involved in the Hippo signaling pathway.

Research conclusions

VGLL3 is overexpressed in GC tissues and associated with a poor prognosis, indicating its potential as a novel prognosis biomarker and therapeutic target for GC.

Research perspectives

The present study suggested that VGLL3 is a novel prognostic biomarker for GC, and the significance of VGLL3 as a promising therapeutic target for GC is highlighted.

REFERENCES

1   **The Lancet**. GLOBOCAN 2018: counting the toll of cancer. *Lancet* 2018; **392**: 985 [PMID: 30264708 DOI: 10.1016/S0140-6736(18)32252-9]

2   **Bray F**, Ferlay J, Soerjomataram I, Siegel RL, Torre LA, Jemal A. Global cancer statistics 2018: GLOBOCAN estimates of incidence and mortality worldwide for 36 cancers in 185 countries. *CA Cancer J Clin* 2018; **68**: 394-424 [PMID: 30207593 DOI: 10.3322/caac.21492]

3   **Siegel RL**, Miller KD, Jemal A. Cancer statistics, 2019. *CA Cancer J Clin* 2019; **69**: 7-34 [PMID: 30620402 DOI: 10.3322/caac.21551]

4   **Gambaro K**, Quinn MC, Wojnarowicz PM, Arcand SL, de Ladurantaye M, Barrès V, Ripeau JS, Killary AM, Davis EC, Lavoie J, Provencher DM, Mes-Masson AM, Chevrette M, Tonin PN. VGLL3 expression is associated with a tumor suppressor phenotype in epithelial ovarian cancer. *Mol Oncol* 2013; **7**: 513-530 [PMID: 23415753 DOI: 10.1016/j.molonc.2012.12.006]

5   **Cody NA**, Shen Z, Ripeau JS, Provencher DM, Mes-Masson AM, Chevrette M, Tonin PN. Characterization of the 3p12.3-pcen region associated with tumor suppression in a novel ovarian cancer cell line model genetically modified by chromosome 3 fragment transfer. *Mol Carcinog* 2009; **48**: 1077-1092 [PMID: 19347865 DOI: 10.1002/mc.20535]

6   **Hélias-Rodzewicz Z**, Pérot G, Chibon F, Ferreira C, Lagarde P, Terrier P, Coindre JM, Aurias A. YAP1 and VGLL3, encoding two cofactors of TEAD transcription factors, are amplified and overexpressed in a subset of soft tissue sarcomas. *Genes Chromosomes Cancer* 2010; **49**: 1161-1171 [PMID: 20842732 DOI: 10.1002/gcc.20825]

7   **Sun X**, Wang T, Zhang C, Ning K, Guan ZR, Chen SX, Hong TT, Hua D. S100A16 is a prognostic marker for colorectal cancer. *J Surg Oncol* 2018; **117**: 275-283 [PMID: 28876468 DOI: 10.1002/jso.24822]

8   **Wang LL**, Chen ZS, Zhou WD, Shu J, Wang XH, Jin R, Zhuang LL, Hoda MA, Zhang H, Zhou GP. Down-regulated GATA-1 up-regulates interferon regulatory factor 3 in lung adenocarcinoma. *Sci Rep* 2017; **7**: 2551 [PMID: 28566697 DOI: 10.1038/s41598-017-02700-5]

9   **Yang S**, Kim CY, Hwang S, Kim E, Kim H, Shim H, Lee I. COEXPEDIA: exploring biomedical hypotheses via co-expressions associated with medical subject headings (MeSH). *Nucleic Acids Res* 2017; **45**: D389-D396 [PMID: 27679477 DOI: 10.1093/nar/gkw868]

10 **Szklarczyk D**, Gable AL, Lyon D, Junge A, Wyder S, Huerta-Cepas J, Simonovic M, Doncheva NT, Morris JH, Bork P, Jensen LJ, Mering CV. STRING v11: protein-protein association networks with increased coverage, supporting functional discovery in genome-wide experimental datasets. *Nucleic Acids Res* 2019; **47**: D607-D613 [PMID: 30476243 DOI: 10.1093/nar/gky1131]

11 **Petrov A**, Beer M, Blome S. Development and validation of a harmonized TaqMan-based triplex real-time RT-PCR protocol for the quantitative detection of normalized gene expression profiles of seven porcine cytokines. *PLoS One* 2014; **9**: e108910 [PMID: 25268123 DOI: 10.1371/journal.pone.0108910]

12 **Sun X**, Wang T, Guan ZR, Zhang C, Chen Y, Jin J, Hua D. FBXO2, a novel marker for metastasis in human gastric cancer. *Biochem Biophys Res Commun* 2018; **495**: 2158-2164 [PMID: 29269301 DOI: 10.1016/j.bbrc.2017.12.097]

13 **Cai X**, Zheng Y, Speck NA. A Western Blotting Protocol for Small Numbers of Hematopoietic Stem Cells. *J Vis Exp* 2018 [PMID: 30199018 DOI: 10.3791/56855]

14 **Wester K**, Wahlund E, Sundström C, Ranefall P, Bengtsson E, Russell PJ, Ow KT, Malmström PU, Busch C. Paraffin section storage and immunohistochemistry. Effects of time, temperature, fixation, and retrieval protocol with emphasis on p53 protein and MIB1 antigen. *Appl Immunohistochem Mol Morphol* 2000; **8**: 61-70 [PMID: 10937051]

15 **Wu J**, Wang F, Liu X, Zhang T, Liu F, Ge X, Mao Y, Hua D. Correlation of IDH1 and B7H3 expression with prognosis of CRC patients. *Eur J Surg Oncol* 2018; **44**: 1254-1260 [PMID: 29871819 DOI: 10.1016/j.ejso.2018.05.005]

16 **Wang Y**, Li J, Xia Y, Gong R, Wang K, Yan Z, Wan X, Liu G, Wu D, Shi L, Lau W, Wu M, Shen F. Prognostic nomogram for intrahepatic cholangiocarcinoma after partial hepatectomy. *J Clin Oncol* 2013; **31**: 1188-1195 [PMID: 23358969 DOI: 10.1200/JCO.2012.41.5984]

17 **Kuang M**, Zheng D, Tao X, Peng Y, Pan Y, Zheng S, Zhang Y, Li H, Yuan C, Zhang Y, Xiang J, Li Y, Chen H, Sun Y. tRNA-based prognostic score in predicting survival outcomes of lung adenocarcinomas. *Int J Cancer* 2019 [PMID: 30838640 DOI: 10.1002/ijc.32250]

18   **Barson NJ**, Aykanat T, Hindar K, Baranski M, Bolstad GH, Fiske P, Jacq C, Jensen AJ, Johnston SE, Karlsson S, Kent M, Moen T, Niemelä E, Nome T, Næsje TF, Orell P, Romakkaniemi A, Sægrov H, Urdal K, Erkinaro J, Lien S, Primmer CR. Sex-dependent dominance at a single locus maintains variation in age at maturity in salmon. *Nature* 2015; **528**: 405-408 [PMID: 26536110 DOI: 10.1038/nature16062]

19   **Tu W**, Wagner EK, Eckert GJ, Yu Z, Hannon T, Pratt JH, He C. Associations between menarche-related genetic variants and pubertal growth in male and female adolescents. *J Adolesc Health* 2015; **56**: 66-72 [PMID: 25287989 DOI: 10.1016/j.jadohealth.2014.07.020]

20   **Liang Y**, Tsoi LC, Xing X, Beamer MA, Swindell WR, Sarkar MK, Berthier CC, Stuart PE, Harms PW, Nair RP, Elder JT, Voorhees JJ, Kahlenberg JM, Gudjonsson JE. A gene network regulated by the transcription factor VGLL3 as a promoter of sex-biased autoimmune diseases. *Nat Immunol* 2017; **18**: 152-160 [PMID: 27992404 DOI: 10.1038/ni.3643]

Retrospective Study

HER2 heterogeneity is a poor prognosticator for HER2-positive gastric cancer

Akio Kaito, Takeshi Kuwata, Masanori Tokunaga, Kohei Shitara, Reo Sato, Tetsuo Akimoto, Takahiro Kinoshita

ORCID number: Akio Kaito (0000-0003-0839-5695); Takeshi Kuwata (0000-0003-0044-953X); Masanori Tokunaga (0000-0002-3183-349X); Kohei Shitara (0000-0001-5196-3630); Reo Sato (0000-0002-2841-0728); Tetsuo Akimoto (0000-0003-0881-1345); Takahiro Kinoshita (0000-0001-7365-8733).

Akio Kaito, Masanori Tokunaga, Reo Sato, Takahiro Kinoshita, Department of Gastric Surgery, National Cancer Center Hospital East, Kashiwa 277-8577, Japan

Akio Kaito, Takeshi Kuwata, Department of Pathology and Clinical Laboratories, National Cancer Center Hospital East, Kashiwa 277-8577, Japan

Akio Kaito, Kohei Shitara, Department of Gastrointestinal Oncology, National Cancer Center Hospital East, Kashiwa 277-8577, Japan

Takeshi Kuwata, Kohei Shitara, Exploratory Oncology Research & Clinical Trial Center (EPOC), National Cancer Center Hospital East, Kashiwa 277-8577, Japan

Tetsuo Akimoto, Juntendo University Graduate School of Medicine, Tokyo 163-8001, Japan

Tetsuo Akimoto, Department of Radiation Oncology, National Cancer Center Hospital East, Kashiwa 277-8577, Japan

Corresponding author: Takeshi Kuwata, MD, PhD, Doctor, Department of Pathology and Clinical Laboratories, National Cancer Center Hospital East, 6-5-1, Kashiwanoha, Kashiwa 277-8577, Japan. tkuwata@east.ncc.go.jp
Telephone: +81-4-71331111
Fax: +81-4-71300190

Abstract

BACKGROUND
The clinical significance of intratumoral human epidermal growth factor receptor 2 (HER2) heterogeneity is unclear for HER2-positive gastric cancer, although it has been reported to be a significant prognosticator for HER2-positive breast cancer, which has received trastuzumab-based chemotherapy.

AIM
To clarify the clinical significance of intratumoral HER2 heterogeneity for HER2-positive gastric cancer, which has received trastuzumab-based chemotherapy.

METHODS
Patients with HER2-positive unresectable or metastatic gastric cancer who received trastuzumab-based chemotherapy as a first line treatment were included. The patients were classified into two groups according to their intratumoral HER2 heterogeneity status examined by immunohistochemistry (IHC) on endoscopic biopsy specimens before treatment, and their clinical

response to chemotherapy and survival were compared.

RESULTS
A total of 88 patients were included in this study, and HER2 heterogeneity was observed in 23 (26%) patients (Hetero group). The overall response rate was significantly better in patients without HER2 heterogeneity (Homo group) (Homo *vs* Hetero: 79.5% *vs* 35.7%, P = 0.002). Progression-free survival of trastuzumab-based chemotherapy was significantly better in the Homo group (median, 7.9 *vs* 2.5 mo, HR: 1.905, 95%CI: 1.109-3.268). Overall survival was also significantly better in the Homo group (median survival time, 25.7 *vs* 12.5 mo, HR: 2.430, 95%CI: 1.389-4.273). Multivariate analysis revealed IHC HER2 heterogeneity as one of the independent poor prognostic factors (HR: 3.115, 95%CI: 1.610-6.024).

CONCLUSION
IHC of HER2 heterogeneity is the pivotal predictor for trastuzumab-based chemotherapy. Thus, HER2 heterogeneity should be considered during the assessment of HER2 expression.

Key words: Human epidermal growth factor receptor 2; Heterogeneity; Trastuzumab; Gastric cancer; Chemotherapy

Core tip: Although intratumoral human epidermal growth factor receptor 2 (HER2) heterogeneity has been reported as an important predictor of trastuzumab-based chemotherapy for HER2-positive breast cancer, the clinical significance of HER2 heterogeneity for gastric cancer had been unclear. We defined intratumoral HER2 heterogeneity as biopsy specimens were taken from two or more different portions of the tumor that showed different HER2 positivity by immunohistochemistry, and HER2 heterogeneity based on this definition was a pivotal poor predictor of tumor shrinkage and poor prognosticator. Thus, intratumoral HER2 heterogeneity should be included in the assessment of HER2 positivity.

INTRODUCTION

Human epidermal growth factor receptor 2 (HER2) was introduced as a predictive biomarker for the treatment of gastric cancer along with trastuzumab[1], and trastuzumab was subsequently recommended to be administered for HER2-positive gastric cancer as a molecular target drug[2,3]. Assessment of HER2 expression was performed by immunohistochemistry (IHC) and in-situ hybridization (ISH), where positive HER2 expression was defined as 3+ on IHC or 2+ on IHC with ISH positive[4]. The strong HER2 intensity of IHC 3+ was reported as a better prognostic factor for HER2-positive gastric cancer treated with trastuzumab-based chemotherapy[1].

The frequency of intratumoral HER2 heterogeneity was reported as 45%-79% by IHC and 23%-54% by ISH for HER2-positive gastric cancers[5-8], which were more frequent than that with HER2-positive breast cancers[9]. Although intratumoral HER2 heterogeneity was reported to be one of the poor predictors for treatment response and poor prognosticator for patients with HER2-positive breast cancer who received trastuzumab-based chemotherapy[10,11], the clinical significance of intratumoral HER2 heterogeneity for HER2 positive gastric cancer treated with trastuzumab has not been well investigated. Recently, Wakatsuki *et al*[12] reported that intratumoral HER2 heterogeneity had a negative survival benefit for patients with surgically resected HER2-positive gastric cancer. However, HER2 assessment before treatment is usually based on the endoscopic biopsy specimen for metastatic gastric cancer, and the

clinical significance of intratumoral HER2 heterogeneity for biopsy specimen is still unknown.

The aim of this study was to clarify the clinical significance of intratumoral HER2 heterogeneity for HER2 positive gastric cancer treated with trastuzumab-based chemotherapy by evaluation of biopsy specimens.

MATERIALS AND METHODS

Patients and data collection

Patients with histologically confirmed HER2-positive metastatic or unresectable adenocarcinoma of the stomach or gastroesophageal junction cancer who received trastuzumab-based chemotherapy as first-line treatment at our hospital between July 2011 and December 2017 were included in this study. The patients were classified into two groups according to intratumoral HER2 heterogeneity, and their clinico-pathological findings, clinical responses, progression-free survival (PFS) and overall survival (OS) were compared. Furthermore, the predictive factor for clinical response and prognostic factor were analyzed using multivariable analyses. We extracted clinicopathological findings such as age, sex, tumor diameter, tumor location, macroscopic tumor type, tumor markers, Eastern Cooperative Oncology Group performance score, TNM stage, metastatic site, chemotherapy regimen, histological type of endoscopic biopsy specimen, HER2 positivity, survival outcomes from our prospectively collected database and medical records. Biopsied specimens stained by IHC were reviewed and assessed for their intratumoral HER2 heterogeneity by two pathologists (A.K. and T.K.).

Patients who received gastrectomy prior to chemotherapy and patients who received chemotherapy without trastuzumab were excluded. Clinical response was evaluated according to new response evaluation criteria in solid tumors (RECIST guideline ver. 1.1) for patients with measurable metastatic lesions[13]. The onset of PFS was defined as the start of chemotherapy, and tumor progression was evaluated by imaging techniques and physical examination. Tumor progression dates for patients who received radical gastrectomy after good clinical response to chemotherapy were defined as the date of first recurrence after surgery. Tumor staging of gastric and EGJ type III tumor followed the Union for International Cancer Control TNM classification of 7th edition for gastric cancer, and tumor staging of EGJ type II tumor followed that for esophageal cancer[14]. Tumor histology was assessed according to the Japanese Classification of Gastric Carcinoma[15], with well and moderately differentiated adenocarcinoma and papillary adenocarcinoma classified as differentiated type, and poorly differentiated adenocarcinoma, signet ring cell carcinoma, and mucinous carcinoma classified as undifferentiated type.

Treatment schedules

Chemotherapy regimens were capecitabine or 5-fluorouracil plus cisplatin with trastuzumab (XPT/FPT) before September 2015 and S-1 plus oxaliplatin with trastuzumab (SOXT) after October 2015. XPT or FPT regimens were followed a ToGA study regimen[1]. SOXT regimen was followed according to the G-SOX study regimen in combination with trastuzumab; oxaliplatin was administered intravenously 100 mg/m^2 on day 1, while S-1 was administered orally 80 mg/m^2 for 14 d followed by a 7-d rest. This schedule was repeated every 3 wk. Trastuzumab was given by intravenous infusion at a dose of 8 mg/kg on day 1 of the first cycle, followed by 6 mg/kg every 3 wk until disease progression[16].

HER2 immunohistochemistry and fluorescence in situ hybridization

All endoscopic biopsy samples were fixed in neutral buffered 10% formalin. Formalin-fixed paraffin-embedded tumor samples were examined for HER2 using IHC and fluorescence in situ hybridization (FISH) when the HER2 score was 2+.

HER2 IHC analyses were performed using the PATHWAY anti-HER-2/neu (4B5) rabbit monoclonal primary antibody (Ventana Medical Systems, Tucson, AZ, United States). IHC HER2 scoring by biopsy specimen was performed as described in the ToGA study[1]. In brief, tumor cell clusters of at least five positive cells with complete basolateral or lateral membranous reactivity was considered HER2-positive for endoscopic biopsy samples irrespective of percentage of tumor cells stained. Tumor cells with strong membranous reactivity were scored 3+, and those with moderate reactivity were scored 2+. HER2 FISH analyses were performed at SRL (Tokyo, Japan) using the Path Vysion HER2 DNA Probe kit (Vysis, Downers Grove, IL, United States). When the ratio of HER2 signals to chromosome 17 centromere signals was 2.0 or greater, the gene was considered amplified (*i.e.*, FISH-positive). HER2 positivity

was defined as IHC score 3+ or IHC score 2+ and FISH positivity, because these criteria were considered to be indications for using trastuzumab by a subset analysis of the ToGA trial[1,3].

Assessment of intratumoral HER2 heterogeneity

Assessment of intratumoral HER2 heterogeneity was conducted on patients who underwent assessment of HER2 positivity from two or more different portions of the same tumor, and three or more biopsy specimens were obtained from each portion. Those patients whose HER2 assessment was performed from only one portion were excluded for further examination. Intratumoral HER2 homogeneity was defined as every portion being HER2-positive by IHC, and if any portion of the tumor was HER2-negative, the tumor was defined as intratumoral HER2 heterogeneity (Figure 1).

Statistical analysis

The baseline characteristics of each group were compared using the χ^2 test or the Fisher's exact test for categorical data, and $P < 0.05$ was considered statistically significant. The median OS rate and PFS rate were estimated by the Kaplan-Meier method. Independent prognostic factors for OS and PFS were evaluated by univariate and multivariable analysis of Cox proportional hazard model and presented as hazard ratio and 95% confidence interval (CI). Evaluated factors in multivariable analysis were those that were significant by univariate analysis. Data were censored on May 31, 2019. All statistical analyses were performed using SPSS Statistics 20 (SPSS Inc., Chicago, IL, United States).

This study was approved by the Institutional Review Board of the National Cancer Center, Japan (IRB file No. 2017-164, approval date: Oct. 11, 2017).

RESULTS

A total of 776 patients with metastatic or unresectable adenocarcinoma of the stomach or gastroesophageal junction were treated in this study period, and HER2 positivity was observed in 127 cases (16.3%). Of these, patients who received upfront gastrectomy before chemotherapy ($n = 5$) or chemotherapy without trastuzumab ($n = 21$), and patients who underwent HER2 assessment from only one portion of the tumor ($n = 13$) were excluded (Figure 2). Finally, a group of 88 patients were evaluated for intratumoral HER2 heterogeneity, in which HER2 homogeneity was observed in 65 (Homo group) and HER2 heterogeneity was observed in 23 (Hetero group) patients.

Patients' backgrounds are shown in Table 1. Intratumoral HER2 heterogeneity was significantly more frequently observed in macroscopically type 3 and type 4 patients than other types, and in patients with IHC 2+ compared to IHC 3+. Other background characteristics such as age, sex, performance status, TNM stage, metastatic site and chemotherapeutic regimens were not significantly different between the groups. Besides, the number of biopsy sites for HER2 assessment was not significantly different, *i.e.*, those numbers more than three was 46% for Homo group and 57% for Hetero group ($P = 0.393$). Waterfall plot for tumor shrinkage and clinical responses for the patients with measurable metastatic lesions ($n = 58$) of both groups are shown in Figure 3. Overall response rate (complete response and partial response) was 79.5% in the Homo group, which was considerably better than that in the Hetero group (35.7%, $P = 0.002$). Kaplan-Meier curves of OS and PFS in both groups are shown in Figure 4. At the time of the analysis, the median follow-up was 18.5 mo (range, 4.7-88.0 mo). The median survival time (MST) in the Hetero group was 12.5 mo, which was considerably worse than that in the Homo group (25.7 mo, HR; 2.430, 95%CI: 1.389-4.273). Median PFS time in the Hetero group was 2.9 mo, which was also significantly worse than that in the Homo group (7.9 mo, HR: 2.000, 95%CI: 1.203-3.333). Multivariate analysis revealed IHC HER2 heterogeneity as one of the independent poor prognostic factors for OS (HR: 3.115, 95%CI: 1.610-6.024) and PFS (HR: 2.123, 95%CI: 1.225-3.676) (Table 2). Undifferentiated histological type (HR: 2.612, 95%CI: 1.388-4.916), number of non-curative factors (HR: 2.252, 95%CI: 1.113-4.553), clinical nodal status (HR: 2.119, 95%CI: 1.165-3.855), hepatic metastasis (HR: 2.084, 95%CI: 1.076-4.036) and HER2 score (2+) (HR: 2.008, 95%CI: 1.094-3.690) were also extracted as independent poor prognostic factors for OS. We compared survival results by the combination of each HER2 score (2+ or 3+) and HER2 heterogeneity (homogeneity or heterogeneity). MST for the Homo group with HER2 3+ was longest (28.2 mo), followed by Hetero group with 3+ (14.6 mo) and Homo group with 2+ (12.9 mo). Hetero group with 2+ had the worst prognosis (MST: 7.2 mo) (Figure 5).
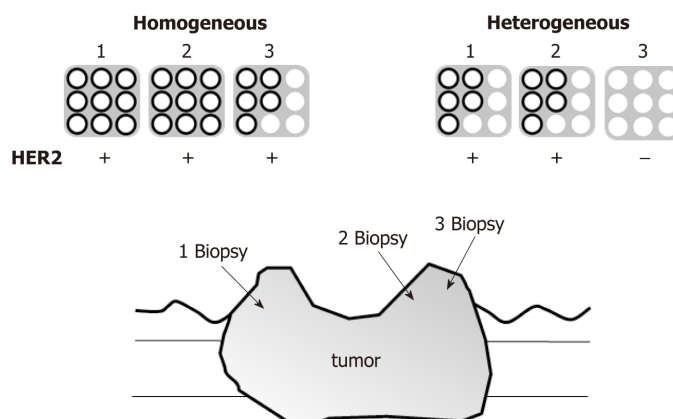
Figure 1 Assessment of intratumoral HER2 heterogeneity. Assessment of intratumoral HER2 heterogeneity was conducted from at least two different portions of the same tumor, and more than three biopsy specimens were obtained from each portion. Homogeneity was defined by all assessed portions showing HER2 positivity, and heterogeneity was defined as a tumor with any portions that did not show HER2 positivity. HER2: Human epidermal growth factor receptor 2.

DISCUSSION

In this study, we examined the effect of intratumoral HER2 heterogeneity by IHC for HER2-positive advanced gastric cancer treated with trastuzumab-based chemotherapy on their therapeutic responses and survival. Intratumoral HER2 heterogeneity by IHC evaluated by biopsy specimen before treatment was one of the independent poor predictive factors for tumor shrinkage and a poor prognosticator.

The definition of intratumoral HER2 heterogeneity for HER2-positive gastric cancer has not been well established. The cut-off value between HER2 homogeneity and heterogeneity of HER2 positive tumor cells varies from 50% to 100% for surgically resected specimens[5,6,12,17] and 30% to 100% for endoscopic biopsy specimens[7,8,18]. The clinical significance of intratumoral HER2 heterogeneity for HER2-positive gastric cancer treated with trastuzumab has not been well investigated, and there have been only a few studies conducted to date. Wakatsuki *et al*[12] defined the cut-off value of HER2 heterogeneity as 100% and reported that HER2 homogeneity group had significantly longer PFS (HR: 0.11, 95%CI: 0.03-0.41) and OS (HR: 0.18, 95%CI: 0.06-0.72). However, their study included only 28 patients who received trastuzumab-based chemotherapy after upfront gastrectomy for resectable gastric cancer, not metastatic cancer.

In post hoc exploratory analyses of the ToGA trial, the proportion of HER2-positive tumor cells in more than 30% of biopsy specimens could not be extracted as a predictive factor for good response to trastuzumab-based chemotherapy[18]. Yagi *et al*[8] recently reported that intratumoral HER2 heterogeneity was a poor predictor for trastuzumab-based chemotherapy and a poor prognosticator with the cut-off value of 100% from the median number of four biopsy specimens. Our current study selected patients in whom HER2 positivity could be assessed from more than two different portions of the tumor, and we defined HER2 heterogeneity as any of those tumor portions being negative for HER2. The number of biopsy specimens examined for each patient in our current study was more than six (*i.e.*, each of the three fragments were obtained from two or more different portions). Although Yagi *et al*[8] adopted the overall proportion of HER2-positive tumor cells to evaluate intratumoral HER2 heterogeneity, we employed the standard criteria of HER2 positivity generally performed in clinical diagnosis, *i.e.*, tumor cell cluster of at least five positive cells with complete basolateral or lateral membranous reactivity. According to our simple definition of intratumoral HER2 heterogeneity, the treatment outcomes were definitively different between the HER2 homogeneity group and heterogeneity group.

The stain intensity for IHC was reported as a significant prognostic factor for HER2-positive gastric cancer in the ToGA trial. The OS was significantly longer in IHC 3+ patients than IHC 2+ patients (MST: 17.9 and 12.3 mo)[1]. Assessment of HER2 positivity for endoscopic biopsy specimen in the ToGA trial was established without consideration of intratumor HER2 heterogeneity, which is now commonly adopted worldwide[4]. Prognostic significance of stain intensity for IHC was also explored in combination with heterogeneity for IHC in our current study. MST of Homo-IHC 3+ patients was 28.2 mo, which was much better than MST of IHC 3+ patients (17.9 mo) in the ToGA trial. Hetero-IHC 3+ and Homo-IHC 2+ patients had comparable
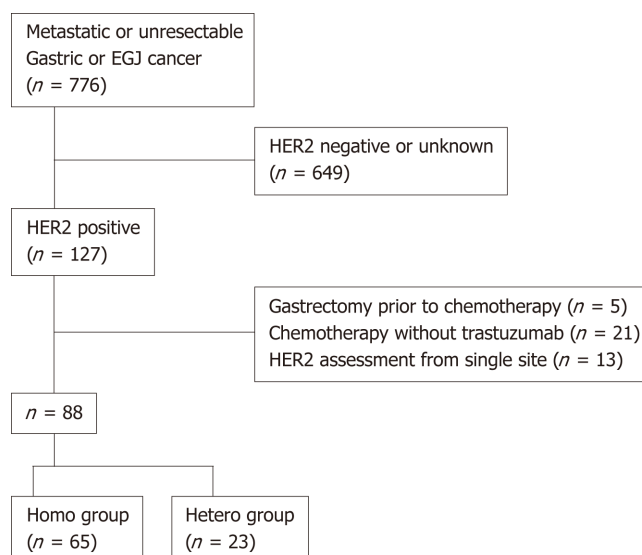
Figure 2 Patient flow chart. HER2 positivity was observed in 127 (16.3%) of 776 patients with metastatic or unresectable adenocarcinoma. After exclusion of 39 patients for the listed reasons, HER2 homogeneity was observed in 65 (Homo group) and HER2 heterogeneity was observed in 23 (Hetero group). HER2: Human epidermal growth factor receptor 2.

survival (14.6 and 12.9 mo), while Hetero-IHC 2+ patients had poorer survival (7.2 mo) compared to IHC 2+ patients (12.3 mo) in the ToGA trial. These results suggest that intratumoral HER2 heterogeneity should be included in the assessment of HER2 positivity in addition to the stain intensity for IHC, and patients with Homo-IHC 3+ might be the most responsive to further anti-HER2 agents. The survival benefits for anti-HER2 drugs such as lapatinib or pertuzumab in combination with trastuzumab and adjuvant therapy of trastuzumab or trastuzumab beyond progression have been demonstrated for breast cancers[19-22]. However, the efficacy of those anti-HER2 agents has not been shown for gastric cancers, and intratumoral HER2 heterogeneity may be one of the reasons for the difference of these results between breast and gastric cancers[23,24].

Although the intrinsic mechanism underlying the correlation between HER2 heterogeneity and poor efficacy of trastuzumab-based chemotherapy is still unclear, chemo-resistance can be one of the main reasons for the treatment failure. Fabi *et al*[25] reported that the discordances of HER2 positivity between primary and metastatic lesions may be a possible cause of chemo-resistance of trastuzumab for metastatic breast cancers. Park *et al*[26] reported these discordances between primary and metastatic lesions could also be observed in HER2-positive gastric cancers, and HER2 heterogeneity of primary lesions existed in such cases with discordances of HER2 positivity. Another explanation for the poor efficacy of trastuzumab might be genomic alterations. Pietrantonio *et al*[27] reported that chemo-resistance against trastuzumab was more frequently observed in patients with genomic alternations including *EGFR*/*MET*/*KRAS*/*PI3K*/*PTEN* mutations than those without. They stated such genomic mutations were correlated with IHC 2+, *i.e.*, the existence of HER2 heterogeneity.

Our study has several limitations. First, concordance of intratumoral HER2 heteroge-neity between endoscopic biopsy specimen and whole tumor tissues was not investigated in the current study. The concordance of HER2 positivity between biopsy specimens and surgically resected specimens was reported to be 80%-91% for IHC 3+ and 25%-57% for IHC 2+ patients[28-30], thus the interpretation of HER2 heterogeneity for IHC 2+ patients must be made with care. In breast cancer, similar results have been reported comparing core needle biopsy specimens and surgically resected specimens[31], and repeat testing or reflex testing using an alternative assay (IHC or ISH) are recommended for IHC equivocal cases[32]. Secondly, there was no common standard of adequate numbers and portions for the assessment of intratumoral HER2 heterogeneity. In this study, the assessment of intratumoral HER2 heterogeneity was performed from at least two portions of the tumor. Ohno *et al*[33] reported that HER2 positivity was different in different tumor regions, *i.e.*, the frequency of HER2 positivity in the biopsy specimen from the superficial spreading portion, ulcer mound, and mass portion was as high as 90% to 100%, while these from ulcer bed was only 45% due to the presence of concomitant necrotic tissues and associated

Table 1 Patients' demographic information

	Homo, *n* = 65	Hetero, *n* = 23	*P*-value
Age in yr	69 (42-81)	67.0 (45-82)	
< 70	34 (52%)	15 (65%)	0.284
≥ 70	31 (48%)	8 (35%)	
Sex			
Male	43 (66%)	18 (78%)	0.279
Female	22 (34%)	5 (22%)	
ECOG performance status			
0	61 (94%)	20 (87%)	0.152
1	2 (3%)	3 (13%)	(0 *vs* ≥ 1)
2	2 (3%)	0	
Macroscopic type			
1	7 (11%)	1 (5%)	0.008
2	28 (43%)	4 (17%)	(type 1/2 *vs* 3/4)
3	23 (35%)	16 (69%)	
4	7 (11%)	2 (9%)	
Tumor location			
Upper	27 (42%)	11 (48%)	0.601
Middle / lower	38 (58%)	12 (52%)	
Histology			
Well differentiated	48 (74%)	14 (61%)	0.31
Poorly differentiated	15 (23%)	9 (39%)	
Other/unknown	2 (3%)	0	
T status			
cT2	2 (3%)	0	0.267
cT3	17 (26%)	4 (17%)	(cT2/3 *vs* cT4)
cT4	46 (71%)	19 (83%)	
N status			
cN0	5 (8%)	2 (9%)	0.748
cN1	5 (8%)	1 (4%)	(≤cN2 *vs* cN3)
cN2	32 (49%)	11 (48%)	
cN3	23 (35%)	9 (39%)	
Number of non-curative factor			
0	1 (1%)	1 (4%)	0.404
1	32 (49%)	13 (57%)	(≤1 *vs* >1)
2	29 (45%)	9 (39%)	
>2	3 (5%)	0	
Non-curative factor			
Lymph node	34 (52%)	10 (43%)	
Peritoneal	22 (34%)	6 (26%)	
Hepatic	27 (42%)	12 (52%)	
Other	9 (14%)	1 (5%)	
Number of HER2 assessment			
2	35 (54%)	10 (43%)	0.393
3	27 (42%)	13 (57%)	
>3	3 (4%)	0	
HER2 score			
3+	53 (82%)	10 (43%)	0.001
2+	12 (18%)	13 (57%)	
Upfront chemotherapy			
SOXT	33 (50%)	12 (52%)	
XPT	25 (37%)	7 (30%)	
SPT	3 (5%)	2 (9%)	

FPT	1 (2%)	2 (9%)
FLT	1 (2%)	
PTXT	1 (2%)	
DCST	1 (2%)	

ECOG: Eastern Cooperative Oncology Group; SOXT: S-1 oxaliplatin capecitabine trastuzumab; XPT: capecitabine cisplatin trastuzumab; SPT: S-1 cisplatin trastuzumab; FPT: 5-Fluorouracil cisplatin trastuzumab; FLT: 5-Fluorouracil leucovorin trastuzumab; PTXT: Paclitaxel trastuzumab; DCST: Docetaxel cisplatin S-1 trastuzumab.

inflammation[34]. These results suggest that the assessment of HER2 heterogeneity should be based on biopsy specimens taken from the appropriate portion of the tumor. Thirdly, this study did not include the intratumoral heterogeneity of *HER2* gene amplification. Intratumoral heterogeneity of *HER2* gene amplification has been reported to be a significant prognostic factors for metastatic or resectable advanced breast cancers[9,11]. The significance of intratumoral heterogeneity of *HER2* gene amplification should also be clarified in further investigations.

In conclusion, intratumoral HER2 heterogeneity by IHC was a significant predictor of clinical response and a poor prognosticator for trastuzumab-based chemotherapy. Thus, intratumoral HER2 heterogeneity would be useful to further stratify patients with HER2-positive gastric cancer, and thus should be taken into account in future clinical trials.

**Table 2 Prognostic factors for overall survival and progression-free survival**

| Covariates | Overall survival | | | | Progression-free survival | | | |
| | Univariate analysis | | Multivariable analysis | | Univariate analysis | | Multivariable analysis | |
	HR (95%CI)	*P*-value	HR (95%CI)	*P*-value	HR (95%CI)	*P*-value	HR (95%CI)	*P*-value
Age, ≥ 80 *vs* < 80	1.31 (0.473-3.625)	0.604			1.138 (0.492-2.633)	0.762		
Sex, female *vs* male	1.057 (0.621-1.798)	0.838			1.005 (0.615-1.642)	0.985		
Macroscopic type, type 3,4 *vs* 1,2	1.72 (1.027-2.881)	0.039			1.641 (1.037-2.598)	0.034		
Clinical tumor depth, cT4 *vs* ≤ cT3	1.838 (0.992-3.405)	0.053			1.408 (0.826-2.401)	0.209		
Clinical nodal status, cN3 *vs* ≤ cN2	2.026 (1.184-3.466)	0.01	2.119 (1.165-3.855)	0.014	1.691 (1.056-2.708)	0.029	1.622 (0.951-2.764)	0.076
Histology, undiff. *vs* diff.	1.884 (1.090-3.255)	0.023	2.612 (1.388-4.916)	0.003	1.643 (1.031-2.618)	0.037	1.902 (1.117-3.237)	0.018
HER2 score, 2+ *vs* 3+	2.331 (1.353-4.016)	0.002	2.008 (1.094-3.690)	0.024	1.828 (1.110-3.012)	0.018	1.612 (0.940-2.770)	0.083
HER2 heterogeneity, hetero *vs* homo	2.439 (1.389-4.274)	0.002	3.115 (1.610-6.024)	0.001	2 (1.203-3.333)	0.008	2.123 (1.225-3.676)	0.007
No. of non-curative factors, ≥ 2 *vs* 1	1.904 (1.138-3.186)	0.014	2.252 (1.113-4.553)	0.024	1.875 (1.185-2.965)	0.007	1.871 (1.023-3.424)	0.042
M1, lymph node	0.687 (0.410-1.150)	0.154			0.568 (0.358-0.902)	0.017		
M1, peritoneal	1.207 (0.699-2.086)	0.5			1.327 (0.828-2.127)	0.24		
M1, hepatic	1.902 (1.141-3.173)	0.014	2.084 (1.076-4.036)	0.029	1.974 (1.244-3.132)	0.004	2.053 (1.151-3.664)	0.015

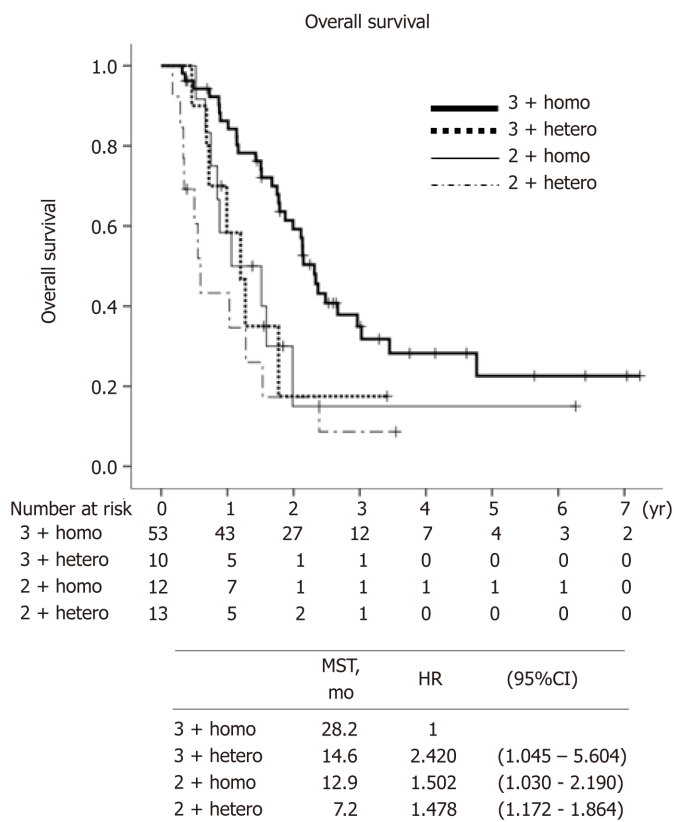HER2: Human epidermal growth factor receptor 2; HR: Hazard ratio.
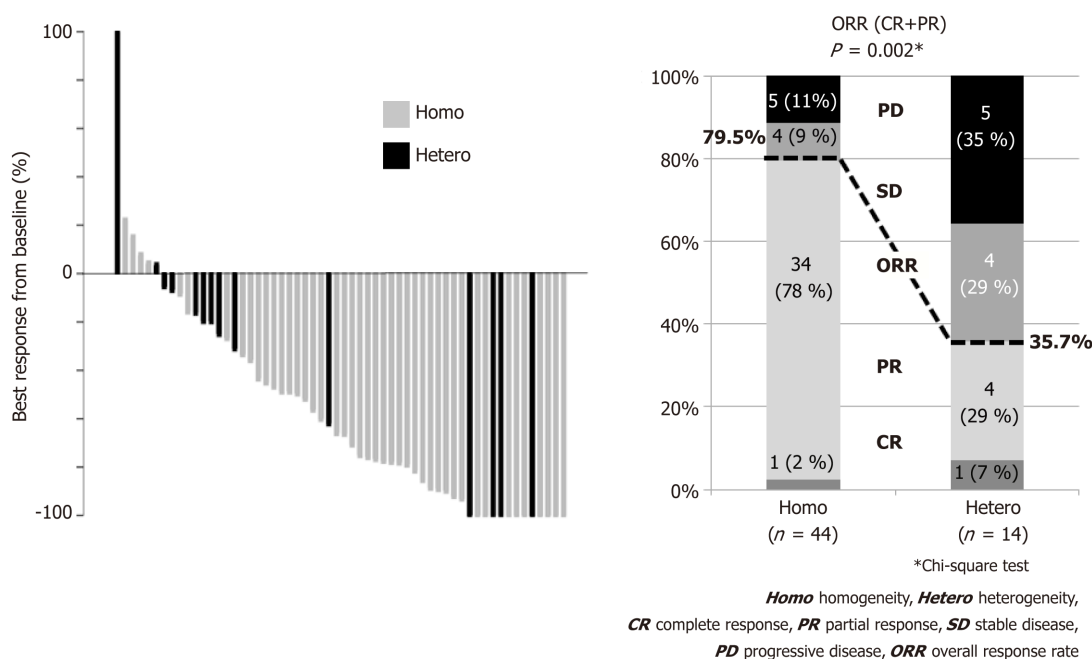
Figure 3 Clinical response for patients with or without intratumoral human epidermal growth factor receptor 2 heterogeneity. Tumor shrinkage (left) and clinical response (right) was evaluated by RECIST ver. 1.1 for 58 patients who have measurable metastatic lesions. ORR was 79.5% in the Homo group, which was significantly higher than that in the Hetero group (35.7%, *P* = 0.002). CR: Complete response; PR: Partial response; SD: Stable disease; PD: Progressive disease; ORR: Overall response rate (CR plus PR).
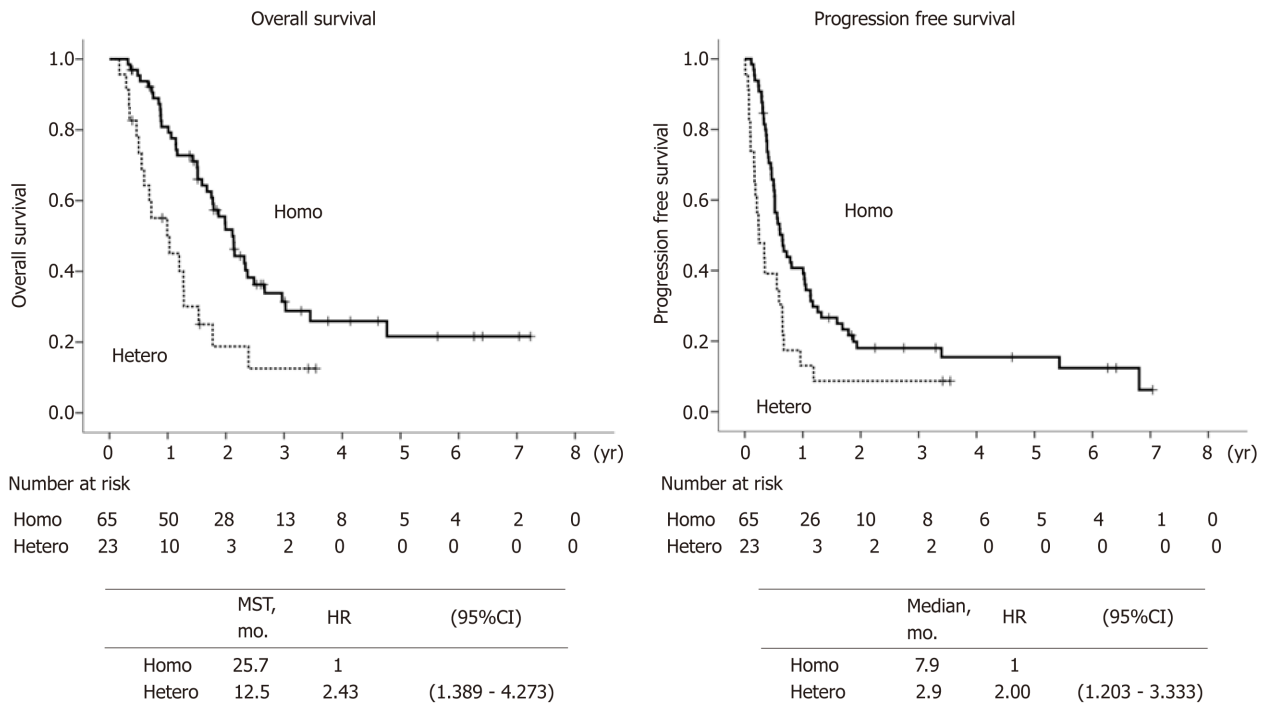
Figure 4 OS and PFS with or without intratumoral human epidermal growth factor receptor 2 heterogeneity. Kaplan-Meier curves of OS (left) and PFS (right) in both groups was shown with the median follow-up of 18.5 mo (range, 4.7-88.0 mo). MST and median PST in the Hetero group were significantly worse than those in the Homo group. MST: Median survival time; HR: Hazard ratio; CI: Confidence interval; OS: Overall survival; PFS: Progression-free survival.

Figure 5 Overall survival by HER2 score and intratumoral HER2 heterogeneity. MST for the Homo group with HER2 3+ was longest (28.2 mo), followed by Hetero group with 3+ (14.6 mo), Homo group with 2+ (12.9 mo) and Hetero group with 2+ (7.2 mo). MST: Median survival time; HR: Hazard ratio; CI: Confidence interval; HER2: Human epidermal growth factor receptor 2.

ARTICLE HIGHLIGHTS

Research background

Human epidermal growth factor receptor 2 (HER2) was introduced as a predictive biomarker for the treatment of gastric cancer along with trastuzumab, and the strong HER2 intensity of immunohistochemistry (IHC) 3+ was reported as a better prognostic factor for HER2-positive gastric cancer treated with trastuzumab-based chemotherapy. Intratumoral HER2 heterogeneity for HER2-positive gastric cancers was reported to be more frequent than in HER2-positive breast cancers. Although intratumoral HER2 heterogeneity was reported to be one of the poor predictors for the treatment response and poor prognosticator for patients with HER2-positive breast cancer who received trastuzumab-based chemotherapy, the clinical significance of intratumoral HER2 heterogeneity for HER2-positive gastric cancer treated with trastuzumab has not been well investigated. Furthermore, even the definitions of HER2 heterogeneity for HER2-positive gastric cancer have not been established. In this study, we established the definition of intratumoral HER2 heterogeneity and clarified the clinical significance of HER2 heterogeneity for HER2-positive gastric cancer.

Research motivation

HER2 heterogeneity may be a pivotal predictor for the efficacy of trastuzumab-based chemotherapy. Authors have previously reported that intratumoral HER2 heterogeneity had a negative survival benefit for patients with surgically resected HER2-positive gastric cancer. However, HER2 assessment before treatment is usually based on endoscopic biopsy specimen for metastatic gastric cancer, and the clinical significance of intratumoral HER2 heterogeneity for biopsy specimen is still unknown. If these clinical significances are clarified, HER2 heterogeneity might be introduced to the assessment of HER2 positivity for gastric cancer in the future.

Research objectives

The aim of this study was to clarify the clinical significance of intratumoral HER2 heterogeneity for HER2-positive gastric cancer treated with trastuzumab-based chemotherapy by evaluation of biopsy specimens.

Research methods

Patients with HER2-positive metastatic or unresectable adenocarcinoma of the stomach or gastroesophageal junction who received trastuzumab-based chemotherapy as first-line treatment at our hospital were included. The patients were classified into two groups (Homo- and Hetero-group) according to intratumoral HER2 heterogeneity, and their clinicopathological findings, clinical responses, progression-free survival (PFS) and overall survival (OS) were compared. Furthermore, the predictive factor for clinical response and prognostic factor were analyzed using multivariable analyses. Assessment of intratumoral HER2 heterogeneity was conducted on patients who underwent assessment of HER2 positivity from two or more different portions of the same tumor, and three or more biopsy specimens were obtained from each portion. Those patients whose HER2 assessment was performed from only one portion were excluded. We defined intratumoral HER2 homogeneity as every portion of the tumor being HER2-positive by IHC, and any portion of the tumor staining negative for HER2 was defined as intratumoral HER2 heterogeneity.

Research results

A total of 776 patients with metastatic or unresectable adenocarcinoma of the stomach or gastroesophageal junction were treated in the study period, and HER2 positivity was observed in 127 patients (16.3%). Intratumoral HER2 heterogeneity was significantly more frequently observed in macroscopically type 3 and type 4 patients than other types, and patients with IHC 2+ than IHC 3+. Tumor shrinkage and clinical responses for the patients with measurable metastatic lesions were evaluated, and overall response rate (complete response and partial response) was considerably better in the Homo group than in the Hetero group. Median survival time in the Hetero group was 12.5 mo, which was considerably worse than that in the Homo group (25.7 mo, HR; 2.430, 95%CI: 1.389-4.273). Median PFS time in the Hetero group was 2.9 mo, which was also significantly worse than that in the Homo group (7.9 mo, HR: 2.000, 95%CI: 1.203-3.333). Multivariate analysis revealed IHC HER2 heterogeneity as one of the independent poor prognostic factors for OS (HR: 3.115, 95%CI: 1.610-6.024) and PFS (HR: 2.123, 95%CI: 1.225-3.676).

Research conclusions

In this study, we examined the effect of intratumoral HER2 heterogeneity by IHC for HER2-positive advanced gastric cancer treated with trastuzumab-based chemotherapy on their therapeutic responses and survival. Intratumoral HER2 heterogeneity by IHC evaluated by biopsy specimen before treatment was one of the independent poor predictive factors for tumor shrinkage and a poor prognosticator. Our current study selected patients in whom HER2 positivity could be assessed from more than two different portions of the tumor, and we newly defined HER2 heterogeneity as any of those portions of the tumor that did not show HER2 positivity. We employed the standard criteria of HER2 positivity generally performed in clinical diagnosis, *i.e.*, tumor cell cluster of at least five positive cells with complete basolateral or lateral membranous reactivity. According to our simple definition of intratumoral HER2 heterogeneity, the treatment outcomes were definitively different between the HER2 homogeneity group and heterogeneity group. Assessment of HER2 positivity for endoscopic biopsy specimen in the ToGA trial was established without consideration of intratumor HER2 heterogeneity. Our

current study suggests that the combination of heterogeneity and IHC might be beneficial to predict the efficacy of trastuzumab-based chemotherapy.

Research perspectives

HER2 heterogeneity is a pivotal predictor for the efficacy of HER2-positive gastric cancers. However, there are still some problems that need to be solved in the future. First, concordance of intratumoral HER2 heterogeneity between endoscopic biopsy specimen and whole tumor tissues has not been investigated in the current study. Secondly, there was no common standard of adequate numbers and portions for the assessment of intratumoral HER2 heterogeneity. Thirdly, this study did not include the intratumoral heterogeneity of HER2 gene amplification. Intratumoral heterogeneity of *HER2* gene amplification has been reported to be one of the significant prognostic factors for metastatic or resectable advanced breast cancers. The significance of intratumoral heterogeneity of *HER2* gene amplification should also be clarified by further investigations. The survival benefits for anti-HER2 drugs such as lapatinib or pertuzumab in combination with trastuzumab and adjuvant therapy of trastuzumab or trastuzumab beyond progression were demonstrated for breast cancers. However, the efficacy of those anti-HER2 agents had not been proven for gastric cancers, and intratumoral HER2 heterogeneity may be considered as one of the reasons for the difference of these results between breast and gastric cancers. If more detailed clinical significance of intratumoral HER2 heterogeneity is solved in the future, anti-HER2 drugs other than trastuzumab can be adopted, and treatment outcomes of HER2-positive gastric cancers would be improved.

REFERENCES

1 **Bang YJ**, Van Cutsem E, Feyereislova A, Chung HC, Shen L, Sawaki A, Lordick F, Ohtsu A, Omuro Y, Satoh T, Aprile G, Kulikov E, Hill J, Lehle M, Rüschoff J, Kang YK; ToGA Trial Investigators. Trastuzumab in combination with chemotherapy versus chemotherapy alone for treatment of HER2-positive advanced gastric or gastro-oesophageal junction cancer (ToGA): a phase 3, open-label, randomised controlled trial. *Lancet* 2010; **376**: 687-697 [PMID: 20728210 DOI: 10.1016/S0140-6736(10)61121-X]

2 **Japanese Gastric Cancer Association**. Japanese gastric cancer treatment guidelines 2014 (ver. 4). *Gastric Cancer* 2017; **20**: 1-19 [PMID: 27342689 DOI: 10.1007/s10120-016-0622-4]

3 **Ajani JA**, D'Amico TA, Almhanna K, Bentrem DJ, Chao J, Das P, Denlinger CS, Fanta P, Farjah F, Fuchs CS, Gerdes H, Gibson M, Glasgow RE, Hayman JA, Hochwald S, Hofstetter WL, Ilson DH, Jaroszewski D, Johung KL, Keswani RN, Kleinberg LR, Korn WM, Leong S, Linn C, Lockhart AC, Ly QP, Mulcahy MF, Orringer MB, Perry KA, Poultsides GA, Scott WJ, Strong VE, Washington MK, Weksler B, Willett CG, Wright CD, Zelman D, McMillian N, Sundar H. Gastric Cancer, Version 3.2016, NCCN Clinical Practice Guidelines in Oncology. *J Natl Compr Canc Netw* 2016; **14**: 1286-1312 [PMID: 27697982]

4 **Bartley AN**, Washington MK, Colasacco C, Ventura CB, Ismaila N, Benson AB, Carrato A, Gulley ML, Jain D, Kakar S, Mackay HJ, Streutker C, Tang L, Troxell M, Ajani JA. HER2 Testing and Clinical Decision Making in Gastroesophageal Adenocarcinoma: Guideline From the College of American Pathologists, American Society for Clinical Pathology, and the American Society of Clinical Oncology. *J Clin Oncol* 2017; **35**: 446-464 [PMID: 28129524 DOI: 10.1200/JCO.2016.69.4836]

5 **Lee HE**, Park KU, Yoo SB, Nam SK, Park DJ, Kim HH, Lee HS. Clinical significance of intratumoral HER2 heterogeneity in gastric cancer. *Eur J Cancer* 2013; **49**: 1448-1457 [PMID: 23146959 DOI: 10.1016/j.ejca.2012.10.018]

6 **Kurokawa Y**, Matsuura N, Kimura Y, Adachi S, Fujita J, Imamura H, Kobayashi K, Yokoyama Y, Shaker MN, Takiguchi S, Mori M, Doki Y. Multicenter large-scale study of prognostic impact of HER2 expression in patients with resectable gastric cancer. *Gastric Cancer* 2015; **18**: 691-697 [PMID: 25224659 DOI: 10.1007/s10120-014-0430-7]

7 **Ahn S**, Ahn S, Van Vrancken M, Lee M, Ha SY, Lee H, Min BH, Lee JH, Kim JJ, Choi S, Jung SH, Choi MG, Lee JH, Sohn TS, Bae JM, Kim S, Kim KM. Ideal number of biopsy tumor fragments for predicting HER2 status in gastric carcinoma resection specimens. *Oncotarget* 2015; **6**: 38372-38380 [PMID: 26460823 DOI: 10.18632/oncotarget.5368]

8 **Yagi S**, Wakatsuki T, Yamamoto N, Chin K, Takahari D, Ogura M, Ichimura T, Nakayama I, Osumi H, Shinozaki E, Suenaga M, Fujisaki J, Ishikawa Y, Yamaguchi K, Namikawa K, Horiuchi Y. Clinical significance of intratumoral HER2 heterogeneity on trastuzumab efficacy using endoscopic biopsy specimens in patients with advanced HER2 positive gastric cancer. *Gastric Cancer* 2019; **22**: 518-525 [PMID: 30328533 DOI: 10.1007/s10120-018-0887-x]

9 **Lee HJ**, Kim JY, Park SY, Park IA, Song IH, Yu JH, Ahn JH, Gong G. Clinicopathologic Significance of the Intratumoral Heterogeneity of HER2 Gene Amplification in HER2-Positive Breast Cancer Patients Treated With Adjuvant Trastuzumab. *Am J Clin Pathol* 2015; **144**: 570-578 [PMID: 26386078 DOI: 10.1309/AJCP51HCGPOPWSCY]

10 **Seol H**, Lee HJ, Choi Y, Lee HE, Kim YJ, Kim JH, Kang E, Kim SW, Park SY. Intratumoral heterogeneity of HER2 gene amplification in breast cancer: its clinicopathological significance. *Mod Pathol* 2012; **25**: 938-948 [PMID: 22388760 DOI: 10.1038/modpathol.2012.36]

11 **Lee HJ**, Seo AN, Kim EJ, Jang MH, Suh KJ, Ryu HS, Kim YJ, Kim JH, Im SA, Gong G, Jung KH, Park IA, Park SY. HER2 heterogeneity affects trastuzumab responses and survival in patients with HER2-positive metastatic breast cancer. *Am J Clin Pathol* 2014; **142**: 755-766 [PMID: 25389328 DOI: 10.1309/AJCPIRL4GUVGK3YX]

12 **Wakatsuki T**, Yamamoto N, Sano T, Chin K, Kawachi H, Takahari D, Ogura M, Ichimura T, Nakayama I, Osumi H, Matsushima T, Suenaga M, Shinozaki E, Hiki N, Ishikawa Y, Yamaguchi K. Clinical impact of intratumoral HER2 heterogeneity on trastuzumab efficacy in patients with HER2-positive gastric cancer. *J Gastroenterol* 2018; **53**: 1186-1195 [PMID: 29633013 DOI: 10.1007/s00535-018-1464-0]

13 **Eisenhauer EA**, Therasse P, Bogaerts J, Schwartz LH, Sargent D, Ford R, Dancey J, Arbuck S, Gwyther S, Mooney M, Rubinstein L, Shankar L, Dodd L, Kaplan R, Lacombe D, Verweij J. New response evaluation criteria in solid tumours: revised RECIST guideline (version 1.1). *Eur J Cancer* 2009; **45**: 228-

247 [PMID: 19097774 DOI: 10.1016/j.ejca.2008.10.026]

14   **Sobin LH**, Gospodarowicz MK, Wittekind C. TNM classification of malignant tumors, 7th ed. Wiley-Blackwell, A John Wiley & Sons, Ltd. 2009

15   **Japanese Gastric Cancer Association**. Japanese classification of gastric carcinoma: 3rd English edition. *Gastric Cancer* 2011; **14**: 101-112 [PMID: 21573743 DOI: 10.1007/s10120-011-0041-5]

16   **Koizumi W**, Takiuchi H, Yamada Y, Boku N, Fuse N, Muro K, Komatsu Y, Tsuburaya A. Phase II study of oxaliplatin plus S-1 as first-line treatment for advanced gastric cancer (G-SOX study). *Ann Oncol* 2010; **21**: 1001-1005 [PMID: 19875759 DOI: 10.1093/annonc/mdp464]

17   **Motoshima S**, Yonemoto K, Kamei H, Morita M, Yamaguchi R. Prognostic implications of HER2 heterogeneity in gastric cancer. *Oncotarget* 2018; **9**: 9262-9272 [PMID: 29507688 DOI: 10.18632/onco-target.24265]

18   **Van Cutsem E**, Bang YJ, Feng-Yi F, Xu JM, Lee KW, Jiao SC, Chong JL, López-Sanchez RI, Price T, Gladkov O, Stoss O, Hill J, Ng V, Lehle M, Thomas M, Kiermaier A, Rüschoff J. HER2 screening data from ToGA: targeting HER2 in gastric and gastroesophageal junction cancer. *Gastric Cancer* 2015; **18**: 476-484 [PMID: 25038874 DOI: 10.1007/s10120-014-0402-y]

19   **Johnston SRD**, Hegg R, Im SA, Park IH, Burdaeva O, Kurteva G, Press MF, Tjulandin S, Iwata H, Simon SD, Kenny S, Sarp S, Izquierdo MA, Williams LS, Gradishar WJ. Phase III, Randomized Study of Dual Human Epidermal Growth Factor Receptor 2 (HER2) Blockade With Lapatinib Plus Trastuzumab in Combination With an Aromatase Inhibitor in Postmenopausal Women With HER2-Positive, Hormone Receptor-Positive Metastatic Breast Cancer: ALTERNATIVE. *J Clin Oncol* 2018; **36**: 741-748 [PMID: 29244528 DOI: 10.1200/JCO.2017.74.7824.]

20   **Swain SM**, Baselga J, Kim SB, Ro J, Semiglazov V, Campone M, Ciruelos E, Ferrero JM, Schneeweiss A, Heeson S, Clark E, Ross G, Benyunes MC, Cortés J; CLEOPATRA Study Group. Pertuzumab, trastuzumab, and docetaxel in HER2-positive metastatic breast cancer. *N Engl J Med* 2015; **372**: 724-734 [PMID: 25693012 DOI: 10.1056/NEJMoa1413513]

21   **Gianni L**, Eiermann W, Semiglazov V, Lluch A, Tjulandin S, Zambetti M, Moliterni A, Vazquez F, Byakhov MJ, Lichinitser M, Climent MA, Ciruelos E, Ojeda B, Mansutti M, Bozhok A, Magazzù D, Heinzmann D, Steinseifer J, Valagussa P, Baselga J. Neoadjuvant and adjuvant trastuzumab in patients with HER2-positive locally advanced breast cancer (NOAH): follow-up of a randomised controlled superiority trial with a parallel HER2-negative cohort. *Lancet Oncol* 2014; **15**: 640-647 [PMID: 24657003 DOI: 10.1016/S1470-2045(14)70080-4]

22   **von Minckwitz G**, du Bois A, Schmidt M, Maass N, Cufer T, de Jongh FE, Maartense E, Zielinski C, Kaufmann M, Bauer W, Baumann KH, Clemens MR, Duerr R, Uleer C, Andersson M, Stein RC, Nekljudova V, Loibl S. Trastuzumab beyond progression in human epidermal growth factor receptor 2-positive advanced breast cancer: a german breast group 26/breast international group 03-05 study. *J Clin Oncol* 2009; **27**: 1999-2006 [PMID: 19289619 DOI: 10.1200/JCO.2008.19.6618]

23   **Tabernero J**, Hoff PM, Shen L, Ohtsu A, Shah MA, Cheng K, Song C, Wu H, Eng-Wong J, Kim K, Kang YK. Pertuzumab plus trastuzumab and chemotherapy for HER2-positive metastatic gastric or gastro-oesophageal junction cancer (JACOB): final analysis of a double-blind, randomised, placebo-controlled phase 3 study. *Lancet Oncol* 2018; **19**: 1372-1384 [PMID: 30217672 DOI: 10.1016/S1470-2045(18)30481-9]

24   **Satoh T**, Xu RH, Chung HC, Sun GP, Doi T, Xu JM, Tsuji A, Omuro Y, Li J, Wang JW, Miwa H, Qin SK, Chung IJ, Yeh KH, Feng JF, Mukaiyama A, Kobayashi M, Ohtsu A, Bang YJ. Lapatinib plus paclitaxel versus paclitaxel alone in the second-line treatment of HER2-amplified advanced gastric cancer in Asian populations: TyTAN--a randomized, phase III study. *J Clin Oncol* 2014; **32**: 2039-2049 [PMID: 24868024 DOI: 10.1200/JCO.2013.53.6136]

25   **Fabi A**, Di Benedetto A, Metro G, Perracchio L, Nisticò C, Di Filippo F, Ercolani C, Ferretti G, Melucci E, Buglioni S, Sperduti I, Papaldo F, Cognetti F, Mottolese M. HER2 protein and gene variation between primary and metastatic breast cancer: significance and impact on patient care. *Clin Cancer Res* 2011; **17**: 2055-2064 [PMID: 21307144 DOI: 10.1158/1078-0432.CCR-10-1920]

26   **Park SR**, Park YS, Ryu MH, Ryoo BY, Woo CG, Jung HY, Lee JH, Lee GH, Kang YK. Extra-gain of HER2-positive cases through HER2 reassessment in primary and metastatic sites in advanced gastric cancer with initially HER2-negative primary tumours: Results of GASTric cancer HER2 reassessment study 1 (GASTHER1). *Eur J Cancer* 2016; **53**: 42-50 [PMID: 26693898 DOI: 10.1016/j.ejca.2015.09.018]

27   **Pietrantonio F**, Fucà G, Morano F, Gloghini A, Corso S, Aprile G, Perrone F, De Vita F, Tamborini E, Tomasello G, Gualeni AV, Ongaro E, Busico A, Giommoni E, Volpi CC, Laterza MM, Corallo S, Priscifandaro M, Antista M, Pellegrinelli A, Castagnoli L, Pupa SM, Pruneri G, de Braud F, Giordano S, Cremolini C, Di Bartolomeo M. Biomarkers of Primary Resistance to Trastuzumab in HER2-Positive Metastatic Gastric Cancer Patients: the AMNESIA Case-Control Study. *Clin Cancer Res* 2018; **24**: 1082-1089 [PMID: 29208673 DOI: 10.1158/1078-0432.CCR-17-2781]

28   **Yoshida H**, Yamamoto N, Taniguchi H, Oda I, Katai H, Kushima R, Tsuda H. Comparison of HER2 status between surgically resected specimens and matched biopsy specimens of gastric intestinal-type adenocarcinoma. *Virchows Arch* 2014; **465**: 145-154 [PMID: 24889042 DOI: 10.1007/s00428-014-1597-3]

29   **Fazlollahi L**, Remotti HE, Iuga A, Yang HM, Lagana SM, Sepulveda AR. HER2 Heterogeneity in Gastroesophageal Cancer Detected by Testing Biopsy and Resection Specimens. *Arch Pathol Lab Med* 2018; **142**: 516-522 [PMID: 28782986 DOI: 10.5858/arpa.2017-0039-OA]

30   **Kanayama K**, Imai H, Yoneda M, Hirokawa YS, Shiraishi T. Significant intratumoral heterogeneity of human epidermal growth factor receptor 2 status in gastric cancer: A comparative study of immunohistochemistry, FISH, and dual-color in situ hybridization. *Cancer Sci* 2016; **107**: 536-542 [PMID: 26752196 DOI: 10.1111/cas.12886]

31   **Tsuda H**, Kurosumi M, Umemura S, Yamamoto S, Kobayashi T, Osamura RY. HER2 testing on core needle biopsy specimens from primary breast cancers: interobserver reproducibility and concordance with surgically resected specimens. *BMC Cancer* 2010; **10**: 534 [PMID: 20925963 DOI: 10.1186/1471-2407-10-534]

32   **Wolff AC**, Hammond ME, Hicks DG, Dowsett M, McShane LM, Allison KH, Allred DC, Bartlett JM, Bilous M, Fitzgibbons P, Hanna W, Jenkins RB, Mangu PB, Paik S, Perez EA, Press MF, Spears PA, Vance GH, Viale G, Hayes DF; American Society of Clinical Oncology; College of American Pathologists. Recommendations for human epidermal growth factor receptor 2 testing in breast cancer: American Society of Clinical Oncology/College of American Pathologists clinical practice guideline update. *J Clin Oncol* 2013; **31**: 3997-4013 [PMID: 24101045 DOI: 10.1200/JCO.2013.50.9984]

33   **Oono Y**, Kuwata T, Takashima K, Yoda Y, Ikematsu H, Shitara K, Kinoshita T, Yano T. Clinicopathological features and endoscopic findings of HER2-positive gastric cancer. *Surg Endosc* 2018; **32**: 3964-3971 [PMID: 29500656 DOI: 10.1007/s00464-018-6138-8]

34   **Gullo I**, Grillo F, Molinaro L, Fassan M, De Silvestri A, Tinelli C, Rugge M, Fiocca R, Mastracci L. Minimum biopsy set for HER2 evaluation in gastric and gastro-esophageal junction cancer. *Endosc Int Open* 2015; **3**: E165-E170 [PMID: 26135662 DOI: 10.1055/s-0034-1391359]

Case Control Study

Changes in corneal endothelial cell density in patients with primary open-angle glaucoma

Zi-Yan Yu, Ling Wu, Bo Qu

ORCID number: Zi-Yan Yu (0000-0003-1091-428X); Ling Wu (0000-0003-3057-6302); Bo Qu (0000-0002-2261-8464).

Author contributions: All authors helped to perform the research; Qu B drafted the manuscript; Yu ZY and Wu L reviewed the published articles and analyzed the data; All authors read and approved the final manuscript.

Institutional review board statement: This study was reviewed and approved by the Ethics Committee of the 4th Affiliated Hospital of China Medical University, No. EC-2019-KS-018.

Informed consent statement: Written informed consent was obtained from all of the patients.

Conflict-of-interest statement: The authors have stated that they have no conflicts of interest.

Data sharing statement: The datasets of this study are readily available from the corresponding author upon reasonable request.

STROBE statement: The guidelines of the STROBE statement have been adopted.

Zi-Yan Yu, Bo Qu, Department of Ophthalmology, 4th Affiliated Hospital of China Medical University, Eye hospital of China Medical University, Key Laboratory of Lens Research of Liaoning Province, Shenyang 110005, Liaoning Province, China

Ling Wu, Department of Ophthalmology, the 4th people's Hospital of Shenyang, Shenyang 110005, Liaoning Province, China

Corresponding author: Bo Qu, MD, PhD, Associate Professor, Dr., Department of Ophthalmology, 4th affiliated Hospital of China Medical University, Eye Hospital of China Medical University, Key Laboratory of Lens Research of Liaoning Province, Shenyang 110005, Liaoning Province, China. dolphinemu@foxmail.com
Telephone: +86-130-66660193
Fax: +86-024-62037227

Abstract

BACKGROUND
Glaucoma is a group of diseases characterized by a specific pattern of optic nerve neuropathy and retinopathy. Increasing evidence demonstrates glaucoma associated corneal endothelium loss. Direct-compression mechanism due to elevated intraocular pressure (IOP), cell toxicity after long term exposure to preservatives and glaucoma surgery have been reported to be the possible mechanism. Herein, we compare the specular endothelial microscopy in primary open-angle glaucoma (POAG) patients and healthy controls of the same age group to observe the corneal endothelium changes and the correlations to the mean IOP in a Chinese case control study.

AIM
To investigate corneal endothelial cell density in Chinese patients with POAG.

METHODS
A case control study was performed on 60 eyes of 60 patients with POAG. Exclusion criteria included history of corneal diseases, intraocular diseases, contact lens use, ocular trauma or surgery (including intraocular surgery and laser treatment), congenital abnormalities or systemic diseases such as diabetes. Intraocular pressure was measured using Goldmann tonometry. Indirect specular microscopy (TOPCON SP-2000P) was performed on central corneas and endothelial images were acquired. Endothelial cell density, area and cell counts were analyzed.

RESULTS

Endothelial cell density was 2959 ± 236 cells/mm^2 in healthy controls and 2757 ± 262 cells/mm^2 in patients with POAG. The POAG eyes had significantly lower endothelial cell density compared to healthy control eyes ($P < 0.001$). In the POAG group, endothelial cell density was 2686 ± 233 cells/mm^2 in the patients receiving medication and 2856 ± 272 cells/mm^2 in the untreated subgroup. The eyes receiving medication had significantly lower endothelial cell density compared to untreated eyes. There was a negative correlation between cell density and mean IOP ($r = -0.286$, $P = 0.004$), positive correlation between the average cell area and mean IOP ($r = 0.228$, $P = 0.022$), maximum cell area and mean IOP ($r = 0.218$, $P = 0.029$) and minimum cell area and mean IOP ($r = 0.290$, $P = 0.003$). The percentage of hexagonal cells was not correlated with mean IOP.

CONCLUSION
Patients with POAG have lower corneal endothelial cell density than healthy controls of the same age. This may be attributed to mechanical damage from elevated IOP and toxicity of glaucoma medications.

Key words: Corneal endothelium; Primary open angle glaucoma; Intraocular pressure

Core tip: Loss of corneal endothelial cells have been reported in primary open-angle glaucoma (POAG) patients. Elevated intraocular pressure, cell toxicity after long-term exposure to preservatives and glaucoma surgery have been reported to be possible mechanisms for endothelial damage. In this study, we aimed to document the corneal endothelial changes and their correlations with mean intraocular pressure between POAG patients and normal controls. We found that the corneal endothelial cell density in POAG patients is decreased and the average endothelial cell area is increased compared with those in healthy controls. High intraocular pressure and anti-glaucoma medication in POAG may be the main causes of corneal endothelial cell damage.

INTRODUCTION

The corneal endothelial monolayer maintains corneal clarity by actively regulating stromal hydration through its barrier and pump functions. Corneal endothelial cells (CECs) have limited proliferative capacity *in vivo*[1,2], thus damage to the corneal endothelium is irreversible. Loss of CECs occurs as a consequence of intraocular surgery, trauma or diseases such as diabetes and glaucoma[3-8]. At the early stage of endothelial damage, neighboring cells spread and/or migrate to compensate for the cell loss, which results in an increase in cell size and/or alteration of cell shape. Progression of cell loss further compromises corneal transparency and causes corneal edema, bullous keratopathy and impaired visual acuity.

Glaucoma is a group of diseases characterized by a specific pattern of optic nerve neuropathy and retinopathy[6,7,9]. There is increasing evidence of glaucoma-associated corneal endothelial changes. Loss of CECs has been reported in various types of glaucoma such as primary angle-closure glaucoma, primary open-angle glaucoma (POAG) and some types of secondary glaucoma[7,9-15]. Endothelial cell loss is attributed to both glaucoma itself and treatment that lowers intraocular pressure (IOP). A direct-compression mechanism due to elevated IOP has been proposed in CEC loss in acute angle-closure glaucoma[11,16]. In addition, cell toxicity after long-term exposure to preservatives in ocular hypotensive drugs is considered another possible mechanism for endothelial damage[13,17]. Moreover, endothelial cell loss caused by glaucoma surgery has been reported in patients after application of antiproliferative medications in filtration surgery and aqueous shunt implantation[18-21].

In this study, we aimed to document the corneal endothelial changes and their correlations with mean IOP by comparing specular endothelial microscopy in patients

of similar age with and without glaucoma.

MATERIALS AND METHODS

Study subjects
Case control study. We recruited 60 POAG patients (32 male, 28 female; mean age 63 ± 13 years, age range 50-80 years) who visited the Glaucoma Division at the Fourth Affiliated Hospital, China Medical University between February and March 2019 and 60 age-matched healthy controls (28 male, 32 female; mean age 61 ± 12 years, age range 50–80 years). We retrospectively analyzed with regard to their pre-treatment characteristics. There was no significant difference of age between the two groups. Only one eye from each patient or healthy control was analyzed. All study procedures adhered to the Declaration of Helsinki for research involving human participants. The exclusion criteria included: previous ocular (including laser peripheral iridotomy), orbital or palpebral surgery; previous ocular trauma; previous or present contact lens use; other ocular diseases (such as corneal endothelial dystrophy, intraocular inflammation and infection) that could affect the corneal endothelium; and systemic diseases (such as diabetes and congenital abnormalities) that could affect the corneal endothelium.

Specular microscopy
Indirect specular microscopy (SP-2000P; TOPCON, Tokyo, Japan) was performed on each subject. Images were captured from the central cornea and analyzed using IMAGEnet 2000 software (TOPCON). Endothelial cell density (ECD), percentage of hexagonal cells, average cell area, maximum cell area, minimum cell area, standard deviation of cell area (SD) and coefficient of variation in cell area were determined. All examinations were performed by the same examiner.

IOP evaluation
The IOP of all subjects was measured using Goldmann tonometry every 2 h from 08:00 to 18:00 h. The average of all measurements was determined and used for analysis.

Statistical analysis
Statistical analysis was performed using SPSS version 19.0 (SPSS, Chicago, IL, United States). The unpaired Student's *t* test was used to compare the means between normal subjects and patients with POAG. The Chi-square test was applied to the comparison between untreated patients and patients receiving ophthalmic medication. Correlation between IOP and each characteristic of CECs was assessed by Pearson's correlation coefficient. Data are presented as mean ± SD and the significance level was set at 0.05.

RESULTS

Endothelial cell characteristics of healthy eyes and POAG eyes
ECD was significantly lower in patients with POAG (2757 ± 262 cells/mm^2) compared to the control group (2959 ± 236 cells/mm^2). The average cell area was significantly increased in glaucoma patients (364.37 ± 34.05 μm^2) compared with the control group (322.23 ± 54.69 μm^2). Consistently, glaucoma patients exhibited increased maximum, minimum and SD of cell area. There were no significant differences in the coefficient of variation of cell area and percentage of hexagonal cells between the two groups (Table 1, Figure 1).

The 60 POAG patients were further divided into two subgroups, untreated patients (*n* = 25) and patients receiving ophthalmic medications (*n* = 35) at the time of the study. No significant difference in age and gender was found between the subgroups. The patients receiving medication had significantly lower ECD (2686 ± 233 cells/mm^2) compared to the untreated subgroup (2856 ± 272 cells/mm^2). Both subgroups had lower cell densities compared to the controls; however, only the difference between patients receiving medication and healthy controls was significant. The maximum, minimum and SD of cell area and percentage of hexagonal cells did not differ between the subgroups (Table 2).

Correlations between endothelial cell characteristics and IOP
The mean IOP in POAG patients (24 ± 5 mmHg) was significantly higher than that in healthy controls (15 ± 2 mmHg). There was a negative correlation between ECD and mean IOP (*r* = −0.286, *P* = 0.004). Positive correlations were found between the

Table 1 Endothelial cell characteristics of study groups

	POAG, *n* = 60	Control, *n* = 60	*P* value
CD, cells/mm²	2757 ± 262	2959 ± 236	< 0.001
SD, μm²	153.87 ± 29.13	140.65 ± 19.53	0.008
CV, %	43.48 ± 7.71	43.06 ± 5.65	0.749
6A, %	49.45 ± 8.23	49.08 ± 9.11	0.831
AVE, μm²	364.37 ± 34.05	322.23 ± 54.69	< 0.001
MAX, μm²	963.52 ± 214.04	827.57 ± 198.18	0.002
MIN, μm²	78.10 ± 16.59	69.37 ± 17.33	0.013

POAG: primary open-angle glaucoma; CD: Cell density; SD: Standard deviation; CV: Coefficient of variation; 6A: Percentage of hexagonal cells; AVE: Average cell area; MAX: Maximum cell area; MIN: Minimum cell area.

average cell area and mean IOP (r = 0.228, P = 0.022), maximum cell area and mean IOP (r = 0.218, P = 0.029) and minimum cell area and mean IOP (r = 0.290, P = 0.003). The percentage of hexagonal cells was not correlated with mean IOP (Figure 2).

DISCUSSION

In Asian populations, primary angle-closure glaucoma is the major type of glaucoma[22,23]. However, a higher prevalence of POAG than primary angle-closure glaucoma has been reported in recent studies in Chinese populations[24,25]. Our data demonstrate that, in a Chinese case control study, patients with POAG had a reduction in corneal ECD and an increase in average endothelial cell area compared to age-matched healthy controls. To our knowledge, this is the first report on CEC loss in Chinese patients with POAG. Our data show a 5.47% reduction in ECD in POAG patients compared to healthy controls. Possible explanations include direct mechanical damage, elevated IOP, cytotoxic effects of ocular hypotensive eye drops, impaired endothelial metabolism due to disruptive aqueous humor circulation and congenital endothelial abnormalities.

Correlation between ECD loss and elevated IOP has been investigated[10]. High IOP directly damages the physical barrier function of CECs and affects the function of the endothelial pump leading to changes in aqueous humor dynamics, which cause corneal stromal edema[13]. Gagnon *et al*[13] hypothesized that the mechanism of IOP damage to CECs is as pressure dependent as damage to the optic nerve. Gagnon *et al*[13] showed that corneal ECD is inversely proportional to mean IOP. Some researchers hypothesized that CEC changes are not associated with high IOP[26-27]. Our data showed that the glaucoma and normal control groups had significant differences in corneal ECD, consistent with Gagnon *et al*'s[13] research.

Our results indicated the negative correlation between mean IOP and corneal ECD and the positive correlation between mean IOP and CEC area (Figure 2. High IOP may be an important factor in corneal endothelial injury. In a high IOP animal model, CEC density decreased by an average 5.8% compared with the normal control eyes[13]. CEC ultrastructure was observed by transmission electron microscopy, and mitochondrial swelling and vacuolar degeneration were observed after 3 d of high IOP, indicating that IOP damaged the physical barrier of endothelial cells. CEC dysfunction allows large amounts of water to enter the cells without any damage and cause endothelial cell edema. However, there was no significant change in intracellular nuclei compared to normal cells. However, if high IOP lasted for 2 wk, the mitochondrial vacuolization and dilated endoplasmic reticulum of CECs indicated aggravation of cell edema. Mild or moderate cell damage can return to normal after the cause of the damage is eliminated, or irreversible damage by cell necrosis may occur. Electron microscopic observation of CECs in a model with high IOP for 4 wk showed irreversible loss of heterochromatin edge, multiple nuclear membrane rupture, and nuclear efflux, showing signs of cell necrosis.

The above observations show that the longer the duration of high IOP, the more severe the ultrastructural destruction of CECs, which have some tolerance to high IOP. Within a certain range, if high IOP is controlled and the damage factor is removed, CECs can recover their structure and function and transparency. The longer high IOP persists, the less the healing capacity of CECs. When the damage exceeds its limit, irreversible damage occurs leading to moderate corneal edema and visual
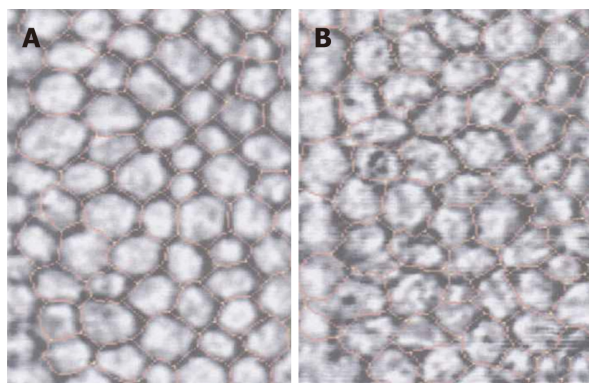
Figure 1 Indirect specular microscopy images of corneal endothelium in normal eyes and eyes with primary open-angle glaucoma. A: Corneal endothelial cells showed regular hexagonal monolayer with clear cell borders in normal eyes; B: Endothelial cells showed irregular and indistinct cell borders with guttae like dark cells in patients with glaucoma.

dysfunction.

It has been shown that damage to CECs can be caused by toxicity of anti-glaucoma medicine[28,29]. The preservative commonly used in anti-glaucoma medication, benzalkonium chloride, plays an important role in ocular surface damage. Its toxic and adverse effects are dose and time dependent and increase in combination and may damage corneal epithelial cells, CECs and central thickness of the cornea[30]. In this study, the corneal ECD of the glaucoma sub groups was compared, and covariance analysis was used to exclude the interference factor of average IOP on CECs. The ECD in the glaucoma treated group was significantly reduced compared with that of the untreated groups, which may have been caused by the benzalkonium chloride preservative in the anti-glaucoma medication. However, the difference in CEC area between the treated and untreated groups was not significant, and further large-scale studies are needed.

Aqueous circulation block may affect metabolism of the corneal endothelium and cause hypoxia in the aqueous humor[31]. That study reported that 30 patients with acute angle-closure glaucoma had significant changes in CEC density compared to normal subjects. The longer the duration of high IOP, the more severe the damage to the corneal endothelium was. The decrease in ECD and the increase in CEC area were related to the length of acute attack and high IOP. Meanwhile, patients with a history of acute attacks showed significantly increased cell area and various changes in shape. Even if the morphologically abnormal CECs show normal density, complications such as loss of corneal endothelial function are more likely to occur after surgery. CEC function requires a certain cell density, but more importantly, it depends on cell morphology, which is a more sensitive indicator of functional changes in the CEC membrane.

The normal corneal endothelium is composed of uniform regular hexagonal cells. Once this structure is destroyed, the corneal endothelium is in an unstable state, and the cells are easily damaged, which causes further deformation and loss[32]. High IOP and aqueous humor blockade can affect the metabolism of the corneal endothelium and cause pathological changes. Glaucoma patients may have congenital abnormal development of corneal endothelial cell layer and trabecular meshwork. In the diagnosis and treatment of glaucoma, the function of CECs directly affects visual acuity and tolerance of intraocular surgery as well as the treatment options. In patients with a history of elevated IOP, the risk of decompensation is greater, corneal edema is more likely and irreversible corneal opacity can be a perioperative or postoperative complication during or after intraocular surgery[33].

The corneal ECD in POAG patients is decreased and the average endothelial cell area is increased compared with those in healthy controls. High IOP and anti-glaucoma medication in POAG may be the main causes of CEC damage. Therefore, for glaucoma patients, quantitative analysis of CEC morphology is necessary, and high IOP should be controlled as soon as possible to prevent corneal endothelial damage.

Table 2 Endothelial cell characteristics of glaucoma subgroups

	With medication, *n* = 35	Untreated, *n* = 25	*P* value
CD, cells/mm²	2686 ± 233	2856 ± 272	0.043
6A, %	49.80 ± 8.32	48.96 ± 8.25	0.929
AVE, µm²	364.31 ± 34.41	364.44 ± 34.24	0.998
MAX, µm²	963.70 ± 187.97	963.26 ± 250.14	0.922
MIN, µm²	80.47 ± 16.28	74.78 ± 16.77	0.089

CD: Cell density; 6A: Percentage of hexagonal cells; AVE: Average cell area; MAX: Maximum cell area; MIN: Minimum cell area.
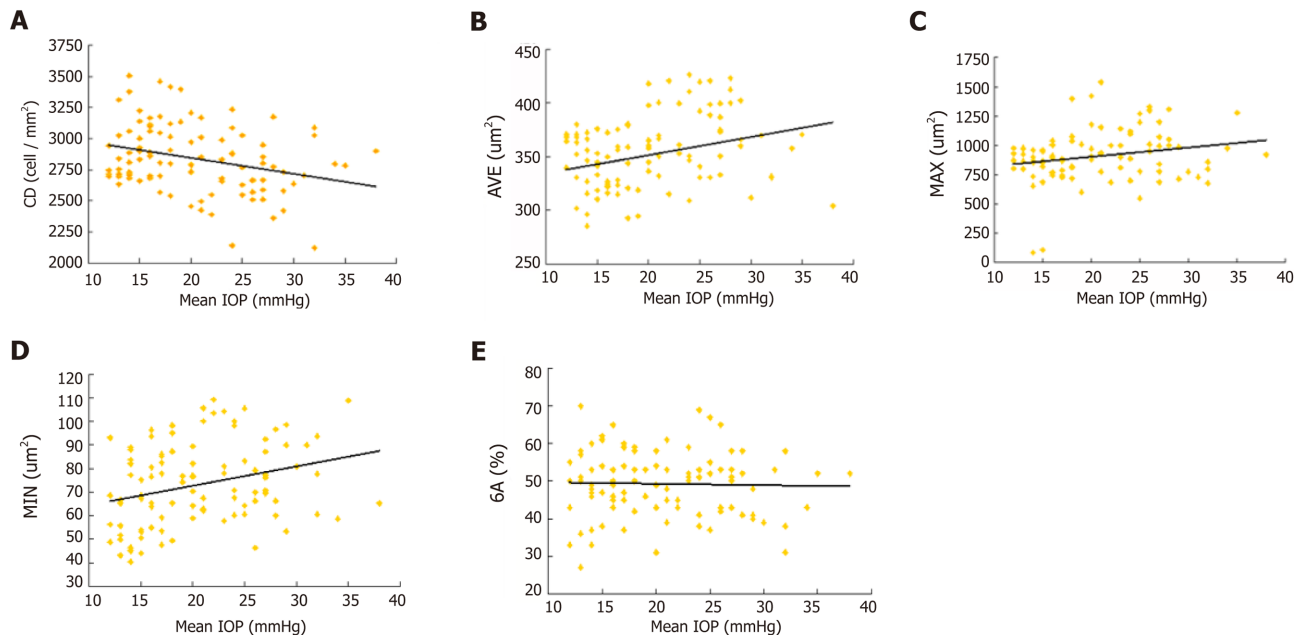
Figure 2 Correlations between endothelial cell characteristics and intraocular pressure. Scatterplots showing the relationship between corneal endothelial cell characteristics and intraocular pressure (IOP). A: There was a negative correlation between cell density and mean IOP (r = -0.286, P = 0.004); B: Positive correlations were found between the average of cell area and mean IOP (r = 0.228, P = 0.022); C: Maximum cell area and mean IOP (r = 0.218, P = 0.029); D: Minimum cell area and mean IOP (r = 0.290, P = 0.003); E: The percentage of hexagonal cells was not correlated with mean IOP. CD: Endothelial cell density; AVG: Average of cell area; MAX: Maximum cell area; MIN: Minimum cell area; GA: Percentage of hexagonal cells.

ARTICLE HIGHLIGHTS

Research background
The corneal endothelial monolayer maintains corneal clarity, and its damage is irreversible. Cornea endothelial cell loss is attributed to open-angle glaucoma, medicine and surgery treatments.

Research motivation
The main topic is the changes in corneal endothelial cell density in primary open-angle glaucoma (POAG) patients.

Research objectives
To investigate the corneal endothelium changes and the correlations to the mean intraocular pressure (IOP) in POAG patients.

Research methods
Sixty POAG patients were selected as the patient group (32 male, 28 females; mean age 63 ± 13 years, age range 50-80 years). Meanwhile, 60 age-matched healthy controls who underwent physical examination were selected. IOP was measured by Goldmann tonometry. Corneal endothelial cell density, percentage of hexagonal cells, average cell area, maximum cell area, minimum cell area, standard deviation of cell area and coefficient of variation in cell area were measured by specular microscopy.

Research results

Endothelial cell density was 2959 ± 236 cells/mm^2 in healthy controls and 2757 ± 262 cells/mm^2 in patients with POAG. The POAG eyes had significantly lower endothelial cell density compared to healthy control eyes ($P < 0.001$). In the POAG group, endothelial cell density was 2686 ± 233 cells/mm^2 in the patients receiving medication and 2856 ± 272 cells/mm^2 in the untreated subgroup. The eyes receiving medication had significantly lower endothelial cell density compared to untreated eyes. There was a negative correlation between cell density and mean IOP ($r = -0.286$, $P = 0.004$) and positive correlation between the average cell area and mean IOP ($r = 0.228$, $P = 0.022$), maximum cell area and mean IOP ($r = 0.218$, $P = 0.029$) and minimum cell area and mean IOP ($r = 0.290$, $P = 0.003$). The percentage of hexagonal cells was not correlated with mean IOP.

Research conclusions

For glaucoma patients, quantitative analysis of CEC morphology is necessary, and high IOP should be controlled as soon as possible to prevent corneal endothelial damage.

Research perspectives

Patients with POAG have lower corneal endothelial cell density than healthy controls of the same age. This may be attributed to mechanical damage from elevated IOP and toxicity of glaucoma medications.

REFERENCES

1   **Murphy C**, Alvarado J, Juster R, Maglio M. Prenatal and postnatal cellularity of the human corneal endothelium. A quantitative histologic study. *Invest Ophthalmol Vis Sci* 1984; **25**: 312-322 [PMID: 6698749]

2   **Hollingsworth J**, Perez-Gomez I, Mutalib HA, Efron N. A population study of the normal cornea using an in vivo, slit-scanning confocal microscope. *Optom Vis Sci* 2001; **78**: 706-711 [PMID: 11700964 DOI: 10.1097/00006324-200110000-00010]

3   **Urban B**, Bakunowicz-Łazarczyk A, Michalczuk M, Krętowska M. Evaluation of corneal endothelium in adolescents with juvenile glaucoma. *J Ophthalmol* 2015; **2015**: 895428 [PMID: 25642345 DOI: 10.1155/2015/895428]

4   **Cho SW**, Kim JM, Choi CY, Park KH. Changes in corneal endothelial cell density in patients with normal-tension glaucoma. *Jpn J Ophthalmol* 2009; **53**: 569-573 [PMID: 20020233 DOI: 10.1007/s10384-009-0740-1]

5   **Buettner H**, Bourne WM. Effect of trans pars plana surgery on the corneal endothelium. *Dev Ophthalmol* 1981; **2**: 28-34 [PMID: 7262410 DOI: 10.1159/000395299]

6   **Kim KN**, Lee SB, Lee YH, Lee JJ, Lim HB, Kim CS. Changes in corneal endothelial cell density and the cumulative risk of corneal decompensation after Ahmed glaucoma valve implantation. *Br J Ophthalmol* 2016; **100**: 933-938 [PMID: 26508781 DOI: 10.1136/bjophthalmol-2015-306894]

7   **Kusakabe A**, Okumura N, Wakimasu K, Kayukawa K, Kondo M, Koizumi N, Sotozono C, Kinoshita S, Mori K. Effect of Trabeculotomy on Corneal Endothelial Cell Loss in Cases of After Penetrating-Keratoplasty Glaucoma. *Cornea* 2017; **36**: 317-321 [PMID: 28151811 DOI: 10.1097/ICO.0000000000001088]

8   **Aldrich BT**, Schlötzer-Schrehardt U, Skeie JM, Burckart KA, Schmidt GA, Reed CR, Zimmerman MB, Kruse FE, Greiner MA. Mitochondrial and Morphologic Alterations in Native Human Corneal Endothelial Cells Associated With Diabetes Mellitus. *Invest Ophthalmol Vis Sci* 2017; **58**: 2130-2138 [PMID: 28395029 DOI: 10.1167/iovs.16-21094]

9   **Setälä K**. Corneal endothelial cell density after an attack of acute glaucoma. *Acta Ophthalmol (Copenh)* 1979; **57**: 1004-1013 [PMID: 545996 DOI: 10.1111/j.1755-3768.1979.tb00531.x]

10 **Malaise-Stals J**, Collignon-Brach J, Weekers JF. Corneal endothelial cell density in acute angle-closure glaucoma. *Ophthalmologica* 1984; **189**: 104-109 [PMID: 6493688 DOI: 10.1159/000309393]

11 **Bigar F**, Witmer R. Corneal endothelial changes in primary acute angle-closure glaucoma. *Ophthalmology* 1982; **89**: 596-599 [PMID: 7122040 DOI: 10.1016/S0161-6420(82)34744-2]

12 **Knorr HL**, Händel A, Naumann GO. [Morphometric and qualitative changes in corneal endothelium in primary chronic open angle glaucoma]. *Fortschr Ophthalmol* 1991; **88**: 118-120 [PMID: 1855725]

13 **Gagnon MM**, Boisjoly HM, Brunette I, Charest M, Amyot M. Corneal endothelial cell density in glaucoma. *Cornea* 1997; **16**: 314-318 [PMID: 9143804 DOI: 10.1097/00003226-199705000-00010]

14 **Knorr HL**, Jünemann A, Händel A, Naumann GO. [Morphometric and qualitative changes in corneal endothelium in pseudoexfoliation syndrome]. *Fortschr Ophthalmol* 1991; **88**: 786-789 [PMID: 1794803]

15 **Vannas A**, Setälä K, Ruusuvaara P. Endothelial cells in capsular glaucoma. *Acta Ophthalmol (Copenh)* 1977; **55**: 951-958 [PMID: 579548 DOI: 10.1111/j.1755-3768.1977.tb05676.x]

16 **Chen MJ**, Liu CJ, Cheng CY, Lee SM. Corneal status in primary angle-closure glaucoma with a history of acute attack. *J Glaucoma* 2012; **21**: 12-16 [PMID: 21048505 DOI: 10.1097/IJG.0b013e3181fc800a]

17 **Baratz KH**, Nau CB, Winter EJ, McLaren JW, Hodge DO, Herman DC, Bourne WM. Effects of glaucoma medications on corneal endothelium, keratocytes, and subbasal nerves among participants in the ocular hypertension treatment study. *Cornea* 2006; **25**: 1046-1052 [PMID: 17133051 DOI: 10.1097/01.ico.0000230499.07273.c5]

18 **Pastor SA**, Williams R, Hetherington J, Hoskins HD, Goodman D. Corneal endothelial cell loss following trabeculectomy with mitomycin C. *J Glaucoma* 1993; **2**: 112-113 [PMID: 19920497 DOI: 10.1097/00061198-199300220-00008]

19 **Smith DL**, Skuta GL, Lindenmuth KA, Musch DC, Bergstrom TJ. The effect of glaucoma filtering surgery on corneal endothelial cell density. *Ophthalmic Surg* 1991; **22**: 251-255 [PMID: 1852377]

20 **Souza C**, Tran DH, Loman J, Law SK, Coleman AL, Caprioli J. Long-term outcomes of Ahmed glaucoma valve implantation in refractory glaucomas. *Am J Ophthalmol* 2007; **144**: 893-900 [PMID: 17916318 DOI: 10.1016/j.ajo.2007.07.035]

21 **Ates H**, Palamar M, Yagci A, Egrilmez S. Trabeculectomy Versus EX-PRESS Shunt Versus Ahmed Valve Implant: Short-term Effects on Corneal Endothelial Cells. *Am J Ophthalmol* 2016; **162**: 201-202

[PMID: 26654385 DOI: 10.1016/j.ajo.2015.11.012]

22   **Sun J**, Zhou X, Kang Y, Yan L, Sun X, Sui H, Qin D, Yuan H. Prevalence and risk factors for primary open-angle glaucoma in a rural northeast China population: a population-based survey in Bin County, Harbin. *Eye (Lond)* 2012; **26**: 283-291 [PMID: 22157917 DOI: 10.1038/eye.2011.243]

23   **Cheng JW**, Cheng SW, Ma XY, Cai JP, Li Y, Wei RL. The prevalence of primary glaucoma in mainland China: a systematic review and meta-analysis. *J Glaucoma* 2013; **22**: 301-306 [PMID: 22134352 DOI: 10.1097/IJG.0b013e31824083ca]

24   **Baskaran M**, Foo RC, Cheng CY, Narayanaswamy AK, Zheng YF, Wu R, Saw SM, Foster PJ, Wong TY, Aung T. The Prevalence and Types of Glaucoma in an Urban Chinese Population: The Singapore Chinese Eye Study. *JAMA Ophthalmol* 2015; **133**: 874-880 [PMID: 25974263 DOI: 10.1001/jamaophthalmol.2015.1110]

25   **Zhong H**, Li J, Li C, Wei T, Cha X, Cai N, Luo T, Yu M, Yuan Y. The prevalence of glaucoma in adult rural Chinese populations of the Bai nationality in Dali: the Yunnan Minority Eye Study. *Invest Ophthalmol Vis Sci* 2012; **53**: 3221-3225 [PMID: 22511635 DOI: 10.1167/iovs.11-9306]

26   **Lee JH**, Oh SY. Corneal endothelial cell loss from suture fixation of a posterior chamber intraocular lens. *J Cataract Refract Surg* 1997; **23**: 1020-1022 [PMID: 9379371 DOI: 10.1016/S0886-3350(97)80074-0]

27   **Verma S**, Nongpiur ME, Husain R, Wong TT, Boey PY, Quek D, Perera SA, Aung T. Characteristics of the Corneal Endothelium Across the Primary Angle Closure Disease Spectrum. *Invest Ophthalmol Vis Sci* 2018; **59**: 4525-4530 [PMID: 30208420 DOI: 10.1167/iovs.18-24939]

28   **Yee RW**. The effect of drop vehicle on the efficacy and side effects of topical glaucoma therapy: a review. *Curr Opin Ophthalmol* 2007; **18**: 134-139 [PMID: 17301615 DOI: 10.1097/ICU.0b013e328089f1c8]

29   **Schehlein EM**, Novack G, Robin AL. New pharmacotherapy for the treatment of glaucoma. *Expert Opin Pharmacother* 2017; **18**: 1939-1946 [PMID: 29172818 DOI: 10.1080/14656566.2017.1408791]

30   **Chen W**, Li Z, Hu J, Zhang Z, Chen L, Chen Y, Liu Z. Corneal alternations induced by topical application of benzalkonium chloride in rabbit. *PLoS One* 2011; **6**: e26103 [PMID: 22022526 DOI: 10.1371/journal.pone.0026103]

31   **Sandoval HP**, Al Sarraf O, Vroman DT, Solomon KD. Corneal endothelial cell damage after lens extraction using the fluid-based system compared to ultrasound phacoemulsification in human cadaver eyes. *Cornea* 2004; **23**: 720-722 [PMID: 15448500 DOI: 10.1097/01.ico.0000130184.56514.51]

32   **Niederer RL**, Perumal D, Sherwin T, McGhee CN. Age-related differences in the normal human cornea: a laser scanning in vivo confocal microscopy study. *Br J Ophthalmol* 2007; **91**: 1165-1169 [PMID: 17389741 DOI: 10.1136/bjo.2006.112656]

33   **Sheng H**, Bullimore MA. Factors affecting corneal endothelial morphology. *Cornea* 2007; **26**: 520-525 [PMID: 17525643 DOI: 10.1097/ICO.0b013e318033a6da]

Observational Study

Myocardial bridge-related coronary heart disease: Independent influencing factors and their predicting value

Dong-Hui Zhao, Qian Fan, Jun-Xia Ning, Xin Wang, Jia-Yu Tian

ORCID number: Dong-Hui Zhao (0000-0001-7836-7425); Qian Fan (0000-0001-7741-1289); Jun-Xia Ning (0000-0002-5969-3269); Xin Wang (0000-0001-5847-9871); Jia-Yu Tian (0000-0003-1701-7784).

Author contributions: Zhao DH, Fan Q, and Ning JX designed the research; Zhao DH, Wang X, and Tian JY performed the research; Fan Q and Ning JX contributed new reagents/analytic tools; Zhao DH, Wang X, and Tian JY analyzed the data; and Zhao DH, Ning JX, and Tian JY wrote the paper.

Dong-Hui Zhao, Qian Fan, Xin Wang, Jia-Yu Tian, Department of Cardiology, Beijing Anzhen Hospital Affiliated to Capital Medical University, Beijing 100029, China

Jun-Xia Ning, Department of Cardiology, The First People's Hospital of Pingyuan County, Dezhou 253100, Shandong Province, China

Corresponding author: Dong-Hui Zhao, MD, Doctor, Department of Cardiology, Beijing Anzhen Hospital, Capital Medical University, No. 2, Anzhen Road, Chaoyang District, Beijing 100029, China. zhaodonghui3486@126.com
Telephone: +86-10-64456548

Abstract

BACKGROUND
Myocardial bridge (MB) will compress the mural coronary artery (MCA) during the systole and cause myocardial ischemia. In the diagnosis of coronary heart disease (CHD), because the structure of MB is difficult to be observed by coronary angiography (CAG), the clinical study of the influence of MB on CHD is lacking. With the advancement of computed tomography coronary angiography technology, detailed observations of the MB anatomy have realized.

AIM
To explore the main influencing factors of MB-related CHD and to find potential indicators for predicting MB-related CHD.

METHODS
A total of 1718 patients with suspected CHD due to the symptoms of myocardial ischemia were enrolled as subjects. Patients diagnosed with CHD were included in a CHD group, and patients with no significant abnormalities were included in a control group. In the CHD group, patients were divided into an MB-CHD subgroup if MB-related CHD was found. In the control group, patients were divided into a simple MB subgroup if MB was found. The patient's clinical data and MB-related indicators, including the branch of MB, MB type (superficial/deep type), MB length, MB thickness, systolic and diastolic compression of the MCA, and MCA systolic stenosis rate were recorded and compared. Logistic regression analysis was used to explore the independent influencing factors of MD-related CHD. ROC curve was used to analyze the diagnostic efficacy of potential indicators for MB-related CHD.

RESULTS
There were 1060 cases in the CHD group and 658 cases in the control group, and

there were 236 cases in the MB-CHD subgroup and 52 cases in the simple MB subgroup. Multivariate logistic regression analysis showed that the combined MB had a significant effect on the occurrence of CHD ($P < 0.05$). MB thickness, systolic compression, diastolic compression, and MCA systolic stenosis rate had significant effects on the occurrence of MB-related CHD ($P < 0.05$). The area under the curve (AUC) of the combination of these influencing factors for the diagnosis of MB-related CHD was 0.959, which was significantly higher than the AUCs of the four indicators separately ($P < 0.05$). The sensitivity was 97.06% and the specificity was 87.63%.

CONCLUSION
MB thickness, systolic compression, diastolic compression, and MCA systolic stenosis are independent influencing factors for MB-related CHD. The combination of these factors has potential diagnostic value for MB-related CHD.

Key words: Myocardial bridge; Coronary heart disease; Mural coronary artery; Computed tomography coronary angiography; Independent influencing factor

Core tip: With the deep understanding of myocardial bridge (MB), it is considered to be the reason of such complications as acute myocardial infarction, ventricular tachycardia, syncope, and sudden cardiac death. Currently, how MB affects coronary heart disease remains unclear. Computed tomography coronary angiography can directly measure MB-related coronary heart disease (CHD), which was used to explore the relationship between MB and CHD. In this study, MB thickness, systolic compression, diastolic compression, and mural coronary artery systolic stenosis were proved to be the independent influencing factors for MB-related CHD. The combination of these factors has potential diagnostic value for MB-related CHD.

INTRODUCTION

Myocardial fiber bundle covering the mural coronary artery (MCA) is called myocardial bridge (MB)[1-3]. With the development of computed tomography coronary angiography (CTA), studies have reported that MB can compress the MCA during systole, causing myocardial ischemia such as angina pectoris and myocardial infarction[4-7]. It is called MB-related coronary heart disease (CHD)[8]. Because the low detection rate of MB and the inconspicuous myocardial ischemia symptoms in most patients with MB, and common risk factors for CHD including age, dyslipidemia, hypertension, smoking, diabetes, obesity, and family history are numerous[9-12], clinicians pay insufficient attention to MB and the studies on MB-related CHD are few. Currently, although coronary angiography (CAG) cannot specifically observe the detailed anatomical structure of MB, CTA has been developed to directly measure MB-related indicators in detail[13-16]. Therefore, the present study utilized CTA to assess the association between MB and CHD, in order to explore the main influencing factors of MB-related CHD and to find potential indicators for predicting MB-related CHD.

MATERIALS AND METHODS

Study participants
This study was approved by the Ethics Committee of the Capital Medical University Affiliated to Beijing Anzhen Hospital, and written informed consent was obtained

from all patients. Study participants were recruited from the department of cardiology, Beijing Anzhen Hospital, Capital Medical University due to the symptoms of myocardial ischemia from December 2016 to June 2018. All patients were diagnosed utilizing CAG or CTA. The inclusion criteria were: (1) Patients with myocardial ischemia symptoms such as angina pectoris and ST-T segment changes; and (2) Glomerular filtration rate (GFR) between 30 and 60 mL/min. The exclusion criteria were: (1) Patients with other heart diseases besides CHD; (2) Patients with poor physical condition and multiple organ failure; (3) Patients allergic to contrast agent; and (4) Patients with coagulopathy. Of all the subjects, if the MCA was found in the CAG, CTA would be performed to observe MB. Patients diagnosed with CHD were divided into a CHD group, and patients with no significant abnormalities were divided into a control group. In the CHD group, patients were divided into an MB-CHD subgroup if MB-related CHD was found. In the control group, patients were divided into a simple MB subgroup if MB was found.

Clinical data recording

The family history of CHD, hypertension, diabetes, hyperlipidemia, smoking, ECG ST-segment changes, lipoprotein(a) [Lp(a)], homocysteine (HCY), plasminogen activator inhibitor-1 (PAI-1), and fibrinogen conditions of subjects were recorded in this study. The diagnosis of hypertension was based on the 2017 American Diabetes Diagnostic Criteria[17]: Grade 1 hypertension: systolic blood pressure 130-139 mmHg, diastolic blood pressure 80-89 mmHg; Grade 2 hypertension: ≥ 140/90 mmHg. The diagnosis of diabetes was based on the 2017 American Diabetes Association diagnostic criteria[18]: Fasting blood glucose ≥ 7.0 mmol/L; random blood glucose ≥ 11.1 mmol/L and patients with diabetic symptoms; 2 h postprandial blood glucose ≥ 11.1 mmol/L in the glucose tolerance test. Patients with atypical symptoms needed to repeat the test to determine the presence of diabetes according to the above criteria. The diagnosis of hyperlipidemia was based on: serum total cholesterol (TC) > 5.2 mmol/L; triglyceride (TG) > 1.7 mmol/L; serum low-density lipoprotein cholesterol (LDL-C) > 3.64 mmol/L[19].

CAG examination

Selective CAG (Siemens Artis Zee floor) was performed in this study. The left coronary angiography was routinely performed in a spider position (left front oblique 45° + foot position 30°), left shoulder position (left front oblique 45° + head position 30°), head position (positive head position 30°), right shoulder position (right front oblique 30° + head position 30°), and liver position (right front oblique 30° + foot position 30°). The right CAG was performed with left front oblique 45° and right front oblique 30°[20].

CTA examination

The scanning was performed using TOSHIBA AQUILION ONE TSX-301A. The ECG was placed on the patient's chest before scanning. ECG-gated scanning was used to scan from the bottom of the heart (marked by tracheal carina) to the whole heart. For enhanced scanning, a double-tube high-pressure syringe was used and the bolus tracking technique was adopted. The contrast agent iohexol 350 was injected through the middle of the elbow vein. The injection speed was 5 mL/s, and the total amount was 60-80 mL. Subsequently, 50 mL of physiological saline was injected at the same rate. After the images were acquired, the resulting data were delivered to the workstation for further analysis. In the section along the longitudinal axis of the coronary artery, if a certain coronary artery was distributed in a certain myocardium, it can be diagnosed as an MB. The branch of the MB was observed and recorded. MB type (superficial/deep type), MB length, MB thickness, MCA end-systolic diameter, and end-diastolic diameter were measured. The MCA systolic stenosis rate was calculated as (MCA end-diastolic diameter - MCA end-systolic diameter)/MCA end-diastolic diameter. The diameter method was used to estimate the systolic and diastolic compression of the MCA.

Statistical analysis

Statistical analyses were performed using SPSS software (version 19.0; Chicago, IL, USA). The numerical data are expressed as the mean ± SD and the comparison between the two groups was compared using the *t*-test. The categorical variables are expressed as number and percentage and the comparison between the two groups was performed by the chi-square test. Logistic regression was used for multivariate analysis to screen out the potential independent influencing factors of MB-related CHD. ROC curve was used to analyze the diagnostic efficacy of potential indicators for MB-related CHD. Statistical significance was defined as 2-tailed $P < 0.05$ for all tests.

RESULTS

Totally 1718 patients who underwent CTA or CAG were enrolled. Of all the participants, 1060 patients diagnosed with CHD were included in the CHD group, and the remaining 658 patients were included in the control group. There were 288 MB patients found in the present study. Totally 236 patients diagnosed with MB-related CHD were divided in the MB-CHD subgroup. It included 121 males and 115 females, and the average age was 60.25 ± 15.34 years. The remaining 52 patients diagnosed with simple MB were divided into the simple MB subgroup. It included 32 males and 20 females, and the average age was 52.65 ± 12.86 years. The lesions of 288 MB were all located in the left anterior descending wall coronary artery, as shown in Figure 1.

Analysis of risk factors for CHD

Clinical characteristics of the CHD group and the control group are shown in Table 1. The ratio of gender, family history of CHD, abnormal TC, HDL-C, TG, Lp(a), HCY, PAI-1, and fibrinogen were comparable in the two groups ($P > 0.05$). The average age, percentage of patients with abnormal hypertension, diabetes, smoking, ECG ST-segment changes, LDL-C, and combined MB in the CHD group were significantly higher than those in the control group ($P < 0.05$). Multivariate logistic regression analysis indicated that the occurrence of CHD was influenced remarkably by hypertension, ECG ST-segment changes, diabetes, LDL-C, and combined MB ($P < 0.05$) except for age and smoking ($P > 0.05$). The further analysis revealed that factors affecting CHD ranked based on OR values as follows: hypertension, diabetes, MB, LDL-C, and ECG ST-segment changes (Table 2).

Comparison of MB-related parameters between the MB-CHD subgroup and simple MB subgroup

The results of the comparisons between the MB-CHD subgroup and the simple MB subgroup showed that the difference of the MB length between the two groups was similar ($P > 0.05$). The proportion of deep MB type, MB thickness, systolic compression, diastolic compression, and MCA systolic stenosis rate in the MB-CHD subgroup were significantly higher than those in the simple MB subgroup ($P < 0.05$, Table 3).

Multivariate analysis of independent influencing factors of MB-related CHD

MB type, thickness, systolic compression, diastolic compression, and MCA systolic stenosis rate were included in the logistic regression analysis. The results showed that MB type had no effect on the occurrence of MB-related CHD ($P > 0.05$). MB thickness, systolic compression, diastolic compression, and MCA systolic stenosis rate had obvious effects on the occurrence of MB-related CHD ($P < 0.05$). The further study revealed that the factors influencing the occurrence of MB-related CHD were as follows in descending order: diastolic compression, MB thickness, MCA systolic stenosis rate, and systolic compression (Table 4).

Effectiveness analysis of MB-related parameters in diagnosing MB-related CHD

The results of ROC curve analysis for the diagnosis of MB-related CHD by MB thickness, systolic compression, diastolic compression, and MCA systolic stenosis rate are shown in Table 5 and Figure 2.The area under the curve (AUC) of diastolic compression was the highest, and its sensitivity reached 95.10%, followed by MB thickness, MCA systolic stenosis rate, and systolic compression. However, the AUC of each indicator did not exceed 0.9. Based on the logistic regression model, we established a combined diagnosis of four indicators, and found that the AUC of the combined diagnosis was 0.959, which was significantly higher than the AUCs of the four indicators separately ($P < 0.05$). The sensitivity was 97.06% and the specificity was 87.63%.

Logistic regression analysis of the effect of the combination of four factors on MB-related CHD

Since the combination of four indicators was the best indicator for the diagnosis of MB-related CHD in this study. We used logistic regression to analyze its effect on MB-related CHD using its optimal diagnostic point. The results showed that when the combination was > 0.275, the risk of the occurrence of MB-related CHD was 15.963 times higher than that when the combination was ≤ 0.275 (Table 6).

DISCUSSION
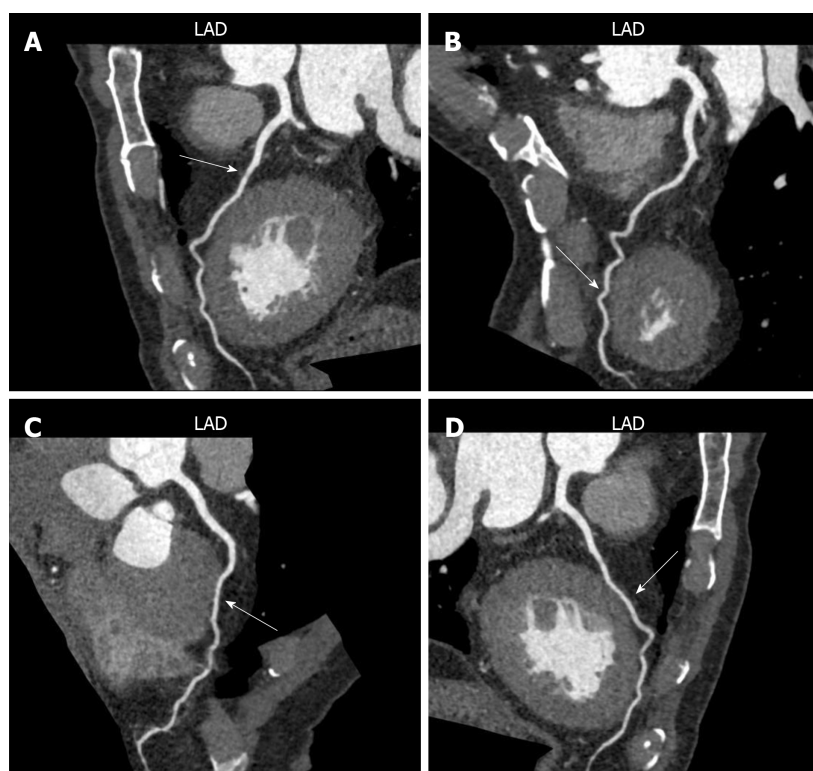
Figure 1 Computed tomography coronary angiography images of myocardial bridge lesions. Myocardial bridge (MB) was marked by the arrow in figures. A and B: MB in the left anterior descending coronary artery; C: MB in the anterior descending coronary artery; D: MB in the right anterior descending coronary artery.

Studies have reported that some patients with sudden cardiac death did not die from myocardial infarction caused by coronary atherosclerosis, but related to MB[8,21-24]. MB may compress coronary arteries during the systolic period, which can cause angina pectoris, myocardial infarction, left ventricular dysfunction, paroxysmal atrioventricular block, myocardial ischemia during exertion, sudden cardiac death, *etc*[25]. With the rapid development of imaging diagnostic technology, the detection rate of myocardial ischemia caused by MB has increased recently[26,27]. CTA has been widely used in MB detection, and it has been proved to non-invasively measure the length and thickness of MB, the systolic and diastolic pressure on MCA, and other MB anatomical features[28,29]. Therefore, in the present study, 288 patients with MB were screened from 1718 patients with suspected CHD. The detailed analyses of MB were performed by CTA in order to explore the effect of MB on CHD.

This study first compared the general data of CHD patients and patients without CHD. In addition to age, hypertension, diabetes, smoking, ECG ST segment changes, and LDL-C, which known as CHD influencing factors, the number of patients with combined MB in the CHD group was significantly higher than that in the control group. Further multivariate analysis showed that combined MB was an independent factor affecting CHD. Furthermore, its influencing effect was second only to the effect of diabetes on CHD. This finding indicates that patients with MB are more likely to suffer with CHD. It is indeed necessary to observe MB in detail and take action to prevent CHD.

In order to fully analyze the MB using CTA, we analyzed various anatomical features of MB including MB type (superficial/depth), MB length, thickness, systolic compression, and diastolic compression. The results showed that the proportion of deep MB, MB thickness, systolic compression, diastolic compression, and MCA systolic stenosis rate in the MB-CHD subgroup were significantly greater than those in the simple MB subgroup. To further explore the effects of MB anatomical features on CHD, we performed a multivariate regression analysis using a logistic regression model. The results showed that MB thickness, systolic compression, diastolic compression, and MCA systolic stenosis were four independent influencing factors on the occurrence of MB-related CHD. The diastolic compression and MB thickness had the greatest influence on MB-related CHD, suggesting that thicker MB will compress MCA during the diastolic phase, affecting MCA perfusion and leading to coronary ischemia.

To better analyze the clinical value of the above four MB anatomical features in the

Table 1 Comparison of clinical characteristics between the coronary heart disease group and the control group, *n* (%)

Characteristic	CHD group (*n* =1060)	Control group (*n* = 658)	*t/X^2* value	*P*-value
Age	60.25 ± 13.25	52.65 ± 10.86	12.360	0.000
Gender (Male/Female)	592/468	388/270	1.610	0.204
Family history of CHD	215 (20.3)	113 (17.2)	2.542	0.111
Hypertension	707 (66.7)	352 (53.5)	29.929	0.000
Diabetes	424 (40.0)	102 (15.5)	114.702	0.000
Smoking	286 (27.0)	122 (18.5)	15.970	0.000
ST-segment changes	456 (43.0)	72 (10.9)	196.224	0.000
Abnormal TC	445 (42.0)	264 (40.1)	0.579	0.447
Abnormal LDL-C	583 (55.0)	260 (39.5)	38.960	0.000
Abnormal HDL-C	456 (43.0)	270 (41.0)	0.656	0.418
Abnormal TG	472 (44.5)	289 (43.9)	0.061	0.805
Abnormal Lp(a)	311 (29.3)	182 (27.7)	0.560	0.454
Abnormal HCY	225 (21.2)	115 (17.5)	3.595	0.058
Abnormal PAY-1	178 (16.8)	99 (15.0)	0.916	0.339
Abnormal fibrinogen	157 (14.8)	87 (13.2)	0.842	0.359
Combined MB	235 (22.2)	53 (8.1)	57.969	0.000

CHD: Coronary heart disease; MB: Myocardial bridge; TC: Total cholesterol; TG: Triglyceride; LDL-C: Low-density lipoprotein cholesterol; Lp(a): Lipoprotein(a); HCY: Homocysteine; PAI-1: Plasminogen activator inhibitor-1.

diagnosis of MB-related CHD. The MB thickness, systolic compression, diastolic compression, MCA systolic stenosis rate, and their combination were included in the ROC curve analysis. The results showed that the AUC of the diastolic compression was the largest when the four indicators were used for diagnosis separately, which was 0.870. The AUC of the other three anatomical features were not high. Although the specificity of the systolic compression was close to 100%, the sensitivity was only 37.25%. It cannot be used as a reliable indicator for the diagnosis of CHD. Similarly, although the sensitivity of diastolic compression was very high, reaching 95.1%, the specificity was only 68.28%. The AUC of combined diagnosis increased to 0.959, suggesting that the accuracy of the combination of the four features for diagnosing MB-related CHD was the best. Logistic regression showed that when the probability distribution of the combination of the four MB anatomical features was > 0.275, the risk of occurrence of MB-related CHD was 15.963 times higher than that when the value was ≤ 0.275. It is suggested that the combination of the four MB anatomical features has potential diagnostic value for MB-related CHD.

The results of this study are unable to be used as clinical criteria currently due to its limited sample size and single-center research. We suggest that a multi-center and large-scale study should be performed to obtain effective indicators for MB-related CHD, in order to improve patients' life quality.

In conclusion, this study found that MB thickness, systolic compression, diastolic compression, and MCA systolic stenosis were independent risk factors for MB-related CHD. The combination of the four MB anatomical features has potential diagnostic value for MB-related CHD. Clinical attention should be paid to MB, and the diagnostic value of MB anatomical features for MB-related CHD should be further explored.

Table 2 Multivariate logistic regression analysis factors affecting the development of coronary heart disease

Risk factor	B	SE	Wald	*P*	OR	95%CI	
						Lower limit	Upper limit
Age	0.622	0.127	3.902	0.048	1.863	1.452	2.390
Hypertension (Yes = 1, No = 0)	1.831	0.227	9.824	0.001	6.238	3.998	9.734
Diabetes (Yes = 1, No = 0)	1.450	0.127	6.205	0.012	4.263	3.324	5.468
Smoking (Yes = 1, No = 0)	0.257	0.228	0.245	0.089	1.293	0.827	2.022
ST-segment changes (Yes = 1, No = 0)	0.638	0.311	5.079	0.023	1.892	1.028	3.481
LDL-C (Abnormal = 1, Normal = 0)	0.790	0.384	4.357	0.036	2.204	1.038	4.678
MB (with = 1, without = 0)	1.260	0.012	10.262	0.000	3.524	3.442	3.608

LDL-C: Low-density lipoprotein cholesterol; MB: Myocardial bridge.

Table 3 Comparison of myocardial bridge parameters between the myocardial bridge-coronary heart disease subgroup and the simple myocardial bridge subgroup

Parameter	Group		*t*/X^2 value	*P*-value
	MB-CHD subgroup (*n* = 236)	Simple MB subgroup (*n* = 52)		
MB type (Superficial /Deep)	125/111	38/14	7.016	0.008
Systolic compression (%)	50.28 ± 11.24	39.86 ± 12.08	7.326	0
Diastolic compression (%)	34.25 ± 10.20	24.74 ± 10.75	7.424	0
MCA systolic stenosis rate (%)	44.35 ± 9.43	32.92 ± 6.60	10.865	0

MB: Myocardial bridge; MCA: Mural coronary artery; CHD: Coronary heart disease.

Table 4 Multivariate analysis of independent influencing factors of myocardial bridge-related coronary heart disease

	B	SE	Wald	*P*	OR	95.0%CI	
						Lower limit	Upper limit
MB type (Deep = 1, Superficial = 0)	0.459	0.316	2.858	0.072	1.582	0.852	2.939
MB thickness	1.001	0.274	10.420	0.000	2.722	1.591	4.657
Systolic compression	0.514	0.162	12.341	0.000	1.672	1.217	2.297
Diastolic compression	1.266	0.347	18.226	0.000	3.548	1.797	7.004
MCA systolic stenosis rate	0.602	0.242	9.854	0.001	1.825	1.136	2.933

MB: Myocardial bridge; MCA: Mural coronary artery.

Table 5 Receiver operating characteristic curve analysis of myocardial bridge indexes for diagnosis of coronary heart disease

	AUC	95%CI	Cut-off point	Sensitivity	Specificity
MB thickness	0.814[a]	0.764 - 0.857	21.54 mm	78.43%	70.97%
Systolic compression	0.755[a]	0.701 - 0.803	45.04%	37.25%	99.46%
Diastolic compression	0.870[a]	0.826 - 0.907	48.65%	95.10%	68.28%
MCA systolic stenosis rate	0.795[a]	0.744 - 0.840	43.45%	77.45%	67.74%
Combination	0.959	0.925 - 0.972	0.275	97.06%	87.63%

[a]*P*< 0.05 *vs* Combination. MB: Myocardial bridge; MCA: Mural coronary artery.

Table 6 Logistic regression analysis of the effect of the combination of the four indicators on myocardial bridge-related coronary heart disease

	B	SE	Wald	*P*	OR	95.0%CI	
						Lower limit	Upper limit
Combination (> 0.275 = 1, < 0.275 = 0)	2.770	0.226	9.752	0.001	15.953	10.244	24.844
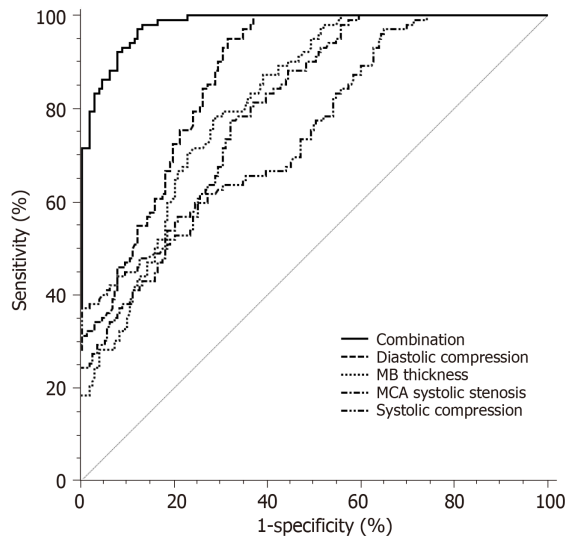
Figure 2 Efficacy of myocardial bridge related indicators and their combination in the diagnosis of myocardial bridge-related coronary heart disease. MB: Myocardial bridge; MCA: Mural coronary artery.

ARTICLE HIGHLIGHTS

Research background

More and more reports indicate that myocardial bridge (MB) can compress the mural coronary artery during cardiac contraction, causing myocardial ischemia such as angina pectoris and myocardial infarction. It is clinically called MB-related coronary heart disease (CHD). Therefore, the relationship between MB and CHD has an important influence on the diagnosis of MB-related CHD. Currently, only when the MB reaches a certain thickness, it can be found in coronary angiography (CAG), which results in a high missing diagnosis rate.

Research motivation

Currently, CAG cannot specifically observe MB-related details. Computed tomography coronary artery (CTA) has become an important means of non-invasive diagnosis of CHD. Studies have shown that CTA can directly show the anatomical relationship between the coronary artery and myocardium. Therefore, this study used CTA to assess the association between MB and coronary atherosclerosis, in order to explore the effect of MB on patients with CHD and improve the detection rate of MB-related CHD.

Research objectives

In this study, CTA was used to observe the anatomy of MB and analyzed the effects of MB thickness, systolic compression, diastolic compression, and MCA systolic stenosis rate on CHD. The purpose of this study was to evaluate the relationship between MB and coronary atherosclerosis by CTA.

Research methods

CHD patients who underwent CTA or CAG were defined as the CHD group and the control group, respectively. CHD patients with combined MB were defined as the MB-CHD subgroup. Patients with simple MB were defined as the simple MB subgroup. The anatomical features of patients with MB were analyzed by multi-factor logistic regression. The ROC curve was used to analyze the diagnostic efficacy of the potential indicators for MB-related CHD.

Research results

MB thickness, systolic compression, diastolic compression, and MCA systolic stenosis had significant effects on the incidence of MB-related CHD ($P < 0.05$). The areas under the ROC curves for the four indicators in diagnosing CHD were 0.814, 0.755, 0.870, and 0.795, respectively. The efficacy of diastolic compression in the diagnosis of CHD was the highest. When the degree

of MB diastolic compression was > 48.68%, the risk of CHD was 15.953 times than that when the value was ≤ 48.68% (P < 0.05).

Research conclusions

MB length, MB thickness, systolic and diastolic compression of MCA have significant effects on the occurrence of MB-related CHD.

Research perspectives

CTA is a non-invasive economic examination that can directly display the anatomical relationship between the coronary arteries and myocardium. The combination of the four MB anatomical features has potential diagnostic value for MB-related CHD. However, the results of this study cannot be regarded as the clinical criteria because of the limited sample size. We suggest that further multi-center study should be performed to obtain the effective indicators for MB-related CHD, in order to provide a reference for early diagnosis of MB.

REFERENCES

1   **Cerrato E**, Barbero U, D'Ascenzo F, Taha S, Biondi-Zoccai G, Omedè P, Bianco M, Echavarria-Pinto M, Escaned J, Gaita F, Varbella F. What is the optimal treatment for symptomatic patients with isolated coronary myocardial bridge? A systematic review and pooled analysis. *J Cardiovasc Med (Hagerstown)* 2017; **18**: 758-770 [PMID: 28834785 DOI: 10.2459/JCM.0000000000000551]

2   **An JW**, Zhao XB, Zhao HL, Zhou W. [Correlation of Coronary Artery Tortuosity Caused by Myocardial Bridge with Coronary Atherosclerosis]. *Zhongguo Yi Xue Ke Xue Yuan Xue Bao* 2018; **40**: 151-157 [PMID: 29724303]

3   **Pourhoseini S**, Bakhtiari M, Babaee A, Ostovan MA, Eftekhar-Vaghefi SH, Ostovan N, Dehghani P. Increased risk of coronary perforation during percutaneous intervention of myocardial bridge: What histopathology says. *J Cardiovasc Thorac Res* 2017; **9**: 108-112 [PMID: 28740631 DOI: 10.15171/jcvtr.2017.18]

4   **Ding SJ**, Huang RC, Jia CF, Zhong L, An P, Wang ZQ, Zhu H, Wu BL, Zhou XC. [The relationship between myocardial bridge in mural coronary artery segment and coronary atherosclerosis]. *Zhonghua Xin Xue Guan Bing Za Zhi* 2016; **44**: 873-878 [PMID: 27903374 DOI: 10.3760/cma.j.issn.0253-3758.2016.10.009]

5   **Saito Y**, Kitahara H, Shoji T, Tokimasa S, Nakayama T, Sugimoto K, Fujimoto Y, Kobayashi Y. Relation between severity of myocardial bridge and vasospasm. *Int J Cardiol* 2017; **248**: 34-38 [PMID: 28712560 DOI: 10.1016/j.ijcard.2017.07.002]

6   **Yu M**, Zhang Y, Li Y, Li M, Li W, Zhang J. Assessment of Myocardial Bridge by Cardiac CT: Intracoronary Transluminal Attenuation Gradient Derived from Diastolic Phase Predicts Systolic Compression. *Korean J Radiol* 2017; **18**: 655-663 [PMID: 28670160 DOI: 10.3348/kjr.2017.18.4.655]

7   **Nishimiya K**, Matsumoto Y, Wang H, Piao Z, Ohyama K, Uzuka H, Hao K, Tsuburaya R, Takahashi J, Ito K, Shimokawa H. Absence of adventitial vasa vasorum formation at the coronary segment with myocardial bridge - An optical coherence tomography study. *Int J Cardiol* 2018; **250**: 275-277 [PMID: 28993001 DOI: 10.1016/j.ijcard.2017.09.211]

8   **Rogers IS**, Tremmel JA, Schnittger I. Myocardial bridges: Overview of diagnosis and management. *Congenit Heart Dis* 2017; **12**: 619-623 [PMID: 28675696 DOI: 10.1111/chd.12499]

9   **Cademartiri F**, Nistri S, Tarantini G, Maffei E. Management of coronary artery disease with cardiac CT beyond gatekeeping. *Heart* 2017; **103**: 975-976 [PMID: 28446549 DOI: 10.1136/heartjnl-2016-310473]

10   **Swerdlow DI**, Humphries SE. Genetics of CHD in 2016: Common and rare genetic variants and risk of CHD. *Nat Rev Cardiol* 2017; **14**: 73-74 [PMID: 28054577 DOI: 10.1038/nrcardio.2016.209]

11   **Liu Y**, Zhu B, Zhuo L, He MY, Xu Y, Wang TT, Cai QQ, Hu B, Xu JC, Zhang WH. [Risk factors for congenital heart disease in Chinese neonates: a Meta analysis]. *Zhongguo Dang Dai Er Ke Za Zhi* 2017; **19**: 754-758 [PMID: 28697826]

12   **Oliver JM**, Gallego P, Gonzalez AE, Garcia-Hamilton D, Avila P, Yotti R, Ferreira I, Fernandez-Aviles F. Risk factors for excess mortality in adults with congenital heart diseases. *Eur Heart J* 2017; **38**: 1233-1241 [PMID: 28077469 DOI: 10.1093/eurheartj/ehw590]

13   **Aksoy F**, Baş HA, Altınbaş A. Nonsymptomatic myocardial bridge causing systolic total narrowing of circumflex artery. *J Saudi Heart Assoc* 2018; **30**: 153-156 [PMID: 29910588 DOI: 10.1016/j.jsha.2017.06.002]

14   **Xu R**, He Y, Xie LJ, Yang MX, Yang ZG, Guo YK. Myocardial bridging in left main coronary artery. *Coron Artery Dis* 2018; **29**: 274-275 [PMID: 29016382 DOI: 10.1097/MCA.0000000000000566]

15   **Boyd JH**, Pargaonkar VS, Scoville DH, Rogers IS, Kimura T, Tanaka S, Yamada R, Fischbein MP, Tremmel JA, Mitchell RS, Schnittger I. Surgical Unroofing of Hemodynamically Significant Left Anterior Descending Myocardial Bridges. *Ann Thorac Surg* 2017; **103**: 1443-1450 [PMID: 27745841 DOI: 10.1016/j.athoracsur.2016.08.035]

16   **Han R**, Sun K, Lu B, Zhao R, Li K, Yang X. Diagnostic accuracy of coronary CT angiography combined with dual-energy myocardial perfusion imaging for detection of myocardial infarction. *Exp Ther Med* 2017; **14**: 207-213 [PMID: 28672916 DOI: 10.3892/etm.2017.4485]

17   **Ioannidis JPA**. Diagnosis and Treatment of Hypertension in the 2017 ACC/AHA Guidelines and in the Real World. *JAMA* 2018; **319**: 115-116 [PMID: 29242891 DOI: 10.1001/jama.2017.19672]

18   **American Diabetes Association**. 2. Classification and Diagnosis of Diabetes. *Diabetes Care* 2017; **40**: S11-S24 [PMID: 27979889 DOI: 10.2337/dc17-S005]

19   **O'Brien SH**, Vesely SK, Schwarz EB. Response to Comment on O'Brien *et al*. Hormonal Contraception and Risk of Thromboembolism in Women With Diabetes. Diabetes Care 2017;40:233-238. *Diabetes Care* 2017; **40**: e62 [PMID: 28428328 DOI: 10.2337/dci17-0004]

20   **Aikawa Y**, Kataoka Y, Kanaya T, Amaki M, Tahara Y, Asaumi Y, Kanzaki H, Noguchi T, Fujita T, Kobayashi J, Yasuda S. Procedural challenge of coronary catheterization for ST-segment elevation myocardial infarction in patient who underwent transcatheter aortic valve replacement using the CoreValveTM. *Cardiovasc Diagn Ther* 2018; **8**: 190-195 [PMID: 29850412 DOI: 10.21037/cdt.2018.04.02]

21   **Kocovski L**, Lee JD, Parpia S, Fernandes J, Nair V. Association of Waist-Hip Ratio to Sudden Cardiac Death and Severe Coronary Atherosclerosis in Medicolegal Autopsies. *Am J Forensic Med Pathol* 2017; **38**: 226-228 [PMID: 28692479 DOI: 10.1097/PAF.0000000000000330]

22   **Finocchiaro G**, Papadakis M, Sharma S, Sheppard M. Sudden Cardiac Death. *Eur Heart J* 2017; **38**: 1280-1282 [PMID: 28938708 DOI: 10.1093/eurheartj/ehx194]

23   **Basso C**, Aguilera B, Banner J, Cohle S, d'Amati G, de Gouveia RH, di Gioia C, Fabre A, Gallagher PJ, Leone O, Lucena J, Mitrofanova L, Molina P, Parsons S, Rizzo S, Sheppard MN, Mier MPS, Kim Suvarna S, Thiene G, van der Wal A, Vink A, Michaud K; Association for European Cardiovascular Pathology. Guidelines for autopsy investigation of sudden cardiac death: 2017 update from the Association for European Cardiovascular Pathology. *Virchows Arch* 2017; **471**: 691-705 [PMID: 28889247 DOI: 10.1007/s00428-017-2221-0]

24   **Agrawal H**, Sexson-Tejtel SK, Qureshi AM, Alam M, Masand P, Fraser CD, Molossi S, Mery CM. Aborted Sudden Cardiac Death After Unroofing of Anomalous Left Coronary Artery. *Ann Thorac Surg* 2017; **104**: e265-e267 [PMID: 28838524 DOI: 10.1016/j.athoracsur.2017.03.016]

25   **Nam P**, Choi BG, Choi SY, Byun JK, Mashaly A, Park Y, Jang WY, Kim W, Choi JY, Park EJ, Na JO, Choi CU, Lim HE, Kim EJ, Park CG, Seo HS, Oh DJ, Rha SW. The impact of myocardial bridge on coronary artery spasm and long-term clinical outcomes in patients without significant atherosclerotic stenosis. *Atherosclerosis* 2018; **270**: 8-12 [PMID: 29407892 DOI: 10.1016/j.atherosclerosis.2018.01.026]

26   **Wu NQ**, Evora M, Lam UP, Ip MF, Li JJ. Acute myocardial infarction caused by myocardial bridging alone confirmed by using intravascular ultrasonography. *Chronic Dis Transl Med* 2017; **3**: 260-262 [PMID: 29354809 DOI: 10.1016/j.cdtm.2017.05.001]

27   **Kikuchi S**, Okada K, Hibi K, Maejima N, Matsuzawa Y, Konishi M, Kimura Y, Kosuge M, Iwahashi N, Ebina T, Tamura K, Kimura K. Myocardial Infarction Caused by Accelerated Plaque Formation Related to Myocardial Bridge in a Young Man. *Can J Cardiol* 2018; **34**: 1687.e13-1687.e15 [PMID: 30527161 DOI: 10.1016/j.cjca.2018.08.023]

28   **Li Y**, Yu M, Zhang J, Li M, Lu Z, Wei M. Non-invasive imaging of myocardial bridge by coronary computed tomography angiography: the value of transluminal attenuation gradient to predict significant dynamic compression. *Eur Radiol* 2017; **27**: 1971-1979 [PMID: 27565800 DOI: 10.1007/s00330-016-4544-7]

29   **McElwee SK**, Velasco A, Doppalapudi H. Mechanisms of sudden cardiac death. *J Nucl Cardiol* 2016; **23**: 1368-1379 [PMID: 27457531 DOI: 10.1007/s12350-016-0600-6]

Observational Study

Clinical significance and role of up-regulation of SERPINA3 expression in endometrial cancer

Mian-Li Zhou, Fang-Shan Chen, Hui Mao

ORCID number: Mian-Li Zhou (0000-0002-2456-6768); Fang-Shan Chen (0000-0001-9801-140X); Hui Mao (0000-0002-9674-4367).

Author contributions: Zhou ML, Chen FS, and Mao H designed the study and wrote the manuscript.

Institutional review board statement: The study was approved by Hospital of Traditional Chinese Medicine Affiliated to Southwest Medical University on October 28, 2016 (Research ethics No. CHEC2016-111).

Informed consent statement: All subjects gave informed consent prior to study inclusion.

Conflict-of-interest statement: The authors have no conflicts of interest to disclose.

Data sharing statement: No additional data are available.

STROBE statement: The authors have read the STROBE Statement, and the manuscript was prepared and revised according to the STROBE Statement.

Mian-Li Zhou, Fang-Shan Chen, Department of Gynecology and Obstetrics, Traditional Chinese Medicine Hospital Affiliated to Southwest Medical University, Luzhou 646000, Sichuan Province, China

Hui Mao, Department of Oncology, Traditional Chinese Medicine Hospital Affiliated to Southwest Medical University, Luzhou 646000, Sichuan Province, China

Corresponding author: Hui Mao, MD, Professor, Department of Oncology, Traditional Chinese Medicine Hospital Affiliated to Southwest Medical University, No. 182, Chunhui Road, Longmatan District, Luzhou 646000, Sichuan Province, China. 15196087724@163.com
Telephone: +86-830-2397165

Abstract

BACKGROUND
Serpin peptidase inhibitor, clade A member 3 (SERPINA3) belongs to the serpin family with an inhibitory activity against proteases. Its aberrant expression has been observed in a wide range of tumor cells. However, its clinical significance and biological function in endometrial cancer have been rarely studied. We designed a study to determine the levels of SERPINA3 and its significance in patients with endometrial cancer.

AIM
To investigate the clinical significance and role of SERPINA3 expression in endometrial cancer cells.

METHODS
Eighty endometrial tissue samples collected from patients with endometrial cancer were included in an observation group and 80 paraffin-embedded tissues samples collected from patients with normal endometrial tissues undergoing myomectomy were employed as a control group between January 2014 and December 2018. The expression of SERPINA3 mRNA was detected by quantitative polymerase chain reaction (PCR) for all endometrial tissues included in the study.

RESULTS
The positive expression rate of SERPINA3 protein in endometrial cancer cells was 71.25% in the observation group, which was significantly higher than that in the control group (31.25%; $P < 0.05$). There was no correlation between SERPINA3 protein in endometrial cancer cells and the age range at which women experienced menopause ($P > 0.05$). However, it was associated with pathological

grade, clinical stage, vascular invasion, and lymph node metastasis ($P < 0.05$). Pathological grade, clinical stage, vascular invasion, and lymph node metastasis were independent prognostic factors for endometrial cancer.

CONCLUSION
The follow-up study of SERPINA3 can be used as a prognostic biomarker for endometrial cancer and as one of the targets for bio-targeted therapy for endometrial cancer.

Key words: Serpin peptidase inhibitor, clade A member 3; Endometrial cancer; Quantitative polymerase chain reaction; Expression

Core tip: Serpin peptidase inhibitor, clade A member 3 (SERPINA3) is considered to be associated with several cancers. In this study, the clinical significance and role of SERPINA3 expression in endometrial cancer were investigated. It was found that the expression of SERPINA3 was up-regulated in endometrial cancer and expression of SERPINA3 in endometrial cancer was correlated with pathological grade, clinical stage, vascular invasion, and lymph node metastasis. SERPINA3 has the potential to be used as a biomarker for prognosis and a specific target for targeted therapy in patients with endometrial carcinoma.

INTRODUCTION

Endometrial cancer is a common malignancy which affects women in China. The incidence of endometrial cancer is just behind that of cervical cancer. It is also the representative malignant cancer of the female reproductive system with an elevated incidence rate in the United States[1]. Many patients are unaware of its onset and development due to the hidden cause and non-specific signs and symptoms in the early stages of the disease. As a result, a great proportion of women are diagnosed with endometrial cancer at an advanced stage, which causes them to miss the important opportunities for appropriate and effective interventions. In most cases, endometrial cancer presents as vaginal bleeding in postmenopausal women; and in non-menopausal women, it is characterized by increased menstrual loss and longer or irregular periods.

Therefore, cancer detection should be carefully used to effectively control the development of cancer, promote the early management intervention, and improve the prognosis accordingly. Currently, the most basic methods for detection of endometrial cancer include diagnostic curettage, adjuvant detection by B-mode ultrasonography, hysteroscopy, and nuclear resonance imaging[2,3]. Surgical therapy is the main intervention for most women with endometrial cancer. The follow-up intervention should focus on the non-invasive, accurate strategies for detecting the above mentioned therapies. Recently, more studies increased their interest in targeted therapy targeting cancer specific genes. Serpin peptidase inhibitor clade A member 3 (SERPINA3) is one of them. The related studies[4,5] revealed that SERPINA3 and its ectopic expression were identified in several cancers, *e.g.*, liver, prostate, lung, and breast cancers. However, few studies investigated SERPINA3 in patients with endometrial cancer. The present study examined the gene expression of SERPINA3 and its clinical significance in endometrial cancer.

MATERIALS AND METHODS

Sample collection
Eighty endometrial tissue samples collected from patients (aged 54-68 years, mean

age 61.5 ± 3.1 years) with endometrial cancer were included in an observation group and 80 paraffin-embedded tissues samples collected from patients (aged 52-69 years, mean age 60.2 ± 2.9 years) with normal endometrial tissues undergoing myomectomy were employed as a control group between January 2014 and December 2018. The tissue samples (6 cm × 4 cm × 2 cm for both groups) were collected with the informed consent of the donors and relatives and with complete follow-up information and clinical data. All the patients were chemoradiotherapy, hormone therapy, and antitumor therapy naïve.

Tissue microarray construction

Tissue microarrays were constructed and exposed to the dye. The most representative tumor regions were marked on haematoxylin and eosin stained section slides. This step was also applicable for normal endometrial tissues. Two focus points were selected per tissue block. Targeted tissue samples were extracted from the donor blocks by a fine hollow needle of 1.0 mm in diameter and then injected into the recipient paraffin blocks. The placement of each tissue sample on the coordinate grid of the recipient block was done according to the research aim and the requirements for the study. Once the recipient block was filled, it was cut to generate 4 um thick slices for analysis.

Immunohistochemical staining

The slices were baked at 70 °C for a total of 1 h. Xylene was used to remove paraffin wax. Then, hydration was performed in graded ethanol. For antigen retrieval, 0.01 mmpl/L of sodium citrate buffer (pH = 6) was added and incubated at 100 °C for 10 min. The sections were then incubated with rabbit anti-human polyclonal antibody (dilution, 1:50) at 4 °C overnight, followed by incubation with goat anti-rabbit (IgG) secondary antibody (1: 200) at room temperature for 1 h. Diaminobenzidine was used for staining. Hematoxylin stain was applied in the secondary staining step. At last, proper neutral balsam was added to seal the tissue. The scoring criteria were: a score of 0 was considered to reflect the positive expression rate of 0 to 10%, score of 1 reflect 10% to 30%, score of 2 reflect 30% to 60%, and score of 3 reflect >60%. If the staining results were not consistent between the two tissue cores, the higher score was considered only. The expression was scored by two pathologists double-blindly. The consistent sores between the two pathologists were involved in the final analysis. Scores of 0 to 1 were defined as low expression and scores of 2 to 3 were defined as high expression.

Real-time quantitative polymerase chain reaction

Total RNA was extracted using TRIZOL reagent. This step was done by strictly following standard instructions (PrimeScript RT, USA). A Rim eScriptRT kit was used for reverse transcription to obtain cDNA. The reaction condition was 37 °C for 30 min and 85 °C for 5 s. The ABI 7300 real-time PCR system was used for amplification. The primers used are as follows: SERPINA3 upstream primer, 5'-TGC CAG CGC ACT CTT CAT C-3' and SERPINA3 downstream primer, 5'-TGT CGT TCA GGT TAT AGT CCC; GAPDH upstream primer, 5'-TGC GAG TAC TCA ACA CCA ACA-3' and GAPDH downstream primer, 5'-GCA TAT CTT CGG CCC ACA-3'. The overall reaction system consisted of 0.8 µL of GAPDH or AERPINA3 upstream and downstream primers, 7.6 µL of cDNA, 10 µL of SYBR Prem ixEx TaqTM, 0.4 µL of Rox Reference Dye (50×), and 0.4 µL of Rox Reference Dye II (50×). PCR reaction conditions were predenaturation at 95 °C for 30 s and 40 cycles of denaturation at 95 °C for 5 s and annealing at 60 °C for 31 s. The obtained data were input into Excel for calculation and analysis.

Statistical analysis

Statistical analyses were performed with SPSS19.0 software using "χ^2" and "t" reflecting results of the test. The count data are presented using percentages and the measured data are presented as the mean ± standard deviation. Significance level was considered at $P < 0.05$.

RESULTS

Expression of SERPINA3 protein

A comparison of SERPINA3 protein expression between the observation group and the control group showed that the positive expression rate of SERPINA3 protein in endometrial cancer cells was 71.25% (57/80) in the observation group, which was significantly higher than that in the control group (31.25%, 25/80; $P < 0.05$).

Relationship between SERPINA3 expression and pathologic features of endometrial cancer

SERPINA3 protein expression in endometrial cancer cells was associated with pathological grade, clinical stage, vascular invasion, and lymph node metastasis ($P < 0.05$), rather than with the age range at which women experienced menopause ($P > 0.05$, Table 1).

Factors influencing the prognosis of patients with endometrial cancer

Pathological grade, clinical stage, vascular invasion, and lymph node metastasis were independent prognostic factors for endometrial cancer (Table 2).

DISCUSSION

Rising prevalence of endometrial cancer has been reported in China over the last decades, and accordingly the research work on endometrial cancer went further and more detailed. However, the exact cause of endometrial cancer is still unknown[6-8]. Currently, the research of endometrial cancer shows increasing interest in how prognosis can be improved by early diagnosis and effective treatment. The assessment of biomarkers may predict the prognosis of endometrial cancer, and should be further studied and interpreted, and studies of biomarkers and bio-targeted therapy for endometrial cancer should be warranted. SERPINA3, an important member of the serine peptidase inhibitors family, has been identified and validated in several cancer cells. However, very few studies have examined SERPINA3 in endometrial cancer cells[9]. As a typical acute-phase protein, SERPINA3 is regulated by inflammatory cytokines so that its expression is increased in the inflammatory response. The promoter of SERPINA3 is transcriptionally activated by three transcription factors and the transcriptional level of SERPINA3 is influenced by single nucleotide polymorphisms within the promoter[10-12]. Single nucleotide polymorphisms are expressed by regulating the components of genetic sequence when the inflammatory response occurs. Once the inflammatory response occurs, it is benefit for the synthesis of SERPINA3. Nowadays, studies have produced inconsistent and even contradictory results on the expression of SERPINA3. The relevant studies[13-15] showed that overexpression of SERPINA3 predicts that damage tends to occur in the body contributing to decreased cell adhesion ability and inhibition of apoptosis. It is revealed that the up-regulation of SERPINA3 is positively associated with malignant tumors.

Few studies have reported the relationship between SERPINA3 protein expression and the incidence of endometrial cancer in China. The current study revealed that pathological grade, clinical stage, vascular invasion, and lymph node metastasis of endometrial cancer were strongly associated with the expression of SERPINA3 ($P < 0.05$). Recently, many studies demonstrated that SERPINA3 could be used as one of the biomarkers in predicting prognosis of several cancers. For instance, SERPINA3 is one of the proteins in signal transduction pathways of the inflammatory response. A study of clinical relapsed ovarian tumors showed that the up-regulation of SERPINA3 was associated with disease progression and chemical resistance[16]. Moreover, another study showed that methylation of the 5' region may account for up-regulation of SERPINA3 in placental disease. Researchers also found that overexpression of SERPINA3 in JEG-3 human choriocarcinoma cells could prevent apoptosis[17]. Furthermore, one study established that SERPINA3 levels were increased in patients with liver, pancreatic, and prostate cancers. Research studies on endometrial cancer have increased in recent years[18]. What is certain is that p53 mutations and subsequent overexpression of human epidermal growth factor receptor 2 (HER2) were common molecular events in endometrial cancer. According to Villalba *et al*[19], an analysis of SERPINA3 expression in normal tissues and endometrial cancer tissues and in different surgical/pathological stages through immunohistochemistry and fluorescence quantitative real-time polymerase chain reaction (FQ-PCR) suggested that the up-regulation of SERPINA3 was strongly associated with factors such as poor differentiation and high surgical/pathological stage. In addition, it predicted a poor prognosis of endometrial cancer.

Endometrial cancer is a malignant tumor that lacks clear diagnosis and optimal treatment. There is currently no conclusive evidence available for the postoperative healing, and the overall survival rate has not been improved fundamentally, although hysterectomy is performed as the main treatment for most women with this cancer. Alternatively, effective postoperative bio-targeted therapy should be given to improve survival and delay recurrence subsequent to surgery in patients who experienced hysterectomy for endometrial cancer[1,20]. Based on the present study,

Table 1 Relationship between SERPINA3 expression and pathologic features of endometrial cancer

Variable		N	SERPINA3 protein		X^2	P-value
			-	+		
Pathological grade	I	45	19	26	9.774	< 0.05
	II	27	4	23		
	III/IV	8	0	8		
Clinical stage	G1	21	10	11	6.351	< 0.05
	G3	32	5	27		
	G2/G3	27	8	19		
Menopause	Yes	41	20	21	0.864	> 0.05
	No	39	15	24		
Vascular invasion	≤ 50%	52	7	45	16.953	< 0.05
	> 50%	28	16	12		
Lymph node metastasis	Positive	24	1	23	10.115	< 0.05
	Negative	56	22	34		

"-" indicates the negative expression of SERPINA3; "+" indicates the positive expression of SERPINA3.

lymph node metastasis and vascular invasion were independent prognostic factors influencing prognosis of endometrial cancer, and SERPINA3 played an important role in the prognosis of endometrial cancer. This further strengthens that SERPINA3 is one of biomarkers for predicting poor prognosis of endometrial cancer. Estrogen-independent type II carcinoma is the more common type of endometrial cancer. Activity of HER2 is increased and cell growth and apoptosis are regulated through the PI3K/AKT pathway in this population. Whether a synergistic interplay exists between SERPINA3 and HER2 in the development of type II endometrial carcinomas should be further investigated[21,22].

In conclusion, SERPINA3 has the potential to be used as a biomarker for prognosis and a specific target for targeted therapy in patients with endometrial carcinomas based on a deepening understanding of endometrial carcinoma through research.

Table 2 Factors influencing the prognosis of patients with endometrial cancer

Factor	B	SE	df	P	95%CI for Exp (B)
Pathological grade	0.6567	0.0149	1	0.000	0.5385-0.8865
Clinical stage	0.7337	0.0140	1	0.000	0.5689-0.8561
Vascular invasion	0.7685	0.0208	1	0.000	0.4414-0.9836
Lymph node metastasis	0.6605	0.0145	1	0.000	0.5176-0.9074

B: Regression coefficient; CI: Confidence index; Exp (B): Odds ratio.

ARTICLE HIGHLIGHTS

Research background

The expression profile of serpin peptidase inhibitor clade A member 3 (SERPINA3) in patients with endometrial cancer has rarely been studied. In the present study, we detected the protein levels of SERPINA3 in patients with endometrial cancer and the correlation between the expression of SERPINA3 and the prognosis for endometrial cancer. The result revealed that SERPINA3 expression was significantly up-regulated in endometrial cancer and was closely correlated with pathological grade, clinical stage, vascular invasion, and lymph node metastasis. These findings indicated that SERPINA3 can be used as a prognostic biomarker for endometrial cancer and as one of the targets for bio-targeted therapy for endometrial cancer.

Research motivation

The results of the present study may provide insight into the application of SERPINA3 as a predictor of clinical outcomes and a potential therapeutic target for endometrial cancer.

Research objectives

The present study aimed to assess the significance of SERPINA3 levels in patients with endometrial cancer.

Research methods

The present study examined tissue samples which were available from patients with endometrial cancer and patients with normal endometrial tissues. Tissue microarrays were constructed and immunohistochemical staining was performed. The expression of SERPINA3 mRNA was detected by quantitative PCR. The data were analyzed with SPSS19.0 software.

Research results

We found that SERPINA3 expression was higher in endometrial cancer compared to normal tissues and up-regulated SERPINA3 was closely correlated with pathological grade, clinical stage, vascular invasion, and lymph node metastasis in endometrial cancer.

Research conclusions

Assessment of tumor *vs* normal tissues showed that the expression of SERPINA3 was up-regulated in endometrial cancer. The SERPINA3 protein level in endometrial cancer cells was associated with pathological grade, clinical stage, vascular invasion, and lymph node metastasis, rather than with the age range at which women experienced menopause. SERPINA3 has the potential to be used as a biomarker for prognosis and a specific target for targeted therapy in patients with endometrial carcinomas.

Research perspectives

Further studies are warranted to improve our understanding of the role of SERPINA3 in endometrial cancer.

REFERENCES

1   **Santamaria M**, Pardo-Saganta A, Alvarez-Asiain L, Di Scala M, Qian C, Prieto J, Avila MA. Nuclear α1-antichymotrypsin promotes chromatin condensation and inhibits proliferation of human hepatocellular carcinoma cells. *Gastroenterology* 2013; **144**: 818-828.e4 [PMID: 23295442 DOI: 10.1053/j.gastro.2012.12.029]

2   **Banno K**, Kisu I, Yanokura M, Masuda K, Ueki A, Kobayashi Y, Susumu N, Aoki D. Epigenetics and genetics in endometrial cancer: new carcinogenic mechanisms and relationship with clinical practice. *Epigenomics* 2012; **4**: 147-162 [PMID: 22449187 DOI: 10.2217/epi.12.13]

3   **Koual M**, Ngo C, Girault A, Lécuru F, Bats AS. Endometrial cancer in the elderly: does age influence surgical treatments, outcomes, and prognosis? *Menopause* 2018; **25**: 968-976 [PMID: 29762198 DOI: 10.1097/GME.0000000000001119]

4   **Weigelt B**, Banerjee S. Molecular targets and targeted therapeutics in endometrial cancer. *Curr Opin Oncol* 2012; **24**: 554-563 [PMID: 22581357 DOI: 10.1097/CCO.0b013e328354e585]

5   **Connor EV**, Rose PG. Management Strategies for Recurrent Endometrial Cancer. *Expert Rev Anticancer*

Ther 2018; **18**: 873-885 [PMID: 29972650 DOI: 10.1080/14737140.2018.1491311]

6   **Kotula E**, Berthault N, Agrario C, Lienafa MC, Simon A, Dingli F, Loew D, Sibut V, Saule S, Dutreix M. DNA-PKcs plays role in cancer metastasis through regulation of secreted proteins involved in migration and invasion. *Cell Cycle* 2015; **14**: 1961-1972 [PMID: 26017556 DOI: 10.1080/15384101.2015.1026522]

7   **Arend RC**, Jones BA, Martinez A, Goodfellow P. Endometrial cancer: Molecular markers and management of advanced stage disease. *Gynecol Oncol* 2018; **150**: 569-580 [PMID: 29843906 DOI: 10.1016/j.ygyno.2018.05.015]

8   **De Bernardi E**, Buda A, Guerra L, Vicini D, Elisei F, Landoni C, Fruscio R, Messa C, Crivellaro C. Radiomics of the primary tumour as a tool to improve 18F-FDG-PET sensitivity in detecting nodal metastases in endometrial cancer. *EJNMMI Res* 2018; **8**: 86 [PMID: 30136163 DOI: 10.1186/s13550-018-0441-1]

9   **Forde N**, Bazer FW, Spencer TE, Lonergan P. 'Conceptualizing' the Endometrium: Identification of Conceptus-Derived Proteins During Early Pregnancy in Cattle. *Biol Reprod* 2015; **92**: 156 [PMID: 25947061 DOI: 10.1095/biolreprod.115.129296]

10   **Jennings P**, Crean D, Aschauer L, Limonciel A, Moenks K, Kern G, Hewitt P, Lhotta K, Lukas A, Wilmes A, Leonard MO. Interleukin-19 as a translational indicator of renal injury. *Arch Toxicol* 2015; **89**: 101-106 [PMID: 24714768 DOI: 10.1007/s00204-014-1237-3]

11   **Cao LL**, Pei XF, Qiao X, Yu J, Ye H, Xi CL, Wang PY, Gong ZL. SERPINA3 Silencing Inhibits the Migration, Invasion, and Liver Metastasis of Colon Cancer Cells. *Dig Dis Sci* 2018; **63**: 2309-2319 [PMID: 29855767 DOI: 10.1007/s10620-018-5137-x]

12   **Li Y**, Dong X, Cai J, Yin S, Sun Y, Yang D, Jiang C. SERPINA3 induced by astroglia/microglia co-culture facilitates glioblastoma stem-like cell invasion. *Oncol Lett* 2018; **15**: 285-291 [PMID: 29399139 DOI: 10.3892/ol.2017.7275]

13   **Takayama S**, Monma Y, Tsubota-Utsugi M, Nagase S, Tsubono Y, Numata T, Toyoshima M, Utsunomiya H, Sugawara J, Yaegashi N. Food intake and the risk of endometrial endometrioid adenocarcinoma in Japanese women. *Nutr Cancer* 2013; **65**: 954-960 [PMID: 24053697 DOI: 10.1080/01635581.2013.818158]

14   **Péré-Brissaud A**, Blanchet X, Delourme D, Pélissier P, Forestier L, Delavaud A, Duprat N, Picard B, Maftah A, Brémaud L. Expression of SERPINA3s in cattle: focus on bovSERPINA3-7 reveals specific involvement in skeletal muscle. *Open Biol* 2015; **5**: 150071 [PMID: 26562931 DOI: 10.1098/rsob.150071]

15   **Chelbi ST**, Wilson ML, Veillard AC, Ingles SA, Zhang J, Mondon F, Gascoin-Lachambre G, Doridot L, Mignot TM, Rebourcet R, Carbonne B, Concordet JP, Barbaux S, Vaiman D. Genetic and epigenetic mechanisms collaborate to control SERPINA3 expression and its association with placental diseases. *Hum Mol Genet* 2012; **21**: 1968-1978 [PMID: 22246292 DOI: 10.1093/hmg/dds006]

16   **Akhmadishina LZ**, Korytina GF, Kochetova OV, Viktorova EV, Viktorova TV. [Analysis of polymorphisms of genes associated with immune response and tissue remodeling in occupational chronic bronchitis]. *Genetika* 2014; **50**: 1363-1373 [PMID: 25739290 DOI: 10.1134/S1022795414110027]

17   **Sohn EH**, Khanna A, Tucker BA, Abràmoff MD, Stone EM, Mullins RF. Structural and biochemical analyses of choroidal thickness in human donor eyes. *Invest Ophthalmol Vis Sci* 2014; **55**: 1352-1360 [PMID: 24519422 DOI: 10.1167/iovs.13-13754]

18   **Haynes BP**, Viale G, Galimberti V, Rotmensz N, Gibelli B, Smith IE, Dowsett M. Differences in expression of proliferation-associated genes and RANKL across the menstrual cycle in estrogen receptor-positive primary breast cancer. *Breast Cancer Res Treat* 2014; **148**: 327-335 [PMID: 25367875 DOI: 10.1007/s10549-014-3181-6]

19   **Villalba M**, Rathore MG, Lopez-Royuela N, Krzywinska E, Garaude J, Allende-Vega N. From tumor cell metabolism to tumor immune escape. *Int J Biochem Cell Biol* 2013; **45**: 106-113 [PMID: 22568930 DOI: 10.1016/j.biocel.2012.04.024]

20   **Yang GD**, Yang XM, Lu H, Ren Y, Ma MZ, Zhu LY, Wang JH, Song WW, Zhang WM, Zhang R, Zhang ZG. SERPINA3 promotes endometrial cancer cells growth by regulating G2/M cell cycle checkpoint and apoptosis. *Int J Clin Exp Pathol* 2014; **7**: 1348-1358 [PMID: 24817931]

21   **Sun YP**, Lv XP, Wang JD, Fang ZH. Expression analysis of PELP1 in type II endometrial carcinoma and its correlation with ER. *Xiandai Fuchanke Jinzhan* 2017; **26**: 270-272, 275

22   **Xue Y**, Sun XL, Wang JL, Wei LH. The preliminary research on the relationship of the expression and regulation between TLR2 and beta-arrestin 2 in endometrial carcinoma. *Xiandai Fuchanke Jinzhan;* 2014; **5**: 337-340

Observational Study

Evaluation of right ventricular volume and systolic function in normal fetuses using intelligent spatiotemporal image correlation

Jia-Xing Sun, Ai-Lu Cai, Li-Mei Xie

ORCID number: Jia-Xing Sun (0000-0002-7667-6686); Ai-Lu Cai (0000-0003-0390-8930); Li-Mei Xie (0000-0002-5308-1786).

Author contributions: Sun JX and Xie LM contributed equally to this work; Xie LM designed the research; Sun JX, Cai AL, Xie LM performed research; Sun JX analyzed the data and wrote the paper.

Institutional review board statement: The study was reviewed and approved by Shengjing Hospital of China Medical University.

Informed consent statement: Patients were not required to give informed consent to the study because the analysis used anonymous data.

Conflict-of-interest statement: There are no conflicts of interest to report.

Data sharing statement: No additional data are available.

STROBE statement: The manuscript was written and revised according to the STROBE Statement.

Jia-Xing Sun, Ai-Lu Cai, Li-Mei Xie, Ultrasound Department, Shengjing Hospital of China Medical University, Shenyang 110004, Liaoning Province, China

Li-Mei Xie, Ultrasound Department, Roicare Hospital and Clinics, Shenyang 110004, Liaoning Province, China

Corresponding author: Li-Mei Xie, MD, PhD, Professor, Ultrasound Department, Shengjing Hospital of China Medical University/Roicare Hospital and Clinics, No. 36 Sanhao Street, Shenyang 110004, Liaoning Province, China. xielm72@163.com
Telephone: +86-24-9661574194
Fax: +86-24-9661574194

Abstract

BACKGROUND
Heart defects are the most common congenital malformations in fetuses. Fetal cardiac structure and function abnormalities lead to changes in ventricular volume. As ventricular volume is an important index for evaluating fetal cardiovascular development, an effective and reliable method for measuring fetal ventricular volume and cardiac function is necessary for accurate ultrasonic diagnosis and effective clinical treatment. The new intelligent spatiotemporal image correlation (iSTIC) technology acquires high-resolution volumetric images. In this study, the iSTIC technique was used to measure right ventricular volume and to evaluate right ventricular systolic function to provide a more accurate and convenient evaluation of fetal heart function.

AIM
To investigate the value of iSTIC in evaluating right ventricular volume and systolic function in normal fetuses.

METHODS
Between October 2014 and September 2015, a total of 123 pregnant women received prenatal ultrasound examinations in our hospital. iSTIC technology was used to acquire the entire fetal cardiac volume with off-line analysis using QLAB software. Cardiac systolic and diastolic phases were defined by opening of the atrioventricular valve and the subsequent closure of the atrioventricular valve. The volumetric data of the two phases were measured by manual tracking and summation of multiple slices and recording of the right ventricular end-systolic volume and the right ventricular end-diastolic volume. The data were used to calculate the right stroke volume, the right cardiac output, and the right ejection fraction. The correlations of changes between the above-mentioned indices and

gestational age were analyzed. The right ventricular volumes of 30 randomly selected cases were measured twice by the same sonographer, and the intra-observer agreement measurements were calculated.

RESULTS
Among the 123 normal fetuses, the mean right ventricular end-diastolic volume increased from 0.99 ± 0.34 mL at 22 wk gestation to 3.69 ± 0.36 mL at 35^{+6} wk gestation. The mean right ventricular end-systolic volume increased from 0.43 ± 0.18 mL at 22 wk gestation to 1.36 ± 0.22 mL at 35^{+6} wk gestation. The mean right stroke volume increased from 0.62 ± 0.29 mL at 22 wk gestation to 2.33 ± 0.18 mL at 35^{+6} wk gestation. The mean right cardiac output increased from 92.23 ± 40.67 mL/min at 22 wk gestation to 335.83 ± 32.75 mL/min at 35^{+6} wk gestation. Right ventricular end-diastolic volume, right ventricular end-systolic volume, right stroke volume, and right cardiac output all increased with gestational age and the correlations were linear ($P < 0.01$). Right ejection fraction had no apparent correlation with gestational age ($P > 0.05$).

CONCLUSION
Fetal right ventricular volume can be quantitatively measured using iSTIC technology with relative ease and high repeatability. iSTIC technology is expected to provide a new method for clinical evaluation of fetal cardiac function.

Key words: Ultrasonography; Fetus; Intelligent spatiotemporal image correlation; Right ventricular volume; Cardiac function

Core tip: Heart defects are the most common congenital malformations in fetuses. Fetal cardiac structure and function abnormalities often lead to changes in ventricular volume. Numerous studies have focused on fetal heart functions, which have not been widely accepted. Between October 2014 and September 2015, the intelligent spatiotemporal image correlation technique was used to measure right ventricular volume in 123 normal fetuses and to evaluate right ventricular systolic function to provide a new method for more accurate and convenient evaluation of fetal heart function.

INTRODUCTION

Heart defects are the most common congenital malformations in fetuses with an incidence six times greater than chromosome abnormalities and four times greater than neural tube defects[1,2]. The diagnosis of congenital heart disease is a challenge using prenatal ultrasound and is the focus of perinatal medical research. Congenital heart disease can be divided into structural and functional abnormalities. Indeed, fetal cardiac structure and function abnormalities often lead to changes in ventricular volume. As ventricular volume is an important index for evaluating fetal cardiovascular development, an effective and reliable method for measuring fetal ventricular volume and cardiac function is necessary for accurate ultrasonic diagnosis and effective clinical treatment of congenital heart disease.

Numerous studies have focused on fetal heart function in an effort to evaluate cardiac function in the healthy fetus and in those in states of cardiac decompensation[3]. The accuracy of traditional two-dimensional (2D) ultrasound in the quantitative evaluation of fetal heart function has not been widely accepted[4-15]. Spatiotemporal image correlation (STIC) technology overcomes many of the shortcomings of conventional 2D ultrasound in the measurement of fetal ventricular volume and evaluation of fetal cardiac function. Recently, a number of studies have used STIC technology in combination with organ computer-aided analysis software to

measure fetal ventricular volume and evaluate heart function with proven accuracy and feasibility[4-7,16-27]. However, STIC still has some limitations and the imaging principle determines that STIC is not a real-time three-dimensional (3D) imaging technology. One-way scanning using the sensors during the scanning process execution is slow, which leads to relatively long image acquisition time. Therefore, STIC is vulnerable to the effects of fetal and maternal respiration, resulting in degradation of image quality[21,23].

The new intelligent STIC (iSTIC) technology adopts an electronic matrix type of probe, which is composed of thousands of vibrating bits, thus generating real-time 3D images with acquired data. The new iSTIC technology acquires high-resolution volumetric images of one cardiac cycle in only 2 s, thus reducing the effects of fetal movement on the image. iSTIC realizes real-time 3D visualization of the fetal heart, which has been shown to have many advantages[24,25,27-29]. In the present study, the iSTIC technique was used to measure right ventricular volume in normal fetuses and to evaluate right ventricular systolic function to provide a new method for more accurate and convenient evaluation of fetal heart function.

MATERIALS AND METHODS

General information

One hundred twenty-three healthy gravidas with singleton gestations who visited our hospital for prenatal ultrasonography between October 2014 and September 2015 were included in the study. The maternal age range was 22–36 years (average, 26.60 ± 3.54 years). The gestational age range was 22–35+6 wk (mean, 28 ± 3.79 wk), including 20 cases at 22–23+6 wk, 24 cases at 24–25+6 wk, 20 cases at 26–27+6 wk, 16 cases at 28–29+6 wk, 18 cases at 30–31+6 wk, 15 cases at 32–33+6 wk, and 10 cases at 34–35+6 wk. The inclusion criteria were as follows: (1) singleton pregnancy; (2) fetal biological measurement indicators consistent with the corresponding gestational age; (3) no obvious fetal anatomic abnormalities shown on 2D ultrasound examination; (4) pregnant women were informed of the purpose of the evaluation, and informed consent was obtained before image acquisition; and (5) fetal heart image acquired using real-time 3D iSTIC technology was free of artifacts.

Instruments

An IU22 3D color Doppler ultrasound diagnostic instrument from Philips Company (Bothell, WA, USA) was used with a 2-4 MHz electronic matrix probe. QLAB software was used for image analysis and post-processing.

Data acquisition

The information of the last menstrual period and the gestational age in the pregnant women was obtained and recorded. The women were asked to lie flat, and a fetal echo program was begun with transabdominal scanning using an X6-1 probe. They were advised to hold their breath during the acquisition process to avoid interference of motion artifacts. Using a 3D/4D iSTIC technology model for a 4-chamber view of the fetal heart, the 3D/4D sampling frame location was adjusted and the sampling range assured 3D/4D volume data acquisition. The sampling frame included the entire fetal heart. The fetal heart rate was measured and recorded after completion of data acquisition. All images were stored in a built-in hard disk in the machine for later offline analysis.

Data analysis

(1) Post-processing of 3D image. The image stored in the built-in hard disk in the machine was extracted for analysis using QLAB software. The atrioventricular valve opening and closing framing at end systole and diastole in the entire cardiac cycle were observed to measure the fetal right ventricular volume. End systole was defined as the moment before atrioventricular valve opening, and end diastole was defined as the moment immediately after the atrioventricular valve closed. The center point of the central position of the right ventricle was adjusted using stacked contours to draw a line along the endocardium of the right ventricular apex to the edge of the tricuspid valve, the software was then automatically stratified followed by manual outlining of the contour of each layer of the lining of the heart at the short axis view of the heart including the trabecular muscle and regulating bundle. Computer software automatically calculated the volume of the right ventricle (Figure 1). The right ventricular end-diastolic volume (REDV) and the right ventricular end-systolic volume (RESV) were measured by the same observer three times to obtain the average value.

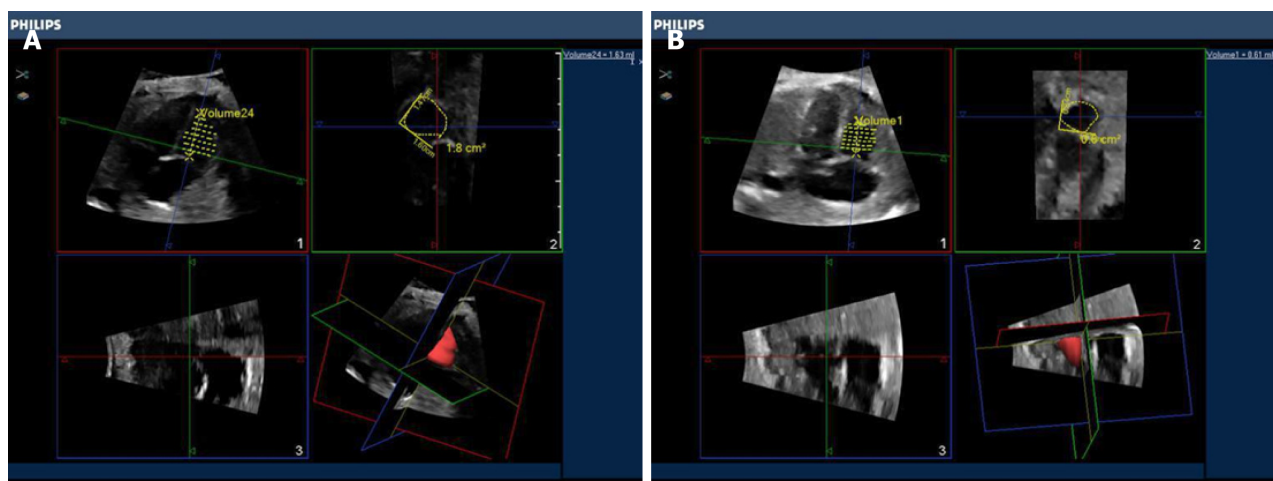(2) The heart function index was calculated as follows: The right stroke volume

Figure 1 Fetal right ventricular end diastolic volume obtained by intelligent spatiotemporal image correlation technique.

(RSV) = REDV- RESV; the right cardiac output (RCO) = RSV × fetal heart rate; the right ejection fraction = RSV/REDV.

(3) The paired Student's *t* test was performed by randomly retrieved images from 30 cases with the fetal right ventricular volume independently measured by two observers (twice for each observer or twice by the same observer) to evaluate the consistency of the measurement. The average value by each observer was compared.

Statistical analysis

Data input and processing were carried out using SPSS 23.0 statistical software. The quantitative data conforming to normal distribution were presented as x ± s. Spearman rank correlation analysis was used to determine the relationship between fetal right ventricular volume and cardiac function parameter changes with gestational age. In addition, the paired Student's *t* test was used to evaluate the consistency of the measurement by the same observer and between different observers. Differences with $P < 0.05$ were considered statistically significant.

RESULTS

Spearman rank correlation analysis

The changes in normal fetal REDV, RESV, RSV, and RCO with gestational age showed significant linear correlations, and the correlation coefficients were 0.903, 0.874, 0.866 and 0.865, respectively ($P < 0.01$, Figure 2, Table 1). Right ejection fraction did not change as gestational age increased, was relatively constant throughout the entire pregnancy, and was not significantly correlated with gestational age ($P > 0.05$, Table 1). Measurement of fetal right ventricular volume and cardiac function was carried out using the iSTIC technique (Table 2).

Paired Student's t test

The intraclass correlation coefficients (ICC) of REDV measured by the same observer was 0.989 with a 95% confidence interval (CI) of 0.978–0.995. The ICC of RESV was 0.978 with a 95%CI of 0.955–0.989. The ICC of REDV measured by different observers was 0.988 with a 95%CI of 0.975–0.944. The ICC of RESV was 0.988 with a 95%CI of 0.900–0.977. There was no statistical difference between the same observer and different observers when applying the iSTIC technique to measure RESV and REDV using the consistency test, and the correlation coefficients were 0.989, 0.951, 0.990, and 0.980, respectively. The results showed that there was particularly good consistency between the same observer and different observers ($P < 0.001$, Table 3).

DISCUSSION

Fetal cardiac function can be affected by a variety of conditions and prenatal interventions. Accurate assessment of fetal cardiac function could help to understand the process of fetal heart disease, improve the accuracy of diagnosis, and determine prenatal interventions[2,5,6,16,19,20,22,23,26,30-39]. Two-dimensional ultrasound is still the

Table 1 The relationship between normal fetal right ventricular end-diastolic volume, right ventricular end-systolic volume, right stroke volume, right cardiac output, and right ejection fraction with gestational ages from 22 to 35^{+6} wk

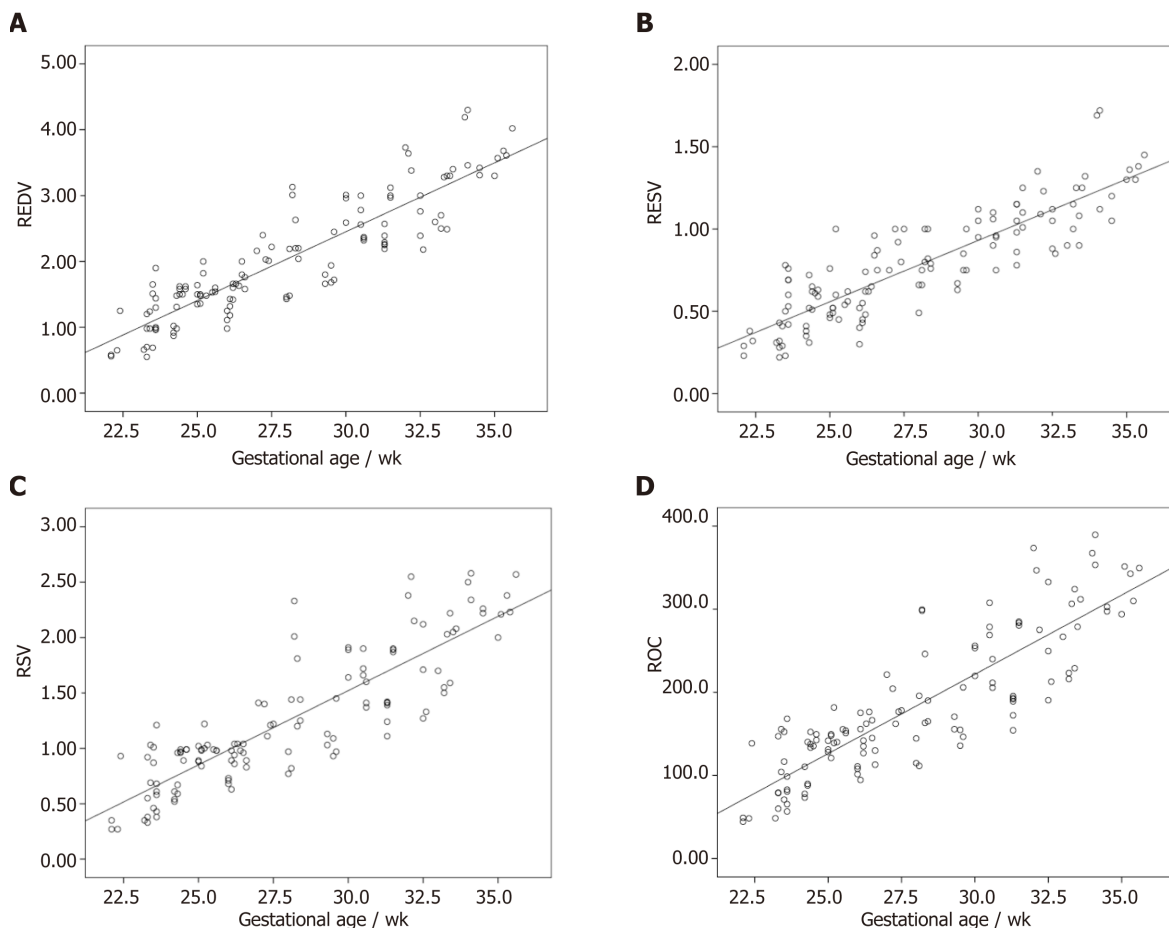| Gestational age	REDV	RESV	RSV	RCO	REF
r	0.903	0.874	0.866	0.865	0.120
P	< 0.001	< 0.001	< 0.001	< 0.001	0.187

REDV: Right ventricular end-diastolic volume; RESV: Right ventricular end-systolic volume; RSV: Right stroke volume; RCO: Right cardiac output; REF: Right ejection fraction.

traditional gold standard for diagnosis of fetal congenital heart diseases[17,20,21] but has a number of limitations in the quantitative evaluation of fetal ventricular volume and cardiac function. When abnormal fetal heart structure causes significant cardiac geometric morphology changes, accurate quantitative assessment of fetal ventricular volume and cardiac function by 2D ultrasound is difficult[3,34].

Application of the STIC imaging technique in fetal heart disorders has been studied extensively, which adds the time factor into the process of 3D data acquisition with continuous unidirectional scanning of the target area by the sensor to obtain the 3D volume data composed of each 2D slice. After completion of volume data acquisition, the software can automatically group 2D sections at the same time to reorganize the image of the entire fetal cardiac cycle, with end-systolic and end-diastolic phases of the cardiac cycle image defined according to opening and closing of the atrioventricular valve in post-processing[3,16,17,20-23,29,36,38-42]. Such technology overcomes the imaginary heart geometry by 2D ultrasound along with a relatively simple image acquisition process and fewer requirements for operator experience. The imaging principle determines that STIC is not a real-time imaging technology but a delayed signal. Therefore, when an abnormality of the fetal heart leads to ventricular desynchrony, the maximum and minimum volume of the fetal ventricle cannot be accurately estimated using this method.

In contrast, iSTIC can generate real-time 3D images with an electronic matrix probe used vertically, and a horizontally-arranged 2D probe to conduct matrix volume imaging. The acoustic beam can automatically rotate for large-range scanning, which can significantly reduce the acquisition time of 3D image data and improve work efficiency. The acquisition time of one image by STIC is usually 8–12 s, but iSTIC only requires 2 s. With the imaging time significantly shortened, iSTIC has solved the contradiction between slow STIC imaging and a rapid fetal heart rate and reduced the effects of fetal and maternal respiration and other factors on the quality of the image. The image resolution is thus increased[29,43,44]. In theory, accuracy of the iSTIC technique in the measurement of fetal ventricular volume is higher than STIC, which also reduces the exposure time of the fetus to ultrasound.

In this study, iSTIC technology was used to evaluate the heart function of 123 normal fetuses. The results showed that the fetal right ventricular volume, right ventricular stroke output, and RCO increased as gestational age increased, thus showing a good correlation with gestational age. Right ejection fraction did not change as the gestational age increased, which was relatively constant throughout the pregnancy and consistent with a previous report[23]. During the entire process of fetal growth and development, the circulatory system plays a critical role. Unlike adults, the fetal right ventricle has the main circulating function. As the right ventricular volume continues to increase, the increased RCO with gestational age can meet the oxygen and nutrient demands for fetal development. In contrast, due to the anatomic and structural characteristics of the right ventricle, which has an irregular shape with the regulation bundle at the apex as well as a rougher endocardial surface compared with the left ventricle, it is particularly important to find an accurate and reliable method to measure fetal right ventricular volume and cardiac function indices.

This study had some shortcomings, such as small sample size and the manual delineation of the lining of the heart in post-processing, which requires clear endocardial imaging and multiple measurements to obtain an average value and reduce measurement errors as far as possible. Due to the rough endocardium surface of the right ventricle, measurement error is inevitable. In addition, there is currently no gold standard for the assessment of fetal heart function to compare the data obtained by iSTIC technology.

In summary, iSTIC technology can be used for the quantitative measurement of fetal right ventricular volume and the evaluation of right ventricular systolic function, which has shown a number of advantages, and the application of iSTIC technology in

Table 2 Measured normal fetal right ventricular end-diastolic volume, right ventricular end-systolic volume, right stroke volume, right cardiac output, and right ejection fraction values with gestational ages between 22 and 35^{+6} wk

Gestational age, wk	Case	REDV, mL	RESV, mL	RSV, mL	RCO, mL/min	REF
22–23^{+6}	20	0.99 ± 0.34	0.43 ± 0.18	0.62 ± 0.29	92.23 ± 40.67	0.58 ± 0.12
24–25^{+6}	24	1.43 ± 0.28	0.55 ± 0.15	0.90 ± 0.18	132.10 ± 26.61	0.62 ± 0.58
26–27^{+6}	20	1.66 ± 0.39	0.69 ± 0.20	0.98 ± 0.22	149.25 ± 34.68	0.59 ± 0.06
28–29^{+6}	16	2.06 ± 0.53	0.77 ± 0.15	1.29 ± 0.44	181.12 ± 57.03	0.61 ± 0.06
30–31^{+6}	18	2.61 ± 0.33	1.00 ± 0.14	1.60 ± 0.26	232.58 ± 45.60	0.61 ± 0.05
32–33^{+6}	15	2.98 ± 0.49	1.10 ± 0.17	1.88 ± 0.39	275.86 ± 55.43	0.63 ± 0.04
34–35^{+6}	10	3.69 ± 0.36	1.36 ± 0.22	2.33 ± 0.18	335.83 ± 32.75	0.63 ± 0.03

REDV: Right ventricular end-diastolic volume; RESV: Right ventricular end-systolic volume; RSV: Right stroke volume; RCO: Right cardiac output; REF: Right ejection fraction. RSV = REDV - RESV; RCO = RSV × fetal heart rate; REF = RSV/REDV.

prenatal diagnosis is worthy of further study and discussion.

Table 3 Consistency between the same observer and different observers

	n	Observer A	Observer B	*t*	*P*	*r*	*P*	ICC	95%CI
REDV	30	1.54 ± 0.82	1.51 ± 0.79	1.417	0.167	0.989	< 0.001	0.988	0.975-0.994
RESV	30	0.62 ± 0.36	0.61 ± 0.37	0.384	0.704	0.951	< 0.001	0.951	0.900-0.977
		First measurement	Second measurement						
REDV	30	1.54 ± 0.81	1.54 ± 0.84	0.196	0.846	0.990	< 0.001	0.989	0.978-0.995
RESV	30	0.63 ± 0.36	0.61 ± 0.37	1.731	0.094	0.980	< 0.001	0.978	0.955-0.989

REDV: Right ventricular end-diastolic volume; RESV: Right ventricular end-systolic volume; ICC: Intraclass correlation coefficients.

Figure 2 Correlations. A: Correlation between right ventricular end diastolic volume and gestational age (wk); B: Correlation between right ventricular end systolic volume and gestational age (wk); C: Correlation between right ventricular stroke volume and gestational age (wk); D: Correlation between right ventricular cardiac output and gestational age (wk). REDV: Right ventricular end-diastolic volume; RESV: Right ventricular end-systolic volume; RSV: Right stroke volume; RCO: Right cardiac output.

ARTICLE HIGHLIGHTS

Research background

Heart defects are the most common congenital malformations in fetuses. Fetal cardiac structure and function abnormalities lead to changes in ventricular volume. As ventricular volume is an important index for evaluating fetal cardiovascular development, an effective and reliable method for measuring fetal ventricular volume and cardiac function is necessary for accurate ultrasonic diagnosis and effective clinical treatment. The new intelligent spatiotemporal image correlation (iSTIC) technology acquires high-resolution volumetric images. Numerous studies have focused on fetal heart function which have not been widely accepted. The iSTIC technique was used to measure right ventricular volume in 123 normal fetuses, and to evaluate right ventricular systolic function to provide a new method for more accurate and convenient evaluation of fetal heart function.

Research motivation

The iSTIC technique was used to provide a new method for more accurate and convenient evaluation of fetal heart function.

Research objectives

One hundred twenty-three healthy gravidas with singleton gestations who visited our hospital for prenatal ultrasonography between October 2014 and September 2015 were included in the study.

Research methods

The women were asked to lie flat, and a fetal echo program was begun with transabdominal scanning using an X6-1 probe. Using a 3D/4D iSTIC technology model for a 4-chamber view of the fetal heart, the 3D/4D sampling frame location was adjusted and the sampling range assured 3D/4D volume data acquisition and the sampling frame included the entire fetal heart. The fetal heart rate was measured and recorded after completion of data acquisition.

Research results

The changes in normal fetal right ventricular end-diastolic volume, right ventricular end-systolic volume, right stroke volume, and right cardiac output with gestational age showed significant linear correlations. Right ejection fraction did not change as gestational age increased, was relatively constant throughout the entire pregnancy, and was not significantly correlated with gestational age.

Research conclusions

iSTIC technology can be used for the quantitative measurement of fetal right ventricular volume and the evaluation of right ventricular systolic function.

Research perspectives

iSTIC can generate real-time 3D images, only requires 2 s, and is the best method now. The direction of the future research is to improve the scanning time.

REFERENCES

1   **Carvalho JS**, Mavrides E, Shinebourne EA, Campbell S, Thilaganathan B. Improving the effectiveness of routine prenatal screening for major congenital heart defects. *Heart* 2002; **88**: 387-391 [PMID: 12231598 DOI: 10.1136/heart.88.4.387]

2   **Tedesco GD**, de Souza Bezerra M, Barros FS, Martins WP, Nardozza LM, Carrilho MC, Moron AF, Carvalho FH, Rolo LC, Araujo Júnior E. Reference Ranges of Fetal Cardiac Biometric Parameters Using Three-Dimensional Ultrasound with Spatiotemporal Image Correlation M Mode and Their Applicability in Congenital Heart Diseases. *Pediatr Cardiol* 2017; **38**: 271-279 [PMID: 27878625 DOI: 10.1007/s00246-016-1509-1]

3   **Godfrey ME**, Messing B, Cohen SM, Valsky DV, Yagel S. Functional assessment of the fetal heart: a review. *Ultrasound Obstet Gynecol* 2012; **39**: 131-144 [PMID: 21611999 DOI: 10.1002/uog.9064]

4   **Simioni C**, Nardozza LM, Araujo Júnior E, Rolo LC, Terasaka OA, Zamith MM, Moron AF. Fetal cardiac function assessed by spatio-temporal image correlation. *Arch Gynecol Obstet* 2011; **284**: 253-260 [PMID: 21188403 DOI: 10.1007/s00404-010-1813-6]

5   **Simioni C**, Araujo Júnior E, Martins WP, Rolo LC, Rocha LA, Nardozza LM, Moron AF. Fetal cardiac output and ejection fraction by spatio-temporal image correlation (STIC): comparison between male and female fetuses. *Rev Bras Cir Cardiovasc* 2012; **27**: 275-282 [PMID: 22996979 DOI: 10.5935/1678-9741.20120058]

6   **Simioni C**, Nardozza LM, Araujo Júnior E, Rolo LC, Zamith M, Caetano AC, Moron AF. Heart stroke volume, cardiac output, and ejection fraction in 265 normal fetus in the second half of gestation assessed by 4D ultrasound using spatio-temporal image correlation. *J Matern Fetal Neonatal Med* 2011; **24**: 1159-1167 [PMID: 21250911 DOI: 10.3109/14767058.2010.545921]

7   **Rolo LC**, Marcondes Machado Nardozza L, Araujo Júnior E, Simioni C, Maccagnano Zamith M, Fernandes Moron A. Reference curve of the fetal ventricular septum area by the STIC method: preliminary study. *Arq Bras Cardiol* 2011; **96**: 386-392 [PMID: 21468533 DOI: 10.1590/s0066-782x2011005000036]

8   **Araujo Júnior E**, Rolo LC, Rocha LA, Nardozza LM, Moron AF. The value of 3D and 4D assessments of the fetal heart. *Int J Womens Health* 2014; **6**: 501-507 [PMID: 24868174 DOI: 10.2147/IJWH.S47074]

9   **Adler DG**, Gabr M, Taylor LJ, Witt B, Pleskow D. Initial report of transesophageal EUS-guided intraparenchymal lung mass core biopsy: Findings and outcomes in two cases. *Endosc Ultrasound* 2018; **7**: 413-417 [PMID: 29786035 DOI: 10.4103/eus.eus_13_18]

10   **Sawada H**, Chen JZ, Wright BC, Sheppard MB, Lu HS, Daugherty A. Heterogeneity of Aortic Smooth Muscle Cells: A Determinant for Regional Characteristics of Thoracic Aortic Aneurysms? *J Transl Int Med* 2018; **6**: 93-96 [PMID: 30425944 DOI: 10.2478/jtim-2018-0023]

11   **Castro-Pocas FM**, Araújo TP, Ferreira ML, Saraiva MM. The role of endoscopic ultrasound in a case of lung cancer with jaundice. *Endosc Ultrasound* 2018; **7**: 279-281 [PMID: 27824020 DOI: 10.4103/2303-9027.193570]

12   **Das UN**. Is Aortic Aneurysm Preventable? *J Transl Int Med* 2017; **5**: 72-78 [PMID: 28721338 DOI: 10.1515/jtim-2017-0022]

13   **Qin C**, Wei B, Ma Z. Endobronchial ultrasound: Echoing in the field of pediatrics. *Endosc Ultrasound* 2018; **7**: 371-375 [PMID: 30289110 DOI: 10.4103/eus.eus_40_18]

14   **Wang J**, Ouyang N, Qu L, Lin T, Zhang X, Yu Y, Jiang C, Xie L, Wang L, Wang Z, Ren S, Chen S, Huang J, Liu F, Huang W, Qin X. Effect of MTHFR A1298C and MTRR A66G Genetic Mutations on Homocysteine Levels in the Chinese Population: A Systematic Review and Meta-analysis. *J Transl Int Med* 2017; **5**: 220-229 [PMID: 29340279 DOI: 10.1515/jtim-2017-0037]

15   **Sahai AV**. EUS is trending! *Endosc Ultrasound* 2018; **7**: 353-355 [PMID: 30168481 DOI: 10.4103/eus.eus_22_18]

16   **Gómez O**, Soveral I, Bennasar M, Crispi F, Masoller N, Marimon E, Bartrons J, Gratacós E, Martinez JM. Accuracy of Fetal Echocardiography in the Differential Diagnosis between Truncus Arteriosus and Pulmonary Atresia with Ventricular Septal Defect. *Fetal Diagn Ther* 2016; **39**: 90-99 [PMID: 26113195 DOI: 10.1159/000433430]

17   **Bravo-Valenzuela NJ**, Peixoto AB, Nardozza LM, Souza AS, Araujo Júnior E. Applicability and technical aspects of two-dimensional ultrasonography for assessment of fetal heart function. *Med Ultrason* 2017; **19**: 94-101 [PMID: 28180202 DOI: 10.11152/mu-934]

18   **He Y**, Wang J, Gu X, Zhang Y, Han J, Liu X, Li Z. Application of spatio-temporal image correlation technology in the diagnosis of fetal cardiac abnormalities. *Exp Ther Med* 2013; **5**: 1637-1642 [PMID: 23837046 DOI: 10.3892/etm.2013.1060]

19   **DeVore GR**. Assessing fetal cardiac ventricular function. *Semin Fetal Neonatal Med* 2005; **10**: 515-541 [PMID: 16257825 DOI: 10.1016/j.siny.2005.08.009]

20   **Araujo Júnior E**, Tonni G, Bravo-Valenzuela NJ, Da Silva Costa F, Meagher S. Assessment of Fetal Congenital Heart Diseases by 4-Dimensional Ultrasound Using Spatiotemporal Image Correlation: Pictorial Review. *Ultrasound Q* 2018; **34**: 11-17 [PMID: 29112643 DOI: 10.1097/RUQ.0000000000000328]

21   **Rocha LA**, Rolo LC, Barros FS, Nardozza LM, Moron AF, Araujo Júnior E. Assessment of Quality of Fetal Heart Views by 3D/4D Ultrasonography Using Spatio-Temporal Image Correlation in the Second and Third Trimesters of Pregnancy. *Echocardiography* 2015; **32**: 1015-1021 [PMID: 25231765 DOI: 10.1111/echo.12743]

22   **Rolo LC**, Nardozza LM, Araujo Júnior E, Simioni C, Zamith MM, Moron AF. [Assessment of the fetal mitral and tricuspid valves areas development by three-dimensional ultrasonography]. *Rev Bras Ginecol Obstet* 2010; **32**: 426-432 [PMID: 21271147 DOI: 10.1590/S0100-72032010000900003]

23   **Zhang J**, Zhou Q, Peng Q, Zhao Y, Gong Z. [Assessment of the right ventricle function of fetus by spatio-temporal image correlation]. *Zhong Nan Da Xue Xue Bao Yi Xue Ban* 2015; **40**: 486-494 [PMID: 26032069 DOI: 10.11817/j.issn.1672-7347.2015.05.005]

24   **Xiong Y**, Liu T, Wu Y, Xu JF, Ting YH, Yeung Leung T, Lau TK. Comparison of real-time three-dimensional echocardiography and spatiotemporal image correlation in assessment of fetal interventricular septum. *J Matern Fetal Neonatal Med* 2012; **25**: 2333-2338 [PMID: 22642553 DOI: 10.3109/14767058.2012.695822]

25   **Xiong Y**, Liu T, Gan HJ, Wu Y, Xu JF, Ting YH, Leung TY, Lau TK. Detection of the fetal conotruncal anomalies using real-time three-dimensional echocardiography with live xPlane imaging of the fetal ductal arch view. *Prenat Diagn* 2013; **33**: 462-466 [PMID: 23494925 DOI: 10.1002/pd.4088]

26   **Zhang J**, Zhou Q, Zhao Y, Peng Q, Gong Z, Long X. Evaluation of right ventricular function in fetal hypoplastic left heart syndrome using spatio-temporal image correlation (STIC). *Cardiovasc Ultrasound* 2016; **14**: 12 [PMID: 27066831 DOI: 10.1186/s12947-016-0056-5]

27   **Xiong Y**, Chen M, Chan LW, Ting YH, Fung TY, Leung TY, Lau TK. Scan the fetal heart by real-time three-dimensional echocardiography with live xPlane imaging. *J Matern Fetal Neonatal Med* 2012; **25**: 324-328 [PMID: 21574902 DOI: 10.3109/14767058.2011.575904]

28   **Lu Y**, Yang T, Luo H, Deng F, Cai Q, Sun W, Song H. Visualization and quantitation of fetal movements by real-time three-dimensional ultrasound with live xPlane imaging in the first trimester of pregnancy. *Croat Med J* 2016; **57**: 474-481 [PMID: 27815938 DOI: 10.3325/cmj.2016.57.474]

29   **Zhu M**, Ashraf M, Zhang Z, Streiff C, Shimada E, Kimura S, Schaller T, Song X, Sahn DJ. Real Time Three-Dimensional Echocardiographic Evaluations of Fetal Left Ventricular Stroke Volume, Mass, and Myocardial Strain: In Vitro and In Vivo Experimental Study. *Echocardiography* 2015; **32**: 1697-1706 [PMID: 25865121 DOI: 10.1111/echo.12939]

30   **Meyer-Wittkopf M**, Cole A, Cooper SG, Schmidt S, Sholler GF. Three-dimensional quantitative echocardiographic assessment of ventricular volume in healthy human fetuses and in fetuses with congenital heart disease. *J Ultrasound Med* 2001; **20**: 317-327 [PMID: 11316309 DOI: 10.1046/j.1469-0705.2001.0180S1019.x]

31   **Blessberger H**, Binder T. NON-invasive imaging: Two dimensional speckle tracking echocardiography: basic principles. *Heart* 2010; **96**: 716-722 [PMID: 20424157 DOI: 10.1136/hrt.2007.141002]

32   **Blessberger H**, Binder T. Two dimensional speckle tracking echocardiography: clinical applications. *Heart* 2010; **96**: 2032-2040 [PMID: 21088126 DOI: 10.1136/hrt.2010.199885]

33   **Zhao L**, Wu Y, Chen S, Ren Y, Chen P, Niu J, Li C, Sun K. Feasibility Study on Prenatal Cardiac Screening Using Four-Dimensional Ultrasound with Spatiotemporal Image Correlation: A Multicenter Study. *PLoS One* 2016; **11**: e0157477 [PMID: 27314236 DOI: 10.1371/journal.pone.0157477]

34   **Rolo LC**, Santana EF, da Silva PH, Costa Fda S, Nardozza LM, Tonni G, Moron AF, Araujo Júnior E. Fetal cardiac interventricular septum: volume assessment by 3D/4D ultrasound using spatio-temporal image correlation (STIC) and virtual organ computer-aided analysis (VOCAL). *J Matern Fetal Neonatal Med* 2015; **28**: 1388-1393 [PMID: 25134922 DOI: 10.3109/14767058.2014.955005]

35   **Hamill N**, Yeo L, Romero R, Hassan SS, Myers SA, Mittal P, Kusanovic JP, Balasubramaniam M, Chaiworapongsa T, Vaisbuch E, Espinoza J, Gotsch F, Goncalves LF, Lee W. Fetal cardiac ventricular volume, cardiac output, and ejection fraction determined with 4-dimensional ultrasound using spatiotemporal image correlation and virtual organ computer-aided analysis. *Am J Obstet Gynecol* 2011; **205**: 76.e1-76.10 [PMID: 21531373 DOI: 10.1016/j.ajog.2011.02.028]

36   **Messing B**, Cohen SM, Valsky DV, Shen O, Rosenak D, Lipschuetz M, Yagel S. Fetal heart ventricular mass obtained by STIC acquisition combined with inversion mode and VOCAL. *Ultrasound Obstet Gynecol* 2011; **38**: 191-197 [PMID: 21370304 DOI: 10.1002/uog.8980]

37   **Barros FS**, Moron AF, Rolo LC, Rocha LA, Martins WP, Tonni G, Nardozza LM, Araujo Júnior E. Fetal myocardial wall area: constructing a reference range by means of spatiotemporal image correlation in the rendering mode. *Fetal Diagn Ther* 2015; **37**: 44-50 [PMID: 25095802 DOI: 10.1159/000363653]

38   **Turan S**, Turan OM, Desai A, Harman CR, Baschat AA. First-trimester fetal cardiac examination using spatiotemporal image correlation, tomographic ultrasound and color Doppler imaging for the diagnosis of complex congenital heart disease in high-risk patients. *Ultrasound Obstet Gynecol* 2014; **44**: 562-567 [PMID: 24585667 DOI: 10.1002/uog.13341]

39   **Tanis JC**, Mohammed N, Bennasar M, Martinez JM, Bijnens B, Crispi F, Gratacos E. Online versus offline spatiotemporal image correlation (STIC) M-mode for the evaluation of cardiac longitudinal annular displacement in fetal growth restriction. *J Matern Fetal Neonatal Med* 2018; **31**: 1845-1850 [PMID:

28508694 DOI: 10.1080/14767058.2017.1330408]

40   **Yagel S**, Cohen SM, Shapiro I, Valsky DV. 3D and 4D ultrasound in fetal cardiac scanning: a new look at the fetal heart. *Ultrasound Obstet Gynecol* 2007; **29**: 81-95 [PMID: 17200988 DOI: 10.1002/uog.3912]

41   **Tedesco GD**, de Souza Bezerra M, Barros FSB, Martins WP, Nardozza LMM, Mattar R, Moron AF, Rolo LC, Araujo Júnior E. Fetal Heart Function by Tricuspid Annular Plane Systolic Excursion and Ventricular Shortening Fraction Using STIC M-Mode: Reference Ranges and Validation. *Am J Perinatol* 2017; **34**: 1354-1361 [PMID: 28571079 DOI: 10.1055/s-0037-1603652]

42   **Messing B**, Gilboa Y, Lipschuetz M, Valsky DV, Cohen SM, Yagel S. Fetal tricuspid annular plane systolic excursion (f-TAPSE): evaluation of fetal right heart systolic function with conventional M-mode ultrasound and spatiotemporal image correlation (STIC) M-mode. *Ultrasound Obstet Gynecol* 2013; **42**: 182-188 [PMID: 23288668 DOI: 10.1002/uog.12375]

43   **Acar P**, Battle L, Dulac Y, Peyre M, Dubourdieu H, Hascoet S, Groussolles M, Vayssière C. Real-time three-dimensional foetal echocardiography using a new transabdominal xMATRIX array transducer. *Arch Cardiovasc Dis* 2014; **107**: 4-9 [PMID: 24364911 DOI: 10.1016/j.acvd.2013.10.003]

44   **Liu J**, Wang Y, Zhao H, Liu W. Spatio-temporal image correlation rendering mode visualizes the specific location and surrounding structure of ventricular septal defect. *Clin Anat* 2019; **32**: 408-420 [PMID: 30623992 DOI: 10.1002/ca.23330]

Observational Study

Correlation between intracoronary thrombus components and coronary blood flow after percutaneous coronary intervention for acute myocardial infarction at different onset time

Ming-Ji Zhang, Xin Liu, Li-Hong Liu, Ning Li, Ning Zhang, Yong-Qing Wang, Xue-Jun Sun, Ping-He Huang, Hong-Mei Yin, Yong-Hui Liu, Hong Zheng

ORCID number: Ming-Ji Zhang (0000-0003-2402-1247); Xin Liu (0000-0002-3125-4850); Li-Hong Liu (0000-0002-7968-7727); Ning Li (0000-0002-5568-2251); Ning Zhang (0000-0002-3791-9323); Yong-Qing Wang (0000-0002-9365-9394); Xue-Jun Sun (0000-0003-3178-738x); Ping-He Hang (0000-0002-1094-0907); Yong-Hui Liu (0000-0003-3736-0029); Hong Zheng (0000-0003-4100-6321).

Ming-Ji Zhang, Xin Liu, Li-Hong Liu, Ning Li, Ning Zhang, Yong-Qing Wang, Xue-Jun Sun, Ping-He Huang, Hong-Mei Yin, Yong-Hui Liu, Hong Zheng, Department of Cardiology, AnSteel Group Hospital, Anshan 114003, Liaoning Province, China

Corresponding author: Ming-Ji Zhang, MAMS, Chief Physician, Department of Cardiology, AnSteel Group Hospital, No. 3 Jianshen Street, Anshan 114003, Liaoning Province, China. asdoctor@163.com
Telephone: +86-412-6706255
Fax: +86-412-6706255

Abstract

BACKGROUND

Acute myocardial infarction (AMI) is a leading cause of mortality. Early reperfusion to restore blood flow is crucial to successful treatment. In the current reperfusion regimen, an increasing number of patients have benefited from direct percutaneous coronary intervention (PCI). In order to understand whether there is a correlation between the components of coronary thrombosis and the absence of reflow or slow blood flow after coronary stent implantation in direct PCI, we collected data on direct PCI cases in our hospital between January 2016 and November 2018.

AIM

To investigate the correlation between intracoronary thrombus components and coronary blood flow after stent implantation in direct PCI in AMI.

METHODS

We enrolled 154 patients (85 male and 69 female, aged 36–81 years) with direct PCI who underwent thrombus catheter aspiration within < 3, 3–6 or 6–12 h of onset of AMI between January 2016 and November 2018. The thrombus was removed for pathological examination under a microscope. The patients of the three groups according to the onset time of AMI were further divided into those with a white or red thrombus. The thrombolysis in myocardial infarction (TIMI) blood flow after stent implantation was recorded based on digital subtraction angiography during PCI. The number of patients with no-reflow and slow blood flow in each group was counted. Statistical analysis was performed based on data such as onset time, TIMI blood flow.

RESULTS

There were significant differences in thrombus components between the patients with acute ST-segment elevation myocardial infarction and non-ST-segment elevation myocardial infarction ($P < 0.01$). In the group with PCI < 3 h after onset of AMI, there was no significant difference in the incidence of no-reflow and slow-flow between the white and red thrombus groups. In the groups with PCI 3-6 and 6-12 h after onset of AMI, there was a significant difference in the incidence of no-reflow and slow-flow between the white and red thrombus groups ($P < 0.01$). There was a significant correlation between the onset time of AMI and the occurrences of no-reflow and slow blood flow during PCI ($P < 0.01$).

CONCLUSION

In direct PCI, the onset time of AMI and color of coronary thrombus are often used to predict whether there will be no reflow or slow blood flow after stent implantation.

Key words: Acute myocardial infarction; Pathological thrombotic component; Direct percutaneous coronary intervention; Blood flow

Core tip: We investigated the correlation between intracoronary thrombus components and coronary blood flow after stent implantation in direct percutaneous coronary intervention (PCI) in acute myocardial infarction (AMI). A total of 154 patients with direct PCI who underwent thrombus catheter aspiration within < 3, 3-6 or 6-12 h of onset of AMI were included. There was a significant correlation between the onset time of AMI and the occurrence of no reflow and slow blood flow during PCI. In direct PCI, the onset time of AMI and color of coronary thrombus may predict whether there will be no reflow or slow blood flow after stent implantation.

INTRODUCTION

Acute myocardial infarction (AMI) is a critical illness with high mortality. Early reperfusion to restore blood flow is the key to successful treatment[1]. In the current reperfusion regimen, an increasing number of patients have benefited from direct percutaneous coronary intervention (PCI). However, as well as some coronary revascularization, there have been some cases of coronary artery no-reflow or slow blood flow after stent implantation in direct PCI[2-6]. In order to understand whether there is a correlation between the components of coronary thrombosis and the absence of reflow or slow blood flow after coronary stent implantation in direct PCI, we collected data on direct PCI cases in our hospital between January 2016 and November 2018.

MATERIALS AND METHODS

Patients

We enrolled 154 patients with AMI who were admitted to our hospital between January 2016 and November 2018. Patients underwent direct PCI within 12 hours of onset of AMI with aspiration catheterization and stent implantation. There were 85 men and 69 women, aged 36–81 years (mean age 59.8 years). There were 116 patients with acute ST-segment elevation myocardial infarction (STEMI), 38 with acute non-ST-segment elevation myocardial infarction (NSTEMI), 85 with right coronary artery

infarction, 47 with left anterior descending artery infarction and 22 with left circumflex artery infarction.

Methods

Grouping: All patients were divided into 3 groups according to the time of AMI onset: < 3, 3-6 and 6-12 h. According to electrocardiography and coronary angiography, the patients were further divided into acute STEMI and acute NSTEMI groups.

Coronary angiography: The coronary condition and thrombolysis in myocardial infarction (TIMI) blood flow were recorded using the JUDKINS method. TIMI blood flow was graded as follows: Level 0, complete occlusion of the diseased blood vessels, no contrast agent was passed, and the distal myocardium was completely non-perfused; Level 1, the diseased blood vessels had a small amount of contrast agent and blood flow, but the distal arterial vascular bed was not fully developed; Level 2, the contrast agent slowly passed through the stenosis or was delayed at the distal end of the stenosis, the distal segment was developed, and the distal myocardium was perfused, that is, the distal vascular bed was fully developed after 3 cardiac cycles; Level 3, the contrast agent rapidly filled the blood vessel and was rapidly emptied, and all distal myocardial perfusion was complete, that is, the distal vascular bed was fully developed within 3 cardiac cycles. Patients with TIMI blood flow Level 0–2 had no reflow and slow blood flow[7]. The severity of coronary thrombosis load was assessed according to the following 6 points: (1) A long thrombus > 3 times the inner diameter of the reference vessel; (2) A strip-shaped thrombus with a length of > 5 mm at the proximal end of the occlusion; (3) A floating thrombus at the proximal end of the occlusion; (4) Inner luminal diameter > 4.0 mm; (5) Occlusion of the proximal vessel without abrupt blunt occlusion; and (6) Contrast agent retention in the distal end of the occluded vessel[8].

PCI: Signed informed consent was obtained from each patient before surgery, and the double-resistance load was given (aspirin 300 mg and ticagrelor 180 mg orally). For patients older than 75 years, aspirin 300 mg and clopidogrel 300 mg were given orally. The appropriate guiding catheter was inserted into the coronary artery associated with the lesion of the offender and guide the wire to the distal end of the coronary artery through the lesion, and the Export AP thrombus aspiration catheter was passed to the lesion through the guiding wire, and pumping was repeated 3 to 5 times from the proximal end to the distal end of the lesion. According to angiography after aspiration of the thrombus, stent implantation was performed in patients with residual stenosis > 75%. The intraoperative TIMI myocardial perfusion grade was recorded and the number of cases without reflow or slow blood flow was recorded. In patients with no reflow or slow blood flow, tirofiban and sodium nitroprusside were given intracoronally through the aspiration catheter to improve blood flow. Typical cases are shown in Figure 1 and Figure 2.

Observation of thrombus components: The thrombus was extracted from the coronary artery and initially observed with the naked eye. The thrombi were classified as white or red, which was confirmed by fixed section microscopy (Figure 3 and Figure 4).

Statistical analysis

Statistical analysis was performed using SPSS version 19.0 software. Normal distribution measurement data are expressed as mean ± SD. The Chi-square test was used to compare the data between the groups. $P < 0.01$ was considered statistically significant.

RESULTS

In the NSTEMI group, 28 cases of white thrombus and 10 of red thrombus were extracted. In the STEMI group, 4 cases of white thrombus and 112 of red thrombus were extracted. There was a significant difference in the thrombus components between the two groups ($P < 0.01$), as shown in Table 1. In the group with PCI at < 3 h after onset of AMI, there were 4 cases of white thrombus (1 had no reflow and slow blood flow), and 27 cases of red thrombus (none had no reflow and slow blood flow). There was no significant difference in the incidence of no reflow and slow blood flow after stent implantation between the two subgroups ($P > 0.05$). In the PCI at 3-6 and 6-12 h after onset of AMI, there were 28 cases of white thrombus (20 patients had no reflow and slow blood flow), and 95 cases of red thrombus (15 patients had no reflow
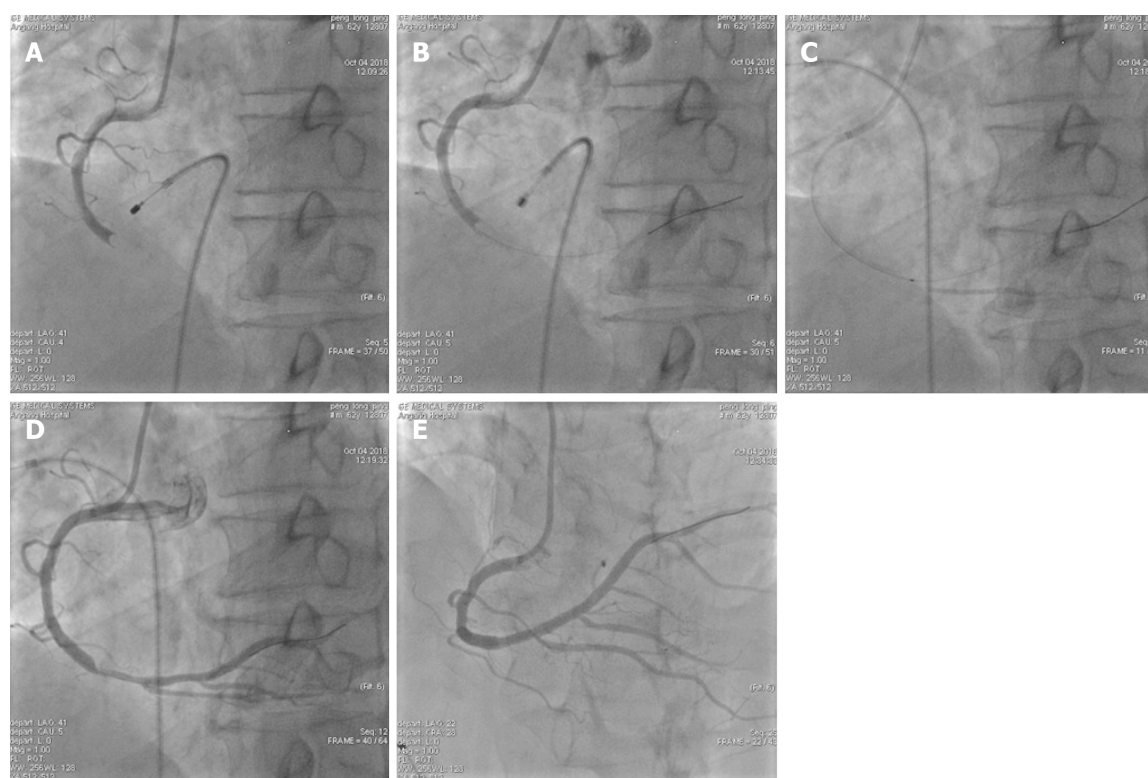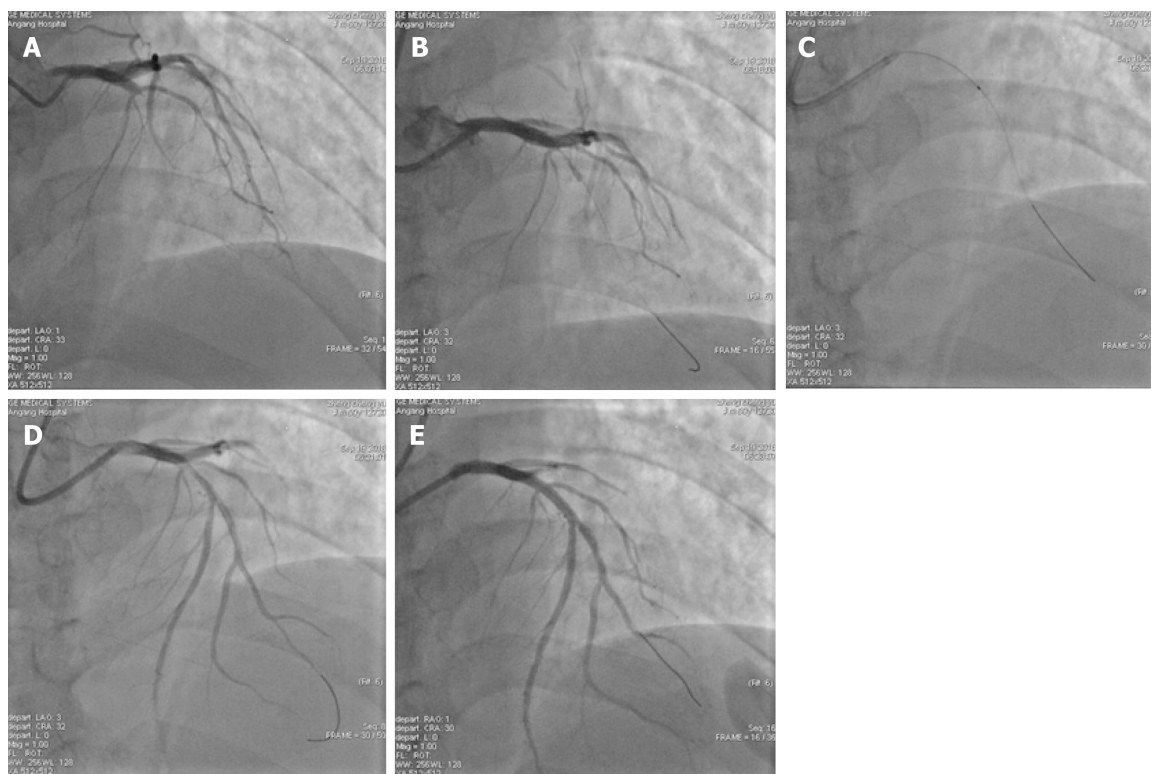
Figure 1 Thrombus aspiration and stent implantation with complete occlusion of the right coronary artery.

and slow blood flow). There was a significant difference in the incidence of no reflow and slow blood flow after stent implantation between these two subgroups ($P < 0.01$), as shown in Table 2. There was a significant correlation between the time of PCI after onset of AMI and the occurrence of no reflow and slow blood flow ($P < 0.01$), as shown in Table 3.

DISCUSSION

The main cause of AMI is acute or secondary occlusion of the coronary artery. Early, effective and continuous opening of infarct-related blood vessels and restoration of effective blood perfusion can reduce the area of necrotic myocardium and reduce mortality[9]. Reperfusion of the myocardium by primary PCI is currently the preferred treatment for AMI. However, with the increasing use of primary PCI, some patients have no reflow or slow blood flow in infarct-related blood vessels after emergency stent implantation[10,11]. No reflow or slow blood flow refers to the phenomenon of no blood flow or slow blood flow after infarction-related coronary artery treatment by stent or balloon, resulting in no perfusion or hypoperfusion of myocardial tissue. The exact mechanism of no reflow or slow blood flow is not fully understood at present. It is not the result of simple mechanical microcirculation embolism, but the comprehensive consequences caused by the interaction of various pathophysiological mechanisms. The main mechanisms are currently considered to include: Myocardial ischemic injury, myocardial reperfusion injury, distal coronary artery embolization and microcirculatory injury. Myocardial ischemia can cause damage to vascular endothelial cells and trigger a cascade of cytokines. Ischemia causes damage to the vascular endothelium, adhesion of neutrophils and platelets, and causes stenosis or occlusion of the lumen, further aggravating microcirculatory disorders. During myocardial reperfusion, a series of changes have occurred, such as calcium overload, increased oxygen free radical production, inflammatory cell infiltration, and activation of apoptotic signaling pathways; these changes aggravate ischemia and form a vicious circle. In patients with AMI undergoing direct PCI, due to balloon pre-expansion or stent implantation, unstable intracoronary plaque rupture or microparticles (such as microthrombus of platelets) decrease, leading to vascular obstruction in the distal coronary artery. When the number of particles is < 25 or the diameter of the particles is < 200 μm, it generally does not cause microvascular obstruction. When the number of particles is 25-200 or the particle diameter is > 200

Figure 2 Thrombus aspiration and stent implantation for complete occlusion of the left anterior descending coronary artery.

μm, it can cause severe microvascular obstruction. At the same time, thromboxane or angiotensin released by the plaque substance may further lead to microcirculatory disorders[12-15]. Different patients have different mechanisms at different pathological stages. Patients with myocardial no reflow after emergency PCI have individual differences, which may be related to genetic susceptibility, and smoking, hypertension, hyperlipidemia and diabetes may also be unfavorable factors for the no-reflow phenomenon[16,17]. The same patient may have multiple different mechanisms at the same time. TIMI blood flow grading is commonly used in clinical evaluation. Coronary artery angiography TIMI blood flow Level 0 is no reflow, while Levels 1 and 2 are slow blood flow. A large number of clinical studies have found that the incidence of no reflow or slow blood flow in primary PCI is estimated to be 20%-30% with TIMI blood flow grading[18]. The rate of no reflow or slow blood flow estimated by microperfusion such as myocardial contrast echo is as high as 34%-39%[19,20], which can cause an increase in myocardial infarct size, continuous reduction of ventricular function, and further increase mortality[21-23]. The incidence is higher in patients with high thromboembolic lesions[24,25].

In conclusion, we found that there was a significant correlation between the onset time of AMI and no reflow and slow blood flow during surgery. The longer onset time of AMI, the higher the incidence of no reflow or slow blood flow. There was a significant difference in the thrombus components between acute STEMI and acute NSTEMI. Patients with acute STEMI had mainly red thrombus, while those with acute NSTEMI had mainly white thrombus, which was closely related to the mechanism of different types of AMI. In patients with PCI at > 3 h after onset of AMI, those with white thrombus were more likely to have no reflow and slower blood flow after stent implantation than patients with red thrombosis. This can predict whether there is no reflow or slow blood flow after stent implantation. At present, the prevention and treatment of microcirculatory disorders and coronary no reflow are limited[26-32]. Therefore, in patients with hyperthrombotic lesions that achieve complete recanalization of infarcted coronary arteries, pre-coronary administration of drugs, such as glycoprotein IIb/IIIa receptor antagonists or sodium nitroprusside, should be fully evaluated based on the nature of the thrombus extracted from the coronary arteries. Calcium antagonists[33,34] are important to reduce the occurrence of slow blood flow or no reflow.

Table 1 Thrombus extraction in patients with percutaneous coronary intervention at different acute myocardial infarction onset time in non-ST-segment elevation myocardial infarction and ST-segment elevation myocardial infarction groups, *n* (%)

Groups	White thrombus	< 3 h	3–6 h	6–12 h
NSTEMI (38 cases)	Yes	3 (50.0)	12 (75.0)	13 (81.25)
	No	3 (50.0)	4 (25.0)	3 (18.75)
STEMI (116 cases)	Yes	1 (4.00)	1 (1.92)	2 (5.13)
	No	24 (96.0)	51 (98.08)	37 (94.87)
Fisher			37.662	29.418
P value		0.016	< 0.001	< 0.001

NSTEMI: Non-ST-segment elevation myocardial infarction; STEMI: ST-segment elevation myocardial infarction.

Table 2 Relationship between different thrombus properties and incidence of no-reflow and slow blood flow after percutaneous coronary intervention at different acute myocardial infarction onset time, *n* (%)

Subgroups	No reflow or slow blood flow	< 3 h	3-6 h	6-12 h
White thrombus (32 cases)	No	3 (75.0)	5 (38.46)	3 (20.0)
	Yes	1 (25.0)	8 (61.54)	12 (80.0)
Red thrombus (122 cases)	No	27 (100)	50 (90.91)	30 (75.0)
	Yes	0 (0)	5 (9.09)	10 (25.0)
Fisher			15.467	13.75
P value		0.143	< 0.001	< 0.001

Table 3 Relationship between acute myocardial infarction onset time and no reflow and slow blood flow during operation, *n* (%)

No reflow or slow blood flow	< 3 h	3-6 h	6-12 h	Chi-square	*P* value
Yes (36 cases)	1 (3.23)	13 (19.12)	22 (40.0)	16.201	< 0.001
No (121 cases)	30 (96.7)7	55 (80.88)	33 (60.0)		
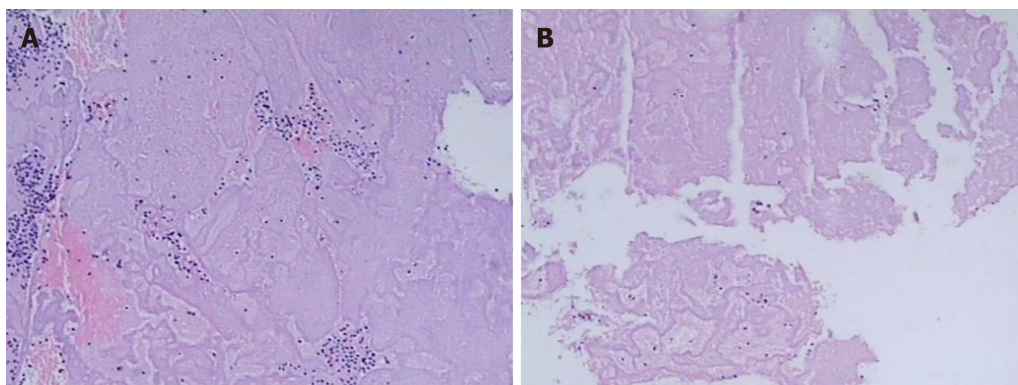
Figure 3 Pathological picture of white thrombus extracted during percutaneous coronary intervention. Hematoxylin and eosin staining, 40×.
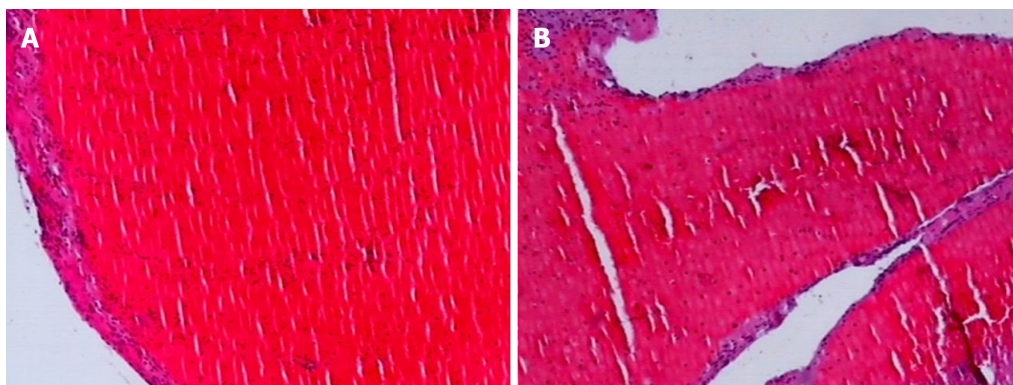
Figure 4 Pathological picture of red thrombus extracted during percutaneous coronary intervention. Hematoxylin and eosin staining, 40×.

ARTICLE HIGHLIGHTS

Research background

Acute myocardial infarction (AMI) is a leading cause of mortality. Early reperfusion to restore blood flow is crucial to successful treatment. An increasing number of patients have benefited from direct percutaneous coronary intervention (PCI). However, coronary artery no-reflow or slow blood flow after stent implantation and coronary revascularization occurred in direct PCI in some cases. The exact mechanism of no reflow or slow blood flow remains unclear

Research motivation

Although in the current reperfusion regimen, an increasing number of patients have benefited from direct PCI, there have been some cases of coronary artery no-reflow or slow blood flow after stent implantation in direct PCI as well as coronary revascularization. The exact mechanism of no reflow or slow blood flow is still unclear. In order to understand whether there is a correlation between the components of coronary thrombosis and the absence of reflow or slow blood flow after coronary stent implantation in direct PCI, we collected data on direct PCI cases in our hospital between January 2016 and November 2018.

Research objectives

This study aims to investigate the correlation between intracoronary thrombus components and coronary blood flow after stent implantation in direct PCI in AMI.

Research methods

A total of 154 patients with direct PCI who underwent thrombus catheter aspiration within < 3, 3–6 or 6–12 h of onset of AMI between January 2016 and November 2018 were included. The thrombus was removed for pathological examination. The patients of three groups according to the onset time of AMI were further divided into those with a white or red thrombus. The thrombolysis in myocardial infarction (TIMI) blood flow after stent implantation was recorded based on digital subtraction angiography during PCI. The number of patients with no-reflow and slow blood flow in each group was counted. Statistical analysis was performed on the onset time, thrombus component, and TIMI blood flow.

Research results

There were significant differences in thrombus components between the patients with acute ST-segment elevation myocardial infarction and non-ST-segment elevation myocardial infarction (P < 0.01). In the group with PCI < 3 h after onset of AMI, there was no significant difference in the incidence of no-reflow and slow-flow between the white and red thrombus groups. In the groups with PCI 3–6 and 6–12 h after onset of AMI, there was a significant difference in the incidence of no-reflow and slow-flow between the white and red thrombus groups (P < 0.01). There was a significant correlation between the onset time of AMI and the occurrence of no-reflow and slow blood flow during PCI (P < 0.01).

Research conclusions

There was a significant correlation between the onset time of AMI and no reflow and slow blood flow during surgery. There was a significant difference in the thrombus components between acute ST-segment elevation myocardial infarction (STEMI) and acute non-ST-segment elevation myocardial infarction (NSTEMI). Patients with acute STEMI had mainly red thrombus, while those with acute NSTEMI had mainly white thrombus, which was closely related to the mechanism of different types of AMI. In patients with PCI at > 3 h after onset of AMI, those with white thrombus were more likely to have no reflow and slower blood flow after stent implantation than patients with red thrombosis. This can predict whether there is no reflow or slow blood flow after stent implantation. In patients with hyperthrombotic lesions that achieve complete recanalization of infarcted coronary arteries, pre-coronary administration of drugs, such as glycoprotein IIb/IIIa receptor antagonists or sodium nitroprusside, should be fully

evaluated based on the nature of the thrombus extracted from the coronary arteries. Calcium antagonists can help reduce the occurrence of slow blood flow or no reflow.

Research perspectives

In direct PCI, the onset time of AMI and color of coronary thrombus are often used to predict whether there will be no reflow or slow blood flow after stent implantation. However, the exact mechanism of no reflow or slow blood flow is not fully understood. Multiple pathophysiological mechanisms might be involved, including myocardial ischemia, myocardial reperfusion injury, distal coronary artery embolization and microcirculatory injury. More prospective studies are needed to be carried out in the future in AMI patients with direct PCI after stent implantation.

REFERENCES

1   **Levine GN**, Bates ER, Blankenship JC, Bailey SR, Bittl JA, Cercek B, Chambers CE, Ellis SG, Guyton RA, Hollenberg SM, Khot UN, Lange RA, Mauri L, Mehran R, Moussa ID, Mukherjee D, Ting HH, O'Gara PT, Kushner FG, Ascheim DD, Brindis RG, Casey DE, Chung MK, de Lemos JA, Diercks DB, Fang JC, Franklin BA, Granger CB, Krumholz HM, Linderbaum JA, Morrow DA, Newby LK, Ornato JP, Ou N, Radford MJ, Tamis-Holland JE, Tommaso CL, Tracy CM, Woo YJ, Zhao DX. 2015 ACC/AHA/SCAI Focused Update on Primary Percutaneous Coronary Intervention for Patients With ST-Elevation Myocardial Infarction: An Update of the 2011 ACCF/AHA/SCAI Guideline for Percutaneous Coronary Intervention and the 2013 ACCF/AHA Guideline for the Management of ST-Elevation Myocardial Infarction: A Report of the American College of Cardiology/American Heart Association Task Force on Clinical Practice Guidelines and the Society for Cardiovascular Angiography and Interventions. *Circulation* 2016; **133**: 1135-1147 [PMID: 26490017 DOI: 10.1161/CIR.0000000000000336]

2   **Bouleti C**, Mewton N, Germain S. The no-reflow phenomenon: State of the art. *Arch Cardiovasc Dis* 2015; **108**: 661-674 [PMID: 26616729 DOI: 10.1016/j.acvd.2015.09.006]

3   **Niccoli G**, Scalone G, Lerman A, Crea F. Coronary microvascular obstruction in acute myocardial infarction. *Eur Heart J* 2016; **37**: 1024-1033 [PMID: 26364289 DOI: 10.1093/eurheartj/ehv484]

4   **Costa RA**, Abizaid A, Lotan C, Dudek D, Silber S, Dizon JM, Maehara A, Dressler O, Brener SJ, Stone GW. Impact of thrombus burden on outcomes after standard versus mesh-covered stents in acute myocardial infarction (from the MGuard for acute ST elevation reperfusion trial). *Am J Cardiol* 2015; **115**: 161-166 [PMID: 25465924 DOI: 10.1016/j.amjcard.2014.10.016]

5   **Barresi L**, Tacelli M, Tarantino I, Cipolletta F, Granata A, Traina M. Improving the yield of EUS-guided histology. *Endosc Ultrasound* 2018; **7**: 301-305 [PMID: 30323157 DOI: 10.4103/eus.eus_45_18]

6   **Dietrich CF**, Bibby E, Jenssen C, Saftoiu A, Iglesias-Garcia J, Havre RF. EUS elastography: How to do it? *Endosc Ultrasound* 2018; **7**: 20-28 [PMID: 29451165 DOI: 10.4103/eus.eus_49_17]

7   **Mahmoud KS**. Left and Right Ventricular Myocardial Performance Index and it,s Relation with TIMI Frame Count in the Coronary Slow Flow Phenomenon. *J Cli Exp Cardiol* 2016; **7**: 1-5 [DOI: 10.4172/2155-9880.1000421]

8   **Van de Werf F**, Bax J, Betriu A, Blomstrom-Lundqvist C, Crea F, Falk V, Filippatos G, Fox K, Huber K, Kastrati A, Rosengren A, Steg PG, Tubaro M, Verheugt F, Weidinger F, Weis M; ESC Committee for Practice Guidelines (CPG). Management of acute myocardial infarction in patients presenting with persistent ST-segment elevation: the Task Force on the Management of ST-Segment Elevation Acute Myocardial Infarction of the European Society of Cardiology. *Eur Heart J* 2008; **29**: 2909-2945 [PMID: 19004841 DOI: 10.1093/eurheartj/ehn416]

9   **Respaud R**, Marchand D, Pelat T, Tchou-Wong KM, Roy CJ, Parent C, Cabrera M, Guillemain J, Mac Loughlin R, Levacher E, Fontayne A, Douziech-Eyrolles L, Junqua-Moullet A, Guilleminault L, Thullier P, Guillot-Combe E, Vecellio L, Heuzé-Vourc'h N. Development of a drug delivery system for efficient alveolar delivery of a neutralizing monoclonal antibody to treat pulmonary intoxication to ricin. *J Control Release* 2016; **234**: 21-32 [PMID: 27173943 DOI: 10.1016/j.jconrel.2016.05.018]

10   **Khan AR**, Binabdulhak AA, Alastal Y, Khan S, Faricy-Beredo BM, Luni FK, Lee WM, Khuder S, Tinkel J. Cardioprotective role of ischemic postconditioning in acute myocardial infarction: a systematic review and meta-analysis. *Am Heart J* 2014; **168**: 512-521.e4 [PMID: 25262261 DOI: 10.1016/j.ahj.2014.06.021]

11   **Eitel I**, Stiermaier T, Rommel KP, Fuernau G, Sandri M, Mangner N, Linke A, Erbs S, Lurz P, Boudriot E, Mende M, Desch S, Schuler G, Thiele H. Cardioprotection by combined intrahospital remote ischaemic perconditioning and postconditioning in ST-elevation myocardial infarction: the randomized LIPSIA CONDITIONING trial. *Eur Heart J* 2015; **36**: 3049-3057 [PMID: 26385956 DOI: 10.1093/eurheartj/ehv463]

12   **Mazhar J**, Mashicharan M, Farshid A. Predictors and outcome of no-reflow post primary percutaneous coronary intervention for ST elevation myocardial infarction. *Int J Cardiol Heart Vasc* 2015; **10**: 8-12 [PMID: 28616509 DOI: 10.1016/j.ijcha.2015.11.002]

13   **Toprak C**, Tabakci MM, Simsek Z, Arslantas U, Durmus HI, Ocal L, Demirel M, Ozturkeri B, Ozal E, Kargin R. Platelet/lymphocyte ratio was associated with impaired myocardial perfusion and both in-hospital and long-term adverse outcome in patients with ST-segment elevation acute myocardial infarction undergoing primary coronary intervention. *Postepy Kardiol Interwencyjnej* 2015; **11**: 288-297 [PMID: 26677378 DOI: 10.5114/pwki.2015.55599]

14   **Camici PG**, d'Amati G, Rimoldi O. Coronary microvascular dysfunction: mechanisms and functional assessment. *Nat Rev Cardiol* 2015; **12**: 48-62 [PMID: 25311229 DOI: 10.1038/nrcardio.2014.160]

15   **Task Force Members**. Montalescot G, Sechtem U, Achenbach S, Andreotti F, Arden C, Budaj A, Bugiardini R, Crea F, Cuisset T, Di Mario C, Ferreira JR, Gersh BJ, Gitt AK, Hulot JS, Marx N, Opie LH, Pfisterer M, Prescott E, Ruschitzka F, Sabaté M, Senior R, Taggart DP, van der Wall EE, Vrints CJ; ESC Committee for Practice Guidelines, Zamorano JL, Achenbach S, Baumgartner H, Bax JJ, Bueno H, Dean V, Deaton C, Erol C, Fagard R, Ferrari R, Hasdai D, Hoes AW, Kirchhof P, Knuuti J, Kolh P, Lancellotti P, Linhart A, Nihoyannopoulos P, Piepoli MF, Ponikowski P, Sirnes PA, Tamargo JL, Tendera M, Torbicki A, Wijns W, Windecker S; Document Reviewers, Knuuti J, Valgimigli M, Bueno H, Claeys MJ, Donner-Banzhoff N, Erol C, Frank H, Funck-Brentano C, Gaemperli O, Gonzalez-Juanatey JR, Hamilos M, Hasdai D, Husted S, James SK, Kervinen K, Kolh P, Kristensen SD, Lancellotti P, Maggioni AP, Piepoli MF, Pries AR, Romeo F, Rydén L, Simoons ML, Sirnes PA, Steg PG, Timmis A, Wijns W,

Windecker S, Yildirir A, Zamorano JL. 2013 ESC guidelines on the management of stable coronary artery disease: the Task Force on the management of stable coronary artery disease of the European Society of Cardiology. *Eur Heart J* 2013; **34**: 2949-3003 [PMID: 23996286 DOI: 10.1093/eurheartj/eht296]

16   **Basso C**, Rizzo S, Thiene G. The metamorphosis of myocardial infarction following coronary recanalization. *Cardiovasc Pathol* 2010; **19**: 22-28 [PMID: 19775915 DOI: 10.1016/j.carpath.2009.06.010]

17   **Yoshino S**, Cilluffo R, Best PJ, Atkinson EJ, Aoki T, Cunningham JM, de Andrade M, Choi BJ, Lerman LO, Lerman A. Single nucleotide polymorphisms associated with abnormal coronary microvascular function. *Coron Artery Dis* 2014; **25**: 281-289 [PMID: 24736300 DOI: 10.1097/MCA.0000000000000104]

18   **Niccoli G**, Burzotta F, Galiuto L, Crea F. Myocardial no-reflow in humans. *J Am Coll Cardiol* 2009; **54**: 281-292 [PMID: 19608025 DOI: 10.1016/j.jacc.2009.03.054]

19   **Joost A**, Stiermaier T, Eitel C, Fuernau G, de Waha S, Desch S, Thiele H, Eitel I. Impact of Initial Culprit Vessel Flow on Infarct Size, Microvascular Obstruction, and Myocardial Salvage in Acute Reperfused ST-Elevation Myocardial Infarction. *Am J Cardiol* 2016; **118**: 1316-1322 [PMID: 27600465 DOI: 10.1016/j.amjcard.2016.07.056]

20   **Gupta S**, Gupta MM. No reflow phenomenon in percutaneous coronary interventions in ST-segment elevation myocardial infarction. *Indian Heart J* 2016; **68**: 539-551 [PMID: 27543480 DOI: 10.1016/j.ihj.2016.04.006]

21   **Ndrepepa G**, Tiroch K, Fusaro M, Keta D, Seyfarth M, Byrne RA, Pache J, Alger P, Mehilli J, Schömig A, Kastrati A. 5-year prognostic value of no-reflow phenomenon after percutaneous coronary intervention in patients with acute myocardial infarction. *J Am Coll Cardiol* 2010; **55**: 2383-2389 [PMID: 20488311 DOI: 10.1016/j.jacc.2009.12.054]

22   **Carrick D**, Oldroyd KG, McEntegart M, Haig C, Petrie MC, Eteiba H, Hood S, Owens C, Watkins S, Layland J, Lindsay M, Peat E, Rae A, Behan M, Sood A, Hillis WS, Mordi I, Mahrous A, Ahmed N, Wilson R, Lasalle L, Généreux P, Ford I, Berry C. A randomized trial of deferred stenting versus immediate stenting to prevent no- or slow-reflow in acute ST-segment elevation myocardial infarction (DEFER-STEMI). *J Am Coll Cardiol* 2014; **63**: 2088-2098 [PMID: 24583294 DOI: 10.1016/j.jacc.2014.02.530]

23   **De Maria GL**, Alkhalil M, Oikonomou EK, Wolfrum M, Choudhury RP, Banning AP. Role of deferred stenting in patients with ST elevation myocardial infarction treated with primary percutaneous coronary intervention: A systematic review and meta-analysis. *J Interv Cardiol* 2017; **30**: 264-273 [PMID: 28370496 DOI: 10.1111/joic.12380]

24   **Izgi A**, Kirma C, Tanalp AC, Dundar C, Oduncu V, Aung SM, Sonmez K, Mutlu B, Mansuroglu D. Predictors and clinical significance of angiographically detected distal embolization after primary percutaneous coronary interventions. *Coron Artery Dis* 2007; **18**: 443-449 [PMID: 17700215 DOI: 10.1097/MCA.0b013e3282a3064e]

25   **Kirma C**, Izgi A, Dundar C, Tanalp AC, Oduncu V, Aung SM, Sonmez K, Mutlu B, Ozdemir N, Erentug V. Clinical and procedural predictors of no-reflow phenomenon after primary percutaneous coronary interventions: experience at a single center. *Circ J* 2008; **72**: 716-721 [PMID: 18441449]

26   **Botta I**, Devriendt J, Rodriguez JC, Morissens M, Carling A, Gutierrez LB, Preseau T, De Bels D, Honore PM, Redant S. Cardiogenic Shock after Nifedipine Administration in a Pregnant Patient: A Case Report and Review of the Literature. *J Transl Int Med* 2018; **6**: 152-156 [PMID: 30425952 DOI: 10.2478/jtim-2018-0029]

27   **Langabeer SE**. Detecting CALR Mutations in Splanchnic Vein Thrombosis: Who and How? *J Transl Int Med* 2018; **6**: 55-57 [PMID: 29984196 DOI: 10.2478/jtim-2018-0015]

28   **Sawada H**, Chen JZ, Wright BC, Sheppard MB, Lu HS, Daugherty A. Heterogeneity of Aortic Smooth Muscle Cells: A Determinant for Regional Characteristics of Thoracic Aortic Aneurysms? *J Transl Int Med* 2018; **6**: 93-96 [PMID: 30425944 DOI: 10.2478/jtim-2018-0023]

29   **Rezkalla SH**, Stankowski RV, Hanna J, Kloner RA. Management of No-Reflow Phenomenon in the Catheterization Laboratory. *JACC Cardiovasc Interv* 2017; **10**: 215-223 [PMID: 28183461 DOI: 10.1016/j.jcin.2016.11.059]

30   **Elgendy IY**, Jneid H. Microvascular obstruction in ST elevation myocardial infarction patients undergoing primary percutaneous coronary intervention: another frontier to conquer? *J Thorac Dis* 2018; **10**: 1343-1346 [PMID: 29708124 DOI: 10.21037/jtd.2018.03.58]

31   **Ito N**, Nanto S, Doi Y, Kurozumi Y, Natsukawa T, Shibata H, Morita M, Kawata A, Tsuruoka A, Sawano H, Okada K, Sakata Y, Kai T, Hayashi T. Beneficial effects of intracoronary nicorandil on microvascular dysfunction after primary percutaneous coronary intervention: demonstration of its superiority to nitroglycerin in a cross-over study. *Cardiovasc Drugs Ther* 2013; **27**: 279-287 [PMID: 23722418 DOI: 10.1007/s10557-013-6456-y]

32   **Zalewski J**, Claus P, Bogaert J, Driessche NV, Driesen RB, Galan DT, Sipido KR, Buszman P, Milewski K, Van de Werf F. Cyclosporine A reduces microvascular obstruction and preserves left ventricular function deterioration following myocardial ischemia and reperfusion. *Basic Res Cardiol* 2015; **110**: 18 [PMID: 25720581 DOI: 10.1007/s00395-015-0475-8]

33   **Abdelaziz HK**, Elkilany W, Khalid S, Sabet S, Saad M. Efficacy and safety of intracoronary verapamil versus sodium nitroprusside for the prevention of microvascular obstruction during primary percutaneous coronary intervention for ST-segment elevation myocardial infarction. *Coron Artery Dis* 2017; **28**: 11-16 [PMID: 27556348 DOI: 10.1097/MCA.0000000000000423]

34   **Lago IM**, Novaes GC, Badran AV, Pavão RB, Barbosa R, Figueiredo GL, Lima MO Filho, Haddad JL, Schmidt A, Marin JA Neto. In-Lab Upfront Use of Tirofiban May Reduce the Occurrence of No-Reflow During Primary Percutaneous Coronary Intervention. A Pilot Randomized Study. *Arq Bras Cardiol* 2016; **107**: 403-410 [PMID: 27982267 DOI: 10.5935/abc.20160149]

Performance of common imaging techniques *vs* serum biomarkers in assessing fibrosis in patients with chronic hepatitis B: A systematic review and meta-analysis

Xue-Ying Xu, Wu-Sheng Wang, Qi-Meng Zhang, Jun-Ling Li, Jin-Bin Sun, Tian-Tian Qin, Hong-Bo Liu

ORCID number: Xue-Ying Xu (0000-0001-5379-0550); Wu-Sheng Wang (0000-0002-1678-4749); Qi-Meng Zhang (0000-0003-3722-5214); Jun-Ling Li (0000-0002-3790-3591); Jin-Bin Sun (0000-0003-4101-0638); Tian-Tian Qin (0000-0001-5355-2261); Hong-Bo Liu (0000-0002-7404-4271).

Xue-Ying Xu, Wu-Sheng Wang, Qi-Meng Zhang, Jun-Ling Li, Jin-Bin Sun, Tian-Tian Qin, Hong-Bo Liu, Department of Epidemiology and Health Statistics, School of Public Health, China Medical University, Shenyang 110122, Liaoning Province, China

Corresponding author: Hong-Bo Liu, PhD, Professor, Research Fellow, Research Scientist, Statistician, Department of Epidemiology and Health Statistics, School of Public Health, China Medical University, No. 77, Puhe Road, Shenyang North New Area, Shenyang 110122, Liaoning Province, China. hbliu@cmu.edu.cn

Abstract

BACKGROUND

Noninvasive biomarkers have been developed to predict hepatitis B virus (HBV) related fibrosis owing to the significant limitations of liver biopsy. Both serum biomarkers and imaging techniques have shown promising results and may improve the evaluation of liver fibrosis. However, most of the previous studies focused on the diagnostic effects of various imaging techniques on fibrosis in all chronic liver diseases.

AIM

To compare the performance of common imaging methods and serum biomarkers for prediction of significant fibrosis caused only by HBV infection.

METHODS

A systematic review was conducted on the records available in PubMed, EMBASE, and the Cochrane Library electronic databases until December 2018. We systematically assessed the effectiveness of two serum biomarkers and three imagine techniques in predicting significant fibrosis solely caused by HBV infection. The serum biomarkers included aspartate aminotransferase-to-platelet ratio index (APRI) and fibrosis index based on the 4 factors (FIB-4). The three imaging techniques included acoustic radiation force impulse (ARFI), FibroScan, and magnetic resonance elastography (MRE). Three parameters, the area under the summary receiver operating characteristic curve (AUSROC), the summary diagnostic odds ratio, and the summary sensitivity and specificity, were used to examine the accuracy of all tests for liver fibrosis.

RESULTS

Out of 2831 articles evaluated for eligibility, 204 satisfied the predetermined inclusion criteria for this current meta-analysis. Eventually, our final data

contained 81 studies. The AUSROCs of serum biomarkers of APRI and FIB-4 were both 0.75. For imaging techniques (ARFI, FibroScan, and MRE), the areas were 0.89, 0.83, and 0.97, respectively. The heterogeneities of ARFI and FibroScan were statistically significant ($I^2 > 50\%$). The publication bias was not observed in any of the serum biomarkers or imaging methods.

CONCLUSION
These five methods have attained an acceptable level of diagnostic accuracy. Imaging techniques, MRE in particular, demonstrate significant advantages in accurately predicting HBV-related significant fibrosis, while serum biomarkers are admissible methods.

Key words: Hepatitis B virus; Diagnostic test; Imaging technology; Liver fibrosis; Meta-analysis

Core tip: Many researchers compared the diagnostic effects for liver fibrosis by new techniques within the domain of imaging techniques separately or focused on fibrosis in all chronic liver diseases. We perform a meta-analysis to compare the effectiveness of both some common imaging methods and serum biomarkers for prediction of significant fibrosis among hepatitis B virus (HBV)-monoinfected patients. The results reveal that imaging techniques have significant advantages in prediction of HBV-related significant fibrosis.

INTRODUCTION

Liver fibrosis is a consequence of the accumulation of extracellular matrix components, caused by persistent liver damage and consequent wound healing reaction[1,2]. It can develop to cirrhosis, even hepatic failure and hepatocellular carcinoma[3]. Approximately one-third of cirrhosis cases worldwide are caused by hepatitis B virus (HBV) infection[2]. It is estimated that about 450 million people are chronically infected with HBV around the world[1], resulting in 600000 to 1000000 deaths annually[4]. Therefore, the accurate diagnosis of the degree of liver fibrosis is essential for the management of chronic hepatitis B (CHB) patients and making clinical decision for doctors.

Liver biopsy is the current reference standard for the evaluation and staging of fibrosis, which is an invasive technique. However, it has several disadvantages, such as patients' reluctance, pain, hemoperitoneum[5], intra- and interobserver variations, and sampling errors[6]. Therefore, several noninvasive methods, including serum biomarkers combining indices/scores and imaging techniques like magnetic resonance imaging (MRI), have been investigated for their potential in assessment of liver fibrosis.

There has been a dramatic increase in developing various noninvasive tests since 1991[7]. There are direct serum noninvasive tests such as hepascore and hyaluronic acid, indirect serum markers which consist of the combination of routine biochemical or haematological tests such as fibrosis index based on the 4 factors (FIB-4), aspartate aminotransferase-to-platelet ratio index (APRI), or Forns index and Fibrotest combined direct and indirect tests[8]. Among all of these tests, APRI and FIB-4, being extensively investigated in numerous studies, demonstrated the greatest potential.

On the other side, with the development of imaging technology, several imaging devices have been developed for the diagnosis and staging of liver fibrosis, which are truly noninvasive methods when compared with serum biomarkers. Historically, radiologists and clinicians have relied on the assessment of morphological changes

associated with liver fibrosis. Other imaging methods depend on changes in physical properties that can be assessed by quantification techniques. These include mechanical properties, texture, $T_1\rho$ lengthening, perfusion, diffusion, and hepatocellular function[9]. Ultrasound (US)-based elastography techniques are portable, relatively inexpensive, fast to acquire, and do not require postprocessing[10]. In particular, 1D transient elastography, commercialized as FibroScan (Echosens, Paris, France), has been widely validated in clinical trials, adopted clinically, and used by clinicians at point of service[9]. Moreover, focal point shear-wave elastography, commercialized as acoustic radiation force impulse (ARFI) (Siemens Medical Solutions, Mountain View, CA), is mapped in 2D using US tracking pulses, and the resulting tissue displacement is measured[11]. It is integrated in a conventional US machine that can be performed with conventional US probes during an abdominal US scan[12,13]. In addition, many MRI techniques for imaging of liver fibrosis are being developed. They typically cover a larger liver volume than US elastography techniques, which may reduce sampling variability and technical failure rate.

These methods have exhibited promising results and may improve the management of liver fibrosis. However, most previous studies compared the diagnostic effects of these new imaging techniques alone and focused on fibrosis in all chronic liver diseases, which might underestimate or overestimate the role of the biomarkers. Therefore, we performed a meta-analysis to compare the pooled performance of some common imaging methods and serum biomarkers for prediction of significant fibrosis among HBV-monoinfected patients.

MATERIALS AND METHODS

Search strategy and selection criteria

Online database search was performed on EMBASE, PubMed, and the Cochrane Library (01/2008-12/2018) for the following terms: Diagnosis test, liver stiffness measurement, LSM, transient elastography, FibroScan, MR elastography, MRE, ARFI, acoustic radiation force impulse, point shear-wave elastography, imaging techniques, hepatitis B virus, HBV, chronic hepatitis B, CHB, and fibrosis. Other studies were identified by a manual search for referenced studies or review articles. EndNote X9 software was used to manage the references.

Studies should be included if they conformed all of the following five criteria: (a) The study evaluated the performance of the APRI and/or ARFI and/or FIB-4 and/or FibroScan and/or MRE for the prediction of fibrosis in HBV infected patients. Studies on patients with other etiologies of liver diseases were also included if data for HBV-infected patients could be independently extracted. Special populations of HBV-infected patients [*e.g*., HBV/HIV, HBV/ hepatitis C virus (HCV), or HBV/ hepatitis D virus (HDV) coinfection] were excluded; (b) Liver biopsy was used to diagnose liver fibrosis as a golden standard; (c) Data could be extracted to construct at least one 2 × 2 table of test performance, based on some cutoff points of the five biomarkers for the significant fibrosis stage; (d) The study assessed the diagnostic accuracy for fibrosis stage F ≥ 2 according to METAVIR or a comparable staging system; and (e) The study included at least 50 patients. Studies of smaller sample sizes were excluded due to concerns on their applicability.

Data extraction and quality assessment

Two reviewers (WWS and XYX) evaluated study eligibility, extracted data from the study, and graded the study quality independently. Any disagreements between the reviewers were resolved by detailed discussions together with a third reviewer (LHB). The parameters in our literature search included author, year of publication, region, age, patient gender , body mass index (BMI), histological scoring system, number of patients, average length of liver specimen, time interval between biopsy and other diagnostic tests, diagnostic method, prevalence of the fibrosis stage, as well as cutoff values to identify the fibrosis stage[14].

XYX and ZQM independently appraised the quality of included studies using the quality assessment of diagnostic accuracy studies questionnaire (QUADAS-2)[15]. It could estimate the internal and external validity of diagnostic accuracy of studies used in systematic reviews.

Statistical analysis and data synthesis

We extracted and tabulated the data in a series of 2 × 2 tables that included sensitivity, specificity, positive predictive value (PPV), and negative predictive value (NPV) at each threshold value. The primary target was to identify significant fibrosis, defined by METAVIR[16], Batts and Ludwig[17], Scheuer[18], and Chinese Hospital system[19], for

stages F2 to F4, and Ishak[20] for stages F3 to F6. This gauge was chosen because significant fibrosis is often considered a threshold for the initiation of antiviral therapy[21]. The method of diagnostic test accuracy was examined in order to provide clinically meaningful results. We examined the area under the summary receiver operating characteristic curve (AUSROC) curve, the summary diagnostic odds ratio (DOR), and the summary sensitivity and specificity to further examine the accuracy of all tests for liver fibrosis.

The heterogeneity of the results between studies was assessed statistically using the Cochran-Q and the quantity I^2. I^2 value can describe the percentage of total variation across studies that is attributable to heterogeneity rather than chance[22]. If there was significant heterogeneity, a meta-regression was conducted to explore the covariates that may induce heterogeneity, according to the following predefined characteristics: (1) Study design (prospective or retrospective); (2) Length of liver specimen (≥ 10 mm, ≥ 15 mm, ≥ 20 mm, or not); (3) Liver biopsy scoring system; (4) Number of centers (single or multicenter); (5) Sample size; (6) Publication year (2014-2018 or 2008-2013); (7) Time interval between biopsy and tests (same day or not); (8) Prevalence of significant fibrosis; (9) BMI; and (10) Location of study.

The potential publication bias was assessed using the Deeks funnel plots[23]. All analyses were performed with Meta-Disc software (v. 1.4) and Stata15.0.

RESULT

Search results
The study selection process is shown in Figure 1. A total of 2831 studies were searched by the described search strategies, of which 2627 were excluded following title and abstract screening. Of those, 81 papers were included in the review following full-text screening (Text S5); 47 studies were related to the APRI[24-70], 11 to the ARFI[29,42,69-77], 32 to the FIB-4[24,25,27,30,35,36,39,40,43-46,48-55,57,58,60,62,63,65-69,78-79], 29 to the FibroScan[28,38,42,52,53,58,60,61,71,73,80-98], and 6 to the MRE[99-104].

Characteristics of the included studies
In the 47 studies of APRI, there were 13725 patients (median age, 37 years; 68.9% of males). The total prevalence of significant fibrosis was 55.9% (range: 16.7%-83.7%). Most studies were conducted in Asia (42 studies). Three studies were from Europe, one from North America, and another from Africa. We did not restrict study participants to any age, but only one study was conducted on children and adolescents exclusively[59]. Twenty-nine studies used the METAVIR score, ten used the Scheuer score, six utilized the Ishak score, and two used the Chinese Hospital System. There were 11179 patients (median age, 37 years; 68.7% of males) in 32 studies evaluating the performance of FIB-4. The total prevalence of significant fibrosis was 57.5% (range: 16.7%-83.7%). Twenty-nine studies were conducted in Asia, two in Europe, and one in North America. All studies included adults only. Seventeen studies used the METAVIR score, nine used the Scheuer score, four utilized the Ishak score, and two used the Chinese Hospital System.

A total of 1527 patients (median age, 36 years; 67.5% of males) were contained in 11 studies on ARFI. The total prevalence of F2 was 54.2% (range: 23.9%-74.3%). Ten studies were conducted in Asia and one in Germany. All the subjects were adults. Six studies used the METAVIR score, two used the Chinese Hospital System, and one used each of the Scheuer score, the Ishak score, and the Batts and Ludwig score.

In the 29 FibroScan studies, a total of 5035 patients (median age, 39 years; 71.4% of males) were included. The overall prevalence of significant fibrosis was 49.4% (range: 14.8%-85%). Twenty-one studies were from Asia, six from Europe, one from Africa, and another from North America. Twenty studies used the METAVIR score, five utilized the Batts and Ludwig score, three utilized the Scheuer score, and one used the Chinese Hospital System.

There were 1228 patients (median age, 49 years; 71.0% of males) used to evaluate the performance of MRE in six studies. The total prevalence of significant fibrosis was 61.4% (range: 45.2%-77.4%). One MRE study was from America and the other five were conducted in Asia. The results of methodological quality assessment according to the QUADAS-2 scale are described for all studies (Figure 2, Text S5).

Performance of serum biomarkers for prediction of significant liver fibrosis
In the 47 studies evaluating the APRI, the area under the ROC curve (AUROC) ranged from 0.54 to 0.87. The AUSROC and the pooled sensitivity, specificity, and DOR are presented in Table 1 and Figure 3. The Cochran-Q was 1199.4 and I^2 > 50%, which indicated significant heterogeneity across the included studies ($P < 0.001$). Meta-
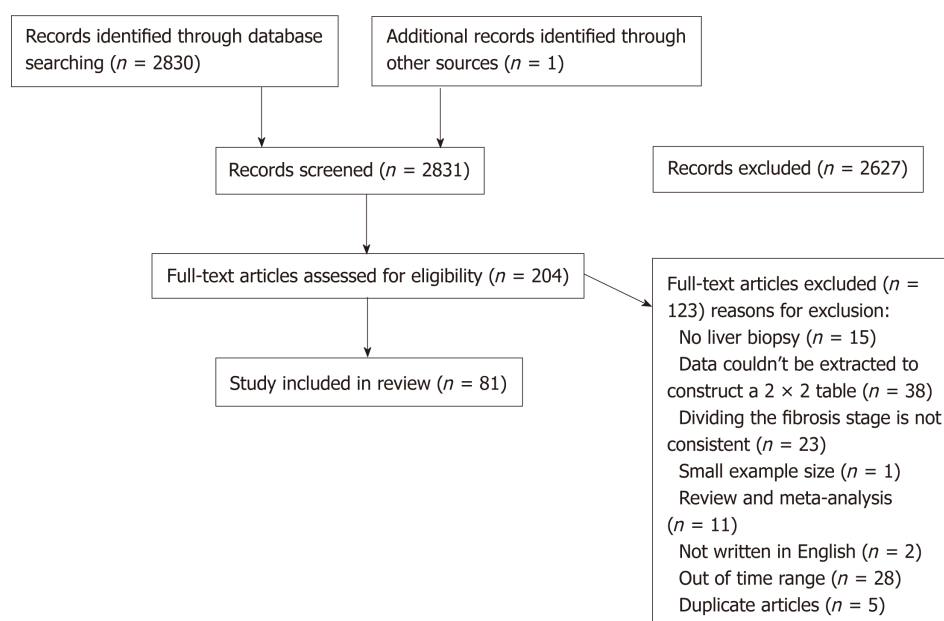
```
┌─────────────────────────────────┐   ┌─────────────────────────────────┐
│ Records identified through      │   │ Additional records identified   │
│ database searching (n = 2830)   │   │ through other sources (n = 1)   │
└─────────────────────────────────┘   └─────────────────────────────────┘
                 │                                    │
                 └──────────────┬─────────────────────┘
                                ▼
                 ┌─────────────────────────────┐      ┌──────────────────────────────┐
                 │ Records screened (n = 2831)  │      │ Records excluded (n = 2627)  │
                 └─────────────────────────────┘      └──────────────────────────────┘
                                │
                                ▼
       ┌────────────────────────────────────────────┐   ┌──────────────────────────────────┐
       │ Full-text articles assessed for eligibility │   │ Full-text articles excluded (n = │
       │ (n = 204)                                   │   │ 123) reasons for exclusion:      │
       └────────────────────────────────────────────┘   │   No liver biopsy (n = 15)       │
                                │                        │   Data couldn't be extracted to  │
                                ▼                        │ construct a 2 × 2 table (n = 38) │
       ┌────────────────────────────────────────────┐   │   Dividing the fibrosis stage is │
       │ Study included in review (n = 81)           │   │ not consistent (n = 23)          │
       └────────────────────────────────────────────┘   │   Small example size (n = 1)     │
                                                         │   Review and meta-analysis       │
                                                         │ (n = 11)                         │
                                                         │   Not written in English (n = 2)│
                                                         │   Out of time range (n = 28)     │
                                                         │   Duplicate articles (n = 5)     │
                                                         └──────────────────────────────────┘
```

Figure 1 Flow diagram of article selection.

regression analysis was used to explore the heterogeneity of the APRI accuracy for predicting significant fibrosis, which was affected by BMI and prevalence of significant fibrosis with regard to sensitivity and only prevalence of significant fibrosis with regard to specificity (Figure S1). In the 32 studies evaluating the FIB-4 for the prediction of fibrosis stage of F2, the AUROC ranged from 0.56 to 0.85. The AUSROC was 0.75 (0.71-0.78) (Figure 3). The summary sensitivity, specificity, and DOR are shown in Table 1. The score of Cochran-Q was 488.9 ($P < 0.05$) and heterogeneity was statistically significant. The heterogeneity of FIB-4 accuracy was mainly affected by prevalence of significant fibrosis with regard to sensitivity, and prevalence of significant fibrosis and study design with regard to specificity according to the meta-regression analysis (Figure S2). The summary sensitivity and specificity of serum indicators by BMI and prevalence of significant fibrosis are listed in Tables 2 and 3.

Performance of imaging techniques for prediction of liver significant fibrosis

The AUROC ranged from 0.72 to 0.96 in 11 studies evaluating the ARFI. When combined, the AUSROC was 0.89 (0.86-0.91). The summary DOR was 23 (95%CI: 15-38), and the score of Cochran-Q was 27.8 and $I^2 > 50\%$, indicating significant heterogeneity across the included studies ($P < 0.05$). In meta-regression analysis, we found that the causes of the heterogeneity were publishing year and sample size for sensitivity, and prevalence of significant fibrosis and BMI for specificity (Figure S3). In the 29 studies evaluating the FibroScan, the AUROC ranged from 0.61 to 0.94. The AUSROC and the pooled sensitivity, specificity, and DOR are also shown in Table 1 and Figure 3. There was significant heterogeneity across the included studies ($I^2 > 50\%$, $P < 0.001$). The heterogeneity of the FibroScan was mainly affected by prevalence of significant fibrosis and BMI with regard to sensitivity or specificity (Figure S4). In the six studies evaluating the MRE for the prediction of significant fibrosis, the AUROC ranged from 0.98 to 0.99. The AUSROC was 0.97 (0.96-0.98) (Figure 3). The summary sensitivity, specificity, and DOR are listed in Table 1, and the Cochran-Q and I^2 of this measure were 0.44 ($P > 0.05$) and 0, respectively. The result of the heterogeneity was statistically insignificant. The subgroup analysis of imaging methods by BMI and prevalence of significant fibrosis are listed in Tables 2 and 3, respectively.

Publication bias

Funnel plots of these markers are illustrated in Figure S5. Symmetry was noted in the funnel plots and publication bias was not observed in any of the serum biomarkers or the imaging methods.

DISCUSSION

Liver fibrosis progression is common in people infected with HBV. Patients with
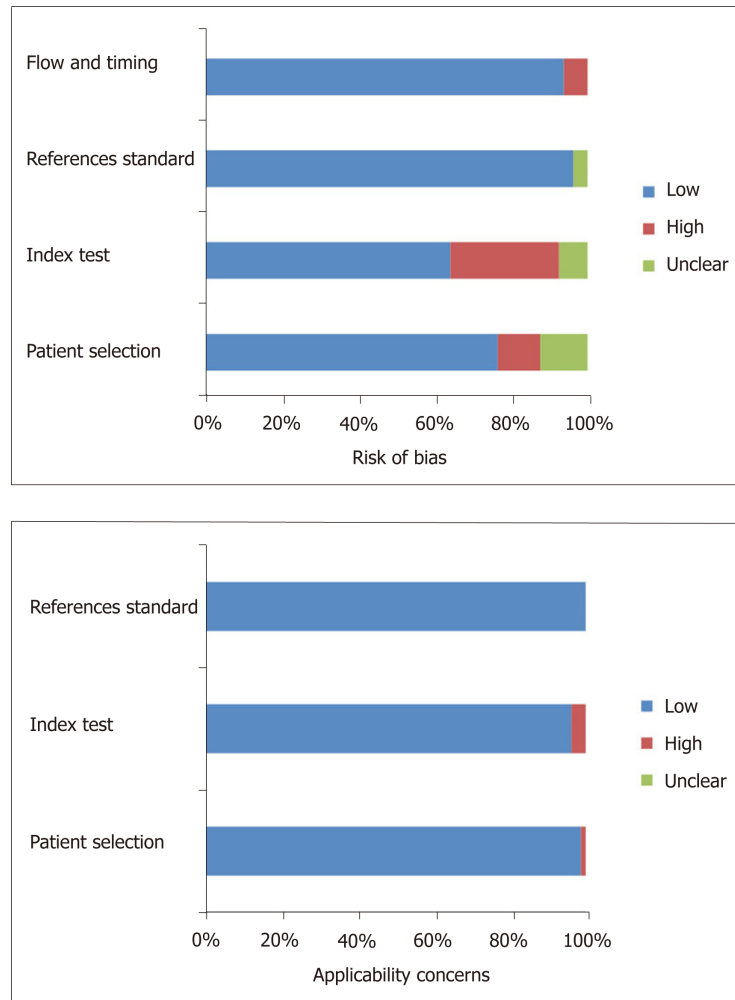
Figure 2 Summary of methodological quality of studies according to QUADAS-2.

significant fibrosis should be considered for clinical therapy, which can potentially reduce and even reverse complications[105]. Considering the risks and limitations of biopsy, researchers should make persistent efforts in researching some noninvasive methods to more conveniently and securely identify patients with significant fibrosis. FIB-4 and APRI are such noninvasive serum biomarkers that they have been gaining increasing acceptance in clinical practice. FibroScan, ARFI, and MRE gradually reveal an advantage with the development of US-based or MRI elastography techniques. These methods may reduce the demand for liver biopsy and also help to monitor the efficacy of treatments[62].

Many scholars have researched the diagnostic effect of APRI and FIB-4 and usually compared them with other new methods. In addition, the World Health Organization (WHO) recommends APRI as the preferred noninvasive test to assess significant fibrosis or cirrhosis and FIB-4 to detect fibrosis stages ≥ F3, considering lower cost, routinely available methods, and untrained staff[106]. Therefore, among all serum biomarkers, only APRI and FIB-4 were singled out in our analysis. Based on the results from an increasing number of studies, the difference between APRI and FIB-4 is not significant in relative diagnostic outcomes, although some articles described that FIB-4 had a higher diagnostic accuracy for cirrhosis when compared with APRI [107]. If only APRI and FIB-4 are available, APRI based on AST, ULN, and platelet count is suggested to diagnose liver significant fibrosis considering resource-limited settings.

With the development of imaging technology, US imaging and MRI devices have been explored to diagnose and stage liver fibrosis, which are truly noninvasive methods. In our meta-analysis, the AUSROCs of imaging techniques are generally bigger than those of APRI and FIB-4. Of these tests, transient elastography performed with FibroScan (Echosens, Paris) has been evaluated widely and has a good performance in predicting cirrhosis, which is corroborated by the Guidelines Development Group. They considered it the most useful test for the assessment of

Table 1 Meta-analysis of hepatitis B-related significant fibrosis

	SEN (95%CI)	SPE (95%CI)	DOR (95%CI)
APRI	0.69 (0.63-0.73)	0.71 (0.66-0.75)	5 (4-6)
FIB-4	0.62 (0.57-0.67)	0.75 (0.71-0.78)	5 (4-5)
ARFI	0.77 (0.70-0.83)	0.87 (0.81-0.92)	23 (15-38)
FibroScan	0.72 (0.68-0.76)	0.82 (0.77-0.86)	12 (9-16)
MRE	0.94 (0.91-0.96)	0.96 (0.93-0.97)	348 (185-656)

SEN: Sensitivity; SPE: Specificity; DOR: Diagnostic odds ratio; CI: Confidence interval; APRI: Aminotransferase-to-platelet ratio index; FIB-4: Fibrosis index based on the 4 factors; ARFI: Acoustic radiation force impulse.

cirrhosis in middle-income countries[106]. In addition, FibroScan acquires information from a much larger portion of the liver tissue compared to biopsy, and therefore, the risk of sampling error is significantly lowered. However, its performance is mediocre for diagnosing moderate liver fibrosis, and the AUSROC ranked in the middle of the five methods. Morbid obesity (BMI > 30), narrow intercostal spaces, and food intake may diminish the accuracy of FibroScan[107]. Because of the limitation of US technology, some researchers advocated that the accuracy of ARFI is similar if not superior to FibroScan for the diagnosis of liver fibrosis[108,109]. Our meta-analysis reveals that ARFI has a higher diagnostic accuracy than FibroScan in identifying HBV-related significant fibrosis. In contrast to FibroScan that has a fixed region of interest box at a fixed insertion depth, ARFI could be performed at variable depths. Furthermore, it can also be performed in obese patients and patients with ascites and integrated in a conventional US system[13]. MRE, the only MRI index, had the best result in prediction of significant fibrosis. The AUSROC of MRE reaches the standard of "best" and even closes to "1"[110]. And the summary sensitivity and specificity have reached 94% and 96%, respectively. It typically covers larger liver tissue than US elastography techniques, which may reduce sampling variability. While MRE has been incorporated into MRI devices, it might be more expensive and require more operator training and expertise. Therefore, it is not widely applied at present, and the number of research articles is limited.

Meta-regression method is a convenient and reliable way for heterogeneity screening. In our study, BMI, prevalence of significant fibrosis, sample size, publishing year, and study design provide heterogeneity in summarizing test results. This is consistent with a range of previous studies[38,111,112]. Some researchers suggested that BMI may reduce the accuracy of ultrasonic technique for detecting significant fibrosis[9,38]. Our results reveal that BMI may affect predicting outcomes of either serum biomarkers or imaging techniques. Imaging technology shows a better predictive effect in the normal weight group, while serum indicators reflect their superiorities in overweight HBV patients (Table 2). The high proportion of fibrosis stage ≥ 2 will reduce the accuracy of evaluating fibrosis by all methods (Table 3). Furthermore, publishing year and sample size are the main contributors to the heterogeneity of ARFI. The AUSROC of ARFI was 0.89 when we excluded the only one article before 2014, the AUSROC of which was 0.75. Therefore, the technology of ARFI, a new diagnostic method, is progressing gradually, and the evaluation effect is increasingly improved. Besides, the AUSROCs in subgroups of sample size between 100 and 300 were much more than others in most cases (Text S6). Although other methods showed no significant differences in the AUSROC among subgroups of sample size, there was a general pattern that the areas were larger in the middle while smaller on both sides (Text S6). This phenomenon is more prominent if the group was changed into three subgroups ($n < 100$, $100 \leq n \leq 300$, and $n > 300$) (Table 4). A few years ago, our team observed that when the sample size was larger than 150, the diagnostic accuracy of predicting fibrosis was noticeably enhanced[111]. Therefore, the sample size of 150-300 will be beneficial to the accuracy of diagnostic tests.

However, there are several limitations in our systematic review. First of all, the cut-off value was not considered due to the absence of threshold effect in all tests (Text S7). Second, the ALT levels were not considered because only a limited number of studies calculated the results by the subgroup of ALT. Third, only the studies published in English and Chinese languages were included. Lastly, other methods, though we have retrieved them, were not considered in this meta-analysis, because the number of articles was not adequate.

In conclusion, these five methods have attained an acceptable level of diagnostic accuracy in our meta-analysis. Imaging techniques are generally better than serum

Table 2 Subgroup analysis of body mass index in prediction of significant fibrosis

Diagnostic test	BMI	Number of studies (*n*)	AUSROC (95%CI)	SEN (95%CI)	SPE (95%CI)
APRI	Overweight	7 (985)	0.78 (0.74-0.81)	0.78 (0.59-0.90)	0.71 (0.61-0.79)
	Normal	13 (2598)	0.75 (0.71-0.79)	0.63 (0.55-0.71)	0.77 (0.68-0.84)
	NA	27 (10142)	0.74 (0.70-0.77)	0.69 (0.62-0.74)	0.68 (0.61-0.74)
FIB-4	Overweight	5 (717)	0.76 (0.72-0.79)	0.58 (0.47-0.70)	0.80 (0.67-0.89)
	Normal	6 (1367)	0.70 (0.66-0.74)	0.58 (0.46-0.69)	0.75 (0.60-0.85)
	NA	21 (9095)	0.75 (0.71-0.79)	0.64 (0.57-0.70)	0.74 (0.69-0.78)
ARFI	Overweight	5 (679)	0.85 (0.82-0.88)	0.76 (0.64-0.85)	0.86 (0.80-0.91)
	Normal[a]	3 (481)	0.91 (0.88-0.95)	0.84 (0.80-0.88)	0.76 (0.64-0.85)
	NA[a]	3 (367)	0.93 (0.85 – 0.99)	0.72 (0.63-0.80)	0.95 (0.91-0.97)
Fibroscan	Overweight	12 (1927)	0.81 (0.77-0.84)	0.68 (0.62-0.74)	0.85 (0.76-0.91)
	Normal	11 (2103)	0.83 (0.79-0.86)	0.73 (0.66-0.79)	0.82 (0.73-0.88)
	NA	6 (1005)	0.85 (0.81-0.88)	0.79 (0.69-0.87)	0.78 (0.72-0.83)

[a]The results were calculated with Meta-Disc software (v. 1.4). BMI: Body mass index; NA: Not assessable; SEN: Sensitivity; SPE: Specificity; CI: Confidence interval; AUSROC: The area under the summary receiver operating characteristic curve; APRI: Aminotransferase-to-platelet ratio index; FIB-4: Fibrosis index based on the 4 factors; ARFI: Acoustic radiation force impulse.

biomarkers in prediction of HBV-related liver significant fibrosis. MRE is a promising indicator and will surprise us with the development of global economy and popularization of technology. If condition allows, ARFI could be a better choice, than FibroScan, for assessment of liver fibrosis in HBV-monoinfected patients with obesity or ascites. The prediction effects of serum markers are generally admissible. Their low cost and easiness in operation make them attractive especially in areas with limited resources and access to imaging technology.

Table 3 Subgroup analysis of prevalence of F2 in prediction of significant fibrosis

Diagnostic test	F2%	Number of studies (*n*)	AUSROC (95%CI)	SEN (95%CI)	SPE (95%CI)
APRI	F2% < 50	16 (4566)	0.72 (0.68-0.76)	0.68 (0.59-0.76)	0.66 (0.57-0.75)
	F2% ≥ 50	31 (9159)	0.77 (0.73-0.81)	0.69 (0.62-0.75)	0.73 (0.68-0.78)
FIB-4	F2% < 50	9 (3234)	0.75 (0.71-0.79)	0.60 (0.47-0.72)	0.76 (0.68-0.83)
	F2% ≥ 50	23 (7945)	0.75 (0.71-0.78)	0.63 (0.57-0.68)	0.74 (0.69-0.78)
ARFI	F2% < 50	4 (554)	0.89 (0.85-0.91)	0.73 (0.62-0.82)	0.93 (0.68-0.97)
	F2% ≥ 50	7 (973)	0.88 (0.85-0.91)	0.80 (0.72-0.87)	0.82 (0.74-0.88)
Fibroscan	F2% < 50	12 (2272)	0.85 (0.81-0.88)	0.77 (0.70-0.83)	0.80 (0.71-0.86)
	F2% ≥ 50	17 (2763)	0.82 (0.78-0.85)	0.69 (0.64-0.74)	0.84 (0.78-0.88)

SEN: Sensitivity; SPE: Specificity; CI: Confidence interval; AUSROC: The area under the summary receiver operating characteristic curve; APRI: Aminotransferase-to-platelet ratio index; FIB-4: Fibrosis index based on the 4 factors; ARFI: Acoustic radiation force impulse.

Table 4 Subgroup analysis of sample size in prediction of significant fibrosis

Diagnostic test	Sample size	Number of studies (N)	AUSROC (95%CI)	SEN (95%CI)	SPE (95%CI)
APRI	*n* < 100	8 (588)	0.73 (0.69-0.77)	0.67 (0.60-0.74)	0.68 (0.61-0.75)
	100 ≤ *n* < 300	27 (5286)	0.77 (0.73-0.80)	0.69 (0.62-0.76)	0.72 (0.65-0.78)
	n ≥ 300	12 (7851)	0.73 (0.69-0.77)	0.67 (0.57-0.76)	0.69 (0.58-0.78)
FIB-4	*n* < 100	6 (411)	0.77 (0.73-0.80)	0.64 (0.54-0.73)	0.77 (0.67-0.85)
	100 ≤ *n* < 300	14 (2917)	0.76 (0.72-0.80)	0.62 (0.53-0.71)	0.77 (0.69-0.83)
	n ≥ 300	12 (7851)	0.74 (0.70-0.77)	0.62 (0.53-0.69)	0.74 (0.67-0.79)
ARFI	*n* < 100	2 (173)	0.72/0.75	0.83/0.50	0.65/0.90
	100 ≤ *n* < 300	9 (1354)	0.90 (0.87-0.92)	0.78 (0.71-0.84)	0.88 (0.82-0.93)
	n ≥ 300	0	-	-	-
Fibroscan	*n* < 100	6 (445)	0.80 (0.76-0.83)	0.70 (0.57-0.80)	0.76 (0.68-0.83)
	100 ≤ *n* < 300	20 (3659)	0.84 (0.81-0.87)	0.74 (0.69-0.79)	0.83 (0.77-0.87)
	n ≥ 300[a]	3 (931)	0.82 (0.69-0.95)	0.62 (0.57-0.66)	0.88 (0.84-0.90)

[a] The results were calculated with Meta-Disc software (v. 1.4). SEN: Sensitivity; SPE: Specificity; CI: Confidence interval; AUSROC: The area under the summary receiver operating characteristic curve; APRI: Aminotransferase-to-platelet ratio index; FIB-4: Fibrosis index based on the 4 factors; ARFI: Acoustic radiation force impulse.
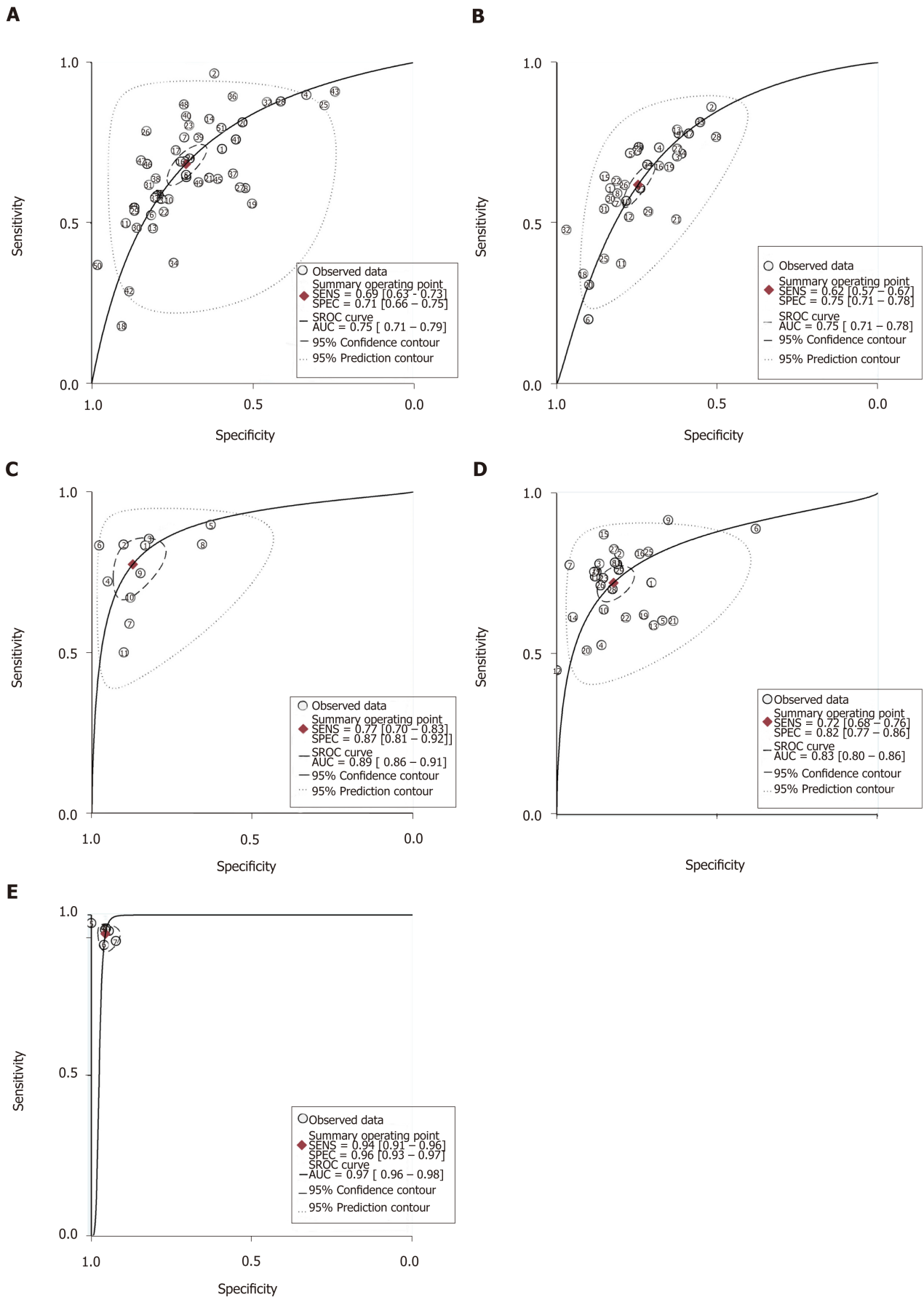
Figure 3 Meta-analysis of hepatitis B-related significant fibrosis. A: Summary receiver operating characteristic (SROC) curve of the aminotransferase-to-platelet ratio index; B: SROC curve of the fibrosis index based on the 4 factors; C: SROC curve of the acoustic radiation force impulse; D: SROC curve of the FibroScan; E: SROC curve of the MRE. SROC: Summary receiver operating characteristic; APRI: Aminotransferase-to-platelet ratio index; FIB-4: Fibrosis index based on the 4 factors; ARFI: Acoustic radiation force impulse.

ARTICLE HIGHLIGHTS

Research background

Liver fibrosis can develop to cirrhosis and even hepatic failure and hepatocellular carcinoma. Approximately one-third of cirrhosis cases worldwide are caused by HBV infection. Therefore, the accurate diagnosis of the extent of liver fibrosis for chronic hepatitis B patients is essential. Many serum biomarkers combining indices/scores and imaging or magnetic resonance imaging techniques have been undergoing dramatic development because of several drawbacks of liver biopsy. These methods have promising results and may improve the management of liver fibrosis. However, most of the previous studies compared the diagnostic effects of these new techniques within the domain of imaging techniques or focused on fibrosis in all chronic liver diseases, which might misestimate the role of these biomarkers. Therefore, we performed a meta-analysis to compare the pooled performance of some common imaging methods with serum biomarkers for prediction of significant fibrosis among HBV-monoinfected patients.

Research motivation

We aimed to assess the accuracy of diagnostic tests for predicting significant fibrosis among patients monoinfected with HBV. Most studies are centered on the domain of imaging techniques and serum biomarkers separately or focused on fibrosis in all chronic liver diseases. Therefore, the key points are that data for HBV infected patients could be extracted independently and we want to integrate and compare the performance of methods of different fields. With the development of medicine and technology, more innovative methods could be invented in the near future. It will provide a boost to precision medicine that chooses a more appropriate and effective method to evaluate liver fibrosis for different populations of patients.

Research objectives

We aimed to compare the pooled performance of some common imaging methods with serum biomarkers for prediction of significant fibrosis among HBV-monoinfected patients. Some serum biomarkers have been calculated and imaging techniques have been developed for the diagnosis of liver fibrosis, respectively. Integrating and comparing the performance of methods of different fields could provide a basis for future research and clinical application and a boost to precision medicine.

Research methods

We examined the areas under the summary receiver operating characteristic curves, the summary diagnostic odds ratios, as well as the summary sensitivities and specificities to further examine the accuracy of all tests for liver fibrosis. Then, we assessed the heterogeneity between studies using the Cochran-Q and I^2. And the Deeks funnel plots were used to assess publication bias. Meta-regression was conducted to further accurately explore the covariates that may induce heterogeneity.

Research results

Our meta-analysis revealed that ARFI showed a higher diagnostic accuracy than FibroScan in identifying HBV-related significant fibrosis. Furthermore, it can also be performed in obese patients and in patients with ascites and be integrated in a conventional ultrasound system. MRE, the only MRI index, had the best result in prediction of significant fibrosis. The area under the SROC curve of MRE reaches the standard of "best" and even closes to "1". The performances of APRI and FIB-4 are poorer than imaging techniques. However, the cut-off value should be considered in future studies.

Research perspectives

Imaging techniques are better than serum biomarkers in prediction of HBV-related liver significant fibrosis in general. MRE is a promising indicator and other serum biomarkers are general.

ACKNOWLEDGEMENTS

REFERENCES

1   **Friedman SL**. Evolving challenges in hepatic fibrosis. *Nat Rev Gastroenterol Hepatol* 2010; **7**: 425-436 [PMID: 20585339 DOI: 10.1038/nrgastro.2010.97]
2   **Kawada N**. Evolution of hepatic fibrosis research. *Hepatol Res* 2011; **41**: 199-208 [PMID: 21338451 DOI: 10.1111/j.1872-034X.2011.00776.x]
3   **Bosch FX**, Ribes J, Cléries R, Díaz M. Epidemiology of hepatocellular carcinoma. *Clin Liver Dis* 2005; **9**: 191-211, v [PMID: 15831268 DOI: 10.1016/j.cld.2004.12.009]
4   **Custer B**, Sullivan SD, Hazlet TK, Iloeje U, Veenstra DL, Kowdley KV. Global epidemiology of hepatitis B virus. *J Clin Gastroenterol* 2004; **38**: S158-S168 [PMID: 15602165 DOI: 10.1097/00004836-200411003-00008]
5   **Bravo AA**, Sheth SG, Chopra S. Liver biopsy. *N Engl J Med* 2001; **344**: 495-500 [PMID: 11172192 DOI:

10.1056/NEJM200102153440706]

6   **Colloredo G**, Guido M, Sonzogni A, Leandro G. Impact of liver biopsy size on histological evaluation of chronic viral hepatitis: the smaller the sample, the milder the disease. *J Hepatol* 2003; **39**: 239-244 [PMID: 12873821 DOI: 10.1016/S0168-8278(03)00191-0]

7   **Poynard T**, Aubert A, Bedossa P, Abella A, Naveau S, Paraf F, Chaput JC. A simple biological index for detection of alcoholic liver disease in drinkers. *Gastroenterology* 1991; **100**: 1397-1402 [PMID: 1672859 DOI: 10.1016/0016-5085(91)90795-M]

8   **Crossan C**, Tsochatzis EA, Longworth L, Gurusamy K, Davidson B, Rodríguez-Perálvarez M, Mantzoukis K, O'Brien J, Thalassinos E, Papastergiou V, Burroughs A. Cost-effectiveness of non-invasive methods for assessment and monitoring of liver fibrosis and cirrhosis in patients with chronic liver disease: systematic review and economic evaluation. *Health Technol Assess* 2015; **19**: 1-409, v-vi [PMID: 25633908 DOI: 10.3310/hta19090]

9   **Petitclerc L**, Sebastiani G, Gilbert G, Cloutier G, Tang A. Liver fibrosis: Review of current imaging and MRI quantification techniques. *J Magn Reson Imaging* 2017; **45**: 1276-1295 [PMID: 27981751 DOI: 10.1002/jmri.25550]

10   **Zhang E**, Wartelle-Bladou C, Lepanto L, Lachaine J, Cloutier G, Tang A. Cost-utility analysis of nonalcoholic steatohepatitis screening. *Eur Radiol* 2015; **25**: 3282-3294 [PMID: 25994191 DOI: 10.1007/s00330-015-3731-2]

11   **Nightingale K**, Soo MS, Nightingale R, Trahey G. Acoustic radiation force impulse imaging: in vivo demonstration of clinical feasibility. *Ultrasound Med Biol* 2002; **28**: 227-235 [PMID: 11937286 DOI: 10.1016/S0301-5629(01)00499-9]

12   **Wang L**, Wang M, Zhao W, Shi Y, Sun Y, Wu X, You H, Jia J. [Key points of 2015 EASL-ALEH clinical practice guidelines: non invasive tests for evaluation of liver severity and prognosis]. *Zhonghua Gan Zang Bing Za Zhi* 2015; **23**: 488-492 [PMID: 26629574]

13   **Frulio N**, Trillaud H, Perez P, Asselineau J, Vandenhende M, Hessamfar M, Bonnet F, Maire F, Delaune J, De Ledinghen V, Morlat P. Acoustic Radiation Force Impulse (ARFI) and Transient Elastography (TE) for evaluation of liver fibrosis in HIV-HCV co-infected patients. *BMC Infect Dis* 2014; **14**: 405 [PMID: 25041708 DOI: 10.1186/1471-2334-14-405]

14   **Adebajo CO**, Talwalkar JA, Poterucha JJ, Kim WR, Charlton MR. Ultrasound-based transient elastography for the detection of hepatic fibrosis in patients with recurrent hepatitis C virus after liver transplantation: a systematic review and meta-analysis. *Liver Transpl* 2012; **18**: 323-331 [PMID: 22140010 DOI: 10.1002/lt.22460]

15   **Whiting PF**, Rutjes AW, Westwood ME, Mallett S, Deeks JJ, Reitsma JB, Leeflang MM, Sterne JA, Bossuyt PM; QUADAS-2 Group. QUADAS-2: a revised tool for the quality assessment of diagnostic accuracy studies. *Ann Intern Med* 2011; **155**: 529-536 [PMID: 22007046 DOI: 10.7326/0003-4819-155-8-201110180-00009]

16   **Intraobserver and interobserver variations in liver biopsy interpretation in patients with chronic hepatitis C**. The French METAVIR Cooperative Study Group. *Hepatology* 1994; **20**: 15-20 [PMID: 8020885 DOI: 10.1002/hep.1840200104]

17   **Batts KP**, Ludwig J. Chronic hepatitis. An update on terminology and reporting. *Am J Surg Pathol* 1995; **19**: 1409-1417 [PMID: 7503362 DOI: 10.1097/00000478-199512000-00007]

18   **Scheuer PJ**. Classification of chronic viral hepatitis: a need for reassessment. *J Hepatol* 1991; **13**: 372-374 [PMID: 1808228 DOI: 10.1016/0168-8278(91)90084-O]

19   **Diseases CSoHaCSoI**. Chinese medical association: Chinese program of prevention and cure for viral hepatitis. *Chin J Intern Med* 2001; **40**: 62-68

20   **Ishak K**, Baptista A, Bianchi L, Callea F, De Groote J, Gudat F, Denk H, Desmet V, Korb G, MacSween RN. Histological grading and staging of chronic hepatitis. *J Hepatol* 1995; **22**: 696-699 [PMID: 7560864 DOI: 10.1016/0168-8278(95)80226-6]

21   **Strader DB**, Wright T, Thomas DL, Seeff LB; American Association for the Study of Liver Diseases. Diagnosis, management, and treatment of hepatitis C. *Hepatology* 2004; **39**: 1147-1171 [PMID: 15057920 DOI: 10.1002/hep.20119]

22   **Higgins JP**, Thompson SG, Deeks JJ, Altman DG. Measuring inconsistency in meta-analyses. *BMJ* 2003; **327**: 557-560 [PMID: 12958120 DOI: 10.1136/bmj.327.7414.557]

23   **Deeks JJ**, Macaskill P, Irwig L. The performance of tests of publication bias and other sample size effects in systematic reviews of diagnostic test accuracy was assessed. *J Clin Epidemiol* 2005; **58**: 882-893 [PMID: 16085191 DOI: 10.1016/j.jclinepi.2005.01.016]

24   **Wang K**, Lu X, Zhou H, Gao Y, Zheng J, Tong M, Wu C, Liu C, Huang L, Jiang T, Meng F, Lu Y, Ai H, Xie XY, Yin LP, Liang P, Tian J, Zheng R. Deep learning Radiomics of shear wave elastography significantly improved diagnostic performance for assessing liver fibrosis in chronic hepatitis B: a prospective multicentre study. *Gut* 2019; **68**: 729-741 [PMID: 29730602 DOI: 10.1136/gutjnl-2018-316204]

25   **Chen YP**, Hu XM, Liang XE, Huang LW, Zhu YF, Hou JL. Stepwise application of fibrosis index based on four factors, red cell distribution width-platelet ratio, and aspartate aminotransferase-platelet ratio for compensated hepatitis B fibrosis detection. *J Gastroenterol Hepatol* 2018; **33**: 256-263 [PMID: 28452125 DOI: 10.1111/jgh.13811]

26   **Celikbilek M**, Dogan S, Gursoy S, Zararsız G, Yurci A, Ozbakır O, Guven K, Yucesoy M. Noninvasive assessment of liver damage in chronic hepatitis B. *World J Hepatol* 2013; **5**: 439-445 [PMID: 24023983 DOI: 10.4254/wjh.v5.i8.439]

27   **Gümüşay O**, Ozenirler S, Atak A, Sönmez C, Ozkan S, Tuncel AF, Yılmaz G, Akyol G. Diagnostic potential of serum direct markers and non-invasive fibrosis models in patients with chronic hepatitis B. *Hepatol Res* 2013; **43**: 228-237 [PMID: 22734888 DOI: 10.1111/j.1872-034X.2012.01057.x]

28   **Li Q**, Chen L, Zhou Y. Diagnostic accuracy of liver stiffness measurement in chronic hepatitis B patients with normal or mildly elevated alanine transaminase levels. *Sci Rep* 2018; **8**: 5224 [PMID: 29588489 DOI: 10.1038/s41598-018-23646-2]

29   **Chen X**, Wen H, Zhang X, Dong C, Lin H, Guo Y, Shan L, Yao S, Yang M, Le X, Liu Y. Development of a Simple Noninvasive Model to Predict Significant Fibrosis in Patients with Chronic Hepatitis B: Combination of Ultrasound Elastography, Serum Biomarkers, and Individual Characteristics. *Clin Transl Gastroenterol* 2017; **8**: e84 [PMID: 28383564 DOI: 10.1038/ctg.2017.11]

30   **Zhang Z**, Wang G, Kang K, Wu G, Wang P. The Diagnostic Accuracy and Clinical Utility of Three Noninvasive Models for Predicting Liver Fibrosis in Patients with HBV Infection. *PLoS One* 2016; **11**: e0152757 [PMID: 27050531 DOI: 10.1371/journal.pone.0152757]

31   **Liang B**, Li Y, Zhao A, Xie F, Guo Z. Clinical utility of serum matrix metalloproteinase-2 and tissue inhibitor of metalloproteinase-2 concentrations in the assessment of liver fibrosis due to chronic hepatitis B. *J Int Med Res* 2012; **40**: 631-639 [PMID: 22613424 DOI: 10.1177/147323001204000225]

32   **Zhou K**, Gao CF, Zhao YP, Liu HL, Zheng RD, Xian JC, Xu HT, Mao YM, Zeng MD, Lu LG. Simpler score of routine laboratory tests predicts liver fibrosis in patients with chronic hepatitis B. *J Gastroenterol Hepatol* 2010; **25**: 1569-1577 [PMID: 20796157 DOI: 10.1111/j.1440-1746.2010.06383.x]

33   **Güzelbulut F**, Sezıklı M, Akkan-Çetınkaya Z, Yaşar B, Özkara S, Kurdaş-Övünç AO. AST-platelet ratio index in the prediction of significant fibrosis and cirrhosis in patients with chronic hepatitis B. *Turk J Gastroenterol* 2012; **23**: 353-358 [PMID: 22965506 DOI: 10.4318/tjg.2012.0348]

34   **Eminler AT**, Ayyildiz T, Irak K, Kiyici M, Gurel S, Dolar E, Gulten M, Nak SG. AST/ALT ratio is not useful in predicting the degree of fibrosis in chronic viral hepatitis patients. *Eur J Gastroenterol Hepatol* 2015; **27**: 1361-1366 [PMID: 26352130 DOI: 10.1097/MEG.0000000000000468]

35   **Liu J**, Zhao J, Zhang Y, Ji Y, Lin S, Dun G, Guo S. Noninvasive Assessment of Liver Fibrosis Stage Using Ultrasound-Based Shear Wave Velocity Measurements and Serum Algorithms in Patients With Viral Hepatitis B: A Retrospective Cohort Study. *J Ultrasound Med* 2017; **36**: 285-293 [PMID: 28039877 DOI: 10.7863/ultra.16.01069]

36   **Yang L**, Ding Y, Rao S, Chen C, Wu L, Sheng R, Fu C, Zeng M. Staging liver fibrosis in chronic hepatitis B with T1 relaxation time index on gadoxetic acid-enhanced MRI: Comparison with aspartate aminotransferase-to-platelet ratio index and FIB-4. *J Magn Reson Imaging* 2017; **45**: 1186-1194 [PMID: 27563840 DOI: 10.1002/jmri.25440]

37   **Li Q**, Li W, Huang Y, Chen L. The gamma-glutamyl transpeptidase-to-platelet ratio predicts liver fibrosis and cirrhosis in HBeAg-positive chronic HBV infection patients with high HBV DNA and normal or mildly elevated alanine transaminase levels in China. *J Viral Hepat* 2016; **23**: 912-919 [PMID: 27375134 DOI: 10.1111/jvh.12563]

38   **Lemoine M**, Shimakawa Y, Nayagam S, Khalil M, Suso P, Lloyd J, Goldin R, Njai HF, Ndow G, Taal M, Cooke G, D'Alessandro U, Vray M, Mbaye PS, Njie R, Mallet V, Thursz M. The gamma-glutamyl transpeptidase to platelet ratio (GPR) predicts significant liver fibrosis and cirrhosis in patients with chronic HBV infection in West Africa. *Gut* 2016; **65**: 1369-1376 [PMID: 26109530 DOI: 10.1136/gutjnl-2015-309260]

39   **Zhou QQ**, Hu YB, Zhou K, Zhang WW, Li MH, Dong P, Ding JG, Hong L, Du QW, Xie Y, Sun QF. Value of non-invasive models of liver fibrosis in judgment of treatment timing in chronic hepatitis b patients with ALT < 2x upperlimit ofnormal. *Zhonghua Gan Zang Bing Za Zhi* 2016; **24**: 665-670

40   **Li Q**, Song J, Huang Y, Li X, Zhuo Q, Li W, Chen C, Lu C, Qi X, Chen L. The Gamma-Glutamyl-Transpeptidase to Platelet Ratio Does not Show Advantages than APRI and Fib-4 in Diagnosing Significant Fibrosis and Cirrhosis in Patients With Chronic Hepatitis B: A Retrospective Cohort Study in China. *Medicine (Baltimore)* 2016; **95**: e3372 [PMID: 27100421 DOI: 10.1097/MD.0000000000003372]

41   **Shin WG**, Park SH, Jang MK, Hahn TH, Kim JB, Lee MS, Kim DJ, Jun SY, Park CK. Aspartate aminotransferase to platelet ratio index (APRI) can predict liver fibrosis in chronic hepatitis B. *Dig Liver Dis* 2008; **40**: 267-274 [PMID: 18055281 DOI: 10.1016/j.dld.2007.10.011]

42   **Liu Y**, Dong CF, Yang G, Liu J, Yao S, Li HY, Yuan J, Li S, Le X, Lin Y, Zeng W, Lin H, Zhang X, Chen X. Optimal linear combination of ARFI, transient elastography and APRI for the assessment of fibrosis in chronic hepatitis B. *Liver Int* 2015; **35**: 816-825 [PMID: 24751289 DOI: 10.1111/liv.12564]

43   **Salkic NN**, Cickusic E, Jovanovic P, Denjagic MB, Iljazovic-Topcic S, Bevanda M, Ahmetagic S. Online combination algorithm for non-invasive assessment of chronic hepatitis B related liver fibrosis and cirrhosis in resource-limited settings. *Eur J Intern Med* 2015; **26**: 628-634 [PMID: 26194460 DOI: 10.1016/j.ejim.2015.07.005]

44   **Erdogan S**, Dogan HO, Sezer S, Uysal S, Ozhamam E, Kayacetin S, Koca Y. The diagnostic value of non-invasive tests for the evaluation of liver fibrosis in chronic hepatitis B patients. *Scand J Clin Lab Invest* 2013; **73**: 300-308 [PMID: 23514016 DOI: 10.3109/00365513.2013.773592]

45   **Kim WR**, Berg T, Asselah T, Flisiak R, Fung S, Gordon SC, Janssen HL, Lampertico P, Lau D, Bornstein JD, Schall RE, Dinh P, Yee LJ, Martins EB, Lim SG, Loomba R, Petersen J, Buti M, Marcellin P. Evaluation of APRI and FIB-4 scoring systems for non-invasive assessment of hepatic fibrosis in chronic hepatitis B patients. *J Hepatol* 2016; **64**: 773-780 [PMID: 26626497 DOI: 10.1016/j.jhep.2015.11.012]

46   **Başar O**, Yimaz B, Ekiz F, Giniş Z, Altınbaş A, Aktaş B, Tuna Y, Çoban S, Delibaş N, Yüksel O. Non-invasive tests in prediction of liver fibrosis in chronic hepatitis B and comparison with post-antiviral treatment results. *Clin Res Hepatol Gastroenterol* 2013; **37**: 152-158 [PMID: 23391746 DOI: 10.1016/j.clinre.2012.07.003]

47   **Dong C**, Feng LY, Li HY, Lu PX, Yao SM, Shan LB, Zhang XY, Chen X. Virtual touch tissue quantification and aspartate aminotransferase to platelet ratio for staging hepatic fibrosis in patients with chronic hepatitis B. *Zhongguo Yixue Yingxiang Jishu* 2016; **32**: 398-402

48   **Li Q**, Lu C, Li W, Huang Y, Chen L. Impact of age on the diagnostic performances and cut-offs of APRI and FIB-4 for significant fibrosis and cirrhosis in chronic hepatitis B. *Oncotarget* 2017; **8**: 45768-45776 [PMID: 28514753 DOI: 10.18632/oncotarget.17470]

49   **Wang J**, Yan X, Yang Y, Chang H, Jia B, Zhao XA, Chen G, Xia J, Liu Y, Chen Y, Wang G, Wang L, Zhang Z, Ding W, Huang R, Wu C. A novel predictive model using routinely clinical parameters to predict liver fibrosis in patients with chronic hepatitis B. *Oncotarget* 2017; **8**: 59257-59267 [PMID: 28938634 DOI: 10.18632/oncotarget.19501]

50   **Lin CL**, Liu CH, Wang CC, Liang CC, Su TH, Liu CJ, Kao JH. Serum Biomarkers Predictive of Significant Fibrosis and Cirrhosis in Chronic Hepatitis B. *J Clin Gastroenterol* 2015; **49**: 705-713 [PMID: 25319739 DOI: 10.1097/MCG.0000000000000250]

51   **Ma XH**, Zang X, You Y, Jiang LL, Zhao J, Ayiguli A, Nie ZG. Diagnostic value of apri combined with fib-4 for significant liver fibrosis in patients with chronic hepatitis b. *Chin J Gastroenterol* 2017; **22**: 544-547 [DOI: 10.3969/j.issn.1008-7125.2017.09.007]

52   **Cao Z**, Li Z, Wang H, Liu Y, Xu Y, Mo R, Ren P, Chen L, Lu J, Li H, Zhuang Y, Liu Y, Wang X, Zhao G, Tang W, Xiang X, Cai W, Liu L, Bao S, Xie Q. Algorithm of Golgi protein 73 and liver stiffness accurately diagnoses significant fibrosis in chronic HBV infection. *Liver Int* 2017; **37**: 1612-1621 [PMID: 28772348 DOI: 10.1111/liv.13536]

53   **Li Y**, Cai Q, Zhang Y, Xie Q, Xu N, Jiang X, Li J, Li X, Zhang Z. Development of algorithms based on serum markers and transient elastography for detecting significant fibrosis and cirrhosis in chronic hepatitis B patients: Significant reduction in liver biopsy. *Hepatol Res* 2016; **46**: 1367-1379 [PMID: 26670087 DOI: 10.1111/hepr.12696]

54   **Liu DP**, Lu W, Zhang ZQ, Wang YB, Ding RR, Zhou XL, Huang D, Li XF. Comparative evaluation of GPR versus APRI and FIB-4 in predicting different levels of liver fibrosis of chronic hepatitis B. *J Viral Hepat* 2018; **25**: 581-589 [PMID: 29230907 DOI: 10.1111/jvh.12842]

55   **Noguchi R**, Kaji K, Namisaki T, Moriya K, Kitade M, Takeda K, Kawaratani H, Okura Y, Aihara Y, Furukawa M, Mitoro A, Yoshiji H. Serum angiotensin-converting enzyme level for evaluating significant fibrosis in chronic hepatitis B. *World J Gastroenterol* 2017; **23**: 6705-6714 [PMID: 29085215 DOI: 10.3748/wjg.v23.i36.6705]

56   **Ren T**, Wang H, Wu R, Niu J. Gamma-Glutamyl Transpeptidase-to-Platelet Ratio Predicts Significant Liver Fibrosis of Chronic Hepatitis B Patients in China. *Gastroenterol Res Pract* 2017; **2017**: 7089702 [PMID: 28831282 DOI: 10.1155/2017/7089702]

57   **Wu X**, Cai B, Su Z, Li Y, Xu J, Deng R, Wang L. Aspartate transaminase to platelet ratio index and gamma-glutamyl transpeptidase-to-platelet ratio outweigh fibrosis index based on four factors and red cell distribution width-platelet ratio in diagnosing liver fibrosis and inflammation in chronic hepatitis B. *J Clin Lab Anal* 2018; **32**: e22341 [PMID: 29251384 DOI: 10.1002/jcla.22341]

58   **Yan LB**, Zhang QB, Zhu X, He M, Tang H. Serum S100 calcium binding protein A4 improves the diagnostic accuracy of transient elastography for assessing liver fibrosis in hepatitis B. *Clin Res Hepatol Gastroenterol* 2018; **42**: 64-71 [PMID: 28688902 DOI: 10.1016/j.clinre.2017.05.013]

59   **Zhijian Y**, Hui L, Weiming Y, Zhanzhou L, Zhong C, Jinxin Z, Hongyan W, Xiangbin D, Weizhi Y, Duoyun L, Xiaojun L, Qiwen D. Role of the Aspartate Transaminase and Platelet Ratio Index in Assessing Hepatic Fibrosis and Liver Inflammation in Adolescent Patients with HBeAg-Positive Chronic Hepatitis B. *Gastroenterol Res Pract* 2015; **2015**: 906026 [PMID: 26236336 DOI: 10.1155/2015/906026]

60   **Bonnard P**, Sombié R, Lescure FX, Bougouma A, Guiard-Schmid JB, Poynard T, Calès P, Housset C, Callard P, Le Pendeven C, Drabo J, Carrat F, Pialoux G. Comparison of elastography, serum marker scores, and histology for the assessment of liver fibrosis in hepatitis B virus (HBV)-infected patients in Burkina Faso. *Am J Trop Med Hyg* 2010; **82**: 454-458 [PMID: 20207872 DOI: 10.4269/ajtmh.2010.09-0088]

61   **Lesmana CR**, Salim S, Hasan I, Sulaiman AS, Gani RA, Pakasi LS, Lesmana LA, Krisnuhoni E, Budihusodo U. Diagnostic accuracy of transient elastography (FibroScan) versus the aspartate transaminase to platelet ratio index in assessing liver fibrosis in chronic hepatitis B: the role in primary care setting. *J Clin Pathol* 2011; **64**: 916-920 [PMID: 21670074 DOI: 10.1136/jclinpath-2011-200044]

62   **Liu HB**, Zhou JP, Zhang Y, Lv XH, Wang W. Prediction on liver fibrosis using different APRI thresholds when patient age is a categorical marker in patients with chronic hepatitis B. *Clin Chim Acta* 2011; **412**: 33-37 [PMID: 20828546 DOI: 10.1016/j.cca.2010.08.032]

63   **Liu XD**, Wu JL, Liang J, Zhang T, Sheng QS. Globulin-platelet model predicts minimal fibrosis and cirrhosis in chronic hepatitis B virus infected patients. *World J Gastroenterol* 2012; **18**: 2784-2792 [PMID: 22719186 DOI: 10.3748/wjg.v18.i22.2784]

64   **Sebastiani G**, Castera L, Halfon P, Pol S, Mangia A, Di Marco V, Pirisi M, Voiculescu M, Bourliere M, Alberti A. The impact of liver disease aetiology and the stages of hepatic fibrosis on the performance of non-invasive fibrosis biomarkers: an international study of 2411 cases. *Aliment Pharmacol Ther* 2011; **34**: 1202-1216 [PMID: 21981787 DOI: 10.1111/j.1365-2036.2011.04861.x]

65   **Ucar F**, Sezer S, Ginis Z, Ozturk G, Albayrak A, Basar O, Ekiz F, Coban S, Yuksel O, Armutcu F, Akbal E. APRI, the FIB-4 score, and Forn's index have noninvasive diagnostic value for liver fibrosis in patients with chronic hepatitis B. *Eur J Gastroenterol Hepatol* 2013; **25**: 1076-1081 [PMID: 23510962 DOI: 10.1097/MEG.0b013e32835fd699]

66   **Wang H**, Xue L, Yan R, Zhou Y, Wang MS, Cheng MJ, Huang HJ. Comparison of FIB-4 and APRI in Chinese HBV-infected patients with persistently normal ALT and mildly elevated ALT. *J Viral Hepat* 2013; **20**: e3-10 [PMID: 23490387 DOI: 10.1111/jvh.12010]

67   **Wang Y**, Xu MY, Zheng RD, Xian JC, Xu HT, Shi JP, Li SB, Qu Y, Dong YW, Lu LG. Prediction of significant fibrosis and cirrhosis in hepatitis B e-antigen negative patients with chronic hepatitis B using routine parameters. *Hepatol Res* 2013; **43**: 441-451 [PMID: 23006433 DOI: 10.1111/j.1872-034X.2012.01094.x]

68   **Wu SD**, Wang JY, Li L. Staging of liver fibrosis in chronic hepatitis B patients with a composite predictive model: a comparative study. *World J Gastroenterol* 2010; **16**: 501-507 [PMID: 20101779 DOI: 10.3748/wjg.v16.i4.501]

69   **Li J**, Yu J, Peng XY, Du TT, Wang JJ, Tong J, Lu GL, Wu XW. Acoustic Radiation Force Impulse (ARFI) Elastography and Serological Markers in Assessment of Liver Fibrosis and Free Portal Pressure in Patients with Hepatitis B. *Med Sci Monit* 2017; **23**: 3585-3592 [PMID: 28735336 DOI: 10.12659/msm.905896]

70   **Dong CF**, Xiao J, Shan LB, Li HY, Xiong YJ, Yang GL, Liu J, Yao SM, Li SX, Le XH, Yuan J, Zhou BP, Tipoe GL, Liu YX. Combined acoustic radiation force impulse, aminotransferase to platelet ratio index and Forns index assessment for hepatic fibrosis grading in hepatitis B. *World J Hepatol* 2016; **8**: 616-624 [PMID: 27190578 DOI: 10.4254/wjh.v8.i14.616]

71   **Dong DR**, Hao MN, Li C, Peng Z, Liu X, Wang GP, Ma AL. Acoustic radiation force impulse elastography, FibroScan®, Forns' index and their combination in the assessment of liver fibrosis in patients with chronic hepatitis B, and the impact of inflammatory activity and steatosis on these diagnostic methods. *Mol Med Rep* 2015; **11**: 4174-4182 [PMID: 25651500 DOI: 10.3892/mmr.2015.3299]

72   **Friedrich-Rust M**, Buggisch P, de Knegt RJ, Dries V, Shi Y, Matschenz K, Schneider MD, Herrmann E, Petersen J, Schulze F, Zeuzem S, Sarrazin C. Acoustic radiation force impulse imaging for non-invasive assessment of liver fibrosis in chronic hepatitis B. *J Viral Hepat* 2013; **20**: 240-247 [PMID: 23490368 DOI: 10.1111/j.1365-2893.2012.01646.x]

73   **Zhang D**, Chen M, Wang R, Liu Y, Zhang D, Liu L, Zhou G. Comparison of acoustic radiation force impulse imaging and transient elastography for non-invasive assessment of liver fibrosis in patients with chronic hepatitis B. *Ultrasound Med Biol* 2015; **41**: 7-14 [PMID: 25308941 DOI: 10.1016/j.ultrasmedbio.2014.07.018]

74   **Ozturker C**, Karagoz E, Sivrioglu AK, Kara K. Clinical usefulness and performance of acoustic radiation force impulse in patients with chronic hepatitis B. *Eur J Gastroenterol Hepatol* 2017; **29**: 663-668 [PMID: 28151749 DOI: 10.1097/MEG.0000000000000842]

75   **Park MS**, Kim SW, Yoon KT, Kim SU, Park SY, Tak WY, Kweon YO, Cho M, Kim BK, Park JY, Kim DY, Ahn SH, Han KH. Factors Influencing the Diagnostic Accuracy of Acoustic Radiation Force Impulse Elastography in Patients with Chronic Hepatitis B. *Gut Liver* 2016; **10**: 275-282 [PMID: 26087790 DOI: 10.5009/gnl14391]

76   **Liu J**, Ji Y, Ai H, Ning B, Zhao J, Zhang Y, Dun G. Liver Shear-Wave Velocity and Serum Fibrosis Markers to Diagnose Hepatic Fibrosis in Patients with Chronic Viral Hepatitis B. *Korean J Radiol* 2016; **17**: 396-404 [PMID: 27134527 DOI: 10.3348/kjr.2016.17.3.396]

77   **Liu F**, Wei L, Wang S, Huang B. Comparison of FibroTouch and acoustic radiation force impulse in diagnosis of liver fibrosis in patients with chronic hepatitis B. *Zhejiang Da Xue Xue Bao Yi Xue Ban* 2016; **45**: 416-421 [PMID: 27868416]

78   **Coskun BD**, Altinkaya E, Sevinc E, Ozen M, Karaman H, Karaman A, Poyrazoglu O. The diagnostic value of a globulin/platelet model for evaluating liver fibrosis in chronic hepatitis B patients. *Rev Esp Enferm Dig* 2015; **107**: 740-744 [PMID: 26671586 DOI: 10.17235/reed.2015.3851/2015]

79   **Zhang YF**, Shi H, Chen LB, Xu QH. [Value of FIB-4 for the diagnosis of liver fibrosis in chronic hepatitis B]. *Zhonghua Shi Yan He Lin Chuang Bing Du Xue Za Zhi* 2010; **24**: 215-217 [PMID: 21186531]

80   **Zhao J**, Zhai F, Cheng J, He Q, Luo J, Yang X, Shao J, Xing H. Evaluating the Significance of Viscoelasticity in Diagnosing Early-Stage Liver Fibrosis with Transient Elastography. *PLoS One* 2017; **12**: e0170073 [PMID: 28107385 DOI: 10.1371/journal.pone.0170073]

81   **Zeng X**, Xu C, He D, Li M, Zhang H, Wu Q, Xiang D, Wang Y. Performance of several simple, noninvasive models for assessing significant liver fibrosis in patients with chronic hepatitis B. *Croat Med J* 2015; **56**: 272-279 [PMID: 26088852 DOI: 10.3325/cmj.2015.56.272]

82   **Leung VY**, Shen J, Wong VW, Abrigo J, Wong GL, Chim AM, Chu SH, Chan AW, Choi PC, Ahuja AT, Chan HL, Chu WC. Quantitative elastography of liver fibrosis and spleen stiffness in chronic hepatitis B carriers: comparison of shear-wave elastography and transient elastography with liver biopsy correlation. *Radiology* 2013; **269**: 910-918 [PMID: 23912619 DOI: 10.1148/radiol.13130128]

83   **Degos F**, Perez P, Roche B, Mahmoudi A, Asselineau J, Voitot H, Bedossa P; FIBROSTIC study group. Diagnostic accuracy of FibroScan and comparison to liver fibrosis biomarkers in chronic viral hepatitis: a multicenter prospective study (the FIBROSTIC study). *J Hepatol* 2010; **53**: 1013-1021 [PMID: 20850886 DOI: 10.1016/j.jhep.2010.05.035]

84   **Cho HJ**, Seo YS, Lee KG, Hyun JJ, An H, Keum B, Kim JH, Yim HJ, Jeen YT, Lee HS, Chun HJ, Um SH, Kim CD, Ryu HS. Serum aminotransferase levels instead of etiology affects the accuracy of transient elastography in chronic viral hepatitis patients. *J Gastroenterol Hepatol* 2011; **26**: 492-500 [PMID: 21332545 DOI: 10.1111/j.1440-1746.2010.06419.x]

85   **Kim BK**, Kim HS, Park JY, Kim DY, Ahn SH, Chon CY, Park YN, Han KH, Kim SU. Prospective validation of ELF test in comparison with Fibroscan and FibroTest to predict liver fibrosis in Asian subjects with chronic hepatitis B. *PLoS One* 2012; **7**: e41964 [PMID: 22848675 DOI: 10.1371/journal.pone.0041964]

86   **Huang R**, Jiang N, Yang R, Geng X, Lin J, Xu G, Liu D, Chen J, Zhou G, Wang S, Luo T, Wu J, Liu X, Xu K, Yang X. Fibroscan improves the diagnosis sensitivity of liver fibrosis in patients with chronic hepatitis B. *Exp Ther Med* 2016; **11**: 1673-1677 [PMID: 27168788 DOI: 10.3892/etm.2016.3135]

87   **Kumar M**, Rastogi A, Singh T, Bihari C, Gupta E, Sharma P, Garg H, Kumar R, Bhatia V, Tyagi P, Sarin SK. Analysis of discordance between transient elastography and liver biopsy for assessing liver fibrosis in chronic hepatitis B virus infection. *Hepatol Int* 2013; **7**: 134-143 [PMID: 26201627 DOI: 10.1007/s12072-012-9380-5]

88   **Kongtawelert P**, Chanmee T, Pothacharoen P, Wisedopa N, Kranokpiruk P, Poovorawan K, Poovorawan Y, Tangkijvanich P. Diagnostic accuracy of liver stiffness measurement and serum hyaluronic acid for detecting liver fibrosis in chronic hepatitis B with respect to alt levels. *Asian Biomed* 2013; **7**: 609-617

89   **Kim BK**, Kim SU, Kim HS, Park JY, Ahn SH, Chon CY, Cho IR, Joh DH, Park YN, Han KH, Kim DY. Prospective validation of FibroTest in comparison with liver stiffness for predicting liver fibrosis in Asian subjects with chronic hepatitis B. *PLoS One* 2012; **7**: e35825 [PMID: 22536445 DOI: 10.1371/journal.pone.0035825]

90   **Goyal R**, Mallick SR, Mahanta M, Kedia S, Shalimar, Dhingra R, Sharma H, Das P, Datta Gupta S, Panda S, Acharya SK. Fibroscan can avoid liver biopsy in Indian patients with chronic hepatitis B. *J Gastroenterol Hepatol* 2013; **28**: 1738-1745 [PMID: 23808910 DOI: 10.1111/jgh.12318]

91   **Cardoso AC**, Carvalho-Filho RJ, Stern C, Dipumpo A, Giuily N, Ripault MP, Asselah T, Boyer N, Lada O, Castelnau C, Martinot-Peignoux M, Valla DC, Bedossa P, Marcellin P. Direct comparison of diagnostic performance of transient elastography in patients with chronic hepatitis B and chronic hepatitis C. *Liver Int* 2012; **32**: 612-621 [PMID: 22103765 DOI: 10.1111/j.1478-3231.2011.02660.x]

92   **Gaia S**, Carenzi S, Barilli AL, Bugianesi E, Smedile A, Brunello F, Marzano A, Rizzetto M. Reliability of transient elastography for the detection of fibrosis in non-alcoholic fatty liver disease and chronic viral hepatitis. *J Hepatol* 2011; **54**: 64-71 [PMID: 20932598 DOI: 10.1016/j.jhep.2010.06.022]

93   **Fung J**, Lai CL, Chan SC, But D, Seto WK, Cheng C, Wong DK, Lo CM, Fan ST, Yuen MF. Correlation of liver stiffness and histological features in healthy persons and in patients with occult hepatitis B, chronic active hepatitis B, or hepatitis B cirrhosis. *Am J Gastroenterol* 2010; **105**: 1116-1122 [PMID: 19920809 DOI: 10.1038/ajg.2009.665]

94   **Lee HJ**, Seo YS, Kim DJ, Kang HS, An H, Kim JH, Cheong JY, Yim HJ, Yeon JE, Lee HS, Byun KS, Cho SW, Kim DJ, Um SH, Kim CD, Ryu HS. Application of the HALF index obviates the need for liver biopsy in half of all patients with chronic hepatitis B. *J Gastroenterol Hepatol* 2011; **26**: 987-995 [PMID: 21198828 DOI: 10.1111/j.1440-1746.2010.06609.x]

95   **Myers RP**, Elkashab M, Ma M, Crotty P, Pomier-Layrargues G. Transient elastography for the noninvasive assessment of liver fibrosis: a multicentre Canadian study. *Can J Gastroenterol* 2010; **24**: 661-670 [PMID: 21157581 DOI: 10.1155/2010/153986]

96   **Sporea I**, Sirli R, Deleanu A, Tudora A, Popescu A, Curescu M, Bota S. Liver stiffness measurements in patients with HBV *vs* HCV chronic hepatitis: a comparative study. *World J Gastroenterol* 2010; **16**: 4832-4837 [PMID: 20939112 DOI: 10.3748/wjg.v16.i38.4832]

97   **Marcellin P**, Ziol M, Bedossa P, Douvin C, Poupon R, de Lédinghen V, Beaugrand M. Non-invasive assessment of liver fibrosis by stiffness measurement in patients with chronic hepatitis B. *Liver Int* 2009; **29**: 242-247 [PMID: 18637064 DOI: 10.1111/j.1478-3231.2008.01802.x]

98   **Dong H**, Xu C, Zhou W, Liao Y, Cao J, Li Z, Hu B. The combination of 5 serum markers compared to FibroScan to predict significant liver fibrosis in patients with chronic hepatitis B virus. *Clin Chim Acta* 2018; **483**: 145-150 [PMID: 29709450 DOI: 10.1016/j.cca.2018.04.036]

99   **Hennedige TP**, Wang G, Leung FP, Alsaif HS, Teo LL, Lim SG, Wee A, Venkatesh SK. Magnetic Resonance Elastography and Diffusion Weighted Imaging in the Evaluation of Hepatic Fibrosis in Chronic Hepatitis B. *Gut Liver* 2017; **11**: 401-408 [PMID: 27965475 DOI: 10.5009/gnl16079]

100   **Lee JE**, Lee JM, Lee KB, Yoon JH, Shin CI, Han JK, Choi BI. Noninvasive assessment of hepatic fibrosis

in patients with chronic hepatitis B viral infection using magnetic resonance elastography. *Korean J Radiol* 2014; **15**: 210-217 [PMID: 24643284 DOI: 10.3348/kjr.2014.15.2.210]

101   **Wu WP**, Chou CT, Chen RC, Lee CW, Lee KW, Wu HK. Non-Invasive Evaluation of Hepatic Fibrosis: The Diagnostic Performance of Magnetic Resonance Elastography in Patients with Viral Hepatitis B or C. *PLoS One* 2015; **10**: e0140068 [PMID: 26469342 DOI: 10.1371/journal.pone.0140068]

102   **Venkatesh SK**, Wang G, Lim SG, Wee A. Magnetic resonance elastography for the detection and staging of liver fibrosis in chronic hepatitis B. *Eur Radiol* 2014; **24**: 70-78 [PMID: 23928932 DOI: 10.1007/s00330-013-2978-8]

103   **Shi Y**, Guo Q, Xia F, Dzyubak B, Glaser KJ, Li Q, Li J, Ehman RL. MR elastography for the assessment of hepatic fibrosis in patients with chronic hepatitis B infection: does histologic necroinflammation influence the measurement of hepatic stiffness? *Radiology* 2014; **273**: 88-98 [PMID: 24893048 DOI: 10.1148/radiol.14132592]

104   **Chang W**, Lee JM, Yoon JH, Han JK, Choi BI, Yoon JH, Lee KB, Lee KW, Yi NJ, Suh KS. Liver Fibrosis Staging with MR Elastography: Comparison of Diagnostic Performance between Patients with Chronic Hepatitis B and Those with Other Etiologic Causes. *Radiology* 2016; **280**: 88-97 [PMID: 26844364 DOI: 10.1148/radiol.2016150397]

105   **Lavanchy D**. Hepatitis B virus epidemiology, disease burden, treatment, and current and emerging prevention and control measures. *J Viral Hepat* 2004; **11**: 97-107 [PMID: 14996343 DOI: 10.1046/j.1365-2893.2003.00487.x]

106   **World Health Organization**. *Guidelines for the prevention, care and treatment of persons with chronic hepatitis B infection* 2015; Available from: https://www.who.int/hiv/pub/hepatitis/hepatitisb-guidelines/en/

107   **Kim BK**, Kim DY, Park JY, Ahn SH, Chon CY, Kim JK, Paik YH, Lee KS, Park YN, Han KH. Validation of FIB-4 and comparison with other simple noninvasive indices for predicting liver fibrosis and cirrhosis in hepatitis B virus-infected patients. *Liver Int* 2010; **30**: 546-553 [PMID: 20074094 DOI: 10.1111/j.1478-3231.2009.02192.x]

108   **Friedrich-Rust M**, Nierhoff J, Lupsor M, Sporea I, Fierbinteanu-Braticevici C, Strobel D, Takahashi H, Yoneda M, Suda T, Zeuzem S, Herrmann E. Performance of Acoustic Radiation Force Impulse imaging for the staging of liver fibrosis: a pooled meta-analysis. *J Viral Hepat* 2012; **19**: e212-e219 [PMID: 22239521 DOI: 10.1111/j.1365-2893.2011.01537.x]

109   **Sporea I**, Sirli R, Popescu A, Danilă M. Acoustic Radiation Force Impulse (ARFI)--a new modality for the evaluation of liver fibrosis. *Med Ultrason* 2010; **12**: 26-31 [PMID: 21165451]

110   **Lockhart M**, Moore JW. Classical differential and operant conditioning in rabbits (Oryctolagus cuniculus) with septal lesions. *J Comp Physiol Psychol* 1975; **88**: 147-154 [PMID: 1120791 DOI: 10.1136/bmj.323.7305.157]

111   **Xu X**, Su Y, Song R, Sheng Y, Ai W, Wu X, Liu H. Performance of transient elastography assessing fibrosis of single hepatitis B virus infection: a systematic review and meta-analysis of a diagnostic test. *Hepatol Int* 2015; **9**: 558-566 [PMID: 26187292 DOI: 10.1007/s12072-015-9643-z]

112   **Xu XY**, Kong H, Song RX, Zhai YH, Wu XF, Ai WS, Liu HB. The effectiveness of noninvasive biomarkers to predict hepatitis B-related significant fibrosis and cirrhosis: a systematic review and meta-analysis of diagnostic test accuracy. *PLoS One* 2014; **9**: e100182 [PMID: 24964038 DOI: 10.1371/journal.pone.0100182]

Acute bleeding after argon plasma coagulation for weight regain after gastric bypass: A case report

Diogo Turiani Hourneaux de Moura, Amit H Sachdev, Po-Wen Lu, Igor Braga Ribeiro, Christopher C Thompson

Diogo Turiani Hourneaux de Moura, Amit H Sachdev, Christopher C Thompson, Division of Gastroenterology, Hepatology and Endoscopy, Brigham and Women's Hospital, Harvard Medical School, Boston, MA 02115, United States

Diogo Turiani Hourneaux de Moura, Igor Braga Ribeiro, Department of Gastroenterology, Clinics Hospital of São Paulo University, São Paulo 05403-00, Brazil

Po-Wen Lu, Department of Gastroenterology and Hepatology, Linkou Chang Gung Memorial Hospital, Taoyuan City, 33305, Taiwan

Corresponding author: Diogo Turiani Hourneaux de Moura, MD, MSc, PhD, Academic Fellow, Postdoctoral Fellow, Research Fellow, Surgeon, Division of Gastroenterology, Hepatology and Endoscopy, Brigham and Women's Hospital, Harvard Medical School, 75 Francis St, Boston, MA 02115, United States. dthmoura@hotmail.com
Telephone: +1-857-2509586

Abstract

BACKGROUND

Roux-en-Y gastric bypass (RYGB) is the most commonly performed surgical procedure used to treat obesity worldwide. Despite satisfactory results in terms of weight loss, over time many patients experience weight regain. There are many factors that contribute to weight regain after RYGB, including the diameter of the gastric-jejunal anastomosis (GJA). One of the most commonly performed endoscopic procedures for weight regain after RYGB is argon plasma coagulation (APC). We report a case of hematemesis after outlet revision with APC. We highlight several treatment modalities that can be used to treat this complication.

CASE SUMMARY

A 45-year-old female with a history of weight regain after RYGB was referred for possible endoscopic treatment for weight regain. On endoscopic evaluation, the diameter of the GJA was 22 mm. Due to the dilated GJA, treatment with APC was performed. Several months later she reported a return of poor satiety and an increased appetite. A repeat endoscopy was then performed. The GJA was approximately 15 mm and was incompetent. APC was performed. One day post procedure she had four episodes of hematemesis. An endoscopy was performed and a large ulcer with a visible arterial vessel was visualized at the GJA. Coagulation was attempted using a Coagrasper and after initial contact with the vessel, the vessel started oozing. Due to fibrosis and the depth of ulceration in the area, clips and repeat APC could not be used. Therefore, an attempt to inject

epinephrine injection was made. However, persistent oozing was noted. As a result, hemostatic powder was applied to the region of the bleeding vessel. Subsequently, no more bleeding was observed. On follow-up, the patient remained hemodynamically stable and a second look endoscopy was not performed. The patient was discharged three days later.

CONCLUSION
APC revision of the GJA is known to be a relatively safe and effective strategy to manage weight regain post RYGB. Anastomotic site bleeding is an infrequent and potentially life-threatening complication associated with this therapy. Endoscopic management is the first line therapy used to achieve hemostasis in these cases.

Key words: Anastomosis; Roux-en-Y; Argon plasma coagulation; Bariatric; Gastric bypass; Gastrointestinal hemorrhage; Case report

Core tip: We report a case of a patient with weight regain after Roux-en-Y gastric bypass presenting with gastrointestinal bleeding after recent outlet revision with argon plasma coagulation. We highlight several treatment modalities, including mechanical, thermal, and topical endoscopic therapies that can be used to treat this complication.

INTRODUCTION

Roux-en-Y gastric bypass (RYGB) is one of the most commonly performed surgical procedure used to treat obesity worldwide[1]. Despite satisfactory results in terms of weight loss, over time many patients experience weight regain[2]. There are many factors that contribute to weight regain after RYGB, including lack of exercise, medical conditions, psychiatric problems, overeating, medicines known to cause weight gain, poor family support, and dilation of the gastric-jejunal anastomosis (GJA)[2,3].

Among these factors, the diameter of the GJA plays an important role in controlling weight regain post RYGB. Though effective, traditional surgical revision is used in less than 15% of patients because it is associated with relatively high complication rates (between 15% to 50%), longer operative time, increased intraoperative blood loss, and a non-negligible mortality rate (of more than twice that of the original procedure)[4-8].

As a result, endoscopic revision of a dilated GJA was first reported in 2004 and has gained wide acceptance since that time[9]. One of the most commonly performed endoscopic procedures post RYGB is argon plasma coagulation (APC). It is safe, efficient, and easy to learn, and is associated with a low complication rate[10,11]. One associated complication is post APC bleeding.

We report a case of a patient with RYGB presenting with gastrointestinal bleeding after recent outlet revision with APC for weight loss. We highlight several treatment modalities that can be used to treat this complication.

CASE PRESENTATION

Chief complaints
We present a case of a 45-year-old female with obesity and a history of type 2 diabetes mellitus, gastroesophageal reflux disease, hypercholesterolemia, hypertension, and nonalcoholic fatty liver disease who underwent RYGB in 2005.

Her pre-procedure weight was 108 kg [Body Mass Index (BMI): 37.4 kg/m²] and her weight decreased to nadir of 80 kg (BMI: 27.7 kg/m²). However, she regained 27 kg and was referred for possible endoscopic treatment for weight regain in 2017.

FINAL DIAGNOSIS

Weight regain after bariatric surgery.

TREATMENT

On endoscopic evaluation, the gastric pouch extended from 38 to 42 cm and no fistula or ulcers were seen. The diameter of the GJA was 22 mm (Figure 1). Due to the dilated GJA, treatment with APC was performed. Under CO_2 insufflation, tissue at the rim of the GJA was treated with forced APC at 0.8 L/min and 70 W in a 1.0 cm concentric ring (Figure 2). There was no direct contact with the mucosa. The patient was treated with monitored anesthesia care. The procedure was performed without any adverse events.

OUTCOME AND FOLLOW-UP

Following her first APC, our patient stopped gaining weight, however, she had inadequate weight loss (106 kg, BMI: 36.7 kg/m^2). Several months later, she reported a return of poor satiety and an increased appetite. A repeat endoscopy was then performed. At that time, the pouch extended from 38 to 41 cm and the GJA was approximately 15 mm in diameter and was incompetent, without ulceration. APC was performed. The procedure occurred without any adverse events, including bleeding.

One day post procedure she had four episodes of hematemesis with visible clots. She also had one large bowel movement with maroon and bright red blood per rectum. Her hemoglobulin decreased from 12.8 g/dL to 10.5 g/dL but she was hemodynamically stable. A type and cross was obtained and two large bore IV needles were inserted. A repeat upper endoscopy was performed. The esophagus and the pouch mucosa appeared normal, with no signs of active bleeding. There was a large ulcer with a visible arterial vessel that was visualized and located at the GJA (Figure 3). Coagulation was attempted using a CoagrasperTM (Olympus, Tokio, Japan) and after initial contact with the vessel, the vessel started oozing (Figure 4). Subsequently, ipolar coaptive coagulation was attempted, without success. Repeat APC was not performed due to the depth of the ulceration and concern that this could potentially increase the risk of a delayed perforation. Therefore, injection therapy using a solution comprised of 2 mL of a 1:10000 solution of epinephrine was attempted surrounding the protruding vessel. However, persistent oozing was noted, and significant blood clots were observed around the anastomotic site limiting endoscopic visualization of the vessel.

Additionally, due to fibrosis in the area and to the poor visualization caused by the blood clots within the pouch, clips could not be applied. As a result, after cleaning some the blood clots, hemostatic powder [Hemospray® (Cook Medical, Winston-Salem, NC, United States)] was applied to the region of the bleeding vessel. Subsequently, there was no more bleeding from the visible vessel (Figure 5). Vital signs remained stable throughout the procedure and no blood transfusions were necessary. The patient remained on an IV proton pump inhibitor (PPI) and she was made nil per os (NPO). One day post procedure an oral PPI was initiated, and she remained on a liquid diet for 2 d and then was advanced to a regular diet. The patient remained hemodynamically stable and a second look endoscopy was not performed. She was discharged three days later.

DISCUSSION

Over the last decade, dilation of the GJA has been recognized as an important cause of weight regain after RYGB. However, re-operative surgery to reduce the GJA diameter or the pouch size is technically challenging and is associated with a relatively high complication rate. Therefore, many endoscopic methods have been developed to reduce the diameter of the gastric pouch and GJA, which include injection therapy into the anastomotic site, endoscopic suturing and plicating, and thermal ablation therapy using APC[2,12-15].

APC was initially developed as a treatment modality for gastrointestinal hemorrhage. It is a catheter-based system that utilizes a jet of ionized argon gas for non-contact electrocoagulation of tissue that can be applied through a standard endoscope. Because the probe does not have direct contact with the mucosa, the procedure is safe and the depth of coagulation is limited to only a few millimeters.

Figure 1 Dilated gastric-jejunal anastomosis prior to endoscopic treatment for weight regain.

The depth of penetration is associated with power input in watts and the greater the wattage applied the deeper the penetration, which may result in injury to the muscular layer. After APC ablation is performed around the anastomotic ring, tissue contracts and results in scar formation, which reduces the caliber of the GJA. As a result, the goal of delayed emptying and early satiety can be achieved, and this contributes to weight loss. In general, APC is safe with few complications reported in the literature, such as anastomotic stricture, ulcer formation, bleeding, and leakage at the GJA[2,11,15].

In this case, we present a patient with hemorrhage after APC. During endoscopy a visible vessel was observed at the GJA. Due to the fibrotic tissue after APC, a hemoclip was thought to not be a good option. Injection with epinephrine solution and thermal therapy with Coagrasper and bipolar coagulation were used with limited success. APC was also thought to be a poor option due to the depth of ulceration. Ultimately, we were able to control the bleed with Hemospray and to the best of our knowledge, this is the first case reported in the literature in which hemostatic powder was used to control bleeding after a revisional endoscopic procedure in a patient with RYGB.

Hemospray was approved as a hemostatic therapy in 2011 and has been shown to rapidly stop active bleeding with a high success rate. It is a novel inorganic powder with minerals which contains no human or animal proteins or botanicals. The powder can be sprayed via a catheter that can be inserted through the working channel of a standard adult endoscope and forms a cohesive barrier after coming into contact with moisture which leads to a tamponade by concentrating and activating platelets and coagulation factors and promoting thrombus formation. As a spray, it is very useful in the management of bleeding when the active bleeding site cannot be definitively localized. Hemospray is indicated for active bleeding (Forrest 1A and 1B) and can be used as a primary therapy or as a rescue therapy after conventional endoscopic treatments fail. After the powder absorbs fluid, it forms a mechanical barrier over the bleeding site. Hemospray is not absorbed by the body or through blood vessels, and the mechanical barrier formed by Hemospray does not need to be removed. The adherent barrier is designed to pass through the GI tract within 72 hours[16,17]. This device can be used as a definitive therapy as in our case or as a bridge to further interventions after hemodynamic stabilization.

CONCLUSION

APC revision of the GJA is known to be a relatively safe and effective strategy to manage weight regain post RYGB. Anastomotic site bleeding is an infrequent and potentially life-threatening complication associated with this therapy. Endoscopic management is first line therapy to achieve hemostasis in these cases. However, fibrotic ulcerative tissue after recent APC may limit the ability to achieve successful hemostasis with standard endoscopic interventions such as injection therapy, thermal therapy, and hemostatic clip placement. Therefore, as presented in this case, hemostatic powder is a useful therapeutic option to achieve hemostasis. This device may be useful as a primary or as a rescue therapy in this setting. More studies are required to better clarify the role of hemostatic powder for bariatric patients with active bleeding.

Figure 2 Gastric-jejunal anastomosis following argon plasma coagulation treatment for weight regain.
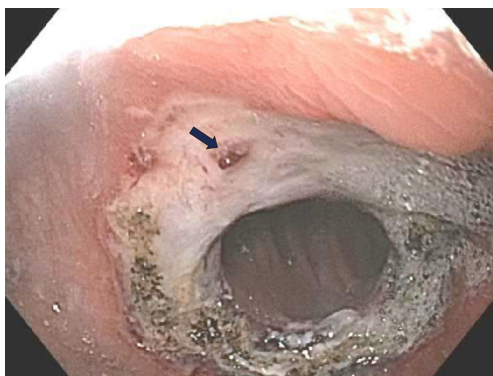
Figure 3 Circumferential ulceration with one protruding vessel at the anastomotic site one day after argon plasma coagulation.
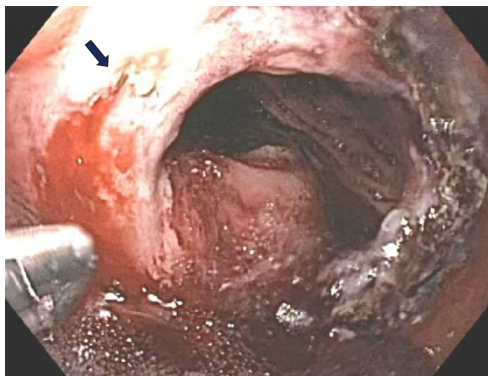
Figure 4 Spurting vessel was noted after thermal therapy with a Coagrasper.

Figure 5 No residual bleeding following Hemospray® with whitish material coverage the ulcer bed.

REFERENCES

1   **Buchwald H**, Avidor Y, Braunwald E, Jensen MD, Pories W, Fahrbach K, Schoelles K. Bariatric surgery: a systematic review and meta-analysis. *JAMA* 2004; **292**: 1724-1737 [PMID: 15479938 DOI: 10.1001/jama.292.14.1724].]

2   **Hourneaux De Moura DT**, Thompson CC. Endoscopic management of weight regain following Roux-en-Y gastric bypass. *Expert Rev Endocrinol Metab* 2019; **14**: 97-110 [PMID: 30691326 DOI: 10.1080/17446651.2019.1571907]

3   **Barhouch AS**, Zardo M, Padoin AV, Colossi FG, Casagrande DS, Chatkin R, Mottin CC. Excess weight loss variation in late postoperative period of gastric bypass. *Obes Surg* 2010; **20**: 1479–1483 [PMID: 20552412 DOI: 10.1007/s11695-010-0202-3]

4   **Linner JH**, Drew RL. Reoperative surgery—indications, efficacy, and long-term follow-up. *Am J Clin Nutr* 1992; **55**: 606S-610S [PMID: 1733138 DOI: 10.1093/ajcn/55.2.606s]

5   **Buchwald H**, Estok R, Fahrbach K, Banel D, Sledge I. Trends in mortality in bariatric surgery: a systematic review and meta-analysis. *Surgery* 2007; **142**: 621-32; discussion 632-5 [PMID: 17950357 DOI: 10.1016/j.surg.2007.07.018]

6   **Livingston EH**. Hospital costs associated with bariatric procedures in the United States. *Am J Surg* 2005; **190**: 816–820 [PMID: 16226964 DOI: 10.1016/j.amjsurg.2005.07.026]

7   **Inabnet WB**, Belle SH, Bessler M, Courcoulas A, Dellinger P, Garcia L, Mitchell J, Oelschlager B, O'Rourke R, Pender J, Pomp A, Pories W, Ramanathan R, Wahed A, Wolfe B. Comparison of 30-day outcomes after non-LapBand primary and revisional bariatric surgical procedures from the Longitudinal Assessment of Bariatric Surgery study. *Surg Obes Relat Dis* 2010; **6**: 22-30 [PMID: 20129303 DOI: 10.1016/j.soard.2009.10.007]

8   **Dapri G**, Cadière GB, Himpens J. Laparoscopic conversion of adjustable gastric banding and vertical banded gastroplasty to duodenal switch. *Surg Obes Relat Dis* 2009; **5**: 678-683 [PMID: 19767245 DOI: 10.1016/j.soard.2009.07.001]

9   **Thompson CC**. Novel endoscopic approaches to common bariatric postoperative complications. *Presented at the ASGE Video Forum*. New Orleans: Digestive Diseases Week; 2004;

10 **Hourneaux de Moura DT**, Hathorn KE, Thompson CC. You Just Got Burned! What Is Wrong With This Gastric Pouch? *Gastroenterology* 2019; **156**: 2139-2141 [PMID: 30716322 DOI: 10.1053/j.gastro.2019.01.255]

11 **Moon RC**, Teixeira AF, Neto MG, Zundel N, Sander BQ, Ramos FM, Matz F, Baretta GA, de Quadros LG, Grecco E, Souza T, Barrichello SA, Filho AC, Usuy EN, de Amorim AMB, Jawad MA. Efficacy of Utilizing Argon Plasma Coagulation for Weight Regain in Roux-en-Y Gastric Bypass Patients: a Multi-center Study. *Obes Surg* 2018; **28**: 2737-2744 [PMID: 29627948 DOI: 10.1007/s11695-018-3229-5]

12 **Higa KD**, Boone K, Nimeri A, Tercero F, Jackson A, Khan A. Gastric bypass: increased restriction for poor weight loss. *Surg Endosc* 2007; **21**: 1922-1923 [PMID: 17909900 DOI: 10.1007/s00464-007-9540-1]

13 **Thompson CC**, Slattery J, Bundga ME, Lautz DB. Peroral endoscopic reduction of dilated gastrojejunal anastomosis after Roux-en-Y gastric bypass: a possible new option for patients with weight regain. *Surg Endosc* 2006; **20**: 1744-1748 [PMID: 17024527 DOI: 10.1007/s00464-006-0045-0]

14 **Brunaldi VO**, Jirapinyo P, de Moura DTH, Okazaki O, Bernardo WM, Galvão Neto M, Campos JM, Santo MA, de Moura EGH. Endoscopic Treatment of Weight Regain Following Roux-en-Y Gastric Bypass: a Systematic Review and Meta-analysis. *Obes Surg* 2018; **28**: 266-276 [PMID: 29082456 DOI: 10.1007/s11695-017-2986-x]

15 **Baretta GA**, Alhinho HC, Matias JE, Marchesini JB, de Lima JH, Empinotti C, Campos JM. Argon plasma coagulation of gastrojejunal anastomosis for weight regain after gastric bypass. *Obes Surg* 2015; **25**: 72-79 [PMID: 25005812 DOI: 10.1007/s11695-014-1363-2]

16 **Sung JJ**, Chiu PW, Chan FKL, Lau JY, Goh KL, Ho LH, Jung HY, Sollano JD, Gotoda T, Reddy N, Singh R, Sugano K, Wu KC, Wu CY, Bjorkman DJ, Jensen DM, Kuipers EJ, Lanas A. Asia-Pacific working group consensus on non-variceal upper gastrointestinal bleeding: an update 2018. *Gut* 2018; **67**: 1757-1768 [PMID: 29691276 DOI: 10.1136/gutjnl-2018-316276]

17 **Hagel AF**, Albrecht H, Nägel A, Vitali F, Vetter M, Dauth C, Neurath MF, Raithel M. The Application of Hemospray in Gastrointestinal Bleeding during Emergency Endoscopy. *Gastroenterol Res Pract* 2017; **2017**: 3083481 [PMID: 28232848 DOI: 10.1155/2017/3083481]

Left colonic metastasis from primary hepatocellular carcinoma: A case report

Fulvio Tagliabue, Morena Burati, Marco Chiarelli, Alessandro Marando, Matilde De Simone, Ugo Cioffi

ORCID number: Fulvio Tagliabue (0000-0002-4095-017X); Morena Burati (0000-0003-2562-4760); Marco Chiarelli (0000-0003-1729-4925); Alessandro Marando (0000-0002-7569-7135); Matilde De Simone (0000-0002-3763-4416); Ugo Cioffi (0000-0002-5321-5828).

Fulvio Tagliabue, Morena Burati, Marco Chiarelli, Department of Emergency and Robotic Surgery, Ospedale "A Manzoni" Lecco via Dell'Eremo 9/11, Lecco 23900, Italy

Alessandro Marando, Department of Pathology, Ospedale "A Manzoni" Lecco via Dell'Eremo 9/11, Lecco 23900, Italy

Matilde De Simone, Ugo Cioffi, Department of Surgery, University of Milan, Milano 20122, Italy

Corresponding author: Ugo Cioffi, MD, PhD, Full Professor, Professor, Surgeon, Department of Surgery, University of Milan, Via F Sforza 35, Milano 20122, Italy. ugo.cioffi@guest.unimi.it
Telephone: +39-341-253331
Fax: +39-341-489311

Abstract

BACKGROUND
Hepatocellular carcinoma (HCC) accounts for 5-6% of all human cancers. Considering the extrahepatic metastasis, the main organs involved are lymphnodes, lung, bone and adrenal gland. Usually colon metastasis is very rare, especially on the left sided colon.

CASE SUMMARY
We report a case of a 70 years-old man hepatitis B carrier with HCC treated four times with trans-arterial chemoembolization, presented to our surgical department complaining of gastrointestinal bleeding. A colonoscopy revealed a mass of 4 cm of the sigmoid colon with signs of bleeding. The computed tomography showed a mass originated from the sigmoid colon of 3.5 cm, and the presence of HCC in segment VI and VII, without portal vein thrombosis. Due to the large size of the mass and the active bleeding, the patient underwent a left colectomy. The postoperative period was uneventful, and the patient was discharged in fifth post-operative day. Histological examination revealed that the neoplasm was characterized by a diffuse proliferation of epithelial cells with an hepatoid differentiation. So, the presence of a history of HCC of the liver and the histopathological features supported the diagnosis of metastasis from the liver.

CONCLUSION
Although rare, colon metastasis from an HCC can be left-sided and can present with acute bleeding.

Key words: Hepatocellular carcinoma; Colon metastasis; Case report

Core tip: Colon metastasis from hepatocellular carcinoma are extremely rare and, when present, they usually located in the right colon. We present a case of a left sided colon metastasis, which presented with acute bleeding and anemia for which the patient underwent left hemicolectomy.

INTRODUCTION

Hepatocellular carcinoma (HCC) causes more than 1 million deaths annually and the incidence is increasing in the last few years.

Unfortunately, only 30% of patients benefit from resection, percutaneous ablation or liver transplantation.

In a series[1,2], the most involved organs , as extrahepatic metastasis, were lymphnodes, lung, bone and adrenal gland. The involvement of the gastrointestinal tract seldom occurs, being found in only 0.5%-2% of cases[3,4] and 4%-6% in another series[1,2]. Usually colon metastasis is very rare, especially the left sided colon, and mostly occurs through direct invasion.

CASE PRESENTATION

Chief complaints
A 70 years-old man presented to our surgical department complaining of gastrointestinal bleeding.

History of present illness
The patient was hepatitis B carrier with HCC treated four times with trans-arterial chemoembolization (TACE). He presented to the Emergency room after several hours of active gastrointestinal bleeding.

Physical examination
At admission vital signs were stable. Patient's temperature was 36.6 °C and Glasgow Coma Scale (GCS) 15/15. The abdomen was soft, non-tender, and non-distended. No mass could be appreciated. Blumberg sign was negative. The rectal examination showed the presence of blood.

Laboratory examinations
The laboratory findings showed normal haemoglobin level, a slight elevation of transaminase [alanine aminotransferase 56 IU/L, aspartate aminotransferase 62 IU/L], and all other values including coagulation, white blood cell, protein, albumin and bilirubin were within normal limits. The alpha-fetoprotein level was 3 ng/mL (range 5-10 ng/mL).

Imaging examination
The computed tomography (CT) showed a mass originated from the sigmoid colon of 3.5 cm (Figure 1), and the presence of HCC in segment VI and VII, without portal vein thrombosis; at ultrasound the neoplasm seemed characterized by a dense vascular pattern.

Further diagnostic work-up
A colonoscopy revealed a mass of 4 centimeters of the sigmoid colon with signs of bleeding (Figure 2).

Figure 1 Computed tomography scan shows a mass of 3.5 cm.

TREATMENT

Because of the large size of the mass and the fact that it was bleeding, it was decided to subject the patient to a left colectomy. At laparotomy the lesion was situated in the distal sigmoid. No direct contact between the neoplasm and the liver was noticeable. Moreover, the sigmoid was normally placed and no dolichocolon sigmoid was reported.

OUTCOME AND FOLLOW-UP

The postoperative period was uneventful, and the patient was discharged in fifth day post operative day. Histological examination revealed that the neoplasm was characterized by a diffuse proliferation of epithelial cells with an hepatoid differentiation (Figure 3A). In fact, the immunohistochemical reaction for HepPar-1 confirmed this type of differentiation (Figure 3B). The differential diagnosis was between a metastasis of HCC from the liver and an hepatoid adenocarcinoma of the colon, but the complete negativity for CK20 and CDX2 (Figure 3C and D) excluded a primary tumor of the colon[5]. So, the presence of an history of HCC of the liver and the histopathological features supported the diagnosis of metastasis from the liver.

DISCUSSION

HCC is one of the most common malignancies worldwide, and its incidence has been increasing in recent years. The prognosis has improved due to the advances in diagnostic imaging and new treatment modalities, but the management of recurrence is a critical problem[6].

Intrahepatic recurrences can be controlled by different treatment modalities, based on the different clinical conditions of the patients, such as hepatectomy, TACE and percutaneous ethanol injection therapy[7]. Because the incidence of extrahepatic metastases is less than that of intrahepatic metastasis, there are fewer documented treatment strategies for extrahepatic metastasis. At present, the prognosis of patients with extrahepatic metastases from HCC is poor[8]. The most frequent sites of extrahepatic metastases are bone, lung, adrenal gland and lymph nodes. Gastrointestinal involvement of HCC is uncommon. The most common modality of metastasis to the gastrointestinal tract is usually the direct invasion *via* adhesion to the serosal side by bulky tumor mass. The most frequently involved site is the duodenum, stomach, hepatic flexure of the colon and jejunum[3]. HCC may disseminate hematogenously to distant gastrointestinal tracts. Portal vein thrombosis may be the key point of hematogenous spread to other sites[4-9]. In our case, the HCC was localized to segment VI and VII, without portal vein thrombosis and metastasized to the left- sided colon five years after TACE.

Some authors[4] postulated that TACE may predispose to HCC metastasis by altering local vasculature and increasing inflammation.

Hematogenous spread was suggested because the metastatic site was distant and the lymph-nodes negative, Natsuizaka *et al*[8] reported, based on the initial diagnosis of intrahepatic HCC , that patients with advanced HCC develop extrahepatic metastases significantly more frequently than those with less advanced HCC.
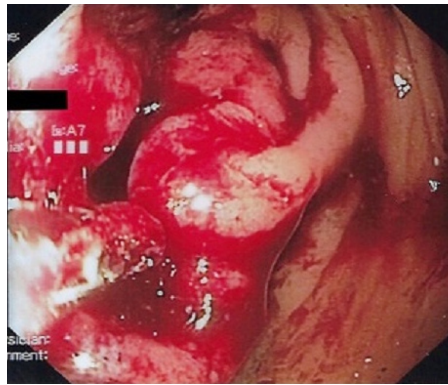
Figure 2 Colonoscopy image: Colonoscopy shows a bleeding mass of the left colon.

There is no standard treatment for extrahepatic metastases of primary HCC, several authors have reported the use of various treatment modalities. However only few HCC patients can undergo surgical resection of extrahepatic metastases because of hepatic reserve or intrahepatic stage. There are reports that suggest that aggressive treatment prolonged survival. Lam *et al*[10] reported that they performed surgical resection in nine patients with pulmonary metastases and that the median survival period of the patients was 42 mo.

In literature there are little datas[11] regarding the efficacy of surgical treatment in patients with colon metastasis from HCC, our case was treated with surgical management because of the size of the colonic mass and the risk of occlusion.

According to the literature, the interval between the diagnosis of HCC and detection of gastrointestinal tract involvement ranged from 3 mo to 8 years[3,4]. Mostly, gastrointestinal metastasis is found in patients with advanced staged HCC. The prognosis is unfortunately poor with a median survival period of 7 mo[8].

However, it was suggested that treatment of extrahepatic metastases may improve survival in some selected patients who have good reserved function, intrahepatic tumor stage (T0-T2), and negative portal vein invasion or occlusion.

CONCLUSION

Even if rare, HCC metastasis must be taken in consideration in those patients with colon carcinoma with medical history positive for hepatocellular cancer or HCV/HBV infection. Even if the prognosis of these patients is usually poor, a hemicolectomy can be a life-saving maneuver and could improve overall survival in some selected cases.
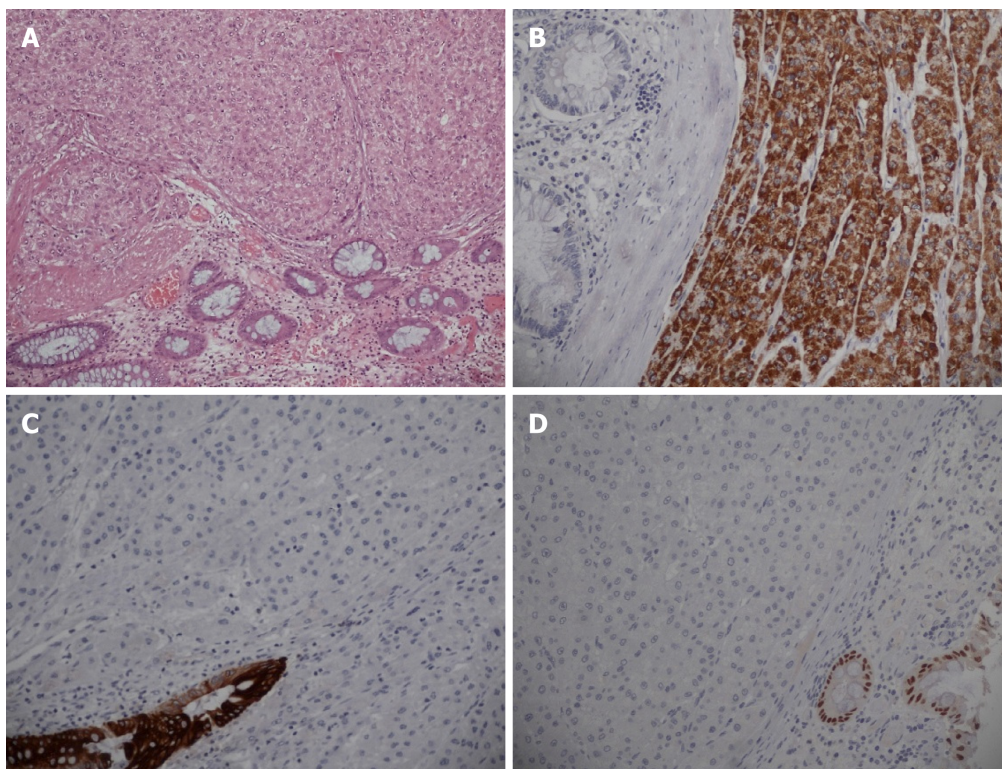
Figure 3 Histology images: Carcinoma with heapthoid differentiation. A: (Hematoxylin-eosin 100 ×); B: Confirmed by the positivity for HepPar-1 (200 ×); C: Negativity for CK20 (200 ×); D: CDX2 (200 ×) excluded the colic origin and it supported the diagnosis of metastasis from the liver.

REFERENCES

1   **Anthony PP**. Primary carcinoma of the liver: a study of 282 cases in Ugandan Africans. *J Pathol* 1973; **110**: 37-48 [PMID: 4353217 DOI: 10.1002/path.1711100105]

2   **Nakashima T**, Okuda K, Kojiro M, Jimi A, Yamaguchi R, Sakamoto K, Ikari T. Pathology of hepatocellular carcinoma in Japan. 232 Consecutive cases autopsied in ten years. *Cancer* 1983; **51**: 863-877 [PMID: 6295617 DOI: 10.1002/1097-0142(19830301)51:5<863]

3   **Lin CP**, Cheng JS, Lai KH, Lo GH, Hsu PI, Chan HH, Hsu JH, Wang YY, Pan HB, Tseng HH. Gastrointestinal metastasis in hepatocellular carcinoma: radiological and endoscopic studies of 11 cases. *J Gastroenterol Hepatol* 2000; **15**: 536-541 [PMID: 10847441]

4   **Chen LT**, Chen CY, Jan CM, Wang WM, Lan TS, Hsieh MY, Liu GC. Gastrointestinal tract involvement in hepatocellular carcinoma: clinical, radiological and endoscopic studies. *Endoscopy* 1990; **22**: 118-123 [PMID: 2162757 DOI: 10.1055/s-2007-1012815]

5   **Armaghani A**, Hernandez Gonzalo D, Daily K. Hepatoid adenocarcinoma of the colon. *BMJ Case Rep* 2015; 2015 [PMID: 25883249 DOI: 10.1136/bcr-2014-206222]

6   **Shuto T**, Hirohashi K, Kubo S, Tanaka H, Tsukamoto T, Yamamoto T, Ikebe T, Kinoshita H. Changes and results of surgical strategies for hepatocellular carcinoma: results of a 15-year study on 452 consecutive patients. *Surg Today* 1998; **28**: 1124-1129 [PMID: 9851619 DOI: 10.1007/s005950050299]

7   **Poon RT**, Fan ST, Lo CM, Ng IO, Liu CL, Lam CM, Wong J. Improving survival results after resection of hepatocellular carcinoma: a prospective study of 377 patients over 10 years. *Ann Surg* 2001; **234**: 63-70 [PMID: 11420484 DOI: 10.1097/00000658-200107000-00010].]

8   **Natsuizaka M**, Omura T, Akaike T, Kuwata Y, Yamazaki K, Sato T, Karino Y, Toyota J, Suga T, Asaka M. Clinical features of hepatocellular carcinoma with extrahepatic metastases. *J Gastroenterol Hepatol* 2005; **20**: 1781-1787 [PMID: 16246200 DOI: 10.111/j-1440-1746.2005.03919]

9   **Yang PM**, Sheu JC, Yang TH, Chen DS, Yu JY, Lee CS, Hsu HC, Sung JL. Metastasis of hepatocellular carcinoma to the proximal jejunum manifested by occult gastrointestinal bleeding. *Am J Gastroenterol* 1987; **82**: 165-167 [PMID: 3028129]

10 **Lam CM**, Lo CM, Yuen WK, Liu CL, Fan ST. Prolonged survival in selected patients following surgical resection for pulmonary metastasis from hepatocellular carcinoma. *Br J Surg* 1998; **85**: 1198-1200 [PMID: 9752858 DOI: 10.1046/j.1365-2168,1998.00846.x]

11 **Mitsialis V**, Lee LS. Metastasis of Hepatocellular Carcinoma to Distal Colon Associated With Inferior Mesenteric Arteriovenous Fistula and Tumor Thrombus: a Case Report. *Am J Gastroenterol* 2018; **113**: 916-918 [PMID: 29880968 DOI: 10.1038/s41395-018-0101-0]

CASE REPORT

ALK-positive anaplastic large cell lymphoma presenting multiple lymphomatous polyposis: A case report and literature review

Makoto Saito, Koh Izumiyama, Reiki Ogasawara, Akio Mori, Takeshi Kondo, Masanori Tanaka, Masanobu Morioka, Kencho Miyashita, Mishie Tanino

ORCID number: Makoto Saito (0000-0002-2683-9475); Koh Izumiyama (0000-0002-0762-6255); Reiki Ogasawara (0000-0002-1136-5035); Akio Mori (0000-0002-2064-2145); Takeshi Kondo (0000-0001-7455-5824); Masanori Tanaka (0000-0002-8173-6620); Masanobu Morioka (0000-0002-0784-8114); Kencho Miyashita (0000-0002-3779-2166); Mishie Tanino (0000-0003-3370-0452).

Makoto Saito, Koh Izumiyama, Reiki Ogasawara, Akio Mori, Takeshi Kondo, Masanori Tanaka, Masanobu Morioka, Department of Internal Medicine and Hematology, Aiiku Hospital, Sapporo 0640804, Japan

Kencho Miyashita, Department of Gastroenterology, Aiiku Hospital, Sapporo 0640804, Japan

Mishie Tanino, Department of Surgical Pathology, Asahikawa Medical University Hospital (formerly Department of Cancer Pathology, Hokkaido University, Faculty of Medicine), Asahikawa 0788510, Japan

Corresponding author: Makoto Saito, MD, PhD, Doctor, Department of Internal Medicine and Hematology, Aiiku Hospital, Minami 4 Nishi 25 Chuo-ku, Sapporo 0640804, Japan. ikyoku@aiiku-hp.or.jp
Telephone: +8-111-5632211

Author contributions: All authors collected and analyzed the patient's clinical data; Miyashita K involved in endoscopic procedure; Tanino M involved in pathological procedure; Saito M designed and wrote the manuscript; and all authors agree to be accountable for all aspects of the work.

Informed consent statement: Informed written consent was obtained from the patient for publication of this report and any accompanying images.

Conflict-of-interest statement: The authors declare that they have no conflict of interest in this work.

CARE Checklist (2016) statement: The manuscript was prepared according to the CARE Checklist (2016).

Open-Access: This article is an open-access article which was selected by an in-house editor and fully peer-reviewed by external reviewers. It is distributed in accordance with the Creative Commons Attribution Non Commercial (CC BY-NC 4.0)

Abstract

BACKGROUND

Anaplastic large cell lymphoma (ALCL) is a type of T-cell lymphoma that can be divided into two categories: anaplastic lymphoma kinase-positive (ALK+) and ALK-negative. Gastrointestinal ALK+ ALCL is rare. Multiple lymphomatous polyposis (MLP) is thought to be a representative form of gastrointestinal lesion in mantle cell lymphoma, and T-cell lymphomas seldom show this feature. Here, we report the first known case of ALK+ ALCL with gastroduodenal involvement to present with MLP.

CASE SUMMARY

The patient was a 43-year-old man who was complained of a mass in the left inguinal area and was performed open biopsy. ALK+ ALCL was diagnosed pathologically. Computed tomography scan demonstrated multiple lymph node lesions in the abdomen - pelvis/inguinal region, and scattered nodular lesions in both lung fields. He did not complain of gastrointestinal symptoms. While, esophagogastroduodenoscopy identified MLP lesions from the antrum of the stomach to the descending portion of the duodenum and mild thickened folds on the corpus of the stomach, and biopsy showed invasion of ALK+ ALCL. We treated this patient with six cycles of CHOEP (Cyclophosphamide, Doxorubicin, Vincristine, Etoposide, and Prednisone) chemotherapy. At the conclusion of treatment, there was complete remission. Numerous white scars were found on the stomach, endoscopically consistent with a remission image of lymphoma. The endoscopic features of this case were thought to be similar to those of MCL.

CONCLUSION
The macroscopic/endoscopic features of gastrointestinal ALK+ ALCL may be more similar to those of B-cell lymphomas rather than T-cell lymphomas.

Key words: Anaplastic large-cell lymphoma; Anaplastic lymphoma kinase; Multiple lymphomatous polyposis; T-cell lymphoma; Gastrointestinal involvement

Core tip: Anaplastic large cell lymphoma (ALCL) encompasses two distinct categories: anaplastic lymphoma kinase-positive (ALK+) and ALK-negative. ALK+ ALCL cases rarely involve the gut. However, in a very small number of case reports, gastrointestinal ALK+ ALCL exhibits a fungating growth pattern, similar to that of B-cell lymphomas rather than T-cell lymphomas. Multiple lymphomatous polyposis (MLP) is thought to be a typical form of gastrointestinal lesion in mantle cell lymphoma, but it develops in other B-cell lymphomas. T-cell lymphomas seldom present with MLP. Here, we report the first known case in the world of ALK+ ALCL with gastroduodenal involvement presenting with MLP.

INTRODUCTION

Anaplastic large cell lymphoma (ALCL) was first described in 1985 by Stein *et al*[1]. According to the 4th edition (2008) of the WHO classification[2], primary systemic ALCL can be divided into two distinct categories: anaplastic lymphoma kinase-positive (ALK+) and ALK-negative. Majority of ALK+ ALCL contain a t(2;5) chromosomal translocation. The t(2;5) translocation fuses a distal part of the *ALK* gene on chromosome 2p23 with the promoter and a proximal domain of the nucleophosmin (*NPM1*) gene on chromosome 5q35[3]. The most common extranodal sites of ALK+ ALCL are the skin, bone and soft tissue. ALK+ ALCL cases involving the gut are rare[2].

Multiple lymphomatous polyposis (MLP) is thought to be a representative form of gastrointestinal lesion in mantle cell lymphoma (MCL)[2,4,5]. Here, we report an extremely rare case of ALK+ ALCL with gastroduodenal involvement presenting as MLP.

CASE PRESENTATION

Chief complaints
A 43-year-old Japanese man suffering from fever, night sweats, general fatigue and weight loss complained of a mass in the left inguinal area. The patient did not complain of gastrointestinal symptoms.

History of present illness
The patient was admitted to a local hospital. Computed tomography (CT) scan demonstrated multiple lymph node lesions continuing to the mesentery and para-aortic/left common iliac artery/left inguinal region (Figure 1). Scattered nodular lesions were found in both lung fields (Figure 1). Following needle biopsy of the left inguinal lesion, malignant lymphoma was suspected, and the patient was transferred to our department.

History of past illness
He had no chronic illness.
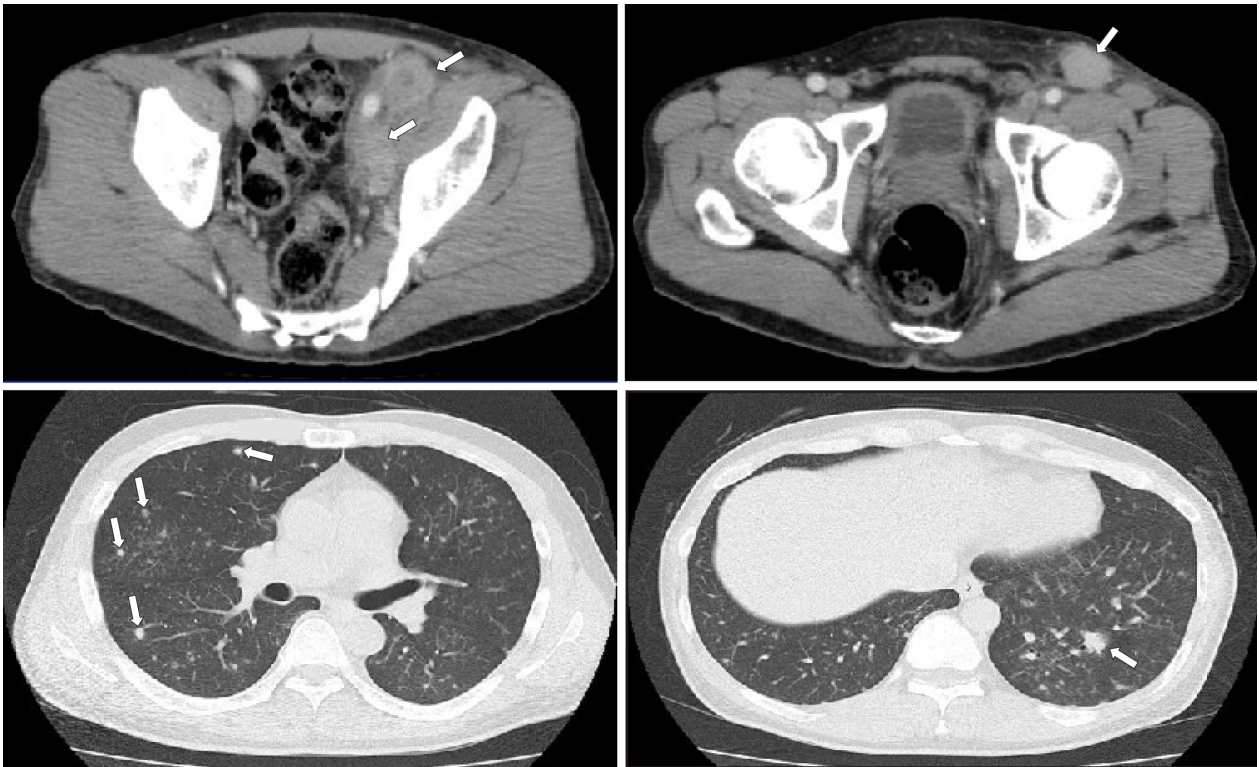
Figure 1 Computed tomography images. (Upper row) Pelvic computed tomography scan demonstrated multiple lymph node lesions (arrows) continuing to the left common iliac artery (left)/left inguinal region (right). (Lower row) Scattered nodular lesions were found in both lung fields (arrows).

Physical examination upon admission

Left inguinal lymph nodes were significantly swollen.

Laboratory examinations

WBC and CRP showed markedly high values, and elevated platelet count, liver dysfunction, and hypoalbuminemia were also observed. In addition, the level of soluble interleukin-2 receptor (normal range: 121-613 U/mL), which was severely elevated according to the measurement of the previous hospital, had further increased over approximately one week (7120 → 12500 U/mL) (Table 1).

Imaging examinations

As measured by positron emission tomography (PET)/CT scan, the mean standardized uptake value was 18.1 in the abdomen – pelvis/inguinal nodes and 3.5 in the lung fields and the mediastinal nodes (Figure 2).

Esophagogastroduodenoscopy findings: In the descending portion of the duodenum, multiple polypoid lesions of 2-3 mm in diameter were observed (Figure 3A). Various large and small polypoid lesions were observed in the antrum of the stomach (Figure 3B and Figure 3C). These lesions are consistent with MLP continuously extending from the antrum of the stomach to the descending portion of the duodenum. Mucosal folds in the corpus of the stomach were slightly thickened, and its surface had changed to a white tone (Figure 3D).

The biopsies of both gastric and duodenal lesions proved the invasion of lymphoma cells, as below mentioned. These lesions could not be detected by PET/CT scan. Colonoscopy and bone marrow aspiration showed no involvement of lymphoma lesions.

Pathological examinations

Left inguinal lymph nodes were examined by open biopsy. Medium to large-sized abnormal lymphoid cells were observed to be invasively proliferating. CD25, CD30, T-cell intracellular antigen-1, and ALK tested positive by immunostaining. Meanwhile, CD3, CD20 and the Epstein-Barr encoding region *in situ* hybridization tested negative. Based on the histopathology, ALK+ ALCL was diagnosed. In the gastric and duodenal biopsy samples, abnormal lymphoid cells with irregular nuclei grew diffusely (Figure 4A), and mitotic figures were observed in high numbers (Figure 4B). Immunohistochemically, CD30 tested strongly positive (Figure 4C), ALK

Table 1 Results of laboratory examinations on admission			
WBC	21.5×10^9/L	TP	5.8 g/dL
St	3%	Alb	2.3 g/dL
Seg	73%	GOT	117 IU/L
Lym	16%	GPT	252 IU/L
Mon	4%	LDH	275 IU/L
Eos	4%	ALP	753 IU/L
RBC	3.99×10^{12}/L	γ-GTP	170 IU/L
Hb	12.1 g/dL	T-Bil	0.2 mg/dL
Hct	36.3%	CRP	13.00 mg/dL
Plt	695×10^9/L	s-IL-2R	12500 U/mL

St: Stab; Seg: Segmented; Lym: Lymphocytes; Mon: Monocytes; Eos: Eosinophil; Hb: Hemoglobin; Hct: Hematocrit; TP: Total protein; sIL-2R: Soluble interleukin-2 receptor.

(monoclonal antibody, ALK1) tested positive in nuclear and cytoplasmic pattern (Figure 4D), and the Ki-67 proliferative (MIB1) index was > 80% (not shown).

FINAL DIAGNOSIS

ALK+ ALCL that involved multiple lymph node lesions in the abdomen - pelvis/inguinal region and mediastinum, also both lung fields and the gastroduodenal lesions (Stage IV).

TREATMENT

We treated this patient with six cycles of CHOEP chemotherapy (Cyclophosphamide 750 mg/m², Doxorubicin 50 mg/m², Vincristine 1.4 mg/m², Etoposide 100 mg/m² x 3 d, and Prednisone 50 mg/m² x 5 d) every three weeks. After administration of two cycles, the lymphoma lesions including lung field nodules shrank remarkably and disappeared at CT examination.

OUTCOME AND FOLLOW-UP

At the conclusion of treatment, there was complete remission. Numerous white scars were found in the stomach, endoscopically consistent with a remission image of lymphoma (Figure 3E). He is followed-up as outpatient with no treatment. There was no evidence of recurrence for more than 1 year and 10 mo since the end of the final treatment.

DISCUSSION

ALCL is a clinically, morphologically, and immunophenotypically heterogeneous T-cell lymphoma. Depending on the presence or absence of ALK expression, ALK+ ALCL was classified as a biologically homogeneous disease unit independent of ALK-negative ALCL in the 4th edition (2008) of the WHO classification[2]. ALK+ ALCL is more prevalent in children and young adults, and the ALK fusion protein is associated with a good prognosis[6]. In contrast, ALK-negative ALCL has a poor prognosis similar to peripheral T-cell lymphoma, not otherwise specified, and angioimmunoblastic T-cell lymphoma[7]. ALK staining pattern is nuclear and cytoplasmic in cases of t(2;5)/NPM-ALK translocation, and membranous or diffuse/granular cytoplasmic in the remaining cases with a variant translocation involving at 2p23[2,8]. ALK staining in our patient showed a nuclear and cytoplasmic pattern. G-banded karyotype of the lymph node lesions showed complex chromosomal abnormalities with +2, der(2;21)(q10;q10),+7, however, translocation at 2p23 could not be confirmed. ALK+ ALCL frequently involves both lymph nodes and extranodal sites. The most commonly involved extranodal sites include the skin, bone, soft tissue, liver and lungs as we reported here[2].
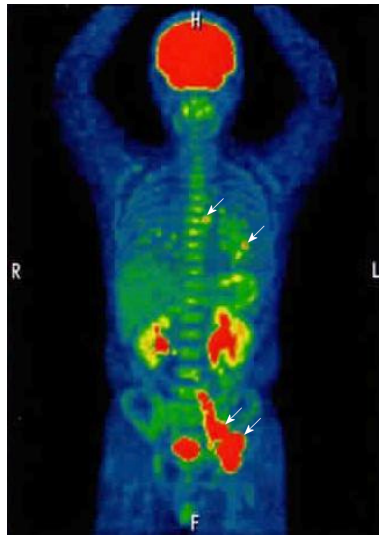
Figure 2 Positron emission tomography/computed tomography (longitudinal) image. Arrows indicate lymphoma lesions. The mean of the standardized uptake value was 18.1 in the multiple lymph node lesions continuing to the mesentery and para-aortic/left common iliac artery/left inguinal, 3.5 in the lesions of the lung fields and the mediastinal nodes. No uptake in the stomach and duodenum.

Because gastrointestinal T-cell lymphomas are rare, little is known about the clinicopathological characteristics of primary gastrointestinal T-cell lymphomas. Kim *et al*[9] investigated the endoscopic differences between B- and T-cell lymphomas and observed that B-cell lymphomas presented more often as fungating (54% of cases), while T-cell lymphomas were frequently ulcerative (47%), and only 13% showing a fungating pattern. Regardless of ALK expression, primary gastrointestinal ALCL is rarer[10]. According to a recent review on gastrointestinal ALCL, the rate of ALK expression among gastrointestinal ALCL was low at 24%[11]. As far as we can determine, ALK+ ALCL of the gut has been reported in only eleven cases[11-20]. The clinical features are summarized in Table 2 for a total of 12 gastrointestinal ALK+ ALCL cases, including our patient. Of these, four cases were reported to involve the esophagus[12-15], all showing fungating tumors. Of the remaining cases, two involved the stomach[11,16], one involved the duodenum[17], one involved both the stomach and duodenum[18], and three involved the small intestine (jejunum/ileum)[11,19,20]. Only three of these last seven cases showed macroscopic findings by resection or endoscopy; the morphology showed a mass formation pattern, such as a submucosal or bulky tumor. Although the number of cases is very small, gastrointestinal ALK+ ALCL often seems to involve the esophagus, in which lymphomas rarely develop, and frequently exhibits a fungating growth pattern similar to that of B-cell lymphomas.

The term ''MLP'' was introduced in 1961 by Cornes to describe malignant lymphoma that presented as multiple polypoid tumors, from 2 mm to several centimeters, affecting long segments of the gastrointestinal tract[21]. Histopathologically, these polyps originate from the mantle zone of the lymphoid follicle of the mucosa-associated lymphoid tissue (MALT)[22]. Therefore, the most frequent lymphoma presenting with MLP is MCL[4,5], and it also develops in other B-cell lymphomas, such as MALT lymphoma and follicular lymphoma[23]. Furthermore, T-cell lymphomas seldom show this feature (11%)[24]. Several cases of adult T-cell leukemia/lymphoma presenting with MLP have been reported in Japan, which is an endemic area of human T-cell lymphotropic virus type 1 infection[25,26]. To the best of our knowledge, including ALK-negative, our case is the first observation of ALCL presenting with MLP. However, in contrast to what has been seen in MCL, the MLP presented in this case with, irregular sized-polyps arranged irregularly. In addition, no MLP lesion was found in the large intestine, which is frequently involved in MCL[27]. In our case, MLP lesions could not be detected with PET/CT scans. As we previously reported in a case of MCL[28], it appears that MLP lesions do not infiltrate the deep layer and instead maintain involvement with the surface layer of the gastrointestinal mucosa, even in the case of ALCL. The characteristic endoscopic findings of MCL are not only MLP, but also thickening of gastric mucosal folds has been reported[5]. In our case, thickened folds of the stomach were also seen, and the endoscopic features were thought to be similar to those of MCL.
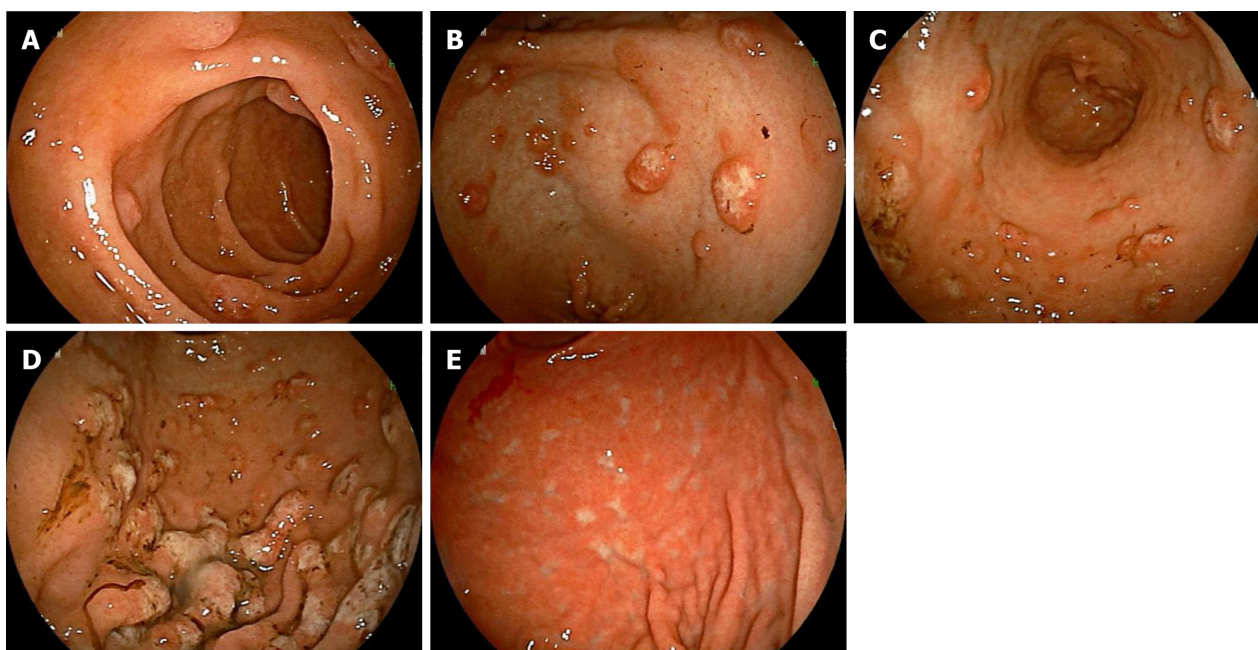
Figure 3 Esophagogastroduodenoscopy findings. Multiple polypoid lesions of 2-3 mm in diameter were seen in the descending portion of the duodenum (A). Various large and small polypoid lesions were seen in the antrum of the stomach (B; lesser curvature side, C; extensive curvature side), accompanied by a change in white tone at the center. Mucosal folds in the corpus of the stomach at the extensive curvature side were slightly thickened, and its surface had changed to a white tone (D). After treatment, numerous white scars were found, and the thickened mucosal folds were improved in the stomach (E).

CONCLUSION

We reported a case of gastroduodenal ALK+ ALCL presenting with MLP. Although there is a limit in considering the macroscopic/endoscopic features of gastrointestinal ALK+ ALCL patients through this very rare case, the morphological features of gastrointestinal ALK+ ALCL may be similar to those of B-cell lymphomas rather than T-cell lymphomas. It is necessary to further accumulate and study the gastrointestinal ALK+ ALCL patients.

Table 2 Clinical features of gastrointestinal anaplastic lymphoma kinase-positive anaplastic large cell lymphoma

Case	Age / sex	Ref.	Occurrence site	Gross/ Endoscopic findings	ALK staining pattern	2p23(FISH /RT-PCR)	Treatment	Outcome
1	56/M	[12]	Esophagus	Large mass	Cytoplasmic		chemo. + auto-SCT	Alive (3 mo)
2	34/F	[13]	Esophagus	Fungating tumor	Nuclear and cytoplasmic		chemo. + auto-SCT	Alive (24 mo)
3	37/M	[14]	Esophagus	Submucosal mass	Nuclear and cytoplasmic		resection + chemo.	Alive (14 mo)
4	3/M	[15]	Esophagus	Wall thickening	Nuclear and cytoplasmic		chemo.	(undescribed)
5	53/M	[11]	Stomach	(Undescribed)	Cytoplasmic		resection + chemo.	Alive (84 mo)
6	72/F	[16]	Stomach	(Undescribed)	(Undescribed)	+ (FISH)	resection	Alive (84 mo)
7	36/M	[17]	Duodenum	(Undescribed)	Nuclear and cytoplasmic	+ (RT-PCR)	resection + chemo.	Alive (24 mo)
8	21/M	[18]	Stomach and Duodenum	Submucosal tumor	Nuclear and cytoplasmic		chemo.	(undescribed)
9	10/M	[11]	Small intestine	(Undescribed)	Nuclear and cytoplasmic		resection + chemo.	Alive (75 mo)
10	17/M	[19]	Jejunum	Polypoidal mass	Cytoplasmic		resection + chemo.	Alive (18 mo)
11	32/M	[20]	Jejunum/Ileum (junction)	Massive tumor	Nuclear and cytoplasmic		resection + chemo.	Alive (5 mo)
12	43/M	Our case	Stomach and Duodenum	MLP and gastric mocosal thickening	Nuclear and cytoplasmic		chemo.	Alive (22 mo)

ALK: Anaplastic lymphoma kinase; FISH: Fluorescence *in situ* hybridization; RT-PCR: Reverse transcription polymerase chain reaction; chemo.: Chemotherapy; auto-SCT: Autologous stem cell transplantation.
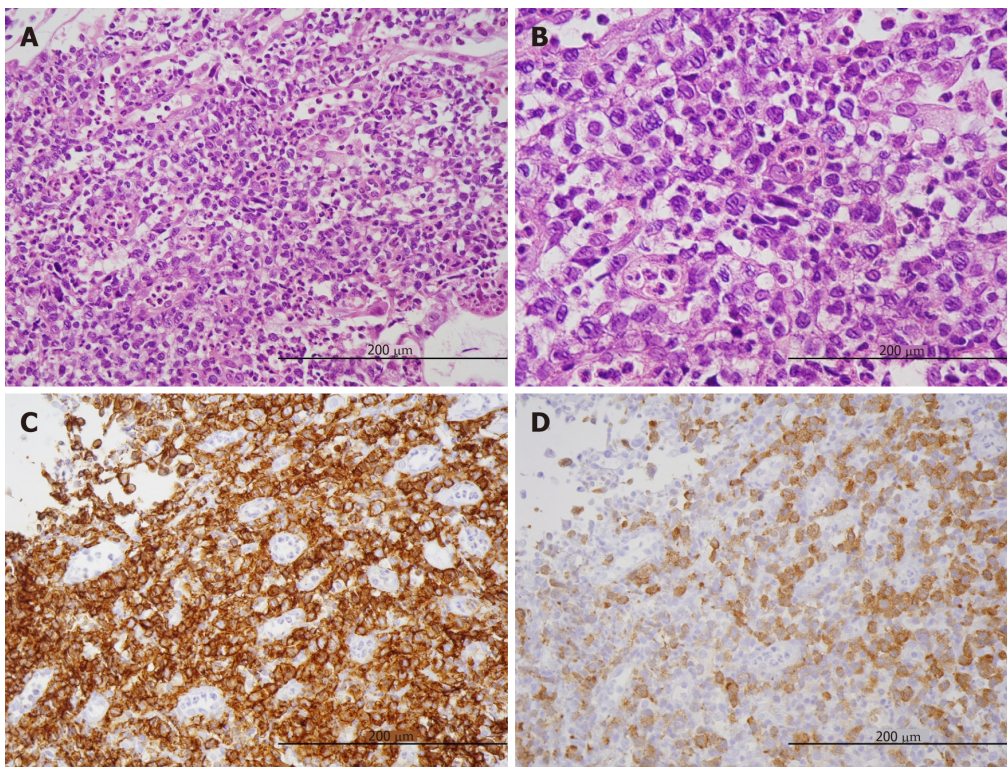
Figure 4 Histopathological findings in biopsy samples (x 200), Medium to large-sized abnormal lymphoid cells with irregular nuclei grew diffusely (A), and mitotic figures were observed in high numbers (B). In immunostaining of lymphoma cells, CD30 was strongly positive (C), and ALK showed positive in nuclear and cytoplasmic patterns (D).

REFERENCES

1   **Stein H**, Mason DY, Gerdes J, O'Connor N, Wainscoat J, Pallesen G, Gatter K, Falini B, Delsol G, Lemke H. The expression of the Hodgkin's disease associated antigen Ki-1 in reactive and neoplastic lymphoid tissue: evidence that Reed-Sternberg cells and histiocytic malignancies are derived from activated lymphoid cells. *Blood* 1985; **66**: 848-858 [PMID: 3876124]

2   **Delsol G**, Jaffe ES, Falini B, Gascoyne RD, Müller-Hermelink HK, Stein H, Campo E, Kinney MC, Swerdlow SH, Campo E, Harris NL, Jaffe ES, Pileri SA. Anaplastic large cell lymphoma (ALCL), ALK-positive. Swerdlow SH, Campo E, Harris NL, Jaffe ES, Pileri SA. *WHO Classification of Tumours of Haematopietic and Lymphoid Tissues*. Lyon, France: IARC press; 2008: 312-316

3   **Morris SW**, Kirstein MN, Valentine MB, Dittmer KG, Shapiro DN, Saltman DL, Look AT. Fusion of a kinase gene, ALK, to a nucleolar protein gene, NPM, in non-Hodgkin's lymphoma. *Science* 1994; **263**: 1281-1284 [PMID: 8122112]

4   **Ruskoné-Fourmestraux A**, Audouin J. Primary gastrointestinal tract mantle cell lymphoma as multiple lymphomatous polyposis. *Best Pract Res Clin Gastroenterol* 2010; **24**: 35-42 [PMID: 20206107 DOI: 10.1016/j.bpg.2009.12.001]

5   **Saito M**, Mori A, Irie T, Tanaka M, Morioka M, Ozasa M, Kobayashi T, Saga A, Miwa K, Tanaka S. Endoscopic follow-up of 3 cases with gastrointestinal tract involvement of mantle cell lymphoma. *Intern Med* 2010; **49**: 231-235 [PMID: 20118601 DOI: 10.2169/internalmedicine.49.2766]

6   **Stein H**, Foss HD, Dürkop H, Marafioti T, Delsol G, Pulford K, Pileri S, Falini B. CD30(+) anaplastic large cell lymphoma: a review of its histopathologic, genetic, and clinical features. *Blood* 2000; **96**: 3681-3695 [PMID: 11090048]

7   **ten Berge RL**, de Bruin PC, Oudejans JJ, Ossenkoppele GJ, van der Valk P, Meijer CJ. ALK-negative anaplastic large-cell lymphoma demonstrates similar poor prognosis to peripheral T-cell lymphoma, unspecified. *Histopathology* 2003; **43**: 462-469 [PMID: 14636272]

8   **Falini B**, Pulford K, Pucciarini A, Carbone A, De Wolf-Peeters C, Cordell J, Fizzotti M, Santucci A, Pelicci PG, Pileri S, Campo E, Ott G, Delsol G, Mason DY. Lymphomas expressing ALK fusion protein(s) other than NPM-ALK. *Blood* 1999; **94**: 3509-3515 [PMID: 10552961]

9   **Kim YH**, Lee JH, Yang SK, Kim TI, Kim JS, Kim HJ, Kim JI, Kim SW, Kim JO, Jung IK, Jung SA, Jung MK, Kim HS, Myung SJ, Kim WH, Rhee JC, Choi KY, Song IS, Hyun JH, Min YI. Primary colon lymphoma in Korea: a KASID (Korean Association for the Study of Intestinal Diseases) Study. *Dig Dis Sci* 2005; **50**: 2243-2247 [PMID: 16416168 DOI: 10.1007/s10620-005-3041-7]

10 **Kim DH**, Lee D, Kim JW, Huh J, Park SH, Ha HK, Suh C, Yoon SM, Kim KJ, Choi KD, Ye BD, Byeon JS, Song HJ, Jung HY, Yang SK, Kim JH, Myung SJ. Endoscopic and clinical analysis of primary T-cell lymphoma of the gastrointestinal tract according to pathological subtype. *J Gastroenterol Hepatol* 2014; **29**: 934-943 [PMID: 24325295 DOI: 10.1111/jgh.12471]

11 **Lee YY**, Takata K, Wang RC, Yang SF, Chuang SS. Primary gastrointestinal anaplastic large cell lymphoma. *Pathology* 2017; **49**: 479-485 [PMID: 28693749 DOI: 10.1016/j.pathol.2017.05.007]

12 **Joshi A**, Fields P, Simo R. Anaplastic lymphoma of the cervical esophagus presenting as a tracheoesophageal fistula. *Head Neck* 2008; **30**: 1264-1268 [PMID: 18228520 DOI: 10.1002/hed.20774]

13 **Yaakup H**, Sagap I, Fadilah SA. Primary oesophageal Ki (CD30)-positive ALK+ anaplastic large cell lymphoma of T-cell phenotype. *Singapore Med J* 2008; **49**: e289-e292 [PMID: 18946602]

14 **Wu N**, Pang L, Chen Z, Wang Y, Ma Q, Chen G, Chen J, Huang J. Primary esophageal CD30-positive ALK-positive anaplastic large cell lymphoma: a case report and literature review. *J Gastrointest Cancer* 2011; **42**: 57-60 [PMID: 20524084 DOI: 10.1007/s12029-010-9147-y]

15 **Hryhorczuk AL**, Harris MH, Vargas SO, Lee EY. Anaplastic large cell lymphoma of the esophagus in a pediatric patient. *Pediatr Radiol* 2012; **42**: 627-631 [PMID: 21877113 DOI: 10.1007/s00247-011-2236-7]

16 **Iwamizu-Watanabe S**, Yamashita Y, Yatabe Y, Nakamura S, Mori N. Frequent expression of CD30 antigen in the primary gastric non-B, non-Hodgkin lymphomas. *Pathol Int* 2004; **54**: 503-509 [PMID: 15189504]

17 **Carey MJ**, Medeiros LJ, Roepke JE, Kjeldsberg CR, Elenitoba-Johnson KS. Primary anaplastic large cell lymphoma of the small intestine. *Am J Clin Pathol* 1999; **112**: 696-701 [PMID: 10549257]

18 **Ishii H**, Isomoto H, Taniguchi H, Kinoshita N, Matsushima K, Taguchi J, Miyazaki Y, Nakao K. Education and Imaging: Gastrointestinal: gastroduodenal involvement of ALK-positive anaplastic large cell lymphoma. *J Gastroenterol Hepatol* 2011; **26**: 933 [PMID: 21488949 DOI: 10.1111/j.1440-1746.2011.06665.x]

19 **Sadiya N**, Ghosh M. Primary ALK positive anaplastic large cell lymphoma of T-cell type of jejunum: Report of a rare extranodal entity with review of literature. *Arch Int Surg* 2014; **4**: 50-53 [DOI: 10.4103/2278-9596.136716]

20 **Cao Q**, Liu F, Li S, Liu N, Li L, Li C, Peng T. Primary rare anaplastic large cell lymphoma, ALK positive in small intestine: case report and review of the literature. *Diagn Pathol* 2016; **11**: 83 [PMID: 27612448 DOI: 10.1186/s13000-016-0539-6]

21 **Cornes JS**. Multiple lymphomatous polyposis of the gastrointestinal tract. *Cancer* 1961; **14**: 249-257 [PMID: 13695582]

22 **Isaacson PG**, MacLennan KA, Subbuswamy SG. Multiple lymphomatous polyposis of the gastrointestinal tract. *Histopathology* 1984; **8**: 641-656 [PMID: 6479906]

23 **Kodama T**, Ohshima K, Nomura K, Taniwaki M, Nakamura N, Nakamura S, Kohno S, Yamamoto J, Karube K, Yamasita Y, Shirakusa T, Kikuchi M. Lymphomatous polyposis of the gastrointestinal tract, including mantle cell lymphoma, follicular lymphoma and mucosa-associated lymphoid tissue lymphoma. *Histopathology* 2005; **47**: 467-478 [PMID: 16241994 DOI: 10.1111/j.1365-2559.2005.02225.x]

24 **Vetro C**, Bonanno G, Giulietti G, Romano A, Conticello C, Chiarenza A, Spina P, Coppolino F, Cunsolo R, Raimondo FD. Rare gastrointestinal lymphomas: The endoscopic investigation. *World J Gastrointest Endosc* 2015; **7**: 928-949 [PMID: 26265987 DOI: 10.4253/wjge.v7.i10.928]

25 **Itsuno M**, Makiyama K, Muta K, Furukawa K, Hara K, Tabata S, Soda H, Ikeda S, Takashima H, Fukuda Y. Adult T-cell leukemia with multiple lymphomatous polyposis of the gastrointestinal tract. *Endoscopy* 1995; **27**: 700-703 [PMID: 8903987]

26 **Hokama A**, Tomoyose T, Yamamoto Y, Watanabe T, Hirata T, Kinjo F, Kato S, Ohshima K, Uezato H, Takasu N, Fujita J. Adult T-cell leukemia/lymphoma presenting multiple lymphomatous polyposis. *World J Gastroenterol* 2008; **14**: 6584-6588 [PMID: 19030219 DOI: 10.3748/wjg.14.6584]

27 **Romaguera JE**, Medeiros LJ, Hagemeister FB, Fayad LE, Rodriguez MA, Pro B, Younes A, McLaughlin P, Goy A, Sarris AH, Dang NH, Samaniego F, Brown HM, Gagneja HK, Cabanillas F. Frequency of

gastrointestinal involvement and its clinical significance in mantle cell lymphoma. *Cancer* 2003; **97**: 586-591 [PMID: 12548600]

28   **Saito M**, Miyazaki M, Tanino M, Tanaka S, Miyashita K, Izumiyama K, Mori A, Irie T, Tanaka M, Morioka M, Tsukamoto E. ¹F-FDG PET/CT imaging for a gastrointestinal mantle cell lymphoma with multiple lymphomatous polyposis. *World J Gastroenterol* 2014; **20**: 5141-5146 [PMID: 24803832 DOI: 10.3748/wjg.v20.i17.5141]

Modified Tong Xie Yao Fang relieves solitary rectal ulcer syndrome: A case report

Li-Li Zhang, Wan-Shan Hao, Meng Xu, Chang Li, Yuan-Yuan Shi

ORCID number: Li-Li Zhang (0000-0002-6906-8893); Wan-Shan Hao (0000-0002-1222-6723); Meng Xu (0000-0003-3070-0123); Chang Li (0000-0003-4008-0167); Yuan-Yuan Shi (0000-0003-2997-4573).

Li-Li Zhang, Meng Xu, Yuan-Yuan Shi, School of Life Sciences, Beijing University of Chinese Medicine, Beijing 100029, China

Wan-Shan Hao, Teaching and Research Section of Shanghan, Beijing University of Chinese Medicine, Beijing 100029, China

Chang Li, Traditional Chinese Medicine Department, Beijing Baicaoyuan Hospital of Traditional Chinese Medicine, Beijing 100107, China

Corresponding author: Yuan-Yuan Shi, PhD, Professor, School of Life Sciences, Beijing University of Chinese Medicine, No. 11 East road, North 3rd Ring Road, Beijing 100029, China. yshi@bucm.edu.cn
Telephone: +86-10-53912150
Fax: +86-10-64286651

Abstract

BACKGROUND
Solitary rectal ulcer syndrome (SRUS) is a rare rectal disorder characterized by bloody mucus in the stool, difficulty in defecation, pain, and anal swelling. To date, the etiology of this syndrome remains not well understood and the diagnosis is frequently confused with other disorders, making treatment a clinical challenge.

CASE SUMMARY
A 50-year-old woman presented to our hospital with a 40-d history of bloody mucus in the stool and anal swelling. SRUS was suspected. Rectoscopy revealed a large, severe ulcerous lesion. Histologically, the lesion was characterized as chronic ulcer without clear tumor cells, and the final diagnosis of SRUS was made. The patient was treated with Chinese medicine therapy, with administration of Tong Xie Yao Fang. After 3 wk of treatment, the symptoms improved significantly. At 2-mo follow-up, rectoscopy in a local hospital showed healed ulcer scars without obvious protrusion 3 cm from the anal verge.

CONCLUSION
Chinese medicine therapy represents a potential treatment of SRUS with predominant rectal bleeding, mucinous discharge, and anal swelling pain.

Key words: Solitary rectal ulcer syndrome; Chinese formulas; Tong Xie Yao Fang; Er Shen Wan; Ding Zhi Xiao Wan; Chinese medicine therapy; Case report

Core tip: Solitary rectal ulcer syndrome (SRUS) is a benign but uncommon rectal disorder. We present the case of a 50-year-old woman who suffered from SRUS for 40 d, with the symptoms of bloody mucous in the stools and anal swelling. Following our success of treatment with modified Tong Xie Yao Fang, we discuss how this traditional Chinese medicine prescription might be an effective treatment strategy for SRUS with this symptom profile.

INTRODUCTION

Solitary rectal ulcer syndrome (SRUS) is a chronic, benign, uncommon and under-diagnosed disease. It is estimated that the annual incidence of SRUS is one of 100000 people, mainly affecting men in the third decade of life and women in the fourth decade[1]. Its symptomological profile consists of intestinal symptoms, primarily constipation, feeling of incomplete defecation, bloody or purulent stools, discomfort with falling anus, and rectal ulcers.

The diagnosis of SRUS is largely based on findings in rectoscopy and analysis of tissue biopsy. The treatment of SRUS includes local medication, improvement of bowel defecation habits, biofeedback, and surgical operation[2]. We report herein the case of a 50-year-old woman with SRUS and describe its appearance on rectoscopy and in analysis of the gross specimen following Chinese medicine therapy. The purpose of publishing this case is to report and discuss the effects of herbal therapy on SRUS.

CASE PRESENTATION

Chief complaints

A 50-year-old woman presented to our hospital with a 2-year history of intermittent dull pain in her left lower abdomen, a 40-d history of rectal swelling and discomfort, and a 20-d history of mucinous and bloody, loose stools.

History of present illness

The patient was sent to our Chinese medicine hospital on September 5, 2018. She reported having had developed intermittent left lower abdominal dull pain 2 years prior, after suffering from cold and eating irritating food. She reported no obvious cause of the rectal swelling discomfort that had developed 2 mo previously nor of the mucinous bloody, loose stools (occurring three or four times a day) 40 d prior. She also reported insomnia, and we observed her tongue to be red in color with white and thick fur, and a thin pulse.

History of past illness and family history

The patient had undergone hemorrhoid surgery in 2009 and polypectomy of the cervical canal in 2011. Her father had died of a femoral fracture in the neck; otherwise, there was no medical family history.

Physical examination upon admission

Physical examination showed no obvious abnormality, except for a tough ulcerative mass, about 2 cm × 2 cm on the wall of the rectum at 3 cm from the anal verge. The remaining rectal mucosa showed smooth surface. Blood stains were detected on the doctor's disposable glove after examination of the patient.

Laboratory examinations

Laboratory examinations provided the following findings: Gram-positive bacilli of 40.0% (normal range: 50%-71%); Gram-negative bacilli of 45.0% (normal range: 24%-44%); antigen-stimulated interferon A of 15.0 SFCs/2.5 × 10^6 (normal: < 6 SFCs/2.5 ×

10^6); specific gravity of urine of 1.008 (normal range: 1.015-1.025); total cholesterol of 5.2 mmol/L (normal: < 5.18 mmol/L); and complement C1q of 149.0 mg/L (normal range: 159-233 mg/L). The white blood cell count (5.99 × 10^9/L) and platelet count (4.03 × 10^{12}/L) were normal. Findings for stool samples' cultures, fecal occult blood, parasite eggs, and amoeba trophozoites were negative.

Imaging examinations

Colonoscopy revealed an irregular nodule, occupying 1/2 of the lumen, at 5 cm from the anal verge. The central ulcer was sunken, with blood stasis spotting and sloughing on the surface, as well as being brittle and bleeding easily (Figure 1A). Rectoscope showed a large ulcerative lesion at 2-4 cm from the anal margin of the rectum, occupying 3/5 of the lumen, covered by a white and bloody sloughing of tissue with central ulcer depression, as well as being brittle and prone to bleeding (Figure 1B). The pathological report noted chronic colonic mucositis, rectal mucosal erosion, and inflammatory granulation (Figure 1C).

FINAL DIAGNOSIS

The patient was diagnosed with SRUS, based on the findings from endoscopy of the rectum and colon (Figure 1A, B) and histology of the biopsy (Figure 1C). Her condition was deemed to be serious. Diagnosis of Traditional Chinese Medicine (TCM) was diarrhea (liver stagnation and spleen deficiency), according to the patient's main clinical symptoms.

TREATMENT

Treatment of modified Tong Xie Yao Fang (TXYF) was administered to soothe the qi, fortify the spleen, quiet the heart, astringe the intestines, regulate the diarrhea, and relieve the pain. The prescription was composed of Chenpi (tangerine peel; 15 g), Baishao (Radix Paeoniae Alba; 20 g), Fangfeng (Radix Saposhnikoviae; 20 g), Gaoben (Ligusticum; 10 g), Baizhu [Rhizoma Atractylodis Macrocephalae (AM); 15 g], Roudoukou (Myristica fragrans; 10 g), Buguzhi (Psoralea corylifolia; 10 g), Paojiang (prepared ginger; 10 g), Pugongying (Mongolian dandelion; 20 g), Dangshen (Radix Codonopsis; 15 g), Yuanzhi (Polygala Tenuifolia; 12 g), Shichangpu (Acorus Tatarinowii; 10 g), and Gancao (licorice; 10 g). The daily dose was decocted with water and taken at 30 min after food intake in the morning and evening. After 7 d, on September 12, 2018, the patient's symptoms were alleviated but the patient woke early in the morning, with the continued red tongue with white and thick fur, and thin, wiry pulse. Suanzaoren (spine date seed; 20 g), Hehuanpi (Silktree Albizia bark; 10 g), and Fuling (Poria Cocos; 15 g) were added into the original prescription. The decoction and delivery method was the same as the initial ones. TCM treatment had been insisted on by the patient, who only wanted Chinese herbal medicine and no Western medicine treatment for 21 d.

OUTCOME AND FOLLOW-UP

On September 30, 2018, the patient was examined in the Third Affiliated Hospital of Beijing University. Rectoscopy showed an irregular shaped ulcer, 3 cm from the anal verge, about 1.0 cm × 1.2 cm in size, less white fur on the surface, flat bottom, concentrated folds around the rectum, and fusion, thickening and interruption near the ulcer; the biopsy specimen was tough, with no stenosis (Figure 2A). The pathological report noted chronic rectal ulcer mucosal inflammation, with focal lymphocyte aggregation (Figure 2B). The results suggested that the ulcer surface tended to be scarred, having improved and healed without prescribed Western medicine. The improvement of rectal symptoms in this patient should be attributed to the role of the 21 herbs administered.

During hospitalization, the patient underwent a series of examinations. Although the cause of SRUS was not found, the ulcer improved gradually with treatment. After discharge, the woman adhered to TCM treatment and also used Titanoreine, a kind of anal suppository the covers the surface of the anal and rectal mucosa with a protective membrane. On December 8, 2018, re-examination by rectoscopy in a local hospital showed that the ulcer scars had healed, without obvious protrusion, at 3 cm from the anal verge. A polyp, about 0.3 cm × 0.3 cm, was found at 3 cm from the anal verge. The surface of the mucosa was found to be smooth (Figure 2C).
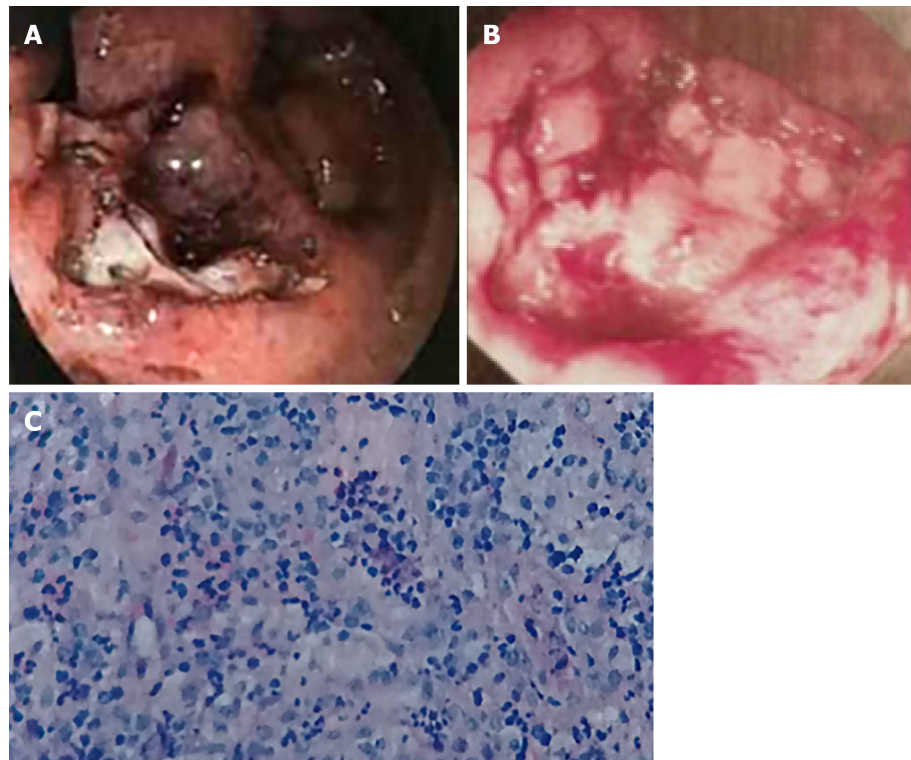
Figure 1 Endoscopic images and corresponding histological findings from before the Traditional Chinese Medicine treatment. A: Colonoscopy image showing actively bleeding, deep ulcerations; B: Rectoscope image showing a large ulcerative lesion covered by a white and bloody sloughing tissue; C: Hematoxylin-eosin-stained rectal ulcers.

DISCUSSION

The pathogenesis of SRUS is not clear, and it is often believed that SRUS might be associated with rectal prolapse and trauma from straining[3,4]. Clinically, SRUS is easy to be suspected as colorectal cancer, based on the similar symptomatic profiles and endoscopic features, which include bleeding or mucus at defecation, anal or rectal pain and discomfort, increased frequency of defecation, and colorectal masses or ulcers[1,5]. Histological features are helpful to distinguish SRUS from malignancy. The key histological features that distinguish SRUS from colorectal cancer are the architectural distortion, fibromuscular obliteration of lamina propria, and absence of tumor cell infiltration[6].

The therapeutic regimens for SRUS include conservative treatment, medical therapy, biofeedback therapy, and surgery[2]. The choice of treatment depends upon the severity of symptoms and the presence of rectal prolapse. In our case, TCM may have played a role in the successful treatment of SRUS and highlights the potential of such as a supplementary and alternative therapy. Some studies have suggested that fruits, vegetables and grains have protective effects against adenoma and colorectal cancer. Probiotics may also have preventive effects on colorectal cancer but the actual beneficial effects remain to be definitively evidenced[7,8]. Conservative treatment (high-fiber diet, laxatives, change in defecatory habits, and biofeedback treatment) were shown to induce a symptomatic improvement in 71/91 patients (63.6%) and healing of mucosal lesion in 17/51 patients (33.3%)[9]. According to those reports, SRUS may be prevented and improved by adjusting dietary structures and probiotic levels.

The basic TCM prescription combination consists of three classic Chinese formulas, (TXYF, consisting of tangerine peel, Radix Paeoniae Alba, Radix Saposhnikoviae, and Rhizoma AM), Er Shen Wan (ESW, consisting of Myristica fragrans and Psoralea corylifolia) and Ding Zhi Xiao Wan (DZXW, consisting of Codonopsis, Polygala tenuifolia Willd, Acorus Tatarinowii, and Poria Cocos). In addition, Gancao (licorice) is used to mediate other herbs. Suanzaoren (spine date seed) and Hehuanpi (Silktree Albizia bark) can be added when the patient suffers from insomnia.

TXYF is recorded in the Dan Xi Xin Fa. Form the viewpoint of TCM, it is used to relieve the pain and diarrhea caused by the incompatibility of the liver and spleen. ESW is recorded in the Pu Ji Ben Shi Fang. Differently, it is used for diarrhea due to deficiency of the spleen. At the patient's first hospital visit, she mainly complained of
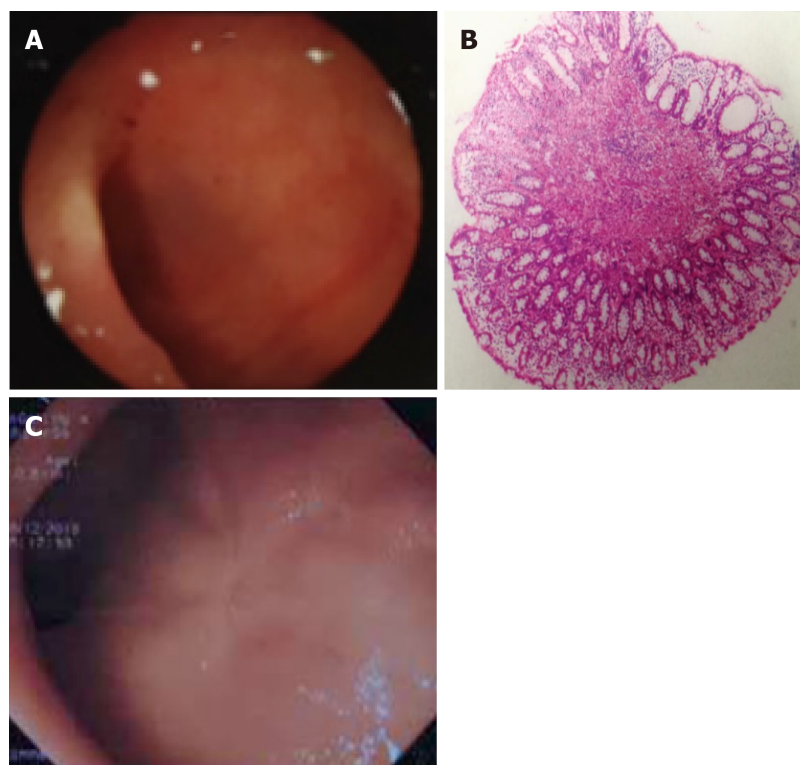
Figure 2 Endoscopic imaging and corresponding histological findings after Traditional Chinese Medicine treatment. A: The improvement of ulcers; B: Hematoxylin-eosin-stained rectal ulcers (× 40); C: The healed ulcers.

pain in her left abdomen, diarrhea, mucinous defecation, and abnormal defecation. Based on TCM theory, her clinical symptoms were categorized as diarrhea. The patient had mild anxiety, depression and insomnia during her illness. DZXW can maintain the ability of learning and memory in depression, and the mechanism involves the promotion of neural stem cell proliferation in hippocampal formation[10].

TXYF is a commonly used Chinese herbal prescription for diarrhea, suggested to be effective in treating diarrhea-predominant irritable bowel syndrome (IBS-D)[11]. 5-hydroxytryptamine (5-HT) is a neurotransmitter that is widely distributed throughout the central nervous system and gastrointestinal tract, which may contribute to the symptoms of IBS. Li *et al*[12] demonstrated that TXYF treatment diminishes colonic 5-HT levels and alleviates the symptoms of IBS-D by favorably affecting microbiota levels in gut flora communities. Data from a study by Yin *et al*[13] suggested that the activity of the enteric nervous system and the regulation of 5-HT and substance P activities can be modulated by TXYF. Corticotropin-releasing hormone-receptor 2 (known as CRH-R2) is known to activate the intestinal mucosal anti-inflammatory response by regulating migration, proliferation and apoptosis of intestinal epithelial cells, as has been shown in colitis-induced mice[14], and to play an important anti-inflammatory role. Gong *et al*[14] demonstrated that TXYF can facilitate mucosal repair in colitis mice by regulating the CRH-R2. TXYF was also shown to improve the symptoms of postinfectious IBS by alleviating behavioral hyperalgesia and exerting antidiarrheal effects, the underlying mechanism of which involves TXYF inhibition of mucosal mast cells' activation, down-regulation of tryptase and c-Fos expression, and reduction of serum TNF-α and histamine levels[15]. Therefore, it is suspected that TXYF may relieve the symptoms of SRUS by decreasing the defecation frequency and promoting mucosal repair.

AM is the most important herb in TXYF. Studies by Song *et al*[16] reveal that treatment with AM significantly stimulates the migration of intestinal epithelial cells (commonly known as IECs) through the polyamine-Kv1 channel signaling pathway, which can promote healing of intestinal injury. Findings from another study suggested that AM significantly stimulates the migration of IEC-6 cells through a polyamine-dependent mechanism, which could accelerate the healing of intestinal injury[17]. These results provide evidence for the effect of AM in treating intestinal diseases that are characterized by injury and ineffective repair of the intestinal mucosa in clinical practice.

ESW, composed of Myristica fragrans and Psoralea corylifolia, is a classical Chinese formula for astringing intestines and resolving diarrhea. The Myristica fragrans seed

extract has shown protective effects against dextran sulfate sodium-induced colitis in an animal model by inhibiting proinflammatory cytokines in the colon mucosa. This indicates the potential usefulness of Myristica fragrans to address intestinal inflammation in a preventive application[18]. Psoralea corylifolia is a well-known traditional herb used because of its antibacterial activity. Corylifolinin and neobavaisoflavone are two isolated compounds of Psoralea corylifolia. Both of them have significant antibacterial activity against *Staphylococcus aureus*, methicillinresistant *Staphylococcus aureus*, and βlactamase-positive *Staphylococcus aureus*. Corylifolinin has been shown to produce the largest inhibitory zone (18 mm) with *Staphylococcus aureus*, being higher than even that of the positive control[19].

Dandelion polysaccharide has a good effect on clearing heat, resolving toxin presence, dissipating binding, and dispersing swelling. It plays an important role in the treatment of ulcerative colitis by decreasing the level of interleukin (IL)-6, which increases chronic intestinal inflammation[20,21]. Dandelion polysaccharide has also been shown to effectively regulate the expression of the IL-6 receptors (particularly the α form) and the glycoprotein 130 (commonly known as gp130) protein in the IL-6/transcriptional activator 3 (commonly known as STAT3) pathway, and then down-regulating the expressions of STAT3 and IL-6 mRNAs in intestinal tissue (of rats), thereby alleviating the colon inflammation state and protecting and repairing the mucosal tissue[21].

Many neurotransmitters, including dopamine, glutamate, norepinephrine, nitric oxide, and 5-HT and its 5-HT3 and 5-HT4 receptors are expressed in the brain and intestine. Disorder of the bidirectional communication between the intestinal tract and intestinal nervous system and brain (brain-intestinal axis) is regulated by various psychosocial and environmental factors (*i.e.*, infection and inflammation)[22]. Therefore, the addition of spirit-regulating herbs may be useful for the recovery of gastrointestinal function.

Clinical application of TCM, DZXW, spine date seed and Silktree Albizia bark has remarkable effect on quieting the spirit and resolving depression. DZXW has been shown to effectively ameliorate learning-memory impairment in aging rats, improving their learning-memory capacity, and its mechanism may be related to a promotion of the function of the cerebral monoamine nervous system in brain tissue and a reduction in the level of lipid peroxidation in brain tissue[23]. Finally, the aqueous extract of Albizia adianthifolia leaves shows anxiolytic and antidepressant effects, and may confer neuroprotection due to alleviation of oxidative stress in the (rat) amygdala induced by 6-hydroxydopamine injection[24].

CONCLUSION

The case described herein demonstrates that Chinese formulas, specifically modified TXYF, can be effective in relieving the symptoms of SRUS. This finding provides new insight into the treatment of SRUS and a basis for further studies to determine the underlying mechanism.

REFERENCES

1   **Martin CJ**, Parks TG, Biggart JD. Solitary rectal ulcer syndrome in Northern Ireland. 1971-1980. *Br J Surg* 1981; **68**: 744-747 [PMID: 7284739 DOI: 10.1002/bjs.1800681021]
2   **Zhu QC**, Shen RR, Qin HL, Wang Y. Solitary rectal ulcer syndrome: clinical features, pathophysiology, diagnosis and treatment strategies. *World J Gastroenterol* 2014; **20**: 738-744 [PMID: 24574747 DOI: 10.3748/wjg.v20.i3.738]
3   **Meurette G**, Regenet N, Frampas E, Sagan C, Le Borgne J, Lehur PA. The solitary rectal ulcer syndrome. *Gastroenterol Clin Biol* 2006; **30**: 382-390 [PMID: 16633303 DOI: 10.1016/S0399-8320(06)73192-X]
4   **Vaizey CJ**, van den Bogaerde JB, Emmanuel AV, Talbot IC, Nicholls RJ, Kamm MA. Solitary rectal ulcer syndrome. *Br J Surg* 1998; **85**: 1617-1623 [PMID: 9876062 DOI: 10.1046/j.1365-2168.1998.00935.x]
5   **Tjandra JJ**, Fazio VW, Petras RE, Lavery IC, Oakley JR, Milsom JW, Church JM. Clinical and pathologic factors associated with delayed diagnosis in solitary rectal ulcer syndrome. *Dis Colon Rectum* 1993; **36**: 146-153 [PMID: 8425418 DOI: 10.1007/BF02051170]
6   **Chiang JM**, Changchien CR, Chen JR. Solitary rectal ulcer syndrome: an endoscopic and histological presentation and literature review. *Int J Colorectal Dis* 2006; **21**: 348-356 [PMID: 16133006 DOI: 10.1007/s00384-005-0020-6]
7   **Uccello M**, Malaguarnera G, Basile F, D'agata V, Malaguarnera M, Bertino G, Vacante M, Drago F, Biondi A. Potential role of probiotics on colorectal cancer prevention. *BMC Surg* 2012; **12** Suppl 1: S35 [PMID: 23173670 DOI: 10.1186/1471-2482-12-S1-S35]
8   **Waluga M**, Zorniak M, Fichna J, Kukla M, Hartleb M. Pharmacological and dietary factors in prevention of colorectal cancer. *J Physiol Pharmacol* 2018; 69 [PMID: 30149368 DOI: 10.26402/jpp.2018.3.02]
9   **Gouriou C**, Chambaz M, Ropert A, Bouguen G, Desfourneaux V, Siproudhis L, Brochard C. A systematic literature review on solitary rectal ulcer syndrome: is there a therapeutic consensus in 2018? *Int J Colorectal Dis* 2018; **33**: 1647-1655 [PMID: 30206681 DOI: 10.1007/s00384-018-3162-z]

10   **Shan DH**, Chai JY, Wang DS, Wang CT. [Effect of Dingzhixiaowan on Neural Stem Cells of Dentate Gyrus and Learning Memory in Depression Model Rats]. *Zhonghua Zhongyiyao Xuekan* 2005; **23**: 1426-1427

11   **Chen M**, Tang TC, Wang Y, Shui J, Xiao XH, Lan X, Yu P, Zhang C, Wang SH, Yao J, Zheng H, Huang DQ. Randomised clinical trial: Tong-Xie-Yao-Fang granules versus placebo for patients with diarrhoea-predominant irritable bowel syndrome. *Aliment Pharmacol Ther* 2018; **48**: 160-168 [PMID: 29856472 DOI: 10.1111/apt.14817]

12   **Li J**, Cui H, Cai Y, Lin J, Song X, Zhou Z, Xiong W, Zhou H, Bian Y, Wang L. Tong-Xie-Yao-Fang Regulates 5-HT Level in Diarrhea Predominant Irritable Bowel Syndrome Through Gut Microbiota Modulation. *Front Pharmacol* 2018; **9**: 1110 [PMID: 30323765 DOI: 10.3389/fphar.2018.01110]

13   **Yin Y**, Zhong L, Wang JW, Zhao XY, Zhao WJ, Kuang HX. Tong Xie Yao Fang relieves irritable bowel syndrome in rats via mechanisms involving regulation of 5-hydroxytryptamine and substance P. *World J Gastroenterol* 2015; **21**: 4536-4546 [PMID: 25914462 DOI: 10.3748/wjg.v21.i15.4536]

14   **Gong SS**, Fan YH, Wang SY, Han QQ, Lv B, Xu Y, Chen X, He YE. Mucosa repair mechanisms of Tong-Xie-Yao-Fang mediated by CRH-R2 in murine, dextran sulfate sodium-induced colitis. *World J Gastroenterol* 2018; **24**: 1766-1778 [PMID: 29713130 DOI: 10.3748/wjg.v24.i16.1766]

15   **Ma X**, Wang X, Kang N, Chen T, Ji H, Lv L, Yin X, Tian Y, Zheng R, Duan Y, Wang F, Tang X. The Effect of Tong-Xie-Yao-Fang on Intestinal Mucosal Mast Cells in Postinfectious Irritable Bowel Syndrome Rats. *Evid Based Complement Alternat Med* 2017; **2017**: 9086034 [PMID: 28331524 DOI: 10.1155/2017/9086034]

16   **Song HP**, Li RL, Chen X, Wang YY, Cai JZ, Liu J, Chen WW. Atractylodes macrocephala Koidz promotes intestinal epithelial restitution via the polyamine--voltage-gated K+ channel pathway. *J Ethnopharmacol* 2014; **152**: 163-172 [PMID: 24417867 DOI: 10.1016/j.jep.2013.12.049]

17   **Song HP**, Li RL, Zhou C, Cai X, Huang HY. Atractylodes macrocephala Koidz stimulates intestinal epithelial cell migration through a polyamine dependent mechanism. *J Ethnopharmacol* 2015; **159**: 23-35 [PMID: 25446597 DOI: 10.1016/j.jep.2014.10.059]

18   **Kim H**, Bu Y, Lee BJ, Bae J, Park S, Kim J, Lee K, Cha JM, Ryu B, Ko SJ, Han G, Min B, Park JW. Myristica fragrans seed extract protects against dextran sulfate sodium-induced colitis in mice. *J Med Food* 2013; **16**: 953-956 [PMID: 24063406 DOI: 10.1089/jmf.2013.2759]

19   **Wang TX**, Yin ZH, Zhang W, Peng T, Kang WY. [Chemical constituents from Psoralea corylifolia and their antioxidant alpha-glucosidase inhibitory and antimicrobial activities]. *Zhongguo Zhongyao Zazhi* 2013; **38**: 2328-2333 [PMID: 24199566]

20   **Powell N**, Lo JW, Biancheri P, Vossenkämper A, Pantazi E, Walker AW, Stolarczyk E, Ammoscato F, Goldberg R, Scott P, Canavan JB, Perucha E, Garrido-Mesa N, Irving PM, Sanderson JD, Hayee B, Howard JK, Parkhill J, MacDonald TT, Lord GM. Interleukin 6 Increases Production of Cytokines by Colonic Innate Lymphoid Cells in Mice and Patients With Chronic Intestinal Inflammation. *Gastroenterology* 2015; **149**: 456-67.e15 [PMID: 25917784 DOI: 10.1053/j.gastro.2015.04.017]

21   **Wang Q**, Bie YL, Wang D, Fan WT. [Effects of Dandelion polysaccharide on IL-6/STAT3 signaling pathway in ulcerative colitis rats]. *Zhongguo Yingyong Shenglixue Zazhi* 2017; **33**: 422-425 [PMID: 29926586]

22   **Mach T**. The brain-gut axis in irritable bowel syndrome--clinical aspects. *Med Sci Monit* 2004; **10**: RA125-RA131 [PMID: 15173682]

23   **Qu R**, Ma S, Zhan Y, Xia W. [Effect of dingzhi xiaowan on learning and memory function in aging rats]. *Zhongguo Linchuang Kangfu* 2004; **8**: 684-685

24   **Beppe GJ**, Dongmo AB, Foyet HS, Dimo T, Mihasan M, Hritcu L. The aqueous extract of Albizia adianthifolia leaves attenuates 6-hydroxydopamine-induced anxiety, depression and oxidative stress in rat amygdala. *BMC Complement Altern Med* 2015; **15**: 374 [PMID: 26481946 DOI: 10.1186/s12906-015-0912-0]

Hydrogen gas therapy induced shrinkage of metastatic gallbladder cancer: A case report

Ji-Bing Chen, Zhong-Bao Pan, Duan-Ming Du, Wei Qian, Yang-Yang Ma, Feng Mu, Ke-Cheng Xu

ORCID number: Ji-Bing Chen (0000-0001-8596-2126); Zhong-Bao Pan (0000-0001-8315-4264); Duan-Ming Du (0000-0002-3360-9563); Wei Qian (0000-0002-8032-4878); Yang-Yang Ma (0000-0002-6403-7553); Feng Mu (0000-0002-7707-2825); Ke-Cheng Xu (0000-0003-1093-4803).

Ji-Bing Chen, Zhong-Bao Pan, Wei Qian, Yang-Yang Ma, Feng Mu, Ke-Cheng Xu, Central Laboratory, Fuda Cancer Hospital of Jinan University, Guangzhou 510665, Guangdong Province, China

Duan-Ming Du, Intervention Department of Shenzhen Second People's Hospital, Shenzhen 518035, Guangdong Province, China

Corresponding author: Ke-Cheng Xu, MD, Chairman, Central Laboratory, Fuda Cancer Hospital of Jinan University, No. 2, Tangdexi Road, Tianhe District, Guangzhou 510665, Guangdong Province, China. xukc@vip.163.com

Telephone: +86-3899-39668666
Fax: +86-3899-39668666

Abstract

BACKGROUND
We present the case of a 72-year-old female patient with gallbladder cancer (GBC) who developed *in situ* recurrence and liver metastases 9 mo after irreversible electroporation ablation and oral tegafur (a fluoropyrimidine derivative) chemotherapy, which failed to control the progression of the disease. The patient further developed metastases in the lymph nodes around the head of the pancreas. The patient had severe anemia, requiring weekly blood transfusions. The gallbladder tumor invaded the descending part of the duodenum, causing intestinal leakage and hepatic colonic adhesion.

CASE SUMMARY
The patient refused other treatments and began daily hydrogen inhalation therapy. After 1 mo of treatment, the gallbladder and liver tumors continued to progress, and intestinal obstruction occurred. After continuous hydrogen therapy and symptomatic treatments including gastrointestinal decompression and intravenous nutrition support, the intestinal obstruction was gradually relieved. Three months after hydrogen therapy, the metastases in the abdominal cavity gradually reduced in size, her anemia and hypoalbuminemia were corrected, lymphocyte and tumor marker levels returned to normal, and the patient was able to resume normal life.

CONCLUSION
This is the first report of an efficacy and safety study about hydrogen therapy in patient with metastatic GBC and a critical general condition, who has remained stable for more than 4 months.

Core tip: This is the first report of an efficacy and safety study about hydrogen therapy in patient with metastatic gallbladder cancer and a critical general condition, who has remained stable for more than 4 mo.

INTRODUCTION

Gallbladder cancer (GBC) is the sixth most common gastrointestinal cancer and the sixth highest cause of cancer-related deaths in China[1]. Despite improvements in the diagnosis and treatment of GBC, the majority of the patients are usually confirmed as having metastatic GBC (mGBC)[2,3]. Due to the high incidence of lymph node or distant metastasis, the 5-year overall survival (OS) rate for GBC is only 5%[3,4]. In mGBC patients who are not candidates for surgery, the National Comprehensive Cancer Network (NCCN) guidelines reco-mmend the use of biliary drainage, chemotherapy, clinical trials, and the best supportive care available. At present, there are few alternative options, and new and more effective methods are urgently required.

In patients with cancer, the treatment strategy, outcome, and prognosis are strongly dependent on immune status. CD8+ T cells become exhausted by persistent stimu-lation by tumor antigens, resulting in cessation of proliferation, cytokine production, and immune function[5,6]. The preventive and therapeutic effects of hydrogen in various diseases, including cancer, have been investigated in several studies[7-9]. Hydrogen was recently reported to stimulate peroxisome proliferatoractivated receptor γ coactivator 1α[10], which enhances mitochondrial function[11] and thus, may rescue exhausted CD8+ T cells. In an advanced study of the effects of inhaled hydrogen gas in 55 patients with stage IV colorectal cancer[12], Akagi *et al*[12] identified accumulation of terminal programmed cell death 1 (PD1)+ CD8+ T cells as a significant index for poor prognosis, with reduction in terminal PD1+ CD8+ T cells and accumulation of terminal PD1- CD8+ T cells following hydrogen gas treatment found to be significantly associated with improved progression-free survival and OS.

Here, we present the case of a 72-year old Chinese woman with stage IIIA GBC who was treated with irreversible electroporation (IRE) and oral tegafur (a fluoropyrimidine derivative) chemotherapy. Primary recurrence and liver metastases were identified 9 mo later. Obvious shrinkage of the patient's recurrent and metastatic lesions was observed with continuous application of a hydrogen oxygen nebulizer, and a clinically objective response lasting for more than 4 mo was achieved. The patient remained disease-free at the time of writing this report.

CASE PRESENTATION

Chief complaints

We present the case of a 72-year-old female GBC patient, who was admitted to our hospital due to chest tightness in September 2018.

History of present illness

After examination, GBC was found to recur *in situ*, invading the duodenal descending part and causing intestinal fistula and hepatic colon adhesion. In addition, multiple metastases of the liver, lymph node metastasis around the head of the pancreas, severe anemia requiring weekly blood transfusion, and symptoms of heart failure were noted.

History of past illness

In December 2017, the 72-year old Chinese patient underwent IRE following diagnosis as GBC (T3N1M0 stage IIIA) based on computed tomography (CT) imaging and pathological findings of GBC (8.0 cm × 3.9 cm) with multiple hilar lymph node invasion (max 4.7 cm × 3.6 cm). She had elevated levels of a variety of serum tumor markers, including CA19-9 (2556 U/mL) and CEA (607.6 ng/mL).

Personal and family history

After IRE ablation of the gallbladder and hilar lymph nodes, oral tegafur (20 mg bid) chemotherapy was administered for 9 mo. CT re-examination in April 2018 showed liquefactive necrosis at the ablation site. During the treatment period, the patient received intermittent red blood cell (RBC) infusions as supportive care for repeated episodes of anemia.

Physical examination upon admission

Accompanied by a progressive increase in pain in the upper right abdomen, a large area of adhesion between the gallbladder and the descending and horizontal segments of the duodenum was found in addition to compression of the inferior vena cava (October 6, 2018).

Laboratory examinations

She had elevated levels of a variety of serum tumor markers, including CA19-9 (88.18 U/mL), AFP (14.11 IU/mL), and CEA (39.68 ng/mL) in September, 2018.

Imaging examinations

After 2 wk of blood transfusions and anti-infective treatment, CT examination again revealed a bladder tumor (6.3 cm × 4.9 cm), with an adjacent descending duodenal fistula, multiple spotted high-density lesions in the liver parenchyma, and dilatation and gas accumulation in the intrahepatic and extrahepatic bile ducts. Enlarged lymph nodes (2.7 cm × 2.1 cm) were visible around the pancreatic head.

FINAL DIAGNOSIS

Metastatic GBC, severe anemia, infection, and gallbladder-duodenal fistula.

TREATMENT

Hydrogen gas treatment

The hydrogen oxygen nebulizer (AMS-H-01, Asclepius Meditec, Shanghai, China) generates 3 L/min hydrogen gas by water electrolysis. As measured by gas chromatography, the gas generated consisted of 67% hydrogen and 33% oxygen. Using a special mask, the patient continued to inhale hydrogen for 3-6 h a day at rest, with no interruption even after the obvious relief of symptoms.

Best supportive care

Due to the long-term difficulty in reversing the anemia in the early stage of hydrogen inhalation therapy, the patient received weekly (1-2) blood infusions, and her RBC and hemoglobin levels were tested regularly. Daily anti-infection treatment was administered for the gallbladder-duodenal fistula, and white blood cell counts were measured regularly. After 1 mo of hydrogen aspiration therapy, the patient presented with intestinal obstruction, which was treated by gastrointestinal decompression and intravenous nutrition. Analgesics and sedatives were prescribed for pain and insomnia, respectively.

Therapeutic procedure

Due to the lack of currently available conventional treatments combined with the patient's poor condition requiring continuous supportive care, hydrogen gas monotherapy was started on October 24, 2018 (Table 1). At the time of writing this report, the patient still continues to receive daily hydrogen therapy.

Adverse events

According to the Common Terminology Criteria for Adverse Events version 3.0 (National Cancer Institute, Bethesda, MD, United States), adverse events were classified and graded every week for at least 2 mo after the treatment was started[13]. Liver function was evaluated based on the levels of alanine transaminase, aspartate

Table 1 Clinical details and therapeutic procedure

Date		Therapy
2017	December	(A) Symptoms of upper right quadrant distension pain and discomfort were aggravated; (B) Color doppler ultrasound: gallbladder tumor, local liver invasion, and multiple enlarged lymph nodes; (C) Gallbladder tumor aspiration biopsy: gallbladder cancer
2018	January 5	(A) Irreversible electroporation ablation of the gallbladder and hilar lymph nodes; (B) Started oral 5-FU (20 mg bid); (C) Infusion of red blood cells for anemia
	April	CT examination: gallbladder tumors and hilar lymph nodes showed liquefactive necrosis after treatment
	September 20–October 8	(A) Routine blood tests and tumor markers; (B) CT examination: gallbladder tumor invaded the descending duodenum; inferior vena cava was compressed; (C) Infusion of red blood cells for anemia
	October 24	(A) CT examination: gallbladder tumor enlarged, multiple spotted metastases found in the liver, and multiple lymph nodes around the pancreatic head; (B) Started hydrogen gas therapy
	November 26	(A) CT examination: gallbladder and intrahepatic tumors enlarged, duodenal bowel obstruction; (B) Gastrointestinal decompression and intravenous nutrition support
	December 10–24	(A) Routine blood tests and tumor markers; (B) Gastric tube removed, the patient gradually began taking semi-liquid food, and her spirit, appetite, and sleep were good
2019	January 8–11	(A) Routine blood tests and tumor markers; (B) CT examination: gallbladder and intrahepatic tumors, lymph nodes around the pancreatic head all shrank significantly, and obstruction was markedly relieved

CT: Computed tomography.

transaminase, total bilirubin, and gamma-glutamyl transpeptidase on multiple occasions during hydrogen treatment. Bone marrow hematopoietic function was evaluated based on peripheral blood erythrocyte counts and hemoglobin levels. Inflammation caused by infection was assessed based on white blood cell counts.

Curative evaluation

The curative effects of the treatment were evaluated according to several aspects of the patient's general condition. Since patients cannot eat normally, serum total protein and albumin levels were monitored after intravenous nutrition. Due to visceral adhesion, intestinal fistula and obstruction, degrees of pain and relief in the upper abdomen were recorded continuously. Absolute lymphocyte counts and serum tumor markers were measured to reflect changes in immune function and tumor activity.

CT imaging changes

Changes in CT tumor imaging were monitored to evaluate the curative effect of hydrogen gas therapy. According to the RECIST 1.1 guidelines[14], therapeutic effects are categorized as a complete response (CR), characterized as disappearance of tumor detection in all target lesions; partial response (PR), total reduction in the diameter of the target lesions ≥ 30%; stable disease (SD), tumor regression failing to reach PR or progressive disease (PD); or PD, defined as total progression of the tumor diameter ≥ 20%.

OUTCOME AND FOLLOW-UP

Hydrogen gas inhalation was started on October 24, 2018. Within 1 mo of treatment, the patient's condition was relatively stable, and her blood indexes, infection status,

and degree of pain gradually improved. Subsequently, intestinal obstruction occurred at the adhesion site between the gallbladder and duodenum; this was relieved after 1 mo of gastrointestinal decompression and intravenous nutrition. The patient insisted on regular hydrogen therapy throughout the course of this treatment.

Adverse events

The most common adverse reactions recorded included drowsiness or agitation, and no other adverse events were observed. The patient's transaminase levels remained normal throughout the treatment. Occasionally her bilirubin levels exceeded the reference range, but returned to normal after short-term use of hepatoprotective drugs. Despite regular blood transfusions, there was little change in the patient's red blood cell counts and hemoglobin levels during the two weeks before hydrogen treatment was initiated. Both indexes continued to increase after hydrogen therapy and blood transfusions, and both reached the lower limit of the reference range after 2.5 mo of treatment (Figure 1A). The frequency of transfusions was decreased gradually after hydrogen therapy and stopped completely after 2 mo of treatment.

Within 1 mo prior to treatment, the patient had a high inflammatory response to infection and a high white blood cell count (22.1×10^9/L). After anti-infection treatment, the white blood cell count was restored to the upper limit of the reference range (9.8×10^9/L), with no further reduction. After 1.5 mo of hydrogen treatment (with no further anti-infection treatment), the leukocyte count decreased to 4.7×10^9/L (Figure 1C left).

Curative evaluation

Serum total protein levels returned to normal shortly after the start of hydrogen therapy and continued to rise. Because of the intestinal obstruction, the patient received intravenous nutrition for 1-2 mo after treatment. Within 2 wk of the removal of the gastric tube, the patient returned to a normal diet and the total protein remained at the upper limit of the reference range. Serum albumin levels returned to normal after 2 mo of hydrogen therapy and continued to rise (Figure 1B).

Prior to hydrogen therapy, extensive adhesion and compression of gallbladder tumors caused severe pain in the upper abdomen that required daily pain medication; this was stopped when the pain gradually diminished after 2 wk of hydrogen treatment. Subsequent pain-induced administration of analgesics was not necessary, even during ileus.

T and NK cells are the major populations of lymphocytes that mediate anti-tumor immunity; therefore, the total number of lymphocytes is positively correlated with the immune function of patients. Before tumor recurrence and metastasis, the total number of lymphocytes continued to rise (1.2×10^9/L), indicating an increase in immune function. However, the total number of lymphocytes declined rapidly with tumor progression, to significantly below the reference range ($0.8-4 \times 10^9$/L), reaching a minimum (0.7×10^9/L) during intestinal obstruction (1.5 mo after hydrogen therapy). The lymphocyte numbers then rebounded, reaching 1×10^9/L after 2.5 mo of hydrogen treatment (Figure 1C right).

Before the detection of tumor recurrence (September 20, 2018), all three tumor markers were significantly higher than the reference range, but all showed a slight decline, which may be related to the compensation of immune function before treatment failure. After identification of tumor recurrence and metastasis, all three markers began to increase rapidly. This was consistent with the rapid growth of the tumor, which caused obstruction. After 1.5 mo of hydrogen therapy, the levels of all three markers began to decrease rapidly, falling into the reference ranges after 2.5 mo (Figure 2).

CT imaging changes

Before hydrogen gas treatment, the sum of the tumor diameters was 12.2 cm; 1 mo after treatment, the sum was 13.1 cm (37% increase, PD); and 2.5 mo after treatment, the sum was 7.5 cm (6% increase, SD) (Figure 3 and Table 2). At the end of February 2019, no tumor recurrence was detected (very similar to the CT examination at 2.5 mo; images not shown). To date, the patient appears completely well (Karnofsky score 100) and has resumed a normal diet and exercise.

DISCUSSION

In GBC patients who are not candidates for surgery, the NCCN guidelines recommend the use of chemotherapy and best supportive care. Due to the large size of tumor in this patient (stage IIIA), the gallbladder function was completely lost with widespread adhesions to the hilum of the liver. Therefore, it was necessary to choose
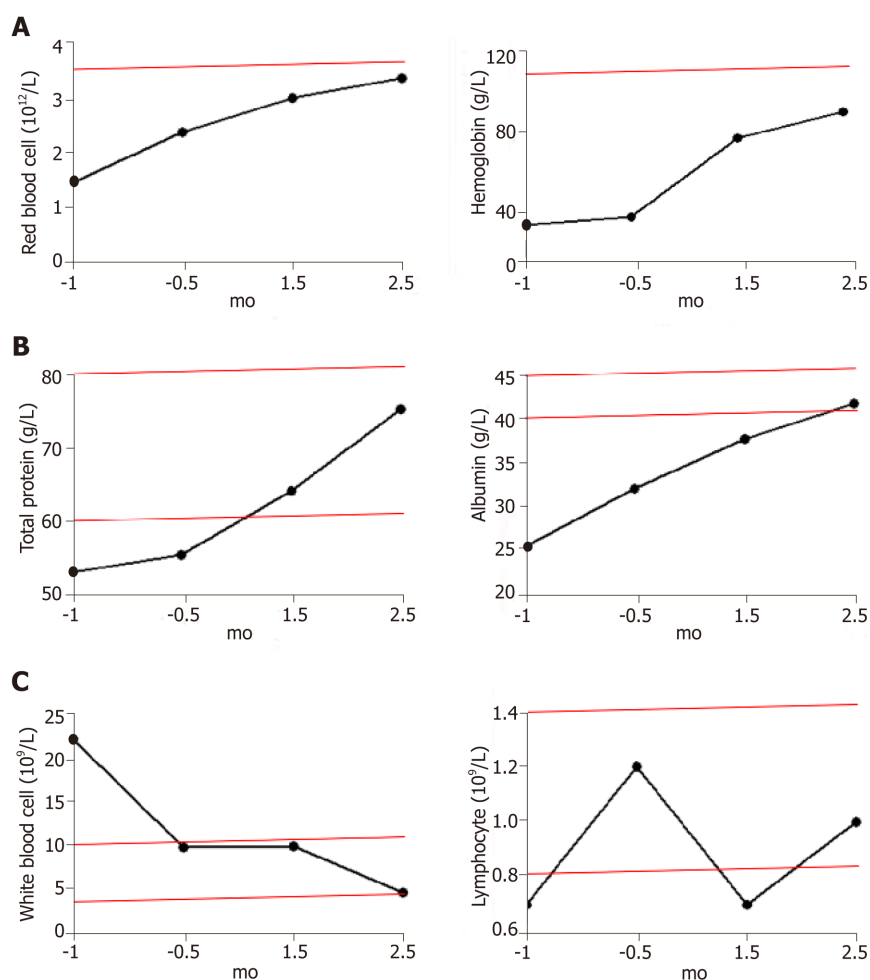
Figure 1 Blood parameters of patients before and after hydrogen treatment. A: Red blood cell counts and hemoglobin levels; the red line in the figures represents the lower limit of the reference range; B: Total protein and albumin concentrations; the red lines in the figures represent the reference range; C: White blood cell and lymphocyte counts; the red lines in the figures represent the reference range.

an ablation method that causes minimal damage to the extrahepatic bile duct system in reducing the tumor size. IRE is a novel ablation technology that utilizes short pulses of high voltage electrical energy to induce tissue necrosis. This technique has many advantages, including short ablation time, preservation of the internal structure of vital organs, and lack of the heat/cold-sink effect[15]. We have previously verified the safety and efficacy of gallbladder ablation in a rabbit model[16]. Although not yet included in the NCCN guidelines, IRE has the potential to be a superior alternative to other ablation techniques for the removal of tumors situated near the gallbladder[17-19].

IRE, combined with oral chemotherapy, effectively controlled the tumors in the gallbladder and the hilar part of the liver, and re-examination after 3 mo of treatment showed that the tumor was basically necrotic. However, for this patient with advanced GBC, palliative treatment could only delay the disease, with continued slow progression of the tumor. In the re-examination after 9 mo of treatment, recurrence of the gallbladder tumor, duodenum fistula, liver metastases, and lymph node metastases around the head of pancreas as well as severe anemia were detected, which indicated that the disease had entered a stage of rapid and life-threatening progression in a short period of time. Best supportive care was the only option at this timepoint, although in general, it is not possible to reverse the progression of such tumors.

Molecular hydrogen, or H_2, can selectively neutralize hydroxyl radicals, but not other reactive oxygen species (ROS)[20]. Hydrogen has been used to treat various states associated with oxidative stress, including trauma[21], neurodegenerative disease[22], inflammatory disease[23], metabolic syndrome[24], adverse reactions to chemotherapy[25], and radiation injury[26]. In addition to the apparent improvement in the immune system[12], there is much evidence that hydrogen directly kills different types of tumors, including cutaneous squamous cell carcinoma[27], leukemia[28], tongue
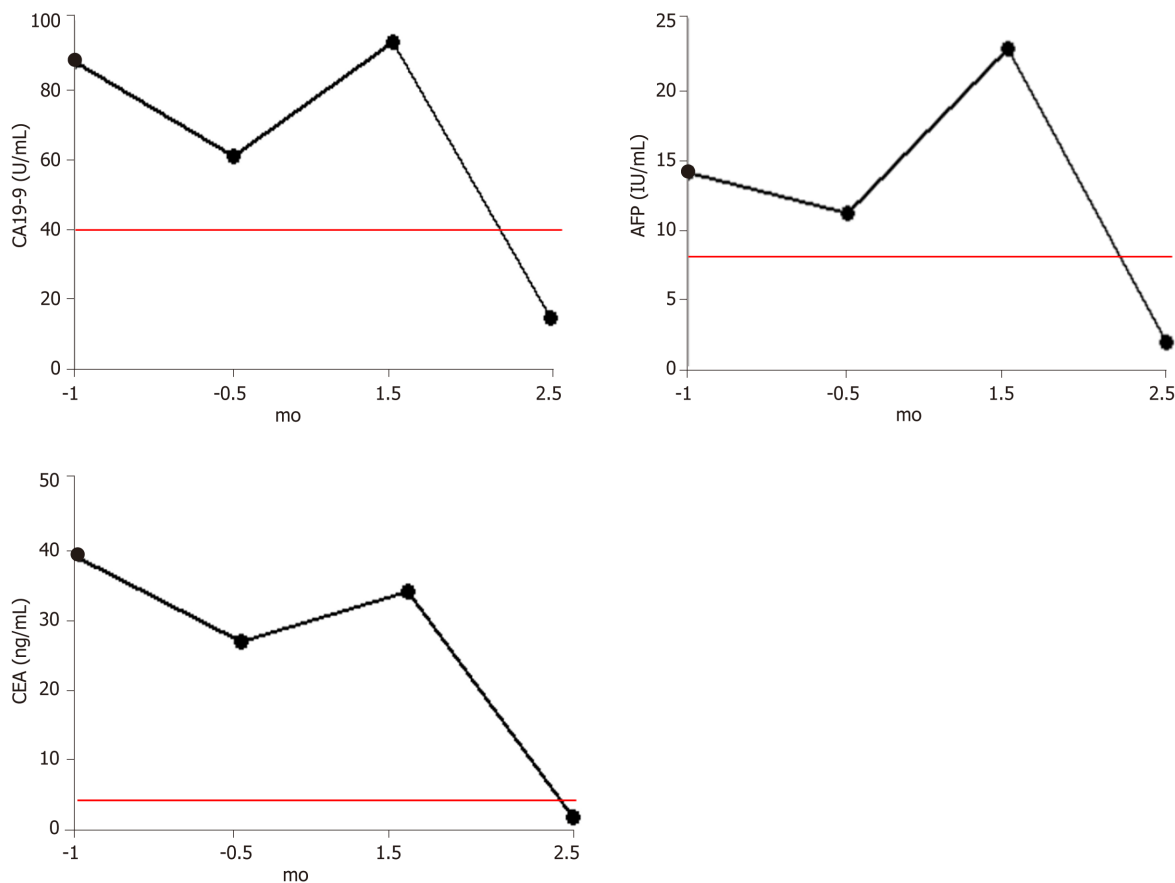
Figure 2 Changes in tumor markers before and after hydrogen treatment. The red lines in the figures represent the upper limit of the reference ranges.

cancer[29,30], and colon cancer[8]. Since there has been no report on the upper limit of hydrogen use, this therapy might be a very safe method.

At the same time as the delivery of optimal supportive care, the patient was enrolled in this clinical study (24 October 2018) with the intention of improving clinical symptoms. One month after the start of hydrogen therapy, the disease continued to progress, and the levels of tumor markers (including CA19-9, AFP, and CEA) continued to rise, although the patient's general status and blood indexes (including total protein, albumin, multiple blood cells count, hemoglobin content, *etc.*) showed continuous improvement, so the patient persisted with the hydrogen treatment. Gradually, the levels of multiple tumor markers began to decline, and multiple hematological indicators continued to improve. The patient underwent gastric tube removal on December 24, and gradually began eating semi-liquid food, with significant improvement in spirit, appetite, and sleep. Subsequent CT examination also confirmed relief of the obstruction, with significant shrinkage of tumors at multiple sites. The reason for the patient's extraordinary recovery, apart from symptomatic treatment, is probably because the persistence of hydrogen therapy; this therapy not only mediates rapid improvement in the physical condition of the patient, but also significantly reduces tumor marker levels, increases lymphocyte counts, and even induces tumor shrinkage.

At present, there is only a temporal connection between hydrogen and improvement of this patient's cancer. The proposed mechanism underlying the anti-cancer properties of hydrogen may involve: (1) Elimination of the high levels of ROS produced by cancer cells, thus inhibiting the proliferation, invasion, and migration of cancer cells[31]; (2) Downregulation of inflammatory factors, elimination of chronic inflammation, and modification of the microenvironment[32]; (3) Protection of mitochondria, which maintains energy generation and help correct hypoxia, thereby transforming the cardiovascular, endocrine, and nervous systems[11]; and (4) Restoration of the function of exhausted cytotoxic T cells, and enhancement of systemic anti-cancer effects[33]. The detailed mechanism remains to be fully elucidated in further follow-up studies, and indications for advanced cancer therapy require verification in studies with greater numbers of patients.

Table 2 Tumor sizes before and after hydrogen gas treatment

	Gallbladder	Liver metastases	Lymph node around the pancreas head	Sum of the tumor diameters
Pretreatment	6.3 cm × 4.9 cm	3.2 cm × 2.6 cm	2.7 cm × 2.1 cm	12.2 cm
1 mo after treatment	6.7 cm × 6.3 cm	4.2 cm × 4.0 cm (large) 3.6 cm × 3.2 cm (small)	2.2 cm × 1.8 cm	16.7 cm
2.5 mo after treatment	3.7 cm × 3.6 cm	4.0 cm × 3.3 cm (large) 3.2 cm × 2.8 cm (small)	2.0 cm × 1.6 cm	12.9 cm

CONCLUSION

This is the first report on the rehabilitation of an advanced GBC patient with a critical general condition, whose disease has gradually improved and has survived for more than 4 mo.
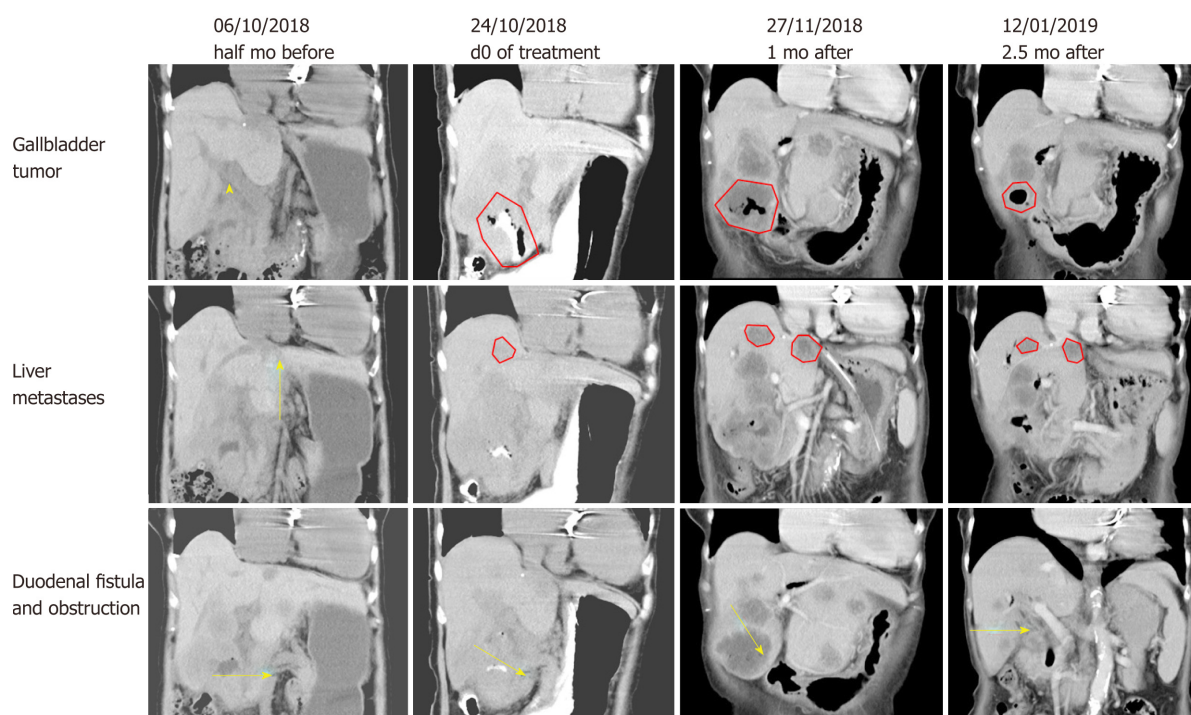
Figure 3 Computed tomography imaging findings at different time points before and after hydrogen treatment. In the first line of figures, the triangle and the contour lines represent the location and range of the gallbladder. In the second line of figures, the contour lines represent the location and range of liver metastases. In the third line of figures, the arrows represent the location of the duodenal fistula or obstruction.

REFERENCES

1   **Chen W**, Zheng R, Baade PD, Zhang S, Zeng H, Bray F, Jemal A, Yu XQ, He J. Cancer statistics in China, 2015. *CA Cancer J Clin* 2016; **66**: 115-132 [PMID: 26808342 DOI: 10.3322/caac.21338]

2   **Shi JS**, Wang JS, Liu G, Yu YL, Lu Y, Jiao XY, Yang YJ, Li GC, Han Y. Early diagnosis of primary gallbladder carcinoma. *Hepatobiliary Pancreat Dis Int* 2002; **1**: 273-275 [PMID: 14612283]

3   **Hueman MT**, Vollmer CM, Pawlik TM. Evolving treatment strategies for gallbladder cancer. *Ann Surg Oncol* 2009; **16**: 2101-2115 [PMID: 19495882 DOI: 10.1245/s10434-009-0538-x]

4   **Hundal R**, Shaffer EA. Gallbladder cancer: epidemiology and outcome. *Clin Epidemiol* 2014; **6**: 99-109 [PMID: 24634588 DOI: 10.2147/CLEP.S37357]

5   **Barber DL**, Wherry EJ, Masopust D, Zhu B, Allison JP, Sharpe AH, Freeman GJ, Ahmed R. Restoring function in exhausted CD8 T cells during chronic viral infection. *Nature* 2006; **439**: 682-687 [PMID: 16382236 DOI: 10.1038/nature04444]

6   **Wherry EJ**. T cell exhaustion. *Nat Immunol* 2011; **12**: 492-499 [PMID: 21739672 DOI: 10.1038/ni.2035]

7   **Ge L**, Yang M, Yang NN, Yin XX, Song WG. Molecular hydrogen: a preventive and therapeutic medical gas for various diseases. *Oncotarget* 2017; **8**: 102653-102673 [PMID: 29254278 DOI: 10.18632/oncotar-get.21130]

8   **Runtuwene J**, Amitani H, Amitani M, Asakawa A, Cheng KC, Inui A. Hydrogen-water enhances 5-fluorouracil-induced inhibition of colon cancer. *PeerJ* 2015; **3**: e859 [PMID: 25870767 DOI: 10.7717/peerj.859]

9   **Wang D**, Wang L, Zhang Y, Zhao Y, Chen G. Hydrogen gas inhibits lung cancer progression through targeting SMC3. *Biomed Pharmacother* 2018; **104**: 788-797 [PMID: 29852353 DOI: 10.1016/j.biopha.2018.05.055]

10 **Kamimura N**, Ichimiya H, Iuchi K, Ohta S. Molecular hydrogen stimulates the gene expression of transcriptional coactivator PGC-1α to enhance fatty acid metabolism. *NPJ Aging Mech Dis* 2016; **2**: 16008 [PMID: 28721265 DOI: 10.1038/npjamd.2016.8]

11 **Handschin C**, Spiegelman BM. Peroxisome proliferator-activated receptor gamma coactivator 1 coactivators, energy homeostasis, and metabolism. *Endocr Rev* 2006; **27**: 728-735 [PMID: 17018837 DOI: 10.1210/er.2006-0037]

12 **Akagi J**, Baba H. Hydrogen gas restores exhausted CD8+ T cells in patients with advanced colorectal cancer to improve prognosis. *Oncol Rep* 2019; **41**: 301-311 [PMID: 30542740 DOI: 10.3892/or.2018.6841]

13 **Basch E**, Reeve BB, Mitchell SA, Clauser SB, Minasian LM, Dueck AC, Mendoza TR, Hay J, Atkinson TM, Abernethy AP, Bruner DW, Cleeland CS, Sloan JA, Chilukuri R, Baumgartner P, Denicoff A, St Germain D, O'Mara AM, Chen A, Kelaghan J, Bennett AV, Sit L, Rogak L, Barz A, Paul DB, Schrag D. Development of the National Cancer Institute's patient-reported outcomes version of the common terminology criteria for adverse events (PRO-CTCAE). *J Natl Cancer Inst* 2014; **106** [PMID: 25265940 DOI: 10.1093/jnci/dju244]

14 **Eisenhauer EA**, Therasse P, Bogaerts J, Schwartz LH, Sargent D, Ford R, Dancey J, Arbuck S, Gwyther S, Mooney M, Rubinstein L, Shankar L, Dodd L, Kaplan R, Lacombe D, Verweij J. New response evaluation criteria in solid tumours: revised RECIST guideline (version 1.1). *Eur J Cancer* 2009; **45**: 228-247 [PMID: 19097774 DOI: 10.1016/j.ejca.2008.10.026]

15   **Wagstaff PG**, Buijs M, van den Bos W, de Bruin DM, Zondervan PJ, de la Rosette JJ, Laguna Pes MP. Irreversible electroporation: state of the art. *Onco Targets Ther* 2016; **9**: 2437-2446 [PMID: 27217767 DOI: 10.2147/OTT.S88086]

16   **Zeng J**, Qin Z, Zhou L, Fang G, Chen J, Li J, Niu L, Liang B, Xu K. Comparison between cryoablation and irreversible electroporation of rabbit livers at a location close to the gallbladder. *Radiol Oncol* 2017; **51**: 40-46 [PMID: 28265231 DOI: 10.1515/raon-2017-0003]

17   **Chen X**, Ren Z, Zhu T, Zhang X, Peng Z, Xie H, Zhou L, Yin S, Sun J, Zheng S. Electric Ablation with Irreversible Electroporation (IRE) in Vital Hepatic Structures and Follow-up Investigation. *Sci Rep* 2015; **5**: 16233 [PMID: 26549662 DOI: 10.1038/srep16233]

18   **Herwald SE**, Chen JH, Arellano RS. Irreversible Electroporation for Treatment of Hepatocellular Carcinoma Adjacent to the Gallbladder. *J Vasc Interv Radiol* 2016; **27**: 1093-1094 [PMID: 27338501 DOI: 10.1016/j.jvir.2016.03.008]

19   **Siddiqui IA**, Kirks RC, Latouche EL, DeWitt MR, Swet JH, Baker EH, Vrochides D, Iannitti DA, Davalos RV, McKillop IH. High-Frequency Irreversible Electroporation: Safety and Efficacy of Next-Generation Irreversible Electroporation Adjacent to Critical Hepatic Structures. *Surg Innov* 2017; **24**: 276-283 [PMID: 28492356 DOI: 10.1177/1553350617692202]

20   **Ohsawa I**, Ishikawa M, Takahashi K, Watanabe M, Nishimaki K, Yamagata K, Katsura K, Katayama Y, Asoh S, Ohta S. Hydrogen acts as a therapeutic antioxidant by selectively reducing cytotoxic oxygen radicals. *Nat Med* 2007; **13**: 688-694 [PMID: 17486089 DOI: 10.1038/nm1577]

21   **Ji X**, Tian Y, Xie K, Liu W, Qu Y, Fei Z. Protective effects of hydrogen-rich saline in a rat model of traumatic brain injury via reducing oxidative stress. *J Surg Res* 2012; **178**: e9-16 [PMID: 22475349 DOI: 10.1016/j.jss.2011.12.038]

22   **Chen T**, Tao Y, Yan W, Yang G, Chen X, Cao R, Zhang L, Xue J, Zhang Z. Protective effects of hydrogen-rich saline against N-methyl-N-nitrosourea-induced photoreceptor degeneration. *Exp Eye Res* 2016; **148**: 65-73 [PMID: 27215478 DOI: 10.1016/j.exer.2016.05.017]

23   **Ren JD**, Ma J, Hou J, Xiao WJ, Jin WH, Wu J, Fan KH. Hydrogen-rich saline inhibits NLRP3 inflammasome activation and attenuates experimental acute pancreatitis in mice. *Mediators Inflamm* 2014; **2014**: 930894 [PMID: 25214720 DOI: 10.1155/2014/930894]

24   **Nakao A**, Toyoda Y, Sharma P, Evans M, Guthrie N. Effectiveness of hydrogen rich water on antioxidant status of subjects with potential metabolic syndrome-an open label pilot study. *J Clin Biochem Nutr* 2010; **46**: 140-149 [PMID: 20216947 DOI: 10.3164/jcbn.09-100]

25   **Kikkawa YS**, Nakagawa T, Taniguchi M, Ito J. Hydrogen protects auditory hair cells from cisplatin-induced free radicals. *Neurosci Lett* 2014; **579**: 125-129 [PMID: 25064701 DOI: 10.1016/j.neulet.2014.07.025]

26   **Watanabe S**, Fujita M, Ishihara M, Tachibana S, Yamamoto Y, Kaji T, Kawauchi T, Kanatani Y. Protective effect of inhalation of hydrogen gas on radiation-induced dermatitis and skin injury in rats. *J Radiat Res* 2014; **55**: 1107-1113 [PMID: 25034733 DOI: 10.1093/jrr/rru067]

27   **Dole M**, Wilson FR, Fife WP. Hyperbaric hydrogen therapy: a possible treatment for cancer. *Science* 1975; **190**: 152-154 [PMID: 1166304 DOI: 10.1126/science.1166304]

28   **Roberts BJ**, Fife WP, Corbett TH, Schabel FM. Response of five established solid transplantable mouse tumors and one mouse leukemia to hyperbaric hydrogen. *Cancer Treat Rep* 1978; **62**: 1077-1079 [PMID: 99233]

29   **Saitoh Y**, Okayasu H, Xiao L, Harata Y, Miwa N. Neutral pH hydrogen-enriched electrolyzed water achieves tumor-preferential clonal growth inhibition over normal cells and tumor invasion inhibition concurrently with intracellular oxidant repression. *Oncol Res* 2008; **17**: 247-255 [PMID: 19192719 DOI: 10.3727/096504008786991620]

30   **Saitoh Y**, Yoshimura Y, Nakano K, Miwa N. Platinum nanocolloid-supplemented hydrogendissolved water inhibits growth of human tongue carcinoma cells preferentially over normal cells. *Exp Oncol* 2009; **31**: 156-162 [PMID: 19783965]

31   **Yang Y**, Zhu Y, Xi X. Anti-inflammatory and antitumor action of hydrogen via reactive oxygen species. *Oncol Lett* 2018; **16**: 2771-2776 [PMID: 30127861 DOI: 10.3892/ol.2018.9023]

32   **Huang L**. Molecular hydrogen: a therapeutic antioxidant and beyond. *Med Gas Res* 2016; **6**: 219-222 [PMID: 28217294 DOI: 10.4103/2045-9912.196904]

33   **Hu Z**, Wu B, Meng F, Zhou Z, Lu H, Zhao H. Impact of molecular hydrogen treatments on the innate immune activity and survival of zebrafish (Danio rerio) challenged with Aeromonas hydrophila. *Fish Shellfish Immunol* 2017; **67**: 554-560 [PMID: 28630014 DOI: 10.1016/j.fsi.2017.05.066]

CASE REPORT

Giant nonfunctional ectopic adrenocortical carcinoma on the anterior abdominal wall: A case report

Dong-Kai Zhou, Zheng-Hao Liu, Bing-Qiang Gao, Wei-Lin Wang

ORCID number: Dong-Kai Zhou (0000-0003-0705-9796); Zheng-Hao Liu (0000-0002-2748-0775); Bing-Qiang Gao (0000-0002-1265-0217); Wei-Lin Wang (0000-0001-9432-2649).

Dong-Kai Zhou, Zheng-Hao Liu, Bing-Qiang Gao, Wei-Lin Wang, Department of Hepatobiliary and Pancreatic Surgery, The Second Affiliated Hospital, School of Medicine, Zhejiang University, Hangzhou 310003, Zhejiang Province, China

Dong-Kai Zhou, Zheng-Hao Liu, Bing-Qiang Gao, Wei-Lin Wang, Key Laboratory of Precision Diagnosis and Treatment for Hepatobiliary and Pancreatic Tumor of Zhejiang Province, The First Affiliated Hospital, School of Medicine, Zhejiang University, Hangzhou 310003, Zhejiang Province, China

Dong-Kai Zhou, Zheng-Hao Liu, Bing-Qiang Gao, Wei-Lin Wang, Clinical Research Center of Hepatobiliary and Pancreatic Diseases of Zhejiang Province, The First Affiliated Hospital, School of Medicine, Zhejiang University, Hangzhou 310003, Zhejiang Province, China

Corresponding author: Wei-Lin Wang, MD, PhD, Doctor, Department of Hepatobiliary and Pancreatic Surgery, The Second Affiliated Hospital, School of Medicine, Zhejiang University, No.88 Jiefang Road, Hangzhou 310003, Zhejiang Provine, China. wam@zju.edu.cn
Telephone: +86-571-87315003
Fax: +86-571-87022776

Abstract

BACKGROUND
Adrenocortical cancer (ACC) is an infrequent and often aggressive malignancy with a very poor prognosis. It can be classified as functional or nonfunctional. Nonfunctional ACC is hampered by the absence of specific signs or symptoms; only abdominal pain with or without incidental adrenal occupation is typically present.

CASE SUMMARY
We report a rare case of a patient with a 30 cm × 15 cm × 8 cm ectopic ACC on the anterior abdominal wall without organ adhesion. A 77-year-old male was admitted to our hospital because of a huge abdominal mass, which, by ultrasonography, had an unclear border with the liver. Computed tomography showed that the mass was not associated with any organ but was adherent to the anterior abdominal wall. The patient underwent tumor resection, and a postoperative pathology examination showed a neuroendocrine tumor, which was diagnosed as ACC. The patient was disease-free at the 9-mo follow up.

CONCLUSION
The anterior abdominal wall is a rare site of ACC growth.

Key words: Adrenocortical carcinoma; Nonfunctional; Ectopic; Abdominal wall; Case

report

Core tip: Aberrant adrenal tissue can be found anywhere, but typically in the testes, ovaries, spermatic cord, and kidneys. The most common site is retroperitoneal fat near the adrenal gland; the bilateral lungs, liver, spleen, pancreas, colon, duodenum, and ovary are less common. This is, to our knowledge, the first report of adrenocortical cancer on the anterior abdominal wall in the English-language literature.

INTRODUCTION

Adrenocortical cancer (ACC) is an infrequent and often aggressive malignancy with a very poor prognosis. According to the Surveillance, Epidemiology and End Results database, ACC has an annual incidence of 0.7-2 per million population[1] and a bimodal age distribution with peaks before 5 years of age and at 40-60 years of age[2].

ACC can be classified as functional or nonfunctional. The early diagnosis and treatment of nonfunctional ACC is hampered by the absence of specific signs or symptoms; only abdominal pain with or without incidental adrenal occupation is typically present. Based on its cost-effectiveness, the American Association of Clinical Endocrinologists guidelines recommend surgery for nonfunctional ACC lesions ≥ 4 cm in diameter[3]. Here, we report the case of a patient with ACC on the abdominal wall. The patient underwent tumor resection and was disease-free at the 9-mo follow up.

CASE PRESENTATION

Chief complaints

A 77-year-old male (body mass index, 24.5 kg/m^2), who 9 mo previously had been admitted to our hepatological surgery department, presented with an enormous exogenous liver occupation that had been detected by ultrasonography in a community hospital 2 d prior. He denied having abdominal pain, nausea, anorexia, or changes in bowel habit.

History of present illness

The patient had no clinical symptoms associated with steroid excess, except for hypertension. He was admitted to our department for diagnosis.

History of past illness

The patient had suffered from hypertension for 40 years but did not have diabetes or cardiovascular disease.

Personal and family history

His medical history and family history were unremarkable.

Physical examination

The results of a physical examination were unremarkable, except for a palpable hard mass and slight tenderness in the hepatic region.

Laboratory examinations

The results of laboratory tests were as follows: CA199, 112.0 U/mL (reference < 37.0 U/mL); alpha fetoprotein, 1.4 ng/mL (reference < 20.0 ng/mL); alanine transaminase, 89 U/L (reference < 35.0 U/L); aspartate transaminase, 49 U/L (reference < 40 U/L); and serum potassium, 4.40 mmol/L (reference 3.50-5.20 mmol/L). The results of the endocrine work-up were negative.

Imaging examinations

Ultrasonography revealed an enormous space-occupying lesion in the right upper abdomen, in which Color Doppler flow imaging showed a small amount of blood flow (Figure 1A). A left-hepatic origin was considered, but contrast-enhanced computed tomography (CT) showed an irregular fat-containing mass in the right upper abdominal cavity of uneven density with an obscure boundary (Figure 1B). The tumor exhibited heterogeneous enhancement in the arterial phase (Figure 1C) and delayed enhancement in the venous phase (Figure 1D).

TREATMENT

A laparotomy was performed. During surgery, a 30 cm × 15 cm × 8 cm tumor was found above the hepatic curvature of the colon in front of the right posterior peritoneum (Figure 2). The liver, pancreas, stomach, colon, and adrenal gland were not infringed, and there was no lymph-node metastasis. The tumor had invaded the local right-abdominal musculature.

FINAL DIAGNOSIS

A postoperative pathology examination indicated that the tumor was hypo-differentiated carcinoma with neuroendocrinalization and so was considered to be ACC. A histopathology examination showed a Weiss score of 6, as cells were distributed in sheets and wide bands, and extensive necrosis was present. The cytoplasm was eosinophilic, the karyotype was irregular, and giant neoplastic cells were present (Figure 3A). The Ki-67 labeling index was > 80% (Figure 3B), and the tumor cells were positive for melan A, vimentin, synaptophysin (Figure 3C-E), CK20, insulin-like growth factor-2 (IGF-2), and EMA; and negative for CK (pan), inhibin a, CgA, and S-100.

OUTCOME AND FOLLOW-UP

The patient underwent regular follow ups involving a physical examination, laboratory testing, and X-ray and CT imaging. He was disease-free at the 9-mo follow up.

DISCUSSION

ACC is a rare malignancy, accounting for about 0.05%-0.2% of all malignant tumors, and has an annual incidence of 1–2 per million[4]. Ectopic adrenal tissue is commonly found in infants and children, but it is less common in adults[5]. ACC is the second most aggressive malignant endocrine tumor after anaplastic thyroid cancer[6]. Aberrant adrenal tissue can be found anywhere, but typically in the testes, ovaries, spermatic cord, and kidneys[6]. The most common site is retroperitoneal fat near the adrenal gland[7,8]; the bilateral lungs[9], liver[7], spleen[8], pancreas[8], colon[8], duodenum[8], and ovary[6] are less common. This is, to our knowledge, the first report of ACC on the anterior abdominal wall in the English-language literature.

The clinical symptoms of primary ACC are dependent on the functional state and volume of the tumor. Around half of patients with ACC are asymptomatic or have symptoms caused by mechanical effects of tumor growth[2], such as abdominal pain, nausea, poor appetite, and back pain[1]. The other half of patients with ACC have symptoms related to elevated levels of steroid hormones-Cushing syndrome, Con syndrome, and feminization. ACC lesions are typically large as they grow rapidly; most are 10-13 cm in diameter, 9%-14% are < 6 cm, and 3% are < 4 cm[1,10,11]. Generally, nonfunctional ACC lesions are small; large nonfunctional ACC lesions are very rare[12].

The pathogenesis of ACC is unclear but is likely to involve IGF-2, tumor protein 53, and β-catenin. ACC can be diagnosed with 100% specificity and 96% sensitivity based on the levels of IGF-2 and Ki-67[13].

Imaging (magnetic resonance imaging or CT) is crucial for identifying adrenal involvement in ACC. In general, ACC is a non-homogeneous tumor with hemorrhage or necrosis and an irregular margin. Nuclear aberrations-comprising a high mitotic count, high nuclear grade, and bizarre mitotic figures—are characteristic histological findings of ACC[13].
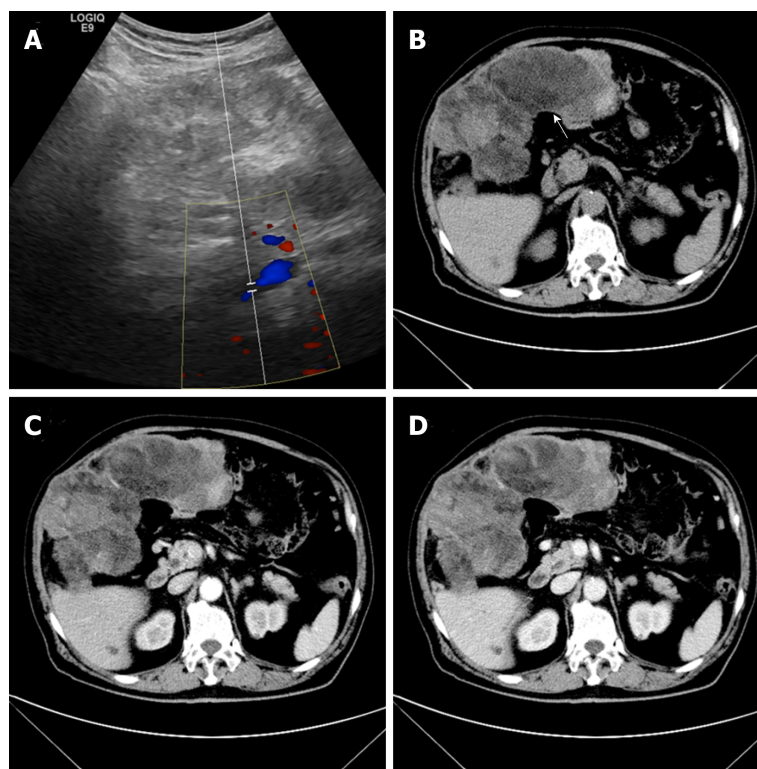
Figure 1 Imaging diagnosis. A: Color Doppler image showing blood flow; B: Computed tomography with contrast (white arrow, fat density); C: Uneven heterogeneous enhancement in the arterial phase; D: Delayed enhancement in the venous phase.

Complete surgical resection is the only potentially curative therapy for ACC; And it is equally important to choose surgical indications according to the latest guidelines for the surgeon[14]. Indeed, complete resection is the most accurate predictor of the outcome. Paton *et al*[11] reported that patients who have complete resection have a higher 5-year survival rate than those who have incomplete resection. In the retrospective study of Terzolo *et al*[15], use of mitotane as adjunct therapy reduced the rates of recurrence and mortality, as did etoposide, doxorubicin and cisplatin plus mitotane, streptozotocin plus mitotane, and gemcitabine plus capecitabine[1,16].

The 5-year overall survival rate of patients with ACC is 37%-47%[1]. For advanced ACC, (*i.e.*, stage III tumor), the mENS®T TNM classification - which comprises the "GRAF" components: grade (G), resection status (R), age (A), and functioning symptoms at diagnosis (defined as tumor or hormone-related symptoms) (F) - is recommended[17]. Rupture of the tumor capsule, metastasis, and a high Ki67 index are associated with reduced disease-free and overall survival.

CONCLUSION

ACC is rare and has a poor prognosis. The 5-year overall survival rate of patients with ACC is 37%-47%, and resection is the optimum treatment modality. We describe a case of a patient with ectopic adrenocortical carcinoma on the anterior abdominal wall and our patient was disease-free at 9 mo after resection of the tumor.
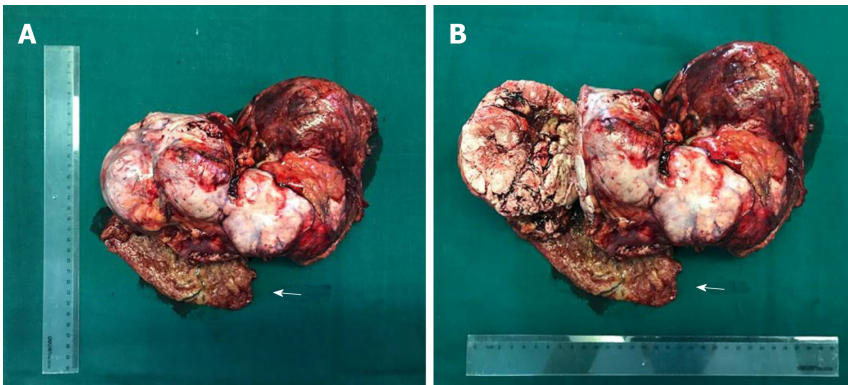
Figure 2 The 30 cm × 15 cm × 8 cm heterogeneous tumor with necrosis (A, B). Arrows invaded abdominal wall tissue.
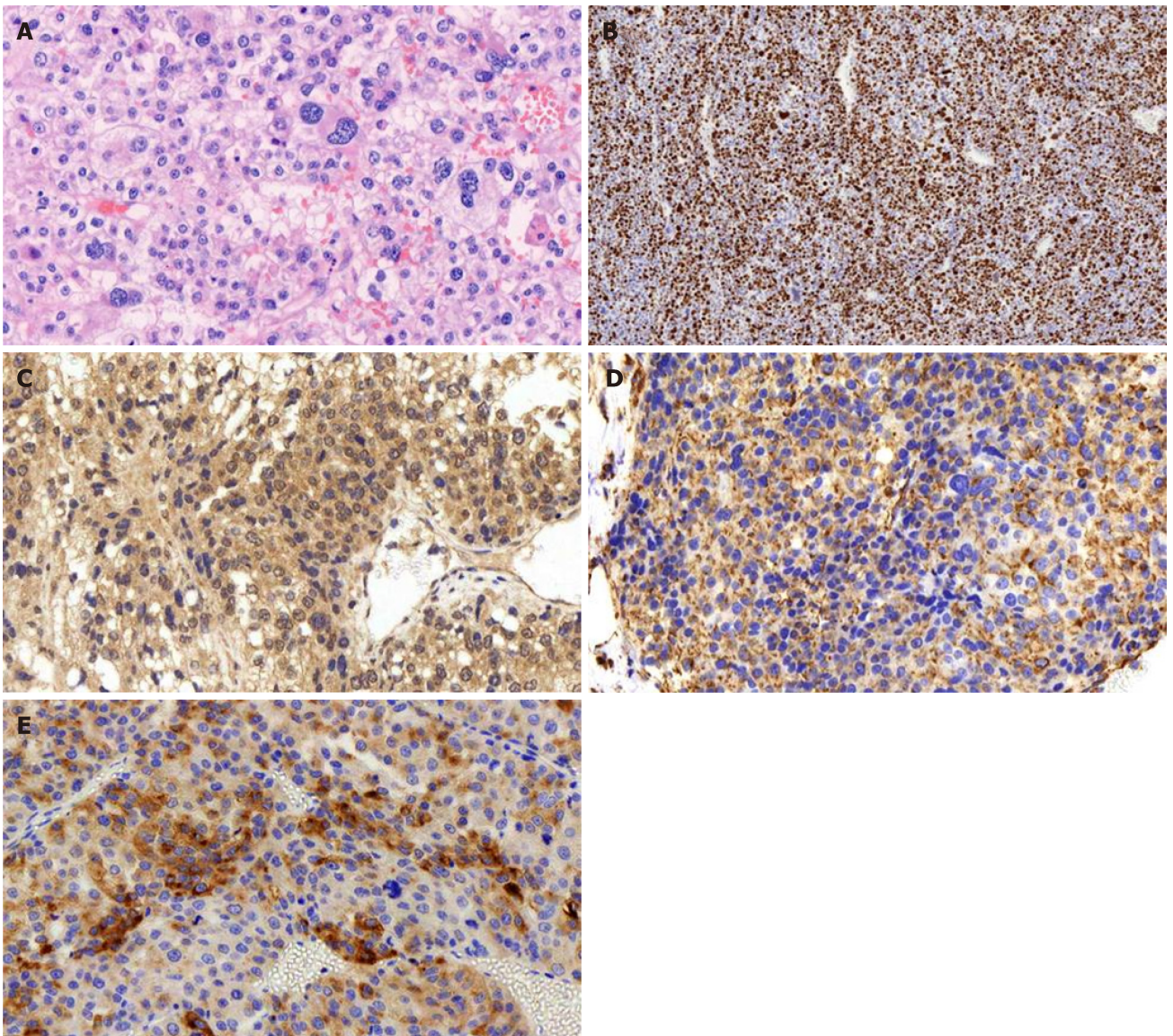
Figure 3 Histological staining. A: Histological staining showing significant nuclear atypia, necrosis, and pleomorphism of the tumor cells (magnification, 200×); B: The Ki-67 labeling index was > 80% (IHC staining; magnification, 50×); C-D: Positive IHC staining for (C) melan-A, (D) vimentin and (E) synaptophysin (magnification, 200×).

REFERENCES

1   **Fassnacht M**, Libé R, Kroiss M, Allolio B. Adrenocortical carcinoma: a clinician's update. *Nat Rev Endocrinol* 2011; **7**: 323-335 [PMID: 21386792 DOI: 10.1038/nrendo.2010.235]

2   **Lam AK**. Update on Adrenal Tumours in 2017 World Health Organization (WHO) of Endocrine Tumours. *Endocr Pathol* 2017; **28**: 213-227 [PMID: 28477311 DOI: 10.1007/s12022-017-9484-5]

3   **Wang TS**, Cheung K, Roman SA, Sosa JA. A cost-effectiveness analysis of adrenalectomy for nonfunctional adrenal incidentalomas: is there a size threshold for resection? *Surgery* 2012; **152**: 1125-1132 [PMID: 22989893 DOI: 10.1016/j.surg.2012.08.011]

4   **Libé R**. Adrenocortical carcinoma (ACC): diagnosis, prognosis, and treatment. *Front Cell Dev Biol* 2015; **3**: 45 [PMID: 26191527 DOI: 10.3389/fcell.2015.00045]

5   **Ayala AR**, Basaria S, Udelsman R, Westra WH, Wand GS. Corticotropin-independent Cushing's syndrome caused by an ectopic adrenal adenoma. *J Clin Endocrinol Metab* 2000; **85**: 2903-2906 [PMID: 10946901 DOI: 10.1210/jcem.85.8.6749]

6   **Chentli F**, Terki N, Azzoug S. Ectopic adrenocortical carcinoma located in the ovary. *Eur J Endocrinol* 2016; **175**: K17-K23 [PMID: 27523914 DOI: 10.1530/EJE-16-0224]

7   **Park WY**, Seo HI, Choi KU, Kim A, Kim YK, Lee SJ, Lee CH, Huh GY, Park DY. Three cases of adrenocortical tumors mistaken for hepatocellular carcinomas/diagnostic pitfalls and differential diagnosis. *Ann Diagn Pathol* 2017; **31**: 9-13 [PMID: 29146062 DOI: 10.1016/j.anndiagpath.2017.05.016]

8   **Marincola Smith P**, Kiernan CM, Tran TB, Postlewait LM, Maithel SK, Prescott J, Pawlik T, Wang TS, Glenn J, Hatzaras I, Shenoy R, Phay J, Shirley LA, Fields RC, Jin L, Weber S, Salem A, Sicklick J, Gad S, Yopp A, Mansour J, Duh QY, Seiser N, Votanopoulos K, Levine EA, Poultsides G, Solórzano CC. Role of Additional Organ Resection in Adrenocortical Carcinoma: Analysis of 167 Patients from the U.S. Adrenocortical Carcinoma Database. *Ann Surg Oncol* 2018; **25**: 2308-2315 [PMID: 29868977 DOI: 10.1245/s10434-018-6546-y]

9   **Arora S**, Damle NA, Aggarwal S, Passah A, Behera A, Arora G, Bal C, Tripathi M. Prostate-Specific Membrane Antigen Expression in Adrenocortical Carcinoma on 68Ga-Prostate-Specific Membrane Antigen PET/CT. *Clin Nucl Med* 2018; **43**: 449-451 [PMID: 29578871 DOI: 10.1097/RLU.0000000000002064]

10   **Sturgeon C**, Shen WT, Clark OH, Duh QY, Kebebew E. Risk assessment in 457 adrenal cortical carcinomas: how much does tumor size predict the likelihood of malignancy? *J Am Coll Surg* 2006; **202**: 423-430 [PMID: 16500246 DOI: 10.1016/j.jamcollsurg.2005.11.005]

11   **Paton BL**, Novitsky YW, Zerey M, Harrell AG, Norton HJ, Asbun H, Kercher KW, Heniford BT. Outcomes of adrenal cortical carcinoma in the United States. *Surgery* 2006; **140**: 914-20; discussion 919-20 [PMID: 17188138 DOI: 10.1016/j.surg.2006.07.035]

12   **Tauchmanovà L**, Colao A, Marzano LA, Sparano L, Camera L, Rossi A, Palmieri G, Marzano E, Salvatore M, Pettinato G, Lombardi G, Rossi R. Andrenocortical carcinomas: twelve-year prospective experience. *World J Surg* 2004; **28**: 896-903 [PMID: 15593464 DOI: 10.1007/s00268-004-7296-5]

13   **Lerario AM**, Moraitis A, Hammer GD. Genetics and epigenetics of adrenocortical tumors. *Mol Cell Endocrinol* 2014; **386**: 67-84 [PMID: 24220673 DOI: 10.1016/j.mce.2013.10.028]

14   **Isik A**, Firat D, Yilmaz I, Peker K, Idiz O, Yilmaz B, Demiryilmaz I, Celebi F. A survey of current approaches to thyroid nodules and thyroid operations. *Int J Surg* 2018; **54**: 100-104 [PMID: 29709542 DOI: 10.1016/j.ijsu.2018.04.037]

15   **Terzolo M**, Angeli A, Fassnacht M, Daffara F, Tauchmanova L, Conton PA, Rossetto R, Buci L, Sperone P, Grossrubatscher E, Reimondo G, Bollito E, Papotti M, Saeger W, Hahner S, Koschker AC, Arvat E, Ambrosi B, Loli P, Lombardi G, Mannelli M, Bruzzi P, Mantero F, Allolio B, Dogliotti L, Berruti A. Adjuvant mitotane treatment for adrenocortical carcinoma. *N Engl J Med* 2007; **356**: 2372-2380 [PMID: 17554118 DOI: 10.1056/NEJMoa063360]

16   **Henning JEK**, Deutschbein T, Altieri B, Steinhauer S, Kircher S, Sbiera S, Wild V, Schlötelburg W, Kroiss M, Perotti P, Rosenwald A, Berruti A, Fassnacht M, Ronchi CL. Gemcitabine-Based Chemotherapy in Adrenocortical Carcinoma: A Multicenter Study of Efficacy and Predictive Factors. *J Clin Endocrinol Metab* 2017; **102**: 4323-4332 [PMID: 29092062 DOI: 10.1210/jc.2017-01624]

17   **Libé R**, Borget I, Ronchi CL, Zaggia B, Kroiss M, Kerkhofs T, Bertherat J, Volante M, Quinkler M, Chabre O, Bala M, Tabarin A, Beuschlein F, Vezzosi D, Deutschbein T, Borson-Chazot F, Hermsen I, Stell A, Fottner C, Leboulleux S, Hahner S, Mannelli M, Berruti A, Haak H, Terzolo M, Fassnacht M, Baudin E; ENSAT network. Prognostic factors in stage III-IV adrenocortical carcinomas (ACC): an European Network for the Study of Adrenal Tumor (ENSAT) study. *Ann Oncol* 2015; **26**: 2119-2125 [PMID: 26392430 DOI: 10.1093/annonc/mdv329]

Oncogenic osteomalacia caused by a phosphaturic mesenchymal tumor of the femur: A case report

Dong Tang, Xiao-Man Wang, Yong-Sheng Zhang, Xiao-Xiao Mi

ORCID number: Dong Tang (0000-0001-5902-8604); Xiao-man Wang (0000-0002-9448-7619); Yong-sheng Zhang (0000-0002-6483-9791); Xiao-xiao Mi (0000-0001-5516-3139).

Dong Tang, Department of Medical Imaging (Radiology), The Affiliated Hospital of Hangzhou Normal University, Hangzhou 310015, Zhejiang Province, China

Xiao-Man Wang, Department of Ultrasound, The Affiliated Hospital of Hangzhou Normal University, Hangzhou 310015, Zhejiang Province, China

Yong-Sheng Zhang, Department of Radiology, Hangzhou Hospital of Traditional Medicine, Hangzhou 310015, Zhejiang Province, China

Yong-Sheng Zhang, Department of Radiology, The Second Affiliated Hospital of Zhejiang Chinese Medical University, Hangzhou 310015, Zhejiang Province, China

Xiao-Xiao Mi, Institute of Translational Medicine, The Affiliated Hospital of Hangzhou Normal University, Hangzhou 310015, Zhejiang Province, China

Corresponding author: Xiao-Xiao Mi, PhD, Chief Technician, Institute of Translational Medicine, The Affiliated Hospital of Hangzhou Normal University, 126 Wenzhou Road, Hangzhou 310015, Zhejiang Province, China. mixiaoxiao1987@163.com
Telephone: +86-571-88303635

Abstract

BACKGROUND
Oncogenic osteomalacia caused by phosphaturic mesenchymal tumors is very difficult to detect. We report a case of tumor-induced osteomalacia caused by a phosphaturic mesenchymal tumor of the left femur in a middle-aged woman after medical imaging and biopsy.

CASE SUMMARY
A 57-year-old woman presented with progressive bone pain for five years. She was diagnosed with hypophosphatemic osteomalacia, as her laboratory data showed low serum phosphorus and low serum calcium. Her knee joint radiography revealed an osteolytic lesion of the left femur. A computed tomography scan showed mixed density shadows in the left femur. Magnetic resonance imaging of the left femur showed the presence of an oval area with a hypointense signal in T1-weighted magnetic resonance imaging (MRI) and high-low mixed signal in T2-weighted MRI. Biopsy samples revealed the presence of short spindle cells, vascularization, and characteristics of phosphaturic mesenchymal tumors. Tumor resection was performed, and the clinical presentations and laboratory abnormalities were reversed.

CONCLUSION
Diagnosis of oncogenic osteomalacia is difficult due to the varieties and

localization of source tumors and absence of pathognomonic biomedical signs. Our case highlights the importance of a combination of medical imaging and biopsy in the diagnosis of oncogenic osteomalacia caused by a phosphaturic mesenchymal tumor.

Key words: Oncogenic osteomalacia; Phosphaturic mesenchymal tumor; Hypophosphatemia; Hypocalcemia; Case report

Core tip: Oncogenic osteomalacia caused by phosphaturic mesenchymal tumors is not easily identifiable or detectable due to its rarity and nonspecific presentations. Herein, we provide a successful example of diagnosis of phopshaturic mesenchymal tumor-induced oncogenic osteomalacia in a female patient who presented progressive bone pain. Our case emphasizes that histologically benign phosphaturic mesenchymal tumors that are responsible for oncogenic osteomalacia can also cause bone destruction.

INTRODUCTION

Oncogenic osteomalacia, also known as tumor-induced osteomalacia, is an uncommon cause of osteomalacia. At present, approximately 140 different tumors have been reported in association with oncogenic osteomalacia, and most osteomalacia-associated tumors are phosphaturic mesenchymal tumors[1,2]. Phosphaturic mesenchymal tumors are found to be commonly associated with phosphaturia and a decreased level of serum 1,2-dihydroxyvitamin D3 that is resistant to vitamin D supplementation. However, oncogenic osteomalacia caused by phosphaturic mesenchymal tumors is not easily identifiable or detectable due to its rarity and nonspecific presentations. The clinical presentations of the patients include nonspecific symptoms of fatigue, bone pain, and musculoskeletal weakness[3]. Although rare, the diagnosis of phosphaturic mesenchymal tumor should be considered in any patient who presents with hypophosphaturic osteomalacia and no other physiologic cause.

In our case, oncogenic osteomalacia was caused by a phosphaturic mesenchymal tumor localized in the patient's left femur. The patient presented with progressive bone pain with no etiology for five years. After X-ray, computed tomography (CT), magnetic resonance imaging (MRI), and biopsy, a diagnosis of oncogenic osteomalacia caused by a phosphaturic mesenchymal tumor was made. Resection of the tumor was performed, and the clinical presentations and laboratory abnormalities were reversed. Here, our case emphasizes that histologically benign phosphaturic mesenchymal tumors that are responsible for oncogenic osteomalacia can also cause bone destruction. Its diagnosis is, thus, reliably achieved by histopathological examination combined with medical imaging.

CASE PRESENTATION

Chief complaints
A 57-year-old woman presented with progressive bone pain of the whole body for three years.

History of present illness
Five years ago, there was no obvious cause for the appearance of pain in her right third toe; pain then developed into the right instep with an associated jerk and then progressively appeared in the right thigh with an associated jerk, thus affecting her ability to walk. Three years ago, systemic pain appeared, especially bone pain. There

was also pain in her muscles and skin. Reduction or even no pain was felt while lying flat. At this time, she also had the ability to do laundry or cook. Two years ago, pain prevented her from daily exercise, and she had to stay in bed. There was no accompanying fever, coma, cough, dizziness, headache, chest tightness, palpitation, nausea, vomiting, or abdominal pain. Five years ago, she was first examined at a hospital, and her laboratory workup showed slightly low levels of serum phosphorus (0.63 mmol/L, reference range: 0.80-1.48 mmol/L) and low serum calcium (1.98 mmol/L, reference range: 2.10-2.60 mmol/L). Bone density examination showed osteoporosis in her left acetabulum and osteopenia in her lumbar spine. Chest and abdomen computed tomographic scans did not reveal any abnormalities. However, the photographs were not available now. She was treated with calcium and vitamin D supplementation. However, her pain persisted. The woman was introduced to our hospital approximately 5 years after the onset of her symptoms.

FINAL DIAGNOSIS

Physical examination showed that palpation on the right upper abdomen was normal; signs such as purple striae, moon face, and central obesity were not observed.

Her laboratory data also revealed slight hypophosphatemia (0.76 mmol/L, reference range: 0.80-1.48 mmol/L) and hypocalcemia (1.86 mmol/L, reference range: 2.10-2.60 mmol/L). Her knee radiographs showed that her bony trabeculae were sparse and her bone density was widely reduced (Figure 1). The X-ray radiograph showed an oval osteolytic lesion in the inferior medullar cavity of the left femur (Figure 1B, arrow). A subsequent CT scan revealed that mixed density shadows were shown in the intramedullary cavity of the left femur (Figure 2, arrow). Non-uniform enhancement in this lesion area was observed. However, no obvious abnormalities were seen in the surrounding soft tissues. MRI of the left knee showed the presence of an intramedullary tumor in the left femur, which showed a hypointense signal on the T1-weighted image (Figure 3A, arrow) and a high-low mixed signal intensity on the T2-weighted image (Figure 3B and C, arrow). Thus, a tumor-induced osteomalacia was confirmed.

TREATMENT AND OUTCOME

The tumor was resected at a local hospital, and the histology revealed a phosphaturic mesenchymal tumor with the presence of spindle cells and prominent blood vessels (Figure 4). Her serum phosphorus and calcium returned to the normal range (phosphorus: 0.89 mmol/L, reference range: 0.80-1.48 mmol/L; calcium: 2.29 mmol/L, reference range: 2.10-2.60 mmol/L), and now the woman can exercise daily and has not had any recent complaints.

DISCUSSION

The existence of tumor-induced osteomalacia is not widely recognized, and its diagnosis can often be delayed[4]. Tumors that are involved in oncogenic osteomalacia include phosphaturic mesenchymal tumors, fibrous dysplasia, osteosarcoma, and others[5-7]. Folpe *et al*[2] revealed that 90% of tumor-induced osteomalacia cases are associated with phosphaturic mesenchymal tumors. Phosphaturic mesenchymal tumors are most often seen in the head and lower extremities, and approximately 53% of them occur in bone, 45% in soft tissue, and 3% in skin[8]. Most phosphaturic mesenchymal tumors are seen in middle-aged adults, with no gender difference[9]. The histology of phosphaturic mesenchymal tumors features proliferation of spindle cells and oval cells, vascularization, a cartilage-like matrix, and giant cells[10]. Although rare, malignant tumors with metastasis and infiltration can also be present[11-13]. The present case of phosphaturic mesenchymal tumor occurred in the left femur and led to hypophosphatemia osteomalacia in a middle-aged woman.

Hypophosphatemia in tumor-induced osteomalacia is caused by the mRNA overexpression of FGF-23, a protein that is produced at low levels by osteocytes[10,14]. FGF-23 plays important roles in phosphate homeostasis and vitamin D metabolism. After binding with the FGFr1 receptor and the transmembrane protein Klotho, FGF-23 exerts bioactivity at the proximal tubules, where it inhibits phosphate resorption. FGF-23 also impairs the activity of hydroxylation of 25-hydroxyvitamin (OH) D3. These mechanisms mainly lead to hypophosphatemia and osteomalacia[15,16]. However, in China, the serum FGF-23 test is not routinely provided in most hospitals.

Figure 1 X-rays of knee joints. A: Anteroposterior view; B: Lateral view. Bone trabeculae of both knees are sparse, bone density is widely reduced, and an oval osteolytic area is shown in the inferior medullary cavity of the left femur (arrow).

This highlights the need for our clinicians to be aware of its entity and to give an appropriate investigation of phosphaturic mesenchymal tumor-induced osteomalacia.

Phosphaturic mesenchymal tumors are often very small in size and grow slowly, which makes them difficult to locate[10]. Malignant tumors and metastasis can often be detected. Infiltration of the surrounding tissue can also happen. Widespread bone metastases may lead to the occurrence of pathological fractures and spinal cord compression, thus significantly affecting patient outcomes. There are no established guidelines for the treatment of metastatic phosphaturic mesenchymal tumors. Complete tumor resection corrects the biochemical abnormalities and remineralization of bone. In our case, we did not observe metastases of the tumors, and resection of the tumor relieved pain and reversed the biochemical abnormalities in the patient. Our case demonstrated that histologically benign phosphaturic mesenchymal tumors can also cause bone pain.

In conclusion, we report a case of oncogenic osteomalacia caused by a phosphaturic mesenchymal tumor of the left femur in a middle-aged woman. Our case emphasizes that histologically benign phosphaturic mesenchymal tumors that are responsible for oncogenic osteomalacia can also cause bone destruction. Its diagnosis is, thus, reliably achieved by histopathological examination combined with medical imaging. We expect that the detailed description of this case presentation of oncogenic osteomalacia will provide a valuable resource to facilitate the diagnosis of such diseases in the future.
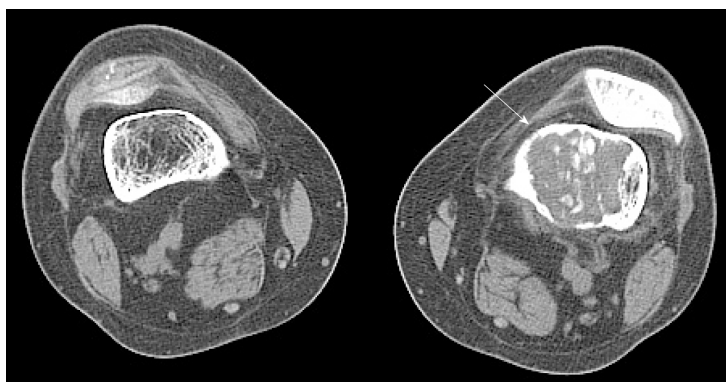
Figure 2 Computed tomography scans of knee joints. Mixed density shadows are shown in the intramedullary cavity of the left femur (arrow). Computed tomography values are 45-70 HU.
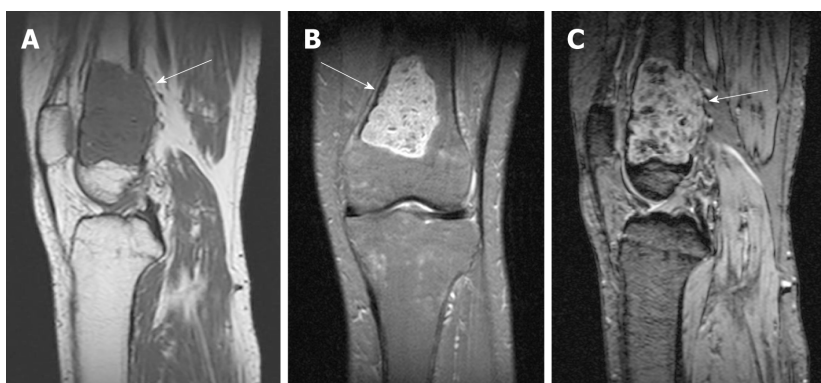
Figure 3 Magnetic resonance imaging of the left knee. A: T1WI sagittal view; B: PDWI coronal view; C: PDWI sagittal view. T1 hypointense (arrow, A) and T2 high-low mixed signal (arrows, B and C) are shown.
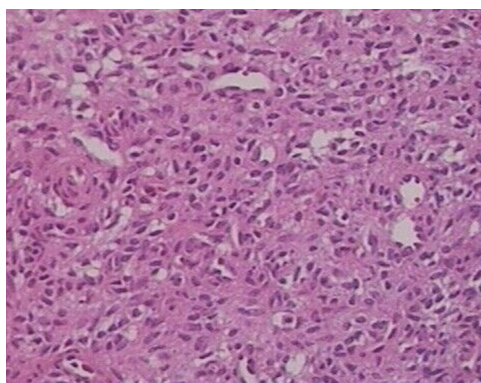
Figure 4 Histology of the resected tumor. Note the presence of short spindle cells and a large number of blood vessels. Some spindle cells grew around blood vessels. HE staining, 100×.

REFERENCES

1   **Rosenberg AE**. WHO Classification of Soft Tissue and Bone, fourth edition: summary and commentary.

Curr Opin Oncol 2013; **25**: 571-573 [PMID: 23942303 DOI: 10.1097/01.cco.0000432522.16734.2d]

2   **Folpe AL**, Fanburg-Smith JC, Billings SD, Bisceglia M, Bertoni F, Cho JY, Econs MJ, Inwards CY, Jan de Beur SM, Mentzel T, Montgomery E, Michal M, Miettinen M, Mills SE, Reith JD, O'Connell JX, Rosenberg AE, Rubin BP, Sweet DE, Vinh TN, Wold LE, Wehrli BM, White KE, Zaino RJ, Weiss SW. Most osteomalacia-associated mesenchymal tumors are a single histopathologic entity: an analysis of 32 cases and a comprehensive review of the literature. *Am J Surg Pathol* 2004; **28**: 1-30 [PMID: 14707860 DOI: 10.1097/00000478-200401000-00001]

3   **Carpenter TO**. Oncogenic osteomalacia--a complex dance of factors. *N Engl J Med* 2003; **348**: 1705-1708 [PMID: 12711747 DOI: 10.1056/NEJMe030037]

4   **Hautmann AH**, Hautmann MG, Kölbl O, Herr W, Fleck M. Tumor-Induced Osteomalacia: an Up-to-Date Review. *Curr Rheumatol Rep* 2015; **17**: 512 [PMID: 25900190 DOI: 10.1007/s11926-015-0512-5]

5   **Boyce AM**, Bhattacharyya N, Collins MT. Fibrous dysplasia and fibroblast growth factor-23 regulation. *Curr Osteoporos Rep* 2013; **11**: 65-71 [PMID: 23532406 DOI: 10.1007/s11914-013-0144-5]

6   **Jiang Y**, Xia WB, Xing XP, Silva BC, Li M, Wang O, Zhang HB, Li F, Jing HL, Zhong DR, Jin J, Gao P, Zhou L, Qi F, Yu W, Bilezikian JP, Meng XW. Tumor-induced osteomalacia: an important cause of adult-onset hypophosphatemic osteomalacia in China: Report of 39 cases and review of the literature. *J Bone Miner Res* 2012; **27**: 1967-1975 [PMID: 22532501 DOI: 10.1002/jbmr.1642]

7   **Weidner N**. Review and update: oncogenic osteomalacia-rickets. *Ultrastruct Pathol* 1991; **15**: 317-333 [PMID: 1755097 DOI: 10.3109/01913129109016242]

8   **Ungari C**, Rocchi G, Rinna C, Agrillo A, Lattanzi A, Pagnoni M. Hypophosphaturic mesenchymal tumor of the ethmoid associated with oncogenic osteomalacia. *J Craniofac Surg* 2004; **15**: 523-527 [PMID: 15111823 DOI: 10.1097/00001665-200405000-00036]

9   **William J**, Laskin W, Nayar R, De Frias D. Diagnosis of phosphaturic mesenchymal tumor (mixed connective tissue type) by cytopathology. *Diagn Cytopathol* 2012; **40** Suppl 2: E109-E113 [PMID: 22927293 DOI: 10.1002/dc.21647]

10   **Chong WH**, Molinolo AA, Chen CC, Collins MT. Tumor-induced osteomalacia. *Endocr Relat Cancer* 2011; **18**: R53-R77 [PMID: 21490240 DOI: 10.1530/ERC-11-0006]

11   **Sidell D**, Lai C, Bhuta S, Barnes L, Chhetri DK. Malignant phosphaturic mesenchymal tumor of the larynx. *Laryngoscope* 2011; **121**: 1860-1863 [PMID: 21721013 DOI: 10.1002/lary.21916]

12   **Uramoto N**, Furukawa M, Yoshizaki T. Malignant phosphaturic mesenchymal tumor, mixed connective tissue variant of the tongue. *Auris Nasus Larynx* 2009; **36**: 104-105 [PMID: 18329207 DOI: 10.1016/j.anl.2008.01.003]

13   **Ogose A**, Hotta T, Emura I, Hatano H, Inoue Y, Umezu H, Endo N. Recurrent malignant variant of phosphaturic mesenchymal tumor with oncogenic osteomalacia. *Skeletal Radiol* 2001; **30**: 99-103 [PMID: 11310207]

14   **Graham R**, Krishnamurthy S, Oliveira A, Inwards C, Folpe AL. Frequent expression of fibroblast growth factor-23 (FGF23) mRNA in aneurysmal bone cysts and chondromyxoid fibromas. *J Clin Pathol* 2012; **65**: 907-909 [PMID: 22933546 DOI: 10.1136/jclinpath-2012-200852]

15   **Hernando N**, Wagner C, Biber J, Murer H. Kidney kinase network regulates renal ion cotransport. *J Clin Invest* 2007; **117**: 3179-3182 [PMID: 17975663 DOI: 10.1172/JCI33859]

16   **Kumar R**. Tumor-induced osteomalacia and the regulation of phosphate homeostasis. *Bone* 2000; **27**: 333-338 [PMID: 10962341 DOI: 10.1016/S8756-3282(00)00334-3]

CASE REPORT

Gastric duplication cyst mimicking large cystic lymphangioma in an adult: A rare case report and review of the literature

Fang-Yi Xv, Alex Sun, Yi Gan, Hong-Jie Hu

ORCID number: Fang-Yi Xv (0000-0002-2791-8941); Alex Sun (0000-0003-1848-9011); Yi Gan (0000-0003-4944-2152); Hong-Jie Hu (0000-0002-9859-5860).

Author contributions: Xv F collected the clinical data of this patient and wrote the manuscript; Gan Y reviewed the histological sections of this case; Sun A and Hu HJ contributed equally to the manuscript polishing; all authors have read and approved the final manuscript.

Informed consent statement: Consent was obtained from the patient.

Conflict-of-interest statement: None declared.

CARE Checklist (2016) statement: The manuscript was prepared and revised according to the CARE Checklist (2016).

Manuscript source: Unsolicited manuscript

Fang-Yi Xv, Hong-Jie Hu, Department of Radiology, Sir Run Run Shaw Hospital, Zhejiang University School of Medicine, Hangzhou 310000, Zhejiang Province, China

Alex Sun, Diagnostic Radiology - Musculoskeletal Imaging, University of California, San Diego, CA 92093, United States

Yi Gan, Department of Pathology, Sir Run Run Shaw Hospital, Zhejiang University School of Medicine, Hangzhou 310000, Zhejiang Province, China

Corresponding author: Hong-Jie Hu, MD, Chief Doctor, Department of Radiology, Sir Run Run Shaw Hospital, Zhejiang University School of Medicine, No. 3, Qingchun East Road, Hangzhou 310000, Zhejiang Province, China. hongjiehu@zju.edu.cn

Abstract

BACKGROUND

Gastric duplication cysts (GDCs) are a relatively uncommon congenital developmental abnormality, mainly occurring in infants but very rarely in adults. Because of the variability in clinical presentation, it is often quite challenging to diagnose GDCs in adults. We are presenting a case report of an adult diagnosed operatively as having a GDC with a literature review to summarize clinical and imaging features and the treatment selections of GDCs in adults so that doctors could have a comprehensive understanding of this disease and make a precise diagnosis and a suitable therapeutic decision for patients.

CASE SUMMARY

A 51-year-old man presented with recurrent epigastric pain and fullness for two years. No significant findings were noted during physical examination and routine blood tests were unremarkable. An abdominal ultrasound revealed a large cyst in the upper left abdominal quadrant. A following contrast-enhanced abdominal computed tomography (CT) scan demonstrated a hypodense cystic lesion between the spleen and stomach. The lesion had scattered calcification in the cyst wall without any significant enhancement. The lesion was initially thought to be a cystic lymphangioma. The patient underwent a surgical resection and intraoperatively it was noted that the lesion was closely adherent to the greater curvature of the stomach. Subsequently, a resection of the gastric mass along with a partial gastrectomy was performed. The patient recovered quickly with a complete symptomatic relief and did not show any further complications during the 8-month follow-up.

CONCLUSION

GDCs are quite rare in adults, with a multitude of symptoms, which is quite

challenging for precise diagnosis before histological examination. Some imaging techniques involving CT, magnetic resonance imaging, and endoscopic ultrasound could provide valuable morphological features for differential diagnosis.

Key words: Gastrointestinal abnormality; Gastric duplication cyst; Computed tomography; Ultrasound; Magnetic resonance imaging; Case report

Core tip: We are presenting a rare case of a duplication cyst in an adult complaining of recurrent upper left abdominal pain and fullness. An abdominal ultrasound and a contrast-enhanced computed tomography scan demonstrated a large cystic lesion along the greater curvature of the stomach with scattered calcification and no significant enhancement was observed. A nutrient vessel arising from the stomach was noted in the cyst wall. Laparoscopic resection of the gastric mass and partial gastrectomy were performed. The patient recovered without any complications.

INTRODUCTION

Gastrointestinal tract duplications are a rare congenital developmental malformation most frequently seen in infants with an incidence of about 1 in 4500 live births and a sex ratio of approximately 2 to 1 (female to male)[1,2]. A gastrointestinal tract duplication is defined as a tubular or spherical structure sharing a common muscular wall and blood supply with normal gastrointestinal tract but having a separate mucosal lining[3], which can appear anywhere along the gastrointestinal tract from the mouth to the anus, with the ileum being the most common location[1,4,5]. Gastric duplication cysts (GDCs), accounting for about less than 10% of gastrointestinal tract duplications, are rarely seen in adults as most cases are diagnosed in childhood, and over 70% cases are discovered before the age of 12[1,4,6]. Although GDCs in adult are a rare entity, they may present with various symptoms including abdominal pain, gastric outlet obstruction, or a palpable abdominal mass.

CASE PRESENTATION

Chief complaints
A 51-year-old man was admitted to our hospital because of a two-year history of repeated episodes of epigastric pain and fullness without any obvious causes.

History of present illness
Two years ago, the patient began to present recurrent upper abdominal pain. The recurrent episodes of pain lasted approximately 1 h and were associated with nausea.

History of past illness
The patient denied any past surgical interventions.

Physical examination
Initial evaluation in the hospital showed no remarkable clinical examination findings.

Laboratory examinations
Laboratory test results were within normal limits.

Imaging examinations
An abdominal ultrasound showed a large cystic lesion in the upper left quadrant

abdomen, which was initially thought to be retroperitoneal (Figure 1A). No significant vascular flow was seen on Doppler (Figure 1B).

A contrast-enhanced abdominal computed tomography (CT) scan was performed for further evaluation (Figure 2). The scan showed a large cystic hypodense lesion, measuring 95 mm × 61 mm × 66 mm, between the spleen and stomach, which was anterior to the left renal fascia and in close proximity to lateral limb of the left adrenal gland. The lesion was lobulated and well-circumscribed with a small amount of wall calcification.

Primary diagnosis

A cystic lymphangioma was the primary diagnostic consideration prior to pathological confirmation according to the imaging examination.

MULTIDISCIPLINARY EXPERT CONSULTATION

Guan-Yu Wang, MD, Chief Doctor, Department of General Surgery, Zhejiang University School of Medicine

Considering recurrent abdominal pain and the imaging findings of an abdominal mass, the patient needed to take surgical treatment into consideration for symptomatic relief.

TREATMENT

The patient chose surgical intervention for symptomatic relief. During the surgery, it was noted that the lesion was adherent to the greater curvature of the proximal stomach, between the superoposterior aspect of the pancreas and splenic hilum. A laparoscopic resection of the perigastric mass and partial gastrectomy were performed.

FINAL DIAGNOSIS

Histological sections showed gastric mucosa-like tissues within the cyst wall and a diagnosis of GDC was made for the patient (Figure 3).

OUTCOME AND FOLLOW-UP

The patient recovered quickly after the surgery without any postoperative complications. There were no recurrent symptoms during his 8-month outpatient follow-up.

DISCUSSION

GDCs are a class of gastrointestinal tract duplications, most commonly occurring in children and very rarely in adults. GDCs have no specific clinical symptoms in adults and the symptoms mainly depend on the lesion location, size, and whether any communication exists with the gastric lumen. Clinical symptoms include nausea, vomiting, abdominal pain, palpable abdominal mass, gastrointestinal bleeding (from ulceration related to ectopic gastric mucosal acid secretion), weight loss, anemia, and failure to thrive[1,6-10]. Some cases are asymptomatic and only incidentally detected during physical examination[7] (Table 1). GDCs can produce all the pathological changes that may occur in the normal gastric lining, including gastritis, gastric ulcer, and even malignant transformation[11,12]. To date, less than 15 cases of malignant transformation arising from GDCs have been reported[7,12-14]. In rare cases, GDCs have been reported to contain ectopic pancreatic tissue[15,16]. Pancreatitis can occur in these cases if the ectopic pancreatic duct is obstructed[16,17]. Laboratory tests in GDCs tend to be unremarkable. Rarely, some cases have abnormally elevated carcinoembryonic antigen (CEA) and CA 19-9[18,19]. These cases may be associated with malignant transformation of GDCs.

GDCs tend to be found along the greater curvature of the stomach[1,4]. It can be divided into intraluminal and extraluminal types according to the location; communicating and non-communicating types according to its connection with
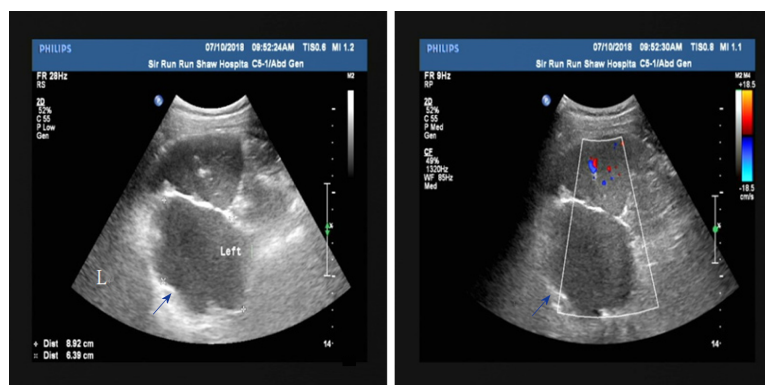
Figure 1 Ultrasound images of the gastric duplication cyst. A large cystic focus (blue arrow) was visible in the space between the spleen, stomach, and left kidney, with no vascularization on Doppler.

gastric lumen; and complete and incomplete duplication according to the degree of deformity. The extraluminal and non-communicating types are more common compared with the intraluminal and non-communicating types, accounting for more than 80% of reported cases[1,4,7]. Complete communicating GDCs are really rare. There has been only one reported case in the past 17 years[1].

The mechanism of GDCs is still unclear but several theories have been proposed to explain the formation of gastrointestinal duplications. Some scholars theorize that gastrointestinal duplications share a similar mechanism with that of diverticulum formations and some believe they are caused by the abnormal development of early embryonic primitive foregut formation and differentiation[1,2,7].

On conventional radiography, intraluminal contrast agent filling can be seen in the communicating type GDCs. In contrast, non-communicating type GDCs would only show gastric wall indentation, indicating a submucous or extraluminal lesion.

CT and magnetic resonance imaging (MRI) are valuable for determining the size, location, and extent of the duplication cyst as well as the relationship to adjacent structures[1,20]. GDCs may be round or lobulated with a thin wall on cross-sectional images[7]. When the duplication cyst is very large and in close proximity to adjacent organs such as the spleen, kidney, or liver, it may be misdiagnosed as a cyst arising from these organs. MRI has high soft tissue resolution and signal changes in multiple phases may present the thin cyst wall usually with slight enhancement, which is useful for distinguishing the origin of the cyst[6]. In our case, no enhanced cystic wall was observed by enhanced CT, but a nutrient vessel arising from the stomach was seen in the cyst wall, which was a helpful imaging feature to identify the origin of the cystic lesion. GDCs occasionally present calcification within the cyst wall, which may be related to the accumulation of secretion or necrosis. Multiple calcifications in the cyst wall were observed in our case and the case reported by D'Journo *et al*[21]. Awan *et al*[22] introduced a special case with multiple calcifications mimicking a staghorn calculus. The contents of most GDCs present fluid density/signal, but bleeding or infection may result in the heterogeneity of density/signal, which can make diagnosis of GDCs in adults complicated[4]. GDCs also need to be distinguished from gastrointestinal stromal tumors (GISTs). GISTs are solid tumors originating from the submucous mesenchymal tissue of the gastrointestinal wall, and vary greatly in size with hemorrhage and necrosis occurring in large tumors and mild or moderate enhancement involving the solid portions of GISTs.

Ultrasound is a noninvasive method widely used for screening in patients with abdominal symptoms. In most cases, ultrasound shows a hypoechoic cystic lesion in the upper abdomen, often adjacent to the stomach, pancreas, and liver.

Endoscopic ultrasound (EUS) is considered a good diagnostic tool for the detection of GDCs because it can show the internal hyperechoic mucosal layer and the hypoechoic smooth muscle layer of the cyst[21]. In recent years, EUS-guided fine-needle aspiration (EUS-FNA) plays an important role in clinical diagnosis of GDCs[5].

On pathology, a GDC must have both a smooth muscle layer and a mucosal epithelial layer (gastrointestinal, gastric, or respiratory mucosa) in the cyst wall[7,14]. Our case had all the layers meeting the diagnostic requirements.

Up to now, there are no well-recognized international guidelines on the treatment of this disease. Several treatment methods have been reported in the literature, including enucleation, formation of cystogastrostomy, and even endoscopic removal[3]. Surgical excision is usually considered the mainstay of treatment for GDCs. Surgical resection is performed not only for the consideration of symptomatic relief
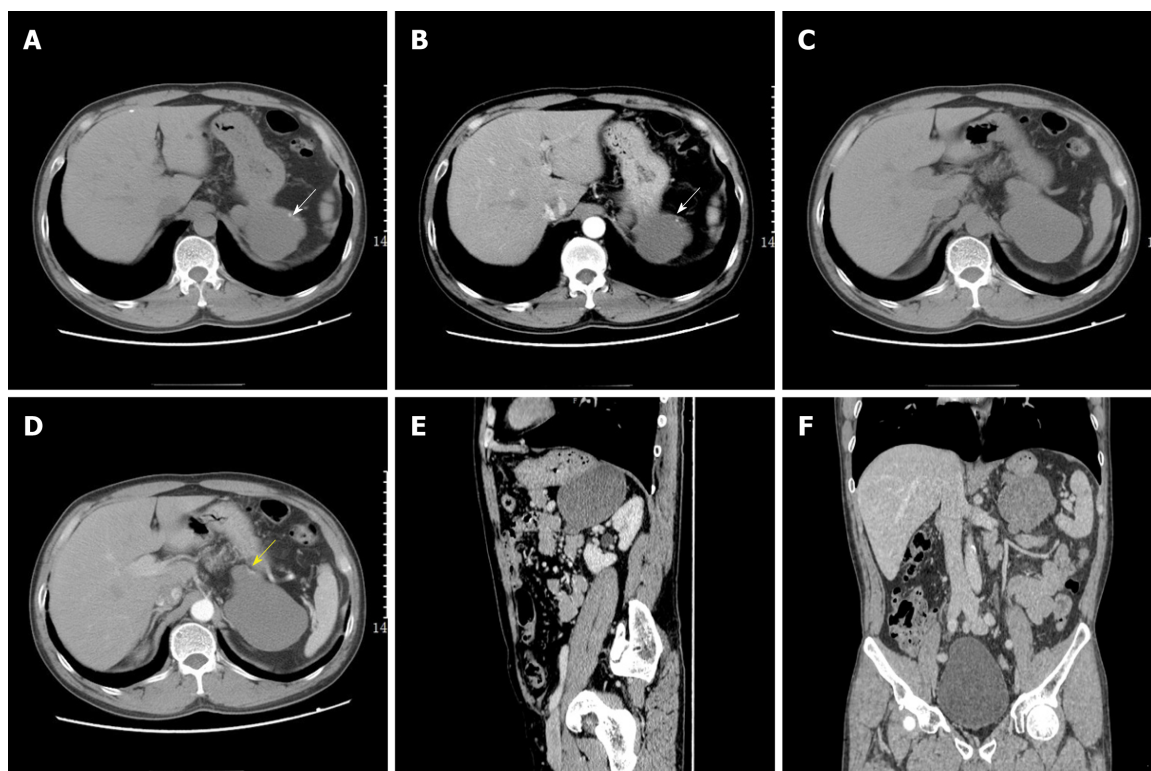
Figure 2 Contrast-enhanced computed tomography images of the gastric duplication cyst. A-F: A large cystic hypodense focus was along the greater curvature of the stomach, measuring 95 mm × 61 mm × 66 mm; A and B: The focus was lobulated and well-circumscribed with a small amount of calcification on its wall (white arrow); C and D: A nutrient vessel from the stomach on the cyst wall was observed on arterial phase images (yellow arrow).

and the prevention of potential complications caused by GDCs such as obstruction, torsion, perforation, bleeding, but also for the risk of malignant transformation in GDCs[3,7]. We performed a review of the English papers about GDCs in the past 17 years on PubMed and found that the majority of those cases had a good prognosis with complete symptomatic relief after surgical resection while only a few cases with malignant transformation developed recurrence or metastasis[11,12,14,23-25].

CONCLUSION

GDCs are a quite rare malformation in adults usually with non-specific clinical symptoms. Some imaging modalities including ultrasound, CT, and MRI are able to figure out morphological features for GDCs diagnosis and EUS could present the exact micro-structure of the cystic wall. We deem that GDCs should be put in the differential list for a cystic mass adjacent to gastric lumen.

Table 1 Teaching points for differential diagnosis

Disease	Age	Teaching points
Gastric duplication cysts (GDCs)	More common in children, rarely seen in adults.	Often present as a cystic focus along the greater curvature and adjacent to stomach with a thin and slightly enhanced wall.
Any cystic lesions from the adjacent organs (liver, biliary ducts, pancreas, and spleen)	Occur at any age.	Ultrasound, CT, and MRI can show the origination of the lesion. History, clinical presentation and laboratory examination could help to lead to the right diagnosis[7].
Gastrointestinal stromal tumors (GISTs)	Present usually in early adulthood[14].	Medical images show masses with solid enhancement arising from the gastric wall which may show cystic or mixed cystic changes[8,14].
Cystic lymphangioma	Occur mostly in children[26].	Mostly seen in the neck and axillae but can be found anywhere in the body[26]. CT and MRI show cystic lesions with the thin wall crawling along the tissue gaps[26,27].

CT: Computed tomography; MRI: Magnetic resonance imaging.
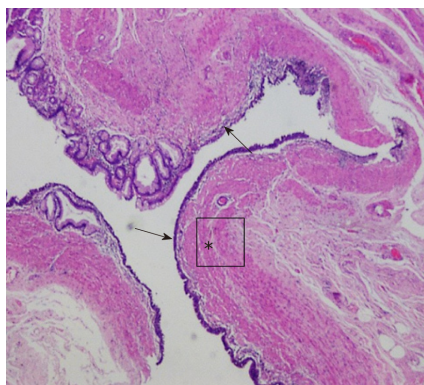
Figure 3 Photomicrograph (hematoxylin and eosin staining, original magnification, ×4) of the surgical specimen demonstrates an inner mucosal layer (arrows) within the cystic mass, along with a continuous muscular layer (asterisk) shared with the stomach.

REFERENCES

1   **Bhatti ZS**, Anderson MA, Wasnik AP. Complete gastric duplication in an adult with associated anomalies. *Clin Imaging* 2016; **40**: 244-246 [PMID: 26995580 DOI: 10.1016/j.clinimag.2015.11.016]

2   **Theodosopoulos T**, Marinis A, Karapanos K, Vassilikostas G, Dafnios N, Samanides L, Carvounis E. Foregut duplication cysts of the stomach with respiratory epithelium. *World J Gastroenterol* 2007; **13**: 1279-1281 [PMID: 17451215]

3   **Hsu HT**, Hsing MT, Chen ML, Chen CJ. A gastric duplication cyst at the splenic hilum mimicking endometriosis clinically in a female adult. *Chin Med J (Engl)* 2009; **122**: 2079-2080 [PMID: 19781401]

4   **Seijo Ríos S**, Lariño Noia J, Abdulkader Nallib I, Lozano León A, Vieites Pérez-Quintela B, Iglesias García J, Domínguez Muñoz JE. [Adult gastric duplication cyst: diagnosis by endoscopic ultrasound-guided fine-needle aspiration (EUS-FNA)]. *Rev Esp Enferm Dig* 2008; **100**: 586-590 [PMID: 19025312]

5   **Maeda H**, Okabayashi T, Nishimori I, Kobayashi M, Morimoto K, Miyaji E, Kohsaki T, Hanazaki K, Onishi S. Diagnostic challenge to distinguish gastric duplication cyst from pancreatic cystic lesions in adult. *Intern Med* 2007; **46**: 1101-1104 [PMID: 17634707]

6   **Abdalkader M**, Al Hassan S, Taha A, Nica I. Complicated Gastric Duplication Cyst in an Adult Patient: Uncommon presentation of an uncommon disease. *J Radiol Case Rep* 2017; **11**: 16-23 [PMID: 29299102 DOI: 10.3941/jrcr.v11i8.3124]

7   **Deesomsak M**, Aswakul P, Junyangdikul P, Prachayakul V. Rare adult gastric duplication cyst mimicking a gastrointestinal stromal tumor. *World J Gastroenterol* 2013; **19**: 8445-8448 [PMID: 24363539 DOI: 10.3748/wjg.v19.i45.8445]

8   **Kamei K**, Yasuda T, Satoi S, Ishikawa H, Sakamoto H, Kitano M, Chikugo T, Nakai T, Takeyama Y. Intrapancreatic gastric duplication cyst mimicking pancreatic cystic tumor. *Clin J Gastroenterol* 2013; **6**: 156-159 [PMID: 26181454 DOI: 10.1007/s12328-013-0367-0]

9   **Feng X**, Liang X, Cai X. A rare case of gastric duplication in an adult mimicking a solid mass. *Chin Med J (Engl)* 2014; **127**: 3516 [PMID: 25269927]

10 **Horne G**, Ming-Lum C, Kirkpatrick AW, Parker RL. High-grade neuroendocrine carcinoma arising in a gastric duplication cyst: a case report with literature review. *Int J Surg Pathol* 2007; **15**: 187-191 [PMID: 17478780 DOI: 10.1177/1066896906295777]

11 **Yamasaki A**, Onishi H, Yamamoto H, Ienaga J, Nakafusa Y, Terasaka R, Nakamura M. Asymptomatic adenocarcinoma arising from a gastric duplication cyst: A case report. *Int J Surg Case Rep* 2016; **25**: 16-20

[PMID: 27289170 DOI: 10.1016/j.ijscr.2016.05.055]

12   **Chan BPH**, Hyrcza M, Ramsay J, Tse F. Adenocarcinoma Arising from a Gastric Duplication Cyst. *ACG Case Rep J* 2018; **5**: e42 [PMID: 29915790 DOI: 10.14309/crj.2018.42]

13   **Kuraoka K**, Nakayama H, Kagawa T, Ichikawa T, Yasui W. Adenocarcinoma arising from a gastric duplication cyst with invasion to the stomach: a case report with literature review. *J Clin Pathol* 2004; **57**: 428-431 [PMID: 15047751]

14   **Passos ID**, Chatzoulis G, Milias K, Tzoi E, Christoforakis C, Spyridopoulos P. Gastric duplication cyst (gdc) associated with ectopic pancreas: Case report and review of the literature. *Int J Surg Case Rep* 2017; **31**: 109-113 [PMID: 28131064 DOI: 10.1016/j.ijscr.2017.01.033]

15   **Oeda S**, Otsuka T, Akiyama T, Ario K, Masuda M, Taguchi S, Shono T, Kawazoe S. Recurrent acute pancreatitis caused by a gastric duplication cyst communicating with an aberrant pancreatic duct. *Intern Med* 2010; **49**: 1371-1375 [PMID: 20647650]

16   **Davies S**, Morris-Stiff G, Lewis MH. Gastric duplication cyst mimicking a pancreatic pseudocyst in a patient with chronic pancreatitis. *Int J Surg* 2008; **6**: e70-e71 [PMID: 17499033 DOI: 10.1016/j.ijsu.2007.03.002]

17   **Johnston J**, Wheatley GH, El Sayed HF, Marsh WB, Ellison EC, Bloomston M. Gastric duplication cysts expressing carcinoembryonic antigen mimicking cystic pancreatic neoplasms in two adults. *Am Surg* 2008; **74**: 91-94 [PMID: 18274440]

18   **Lee LS**, Ong HS. A rare case of two synchronous gastric duplication cysts in an adult. *Singapore Med J* 2013; **54**: e91-e92 [PMID: 23624463]

19   **D'Journo XB**, Moutardier V, Turrini O, Guiramand J, Lelong B, Pesenti C, Monges G, Giovannini M, Delpero JR. Gastric duplication in an adult mimicking mucinous cystadenoma of the pancreas. *J Clin Pathol* 2004; **57**: 1215-1218 [PMID: 15509688 DOI: 10.1136/jcp.2004.019091]

20   **Awan A**, Tiruneh F, Iftikhar H, Samuel G, Awan A. A Gastric Duplication Cyst Initially Mimicking Staghorn Calculus. *J Coll Physicians Surg Pak* 2018; **28**: S26-S27 [PMID: 29482696 DOI: 10.29271/jcpsp.2018.03.S26]

21   **Barussaud ML**, Meurette G, Cassagnau E, Dupasc B, Le Borgne J. Mixed adenocarcinoma and squamous cell carcinoma arising in a gastric duplication cyst. *Gastroenterol Clin Biol* 2008; **32**: 188-191 [PMID: 18496895]

22   **Liu K**, Lin X, Wu J, Liu H, Meng M, Su H, Tai W, Chang H. Peritoneal metastatic adenocarcinoma possibly due to a gastric duplication cyst: a case report and literature review. *BMC Gastroenterol* 2014; **14**: 48 [PMID: 24641252 DOI: 10.1186/1471-230X-14-48]

23   **Fukumoto K**, Suzuki S, Sakaguchi T, Morita Y, Oishi K, Suzuki A, Inaba K, Kamiya K, Miura K, Konno H. Adenocarcinoma arising from gastric duplication: a case report with literature review. *Clin J Gastroenterol* 2008; **1**: 148-152 [PMID: 26193693 DOI: 10.1007/s12328-008-0024-1]

24   **François S**, Martin M, Costa O, Urbain D, Mana F. Cystic Lymphangioma: Are Triglycerides Always Measurable? *Case Rep Gastrointest Med* 2018; **2018**: 9591420 [PMID: 29686910 DOI: 10.1155/2018/9591420]

25   **Wunderbaldinger P**, Paya K, Partik B, Turetschek K, Hörmann M, Horcher E, Bankier AA. CT and MR imaging of generalized cystic lymphangiomatosis in pediatric patients. *AJR Am J Roentgenol* 2000; **174**: 827-832 [PMID: 10701634 DOI: 10.2214/ajr.174.3.1740827]

CASE REPORT

Endometriosis of the duplex appendix: A case report and review of the literature

Ming-Yuan Zhu, Fa-Ming Fei, Jing Chen, Zhong-Cheng Zhou, Bin Wu, Yi-Yu Shen

ORCID number: Ming-Yuan Zhu (0000-0002-1592-7429); Fa-Ming Fei (0000-0003-4616-1830); Jing Chen (0000-0002-8857-5209); Zhong-Cheng Zhou (0000-0003-4489-8847); Bin Wu (0000-0002-1235-0951); Yi-Yu Shen (0000-0002-4454-4275).

Ming-Yuan Zhu, Fa-Ming Fei, Jing Chen, Zhong-Cheng Zhou, Bin Wu, Yi-Yu Shen, Department of General Surgery, The Second Affiliated Hospital of Jiaxing University, Jiaxing 314000, Zhejiang Province, China

Corresponding author: Yi-Yu Shen, MD, Chief Doctor, Department of General Surgery, The Second Affiliated Hospital of Jiaxing University, 1518 Huancheng North Road, Jiaxing 314000, Zhejiang Province, China. jxeysyy01@163.com
Telephone: +86-1570-6701708

Abstract

BACKGROUND
Duplication of the appendix is an infrequent congenital malformation with a complex classification. The horseshoe appendix is a subtype of the duplex appendix and is rarely reported in the literature. Endometriosis is a common gynecological disease that rarely occurs in the appendix. Moreover, horseshoe appendix combined with endometriosis has not been previously reported.

CASE SUMMARY
Here, we describe a 44-year-old woman who was admitted with a 1-d history of migratory lower right quadrant pain. Physical examination was consistent with the signs of acute appendicitis. The patient underwent an emergency exploratory laparotomy. The distal tip of the appendix was in contact with the cecum by another base, or "horseshoe appendix". In addition, a small intestinal mass and an ovarian mass were identified. Subsequently, appendectomy, partial resection of the small intestine, and right oophorectomy were successively performed. The histopathology confirmed the diagnosis of acute inflammation of the duplex appendix with endometriosis, small intestine endometriosis, and ovarian endometriosis.

CONCLUSION
Surgeons need to be aware of the possibility of the duplex appendix when performing an appendectomy, and this study emphasizes the importance of exploring the entire abdomen.

Key words: Duplex appendix; Horseshoe appendix; Endometriosis; Appendectomy; Case report

Core tip: We describe a patient with endometriosis of the duplex appendix, small intestine, and ovary. There are no similar cases reported. Currently, the diagnosis of duplex appendix and endometriosis is difficult before surgery. Our case suggests that serum carbohydrate antigen 125 levels and fecalith of the appendix may be useful signs for the diagnosis of endometriosis and duplex appendix, respectively. However, the most important procedure is the careful exploration of the abdominal cavity during surgery. Serious legal disputes can occur due to neglecting another infected appendix or not carefully exploring other parts of the abdominal cavity.

INTRODUCTION

Acute appendicitis is the most common surgical emergency of the abdomen. The overall lifetime risk for acute appendicitis is 6.7% in females and 8.6% in males[1]. Duplication of the appendix is extremely rare and is usually incidentally found during surgery. A duplication of the appendix was first reported in the form of a case report in 1892[2]. To date, only a total of approximately 100 cases have been reported[3]. Endometriosis, as a common disease in women of childbearing age, predominantly occurs in the adnexa and less frequently in the digestive tract, especially in the small intestine and appendix. Here, we report a unique case of duplex appendix with acute appendicitis coexisting with appendiceal endometriosis in an adult female patient. In addition, endometriosis was found in the small intestine and ovary. The most special of the duplex appendix is the horseshoe appendix. To the best of our knowledge, only the abovementioned 14 cases have been reported thus far[4], but there are no reports of horseshoe appendix combined with endometriosis. The classification, symptoms, and radiological appearance of the duplex appendix with endometriosis have been described in the literature and are discussed in this paper.

CASE PRESENTATION

Chief complaints

A 44-year-old Chinese woman was admitted to the Emergency Department of The Second Affiliated Hospital of Jiaxing University (Jiaxing, China) because of migratory lower right quadrant pain for 1 d associated with nausea, vomiting, and anorexia.

History of present illness

She reported a 1-d medical history of migratory lower right quadrant pain that started as epigastric pain and became localized to the lower right abdominal quadrant, especially at McBurney's point. She also complained about nausea, vomiting, and anorexia.

History of past illness

The patient had an 8-year history of repeated lower abdominal pain that appeared in the first 1-2 d of menstruation and disappeared after the end of menstruation. However, her menstrual cycle was regular, with no menorrhagia or dyspareunia reported. Therefore, she was not regularly seen in the gynecology clinic for several years.

Personal and family history

The last menstrual period ended 5 d before admission. She had a history of caesarean section 18 years ago. No additional family history was presented.

Physical examination upon admission

Her abdominal examination revealed that the abdomen was diffusely soft, nondistended, but presented tenderness, rebound tenderness, and guarding with a voluntary component in the lower right quadrant, and increased pain with coughing

at the McBurney's point, which were consistent with the signs of acute appendicitis. Moreover, Rovsing's sign was positive. No abdominal mass was palpable, and bowel sounds were normoactive.

Laboratory examinations

Hematological examinations, including serum electrolyte levels, human chorionic gonadotropin, and complete blood count were within normal limits, apart from white blood cell count, carbohydrate antigen 125 (CA125), and C-reactive protein concentrations that were mildly elevated at 10.1×10^9/L (77.8% neutrophils), 69.5 U/mL, and 10 mg/mL, respectively.

Imaging examinations

A computed tomography (CT) scan of the abdomen showed that the appendix was markedly swollen and thickened and had obvious periappendicular leaking; additionally, two fecaliths were located at the root of the appendix (Figure 1). Simultaneously, the CT scan also showed a cystic mass in the right ovary (Figure 1). The findings from the patient's abdominal examination and CT scan were consistent with acute fecal appendicitis.

FINAL DIAGNOSIS

Based on the above physical examination features and imaging data, a provisional diagnosis of acute appendicitis and right ovarian cyst was made.

TREATMENT

Laparoscopic examination revealed moderate bloody fluid collections, and the omentum was localized to the right lower abdomen and pelvic cavity. Additionally, a cystic mass with a size of 3.5 cm × 2.5 cm was seen in the right ovary, which was not ruptured and was consistent with the CT scan findings. No evidence of endometrium was found by laparoscopic evaluation of the abdominal and pelvic cavities. Moreover, the appendix appeared unusually atrophic upon itself and measured 3 cm × 2.5 cm at the widest diameter, which was obviously inflamed, hyperemic, and swollen, which agreed with the preoperative diagnosis. However, we found a tight adhesion between the appendix, the lateral abdominal wall, and the posterior peritoneum, resulting in unclear anatomical structures that were difficult to separate. Therefore, a laparotomy was performed *via* an extended McBurney's incision in the lower right abdominal quadrant. After carefully separating the adhesions, an appendix was seen. Then, we attempted to separate the base of the appendix, and we were surprised to find that there were two bases that had their cavities both in contact with the cecum with each other through the appendiceal lumen, or "horseshoe appendix" (Figure 2). The two bases were positioned frontally on the cecum with a central mesoappendix, and the central mesoappendix vessel was fan-shaped. The proximal appendix stump and mesoappendix vessel were divided and ligated, and then the appendix was removed for pathological examination. Unfortunately, because there was no consideration of the rarity of this case, there were not enough intraoperative photographs remaining. Upon gross pathological inspection, the total length of the duplex appendix was approximately 6 cm. There were two cavities in the root of the cecum, both of which led to a swollen inflamed appendix containing a fecalith. Subsequently, a meticulous inspection of distal ileal segments and right tuboovarian structures was performed through palpation, and we unexpectedly found a hard mass, 10 cm proximal to the ileocecal valve, which gave rise to a mild stenosis of the intestine. Additionally, a right ovarian cyst was found, as previously mentioned. Hence, partial resection of the small intestine with end-to-end anastomosis was executed, as well as right oophorectomy by a gynecologist. Grossly, the soft tissue mass had a size of 1.5 cm × 1.5 cm, but the serosal surface and the mucosa were normal. The cut surface revealed hard nodular regions, which contained some small cystic spaces brimmed with both serous fluid and hemorrhage. The ovarian cyst showed that the cut surface also contained several small cystic spaces and was filled with chocolate-like cyst fluid and old bleeding.

OUTCOME AND FOLLOW-UP

Hematoxylin and eosin staining revealed obvious acute and chronic inflammatory cell infiltration within and around the duplex appendix. The lumens of the two
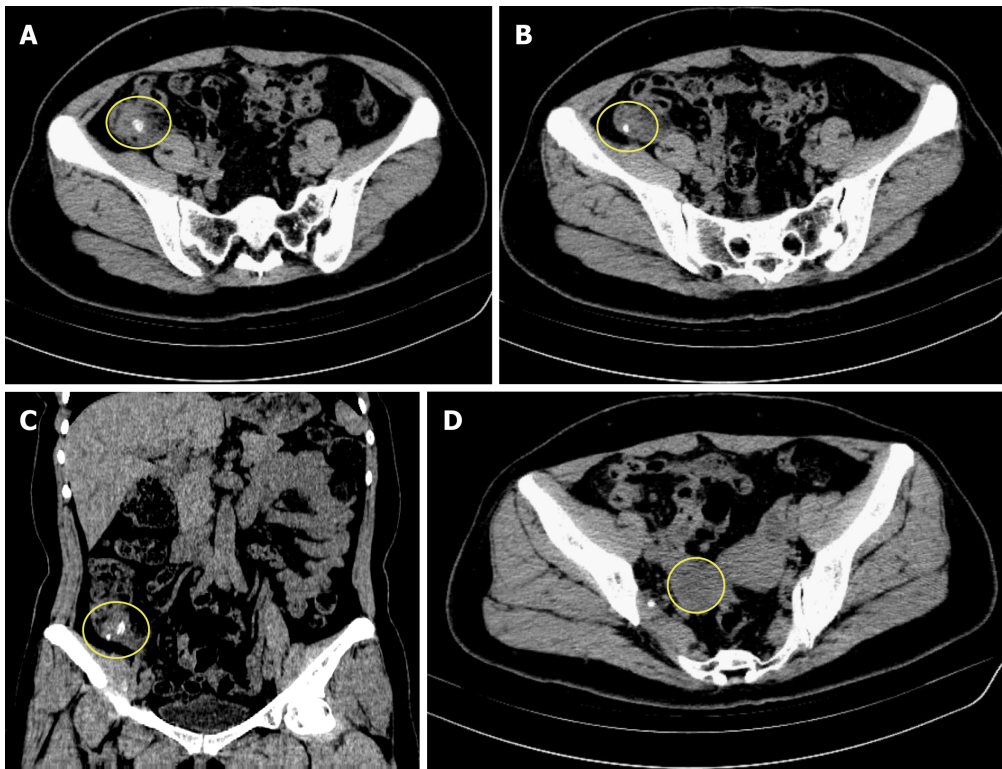
Figure 1 Computed tomography scan of the patient's abdomen. A and B: Transverse sections showing swelling of the appendix with surrounding exudation, and there is a fecalith at the root of the appendix, respectively; C: Coronal section showing swelling of the appendix with exudation and two separate fecaliths at its root; D: Transverse section showing a low density mass located in the right ovary.

appendixes were obstructed with fecalith. Meanwhile, several ectopic endometrial-type glands and stroma were found in the thickened muscularis propria of the duplex appendix (Figure 3), small intestine (Figure 3), and right ovary (Figure 3). Additionally, the glands were dilated, most of which contained hemorrhage within their cavities. Histological diagnoses of duplex appendix with fecalith and endometriosis were made, which caused acute appendicitis, and diagnoses of endometriosis of the small intestine and the right ovary were also made. These results were surprising discoveries. The patient subsequently recovered well with no complications and was discharged from the hospital on the 10th postoperative day. She was referred to a gynecological clinic for further assessment of her endometriosis. At the 6-month follow-up, there were no recurrences of abdominal pain or other clinical symptoms.

DISCUSSION

Duplication of the digestive tract is a rare congenital malformation in adults because more than 80% of cases have serious abdominal or intestinal obstruction before the age of 2 years[5]. Appendiceal duplication is extremely rare and may be related to the duplication of other organs or other anomalies. Colons investigated 50000 pathological specimens of the appendix, and there were only just two cases of duplication[6]. The overall incidence of appendiceal duplication is approximately 0.004%[6]. Appendiceal duplication was first formally classified by Cave in 1936 and divided into three types based on their anatomic locations. Then, this classification was updated and amended in 1962 by Wallbridge[7] and is called the "Cave-Wallbridge" classification. Subsequently, this classification was further improved by Biermann *et al*[8] and Kjossev *et al*[9], respectively. However, there were several cases that could not be classified according to the above classifications, for instance, horseshoe appendix and triplex appendix. We believe that an updated classification system is needed to distinguish appendiceal anomalies or to modify the present system. Therefore, Calotă *et al*[10] proposed a new classification system for appendiceal anomalies in 2010, which was divided into number anomalies and shape anomalies and was modified by Takabatake *et al*[11] again in 2016. The new classification system of appendiceal anomalies is presented in Table 1[4,10-13]. Most cases can be classified on
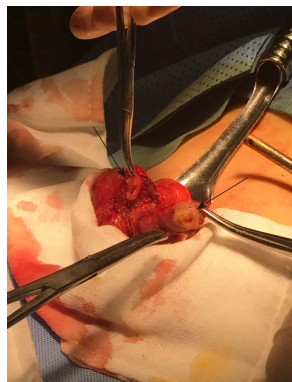
Figure 2 Intraoperative photograph of the patient. The intraoperative photograph shows that there are two bases of the appendix at the end of the cecum, and both of these bases are in contact with the cecum (black arrow).

the basis of the new classification. There have been 22 cases of Type A, 8 cases of Type B1, 46 cases of Type B2, 10 cases of Type C, 2 cases of triple appendix, and 14 cases of horseshoe appendix reported as of the beginning of 2018[3,4]. Although the duplex appendix is rare, surgeons should suspect the possibility of it when performing an appendectomy to prevent adverse consequences and medical disputes. In addition, a differential diagnosis is also necessary, including Meckel's diverticulum, colonic tumor, gastroenteritis, congenital cecal diverticulum, intussusceptions, and inflammatory bowel disease[14]. In the presence of a duplex appendix, the possibility of other congenital malformations should be further explored, especially in cases of Type B1 and Type C. However, Type B2, which is the most common variety and the most likely to be misdiagnosed or mismanaged, is unrelated to any other congenital anomalies[3].

In the classification of duplex appendix, the horseshoe appendix is a rarer congenital malformation. In 1989, Mesko *et al*[15] first depicted the horseshoe appendix. Through a review of the literature, 14 patients with horseshoe appendix have been reported to date[4], and as per our knowledge, our patient was the 15th patient with a reported horseshoe appendix. The etiology and pathogenesis of horseshoe appendix are still unclear because there are extremely limited cases that have been reported thus far. Currently, some theories have been proposed to explain how the horseshoe appendix forms[16]. First, the horseshoe appendix may form by the mutual fusion between the tip of the normal appendix and that of the abnormal appendix. Second, a horseshoe appendix may develop from the fusion between the tip of the appendix and another part of the cecum, which then becomes the second base. Third, in the embryonic period, the base of the appendix split into two parts, each of which develops continuously, resulting in two bases that are also single structures. However, the first two theories do not seem to explain why both appendixes are supplied by a single blood vessel in the mesoappendix, and its branches fan out instead of forming an arcade. The study of the formation mechanism of the duplex appendix revealed that a "transient appendix" at the terminus of the cecum, which was distinct from the normal appendix, was observed during the 6th week of embryonic development and atrophy at the 7th week[17]. If the transient appendix does not disappear, a duplex appendix may form. Additionally, the horseshoe appendix, a subtype of the duplex appendix, may be caused by some abnormalities in the embryonic period. Therefore, the third theory is most likely to explain the formation of a horseshoe appendix. However, more research is needed to support this theory, because of the limited number of cases.

The horseshoe appendix can be divided into two types according to the following new classification system (Table 1): Frontal type, in which both bases of the appendix are not on the tenia, and sagittal type, in which the bases are along the tenia[11]. The malformation of our patient was a horseshoe type with a frontal location. In addition, we must simultaneously pay attention to whether the patient had other malformations because genitourinary, other intestinal, or vertebral malformations have been observed in cases with a duplex appendix. Fortunately, other associated congenital anomalies had not been observed in our patient, except for the endometriosis of the small intestine and ovary. Preoperative diagnosis is extremely difficult, whether it is a horseshoe appendix or other types of duplex appendix. It has been reported that[4] ultrasound and three-dimensional reconstruction may be helpful for the preoperative diagnosis of a horseshoe appendix, but most cases are accidentally discovered during surgery, and only two patients had a clear diagnosis before
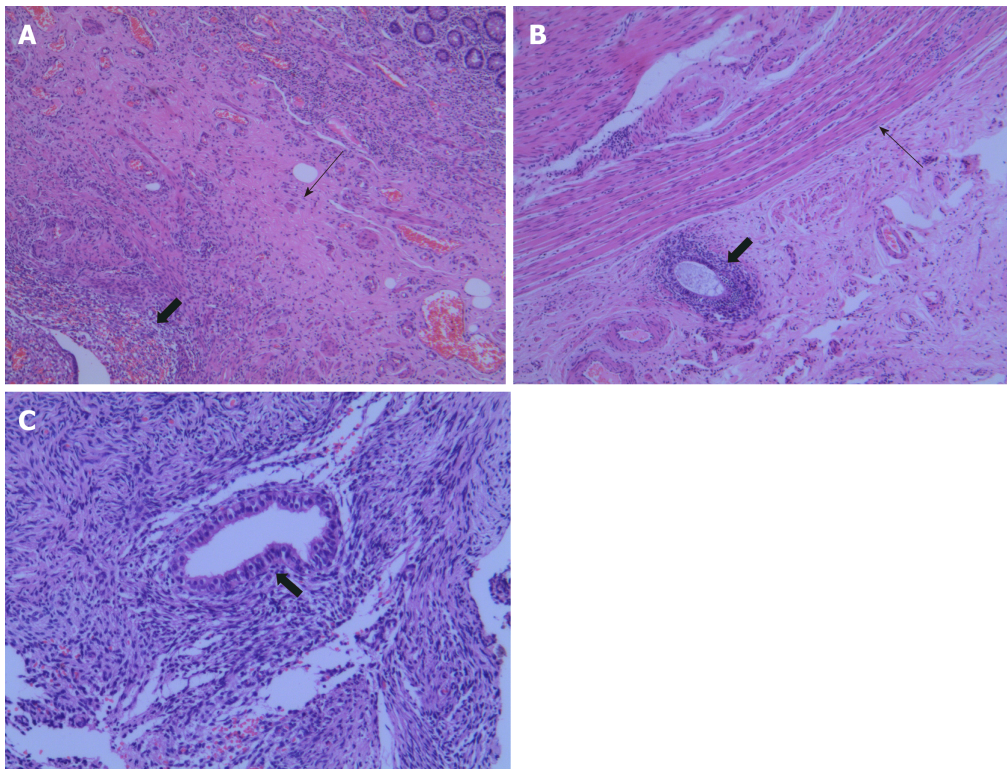
Figure 3 Histopathological appearances of the endometriosis in appendix, small intestine, and ovary. A: Hematoxylin and eosin (HE) staining shows that ectopic endometrial-type glands and stroma (thick arrows) were detected in the muscular layers (thin arrows) of the appendix (×40); B: Ectopic endometrial-type glands and stroma (thick arrows) were observed in the subserosa of the small intestine. The muscular layers are indicated by thin arrows (HE, ×40); C: Higher magnification of endometriosis (thick arrows) in the ovary (HE, ×100).

surgery. In our patient, imaging failed to preoperatively diagnose appendiceal anomalies. However, after surgery, we reviewed the CT scan repeatedly, and the images showed that there were two free fecaliths at the root of the appendix, which may indicate the presence of a duplex appendix (Figure 1). This finding was easily ignored.

Endometriosis, which is defined as the growth of endometrial glands and stroma outside the uterine cavity, is a fairly common disease that affects up to 15% of women in childbearing age. Von Rokitansky first described endometriosis in 1860[18]. Several theories have been proposed to explain the pathogenesis of endometriosis, including retrograde menstruation and implantation theory, coelomic metaplasia theory, lymphovascular spread theory, direct transplantation and dissemination theory, and the cellular immunity theory which was a newly developed theory[19-21]. However, the specific etiology of endometriosis is still unclear. A variety of factors potentially contribute to the disease. Endometriosis can occur anywhere in the body, including pelvis organs, gastrointestinal tract, and pleural and pericardial cavities, but the ambilateral adnexa is the most frequent. Once involving the gastrointestinal tract, endometriosis also commonly involves the recto-sigmoid (72%), recto-vaginal septum (13%), small intestine (7%), cecum (3.6%), and appendix (3%)[18]. Endometriosis of the appendix is a rare disease, and its overall incidence ranges between 0.02% and 36.6%, which is widely variable and depends on the population being evaluated[22]. Our patient not only had rare appendix and ileum involvement but also had a duplex appendix. This dual participation has not been observed thus far.

Clinically, the symptoms of endometriosis are diverse and have been determined by the site of occurrence. Endometriosis of the appendix is usually asymptomatic, but it may also cause acute or chronic pelvic pain, appendicitis, lower gastrointestinal hemorrhage, and intussusception[19,22]. Consistent with some reports (Table 2)[19,23-27], our patient also presented the symptoms of acute appendicitis. Moreover, laparoscopic exploration also showed the presence of bloody fluid in the abdominal cavity. The hemoperitoneum is likely to be related to menstruation, because in these reports (Table 2), patients presented the symptoms of acute appendicitis during the menstrual period. As our patient presented the symptoms of appendicitis on the 5th day after the end of menstruation, we assume it to be related to the appendiceal fecalith. The occurrence of acute appendicitis may be the result of the dual effects of endometriosis and appendiceal fecalith. Moreover, our patient had a history of

Table 1 New classification of appendiceal anomalies

Number anomalies

Agenesis: Absence of appendix

Duplex appendix

Type A: Partial duplication with both appendices sharing a common base like '' Y-shaped'' on a single cecum

Type B: Complete duplication of the appendix on a single cecum

B1 avian type: Two appendices symmetrically placed on either side of the ileocecal valve

B2 tenia coli cecum type: One appendix arising from the usual site of the cecum and the other arising from the cecum along the tenia

B3 tenia coli hepatic flexure type: One appendix arising from the usual site of the cecum and the other arising from the hepatic flexure of the colon along the tenia

B4 tenia coli splenic flexure type: One appendix arising from the usual site of the cecum and the other arising from the splenic flexure of the colon along the tenia

Type C: Duplication of the cecum, each having its own appendix

Triplex appendix: Complete triplication of appendix on the cecum

Horseshoe appendix

With sagittal disposal: The bases of the appendix are along the tenia in sagittal direction

With frontal disposal: The bases of the appendix are not on the tenia

Data from these studies[4,10-13].

repeated lower abdominal pain which was associated with menstruation, consistent with some reports[23,26,27]. It suggests that hemoperitoneum and chronic abdominal pain may be important signs of endometriosis diagnosis, which further validates the theory of retrograde menstruation. Additionally, gastrointestinal endometriosis can present with episodes of abdominal pain, change in bowel habits, abdominal distention, rectal bleeding, and intestinal obstruction[28-30]. Fortunately, although small intestinal endometriosis in our case was asymptomatic, it did not cause intestinal obstruction due to timely detection.

The clinical manifestations of endometriosis are usually nonspecific, leading to the diagnostic dilemma. Therefore, complete preoperative examination is needed, including CT scan, magnetic resonance imaging (MRI), abdominal ultrasonography, and laboratory examination. It was reported that[31] multislice CT has a great potential for detecting alterations in the intestinal wall, especially when combined with enteroclysis. MRI has a high sensitivity (77%-93%) in the diagnosis of bowel endometriosis[32]. Unfortunately, there is currently no gold standard for the imaging diagnosis of endometriosis[20]. The serum CA125 level, which has been used to monitor the progress of endometriosis, may be a useful diagnostic indicator[33]. However, it has also been reported that CA125 is not sensitive enough to the diagnosis of endometriosis[30]. In our patient, the abdominal CT scan did not suggest endometriosis, but she had a high preoperative serum CA125 level of 69.5 U/mL. Therefore, we believe that the presence of endometriosis needs to be suspected when patient have elevated serum CA125 levels. Additionally, except for the hemoperitoneum we have mentioned above, blueberry spot of the peritoneum and nodularity of the appendix may also indicate the presence of endometriosis during surgery[19,23]. Intraoperatively, we only found moderate hemorrhagic peritoneal fluid in our patient. However, the postoperative pathology of our patient confirmed the presence of endometriosis in the appendix, small intestine, and ovary. Therefore, laparoscopy and pathological confirmation remain the gold standard for the diagnosis of endometriosis. Given the nature of endometriosis, patients such as ours should be encouraged to refer to gynecologists for further assessment of the extent of endometriosis and for postoperative follow-up.

CONCLUSION

Acute appendicitis is a common abdominal disease. Although duplex appendix is rare, especially the horseshoe appendix, surgeons who may not encounter it throughout their careers need to be aware of the possibility of it when performing an appendectomy. In particular, preoperative CT showed two separate fecaliths at the root of the appendix, which may be a useful sign for the diagnosis of a duplex appendix. Therefore, a detailed exploration of the cecal pole and retrocecal space is encouraged to avoid misdiagnosis during surgery; misdiagnosis of appendix

Table 2 Clinical features of patients with appendix endometriosis

Ref.	Year	Age	Symptoms	Previous history	Episode time	Hemoperitoneum
Uncu *et al*[25]	2008	45	Abdominal pain and nausea	Not described	The second day of menstruation	Yes
Akbulut *et al*[26]	2009	40	Lower right quadrant pain	Lower right abdominal pain before every menstrual period for 8 or 9 yr	The third day of menstruation	Not described
Uwaezuoke *et al*[23]	2013	29	Right iliac fossa pain	One-year history of recurrent lower abdominal pain	The second day of menstruation	Yes
Curbelo-Peña *et al*[24]	2015	39	Right iliac fossa pain	Not described	Be menstruating at the time	Yes
Shen *et al*[27]	2016	34	Right iliac fossa pain	Repeated abdominal pain associated with menstruation for several months	The second day of menstruation	Yes
St John *et al*[19]	2018	29	Migratory lower right quadrant pain	Not described	The second day of menstruation	Yes
Our case	2019	44	Migratory lower right quadrant pain	Eight-year history of repeated lower abdominal pain	Five days after the last menstrual period ended	Yes

duplication may result in a poor clinical outcome and law dispute. In addition, women of childbearing age who have chronic pelvic pain or elevated CA125 levels need to highly suspect the possibility of endometriosis. In summary, whether laparoscopy or laparotomy is used, careful exploration of the entire abdomen is crucial and occasionally surprises us.

REFERENCES

1   **Addiss DG**, Shaffer N, Fowler BS, Tauxe RV. The epidemiology of appendicitis and appendectomy in the United States. *Am J Epidemiol* 1990; **132**: 910-925 [PMID: 2239906 DOI: 10.1093/oxfordjournals.aje.a115734]

2   **Khanna AK**. Appendix vermiformis duplex. *Postgrad Med J* 1983; **59**: 69-70 [PMID: 6866880 DOI: 10.1136/pgmj.59.687.69]

3   **Nageswaran H**, Khan U, Hill F, Maw A. Appendiceal Duplication: A Comprehensive Review of Published Cases and Clinical Recommendations. *World J Surg* 2018; **42**: 574-581 [PMID: 28799135 DOI: 10.1007/s00268-017-4178-1]

4   **Liu J**, Dong C, Wang H, Sun D, Liang R, Gao Z, Wang L. One type of duplex appendix: horseshoe appendix. *Ther Clin Risk Manag* 2018; **14**: 1987-1992 [PMID: 30349277 DOI: 10.2147/TCRM.S179929]

5   **Macpherson RI**. Gastrointestinal tract duplications: clinical, pathologic, etiologic, and radiologic considerations. *Radiographics* 1993; **13**: 1063-1080 [PMID: 8210590 DOI: 10.1148/radiographics.13.5.8210590]

6   **COLLINS DC**. A study of 50,000 specimens of the human vermiform appendix. *Surg Gynecol Obstet* 1955; **101**: 437-445 [PMID: 13256319]

7   **Wallbridge PH**. Double appendix. *Br J Surg* 1962; **50**: 346-347 [PMID: 13998581 DOI: 10.1002/bjs.18005022124]

8   **Biermann R**, Borský D, Gogora M. Double appendicitis--a rare pathologic entity. *Chirurg* 1993; **64**: 1059-1061 [PMID: 8119095]

9   **Kjossev KT**, Losanoff JE. Duplicated vermiform appendix. *Br J Surg* 1996; **83**: 1259 [PMID: 8983623 DOI: 10.1002/bjs.1800830926]

10   **Calotă F**, Vasile I, Mogoantă S, Zavoi R, Paşalega M, Moraru E, Stoicea C. Horseshoe appendix: a extremely rare anomaly. *Chirurgia (Bucur)* 2010; **105**: 271-274 [PMID: 20540245]

11   **Takabatake K**, Ikeda J, Furuke H, Kato C, Kishimoto T, Kumano T, Imura K, Shimomura K, Kubota T, Taniguchi F, Shioaki Y. A case of a horseshoe appendix. *Surg Case Rep* 2016; **2**: 140 [PMID: 27878571 DOI: 10.1186/s40792-016-0261-3]

12   **Singh CG**, Nyuwi KT, Rangaswamy R, Ezung YS, Singh HM. Horseshoe Appendix: An Extremely Rare Appendiceal Anomaly. *J Clin Diagn Res* 2016; **10**: PD25-26 [PMID: 27134939 DOI: 10.7860/JCDR/2016/16569.7494]

13   **Canbay E**, Akman E. Appendix perforation in appendix duplication in a man: a case report. *J Med Case*

Rep 2011; **5**: 162 [PMID: 21513538 DOI: 10.1186/1752-1947-5-162]

14   **Travis JR**, Weppner JL, Paugh JC 2nd. Duplex vermiform appendix: case report of a ruptured second appendix. *J Pediatr Surg* 2008; **43**: 1726-1728 [PMID: 18779015 DOI: 10.1016/j.jpedsurg.2008.04.023]

15   **Mesko TW**, Lugo R, Breitholtz T. Horseshoe anomaly of the appendix: a previously undescribed entity. *Surgery* 1989; **106**: 563-566 [PMID: 2772830]

16   **DasGupta R**, Reber PU, Patel AG. Horseshoe appendicitis. *Eur J Surg* 1999; **165**: 1095-1096 [PMID: 10595618 DOI: 10.1080/110241599750007973]

17   **Cave AJ**. Appendix Vermiformis Duplex. *J Anat* 1936; **70**: 283-292 [PMID: 17104589]

18   **Saleem A**, Navarro P, Munson JL, Hall J. Endometriosis of the appendix: Report of three cases. *Int J Surg Case Rep* 2011; **2**: 16-19 [PMID: 22096677 DOI: 10.1016/j.ijscr.2010.11.001]

19   **St John BP**, Snider AE, Kellermier H, Minhas S, Nottingham JM. Endometriosis of the appendix presenting as acute appendicitis with unusual appearance. *Int J Surg Case Rep* 2018; **53**: 211-213 [PMID: 30423543 DOI: 10.1016/j.ijscr.2018.10.048]

20   **Charatsi D**, Koukoura O, Ntavela IG, Chintziou F, Gkorila G, Tsagkoulis M, Mikos T, Pistofidis G, Hajiioannou J, Daponte A. Gastrointestinal and Urinary Tract Endometriosis: A Review on the Commonest Locations of Extrapelvic Endometriosis. *Adv Med* 2018; **2018**: 3461209 [PMID: 30363647 DOI: 10.1155/2018/3461209]

21   **Papavramidis TS**, Sapalidis K, Michalopoulos N, Karayanopoulou G, Raptou G, Tzioufa V, Kesisoglou I, Papavramidis ST. Spontaneous abdominal wall endometriosis: a case report. *Acta Chir Belg* 2009; **109**: 778-781 [PMID: 20184068 DOI: 10.1080/00015458.2009.11680536]

22   **Mabrouk M**, Raimondo D, Mastronardi M, Raimondo I, Del Forno S, Arena A, Sutherland N, Borgia A, Mattioli G, Terzano P, Seracchioli R. Endometriosis of the Appendix: When to Predict and How to Manage-A Multivariate Analysis of 1935 Endometriosis Cases. *J Minim Invasive Gynecol* 2019 [PMID: 30849476 DOI: 10.1016/j.jmig.2019.02.015]

23   **Uwaezuoke S**, Udoye E, Etebu E. Endometriosis of the appendix presenting as acute appendicitis: a case report and literature review. *Ethiop J Health Sci* 2013; **23**: 69-72 [PMID: 23559841]

24   **Curbelo-Peña Y**, Guedes-De la Puente X, Saladich-Cubero M, Molinas-Bruguera J, Molineros J, De Caralt-Mestres E. Endometriosis causing acute appendicitis complicated with hemoperitoneum. *J Surg Case Rep* 2015; 2015 [PMID: 26253154 DOI: 10.1093/jscr/rjv097]

25   **Uncu H**, Taner D. Appendiceal endometriosis: two case reports. *Arch Gynecol Obstet* 2008; **278**: 273-275 [PMID: 18236056 DOI: 10.1007/s00404-008-0570-2]

26   **Akbulut S**, Dursun P, Kocbiyik A, Harman A, Sevmis S. Appendiceal endometriosis presenting as perforated appendicitis: report of a case and review of the literature. *Arch Gynecol Obstet* 2009; **280**: 495-497 [PMID: 19169700 DOI: 10.1007/s00404-008-0922-y]

27   **Shen AY**, Stanes A. Isolated Appendiceal Endometriosis. *J Obstet Gynaecol Can* 2016; **38**: 979-981 [PMID: 27720099 DOI: 10.1016/j.jogc.2016.06.006]

28   **Lainas P**, Dammaro C, Rodda GA, Morcelet M, Prevot S, Dagher I. Appendiceal endometriosis invading the sigmoid colon: a rare entity. *Int J Colorectal Dis* 2019; **34**: 1147-1150 [PMID: 30666405 DOI: 10.1007/s00384-019-03242-0]

29   **Sali PA**, Yadav KS, Desai GS, Bhole BP, George A, Parikh SS, Mehta HS. Small bowel obstruction due to an endometriotic ileal stricture with associated appendiceal endometriosis: A case report and systematic review of the literature. *Int J Surg Case Rep* 2016; **23**: 163-168 [PMID: 27153232 DOI: 10.1016/j.ijscr.2016.04.025]

30   **Slesser AA**, Sultan S, Kubba F, Sellu DP. Acute small bowel obstruction secondary to intestinal endometriosis, an elusive condition: a case report. *World J Emerg Surg* 2010; **5**: 27 [PMID: 20846366 DOI: 10.1186/1749-7922-5-27]

31   **Biscaldi E**, Ferrero S, Fulcheri E, Ragni N, Remorgida V, Rollandi GA. Multislice CT enteroclysis in the diagnosis of bowel endometriosis. *Eur Radiol* 2007; **17**: 211-219 [PMID: 16937103 DOI: 10.1007/s00330-006-0364-5]

32   **De Ceglie A**, Bilardi C, Blanchi S, Picasso M, Di Muzio M, Trimarchi A, Conio M. Acute small bowel obstruction caused by endometriosis: a case report and review of the literature. *World J Gastroenterol* 2008; **14**: 3430-3434 [PMID: 18528943 DOI: 10.3748/wjg.14.3430]

33   **Bedaiwy MA**, Falcone T. Laboratory testing for endometriosis. *Clin Chim Acta* 2004; **340**: 41-56 [PMID: 14734195 DOI: 10.1016/j.cccn.2003.10.021]

Fever and neck pain after pacemaker lead extraction: A case report

Shao-Xian Wang, Jian Bai, Rui Ma, Rong-Fang Lan, Jia Zheng, Wei Xu

ORCID number: Shao-Xian Wang (0000-0002-8602-792X); Jian Bai (0000-0002- 1715-794X); Rui Ma (0000-0002-1022-3078); Rong-Fang Lan (0000-0002-0050-9160); Jia Zheng (0000-0002-9544-8064); Wei Xu (0000-0002-3257-2455).

Shao-Xian Wang, Department of Cardiology, Nanjing Drum Tower Hospital, Clinical College of Nanjing Medical University, Nanjing 210008, Jiangsu Province, China

Jian Bai, Rui Ma, Rong-Fang Lan, Jia Zheng, Wei Xu, Department of Cardiology, Nanjing Drum Tower Hospital, Nanjing University Medical School, Nanjing 210008, Jiangsu Province, China

Corresponding author: Wei Xu, MD, Chief Doctor, Professor, Department of Cardiology, Nanjing Drum Tower Hospital, Clinical College of Nanjing Medical University, No. 321, Zhongshan Road, Gulou District, Nanjing 210008, Jiangsu Province, China. 13390900868@163.com
Telephone: +86-25-83106666
Fax: +86-25-68182812

Abstract

BACKGROUND
Venous thrombosis (VT) is one of the minor complications of pacemaker lead extraction. It is often found due to the swelling of the limbs after the extraction. It is easy to be neglected or even misdiagnosed in the absence of typical clinical symptoms. The incidence, risk factors, and long-term impact of this complication are still unclear. Herein, we report a case of deep VT caused by transvenous lead extraction, which is easily misdiagnosed.

CASE SUMMARY
A 66-year-old woman underwent a pacemaker lead extraction at our hospital because of a pacemaker pocket infection. After the extraction, she began to experience intermittent fever accompanied by sweating. The highest body temperature recorded was 37.9 °C. Additionally, she reported migratory pain that made her uncomfortable. The pain was mistakenly thought to be caused by operation trauma. At first, the pain radiated from the left chest to the mandible. Then, the pain in the left chest was alleviated, but pain in the left neck and throat appeared. Finally, the pain was confined to the mandible and a submandibular mass was palpated with no other abnormalities upon physical examination. Computed tomography venography and angiography finally indicated that the fever and pain were the symptoms of thrombophlebitis caused by lead extraction. The patient was then treated with rivaroxaban for more than three months and has shown no symptoms since she left the hospital.

CONCLUSION
The possibility of thrombosis should be considered when pain and recurrent fever occur after pacemaker lead extraction.

Key words: Venous thrombosis; Lead extraction; Neck pain; Fever; Anticoagulants; Case

Core tip: Deep venous thrombosis caused by transvenous lead extraction is easily missed. The exact incidence is still unclear. Thrombosis after lead extraction during hospitalization should be identified early even without typical symptoms such as edema. Additionally, reasonable and standard anticoagulation therapy after lead extraction should be considered in the future.

INTRODUCTION

With the increasing use of cardiovascular implantable electronic devices (CIEDs), increasing attention has been paid to the safety and complications of lead extraction after CIED implantation. The indications of transvenous lead extraction (TLE) include infection, venous stenosis and occlusion, lead malfunction, lead perforation, arrhythmias, as well as radiation therapy[1]. Complications of TLE include cardiac avulsion, vascular laceration, pericardial effusion, hemothorax, pulmonary embolism, pocket hematoma, venous thrombosis (VT), *etc*[1]. Among them, VT caused by TLE is easily missed in the clinic, and the incidence is unclear. The following case shows that VT can be caused by TLE and is characterized by intermittent fever and neck pain.

CASE PRESENTATION

Chief complaints

A 66-year-old woman was admitted to our hospital due to infection of the pacemaker pocket for one month.

History of present illness

The patient was diagnosed with sick sinus syndrome for which she received a dual-chamber pacemaker 10 years ago. One month prior to admission, after carrying a heavy burden, she found redness and swelling at the pocket site, which gradually ulcerated. The local hospital gave her an antiinfection treatment of cephalosporin for a week, but the outcome was not positive. Therefore, she was transferred to our hospital for further treatment.

History of past illness

The patient had a history of hypertension, type 2 diabetes mellitus, and chronic gastric ulcer. She underwent a meningioma resection 7 years earlier and cataract surgery in both eyes 8 years earlier. The patient had no history of hepatitis or tuberculosis.

Personal and family history

The patient had no significant past history or family history.

Physical examination upon admission

The patient's blood pressure and blood glucose were well controlled by medication. Her body temperature was normal three days before the operation.

Except for swelling and ulceration at the pocket site, other physical examination results were normal. There were no abnormalities in the laboratory examination, electrocardiogram, chest X-ray, or preoperative echocardiogram. Multiple blood cultures were negative before the preventative use of vancomycin 0.5 g/q8h.

Laboratory examinations

After excluding the contraindication of operation, the left leads were extracted successfully, and a temporary pacemaker was implanted on the other side. Intraoperative angiography revealed patency of the bilateral subclavian veins (Figure 1). The results of the pacemaker pocket tissue and lead culture showed the presence of

Staphylococcus epidermidis, which is sensitive to vancomycin. Vancomycin was used continuously after the operation. The next day after the operation, the patient complained of pain radiating from the left chest to the mandible, with a pain score of 6. She began to present intermittent fever accompanied by sweating. Therefore, blood cultures were performed at that time; however, the results were negative. The serum concentration of vancomycin was up to standard. Three days after the operation, the patient felt that the pain in the left chest was alleviated, but increased pain in the left neck and throat accompanied by an irregular cough (dry cough, no sputum) appeared. Physical examination showed neck tenderness, normal tonsils, and a normal uvula. A few days later, the patient still had an intermittent low fever with sweating. Laboratory examination showed that routine blood and procalcitonin levels were normal, the erythrocyte sedimentation rate (ESR) was 44 mm/h, and the hypersensitive C-reactive protein (CRP) level was 45.6 mg/L. The operation incision and temporary pacemaker placement site were observed to be dry and clean without redness, burning, effusion, or pus. Seven days after the extraction, the patient felt relieved of pain in the left chest and neck and said that the pain was confined to the mandible. A submandibular mass was found through palpation. Routine blood tests, blood biochemical indexes, and procalcitonin levels were normal. Her ESR was 65 mm/h, hypersensitive CRP was 57.4 mg/L, plasma D-dimers was 9.58 mg/L, and fibrinogen was 5.6 g/L.

Imaging examination

Color Doppler ultrasound showed left internal jugular vein thrombosis. Occlusion of the left common jugular vein, internal and external jugular veins, and subclavian vein was further demonstrated by computed tomography venography (CTV) (Figure 2). The patient refused the intravenous or subcutaneous use of anticoagulants; therefore, rivaroxaban was given.

FINAL DIAGNOSIS

VT after pacemaker lead extraction caused the symptoms of the patient.

TREATMENT

After 2 d of anticoagulant treatment with 15 mg rivaroxaban bid, the patient's temperature returned to normal (Figure 3), and no further neck pain was reported. Permanent pacemaker implantation on the right side was performed 5 d after anticoagulant therapy. Intraoperative angiography revealed occlusion of the left subclavian veins (Figure 4). Anticoagulant drugs were discontinued 24 h before implantation and were resumed 48 h after the operation.

OUTCOME AND FOLLOW-UP

Hypersensitive CRP and ESR showed a downward trend after anticoagulant therapy, and the patient was discharged from the hospital when her condition was stable. Clinical follow-up was conducted by telephone interviews with the patient. Rivaroxaban 15 mg bid was used for 21 d after the thrombosis was found, followed by 20 mg qd. The total rivaroxaban treatment lasted more than three months. The patient has shown no symptoms since she left the hospital.

DISCUSSION

Complications caused by TLE include major complications, minor complications, and death within 48 h after lead extraction[2]. Major complications are life-threatening or fatal complications, such as cardiac avulsion, vascular avulsion, stroke, and bleeding requiring transfusion. Minor complications include hematoma, hemothorax, VT and others that are not life-threatening to the human body. There has been a case report of thrombosis caused by TLE in the past. Hanninen *et al*[3] reported thrombosis extending from the right atrium to the right ventricular outflow after TLE, and the huge thrombus disappeared after anticoagulation treatment. The trauma of TLE might be the cause of thrombosis. Wazni *et al*[4] reported that the incidence of VT caused by TLE was 0.21%. A single-center study by Kennergren *et al*[5] found three patients with postoperative thrombosis in 647 patients, which indicated that the incidence was
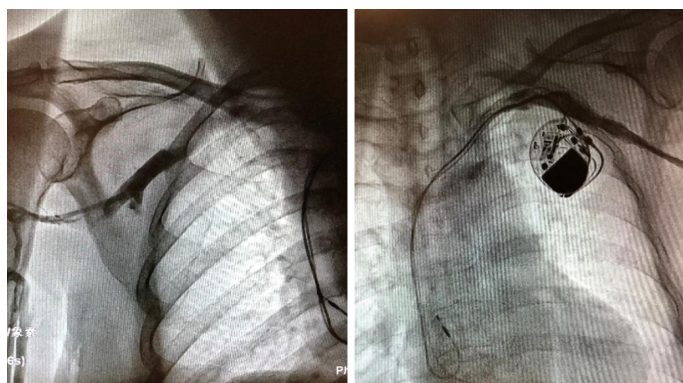
Figure 1 Intraoperative angiography revealed patency of the bilateral subclavian veins before the left lead extraction.

0.5%. Wilkoff *et al*[6] studied TLE in 301 patients, and three of whom presented VT; therefore, the incidence was 1%. However, Bracke *et al*[7] indicated that the incidence of VT caused by TLE was more than 8%. In our center, bilateral venography was performed routinely before TLE and the implantation of a new pacemaker. Since 2013, we have conducted TLEs in 240 patients in our center. This patient was the first to suffer VT after TLE and before the implantation of a new pacemaker. However, we may have underestimated the incidence as we did not follow these patients after the new CIEDs were implanted. The exact incidence of this complication is unclear due to the different follow-up times of each researcher and the underestimation of atypical clinical symptoms caused by this complication. However, neglect of pulmonary embolism and other complications caused by deep VT might increase hospitalization rates and mortality[8].

Edema of the affected extremity is reported as the most typical symptom of upper-extremity deep VT[9]. Some patients may also suffer from pain or erythema, which occurs less often in upper-extremity deep VT[9]. Approximately 5% of deep VT patients are asymptomatic[9]. Similarly, edema is also a symptom with a prompting effect of VT caused by TLE[1,6,10]. CTV and venography can produce a definitive diagnosis.

Fever is reported to have the lowest predictive value of VT[11]. In our center, 82 of 240 patients had newly fever after TLE. Among them, 32 patients had a definite etiology: 13 were due to drug fever, 9 due to pulmonary infections, 5 to bacteremia, and 1 each to hyperthyroidism, cancer, gout, viral infection, and thrombophlebitis. In the remaining 50 people, we did not find a clear cause of fever and the average body temperature of them was lower than 38 °C. They might have suffered from physiological fever caused by operative trauma or neglected pathological fever[12].

The patient we reported lacked typical symptoms. We first considered that the fever that occurred after TLE was caused by infection because infection was the primary post-procedure complication of significance[1]. However, the results of laboratory tests did not support this diagnosis. We also considered that the patient might have a drug fever because previous literature reported that using vancomycin can lead to a drug fever in some patients[13]. However, this was ruled out because the body temperature returned to normal without the cessation of vancomycin. Additionally, we had no evidence to suspect that the fever was caused by tumors or autoimmune diseases because the related examinations were negative. The patient complained of neck pain. First, we only considered that the pain was caused by operation trauma and neglected that the pain might be caused by thrombophlebitis.

In retrospect, the patient had a pacemaker implanted for more than ten years, which might lead to severe adhesion between wire, tissue, and blood vessels. Therefore, thrombophlebitis occurred after the extraction of the leads, resulting in recurrent fever. After thrombosis of the left subclavian vein, it further spread to the left internal jugular vein. Therefore, her neck pain was related to thrombotic occlusion of the internal jugular vein. Venography indicated collateral circulation formation, so there was no swelling of the upper limbs or face. Postoperative fever prevented the implantation of the new pacemaker and prolonged her hospital stay. After anticoagulation treatment, her body temperature returned to normal. However, anticoagulation treatment might increase the risk of hematoma formation after pacemaker implantation[14]. Recent studies have shown that pocket hematoma increases the risk of device-related infection[15,16].

We hypothesize that the incidence of VT caused by TLE is higher than that reported
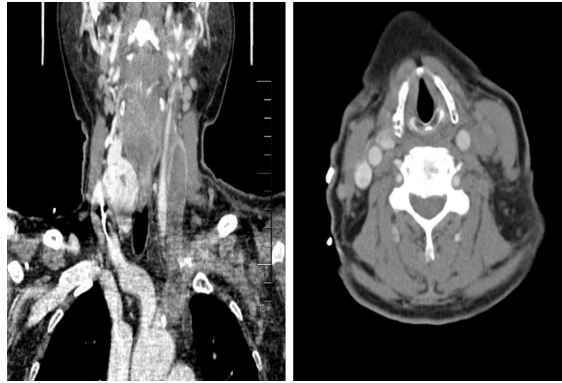
Figure 2 Computed tomography venography showed occlusion of the left common jugular vein, internal and external jugular veins, and subclavian vein.

previously in the literature. We might underestimate the incidence because of the lack of symptoms and short follow-up time. There are no clear guidelines regarding effective and safe anticoagulation strategies for patients with VT after TLE, especially in those who need new CIEDs implanted after TLE. As clinicians, we need to reduce misdiagnoses, and we should be alert to the possibility of VT when patients suffer from recurrent fever and neck pain after TLE.

CONCLUSION

We need pay more attention to the VT caused by pacemaker lead extraction, both in clinical work and in research fields.
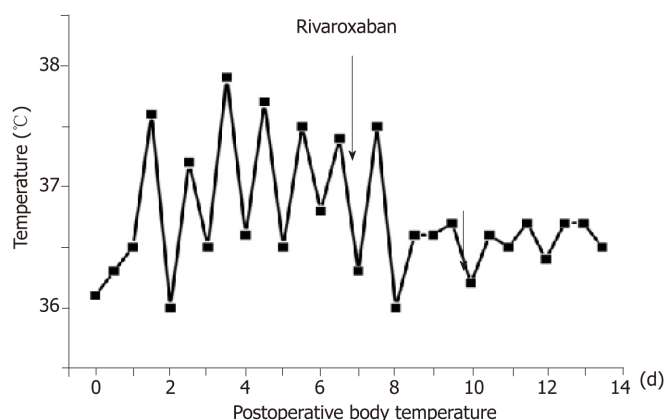
Figure 3 Body temperature returned to normal after administration of rivaroxaban for two days.
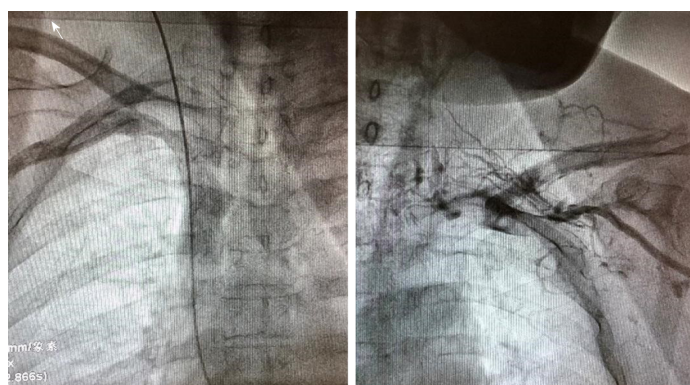
Figure 4 Intraoperative angiography showed that the right subclavian vein was open and the left subclavian vein was occluded accompanied by collateral circulation establishment.

REFERENCES

1 **Kusumoto FM**, Schoenfeld MH, Wilkoff BL, Berul CI, Birgersdotter-Green UM, Carrillo R, Cha YM, Clancy J, Deharo JC, Ellenbogen KA, Exner D, Hussein AA, Kennergren C, Krahn A, Lee R, Love CJ, Madden RA, Mazzetti HA, Moore JC, Parsonnet J, Patton KK, Rozner MA, Selzman KA, Shoda M, Srivathsan K, Strathmore NF, Swerdlow CD, Tompkins C, Wazni O. 2017 HRS expert consensus statement on cardiovascular implantable electronic device lead management and extraction. *Heart Rhythm* 2017; **14**: e503-e551 [PMID: 28919379 DOI: 10.1016/j.hrthm.2017.09.001]

2 **Di Monaco A**, Pelargonio G, Narducci ML, Manzoli L, Boccia S, Flacco ME, Capasso L, Barone L, Perna F, Bencardino G, Rio T, Leo M, Di Biase L, Santangeli P, Natale A, Rebuzzi AG, Crea F. Safety of transvenous lead extraction according to centre volume: a systematic review and meta-analysis. *Europace* 2014; **16**: 1496-1507 [PMID: 24965015 DOI: 10.1093/europace/euu137]

3 **Hanninen M**, Cassagneau R, Manlucu J, Yee R. Extensive Thrombosis Following Lead Extraction: Further Justification for Routine Post-operative Anticoagulation. *Indian Pacing Electrophysiol J* 2014; **14**: 150-151 [PMID: 24920869]

4 **Wazni O**, Epstein LM, Carrillo RG, Love C, Adler SW, Riggio DW, Karim SS, Bashir J, Greenspon AJ, DiMarco JP, Cooper JM, Onufer JR, Ellenbogen KA, Kutalek SP, Dentry-Mabry S, Ervin CM, Wilkoff BL. Lead extraction in the contemporary setting: the LExICon study: an observational retrospective study of consecutive laser lead extractions. *J Am Coll Cardiol* 2010; **55**: 579-586 [PMID: 20152562 DOI: 10.1016/j.jacc.2009.08.070]

5 **Kennergren C**, Bjurman C, Wiklund R, Gäbel J. A single-centre experience of over one thousand lead extractions. *Europace* 2009; **11**: 612-617 [PMID: 19329797 DOI: 10.1093/europace/eup054]

6 **Wilkoff BL**, Byrd CL, Love CJ, Hayes DL, Sellers TD, Schaerf R, Parsonnet V, Epstein LM, Sorrentino RA, Reiser C. Pacemaker lead extraction with the laser sheath: results of the pacing lead extraction with the excimer sheath (PLEXES) trial. *J Am Coll Cardiol* 1999; **33**: 1671-1676 [PMID: 10334441 DOI: 10.1016/s0735-1097(99)00074-1]

7 **Bracke FA**, Meijer A, Van Gelder LM. Symptomatic occlusion of the access vein after pacemaker or ICD lead extraction. *Heart* 2003; **89**: 1348-1349 [PMID: 14594900 DOI: 10.1136/heart.89.11.1348]

8 **Isma N**, Svensson PJ, Gottsäter A, Lindblad B. Upper extremity deep venous thrombosis in the population-based Malmö thrombophilia study (MATS). Epidemiology, risk factors, recurrence risk, and mortality. *Thromb Res* 2010; **125**: e335-e338 [PMID: 20406709 DOI: 10.1016/j.thromres.2010.03.005]

9 **Mai C**, Hunt D. Upper-extremity deep venous thrombosis: a review. *Am J Med* 2011; **124**: 402-407 [PMID: 21531227 DOI: 10.1016/j.amjmed.2010.11.022]

10 **Byrd CL**, Wilkoff BL, Love CJ, Sellers TD, Reiser C. Clinical study of the laser sheath for lead

extraction: the total experience in the United States. *Pacing Clin Electrophysiol* 2002; **25**: 804-808 [PMID: 12049372 DOI: 10.1046/j.1460-]

11   **Diamond PT**, Macciocchi SN. Predictive power of clinical symptoms in patients with presumptive deep venous thrombosis. *Am J Phys Med Rehabil* 1997; **76**: 49-51 [PMID: 9036911 DOI: 10.1097/00002060-199701000-00009]

12   **Rehman T**, deBoisblanc BP. Persistent fever in the ICU. *Chest* 2014; **145**: 158-165 [PMID: 24394828 DOI: 10.1378/chest.12-2843]

13   **Hung YP**, Lee NY, Chang CM, Lee HC, Wu CJ, Chen PL, Lee CC, Chung CH, Ko WC. Tolerability of teicoplanin in 117 hospitalized adults with previous vancomycin-induced fever, rash, or neutropenia: a retrospective chart review. *Clin Ther* 2009; **31**: 1977-1986 [PMID: 19843487 DOI: 10.1016/j.clinthera.2009.09.010]

14   **Chow V**, Ranasinghe I, Lau J, Stowe H, Bannon P, Hendel N, Kritharides L. Peri-procedural anticoagulation and the incidence of haematoma formation after permanent pacemaker implantation in the elderly. *Heart Lung Circ* 2010; **19**: 706-712 [PMID: 20851678 DOI: 10.1016/j.hlc.2010.08.011]

15   **Essebag V**, Verma A, Healey JS, Krahn AD, Kalfon E, Coutu B, Ayala-Paredes F, Tang AS, Sapp J, Sturmer M, Keren A, Wells GA, Birnie DH; BRUISE CONTROL Investigators. Clinically Significant Pocket Hematoma Increases Long-Term Risk of Device Infection: BRUISE CONTROL INFECTION Study. *J Am Coll Cardiol* 2016; **67**: 1300-1308 [PMID: 26988951 DOI: 10.1016/j.jacc.2016.01.009]

16   **Masiero S**, Connolly SJ, Birnie D, Neuzner J, Hohnloser SH, Vinolas X, Kautzner J, O'Hara G, VanErven L, Gadler F, Wang J, Mabo P, Glikson M, Kutyifa V, Wright DJ, Essebag V, Healey JS; SIMPLE Investigators. Wound haematoma following defibrillator implantation: incidence and predictors in the Shockless Implant Evaluation (SIMPLE) trial. *Europace* 2017; **19**: 1002-1006 [PMID: 27353323 DOI: 10.1093/europace/euw116]

CASE REPORT

c.753_754delAG, a novel *CFTR* mutation found in a Chinese patient with cystic fibrosis: A case report and review of the literature

Yu-Qing Wang, Chuang-Li Hao, Wu-Jun Jiang, Yan-Hong Lu, Hui-Quan Sun, Chun-Yan Gao, Min Wu

ORCID number: Yu-Qing Wang (0000-0002-4153-3984); Chuang-Li Hao (0000-0002-1342-8175); Wu-Jun Jiang (0000-0002-1538-9069); Yan-Hong Lu (0000-0002-9447-6493); Hui-Quan Sun (0000-0002-1200-0812); Chun-Yan Gao (0000-0001-6875-9652); Min Wu (0000-0001-9758-9517).

Yu-Qing Wang, Chuang-Li Hao, Wu-Jun Jiang, Yan-Hong Lu, Hui-Quan Sun, Chun-Yan Gao, Min Wu, Department of Respiratory Medicine, Children's Hospital of Soochow University, Suzhou 215000, Jiangsu Province, China

Corresponding author: Yu-Qing Wang, MD, Chief Doctor, Deputy Director, Department of Respiratory Medicine, Children's Hospital of Soochow University, No. 303, Jingde Road , Suzhou 215000, Jiangsu Province, China. wang_yu_qing@126.com
Telephone: +86-512-67788313
Fax: +86-512-67786316

Abstract

BACKGROUND
Cystic fibrosis (CF) is rare in Asian populations relative to the Caucasian population. In this paper, we report the cystic fibrosis transmembrane conductance regulator (CFTR) variation in a family of Chinese CF patients, and systematically review the previous literature.

CASE SUMMARY
Here we report a 30-month-old Chinese girl who was diagnosed with CF based on her history and symptoms such as recurrent productive cough, wheezing with repeated infection of *Pseudomonas aeruginosa*, and parasinusitis. Chest computed tomography (CT) scanning revealed obvious exudative lesions and bilateral bronchiectasis. Liver CT scanning revealed a low-density lesion in the left lobe of the liver. A diagnosis of CF was made based upon *CFTR* gene tests. The *CFTR* gene was sequenced using the blood samples of her and her parents and showed a heterozygous novel missense mutation of c.753_754delAG in exon 7. In addition, a heterozygous c.1240 C>T mutation was found in exon 10 of the *CFTR*. The mutation c.753_754delAG was verified to have been inherited from her mother, and the c.1240 C>T mutation was from her father who was diagnosed with congenital absence of vas deferens.

CONCLUSION
A novel mutation of CFTR, c.753_754delAG, was found in a Chinese CF child. c.2909G>A is the most common mutation among Chinese CF patients.

Key words: Cystic fibrosis; Cystic fibrosis transmembrane conductance regulator; Mutation; Chinese children; Case report

Core tip: Cystic fibrosis (CF) is an autosomal recessive inherited disease caused by mutations in the CF transmembrane conduction regulator (*CFTR*) gene. CF is rare in Chinese. ΔF508 is the most common mutation, accounting for greater than two-thirds of CF alleles worldwide, though it is not a predominant mutation in Chinese CF patients. In this paper, we report a novel homozygous complex rearrangement involving *CFTR* exon 7 deletion (c.753_754delAG chr7-117176607-117176608) in a Chinese child with CF and describe the clinical feature. Moreover, we further review the literature regarding gene mutations in Chinese CF cases from the 1970s to 2017.

INTRODUCTION

Cystic fibrosis (CF) is an autosomal recessive inherited disease caused by mutations in the CF transmembrane conduction regulator (*CFTR*) gene. CF is most common in the Caucasian population, with a prevalence of 1/2500-3500 among those with Northern European ancestry[1,2]. CF was once considered extremely rare among the Chinese population, and to date, only about 60 cases of CF have been diagnosed in China[3]. CFTR is responsible for regulating the flow of chloride ions across the epithelial membrane. Since *CFTR* was first identified as the pathogenic gene of CF in 1989, more than 2000 mutations have been found in CF patients, according to the Cystic Fibrosis Mutation Database (http://www.genet.sickkids.on.ca). ΔF508 is the most common mutation, accounting for greater than two-thirds of CF alleles worldwide, though it is not a predominant mutation in Chinese CF patients[4]. The most common gene mutation in Chinese children with CF is c.2909G-A[5]. With increased awareness of this disease and improvements in diagnostic techniques, we have found that CF is not as rare as once believed in the Chinese population. The novel variants c.699 C-A, c.579+1_579+2insACAT, c.1117-1G>C c.3140-454_c.3367+249del931ins13, and p.R1048_G1123del have been reported in CF patients from China in recent years[6-8]. Interestingly, the gene mutation spectrum of CFTR in Chinese patients with CF is significantly different from that in Caucasian patients. Therefore, it is necessary to establish the Chinese *CFTR* gene mutation database, which will facilitate the genetic diagnosis of CF patients in China. In the present study, we identified a novel homozygous complex rearrangement involving CFTR exon 7 deletion (c.753_754delAG chr7-117176607-117176608) using multiplex ligation-dependent probe amplification analysis in a Chinese child with CF. We further review the literature regarding Chinese CF patients from the 1970s to 2017. The clinical data of all identified CF patients are summarized.

CASE PRESENTATION

Chief complaints

A girl aged 2 years and 10 months was admitted to Children's Hospital of Soochow University in May 2018 due to recurrent productive cough and wheezing lasting for 1 month.

History of past illness

She had experienced recurrent pneumonia (2-3 times every year) beginning 4 mo after birth, with repeated infection by *Pseudomonas aeruginosa* and parasinusitis, but without a history of chronic diarrhea or pancreatic involvement.

Personal and family history

The child was conceived through *in vitro* fertilization. Her father had been diagnosed with congenital absence of vas deferens, and her mother was healthy.

Physical examination

She weighed 11 kg, her height was 89 cm, her body mass index was 13.9, and she

presented with shortness of breath and dyspnea. Crackles and wheezing rales were present in bilateral lungs. The heart and abdomen were normal. No clubbed digits were found.

Laboratory examinations

Blood routine examination showed a white blood cell count of 15.59×10^9/L, a C reactive protein concentration of 55.4 mg/L, and positivity for *Pseudomonas aeruginosa* on bronchoalveolar lavage fluid culture. Findings on other tests, including serum electrolyte measurement, fungus culture, Glactomannan test, T-SPOT tuberculosis test, allergic bronchopulmonary aspergillosis and aspergillus fumigatus specific IgE detection were all negative.

Imaging examinations

Chest computed tomography (CT) scanning revealed obvious exudative lesions and bilateral bronchiectasis (Figures 1 and 2). Sinus CT scanning revealed bilateral parasinusitis. Liver CT scanning revealed a low-density lesion in the left lobe of the liver. In patients with CF, the liver is also the organ affected by the dense secretion of digestive juice. Bile secreted by the liver can clog bile ducts and damage the liver. Ultrasonography of the pancreas was negative.

CFTR gene sequence analysis

Two heterozygous mutations were found in the CF patient by Sanger sequencing analysis. A heterozygous novel missense mutation of c.753_754delAG chr7-117176607-117176608 was identified in exon 7 (Figure 3), which was inherited from her mother based on its identification in the mother's sample as well (Figure 3). This novel mutation has not yet been recorded in the *CFTR* mutation database (http://www.genet.sickkids.on.ca). In addition, a heterozygous c.1240 C>T mutation in exon 10 was observed in *CFTR* of the CF patient (Figure 4), which was inherited from her father and had already been included in the *CFTR* mutation database.

FINAL DIAGNOSIS

CF.

TREATMENT

Her symptoms improved after antibiotic treatment with ceftazidime for 3 wk, expectorant, and nutritional support treatment including fat-soluble vitamins and powdered milk with high calorie.

OUTCOME AND FOLLOW-UP

After being discharged from our hospital, the children were followed monthly in the outpatient clinic. We gave low dose azithromycin anti-inflammatory treatment to eradicate *P. aeruginosa* infection. We did regular examinations of respiratory rate, oxygen saturation, and high-resolution CT of the chest to evaluate the pulmonary disease regression/progression. We introduced regular atomized bronchodilators such as terbutaline and oral secretion expellant including acetylcysteine to help remove respiratory secretions. She had one time of pulmonary infection. The general situation remained well up to date. She weighed 13 kg, her height was 95 cm, and her body mass index was 14.4.

DISCUSSION

CF is characterized by the abnormal transport of ions and fluid across epithelial cell membranes, resulting from mutations on both alleles in the gene encoding the CFTR[9,10]. *CFTR* mutations can cause secretions to obstruct the airway, pancreatic tract, and biliary tract and lead to abnormal secretion by the sweat glands. The most important organ to be invaded in CF is the lung, and lung disease is the most lethal factor (85%)[11]. The pancreas is also an important affected organ in CF. Disorders caused by CF include nutritional disorders (fat, protein malabsorption, and fatty diarrhea) and growth retardation. Low body weight caused by pancreatic insufficiency is negatively correlated with lung function and survival rate, and thus,
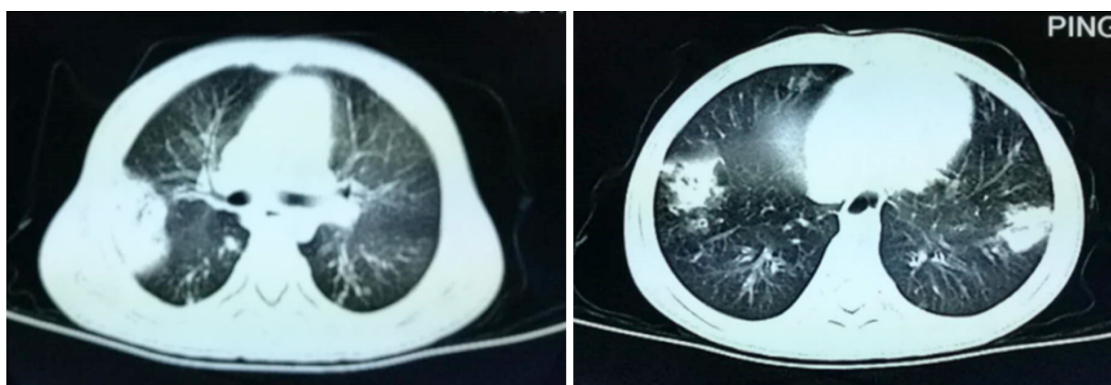
Figure 1 Chest computed tomography images of the cystic fibrosis patient. A chest computed tomography scan showed obvious exudative lesions and bilateral bronchiectasis in the lung of the cystic fibrosis patient.

an important factor for poor prognosis[12]. Malnutrition and gastrointestinal symptoms are relatively mild and atypical in Chinese CF patients. Therefore, it is easy for CF diagnosis to be missed or delayed.

For patients with one or more clinical characteristics, such as chronic sinopulmonary disease, gastrointestinal and nutritional abnormalities, genital abnormalities in males resulting in obstructive azoospermia, and/or a family history of CF, the measurement of sweat electrolyte concentrations has been the mainstay of CF diagnosis since the standardized procedure was introduced[13]. In the CF case reported here, the patient had chronic sinopulmonary disease, and her father had a CF mutation with obstructive azoospermia. These patients should undergo repeat sweat chloride testing and further evaluation, including detailed clinical assessment and more extensive *CFTR* gene mutation analysis. CF in Chinese patients is difficult to diagnose, due to insufficient understanding and because sweat examination as well as genetic testing cannot be carried out in most hospitals. It is necessary to educate Chinese pediatricians concerning the clinical manifestations and diagnostic criteria for CF and to promote the implementation of the sweat chloride test.

CFTR mutations are divided into five general classes: mutations affecting biosynthesis, mutations interfering with protein maturation, mutations influencing Cl- channel regulation, mutations intervening Cl- conductance or channel gating, and mutations that reduce CFTR synthesis[14]. Different types of *CFFR* mutations can cause different clinical phenotypes: I, II, and III mutations are prone to cause pancreatic insufficiency with more serious clinical manifestations. In contrast, because normal Cl- channel function is partially retained, the clinical symptoms of IV and V mutations are relatively mild with pancreatic function remaining normal.

Several studies have demonstrated that p.F508del is the most common mutation in Caucasian CF patients, accounting for approximately 70% of cases[4,5]. The p. F508del mutation is a type II mutation. We review 82 different mutations among 69 Chinese CF patients (40 females and 29 males) reported from the 1970s to 2017. Among them, 53 were from mainland China, 9 from Taiwan, and 4 from Hongkong, with the remaining patients being of Chinese and Vietnamese descent, Chinese and Portuguese descent[7,8,15-40] (Table 1). The age at diagnosis ranged from 0.17 months to 23 years.

Among the Chinese CF patients, the c.2909 G>A variant was the most common mutation type (11%), followed by 1898+5G>T (7.3%), c.293A>G (6.1%), and 2215insG+G2816A and c.263T>G (both 4.9%). Nevertheless, no p.F508del mutation was found in the Chinese patients (Table 1). In addition, with the exceptions of c.3909 C>G, R553X, and c.1000 C>T, none of the *CFTR* mutations in the Chinese patients were present in the common Caucasian *CFTR* mutation-screening panels, indicating that the mutations identified in Chinese CF patients are obviously different from the common gene mutations in Caucasian CF patients. Further, pulmonary lesions were more prominent in Chinese CF patients with or without pancreatic insufficiency[6-8,26,27]. Therefore, it is necessary to establish a Chinese gene mutation database to facilitate genetic diagnosis of CF in China to clarify the relationship between genotype and clinical phenotype.

In the case reported herein, the c.1240C>T mutation resulted in the alteration of amino acid p.Q414* (glutamine > termination). This mutation type has been reported already as a pathogenic mutation in the HGMD pro database[14]. c.753_754A del A.G is a novel mutation (deletion mutation) that results in amino acid changes P.R251Sfs * 6 (frame-shifting mutation - 6 termination). According to the ACMG guidelines, the mutation site c.753_754delAG could be classified as a pathogenic mutation[39]. Both
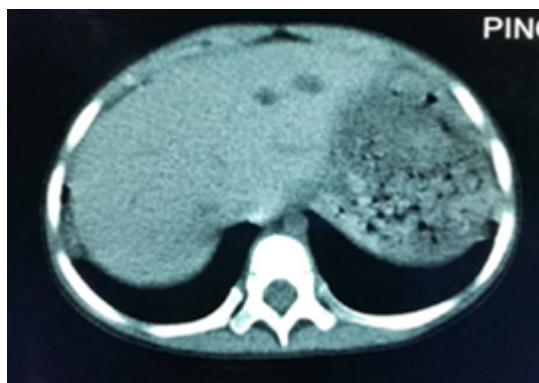
Figure 2 Liver computed tomography image of the cystic fibrosis patient. A liver computed tomography scan revealed a low-density lesion in the left lobe of the liver.

mutations could result in the early termination of CFTR protein translation, which might have a great impact on protein function. The double heterozygous mutation came from the patient's parents separately. As a compound heterozygous mutation, it is consistent with autosomal recessive inheritance and is a theoretically possible cause of disease. This case expands the mutation spectrum of *CFTR* in patients of Chinese origin. Several studies have shown that only pancreatic function correlates well with *CFTR* genotypes[40,41]. According to the pancreatic status of patients, CF mutations can be subdivided into two groups: mild and severe mutations[40]. Patients with pancreatic insufficiency are homozygous or compound heterozygous with two "severe" mutations, whereas patients with pancreatic sufficiency have at least one "mild" allele. As it is not clear from the case if the patient had pancreatic sufficiency or insufficiency, we cannot deduce whether the two mutations were severe mutations or not. Elevated serum lipase, which has not been mentioned before, is not a sign of severe mutation, more of possible pancreatitis which is more commonly seen in heterozygous CF carriers or in those with milder mutations and pancreatic sufficiency.

CONCLUSION

In conclusion, a novel compound heterozygous c.753_754delAG mutation was found in exon 7 of *CFTR* in the case reported herein. The common *CFTR* mutation spectrum in Chinese CF patients is quite different from that in Caucasian patients. Therefore, the Chinese common *CFTR* mutation spectrum provides valuable data for CF diagnosis in Chinese patients and the development of a commercial Chinese *CFTR* genetic screening kit. The relevant Chinese gene mutation database is urgently needed.

Table 1 Characteristics of *CFTR* gene mutations in 69 Chinese cystic fibrosis patients

Reference	Location	*n*	Gender	Age (yr)	Mutation
Wang *et al*[15], 1993	Taiwan China	1	F	0.5	1898+5 G-->T, 2215insG+G2816A
Chen *et al*[16],1995	Mainland China	1	F	—	E2 del about 30 bp
Zielenski *et al*[17], 1995	Taiwan China	1	F	8	1898+5 G-->T, 1898+5 G-->T
Crawford *et al*[18], 1995	Chinese and Portuguese	1	F	3	1898 + 1G>T
Wagner *et al*[19], 1999	Chinese	1	F	23	c.319-326delGCTTCCTA, c. 2909G>A
Wu *et al*[20], 2000	Taiwan China	2	F	14	1898+5 G>T, 2215insG+G2816A
			M	17	1898+5 G>T, 2215insG+G2816A
Alper *et al*[21], 2003	Chinese and Vietnamese	2	M	1.5	G151T, 989-992insA
	Taiwan China		F	0.5	1898+5G>T, 2215insG+G2816A
Chen *et al*[22], 2005	Taiwan China	1	M	3	R553X, R553X
Li *et al*[6], 2006	Mainland China	1	F	14	699C>A, 3821-3823delT
Wang *et al*[23], 2012	Mainland China	1	F	14	W679X
Liu *et al*[24], 2012	Mainland China	2	F	13	2909G>A, 362T>G
			F	10	3196C>T, 3196C>T
Cheng *et al*[25], 2013	Mainland China	1	F	12	W679X, 1342-11TTT>G, 3120+2T>C
Liu *et al*[26], 2015	Mainland China	7	M	12	c.95T>C, c.1657C>T
			M	10	c.293A>G, c.558C>G
			M	16	c.2052 dupA, E18-E20(c.2909-?_3367 + ?del)
			F	16	c.2909G>A, E7-E11†(c.744-?_1584 + ?del)
			F	10	c.1679 + 2T>C, c.2658-1G>C
			F	21	c.293A>G, c.293A>G
			F	28	c.1666A>G
Shen *et al*[27], 2016	Mainland China	19	M	11.58	c.1699G>T, c.3909C>G
			F	10.58	c.263T>G, c.1766+5G>T, c.110C>G
			M	13.25	c.3700A>G, c.960_961insA
			F	13.67	c.263T>G, c.2909G>A
			M	7.17	c.326A>G, c.1000C>T, c.1666A>G
			F	10.67	c.595C>T
			F	7.75	c.223C>T, c.326A>G
			F	7.33	c.1000C>T
			F	10.17	c.263T>G
			F	11.08	c.1666A>G
			M	8.25	c.293A>G, c.558C>G
			F	4.17	c.326A>G, c.2374C>T
			M	3.67	c.1666A>G
			F	12.67	c.293A>G
			M	11	c.648G>A, c.2491-126T>C
			F	10.33	c.3196C>T
			M	11.17	c.414_415insCTA
			F	3.42	c.1075C>T, c.3307delA
			F	14	c.2909G>A
Chu *et al*[28], 2016	Mainland China	1	M	9	C.579+2insACAT, C.F481766+5G>T
Xu *et al*[29], 2016	Mainland China	1	M	0.67	c.595C>T, C.2290C>T
Li *et al*[30], 2016	Mainland China	1	M	0.42	c.214G>G/A, c.650A>A/G,c.3406G>G/A
Tian *et al*[31], 2016	Mainland China	8	F	15	c.2909G>A, c.2374C>T
			F	1	c.2909G>A, c.2125C>T
			M	13	c.3700A>G, c.959–960insA
			M	15	c.3635delT
			F	4	c.2909G>A, c.263T>G
			F	13	c.2909G>A, c.2907A>C
			M	20	c.2909G>A, c.1521_1523delCTT
			F	22	c.2909G>A, c.1997T>G

Leung *et al*[32], 2017	HongKong China	4	M	17	c.1766+5G>T, c.3068T>G
			M	0.5	c.1766+5G>T, c.3140-26A>G
			M	0.17	c.868C>T, c.3068T>G
			F	0.75	c.1657C>T, c.3068T>G
Xie *et al*[33], 2017	Mainland China	2	M	12	c.865A>T,c.3651_3652insAAAT
			M	15	c.865A>T,c.3651_3653insAAAT
Zheng *et al*[34], 2017	Mainland China	2	M	5	c.3196C>T, c.870-1G>C
			F	5	c.3G>A , c.1572C>A
Xu *et al*[7], 2017	Mainland China	4	M	9	c.579+1_579+2insACAT, c.1766+5G>T
			M	5	c.595C>T
			F	6	c.1117-1G>C, c.2909G>A
			M	13	c.4056G>C
Liu *et al*[8], 2017	Mainland China	1	M	11	c.3140-454_c.3367+249del931ins13
Yao *et al*[35], 2017	Mainland China	1	F	0.5	c.532G>A
Sun *et al*[36], 2017	Mainland China	1	F	2	C.1 666A>G
Guo *et al*[37], 2017	Mainland China	1	F	0.75	c.1373G>A(p.G458E), c.271G>A(p.G91R)
Li *et al*[38], 2017	Mainland China	1	F	1.33	R709X, G970D

Figure 3 Genomic sequence of exon 7 of *CFTR*. *CFTR* genomic sequencing results for exon 7 showed a heterozygous mutation of c.753_754delAG chr7-117176607-1171766 08 p.R251Sfs*6 in the cystic fibrosis patient and her mother. Exon 7 of *CFTR* was normal in her father.
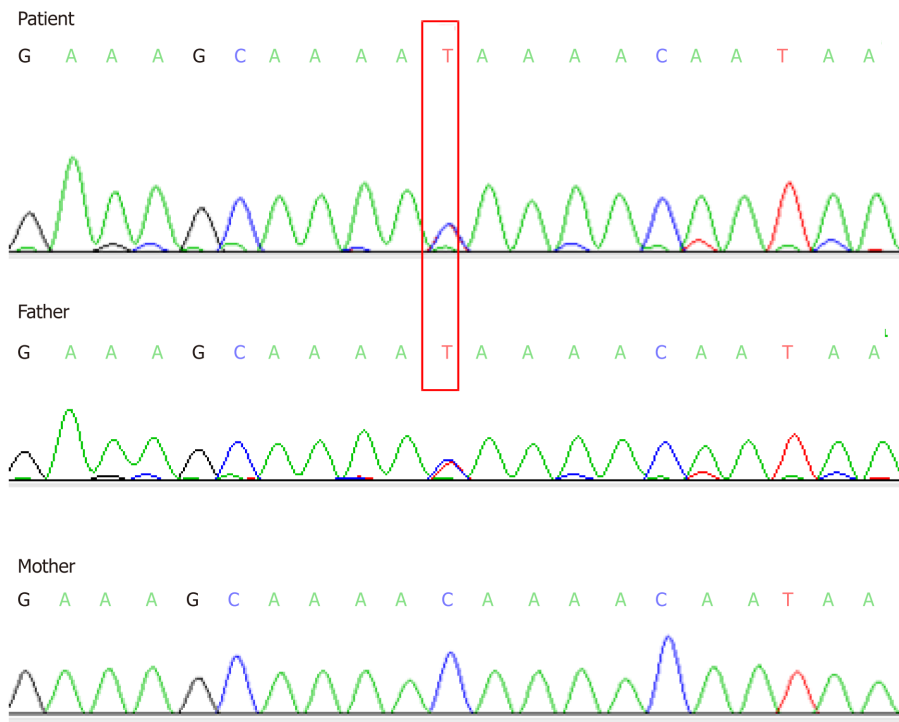
Figure 4 Genomic sequence of exon 10 of *CFTR*. *CFTR* genomic sequencing results of exon 10 revealed a heterozygous mutation of c.1240C>T chr7-117188725 p.Q414* in the cystic fibrosis patient and her father. Exon 10 of her mother was normal.

ACKNOWLEDGEMENTS

REFERENCES

1   **Salvatore D**, Buzzetti R, Baldo E, Forneris MP, Lucidi V, Manunza D, Marinelli I, Messore B, Neri AS, Raia V, Furnari ML, Mastella G. An overview of international literature from cystic fibrosis registries. Part 3. Disease incidence, genotype/phenotype correlation, microbiology, pregnancy, clinical complications, lung transplantation, and miscellanea. *J Cyst Fibros* 2011; **10**: 71-85 [PMID: 21257352 DOI: 10.1016/j.jcf.2010.12.005]
2   **Southern KW**, Munck A, Pollitt R, Travert G, Zanolla L, Dankert-Roelse J, Castellani C; ECFS CF Neonatal Screening Working Group. A survey of newborn screening for cystic fibrosis in Europe. *J Cyst Fibros* 2007; **6**: 57-65 [PMID: 16870510 DOI: 10.1016/j.jcf.2006.05.008]
3   **Singh M**, Rebordosa C, Bernholz J, Sharma N. Epidemiology and genetics of cystic fibrosis in Asia: In preparation for the next-generation treatments. *Respirology* 2015; **20**: 1172-1181 [PMID: 26437683 DOI: 10.1111/resp.12656]
4   **Tabaripour R**, Niaki HA, Douki MR, Bazzaz JT, Larijani B, Yaghmaei P. Poly thymidine polymorphism and cystic fibrosis in a non-Caucasian population. *Dis Markers* 2012; **32**: 241-246 [PMID: 22430190 DOI: 10.3233/DMA-2011-0880]
5   **Boyle MP**, De Boeck K. A new era in the treatment of cystic fibrosis: correction of the underlying CFTR defect. *Lancet Respir Med* 2013; **1**: 158-163 [PMID: 24429096 DOI: 10.1016/S2213-2600(12)70057-7]
6   **Li N**, Pei P, Bu DF, He B, Wang GF. A novel CFTR mutation found in a Chinese patient with cystic fibrosis. *Chin Med J (Engl)* 2006; **119**: 103-109 [PMID: 16454991 DOI: 10.3901/JME.2006.11.103]
7   **Xu J**, Yin Y, Zhang L, Zhang J, Yuan S, Zhang H. Four case reports of Chinese cystic fibrosis patients and literature review. *Pediatr Pulmonol* 2017; **52**: 1020-1028 [PMID: 28608624 DOI: 10.1002/ppul.23744]
8   **Liu K**, Liu Y, Li X, Xu KF, Tian X, Zhang X. A novel homozygous complex deletion in CFTR caused cystic fibrosis in a Chinese patient. *Mol Genet Genomics* 2017; **292**: 1083-1089 [PMID: 28620757 DOI: 10.1007/s00438-017-1334-0]
9   **Riordan JR**, Rommens JM, Kerem B, Alon N, Rozmahel R, Grzelczak Z, Zielenski J, Lok S, Plavsic N, Chou JL. Identification of the cystic fibrosis gene: cloning and characterization of complementary DNA. *Science* 1989; **245**: 1066-1073 [PMID: 2475911 DOI: 10.1126/science.2475911]
10   **Kerem B**, Rommens JM, Buchanan JA, Markiewicz D, Cox TK, Chakravarti A, Buchwald M, Tsui LC. Identification of the cystic fibrosis gene: genetic analysis. *Science* 1989; **245**: 1073-1080 [PMID: 2570460 DOI: 10.1016/0168-9525(89)90156-X]
11   **Davis PB**. Cystic fibrosis since 1938. *Am J Respir Crit Care Med* 2006; **173**: 475-482 [PMID: 16126935 DOI: 10.1164/rccm.200505-840OE]
12   **Stallings VA**, Stark LJ, Robinson KA, Feranchak AP, Quinton H; Clinical Practice Guidelines on Growth

and Nutrition Subcommittee; Ad Hoc Working Group. Evidence-based practice recommendations for nutrition-related management of children and adults with cystic fibrosis and pancreatic insufficiency: results of a systematic review. *J Am Diet Assoc* 2008; **108**: 832-839 [PMID: 18442507 DOI: 10.1016/j.jada.2008.02.020]

13   **Farrell PM**, Rosenstein BJ, White TB, Accurso FJ, Castellani C, Cutting GR, Durie PR, Legrys VA, Massie J, Parad RB, Rock MJ, Campbell PW; Cystic Fibrosis Foundation. Guidelines for diagnosis of cystic fibrosis in newborns through older adults: Cystic Fibrosis Foundation consensus report. *J Pediatr* 2008; **153**: S4-S14 [PMID: 18639722 DOI: 10.1016/j.jpeds.2008.05.005]

14   **Dörk T**, Fislage R, Neumann T, Wulf B, Tümmler B. Exon 9 of the CFTR gene: splice site haplotypes and cystic fibrosis mutations. *Hum Genet* 1994; **93**: 67-73 [PMID: 7505767 DOI: 10.1007/BF00218916]

15   **Wang MC**, Shu SG, Chang SM, Ho WL, Chi CS. Cystic fibrosis in two Chinese infants in Taiwan. *Zhonghua Min Guo Xiao Er Ke Yi Xue Hui Za Zhi* 1993; **34**: 314-321 [PMID: 8213163]

16   **Chen BH**, Zhang SZ, Yang Y. The first case of CF in Mainland China identified by DNA analysis. *Zhonghua Yi Xue Yi Chuan Xue Za Zhi* 1995; **12**: 5-9

17   **Zielenski J**, Markiewicz D, Lin SP, Huang FY, Yang-Feng TL, Tsui LC. Skipping of exon 12 as a consequence of a point mutation (1898 + 5G-->T) in the cystic fibrosis transmembrane conductance regulator gene found in a consanguineous Chinese family. *Clin Genet* 1995; **47**: 125-132 [PMID: 7543385 DOI: 10.1111/j.1399-0004.1995.tb03944.x]

18   **Crawford J**, Labrinidis A, Carey WF, Nelson PV, Harvey JS, Morris CP. A splicing mutation (1898 + 1G-->T) in the CFTR gene causing cystic fibrosis. *Hum Mutat* 1995; **5**: 101-102 [PMID: 7537147 DOI: 10.1002/humu.1380050115]

19   **Wagner JA**, Vassilakis A, Yee K, Li M, Hurlock G, Krouse ME, Moss RB, Wine JJ. Two novel mutations in a cystic fibrosis patient of Chinese origin. *Hum Genet* 1999; **104**: 511-515 [PMID: 10453741 DOI: 10.1007/s004390050996]

20   **Wu CL**, Shu SG, Zielenski J, Chiang CD, Tsui LC. Novel cystic fibrosis mutation (2215insG) in two adolescent Taiwanese siblings. *J Formos Med Assoc* 2000; **99**: 564-567 [PMID: 10925568 DOI: 10.1016/S0885-3924(00)00150-0]

21   **Alper OM**, Shu SG, Lee MH, Wang BT, Lo SY, Lin KL, Chiu YL, Wong LJ. Detection of novel CFTR mutations in Taiwanese cystic fibrosis patients. *J Formos Med Assoc* 2003; **102**: 287-291 [PMID: 12874665 DOI: 10.1016/S0885-3924(03)00065-4]

22   **Chen HJ**, Lin SP, Lee HC, Chen CP, Chiu NC, Hung HY, Chern SR, Chuang CK. Cystic fibrosis with homozygous R553X mutation in a Taiwanese child. *J Hum Genet* 2005; **50**: 674-678 [PMID: 16283068 DOI: 10.1007/s10038-005-0309-x]

23   **Wang B**, Yang L. Cystic Fibrosis Involving Multisystem: A Case Report and Literature Review. *Huaxi Yixue* 2012; **6**: 852-854

24   **Liu JR**, Peng Y, Zhao YH, Wang W, Guo Y, He JX, Zhao SY, Jiang ZF. [Clinical manifestations and gene analysis of 2 Chinese children with cystic fibrosis]. *Zhonghua Er Ke Za Zhi* 2012; **50**: 829-833 [PMID: 23302613 DOI: 10.1007/s11783-011-0280-z]

25   **Cheng Y**, Ning G, Song B, Guo YK, Li XS. A Chinese girl with cystic fibrosis: a case report identified by sweat and genetic tests. *Chin Med J (Engl)* 2012; **125**: 719 [PMID: 22490504 DOI: 10.3760/cma.j.issn.0366-6999.2012.04.031]

26   **Liu Y**, Wang L, Tian X, Xu KF, Xu W, Li X, Yue C, Zhang P, Xiao Y, Zhang X. Characterization of gene mutations and phenotypes of cystic fibrosis in Chinese patients. *Respirology* 2015; **20**: 312-318 [PMID: 25580864 DOI: 10.1111/resp.12452]

27   **Shen Y**, Liu J, Zhong L, Mogayzel PJ, Zeitlin PL, Sosnay PR, Zhao S. Clinical Phenotypes and Genotypic Spectrum of Cystic Fibrosis in Chinese Children. *J Pediatr* 2016; **171**: 269-76.e1 [PMID: 26826884 DOI: 10.1016/j.jpeds.2015.12.025]

28   **Chu JL**, Wang Y, Qian J. Cystic fibrosis with severe pneumonia in children. *Chin Pediatr Emerg Med* 2016; **23**: 501-504 [DOI: 10.3760/cma.j.issn.1673-4912.2016.07.018]

29   **Xu BP**, Wang H, Zhao YH, Liu J, Yao Y, Feng XL, Shen KL. [Molecular diagnosis of two Chinese cystic fibrosis children and literature review]. *Zhonghua Er Ke Za Zhi* 2016; **54**: 344-348 [PMID: 27143075 DOI: 10.3760/cma.j.issn.0578-1310.2016.05.007]

30   **Li L**, Wang NL, Gong JY, Wang JS. [Infantile cholestasis caused by CFTR mutation: case report and literature review]. *Zhonghua Er Ke Za Zhi* 2016; **54**: 851-855 [PMID: 27806795 DOI: 10.3760/cma.j.issn.0578-1310.2016.11.013]

31   **Tian X**, Liu Y, Yang J, Wang H, Liu T, Xu W, Li X, Zhu Y, Xu KF, Zhang X. p.G970D is the most frequent CFTR mutation in Chinese patients with cystic fibrosis. *Hum Genome Var* 2016; **3**: 15063 [PMID: 27081564 DOI: 10.1038/hgv.2015.63]

32   **Leung GK**, Ying D, Mak CC, Chen XY, Xu W, Yeung KS, Wong WL, Chu YW, Mok GT, Chau CS, McLuskey J, Ong WP, Leong HY, Chan KY, Yang W, Chen JH, Li AM, Sham PC, Lau YL, Chung BH, Lee SL. <i>CFTR</i> founder mutation causes protein trafficking defects in Chinese patients with cystic fibrosis. *Mol Genet Genomic Med* 2016; **5**: 40-49 [PMID: 28116329 DOI: 10.1002/mgg3.258]

33   **Xie Y**, Huang X, Liang Y, Xu L, Pei Y, Cheng Y, Zhang L, Tang W. A new compound heterozygous CFTR mutation in a Chinese family with cystic fibrosis. *Clin Respir J* 2017; **11**: 696-702 [PMID: 26471113 DOI: 10.1111/crj.12401]

34   **Zheng B**, Cao L. Differences in gene mutations between Chinese and Caucasian cystic fibrosis patients. *Pediatr Pulmonol* 2017; **52**: E11-E14 [PMID: 27717243 DOI: 10.1002/ppul.23539]

35   **Yao Y**, Feng XL, Xu BP, Shen KL. Pseudo-Bartter Syndrome in a Chinese Infant with Cystic Fibrosis Caused by c.532G>A Mutation in <i>CFTR</i>. *Chin Med J (Engl)* 2017; **130**: 2771-2772 [PMID: 29133775 DOI: 10.4103/0366-6999.218015]

36   **Sun Y**, Zhong YM, Zhu M, Wang SY, Wang J, Zhang H, Zhang L, Shao H. Clinical and radiological manifestations of 5 pediatric cases with cystic fibrosis. *J Clin Pediatr* 2017; **35**: 837-840 [DOI: 10.3969/j.issn.1000-3606.2017.11.009]

37   **Guo ZY**, Shi YY, Qian LL, Wang LB. A case report of infantile cystic fibrosis with pseudo-Bartter syndrome. *Zhongguo Xunzheng Erke Zazhi* 2017; **12**: 471-473 [DOI: 10.3969/j.issn.1673-5501.2017.06.014]

38   **Li J**, Zhang Y, Wang W, Wan WL, Qiu ZQ. One case of cystic fibrosis in children with pseudoBartter syndrome and literature review. *Shandong Yiyao* 2017; **57**: 48-50 [DOI: 10.3969/j.issn.1002-266X.2017.04.015]

39   **Richards S**, Aziz N, Bale S, Bick D, Das S, Gastier-Foster J, Grody WW, Hegde M, Lyon E, Spector E, Voelkerding K, Rehm HL; ACMG Laboratory Quality Assurance Committee. Standards and guidelines for

the interpretation of sequence variants: a joint consensus recommendation of the American College of Medical Genetics and Genomics and the Association for Molecular Pathology. *Genet Med* 2015; **17**: 405-424 [PMID: 25741868 DOI: 10.1038/gim.2015.30]

40   **Kristidis P**, Bozon D, Corey M, Markiewicz D, Rommens J, Tsui LC, Durie P. Genetic determination of exocrine pancreatic function in cystic fibrosis. *Am J Hum Genet* 1992; **50**: 1178-1184 [PMID: 1376016]

41   **Ferrari M**, Cremonesi L. Genotype-phenotype correlation in cystic fibrosis patients. *Ann Biol Clin (Paris)* 1996; **54**: 235-241 [PMID: 8949420 DOI: 10.1016/S0065-2423(08)60428-X]

CASE REPORT

Common iliac artery occlusion with small intestinal transection caused by blunt abdominal trauma: A case report and review of the literature

You-Xin Zhou, Yong Ji, Jing Chen, Xin Yang, Qing Zhou, Jian Lv

ORCID number: You-Xin Zhou (0000-0001-8498-709X); Yong Ji (0000-0002-8043-6589); Jing Chen (0000-0002-0147-1440); Xin Yang (0000-0002-8447-2181); Qing zhou (0000-0001-9214-1246); Jian Lv (0000-0002-9931-1946).

You-Xin Zhou, Yong Ji, Xin Yang, Jian Lv, Department of General Surgery, People's Hospital of Jingjiang, Yangzhou University Medical Academy, Jingjiang 214500, Jiangsu Province, China

Jing Chen, Imaging Department, People's Hospital of Jingjiang, Yangzhou University Medical Academy, Jingjiang 214500, Jiangsu Province, China

Qing Zhou, Department of General Surgery, Affiliated Hospital of Jiangsu University, Zhenjiang 212000, Jiangsu Province, China

Corresponding author: Jian Lv, MD, Doctor, Surgeon, Department of General Surgery, People's Hospital of Jingjiang, Yangzhou University Medical Academy, No. 28, Zhongzhou Road, Jingjiang 214500, Jiangsu Province, China. lvjian11@yahoo.com
Telephone: +86-0523-84995315
Fax: +86-0523-84995315

Abstract

BACKGROUND
Most major abdominal vascular injuries are caused by penetrating injuries. A common iliac artery occlusion caused by blunt force trauma is rare, and very few cases have been reported. Because of this low incidence, atypical symptoms, and frequent association with other severe injuries, the proper diagnosis tends to be missed or delayed. The gold standard for diagnosis is angiography, and treatment remains a challenge.

CASE SUMMARY
We report here the unusual case of a common iliac artery occlusion caused by blunt abdominal compressive trauma, with transection of the small intestine. At presentation, the patient (a 56-year-old man) complained of pain and numbness in the left lower extremity and severe pain in the whole abdomen. Physical examination showed total abdominal tenderness with evidence of peritoneal irritation. The left lower limb was pulseless and cold. Abdominal computed tomography examination revealed digestive tract perforation, and abdominal computed tomography angiography showed left common iliac artery occlusion. The patient was treated successfully by anastomosis of the intestine, percutaneous transluminal angioplasty, and stenting. The patient was followed for more than 11 mo after the operation and showed a good recovery.

CONCLUSION
Patients with abdominal trauma should be suspected of having major vascular

injury. Individualized treatment strategies are needed for this condition.

Key words: Common iliac artery occlusion; Transection of the small intestine; Blunt abdominal trauma; Case report; Percutaneous transluminal angioplasty; Anastomosis of the intestine

Core tip: Most major abdominal vascular injuries are caused by penetrating injuries. As a subset of arterial blunt trauma, the percentage of iliac arterial injury is small. Common iliac artery occlusion in blunt trauma is especially uncommon. We report such a rare case here. Furthermore, we review the reported cases in the English literature and provide a discussion on the mechanism of injury, clinical presentation and signs, diagnosis, surgical modalities, and outcome.

INTRODUCTION

Penetrating rather than blunt trauma causes the greatest majority of vascular injuries. As a subset of arterial blunt trauma, the percentage of iliac arterial injury is small. The largest review of these cases in the literature was published by Tuech *et al*[1], who reviewed 9 patients with common iliac artery occlusion in blunt trauma. We add to these rare cases in the literature by reporting a new case here. Furthermore, we review 7 cases reported between the years of 2001 and 2018, and discuss the mechanism of injury, clinical presentation and signs, diagnosis, surgical modalities, and outcome.

CASE PRESENTATION

Chief complaints
A 56-year-old male steel worker's lower abdomen had been compressed between two forklifts. He was admitted to the People's Hospital of Jingjiang with pain and numbness in the left lower extremity and severe pain throughout the entire abdomen, especially in the lower abdomen.

History of past illness
The patient had no significant medical history.

Family history
The patient had no significant family history.

Physical examination
The patient showed clear consciousness upon presentation. Physical examination showed stable vital signs, including blood pressure of 136/68 mmHg (normal range: 90-140/60-90 mmHg), pulse rate of 95/min (normal range: 60/min-100/min), respiratory rate of 16/min (normal range: 16/min-20/min), and temperature of 37.0 °C (normal range: 36.1°C-37°C). No obvious contusion of the abdominal wall or the left lower limb was noted. He had total abdomen tenderness, with evidence of peritoneal irritation and obvious board-like rigidity of the abdomen. The left lower extremity had good mobility but it was painful and numb, and skin temperature was significantly decreased. Pulsation of the left dorsal pedal artery had disappeared.

Laboratory examination
Laboratory examination revealed a hemoglobin level of 152 g/L (normal range: 130-175 g/L), white blood cell count of 13.2×10^9/L (normal range: 3.5×10^9/L to 9.5×10^9/L), and neutrophil percentage of 94.6% (normal range: 40%-75%).

Imaging examination

Pre-hospitalization abdominal computed tomography examination had revealed a perforation of the digestive tract. Abdominal computed tomography angiography showed occlusion of the left common iliac artery (Figure 1) and atherosclerosis of the abdominal aorta, bilateral iliac artery, and lower right femoral artery.

FINAL DIAGNOSIS

Common iliac artery occlusion with transection of the small intestine caused by blunt abdominal trauma.

TREATMENT

The patient underwent laparotomy under general anesthesia. Surgical findings included transection of the small intestine at about 2 m away from the ileocecus, without bleeding in the mesentery. About 200 mL of pus was found in the pelvic and abdominal cavity. We performed a partial small bowel resection and then a side-to-side small bowel anastomosis using a linear cutting closer (Figure 2A).

The abdominal symptoms of discomfort were completely relieved after the operation; however, the symptom of discomfort in the left leg became more prominent. The patient was immediately transferred to a superior hospital, where arteriography of the left lower extremity was performed, followed by percutaneous transluminal angioplasty with stenting at 4 d later. Unfortunately, the details of those operations were not available.

OUTCOME AND FOLLOW-UP

The postoperative course was uneventful. Physical examination revealed a warm left leg with restoration of pulse and normal sensation. Re-examination by abdominal computed tomography showed good position of the left common iliac artery stent (Figure 2B). The patient was followed for more than 11 mo after the operation and recovered well.

DISCUSSION

Injury to the common iliac artery secondary to blunt trauma is rare[2-6]. The reported rates of incidence of iliac artery injuries from trauma range from 0.4% to 7.1%[2,7]. The rare nature of this injury is largely due to the vessel's position in the retroperitoneal location, where it is protected by the bony pelvic girdle[5,6]. A total of only 8 cases, including our case reported herein, are present in the literature[8-14]. We have summarized the data from these cases on age, sex, causes of injury, location, clinical presentation and signs, findings of auxiliary examination, and associated injuries in Table 1. The data on operative delay time, procedure, fasciotomy, and outcomes are summarized in Table 2. The total 8 patients include 7 males and 1 female, with a mean age of 40 years old (range: 9-74 years). The causes of injury were seatbelt syndrome in 3 of the patients, direct compression injury in 4, and car crash in 1. Common iliac artery occlusion occurred on the left and bilateral sides in 2 cases each and on the right in 4. All 8 cases were diagnosed in time. Except for the youngest case among the total 8 and our case, the other 6 cases were treated immediately after admission. Four cases had a good prognosis. For the other 4 cases, 2 died, 1 suffered paralysis in the right leg, and 1 became paraplegic.

The most common mechanisms of injury appear to be direct anteroposterior compressions[6,15], traction from displaced bone fragments[16], and shearing forces, possibly accentuated by use of a seatbelt[17]. In fact, the mechanism of seatbelt syndrome or deceleration injury can also be understood as a type of abdominal compression. A total of 13 patients have been reported with common iliac artery occlusion due to direct anteroposterior compression[1]. We also found 4 cases of direct anteroposterior compression. It would be reasonable to assume then that abdominal compression is the main cause of common iliac artery occlusion. Blunt trauma-induced abdominal aortic injuries most frequently result in intimal tearing. Atherosclerotic disease has been postulated as a predisposing factor for aortic intimal tearing because of intimal weakening and loss of both elasticity and compliance[15,18].
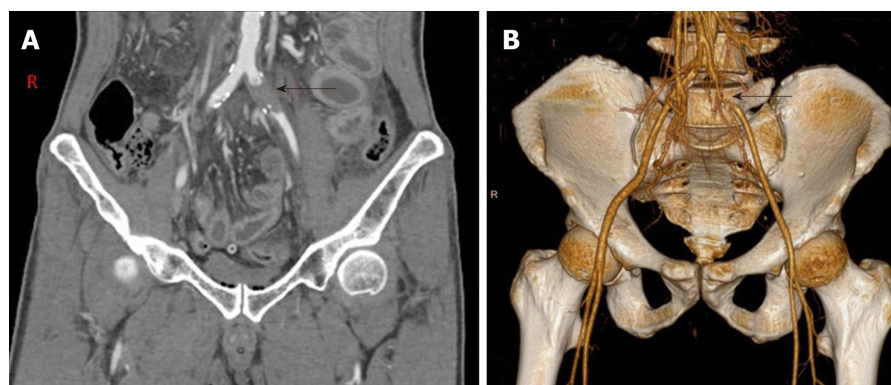
Figure 1 Abdominal computed tomography findings of a common iliac artery occlusion. A: Abdominal computed tomography angiography confirmed a 2.5 cm occlusion of the left common iliac artery, with preservation of the common iliac bifurcation and distal arterial tree. There was no evidence of active arterial bleeding or pseudoaneurysm formation (arrow); B: Three-dimensional computed tomography angiogram reconstruction showed obvious occlusion of the left common iliac artery (arrow).
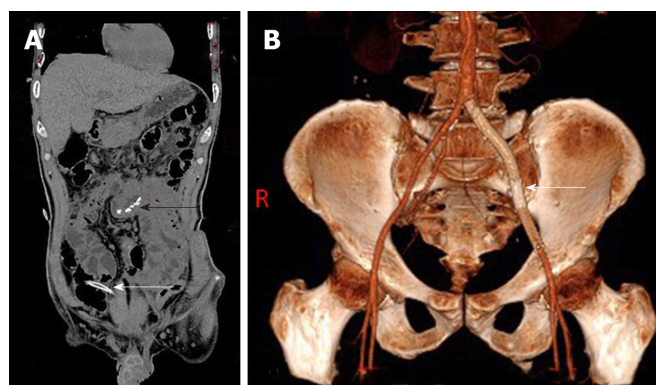
In our patient, abdominal computed tomography angiography examination showed atherosclerosis of the abdominal aorta, bilateral iliac artery, and lower right femoral artery. We can speculate that the occlusion of the left common iliac artery may also have been caused by atherosclerotic plaque rupture. Endometrial tear, atherosclerotic plaque rupture, and intramural hematoma formation can lead to common iliac artery diameter reduction or even occlusion. If the compression force is strong enough, it may lead to transection of the common iliac artery[19].

Because of the low incidence of this injury, its atypical symptoms, and frequent association with other severe injuries, the diagnosis is often missed or delayed. This can cause serious harm to the patients. Therefore, our attention should be focused on proper identification and early diagnosis. The clinical manifestations and signs of acute lower limb ischemia can provide important clues for the diagnosis. It is important to note that acute limb ischemia caused by common iliac artery occlusion from blunt abdominal trauma is rare[2,5] and clinical presentation may be delayed for months or years[6,17]. Tuech *et al*[1] reported the median operative delay time to be 15 d, ranging from 3 d to 36 years. All of the 8 cases we reviewed (including our own) presented acute lower limb ischemia. This may be the main reason why they were able to receive timely diagnosis and treatment. Except for the youngest patient and our patient among these 8 total cases, the other 6 patients were diagnosed and treated shortly after admission. The youngest and our patient were also diagnosed shortly after admission but the surgery was performed 4 d later. For the former, given the patient's young age and incomplete occlusion with severe multiple injuries, a conservative initial approach was decided. For the latter, we delayed operation due to the incomplete occlusion allowing for a longer observation period.

Most patients present with other injuries, such as traumatic intestinal perforation, pelvic fracture, liver and spleen injury, bladder rupture, and contusion of the thoracoabdominal wall, among others. Treating clinicians should be especially careful with these patients because the signs and symptoms of vascular injury may be obscured by the signs and symptoms of other injury, especially in those patients who do not show acute lower limb ischemia. It is very important to inquire about the patient's detailed medical history and to perform a meticulous physical examination. In addition, it is also necessary to go to the bedside frequently, to observe any changes in the patient's condition because changes in emergency patients are dynamic.

Angiography is the gold standard for diagnosis and should be performed when there is a clinical doubt. The development of abdominal computed tomography angiography has allowed for three-dimensional reconstruction of the blood vessels and a clearer assessment of the location and extent of damage, which can help surgeons in deciding on the correct treatment strategies. The precondition of angiography is the hemodynamic stability of the patient. It is generally contrain-dicated in a hemodynamically unstable patient with multisystem injury; for these patients, duplex ultrasonography may be helpful. Among the total 8 cases discussed herein, 6 underwent angiography, 3 of which were given the abdominal computed tomography angiography; the 2 other patients did not undergo any blood vessel examination.

Once injury to the common iliac artery has been determined, operative repair is generally indicated. The surgical procedure includes both open and endovascular

Figure 2 Abdominal computed tomography findings after partial small intestine resection and stent implantation. A: The nail of the linear cutting closer is shown (black arrow) along with the abdominal cavity silicone drainage tube (white arrow); B: Three-dimensional computed tomography angiogram reconstruction confirmed good position of the left common iliac artery stent (white arrow).

approaches. Ligation of the iliac artery results in an unacceptable amputation rate of up to 50%[7]. Major vessels should be ligated only when the procedure is considered to be life-saving or in the presence of gross contamination, where subsequent extra-anatomical grafting is possible[2]. The loss of 1.5 cm of vessel is the maximum length that can be dealt with by mobilization and end-to-end anastomosis[2,13]. Furthermore, the vascular wall must be normal before anastomosis and the anastomotic site must be free of tension. Long segment injury may require substitution of a vascular conduit[20].

Autologous vein grafts and synthetic grafts are available. At present it is still debatable which is better - an autologous vein graft or a synthetic graft. Autologous grafting with the hypogastric artery or saphenous vein on injured iliac arteries may give rise to the problems of size discrepancies and time consumption in harvest, making these grafts unfavorable[1,5]. Synthetic grafts are more favorable as they are available in various sizes, but they are not ideal in cases of peritoneal contamination from concomitant bowel perforation. Several articles have provided evidence that polytetrafluoroethylene grafts may be used in the face of substantial contamination and may be resistant to subsequent infection[21,22].

Extra-anatomic bypass and femorofemoral or axillofemoral bypass are alternatives. Endovascular techniques have been used to treat a variety of endovascular diseases[23-26]. The endovascular approach offers benefits in terms of easier access to the target lesion, reduction in blood transfusion requirement, and obviation of the potential need for systemic heparinization[13]. Among the total 8 patients discussed herein, 5 underwent endovascular stenting and the remaining 3 underwent open surgery. Jovanovic *et al*[11] consider that reinforcement of the posterior aortic wall to the anterior longitudinal ligament should be added to the armamentarium of aortic injury treatment. In our case, the final choice of endovascular therapy may have resulted from consideration of the patient's hemodynamic stability, absence of vessel rupture, and severe abdominal cavity contamination.

Considering that most patients with this injury present with multiple other severe injuries, it is important to remember that the primary purpose of treatment is to save the patient's life. Therefore, the principles of simplicity and efficiency must be satisfied when choosing the therapeutic method. Endovascular therapy has the advantages of being minimally invasive, having little effect on the patient, and producing clear effect, all of which conform to the above two principles. Among the total 8 patients discussed herein, 2 did not receive surgery until 4 d after the diagnosis and neither experienced serious repercussions.

Taking into account the information presented in previous literature reviews of this injury, we noted the consequence of short-term ischemic necrosis of the affected limb to be infrequent. Therefore, within the time allowed, the most serious injury endangering the patient's life should be addressed first, followed by the compression injury of the lower abdomen when the patient's general condition has stabilized. It is important to avoid multi-organ surgery and long anesthesia time associated with a one-stage operation, especially for patients who are elderly, have underlying basic diseases, or are seriously injured. This is consistent with the current damage control theory; however, the premise is to closely observe changes in the patient's condition. Once the limb is found to have the tendency of ischemic necrosis, immediate surgical intervention should be initiated.

Table 1 Demographic and clinical profile of the cases of compression injury of the lower abdomen in the literature

Age (sex)	Cause of injury	Location	Symptom and sign	Auxiliary examination	Associated injuries
44 (M)	Car crash	Right	Cold right lower leg; absent right femoral, popliteal, and pedal pulses; absent left popliteal and pedal pulses	Angiography	Subarachnoid and intraventricular hemorrhage and diffuse axonal injury; subcapsular hematoma of the liver, splenic laceration, comminuted fracture of the left iliac wing, and widening of the left sacroiliac joint; contusion of the mid-abdomen
27 (M)	Crushed between a fork-lift truck and a concrete platform	Bilateral	Cold and loss of motor function for both feet, with the right foot being worse; no femoral or pedal pulse	Doppler scanning; arteriography	Pelvic and right acetabular fracture; retroperitoneal bladder rupture; abdominal wall disruption
74 (F)	Seatbelt injury	Bilateral (aortic bifurcation disruption)	Pulseless and cold	No	Contusion of chest wall and left lung; complete disruption of the lower abdominal muscles; intestinal transection with mesenteric disruption
26 (M)	Abdominal and lumbar spine compression in a metal press	Left	Cold and pale; reduction of power and sensory loss; no pulsation of the femoral artery	ACTA	Contusion of the abdominal wall; retroperitoneal hematoma in the left psoas muscle
9 (M)	Seatbelt-related injury	Right (aortic dissection)	A cold right lower leg	MRA	Intestinal perforation; fractures of the lumbar spine
51 (M)	Abdomen compression by a tractor against a house wall	Right (aortic dissection)	Cold and pale; no palpable artery pulses	ACTA	Traumatic perforations of the ileum and transversal colon
35 (M)	Seatbelt injury	Right	Absent right femoral, popliteal, and posterior tibial pulses	No	Multiple scalp and face lacerations; bowel transections of descending colon and one segment of the small bowel
56 (M)	Lower abdomen compression between two forklifts	Left	Pain; cold and numb; pulsation of the left dorsal pedal artery disappeared	ACTA	Transection of small intestine

ACTA: Abdominal computed tomography angiography; MRA: Magnetic resonance angiography.

Compartment syndrome should be anticipated after revascularization. Postoperative increase in pain in the distal limb, any evidence of decreased perfusion, increasing neurological signs, or limb swelling warrant fasciotomy without delay[2]. Among the total 8 patients discussed herein, delayed fasciotomy occurred in 3. Certainly, close observation and judicious clinical judgment are necessary in every case.

CONCLUSION

All patients with abdominal trauma should be suspected of having major vascular injury, especially those with compression injury of the lower abdomen. Taking detailed medical history and performing a meticulous physical examination are necessary. In addition, the patient should be carefully observed to detect any changes in the overall condition. It is especially important to consider the most simple and effective methods first, to minimize the risk of death. Ultimately, however, individualized treatment strategies based on each patient's condition are needed and will improve outcomes.

Table 2 Treatment details and prognosis of the 8 cases

Operative delay time	Procedure	Fasciotomy	Result
< 4 h	Endovascular stenting	No	Died due to complications of brain injury
Shortly after admission	Endovascular stenting	Right	Right leg paralysis persisted secondary to severe lumbar plexus nerve injury
Shortly after admission	Aortoiliac bypass with spiraled saphenous vein graft	Bilateral	Died due to severe acute respiratory distress syndrome and associated pulmonary sepsis
Shortly after admission	Endovascular stenting	No	Good
After 4 d	Endovascular stenting	Right	Well-perfused right lower limb with normal pulses but paraplegic
Shortly after admission	Use of anterior longitudinal ligament and great saphenous vein graft	No	Good
Approximately 3 h	Segmental excision and internal iliac artery patch angioplasty	No	Good
After 4 d	Endovascular stenting	No	Good

REFERENCES

1 **Tuech JJ**, Villapadierna F, Singland JD, Papon X, Pessaux P, Vergos M. Blunt injury to the common iliac artery. *Eur J Vasc Endovasc Surg* 2000; **20**: 47-50 [PMID: 10906297 DOI: 10.1053/ejvs.2000.1118]

2 **Blacklay PF**, Duggan E, Wood RF. Vascular trauma. *Br J Surg* 1987; **74**: 1077-1083 [PMID: 3322478 DOI: 10.1002/bjs.1800741204]

3 **Ekbom GA**, Towne JB, Majewski JT, Woods JH. Intra-abdominal vascular trauma-a need for prompt operation. *J Trauma* 1981; **21**: 1040-1044 [PMID: 7033558 DOI: 10.1097/00005373-198112000-00007]

4 **Feliciano DV**, Bitondo CG, Mattox KL, Burch JM, Jordan GL, Beall AC, De Bakey ME. Civilian trauma in the 1980s. A 1-year experience with 456 vascular and cardiac injuries. *Ann Surg* 1984; **199**: 717-724 [PMID: 6375595 DOI: 10.1097/00000658-198406000-00010]

5 **Tsai FC**, Wang CC, Fang JF, Lin PJ, Kao CL, Hsieh HC, Chu JJ, Chen RJ, Chang CH. Isolated common iliac artery occlusion secondary to atherosclerotic plaque rupture from blunt abdominal trauma: case report and review of the literature. *J Trauma* 1997; **42**: 133-136 [PMID: 9003272 DOI: 10.1097/00005373-199701000-00024]

6 **Buscaglia LC**, Matolo N, Macbeth A. Common iliac artery injury from blunt trauma: case reports. *J Trauma* 1989; **29**: 697-699 [PMID: 2724390 DOI: 10.1097/00005373-198905000-00029]

7 **DeBAKEY ME**, SIMEONE FA. Battle injuries of the arteries in World War II; an analysis of 2,471 cases. *Ann Surg* 1946; **123**: 534-579 [PMID: 21024586 DOI: 10.1097/00000658-194604000-00005]

8 **Sternbergh WC**, Conners MS, Ojeda MA, Money SR. Acute bilateral iliac artery occlusion secondary to blunt trauma: successful endovascular treatment. *J Vasc Surg* 2003; **38**: 589-592 [PMID: 12947281 DOI: 10.1016/S0741-5214(03)00295-7]

9 **Aerts NR**, Lichtenfels E, Erling N. Seat Belt Syndrome and Aortoiliac Lesion: Case Report and Review of the Literature. *Eur J Trauma Emerg Surg* 2007; **33**: 198-200 [PMID: 26816152 DOI: 10.1007/s00068-006-5134-1]

10 **Poon H**, Patel A, Vijay S, Downing R. Endovascular repair for left common iliac artery occlusion following blunt trauma without associated bony injury: image in vascular surgery. *Vasc Endovascular Surg* 2012; **46**: 179-180 [PMID: 22232330 DOI: 10.1177/1538574411431343]

11 **Jovanovic M**, Radojkovic M, Djordjevic P, Rancic D, Jovanovic N, Rancic Z. Recycling and Reinforcing Intimomedial Flap of the Infrarenal Aorta Using Anterior Longitudinal Ligament in Patients With Acute Trauma With Bowel Injuries. *Vasc Endovascular Surg* 2017; **51**: 501-505 [PMID: 28764607 DOI: 10.1177/1538574417722930]

12 **Mogannam AC**, Cubas RF, Gutierrez IM, Astudillo JA, Abou-Zamzam AM. Blunt Traumatic Occlusion of the Common Iliac Artery Repaired With Segmental Excision and Internal Iliac Artery Patch Angioplasty. *Ann Vasc Surg* 2017; **39**: 284.e1-284.e4 [PMID: 27908816 DOI: 10.1016/j.avsg.2016.08.025]

13 **Lyden SP**, Srivastava SD, Waldman DL, Green RM. Common iliac artery dissection after blunt trauma: case report of endovascular repair and literature review. *J Trauma* 2001; **50**: 339-342 [PMID: 11242303 DOI: 10.1097/00005373-200102000-00024]

14 **Papazoglou KO**, Karkos CD, Kalogirou TE, Giagtzidis IT. Endovascular management of lap belt-related abdominal aortic injury in a 9-year-old child. *Ann Vasc Surg* 2015; **29**: 365.e11-365.e15 [PMID: 25463338 DOI: 10.1016/j.avsg.2014.09.026]

15 **Beless DJ**, Muller DS, Perez H. Aortoiliac occlusion secondary to atherosclerotic plaque rupture as the result of blunt trauma. *Ann Emerg Med* 1990; **19**: 922-924 [PMID: 2372177 DOI: 10.1016/S0196-0644(05)81571-9]

16 **Frank JL**, Reimer BL, Raves JJ. Traumatic iliofemoral arterial injury: an association with high anterior acetabular fractures. *J Vasc Surg* 1989; **10**: 198-201 [PMID: 2760998 DOI: 10.1067/mva.1989.0100198]

17 **Nitecki S**, Karmeli R, Ben-Arieh Y, Schramek A, Torem S. Seatbelt injury to the common iliac artery: report of two cases and review of the literature. *J Trauma* 1992; **33**: 935-938 [PMID: 1474646 DOI: 10.1097/00005373-199212000-00029]

18 **Gupta N**, Auer A, Troop B. Seat belt-related injury to the common iliac artery: case report and review of the literature. *J Trauma* 1998; **45**: 419-421 [PMID: 9715211 DOI: 10.1097/00005373-199808000-00044]

19   **Ko SY**, Tan KH, Cheng-Huang CY, Huang MK, Seow VK, Chen CC. Complete common iliac artery transection: an easily misdiagnosed but fatal complication of blunt abdominal injury. *Am J Emerg Med* 2007; **25**: 251-253 [PMID: 17276845 DOI: 10.1016/j.ajem.2006.11.017]

20   **Feliciano DV**, Mattox KL, Graham JM, Bitondo CG. Five-year experience with PTFE grafts in vascular wounds. *J Trauma* 1985; **25**: 71-82 [PMID: 3965739 DOI: 10.1097/00005373-198501000-00012]

21   **Landreneau RJ**, Lewis DM, Snyder WH. Complex iliac arterial trauma: autologous or prosthetic vascular repair? *Surgery* 1993; **114**: 9-12 [PMID: 8356533]

22   **Shah DM**, Leather RP, Corson JD, Karmody AM. Polytetrafluoroethylene grafts in the rapid reconstruction of acute contaminated peripheral vascular injuries. *Am J Surg* 1984; **148**: 229-233 [PMID: 6465430 DOI: 10.1016/0002-9610(84)90227-7]

23   **Ouchi T**, Kato N, Nakajima K, Higashigawa T, Hashimoto T, Chino S, Sakuma H. Splenic Artery Aneurysm Treated With Endovascular Stent Grafting: A Case Report and Review of Literature. *Vasc Endovascular Surg* 2018; **52**: 663-668 [PMID: 29940816 DOI: 10.1177/1538574418785252]

24   **Kaya U**, Colak A, Becit N, Ceviz M, Kocak H. Endovascular Stent Graft Repair of Localized Acute Aortic Intramural Hematoma: A Case Report and Literature Review. *Eurasian J Med* 2017; **49**: 211-213 [PMID: 29123447 DOI: 10.5152/eurasianjmed.2017.17151]

25   **Zebari S**, Huang DY, Wilkins CJ, Sidhu PS. Acute Testicular Segmental Infarct Following Endovascular Repair of a Juxta-renal Abdominal Aortic Aneurysm: Case Report and Literature Review. *Urology* 2019; **126**: 5-9 [PMID: 30529337 DOI: 10.1016/j.urology.2018.11.030]

26   **Woo EY**, Milner R, Brayman KL, Fairman RM. Successful PTA and stenting for acute iliac arterial injury following pancreas transplantation. *Am J Transplant* 2003; **3**: 85-87 [PMID: 12492717 DOI: 10.1034/j.1600-6143.2003.30116.x]

CASE REPORT

Percutaneous coronary intervention for ostial lesions of the left main stem in a patient with congenital single left coronary artery: A case report

Qiang Wu, Zong-Zhuang Li, Feng Yue, Fang Wei, Chen-Yun Zhang

ORCID number: Qiang Wu (0000-0001-9603-1192); Zong-Zhuang Li (0000-0004-1791-4503); Feng Yue (0000-0001-8690-1130); Fang Wei (0000-0001-8346-9899); Chen-Yun Zhang (0000-0001-5198-0959).

Informed consent statement: The patient gave informed consent for the publication of this case report and any accompanying images.

Conflict-of-interest statement: The authors have no conflicts of interest to disclose.

CARE Checklist (2016) statement: The manuscript was revised according to the CARE checklist.

Qiang Wu, Zong-Zhuang Li, Feng Yue, Fang Wei, Chen-Yun Zhang, Department of Cardiology, Guizhou Provincial People's Hospital, Guiyang, 550002, Guizhou Province, China

Corresponding author: Chen-Yun Zhang, MD, Chief Physician, Department of Cardiology, Guizhou Provincial People's Hospital, No. 83, East Zhongshan Road, Guiyang 550002, Guizhou Province, China. cyzhang5828@163.com
Telephone: +86-851-85937213
Fax: +86-851-85937213

Abstract

BACKGROUND
Single coronary artery (SCA) originating from a solitary ostium in the aorta and perfusing the entire myocardium is a very rare congenital anomaly of the coronary artery. Furthermore, a right coronary artery (RCA) arising from the mid segment of the left anterior descending artery (LAD) is an extremely uncommon variation of SCA.

CASE SUMMARY
A 76-year-old woman presented a 5-mo history of exertional angina. Selective coronary angiography revealed an SCA, with severe ostial stenosis that originated from the left sinus of Valsalva and bifurcated normally into the LAD and circumflex coronary artery. In addition, an anomalous RCA originated from the mid segment of the LAD as a separate branch. Successful balloon angioplasty and stenting for the SCA ostial stenosis were performed on the patient.

CONCLUSION
Percutaneous coronary intervention (PCI) of the main trunk for SCA is very similar to PCI of an unprotected left main coronary artery. Although technical difficulties and risks do exist, PCI for severe ostial stenosis of the main trunk is safe and efficacious in selected SCA patients.

Key words: Coronary anomaly; Single coronary artery; Left main coronary artery; Percutaneous coronary intervention; Case report

Core tip: The right coronary artery arising from the mid segment of the left anterior

descending artery is an extremely uncommon variation of single coronary artery (SCA). In this report, a 76 year-old female presented a 5-month history of exertional angina. Selective coronary angiography revealed an SCA, with severe ostial stenosis. Successful balloon angioplasty and stenting for the SCA ostial stenosis were performed on this case. Although technical difficulties and definite risk do exist, percutaneous coronary intervention for severe ostial stenosis of main trunk is safe and efficacious in selected SCA cases.

INTRODUCTION

Single coronary artery (SCA) that originates from a single ostium in the aortic trunk and perfuses the entire myocardium is an extremely rare congenital anomaly of the coronary artery. The incidence of SCA ranges from 0.016% to 0.066% in the patient population undergoing coronary angiography[1-3]. Myocardial perfusion could be affected in patients with different SCA subtypes, such as SCA arising ectopically from the right aortic sinus and passing between the aorta and pulmonary artery before dividing into the left anterior descending artery (LAD) and left circumflex artery, slit-like ostium due to an acute angle of SCA, or those complicated with proximal atherosclerotic stenosis[4-6]. Coronary artery ostioplasty and bypass grafting are recommended as the first-line revascularization therapeutic strategy for these subtypes of SCA which can cause serious, even fatal, consequences[7,8]. In this case report, a patient with SCA, combined with severe ostial lesions of the left main coronary artery (LM) and significant stenosis of the left anterior descending artery (LAD), was successfully treated by percutaneous coronary intervention (PCI).

CASE PRESENTATION

Chief complaints

A 76-year-old woman with a medical history of hypertension and hypercholesterolemia was admitted with progressive angina over five months.

Examinations of the patient

Electrocardiography showed non-specific ST-T abnormalities. The transthoracic echocardiography findings were normal for left ventricular performance without segmental hypokinesis. Diagnostic coronary angiography performed *via* the transfemoral approach showed that the LM, which normally originates from the left sinus of the Valsalva, had a 95% ostial calcified stenosis and slight shaft lesion. The LM branched into the normal left circumflex artery and the LAD with a diffuse lesion (70%-99%) in its mid segment with delayed distal flow. An anomalous branch without significant lesions arose from the mid-portion of the LAD and perfused the notional area of the right coronary artery (RCA) (Figure 1). The LAD wrapped around the apex, had an extended length, and then supplied to the posterior and inferior wall. Aortography revealed a blunt right and noncoronary sinus without any stumps (Figure 2).

FINAL DIAGNOSIS

The patient was diagnosed with coronary atherosclerotic heart disease with unstable angina; essential hypertension and hypercholesterolemia; and congenital SCA anomaly with branching of the RCA originating from the LAD, complicated with ostial LM lesions and a mid-segment stenosis of the LAD.
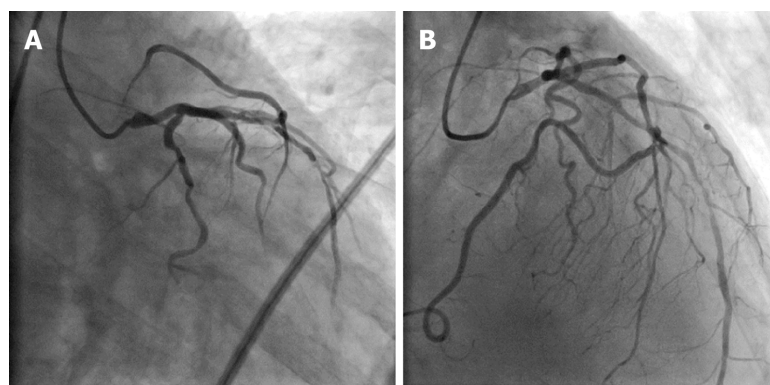
Figure 1 Coronary angiograms. A: Left anterior oblique caudal view; B: Right anterior oblique cranial view. The coronary angiograms show the left main coronary artery with severe ostial stenosis and left anterior descending artery (LAD) with a diffuse lesion in the mid segment and right coronary artery from the midportion of the LAD.

TREATMENT

Based on these findings, surgical treatment was advised for the patient. However, she refused coronary artery bypass grafting and instead accepted PCI. A 6F Judkin's left 4 guiding catheter was used to engage the main trunk and an intra-aortic vacant guide wire was placed to prevent a decrease in blood pressure in the coronary artery. After balloon pre-dilatation of the lesion around the LM and LAD, two sirolimus-eluting stents (2.5 mm × 33 mm and 3.0 mm × 33 mm) were placed at the middle LAD and then a 3.5 mm × 18 mm sirolimus-eluting stent at the ostial and shaft of the single coronary trunk was successfully deployed. Balloon post-dilatations of the entire stented segment were performed per standard procedure. The final angiographic results were satisfactory as demonstrated by thrombolysis in myocardial infarction grade 3 flow (Figure 3). The collaterals from the RCA and left circumflex artery were still visible.

OUTCOME AND FOLLOW-UP

Postoperatively, the patient was treated with guideline-directed medical therapy, which included aspirin, clopidogrel, irbesartan, and atorvastatin. The patient was followed at 6-mo intervals. No myocardial ischemia symptoms, changes in electrocardiography, cardiac dysfunction, or adverse cardiac events were noted during the three-year follow-up period.

DISCUSSION

SCA is a rare congenital anomaly of the coronary artery and is usually found by coronary angiography or necropsy. An SCA may arise with a single ostium from either the left Valsalva sinus or the right sinus. This causes confusion on where to cannulate another coronary artery ostium upon coronary angiography. Multislice computed tomography and magnetic resonance imaging can also aid in the diagnosis of SCA[4,9,10]. Multislice computed tomography may be superior to conventional selective coronary angiography in confirming and visualizing the origin, course, and termination of the SCA. Magnetic resonance coronary angiography, without radiation and contrast medium, has advantages in providing the spatial position of SCA[11,12].

Lipton *et al*[13] originally classified these coronary variations based on the site of origin, anatomical distribution, and course of the branches. Type L or R describes SCA that arises from the sinus of Valsalva and divides them into class I-III. Class I denotes SCA following the normal left or right course. In class II, an anomalous artery arises from the proximal part of the normally located opposite coronary artery and crosses at the base of the heart as a large transverse trunk to supply the contralateral coronary artery. Class III represents the LAD and the circumflex artery originating separately from the proximal part of the normal RCA. In classes II and III, based on the relationship between the anomalous coronary artery, the aorta, and the pulmonary artery, the "A" refers to the anomalous artery passing anterior to the pulmonary artery, and "B" refers to it coursing between the aorta and pulmonary artery, while
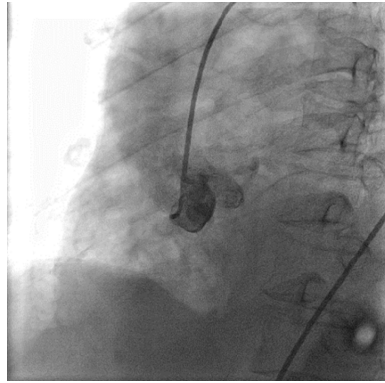
Figure 2 Aortography (left anterior oblique view) reveals a blunt right and noncoronary sinus without coronary origin.

"P" refers to it passing posterior to the large vessels. Yamanaka *et al*[2] and Shirani *et al*[14] modified the classification to describe the origin and course of these coronary anomalies. The anomalous origin of the RCA arose from the midportion of LAD in our patient, which is an extremely rare variation of SCA and does not fall under any subtype of Lipton's classification[15,16]. This kind of congenital anomaly generally remains asymptomatic. However, the origin of the anomalies and the course of the coronary artery are heterogeneous variations of clinical presentations and consequences[17].

CONCLUSION

There has been no consensus regarding the risk for atherosclerosis in patients with SCA. However, the myocardial ischemia symptoms in our patient were caused apparently by atherosclerotic stenosis of the LM and LAD, and not the anomaly itself. Unprotected LM stenosis has been traditionally treated using coronary artery bypass grafting. Improvements in drug-eluting stents and techniques have led to increased use of PCI on unprotected LM[18,19]. Results from randomized clinical trials and registries have confirmed that PCI of the LM lesion is safe and efficacious in selected patients with low or intermediate angiographic risk scores[20,21]. However the PCI procedure for the main trunk ostial lesion of SCA is still a technical challenge for surgeons and may be of high risk. Stenting on the shaft and distal lesions of the LM have been described previously only in three patients[22-24]. However, this report is the first to describe PCI for severe ostial main stem stenosis and SCA with an anomalous origin of the RCA arising from the LAD.

Figure 3 Coronary angiograms after percutaneous coronary intervention. A: Caudal view; B: Right anterior oblique cranial view. The images show excellent stent expansion and no dissection in the left main coronary artery ostia, the mid segment of left anterior descending artery, and right coronary artery with thrombolysis in myocardial infarction grade 3 flow.

REFERENCES

1   **Yildiz A**, Okcun B, Peker T, Arslan C, Olcay A, Bulent Vatan M. Prevalence of coronary artery anomalies in 12,457 adult patients who underwent coronary angiography. *Clin Cardiol* 2010; **33**: E60-E64 [PMID: 21184546 DOI: 10.1002/clc.20588]

2   **Yamanaka O**, Hobbs RE. Coronary artery anomalies in 126,595 patients undergoing coronary arteriography. *Cathet Cardiovasc Diagn* 1990; **21**: 28-40 [PMID: 2208265]

3   **Desmet W**, Vanhaecke J, Vrolix M, Van de Werf F, Piessens J, Willems J, de Geest H. Isolated single coronary artery: a review of 50,000 consecutive coronary angiographies. *Eur Heart J* 1992; **13**: 1637-1640 [PMID: 1289093]

4   **Brothers JA**, Whitehead KK, Keller MS, Fogel MA, Paridon SM, Weinberg PM, Harris MA. Cardiac MRI and CT: differentiation of normal ostium and intraseptal course from slitlike ostium and interarterial course in anomalous left coronary artery in children. *AJR Am J Roentgenol* 2015; **204**: W104-W109 [PMID: 25539262 DOI: 10.2214/AJR.14.12953]

5   **Kim SY**, Seo JB, Do KH, Heo JN, Lee JS, Song JW, Choe YH, Kim TH, Yong HS, Choi SI, Song KS, Lim TH. Coronary artery anomalies: classification and ECG-gated multi-detector row CT findings with angiographic correlation. *Radiographics* 2006; **26**: 317-33; discussion 333-4 [PMID: 16549600 DOI: 10.1148/rg.262055068]

6   **Basso C**, Maron BJ, Corrado D, Thiene G. Clinical profile of congenital coronary artery anomalies with origin from the wrong aortic sinus leading to sudden death in young competitive athletes. *J Am Coll Cardiol* 2000; **35**: 1493-1501 [PMID: 10807452]

7   **Angelini P**, Walmsley RP, Libreros A, Ott DA. Symptomatic anomalous origination of the left coronary artery from the opposite sinus of valsalva. Clinical presentations, diagnosis, and surgical repair. *Tex Heart Inst J* 2006; **33**: 171-179 [PMID: 16878619]

8   **Anuwatworn A**, Karta P, Yee J, Li S, Kumar V, Steffen K. Single Coronary Artery Arising from the Right Sinus of Valsalva and the Role of Coronary Computed Tomography Angiography. *S D Med* 2018; **71**: 130-132 [PMID: 29991101]

9   **Srinivasan KG**, Gaikwad A, Kannan BR, Ritesh K, Ushanandini KP. Congenital coronary artery anomalies: diagnosis with 64 slice multidetector row computed tomography coronary angiography: a single-centre study. *J Med Imaging Radiat Oncol* 2008; **52**: 148-154 [PMID: 18373806 DOI: 10.1111/j.1440-1673.2008.01933.x]

10 **Aldana-Sepulveda N**, Restrepo CS, Kimura-Hayama E. Single coronary artery: spectrum of imaging findings with multidetector CT. *J Cardiovasc Comput Tomogr* 2013; **7**: 391-399 [PMID: 24331935 DOI: 10.1016/j.jcct.2013.11.009]

11 **Taylor AM**, Thorne SA, Rubens MB, Jhooti P, Keegan J, Gatehouse PD, Wiesmann F, Grothues F, Somerville J, Pennell DJ. Coronary artery imaging in grown up congenital heart disease: complementary role of magnetic resonance and x-ray coronary angiography. *Circulation* 2000; **101**: 1670-1678 [PMID: 10758049]

12 **Clemente A**, Del Borrello M, Greco P, Mannella P, Di Gregorio F, Romano S, Morra A. Anomalous origin of the coronary arteries in children: diagnostic role of three-dimensional coronary MR angiography. *Clin Imaging* 2010; **34**: 337-343 [PMID: 20813295 DOI: 10.1016/j.clinimag.2009.08.030]

13 **Lipton MJ**, Barry WH, Obrez I, Silverman JF, Wexler L. Isolated single coronary artery: diagnosis, angiographic classification, and clinical significance. *Radiology* 1979; **130**: 39-47 [PMID: 758666 DOI: 10.1148/130.1.39]

14 **Shirani J**, Roberts WC. Solitary coronary ostium in the aorta in the absence of other major congenital cardiovascular anomalies. *J Am Coll Cardiol* 1993; **21**: 137-143 [PMID: 8417054]

15 **Wilson J**, Reda H, Gurley JC. Anomalous right coronary artery originating from the left anterior descending artery: case report and review of the literature. *Int J Cardiol* 2009; **137**: 195-198 [PMID: 19427707 DOI: 10.1016/j.ijcard.2009.03.140]

16 **Yurtdaş M**, Gülen O. Anomalous origin of the right coronary artery from the left anterior descending artery: review of the literature. *Cardiol J* 2012; **19**: 122-129 [PMID: 22461044]

17 **Angelini P**, Velasco JA, Flamm S. Coronary anomalies: incidence, pathophysiology, and clinical relevance. *Circulation* 2002; **105**: 2449-2454 [PMID: 12021235]

18 **Yang YY**, Wu Q. Two-staged stent-assisted angioplasty treatment strategy for severe left main coronary distal bifurcation stenosis associated with the right coronary chronic total occlusion. *Int J Clin Exp Med* 2014; **7**: 4509-4514 [PMID: 25550977]

19   **Chen SL**, Zhang JJ, Han Y, Kan J, Chen L, Qiu C, Jiang T, Tao L, Zeng H, Li L, Xia Y, Gao C, Santoso T, Paiboon C, Wang Y, Kwan TW, Ye F, Tian N, Liu Z, Lin S, Lu C, Wen S, Hong L, Zhang Q, Sheiban I, Xu Y, Wang L, Rab TS, Li Z, Cheng G, Cui L, Leon MB, Stone GW. Double Kissing Crush Versus Provisional Stenting for Left Main Distal Bifurcation Lesions: DKCRUSH-V Randomized Trial. *J Am Coll Cardiol* 2017; **70**: 2605-2617 [PMID: 29096915 DOI: 10.1016/j.jacc.2017.09.1066]

20   **Xu B**, Redfors B, Yang Y, Qiao S, Wu Y, Chen J, Liu H, Chen J, Xu L, Zhao Y, Guan C, Gao R, Généreux P. Impact of Operator Experience and Volume on Outcomes After Left Main Coronary Artery Percutaneous Coronary Intervention. *JACC Cardiovasc Interv* 2016; **9**: 2086-2093 [PMID: 27765302 DOI: 10.1016/j.jcin.2016.08.011]

21   **Gershlick AH**, Kandzari DE, Banning A, Taggart DP, Morice MC, Lembo NJ, Brown WM, Banning AP, Merkely B, Horkay F, van Boven AJ, Boonstra PW, Dressler O, Sabik JF, Serruys PW, Kappetein AP, Stone GW. Outcomes After Left Main Percutaneous Coronary Intervention Versus Coronary Artery Bypass Grafting According to Lesion Site: Results From the EXCEL Trial. *JACC Cardiovasc Interv* 2018; **11**: 1224-1233 [PMID: 29976358 DOI: 10.1016/j.jcin.2018.03.040]

22   **Roffi M**, Eberli FR, Wyttenbach R, Gallino A. Percutaneous coronary intervention of the left main trunk in congenitally anomalous single coronary artery. *J Invasive Cardiol* 2001; **13**: 808-809 [PMID: 11731695]

23   **Stevens GR**, Kini AS, Sharma SK. Intervention of stenosed right coronary artery and anomalous left main coronary artery: single main coronary trunk. *J Invasive Cardiol* 2008; **20**: E71-E72 [PMID: 18316835]

24   **Kawashima S**, Shiraishi J, Hyogo M, Shima T, Sawada T, Kohno Y. Main trunk crossover stenting in a patient with left internal thoracic artery--protected single coronary artery. *Cardiovasc Interv Ther* 2015; **30**: 307-310 [PMID: 25117026 DOI: 10.1007/s12928-014-0293-1]

Baishideng®